

UNCLASSIFIED

AD NUMBER
AD803509
NEW LIMITATION CHANGE
TO Approved for public release, distribution unlimited
FROM Distribution authorized to U.S. Gov't. agencies only; Administrative/Operational Use; 15 JAN 1964. Other requests shall be referred to Federal Aviation Administration, Washington, DC.
AUTHORITY
FAA notice, 2 Jul 1973

THIS PAGE IS UNCLASSIFIED

AD-803509

A-V

AERODYNAMICS

COMMERCIAL SUPERSONIC TRANSPORT PROPOSAL JANUARY 15, 1964

THE BOEING COMPANY

D6-2400-11

PROPRIETARY INFORMATION

This document contains information proprietary to The Boeing Company and shall be used only by the United States Government and participating airlines for the purpose of evaluating The Boeing Supersonic Transport Proposal. The information contained herein should not be revealed to other than the above without the written permission of The Boeing Company.

Best Available Copy

69

6

Jan 13/64

ERRATA

Volume A V Aerodynamics

Page No. Reads

1	3/6	Should Read	Fig. 3-5, add below horizontal scale: RAMP GROSS WEIGHT - 1000 LBS	9	C/28	Fig. C6-35	Fig. C6-34
2	3/13	Fig. 3-12, horizontal scale: GROSS WEIGHT - 1000 LB	RAMP GROSS WEIGHT - 1000 LB	10	C/29	Fig. C6-34	shown in Table C6-B; no significant differences are found
3	4/11	1st Column Heading: ENGINE LB SEC AIRFLOW	ENGINE LB SEC AIRFLOW	11	C/35	Last Line shown; no significant differences are found	
4	6/15	Last Line: Thrust/Weight - 0.03	Thrust/Weight - 0.03	12	C/38	Fig. C6-47, title: Lift, Drag and Pitching Moment, Wing Sweep	Lift, Drag and Pitching Moment, Wing Sweep - 74°
5	7/51	Fig. 7-42, vertical scale lower plot: ϕ	ϕ	13	C/43	Second line: ϕ (x)	L (x)
6	8/14	Fig. B3-16, horizontal scale: GROSS WEIGHT - 1000 LB	RAMP GROSS WEIGHT - 1000 LB	14	D/1	Column 2, line 7: $\dot{\psi}$ Roll Rate, $d\psi/dt$	$\dot{\psi}$ Yaw Rate, $d\psi/dt$
7	B/51	$S = \int \left(\frac{V}{a_c} \right) dV$ $a_m = \frac{2}{W} (L - W \cos \gamma \cos \alpha)$ $a_c = \frac{2}{W} (F_n \cos \alpha - W \sin \gamma)$	ADD, "SEA LEVEL" to MAXIMUM DRY POWER LINE. $S = \int \left(\frac{V}{a_c} \right) dV$ $a_m = \frac{2}{W} (L - W \cos \gamma + \gamma_n \sin \alpha)$ $a_c = \frac{2}{W} (F_n \cos \alpha - D - W \sin \gamma)$	15	D/1	Column 2, line 8: $\dot{\phi}$ Yaw Rate, $d\phi/dt$	$\dot{\phi}$ Roll Rate, $d\phi/dt$
8	C/17	Fig. C6-16, Title: Measured Camber and Thickness Wave Drag	Measured Camber and Thickness Wave Drag	16	D/2	Column 2, line 15, in equation: C_m	C_m
				17	D/8	Column 2, line 16:	C_m
						$C_m(p_{1st}) = C_m(p_{1st}) + \Delta \frac{dC_m}{d\alpha} (\alpha - \alpha_{1st})$	$C_m(p_{1st}) = C_m(p_{1st}) + \Delta \frac{dC_m}{d\alpha} (\alpha - \alpha_{1st})$
				18	D/13	Figure, Title: Figure D-5, Comparison of Horizontal Tails, Aspect Ratio = 2.2 (top) and 3.5 (lower)	
				19	D/85	Column 1, line 22: Pitching Moment (C_m , C_m)	Pitching Moment (C_m , C_m)
				20	D/89	Column 1, line 29: Aerodynamic Time (lat., - Dir) Value = .3129	Value = 0.0-63

TABLE OF CONTENTS

APPENDIX

4

1.0 SUMMARY

2.0 CONFIGURATION DESCRIPTION A

3.0 AIRPLANE PERFORMANCE B

4.0 GROWTH

5.0 CONFIGURATION DEVELOPMENT

6.0 PERFORMANCE SUBSTANTIATION C

7.0 STABILITY AND CONTROL D

8.0 FLIGHT CRITERIA

REFERENCES

NOTICES

When Government drawings, specifications, or other data are used for any purpose other than in connection with a definitely related Government procurement operation, the United States Government thereby incurs no responsibility nor any obligation whatsoever, and the fact that the Government may have formulated, furnished, or in any way supplied the said drawings, specifications, or other data, is not to be regarded by implication or otherwise as in any manner licensing the holder or any other person or corporation, or conveying any rights or permission to manufacture, use, or sell any patented invention that may in any way be related thereto.

All distribution of this document is controlled. This document may be further distributed by any holder only with specific prior approval of:

Director of Supersonic Transport Development
Federal Aviation Agency
Washington, D. C. 20533

The distribution of this document is limited because it contains technology identifiable with items excluded from export by the Department of State (U. S. Export Control Act of 1949 as amended).

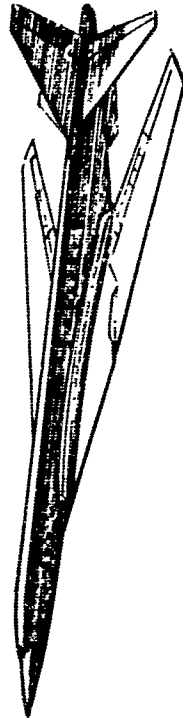
SECTION 1

SUMMARY

TABLE OF CONTENTS

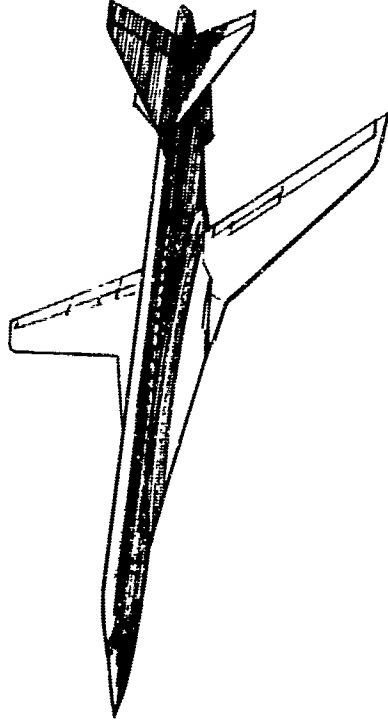
1.0 SUMMARY.....	1/1
1.1 Configuration Description.....	1/3
1.2 Performance.....	1/3
1.3 Growth.....	1/7
1.4 Configuration Development.....	1/8
1.5 Stability and Control.....	1/10

SUPERSONIC



- High sweep (74°), most effective use of camber, twist, and thickness.
- Most efficient planform for supersonic flight.
- Gust alleviation from elastic wing and low lift per unit angle of attack.
- Freedom to choose optimum transonic wing sweep schedule to minimize sonic boom.

SUBSONIC



- High span, efficient low speed flight, low stall speed.
- Conventional subsonic flight characteristics.
- Conventional high lift devices and low landing attitude.

- Inherent balance in all flight regimes, low trim drag and good longitudinal stability without fuel transfer.

1.0 SUMMARY

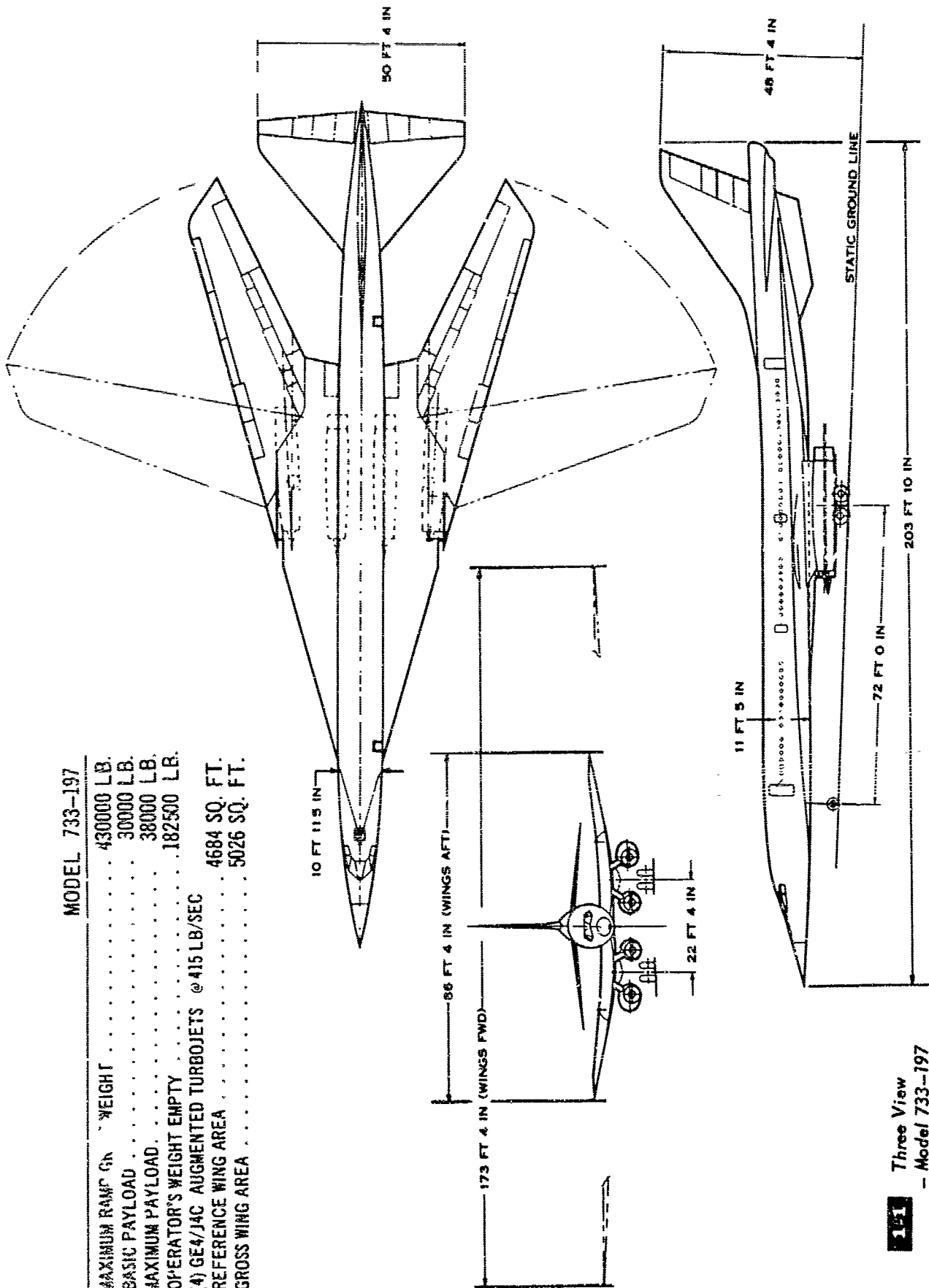
A supersonic transport must be designed to meet the fundamental requirements that are common to all commercial air transports. To fulfill these requirements a design must:

- be *ECONOMICALLY COMPETITIVE* with other forms of air transportation;
- provide the highest possible degree of *SAFETY*;
- provide *OPERATIONAL FLEXIBILITY*;
- be capable of direct *INTEGRATION* into airline operations and air traffic systems.

A variable sweep wing best fulfills the above requirements for a supersonic transport. Following the development in 1959 by the NASA of the variable sweep concept based on a single pivot point, The Boeing Company began its own study of variable sweep. Since then Boeing has invested more than 11,000 hours of wind tunnel testing on variable sweep development for both the TFX program and the supersonic transport.

MODEL 733-197

MAXIMUM RAMP GROSS WEIGHT	430000 LB.
BASIC PAYLOAD	30000 LB.
MAXIMUM PAYLOAD	38000 LB.
OPERATOR'S WEIGHT EMPTY	182500 LB.
(4) GE4/J4C AUGMENTED TURBOJETS @ 415 LB/SEC	
REFERENCE WING AREA	4684 SQ. FT.
GROSS WING AREA	5026 SQ. FT.



1:1 Three View
- Model 733-197

1.1 Configuration Description

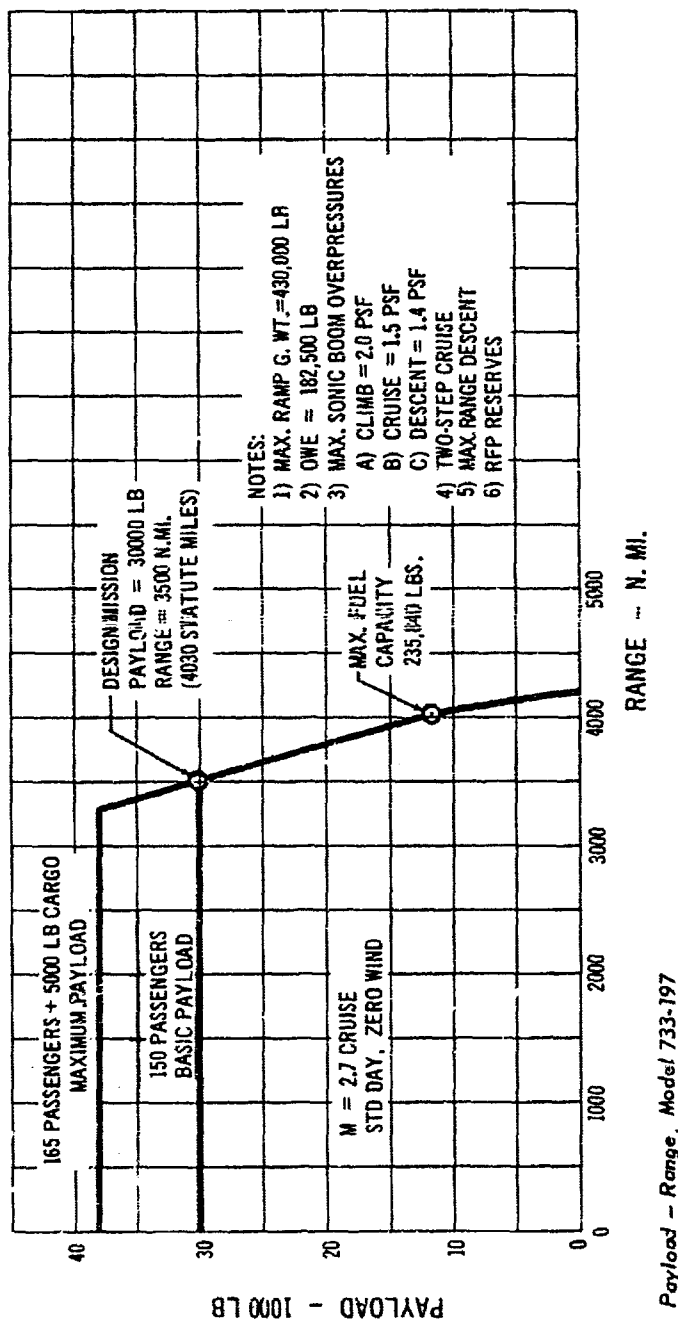
Fig. 1-1 presents a three-view drawing of the Boeing Model 733-197 supersonic transport. The principal features are:

- a variable sweep wing which varies the leading edge sweep from 20 degrees with the wings folded to 74 degrees with the wings fully swept.
- four GE 4/J4C afterburning jet engines mounted in individual pods below the fixed inboard portion of the wing.
- conventional tail and control surfaces.
- conventional tricycle landing gear.

The basic characteristics are tabulated in Fig. 1-1.

1.2 Performance

The Design Mission of the 733-197 consists of a 3500 nautical mile range with a 30,000-pound payload (150 passengers) and ramp gross weight of 430,000 pounds. The airplane cruises at Mach 2.7. Fig. 1-2 shows the payload-range capabilities of the proposed design. Although the basic payload is 30,000 pounds (150 passengers), the payload may be increased to 38,000 pounds (165 passengers plus 5000 pounds of cargo) with no increase in structural weight. This results in a range of 3277 nautical miles with a ramp gross weight of 430,000 pounds.

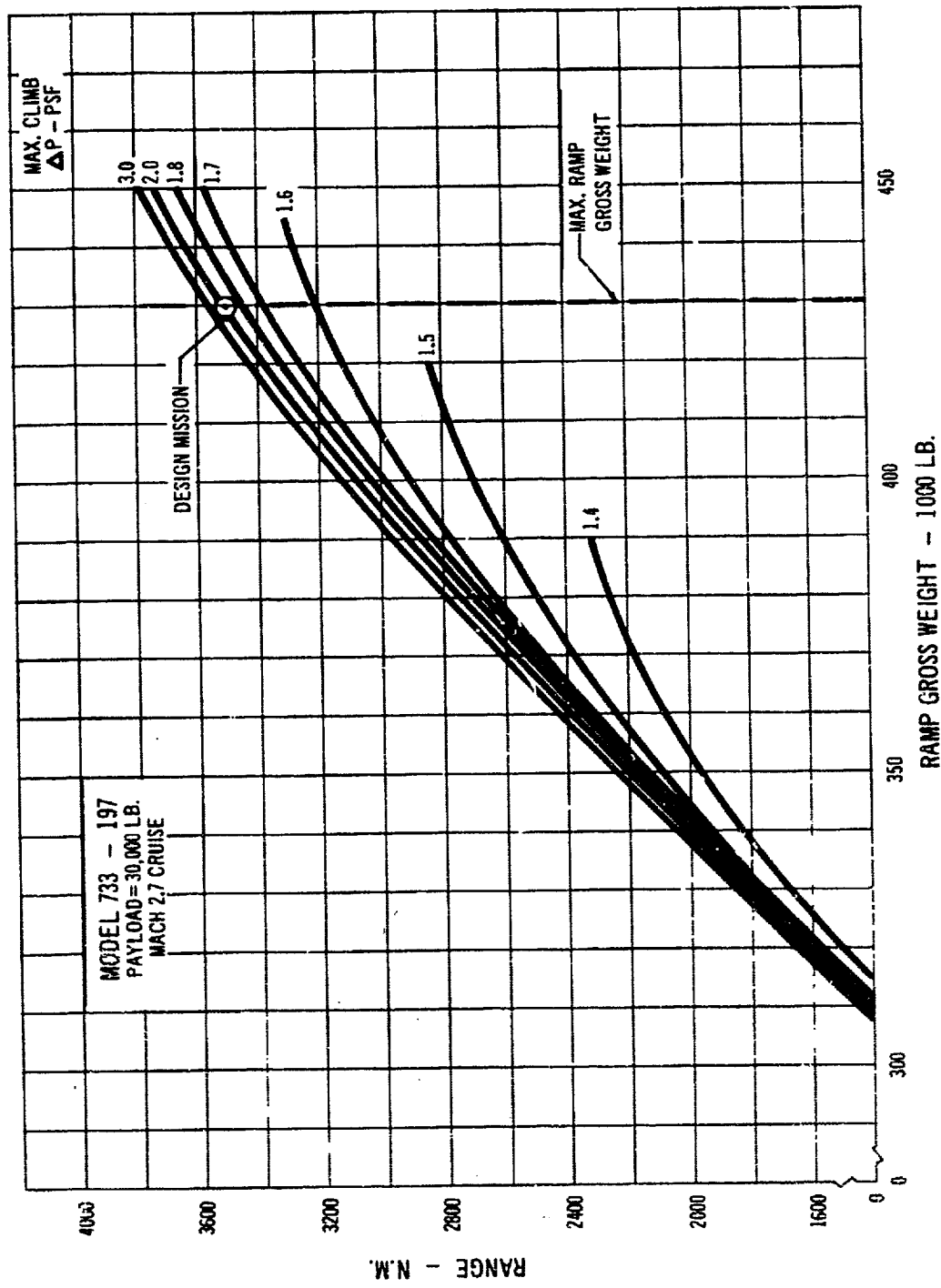


Considerable flexibility is possible in the climb and acceleration phase of a mission. By climbing to a higher altitude for transonic acceleration, one may trade the additional climb fuel required for a lower sonic boom overpressure. The increased climb fuel results in either a decrease in range, because there is less fuel available for cruise, or an increase in the ramp gross weight for a given range.

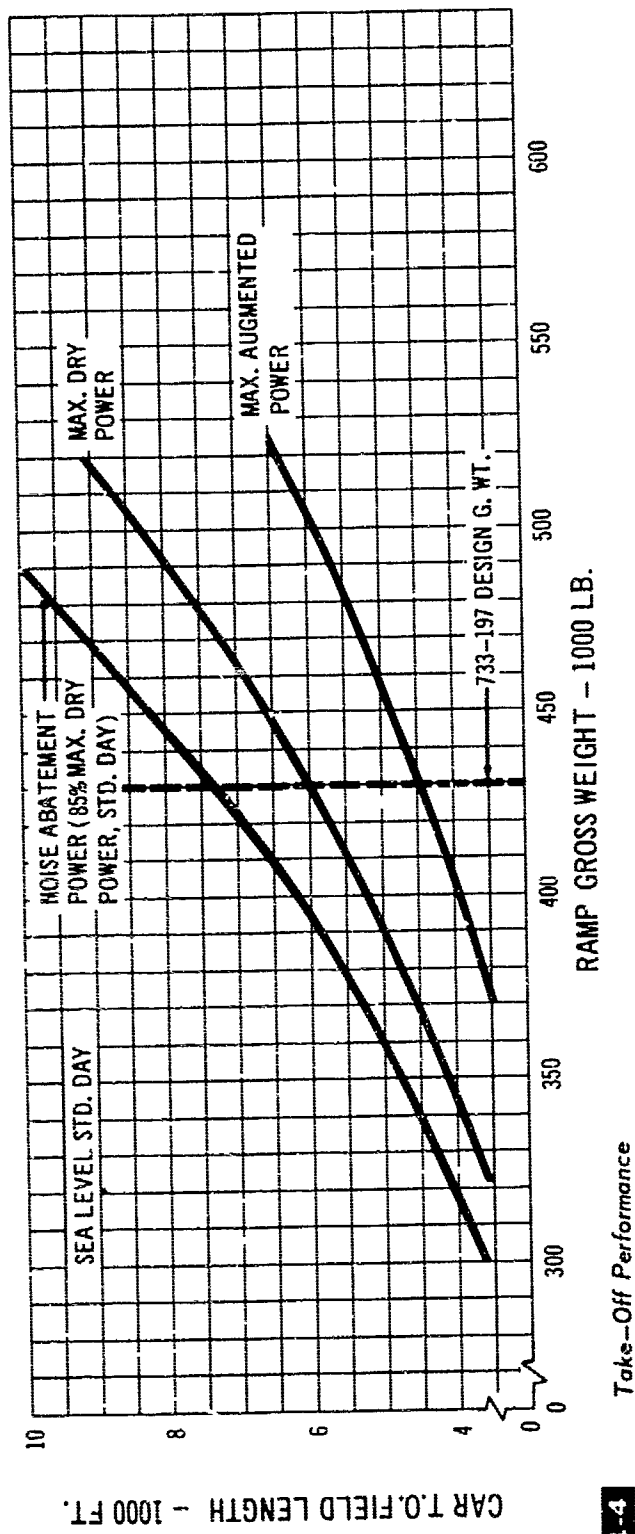
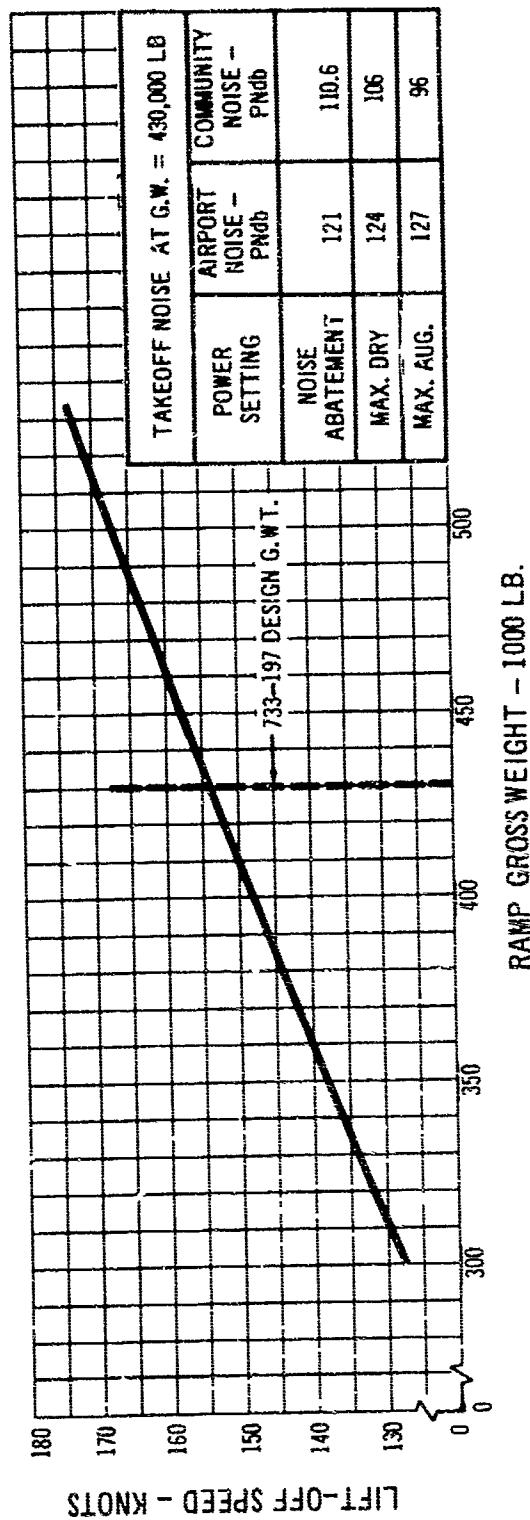
The relationship between ramp gross weight, range, and maximum sonic boom overpressure in climb is shown in Fig. 1-3 for a constant payload of 30,000 pounds. At the design gross weight, the maximum overpressure

may be reduced from 2.0 to 1.8 psf with only a 2 percent decrease in range, and an overpressure of 1.6 psf results in a 3200 nautical mile range. At a typical transcontinental range of 2200 nautical miles, the Model 733-197 has exceptional flexibility with respect to climb schedule and resultant sonic boom overpressure. At the maximum allowable overpressure of 2.0 psf, the ramp gross weight is 350,000 pounds. However, the overpressure may be reduced to 1.5 psf in climb with only a 110 nautical mile reduction in range, or an increase in gross weight of 7000 pounds with no decrease in range. This versatility is especially valuable when sonic boom is an important operational factor.





1-3 Operational Versatility - Sonic Boom in Climb

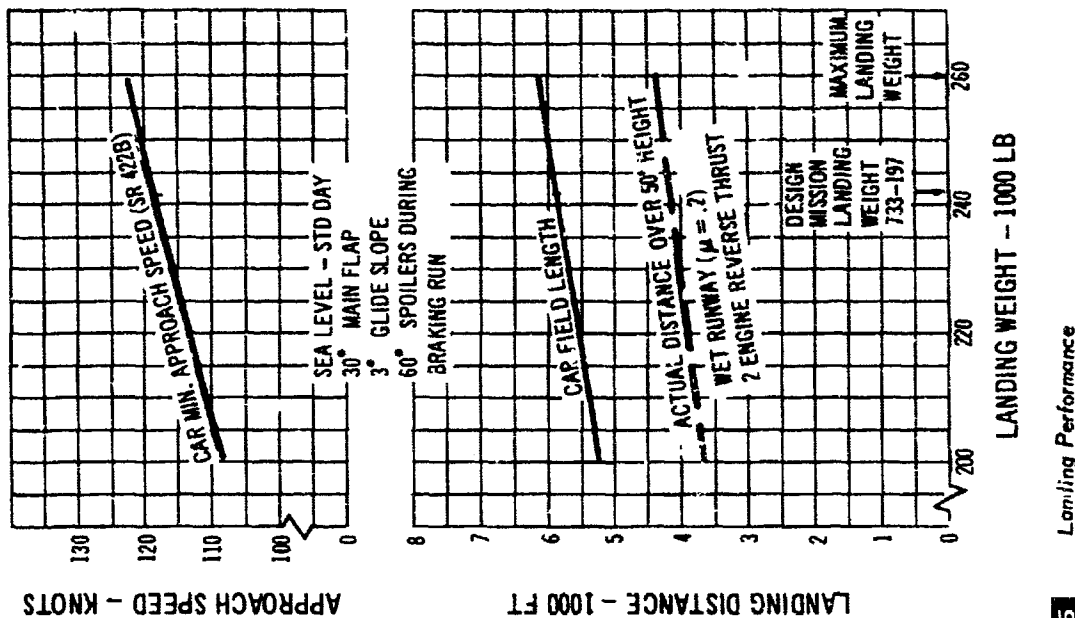


The CAR takeoff field lengths and liftoff speeds are shown in Fig. 1-4. For noise abatement during takeoff, a reduced power setting is used (85 percent maximum dry thrust for sea level standard day conditions). This allows both the airport and community noise restrictions as well as the field length requirement to be met at the same time. As shown in Fig. 1-4 the design mission takeoff field length of 7350 feet may be decreased to 6000 feet by using maximum dry power, and 4500 feet by using maximum augmented power. As the takeoff power is increased, a moderate increase in airport noise is traded for a significant decrease in community noise, because of the shorter field length and more rapid climbout.

The landing performance is presented in Fig. 1-5. At the design mission landing weight, the approach speed is 118 knots and the CAR landing distance is 5850 feet for sea level, standard day conditions. The actual landing distance under wet runway conditions using two-engine reverse thrust is 4150 feet.

1.3 Growth

Variable sweep makes it possible to choose a wing area and engine size with excellent growth potential without compromising the performance of the basic airplane. Fig. 1-6 presents the payload-range curves for two growth versions of the Model 733-197. Both have a maximum payload of 43,000 pounds. A range of 2500 nautical miles, typical for domestic route requirements, is obtained with a gross weight of only 408,000 pounds, and a maximum overpressure of 2.0 psf. For intercontinental routes the range is increased to 3500 nautical miles by raising the gross weight to 520,000 pounds and increasing the overpressure during climb to 2.1 psf. Trades between range, gross weight and sonic boom, similar to those shown in



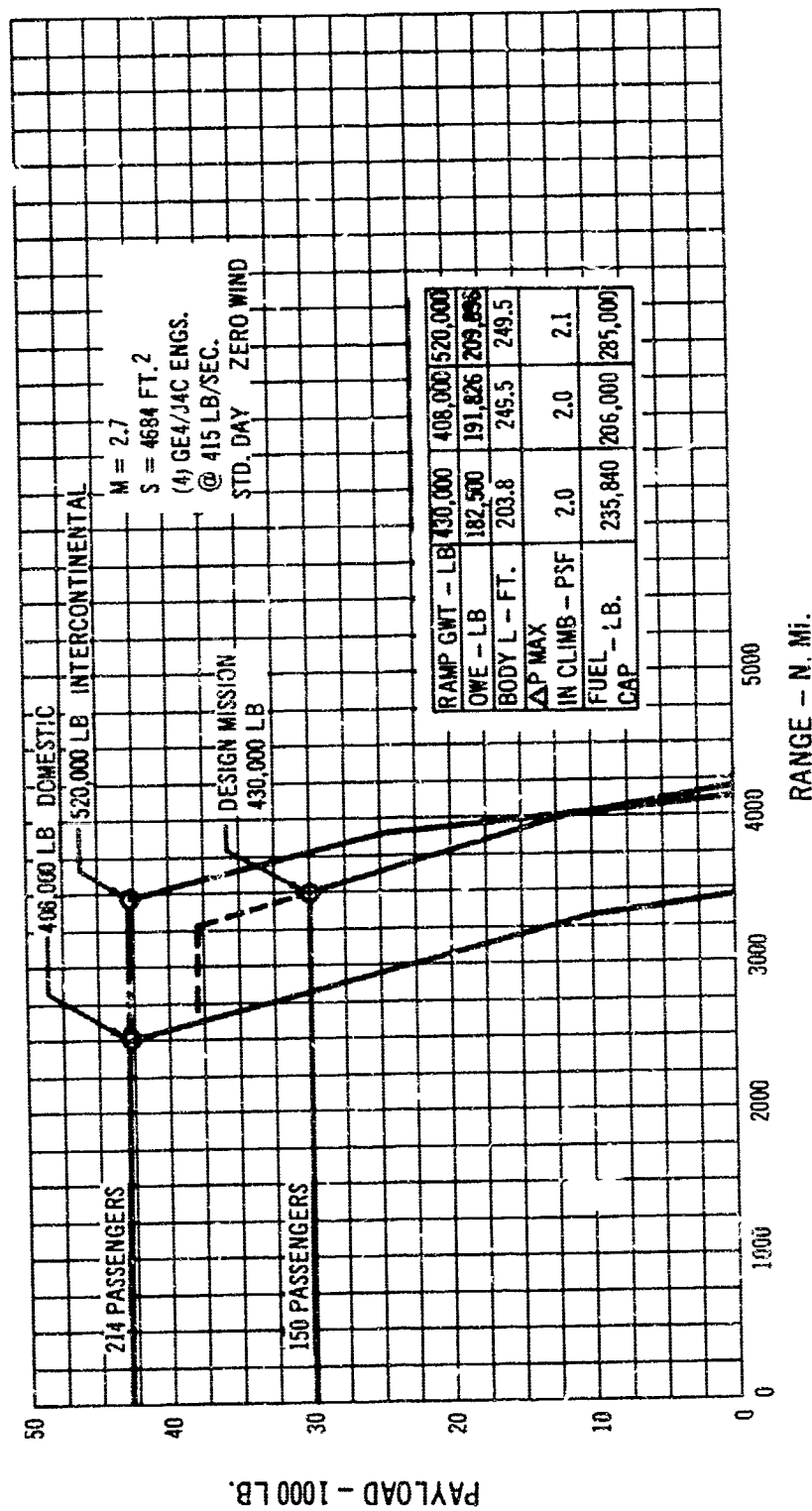
1-5 Landing Performance

Fig. 1-3 for the basic airplane, may also be made for the growth versions.

Because of the inherent growth potential of the Model 733-197 design, airplane growth is achieved primarily by adding fuselage sections to accommodate the increased payload. No change in the basic wing or engine type and size is required. Excellent performance of the growth versions is obtained with no further improvement in the presently proposed engine performance.

1.4 Configuration Development

A successful airplane design must be compatible with every flight regime in which the airplane will operate. The fundamental advantage of variable sweep is that the most favorable geometric and aerodynamic characteristics for both extremes of the flight spectrum are combined in one configuration without compromising the performance in any area.

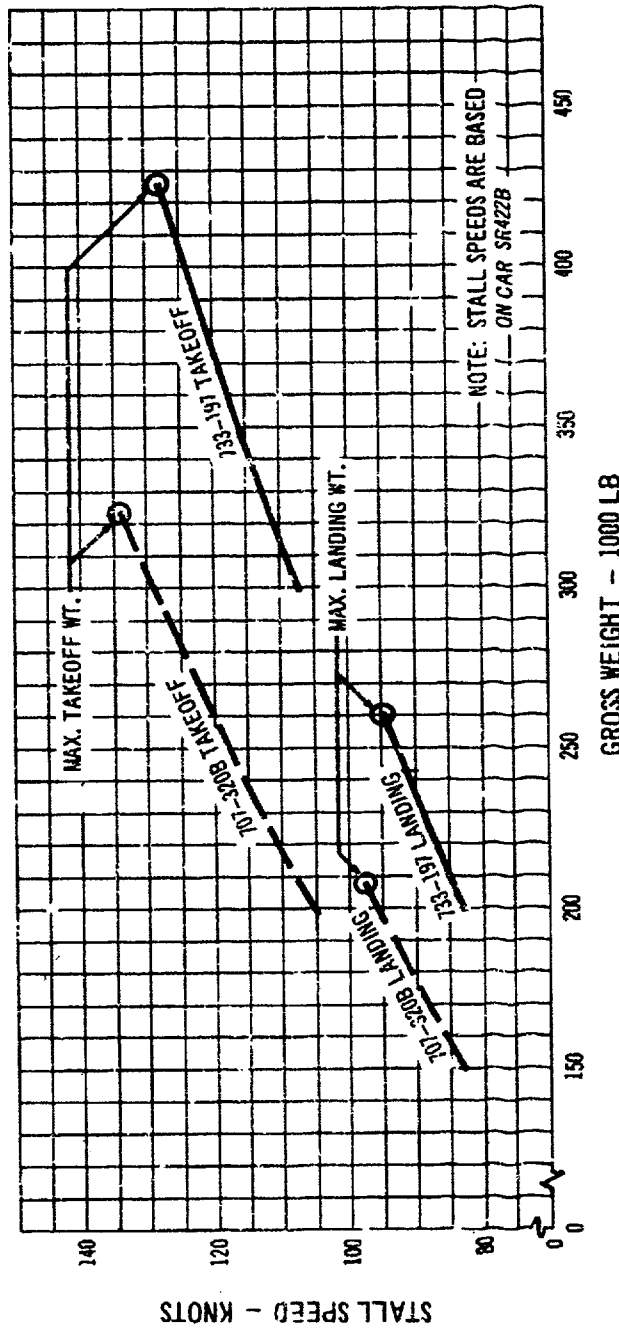


1-6 "GROWTH" Payload-Range

In supersonic cruise, the wing is highly swept, resulting in a subsonic velocity component perpendicular to the leading edge of the wing. Hence the essentially subsonic nature of the flow over the wing permits very effective use of twist and camber, as well as a slightly thicker wing than if the leading edge were supersonic. A favorable spanwise lift distribution is also obtained.

The arrow wing planform of the variable sweep wing has been proven by theory and experiment to be the most efficient supersonic lifting surface. The natural elasticity and low lift per unit angle of attack of the arrow wing contribute to favorable gust response characteristics and a smooth ride.

For efficient low speed flight a very high span wing is desired. As the Model 733-197 wing moves from the fully swept cruise position to the forward landing position, the span more than doubles, resulting in a conventional subsonic configuration. This offers many advantages. Conventional high lift flap systems produce stall speeds equal to or less than the Model 707-320B as shown in Fig. 1-7. This permits the Request for Proposal (RFP) landing and takeoff requirements to be easily met by the Model 733-197. The obvious contribution to safety is further enhanced by a low landing attitude for good pilot visibility as well as the excellent subsonic handling



1-7 Comparison of Stall Speeds with the 707-320B

qualifier. Low holding and approach speeds make the Model 733-197 compatible with air traffic control systems and existing subsonic airplanes.

Operational flexibility is inherent in a variable sweep airplane. The optimum leading edge sweep may be chosen throughout the total flight regime, producing economy and efficient flexibility. Excellent performance is obtained in the areas of:

- subsonic cruise to alternate destinations or for short route segments;
- holding at maximum endurance conditions;
- long range ferry flight for unscheduled maintenance;
- climb and acceleration through transonic Mach numbers.

The efficient subsonic cruise and holding capability of a variable sweep airplane greatly improves potential use of the trip fuel reserves.

The efficiency of a variable sweep wing at all Mach numbers permits flexibility in the initial selection of engine size and wing area. As Section 5.0 discusses in detail, it is possible to choose a relatively larger engine size and wing area than dictated by parametric optimization studies, without compromising the performance of the design mission. Thus, efficient operation of the airplane is not restricted to the design mission alone, but is extended to many off-design conditions. Economic operation is assured over a wide variety of routes.

For example, the minimum thrust to drag ratio during the design mission climb and acceleration is equal to 1.54. This high available thrust margin greatly reduces the influence of operational variations on mission performance. The design mission specifies a maximum sonic boom overpressure of 2.0 psf in climb in accordance with the RFP requirement. However, as discussed previously in Section 1.2, the maximum overpressure may be reduced to 1.8 psf with less than a 2 percent reduction in range. A range of 3200 nautical miles is possible with a

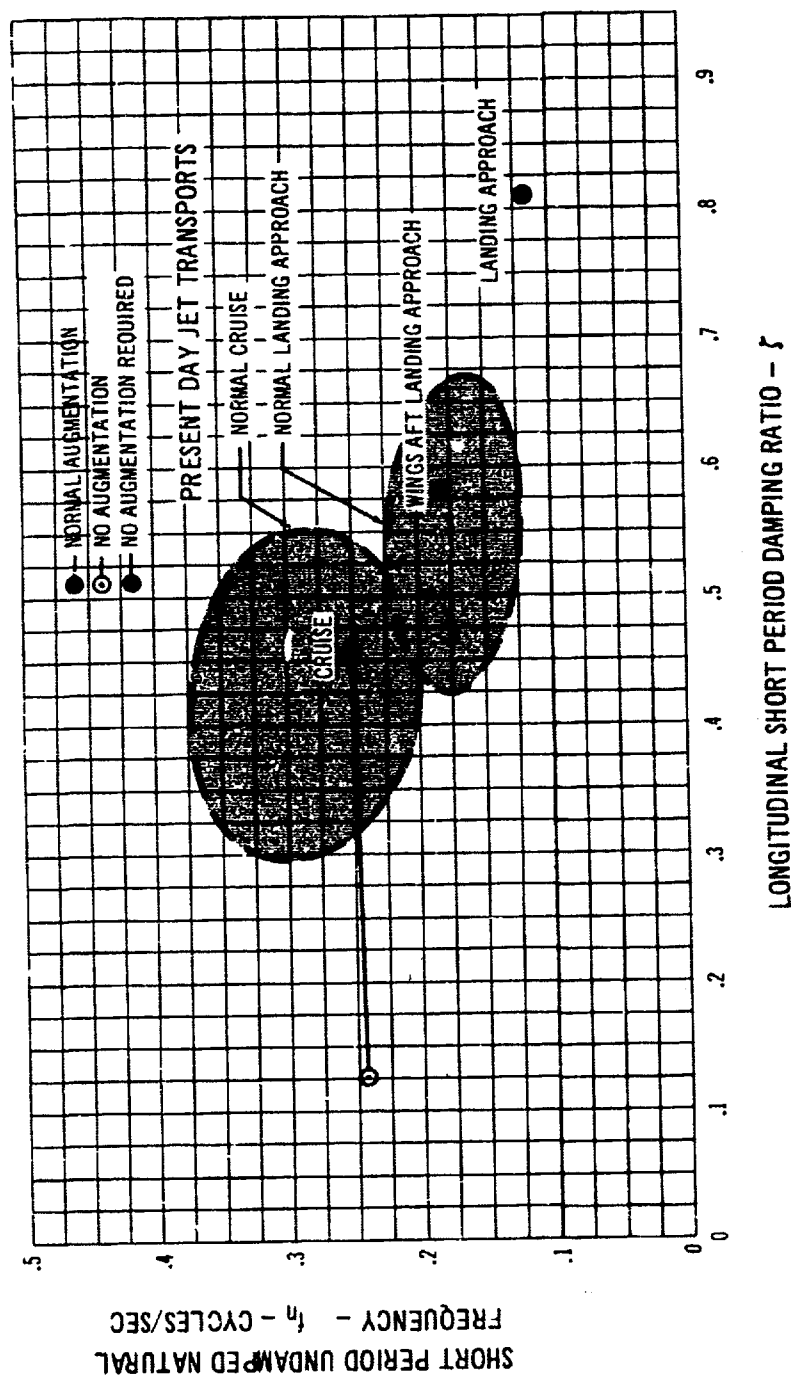
maximum overpressure of only 1.6 psf and a 30,000-pound payload.

The good low speed performance of a variable sweep configuration helps to maintain low noise levels. The Model 733-197 satisfies all noise restrictions specified by the RFP. A high lift-drag ratio results in a low thrust level during landing approach and correspondingly low landing noise. At takeoff, high maximum lift coefficient and high lift-drag ratio permits (1) takeoff in a short distance with a low power setting, giving a low airport noise level, and (2) a rapid climb resulting in low noise levels in community areas under the flight path. Complete data on the relationships between noise levels and takeoff and landing performance are given in Sections 3.3 and 3.4.

1.5 Stability and Control

The Model 733-197 has stability and control characteristics similar or superior to current subsonic jet transports. The flexible, variable sweep wing compensates for the shift of the lift center from subsonic to supersonic flight resulting in good longitudinal stability in all flight regimes without fuel transfer. Furthermore, in cases of emergency, such as cabin depressurization, a rapid transition from supersonic to subsonic flight can be safely made with no change in wing sweep, and without fuel transfer.

The airplane motion is damped in all flight conditions. Aerodynamic damping is high enough that the airplane may be safely flown throughout the flight envelope without stability augmentation. Figs. 1-8 and 1-9 show the longitudinal and lateral-directional dynamic characteristics of the Model 733-197 compared with current Boeing Model 707 subsonic jet characteristics. In every flight condition the augmented and unaugmented performance of the Model 733-197 equals or exceeds that of the Model 707. In the landing approach condition longitudinal augmentation is not required with the wing in any sweep position.



1-8 Boeing SST Longitudinal Dynamic Characteristics

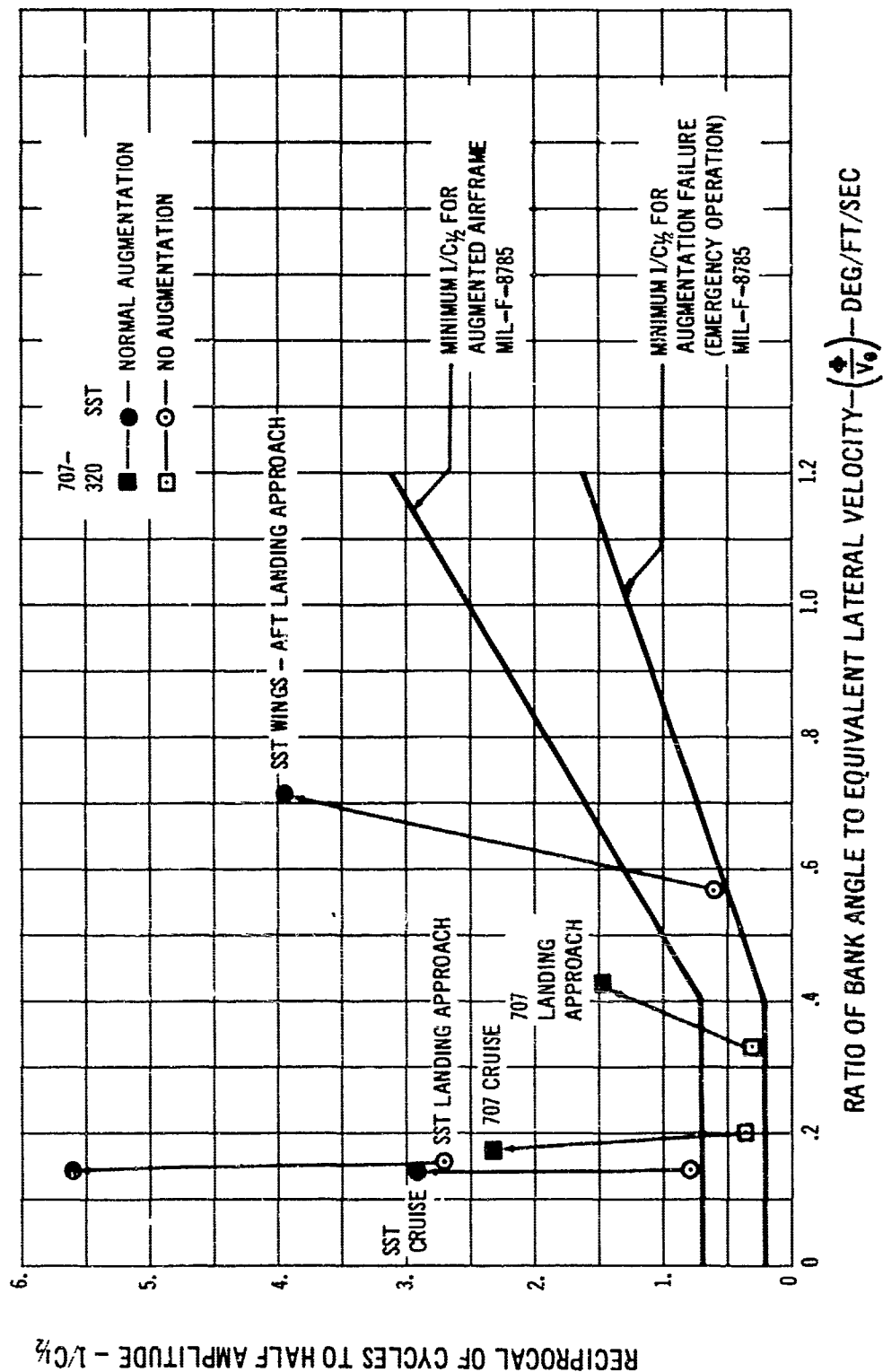
Engine failure will not result in either an unsafe airplane attitude or an unsafe control situation in any flight condition, including takeoff at maximum unaugmented thrust and high thrust conditions at Mach 2.7.

Although best low speed handling qualities and performance are obtained with the wings forward in the landing position, the Model 733-197 may be safely landed

with the wings at any sweep angle. Safe go-around capability is provided even with the wings fully swept.

At the design mission landing weight, the wings-aft landing distance is 6450 feet, for sea level, standard day, wet runway conditions, and two-engine reverse thrust. The corresponding approach speed is 184 knots, with a body attitude of 7 degrees on a 3-degree glide slope.

The complete basic performance data for the Model 733-197 are found in the body of this document. More detailed supplementary data are presented in the Appendices.



1-9 Boeing SST Lateral-Directional Dynamic Characteristics

SECTION 2

CONFIGURATION DESCRIPTION

TABLE OF CONTENTS

2.0 CONFIGURATION DESCRIPTION.....2/1

A2.0 APPENDIX A.....A/1

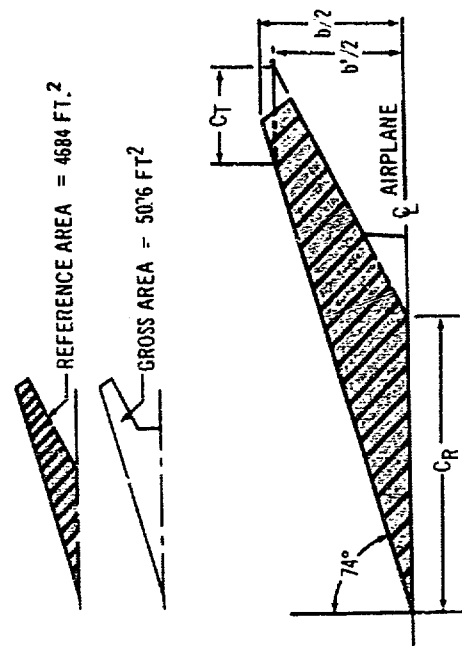
2.0 CONFIGURATION DESCRIPTION (RFP 3.2.6)

The Boeing Model 733-197 supersonic transport configuration is shown in Figs. 2-2 and 2-3. Additional descriptive data are given in the Appendix A 2.0. The airplane has a variable sweep wing of modified arrow planform joined to the lower fuselage below the passenger floor. Four propulsion pods are mounted beneath the wing and a conventional vertical fin, ventral fin, and horizontal stabilizer are located on the aft body. The airplane is 203 feet 10 inches long and provides accommodations for 150 passengers, baggage, passenger service areas, and the flight crew in the basic configuration. Volume is provided for 6,750 pounds of cargo. Alternate payload arrangements are shown in Volumes A-III and M-VII. The design range of 3500 nautical miles is achieved at a gross weight of 430,000 pounds for the design cruise Mach number of 2.70.

The variable sweep wing allows a variation in leading edge sweep angle between 20 degrees and 74 degrees. The 74 degree sweep position (86 feet 4 inch span) is used for supersonic cruise. Takeoff and landing are accomplished with a leading edge sweep angle of 20 degrees (173 feet 4 inch span). Intermediate sweep positions are used for subsonic flight and acceleration to supersonic cruise. The gross wing area is 5026 square feet, including the trailing edge extension. A reference wing area of 4684 square feet, derived from the basic arrow planform as shown in Fig. 2-1, has been used for aerodynamic analysis.

High lift mechanical flaps are located on the wing leading and trailing edges to provide the excellent takeoff and landing characteristics of the airplane. High and low speed spoilers and low speed ailerons are used for lateral control.

The leading edges of the fixed inboard portion of the wing contain a leading edge flap, a streamwise notch, and a wing fence to aid the high lift stability characteristics of the airplane.



2-1. Wing Area Definition

The propulsion pods consist of four General Electric GE4/J4C augmented turbojet engines, utilizing axisymmetric spike inlets, strut mounted beneath the wing. Thrust reversal capability is provided on each engine. The engines are sized for 415 lb/sec airflow each.

The main landing gear is trunnion supported from the wing center section structure and retracts forward into the strake and wheel fairing beneath the wing. The tread of the main landing gear is 22 feet 4 inches. Each main gear mounts four 49 x 18 Type VII tires. Brakes are provided on all main gear wheels.

The nose landing gear is trunnion supported from primary fuselage structure and retracts forward into the wheel cavity provided in the forward fuselage. The gear mounts two 34 x 13 Type VII tires and has steering capability of $+74^\circ$.

The horizontal stabilizer is used for longitudinal trim

with segmented elevators for control. The maximum angular travel for the elevator surface is $+30$ degrees. The stabilizer has an angular travel of $+10$ to -20 degrees.

The vertical tail is fixed and incorporates segmented rudders for control. The maximum angular travel for the rudders is $+25^\circ$.

The gross weight of the airplane is 430,000 pounds. The major elements of the weight breakdown are:

Operator's Weight Empty	182,500 lbs.
Payload	30,000 lbs.
(150 passengers & baggage)	
Fuel	217,500 lbs.
GROSS WEIGHT	430,000 lbs.
Maximum Fuel Volume	35,200 gal.
(235,840 at 6.7 lb./gal.)	

More detailed configuration data, including a complete geometrical description of the aerodynamic surfaces and controls, are given in Appendix A2.0

FOLD OUT



WEIGHTS

MAX. RAMP WEIGHT _____ 430,000 LBS
 PAYLOAD _____ 30,000 LBS
 OPERATOR'S WEIGHT EMPTY _____ 182,500 LBS
 FUEL CAPACITY _____ 235,840 LBS

CENTER OF GRAVITY DATA

Most Fwd C.G. _____ 40% M.A.C. (Gear Up, Wing Fwd)
 Most Aft C.G. _____ 48% M.A.C. (Gear Up, Wing Aft)
 Operator's Weight Empty _____ 45.5% M.A.C. (Vertical C.G. @ W.L. 323 (Wing Fwd, Gear Down)
 Maximum Ramp Weight _____ 47.0% M.A.C. (Vertical C.G. @ W.L. 330 (Gear Down, Wing Aft)

WING

Ref Wing Area _____ 4684 FT²
 Gross Wing Area _____ 5026 FT²
 @ $\Delta LE = 74^\circ$
 Span _____ 86.33 FT.
 Mean Aerodynamic Chord, Ref Area = 4684 FT² _____ 64.52 FT
 Aspect Ratio _____ 1.59
 Taper Ratio _____ .354
 Pivot Location _____ .455 Chord and .378 Semi-span
 Dihedral Angle _____ 0
 Angle of Incidence of Root to Fuselage Ref. Line _____ -1°
 Angle of Incidence of Tip to Fuselage Ref. Line _____ -5.174° (Defined @ .90 Semi-span)
 Airfoil Section at Side of Body _____ B733-1 1/c Max = .041
 Airfoil Section at .378 b/2 _____ B733-2 1/c Max = .0506
 Airfoil Section at 0.65 b/2 _____ B733-3 1/c Max = .025

FLAPS AND CONTROL SURFACES (DEFINED FOR LEADING EDGE SWEEP = 20°)

Surface Type	INBOARD T.E. FLAPS		OUTBOARD T.E. FLAPS		L.E. SLATS		AILERONS		SPOILERS SEGMENTED
	PLAIN	DOUBLE SLOTTED	PLAIN	DOUBLE SLOTTED					
Distance from \bar{C} of Airplane to Inb'd Edge	3.75 FT	19.50 FT	25.8 FT	63 FT	63 FT	2.9 FT			
Distance from \bar{Q} of Airplane to Outb'd Edge	9.0 FT	63 FT	84 FT	82 FT	63 FT				
Max Deflection	40°	$30^\circ/50^\circ$	40°	-25°	60°				
Deflection for Takeoff	8°	$8^\circ/23^\circ$	30°						
Deflection for Landing	40°	$20^\circ/40^\circ$	40°						
% Wing Chord	7 FT. Avg	$30\%/12\%$	2.6 FT Avg	34%	15%				
% Wing Area Affected		68%							

2.2 General Arrangement Data

HORIZONTAL TAIL

Area (Projected) (Exposed) _____ 950 FT²
 Span, Total _____ 50.35 FT
 Aspect Ratio (P based on Projected Area) _____ 2.086
 Incidence to Fuselage Ref-Line (Neutral Position) _____ Variable +10° to -20°
 Airfoil Section _____ Bi-Convex
 Thickness Ratio _____ .03
 Sweep Angle (Leading Edge) _____ 50°
 Mean Aerodynamic Chord (M.A.C.) _____ 24.2 FT
 Distance to Leading Edge M.A.C. from Leading Edge Root Chord _____ 10.316 FT
 Location of M.A.C. from Thrust Line _____ 6 FT Above
 Dihedral Angle _____ -5°
 Taper Ratio _____ .20

VERTICAL TAIL

Area _____ 471.70 FT²
 Span _____ 22.92 FT
 Aspect Ratio _____ 1.113
 Airfoil Section _____ Bi-Convex
 Thickness Ratio at Body _____ .0648
 Thickness Ratio at .25 Span _____ .030
 Thickness Ratio at .50 Span _____ .024
 Thickness Ratio at .75 Span _____ .020
 Thickness Ratio at 1.0 Span _____ .020
 Sweep Angle (Leading Edge) _____ 55°
 Mean Aerodynamic Chord (M.A.C.) _____ 23.05 FT
 Distance to Leading Edge M.A.C. from Leading Edge Root Chord _____ 13.118 FT
 Location of M.A.C. from Thrust Line (of outboard engine) _____ 20.00 FT.
 Taper Ratio _____ .254

WETTED AREA (EXPOSED SURFACE AREA)

Fuselage _____ 5339 FT.²
 Wing (Including Strake) _____ 8144 FT.²
 Tail _____ 3056 FT.²
 Propulsion Pods _____ 2169 FT.²
 Total _____ 18708 FT.²

WING SPOILERS
 SEGMENTED
 63 FT _____ 20 FT
 62 FT _____ 63 FT
 25° _____ 60°
 34% _____ 15%

1 2 3 4 5 6 7 8 9 10 11 12 13 14 15 16 17 18 19 20 21 22 23 24 25 26 27 28 29 30 31 32



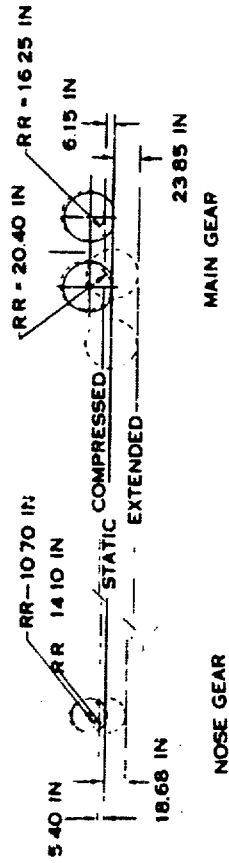
DATA MODEL 733-197

POWER PLANTS—(4) GE 4/J4C AUGMENTED TURBOJETS
TOTAL ENGINE AIRFLOW 1660 LB/SEC

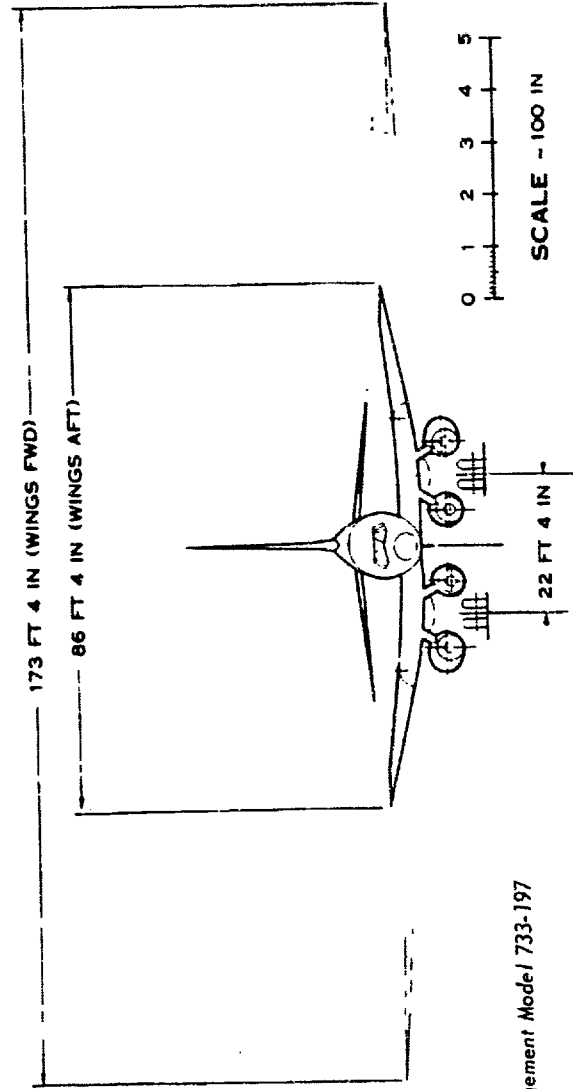
MAXIMUM RAMP WEIGHT 430,000 LBS
BASIC PAYLOAD 30,000 LBS
OPERATOR'S WEIGHT EMPTY 182,500 LBS
FUEL CAPACITY 35,200 GALLONS
235,840 @ 6.7 LBS/GAL

MAIN GEAR 8—49X18 TIRES TYPE VII
NOSE GEAR 2—34X13 TIRES TYPE VII

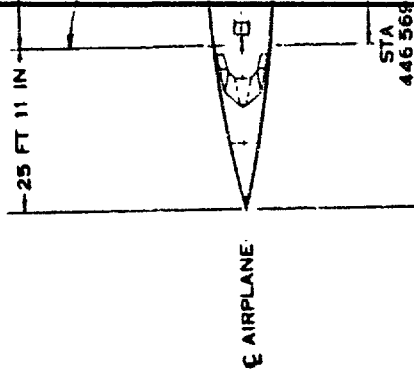
DESIGN GROSS WEIGHT CG LIMITS—GEAR DOWN
MOST FORWARD CG 40.5% MAC WINGS FWD
MOST AFT CG 48.0% MAC WINGS AFT



DEFLECTIONS



2-3 General Arrangement Model 733-197



STA 135

146
STRAIGHT
AHEAD
HORIZONTAL
REF LINE

A

B

SECTION 3
AIRPLANE PERFORMANCE
TABLE OF CONTENTS

3.0 AIRPLANE PERFORMANCE	3/1
3.1 Payload—Range Capability.....	3/1
3.2 Flight Limits.....	3/8
3.2.1 Climb and Cruise Speed Limits.....	3/8
3.3 Takeoff Performance.....	3/10
3.3.1 Takeoff Field Lengths and Community Noise Levels.....	3/11
3.3.2 Takeoff Speeds.....	3/14
3.3.3 Takeoff Climb Gradients.....	3/15
3.4 Approach and Landing Performance.....	3/15
3.4.1 Landing Approach Noise Trade Factors.....	3/15
3.4.2 CAR Approach Speeds and Climb Gradients.....	3/15
3.4.3 CAR Landing Distance.....	3/17
3.4.4 Landing Distances, Wet Runway.....	3/18
B3.0 APPENDIX B	B/1

3.0 AIRPLANE PERFORMANCE (RFP 2.2-2.8, 3-27)

The Boeing Model 733-197 meets or exceeds all the performance design objectives and requirements in the RFP. The design mission capability of the Model 733-197 at a ramp gross weight of 430,000 pounds is 3500 nautical miles (4030 statute miles) with a 30,000-pound payload (150 passengers) at a cruise speed of Mach 2.7. The maximum payload capability is 38,000 pounds (165 passengers plus 5,000 pounds cargo). The airplane meets the sonic boom overpressure requirements of 2.0 psf maximum in climb and 1.5 psf maximum in cruise or descent with only pressures significantly lower can be achieved with only small range penalties. Noise in the vicinity of airports resulting from takeoff and landing operations meet the RFP requirements, without undue maneuvering or critical speed limiting maneuvers. The CAR takeoff field length at maximum gross weight at sea level in an ISA + 15 degrees Centigrade hot day atmosphere is only 8,000 feet (RFP objective 10,500 feet) and the corresponding lift-off speed is 154 knots EAS (RFP objective 160 knots EAS). For the same atmospheric conditions the landing distance over a 50-foot obstacle at maximum landing weight on a wet runway is only 4500 feet with reverse thrust on two engines (RFP objective 8000 feet) and the CAR minimum approach speed is 123 knots EAS (RFP objective 135 knots EAS). All CAR takeoff and landing climb gradient requirements are bettered by a large margin. The excellent takeoff and landing performance of the Model 733-197 and its low airport and community noise levels are due to the variable sweep wing characteristics. This same feature provides high subsonic cruise efficiency. Together they provide a high degree of operational versatility for the Model 733-197 and ensure its compatibility with the air traffic control system utilized by subsonic jets.

This section presents the major performance capabilities of the Model 733-197 airplane. Sufficient performance data are given in the appendix to this section (Ap-

pendix B) to conduct airline route analyses and to compute off-design performance. In addition, miscellaneous performance data are shown. A table of contents precedes the appendix to facilitate use of the data. All performance data are based on the U. S. Standard Atmosphere, 1962. The engine data used in the performance calculations can be found in the Propulsion Report, Volume A-VI.

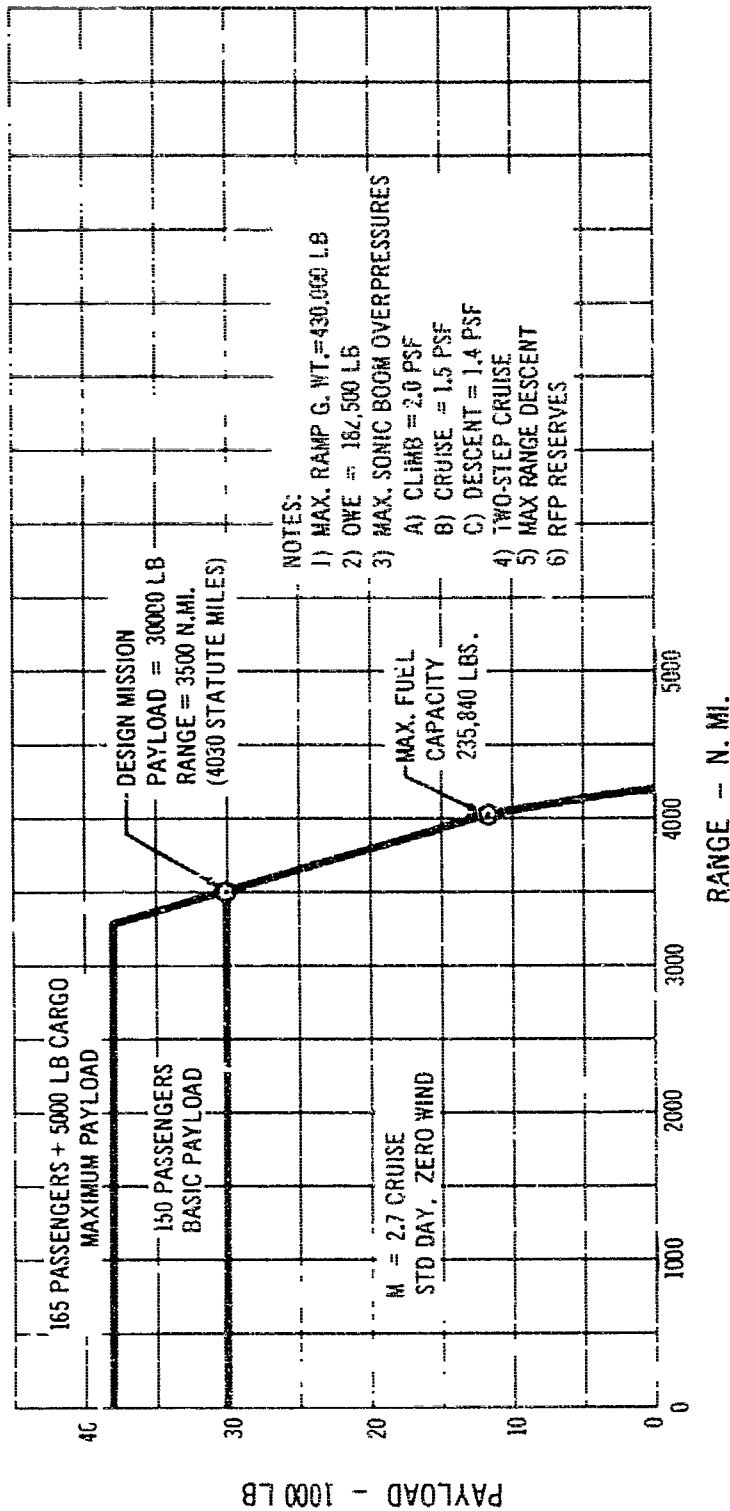
3.1 Payload-Range Capability

Fig. 3-1 shows the payload-range capability of the Model 733-197 for standard day, zero wind conditions at the design cruise speed of Mach 2.7. The range is 3277 nautical miles with the maximum design payload of 165 passengers plus 5000 pounds cargo (38,000 pounds payload) while at maximum fuel capacity and zero payload the maximum range is 4205 nautical miles. These data are based upon a constant altitude two-step climb cruise technique and a maximum range descent. Sonic boom overpressures are limited to 2.0 psf in climb, 1.5 psf in cruise and 1.4 psf in descent.

A detailed breakdown of the design mission flight profile is presented in Fig. 3-2. The fuel used, weight, time and distance for each segment of the mission are given. Taxi, takeoff, approach and landing fuel allowances as well as the mission reserves are shown in detail.

The sonic boom overpressures under the flight path and the flight profile required to attain the design overpressure requirements are shown in Fig. 3-3 for the design mission. The altitude required to achieve an overpressure of 2.0 psf at Mach 1.5 is 44,900 feet and the altitude required for 1.5 psf at Mach 2.7 is 59,600 feet. The normal descent schedule causes a maximum overpressure of 1.4 psf. These data also show that during climb the sonic boom intensities greater than 1.5 psf are confined to a corridor approximately 13 to 17 nautical miles wide and 150 nautical miles long.

Fig. 3-4 shows the range capability of the Model 733-197 versus gross weight for standard day, zero wind



351 Payload - Range

conditions. Data are shown for both the design payload of 30,000 pounds and the maximum payload of 38,000 pounds. The climb schedule is the same for all gross weights and is the schedule which gives a maximum overpressure of 2 psf for the design gross weight case. The maximum overpressures occurring in both climb and cruise are also shown. These data show that for a typical transcontinental range of 2200 nautical miles the maximum payload of 38,000 pounds can be carried at a ramp gross weight of 364,000 pounds with maximum overpressures of 1.91 and 1.31 in climb and cruise, respectively. The design pay-

load of 30,000 pounds can be carried at a ramp gross weight of 350,000 pounds with maximum overpressures of 1.89 and 1.29 in climb and cruise, respectively.

Fig. 3-5 shows the versatility available in the Model 733-197 with regard to sonic boom overpressures in climb for the design payload case. These data show that lowering the maximum sonic boom overpressure 10 percent to 1.8 psf would result in a range loss of about 60 nautical miles (2 percent) for the design mission. For a typical transcontinental range of 2200 nautical miles lowering the sonic boom 20 percent to 1.5 psf would result in a range

RAMP GROSS WL. = 430,000 Lb.

$S_w = 4,684 \text{ FL}^2$

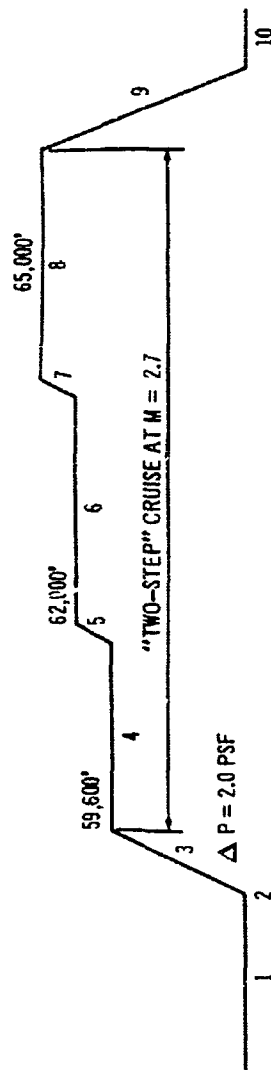
$W_a = 1,660 \text{ Lb./Sec.}$

$CWE = 182,500 \text{ Lb.}$

$PL = 30,000 \text{ Lb.}$

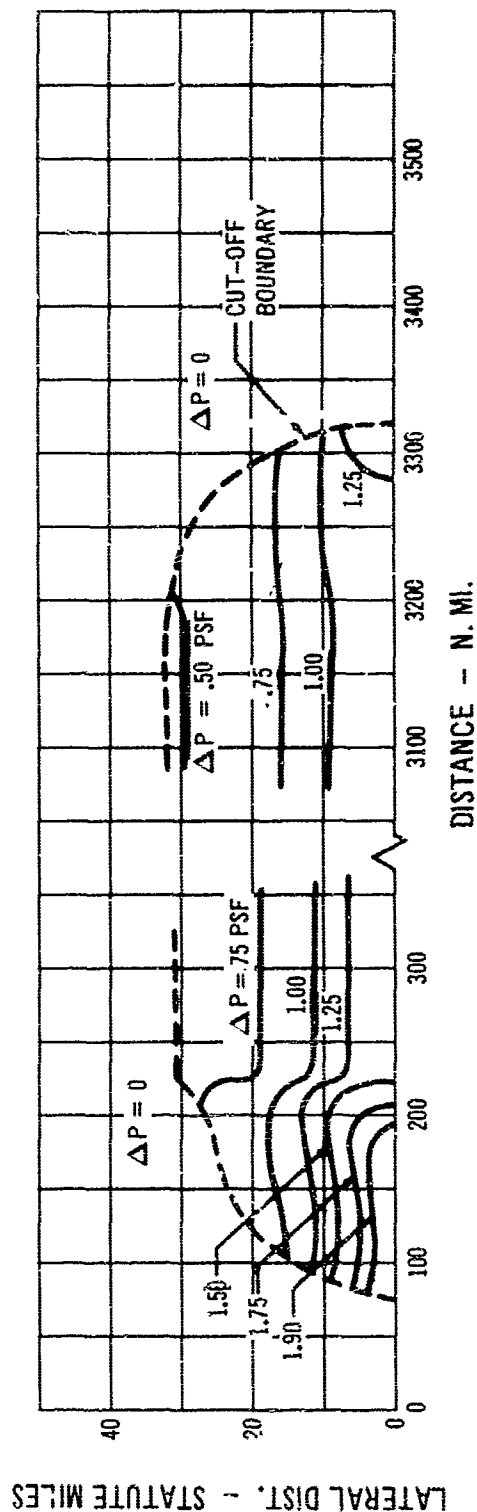
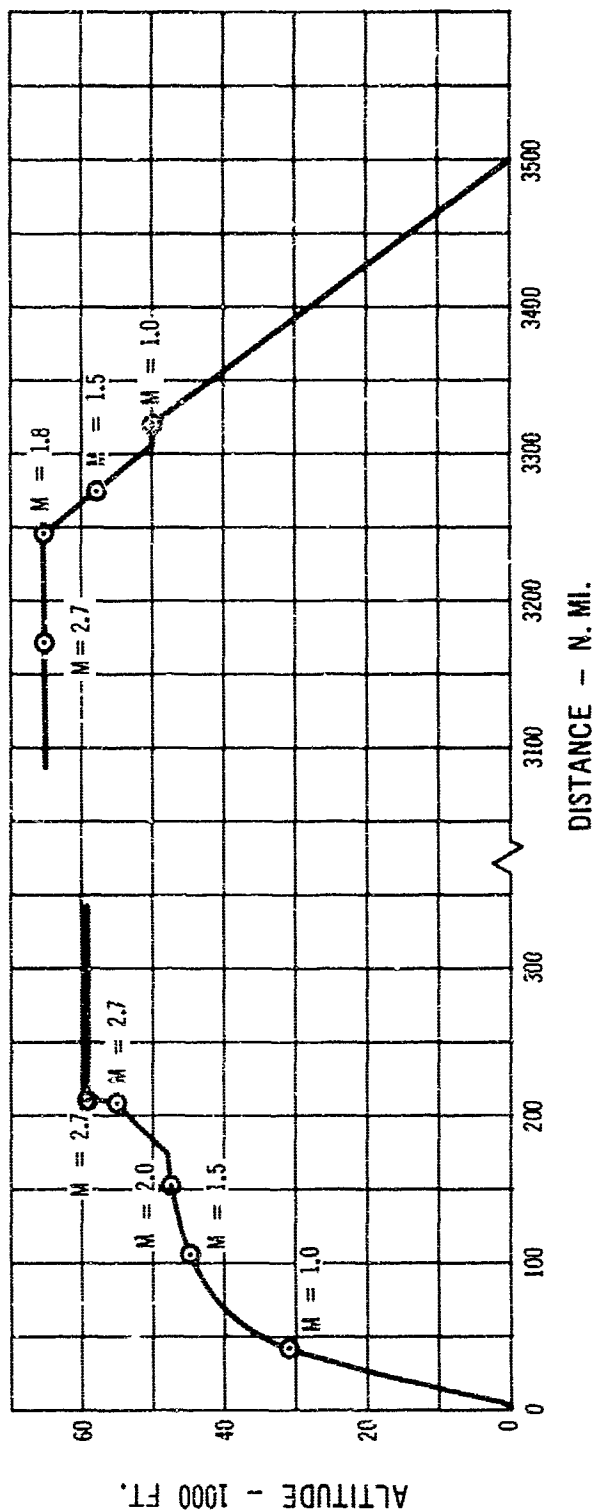
GE4/J4C

STD. DAY, ZERO WIND

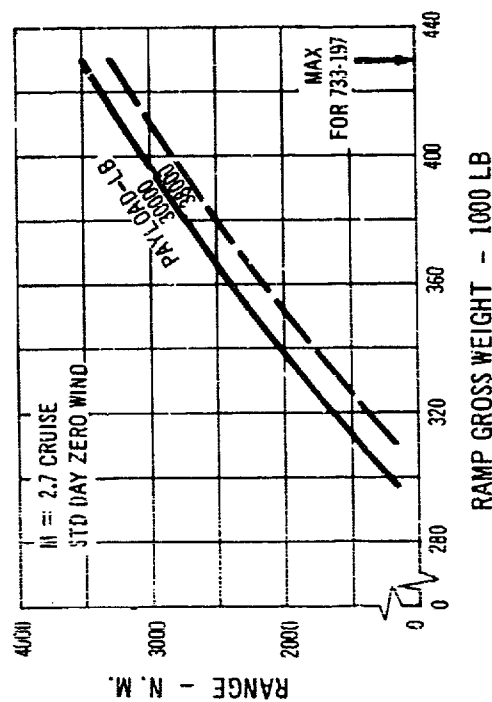
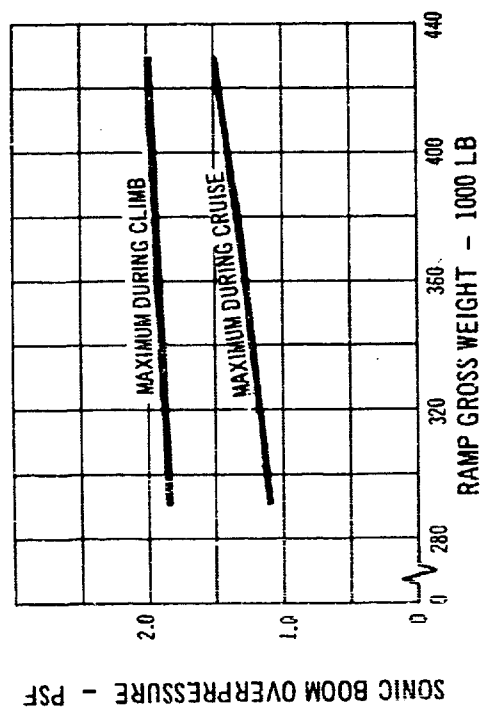


		FUEL USED - LB.	FUEL REMAINING - LB.	WEIGHT AT END OF OPER- ATION - LB.	TIME - HR.	DISTANCE - N. MI.
1. Take-off	Taxi (10 Minutes)	3,290	214,210	426,710	0	0
	T.O. Run	1,640	212,570	425,070	0	0
2. S.L. Acceleration		2,240	210,330	422,830	.0127	4
3. Climb and Acceleration		43,830	166,500	379,000	.2603	209
4. M 2.7 Cruise at 59,500 Ft.		39,000	127,500	340,000	.501	776
5. M 2.7 Climb to 62,000 Ft.		1,500	126,000	338,500	.017	27
6. M 2.7 Cruise at 62,000 Ft.		43,500	82,500	295,000	.626	970
7. M 2.7 Climb to 65,000 Ft.		1,630	80,870	293,370	.021	33
8. M 2.7 Cruise at 65,000 Ft.		45,525	35,345	247,845	.743	1152
9. Descent from 65,000 Ft.		3,330	32,015	244,515	.669	329
10. Approach and Landing (6 Min. at S.L.)		2,300	29,715	242,215	0	0
		<u>187,785</u>			2.8500	3500
RESERVES:						
a. 7% trip fuel		12,915		229,300		
b. 260 N.MI. Altn. Cruise M = .85, $\lambda = 42^\circ$		8,000		221,300		
c. Holding at 15,000 ft., $\frac{1}{2}$ hr., $\lambda = 30^\circ$		8,800		212,500		
TOTAL RESERVES		29,715				
TOTAL FUEL		217,500				

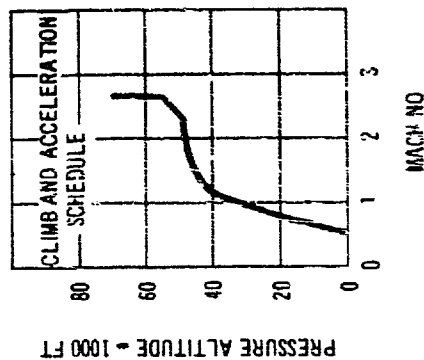
3-2 Design Mission Flight Profile



3-3 Design Mission Sonic Boom Overpressures

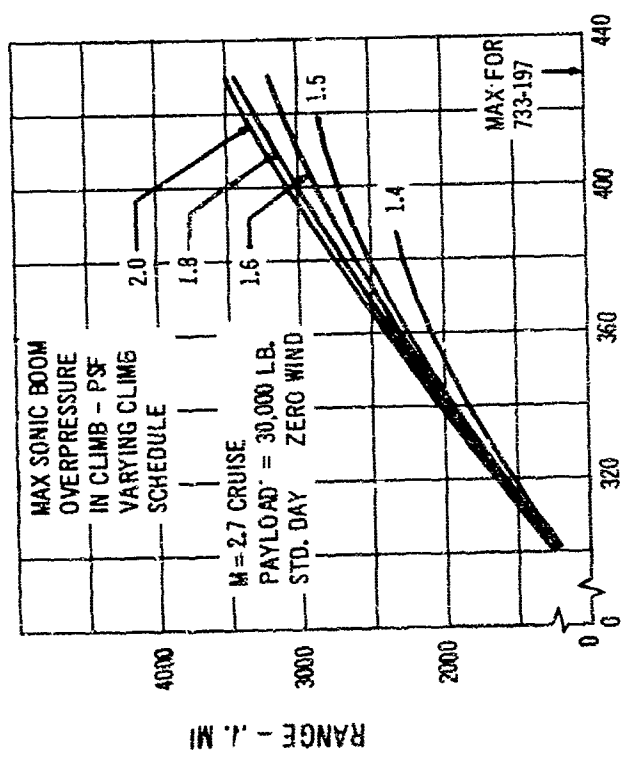
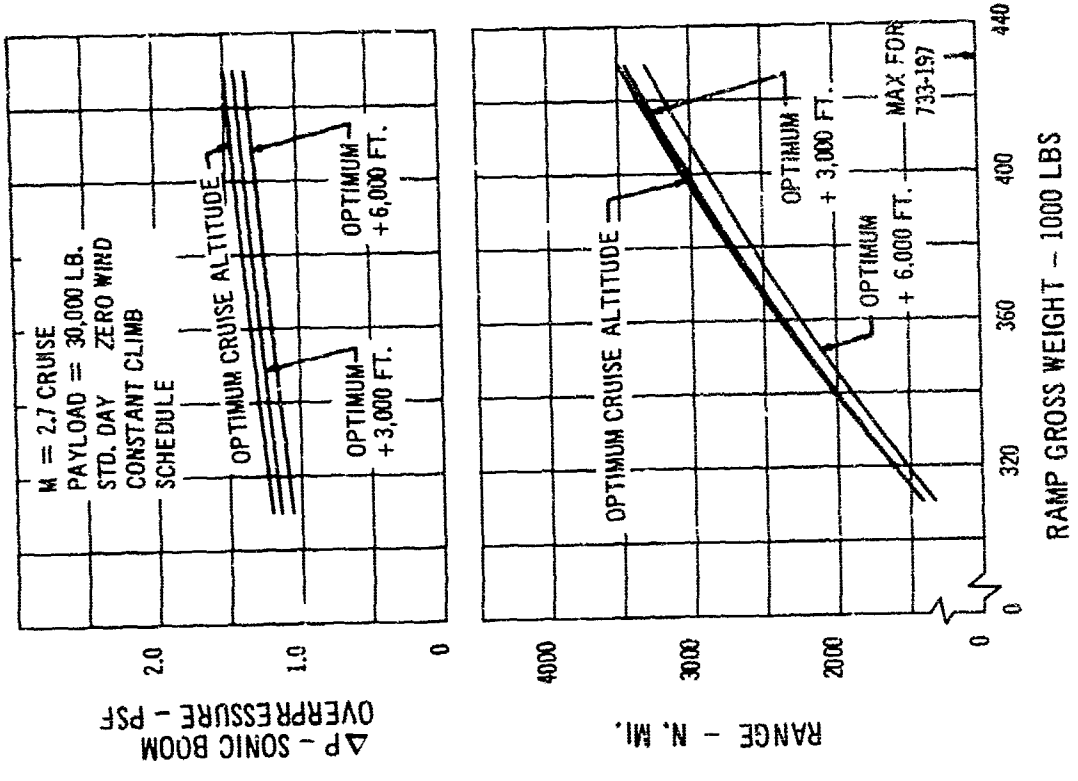


3-4 Range versus Gross Weight



loss of 110 nautical miles (3 percent) or, alternately, an increase in gross weight to 357,000 pounds. Fig. 3-6 shows the versatility available with regard to sonic boom overpressures in cruise for the design payload case. These data show that lowering the maximum sonic boom overpressures in cruise 10 percent to 1.35 psf results in a range loss of about 200 nautical miles; (6 percent) for the design mission case. For a typical transcontinental range of 2200 nautical miles lowering the maximum sonic boom overpressures in cruise 10 percent to 1.16 psf would result in a range loss of 130 nautical miles (4 percent) or alternately, an increase in gross weight to 357,000 pounds.

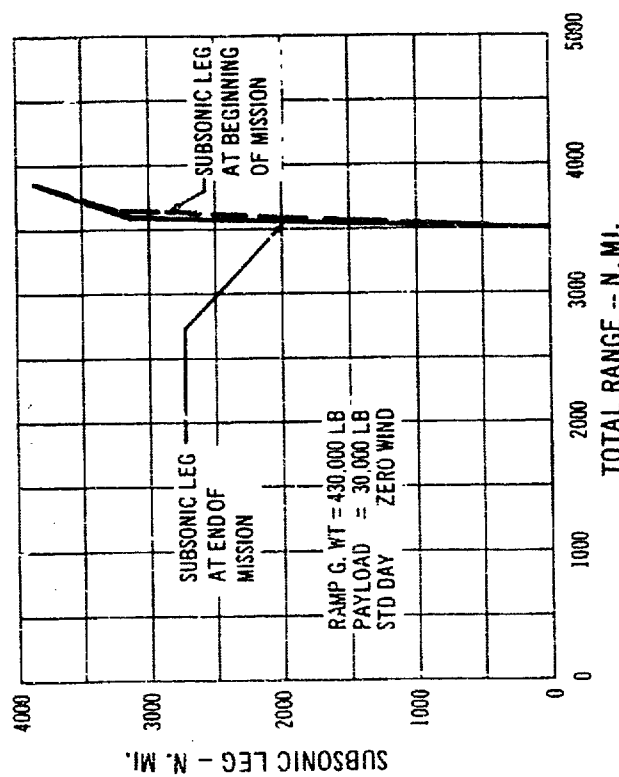
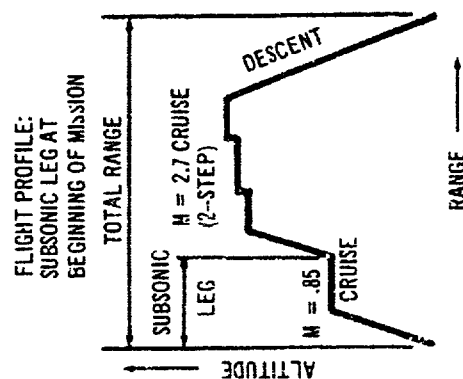
It is possible that supersonic flight will be prohibited over certain areas for a variety of reasons. In this event, subsonic legs at the beginning or the end of a mission will be required and possibly at both ends of the mission. Fig. 3-7 shows the capabilities of the Model 733-197 in this respect. These data show that subsonic cruise legs increase the range capability of the airplane. This is due to the variable sweep wing which provides excellent subsonic cruise capability with the wing sweep at 42 degrees.



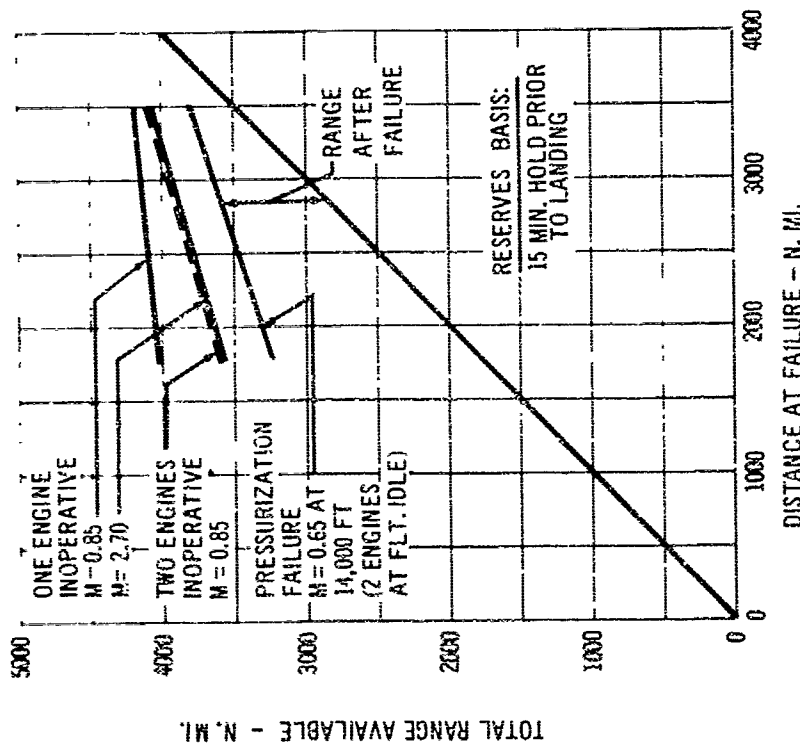
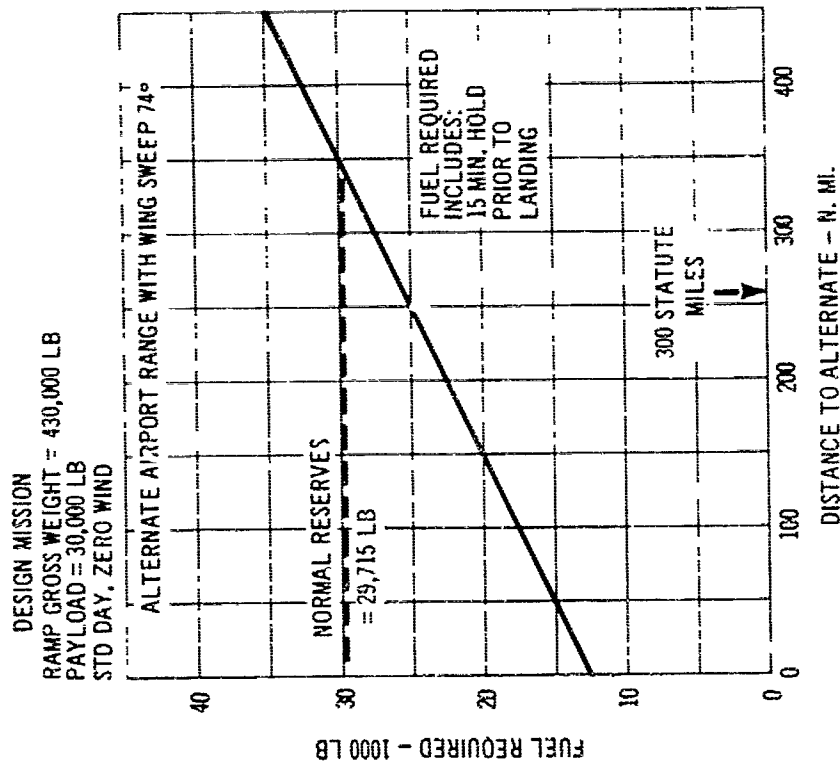
3-5 Operational Versatility - Sonic Boom in Climb

3-6 Operational Versatility - Sonic Boom in Cruise

The variable-sweep wing on the Model 733-197 provides for a high degree of operational reliability and safety. Fig. 3-8 shows the effects of several types of failures for the design mission case. These data show that for the most severe case, a cabin pressurization failure at mid-range (regarded as an extremely remote probability) the alternate distance available is 1480 nautical miles, more than adequate on most routes, i.e., on the New York to Paris route, Gander and Shannon are only 850 nautical miles away. Fig. 3-8 also shows that if a wing sweep failure occurs at the end of the normal cruise (also regarded as an extremely remote probability), the normal



3-7 Operational Versatility - Subsonic Cruise Legs



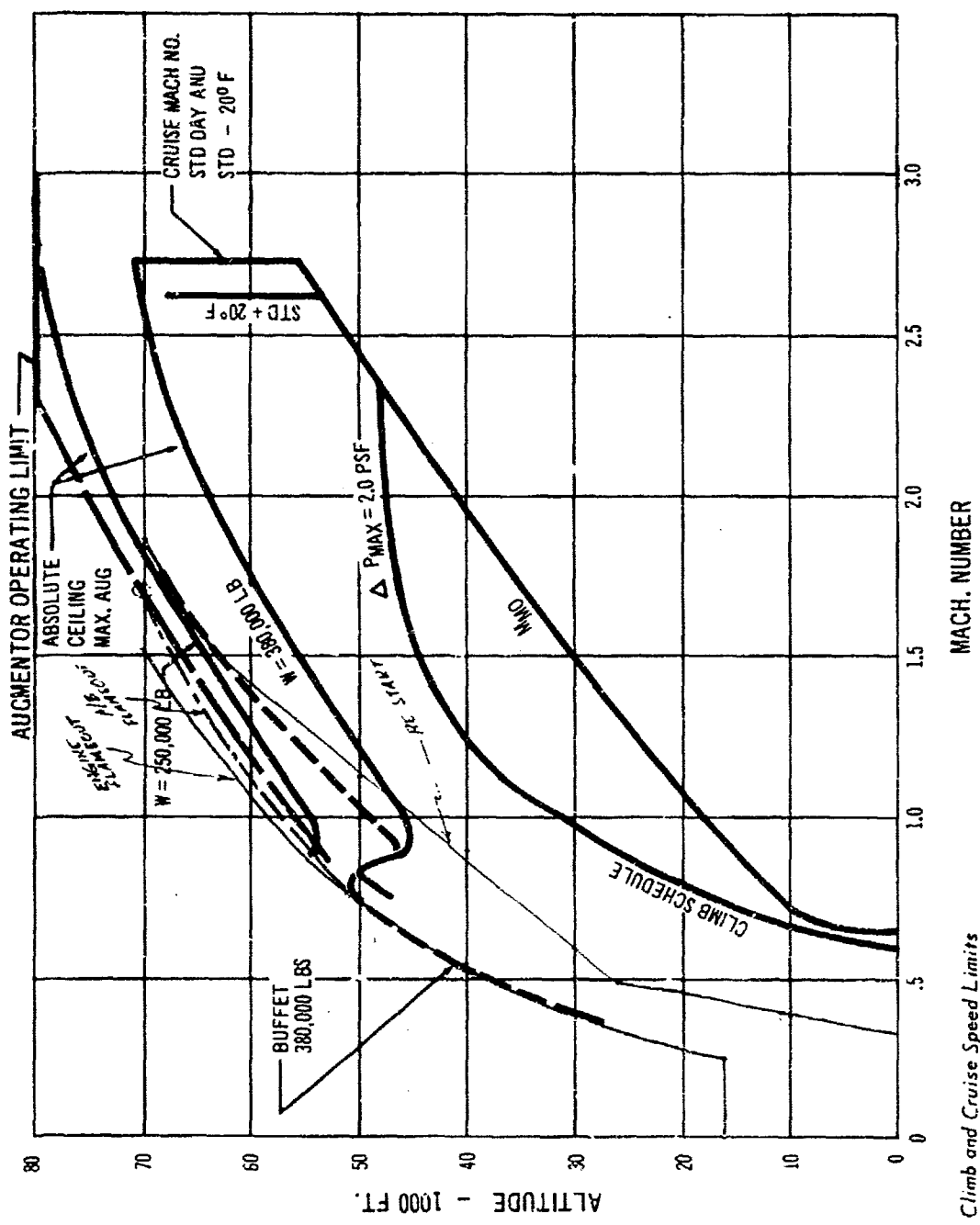
3.8 Operational Reliability and Safety

reserves provide an alternate airport capability of about 340 nautical miles. The fuel reserves assumed for these emergency missions consist of a 15-minute hold prior to landing in addition to the normal landing and approach fuel allowance of 2300 pounds.

3.2 Flight Limits

3.2.1 Climb and Cruise Speed Limits

Climb and cruise speed limits as a function of Mach number and pressure altitude are presented in Fig. 3-9. The



3.9 Climb and Cruise Speed Limits

sonic boom climb schedule is shown for the design mission. The maximum operating Mach number (M_{MO}) is shown indicating the operating limits of the configuration. The design stagnation temperature of 500 degrees occurs at a cruise Mach number of 2.7 for standard day and at a Mach number of 2.6 for a temperature of standard + 20 degrees Fahrenheit.

Absolute ceiling and buffet altitudes are shown for standard day conditions using the climb and descent sweep schedule.

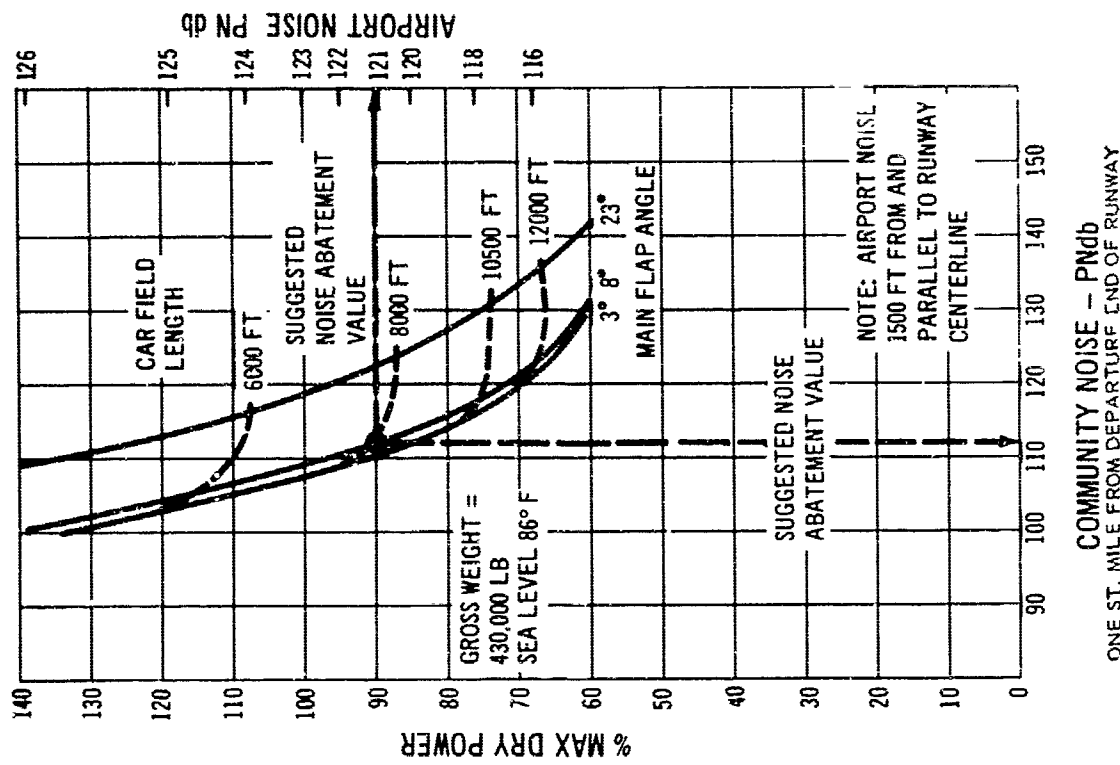
3.3 Takeoff Performance

The Boeing Supersonic Commercial Transport will have an excellent takeoff performance capability using thrust levels chosen to minimize perceived noise on the ground. Further, a high degree of operational flexibility exists in the Model 733-197 design in that:

- field length and community noise under the takeoff path may be reduced by taking off at higher thrusts than the noise-abatement power;
- field length may be further reduced by taking off at higher flap angles;
- very high climb gradients are possible where obstacle clearance is important, using moderate flap angles and high takeoff thrust.

In the sections immediately following, takeoff performance is shown for power settings chosen to give low airport and community noise levels during takeoff at sea level with an air temperature of standard + 15 degrees Centigrade (86 degrees Fahrenheit). A main flap angle of 8 degrees is used and engines are throttled back to give a climb rate of 500 feet per minute at one mile beyond the departure end of the runway.

Choice of this mode of operation was based on the data shown in Fig. 3-10 in which the possible trades between ground noise, climb (community) noise, field length, and takeoff power are shown for the design ramp



3-10 Take-Off Noise

gross weight of 430,000 pounds at sea level, hot day conditions.

On a standard day at sea level, the noise abatement takeoff power will be 85 percent Max. Dry; the community noise level will be reduced to 110.6 PNdb (RFP requirement, 112 PNdb) and field length will be 7350.

The noise levels shown are based on a Boeing evaluation of unsuppressed GE4/J4C engines. These are 3 PNdb greater than a General Electric estimate which was provided as a supplement to their specification. It is estimated that sound suppressors, which will be studied in Phases II and III, will result in a reduction of 2 to 5 PNdb from the values shown.

A typical takeoff profile designed to minimize noise is shown in Fig. 3-11. This figure depicts distances, and climb angles appropriate to takeoff at a gross weight of 430,000 pounds on a standard +15 degrees Centigrade day at sea level. Noise abatement power is selected; rotation, lift-off, and flare to climb attitude follow conventional practices as per 4T.114 of SR 422B. Lift-off is at 154 knots, and the steady climb at 163 knots with a climb rate of 2270 feet per minute. One statute mile beyond the end of the runway, at an altitude of 1140 feet, the throttles are eased back to reduce the rate of climb to 500 feet per minute. After passing over the densely populated area, power is increased to a climb setting and flap retraction is initiated when a suitable speed margin has been gained.

3.3.1 TAKEOFF FIELD LENGTHS AND COMMUNITY NOISE LEVELS

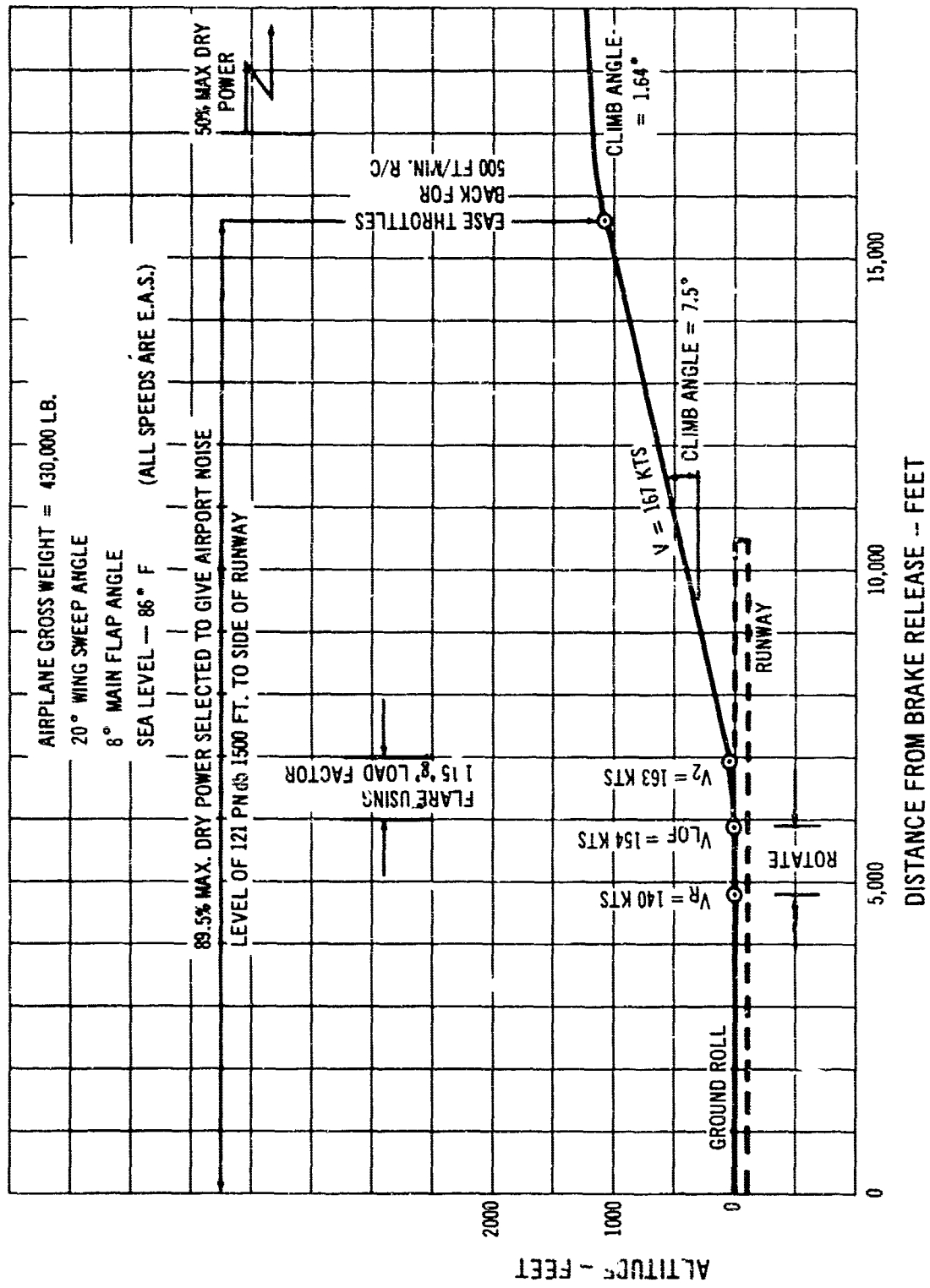
C.A.R. takeoff field lengths for the 733-197 configuration are plotted in Fig. 3-12 for a constant 86 degrees Fahrenheit temperature, at several altitudes. A range of takeoff weights, from 300,000 to 500,000 pounds, and altitudes, from sea level to 8000 feet, are covered. The corresponding community noise levels are also indicated. The field lengths are for the aircraft trimmed at the most forward c.g. posi-

tion (.4 MAC).

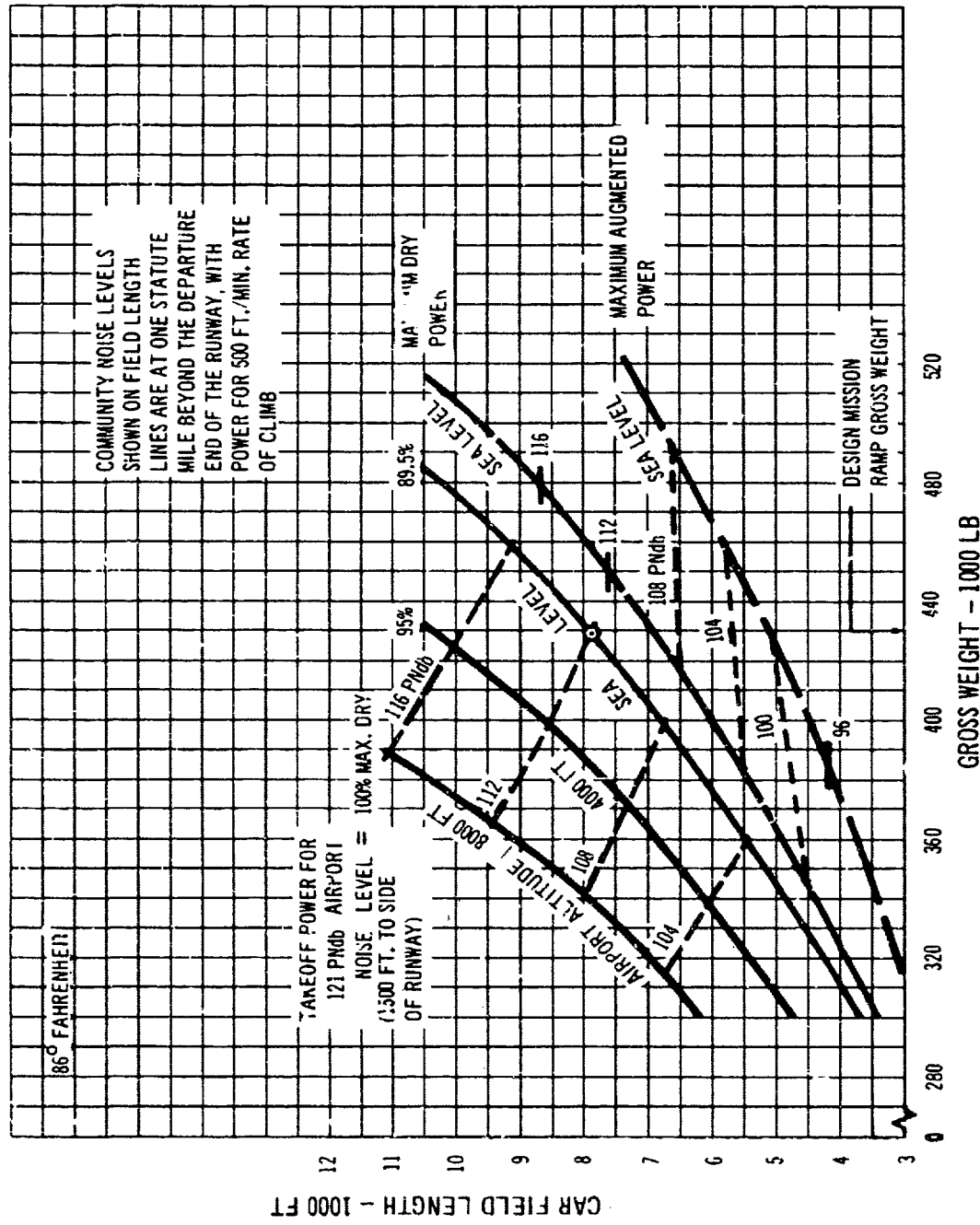
As indicated in Fig. 3-12, using the noise abatement thrust setting at sea level and a hot day temperature of 86 degrees Fahrenheit, the 733-197 airplane has a C.A.R. takeoff field length of 8000 feet and a community noise level of 112 PNdb at the design gross weight of 430,000 pounds. The noise abatement thrust level upon which the field lengths are based is selected to provide an airport ground noise level of 121 PNdb 1500 feet to the side of the takeoff path. This somewhat arbitrary criterion has been selected in order to illustrate the effect of a noise abatement procedure on performance. However, experience indicates that 121 PNdb at 1500 feet is well within the tolerable range for normal airport operations. Thus, all takeoff requirements specified in Paragraphs 2.6.1, 2.6.3, and 2.8.9 of the Request for Proposal are met or exceeded.

Fig. 3-12 also includes curves for sea level takeoffs using maximum dry and augmented thrust. As is to be expected, the field lengths for this thrust setting are considerably shorter than the corresponding field lengths for noise-abatement thrust settings. The airport ground noise for a takeoff using maximum augmented thrust is 126 PNdb; however, a reduction in community noise is realized compared to that corresponding to a takeoff using the noise abatement thrust setting, since the height of the airplane above the community is increased. All community noise levels shown are based on a thrust setting which provides a rate of climb of 500 feet per minute at a constant speed and at a height which results when the throttles are eased back to this condition at a point one statute mile beyond the departure end of the runway.

By using maximum augmented thrust, a takeoff field length of less than the maximum of 10,500 feet, permitted by Par. 2.8.9 of the Request for Proposal, is obtained for the maximum design ramp weight of 430,000 pounds for even the most severe condition considered (8000-foot altitude and 86 degrees Fahrenheit hot day temperature).



311 Typical Take-Off Profile

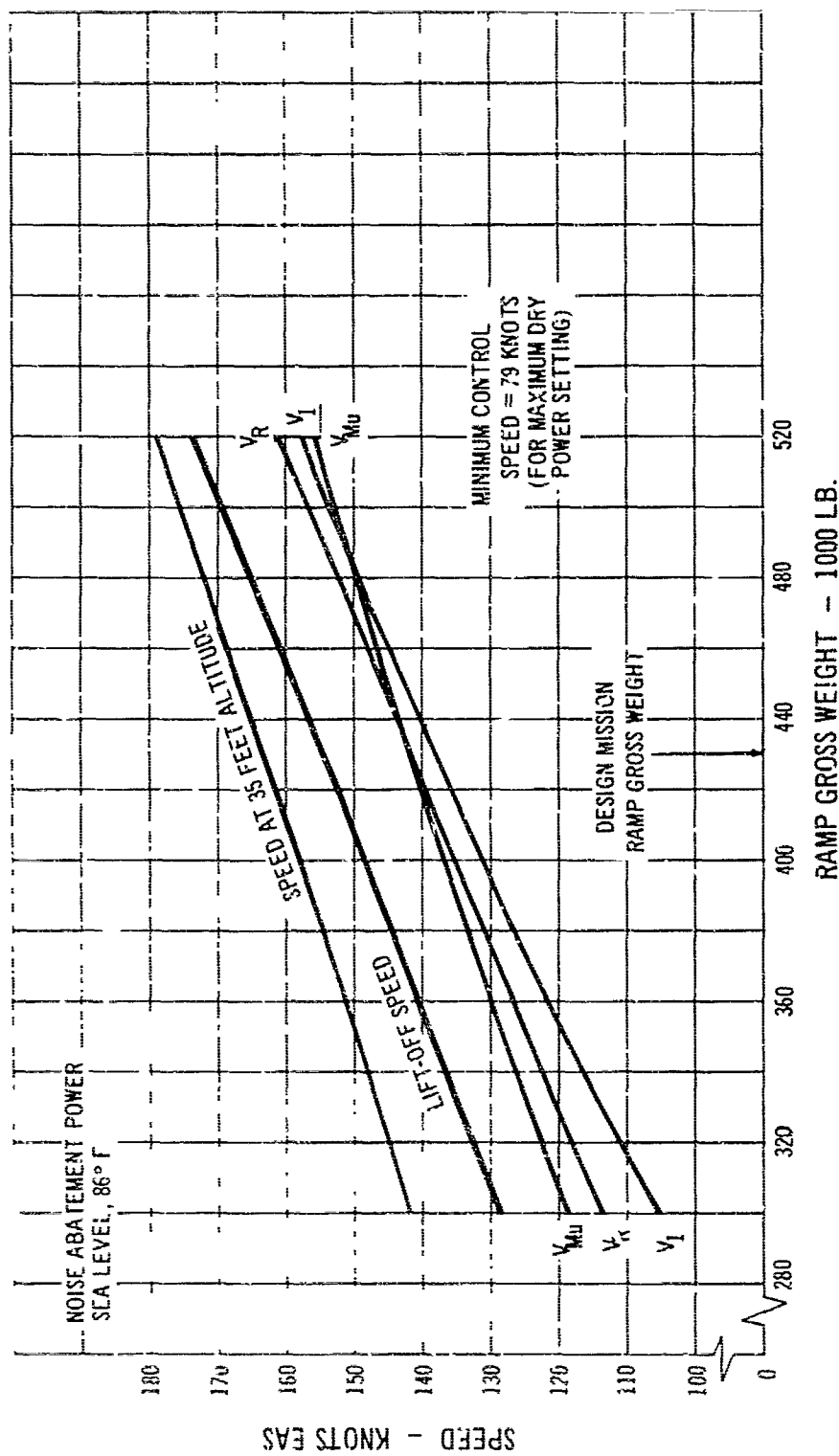


3-12 Take-Off Distance - 86° F

3.3.2 TAKEOFF SPEEDS

All speeds used in evaluating takeoff performance have been chosen to meet the applicable requirements of special C.A.R. No. SR 422D, together with the further Tentative Airworthiness Objectives and Standards for Supersonic

Transport Design Proposals (the latter dated August 15, 1963). The minimum control speed (V_{MC}), takeoff refusal speed (V_I), rotation speed (V_R), minimum unstick speed (V_{MU}), liftoff speed (V_{LOF}), and the speed at 35 feet altitude are shown in Fig. 3-13 as functions of take-off weight for the noise-abatement takeoff thrust at sea



3-13 Take-Off Speeds

level. These speeds correspond to the aircraft trimmed with the c.g. in the most forward position and thus are conservative. With the engines mounted close to the airplane centerline, control with a critical engine failed presents no difficulty. V_{NE} is shown at maximum dry power, a thrust which may be obtained rapidly on advancing the throttles after an engine failure. The extra climb performance resulting from using this thrust is a good safety feature on this airplane.

Lift-off speed has been determined either by the geometry-limited, minimum unstick speed, or by the requirement to reach the takeoff safety speed at 35 feet altitude, depending on the airplane thrust-to-weight ratio.

The lift-off speed for the design ramp gross weight of 430,000 pounds is 154 knots EAS.

3.3.3 TAKEOFF CLIMB GRADIENTS

All takeoff climb gradient requirements outlined in Special Civil Air Regulation No. SR 422B, Par. 4T.120, are easily met by the 733-197 configuration with the critical engine inoperative and the remaining engines at the noise abatement thrust setting. For an altitude of 8,000 feet and a temperature of 86 degrees Fahrenheit — the most severe condition considered — the airplane would become second-segment climb-gradient limited at a weight of 450,000 pounds.

3.4 Approach and Landing Performance

Landing approach speeds, climb gradients, field lengths, and approach noise levels, are presented in this section. The performance shown is based on an approach at $1.3V_{S0}$ unless otherwise stated. V_{S0} is the 1 "g" stall speed, with the aircraft trimmed for the c.g. in the most forward (most conservative) position.

For a sea level, standard day landing at the normal mission landing weight of 242,215 pounds, the landing approach speed is 125 knots, the C.A.R. landing field length is 5,850 feet, the actual landing distance over a

50-foot obstacle is 4,500 feet for a wet runway condition, and a noise level of approximately 119.5 PNdb will be perceived directly under the flight path at a point one statute mile from the airport runway.

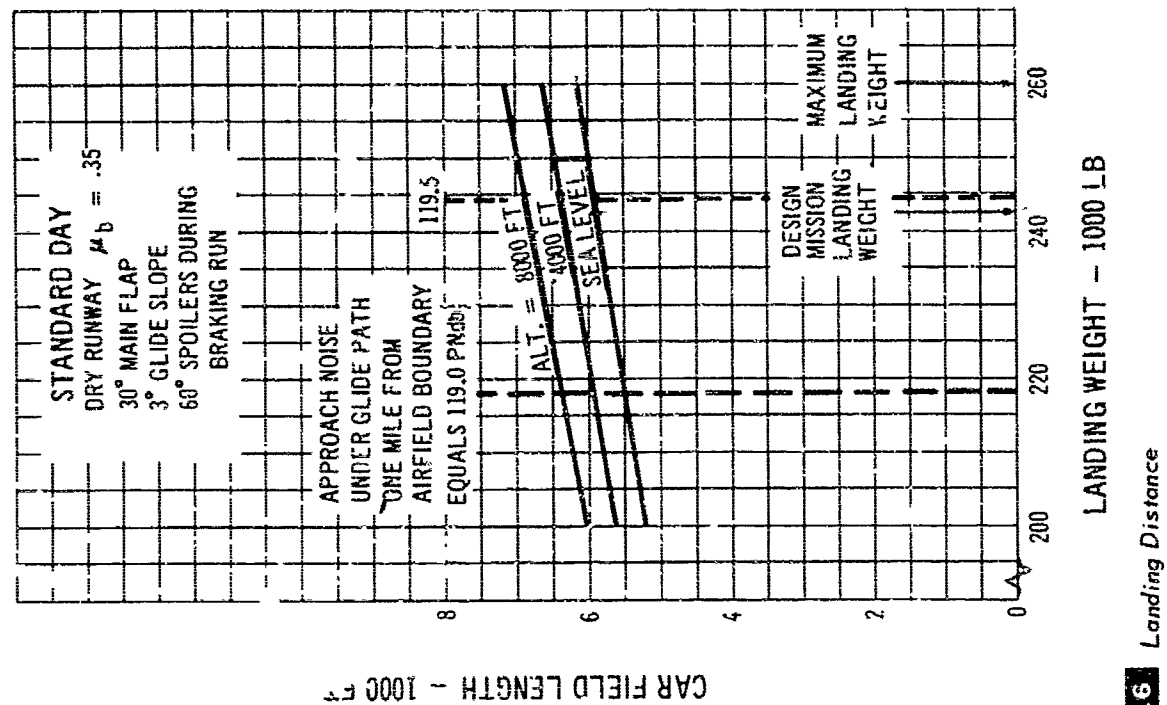
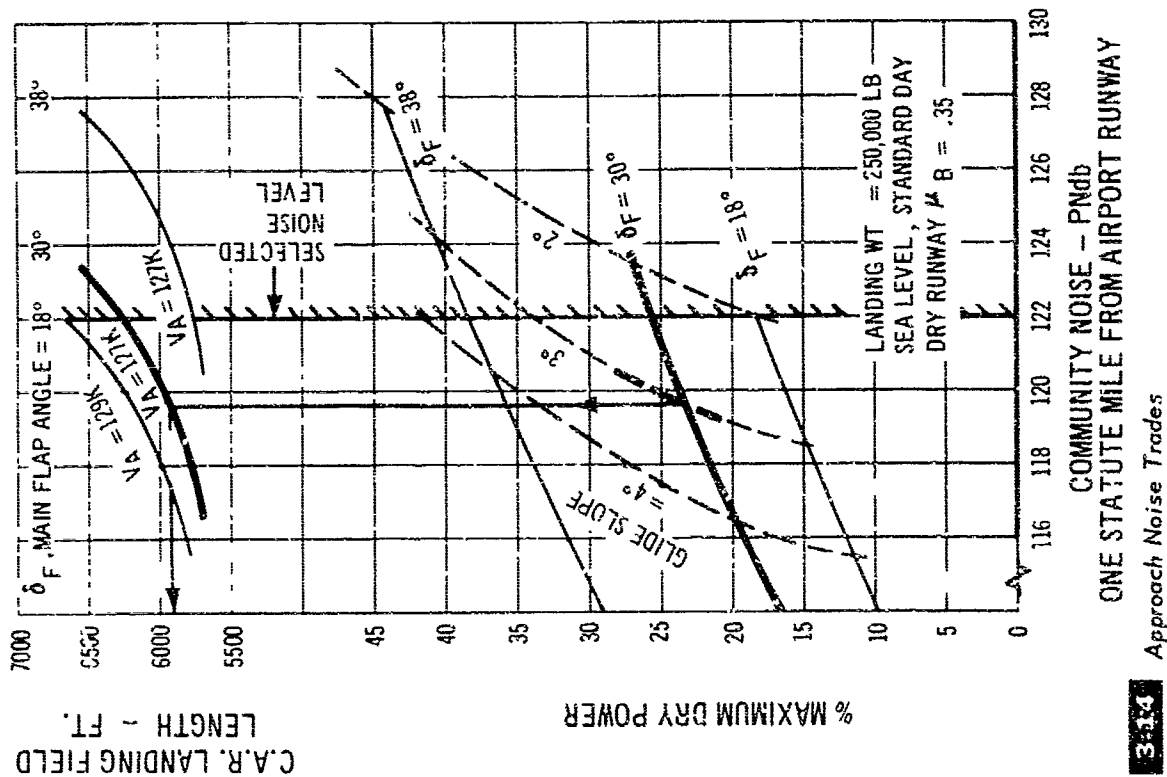
3.4.1 LANDING APPROACH NOISE TRADE FACTORS

The subject of community noise levels in the landing approach has been thoroughly explored. For purposes of comparison with existing airplane approach noise levels, the perceived noise directly under the flight path at a point one statute mile from the airport runway has been chosen as reference. As discussed in Section 8 of Volume A-VII, 122 PNdb has been selected as a maximum level for approach noise.

Some of the trades possible are shown in Fig. 3-14, where glide angle and flap angle (the latter affects L/D ratio and approach speed) are the primary variables. Glide slope and L/D are potent factors in fixing the perceived noise levels. Approach speed is a further variable. The chart has been prepared for a landing weight of 250,000 pounds. A reference point on the chart is shown for a 3-degree glide slope at 30 degrees main flap angle. This gives a noise level of 119.6 PNdb, an approach speed of 127 knots (minimum approach speed per SR422B is 120 knots), and a field length of 5950 feet. Use of a 2.5 degree glide slope would increase the noise level to 121.7 PNdb and the field length to 6200 feet. Noise levels may be reduced by increasing the glide slope, since less thrust is then needed on the approach, or by reducing main flap angle, which has the same effect. The latter, however, affects the field length adversely.

3.4.2 C.A.R. APPROACH SPEEDS AND CLIMB GRADIENTS

Landing approach speeds are shown in Fig. 3-15 for a range of landing weights, where they are compared with



the minimum approach speeds, $1.3V_s$, permitted by the present Civil Air Regulations of SR422B. Typically, the latter are smaller by about 7 knots.

Body reference angle-of-attack during approach will be 3.6 degrees, placing the body at 0.6 degrees nose-up relative to horizontal when approaching down a 3 degree glide path. This will give excellent visibility, making accurate touchdowns possible in low weather minimums.

In the event of a go-around, 90 percent of maximum dry thrust is available in seven seconds from the time the throttles are advanced from idle. With the operating engines at this power, all landing and approach climb-gradient requirements of FAA SR-422B are easily met by the 733-197 airplane.

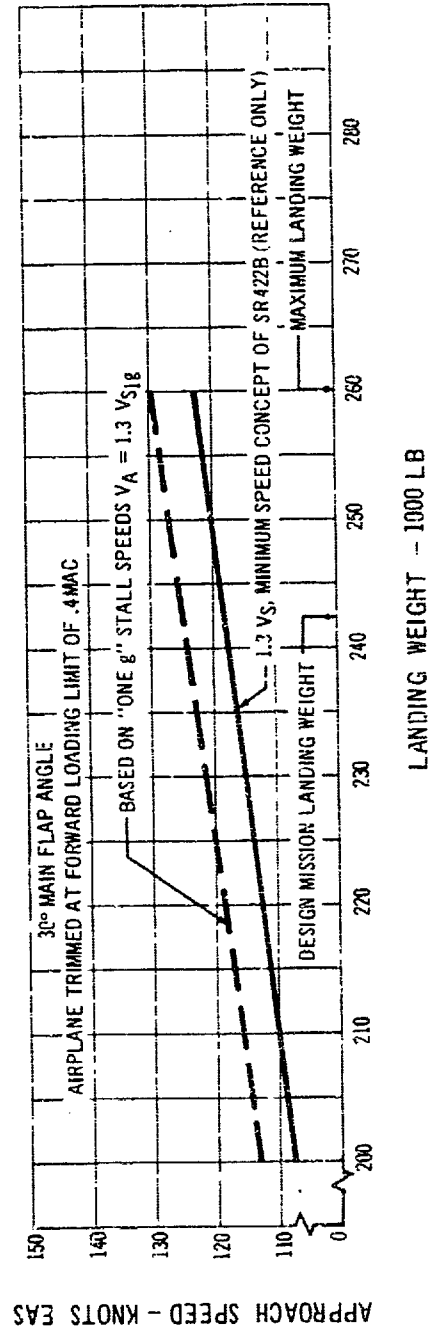
3.4.3 C.A.R. LANDING DISTANCE

Fig. 3-16 shows the C.A.R. landing field lengths for a range of landing weights. Altitudes of 0, 4000 and 8000

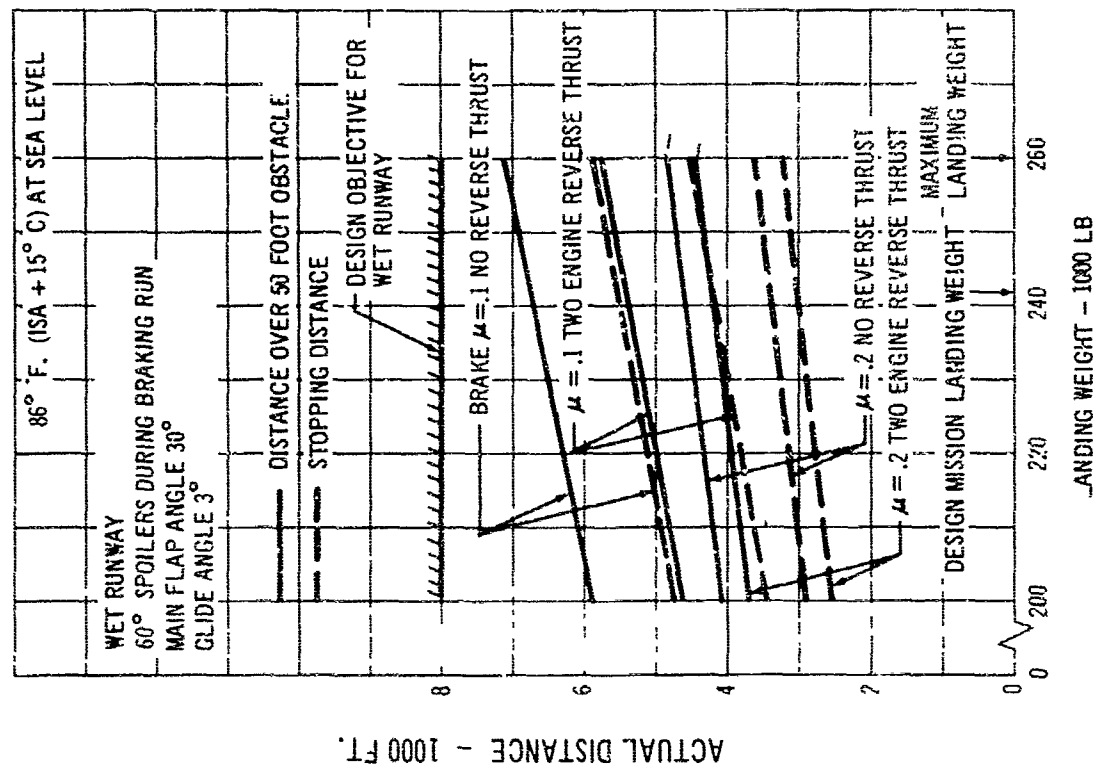
feet are covered at a standard day ambient temperature. A 3 degree glide slope was chosen to illustrate the distances because of its suitability for reasonably low community noise levels during landing approach. The distances shown would be increased by about 250 feet with a 2.5 degree glide slope.

A braking μ of 0.35, a value already proven on Boeing 707 airplanes, was used in computing ground roll; wing spoilers are also utilized after braking commences.

At sea level, the landing field length is 5850 feet at the normal landing weight of 242,215 pounds. At maximum landing weight of 260,000 pounds the distance increases to 6100 feet. Landing field lengths would be reduced by some 400 to 500 feet if the minimum approach speed, $1.3V_s$, permitted by the present Civil Air Regulations of SR-422B, were used. Community noise levels during approach, at one statute mile from the airport are about 119.5 PNdb.



3-15 Landing Approach Speed



3-17 Landing Distance, Wet Runway

3.4.4 LANDING DISTANCES, WET RUNWAY

Actual landing field length over a 50-foot obstacle is shown on Fig. 3-17 for a wet runway surface at sea level, 86 degrees Fahrenheit air temperature. Braking friction coefficients, μ_B , of 0.1 and 0.2 have been used, both with and without reverse thrust on two engines. A μ_B of 0.2 has been obtained, under wet runway conditions, on Boeing 707-type aircraft using individually modulated anti-skid units.

The actual field length is equal to 4500 feet at a landing weight of 260,000 pounds, with $\mu_B = .2$ and two engine reverse thrust used for stopping. This provides a handsome margin for operational factors in meeting the RFP requirement for 8000-foot distance. Full reverse thrust is used only above 50 knots speed to avoid hot gas reingestion by the engines.



SECTION 4

GROWTH

TABLE OF CONTENTS

4.0 GROWTH	4/1
4.1 Range-Payload Trades	4/1
4.2 Sonic Boom Trades	4/1
4.3 Low Speed Performance and Noise Trades	4/1
4.4 Performance Summary	4/8

4.0 GROWTH

In this section, the performance trades of two growth versions of the Model 733-197 are considered. The external geometry differs from the basic model only in body length. (The growth versions have a body length of 249 feet versus 204 feet for the basic model.) The wing area, engine type, and engine size are the same. A three-view drawing of the growth versions is given in Fig. 4-1. The models were selected in order to meet the requirements of (1) a domestic operator and (2) an intercontinental operator.

4.1 Range-Payload Trades

Using the basic airframe and engine size selected for the Model 733-197, the trades of range and payload by lengthening the body were studied. The results are presented in Fig. 4-2. Fig. 4-2 (left) shows the trades where the design sonic boom overpressure during climb is 2 psf. From this trade study, the domestic operator's version was selected. The design characteristics are: ramp gross weight, 408,000 pounds; range, 2500 nautical miles; payload, 43,000 pounds (214 passengers).

Fig. 4-2 (right) shows data from which the intercontinental version was selected. In order to provide an adequate thrust margin during climb and acceleration, the overpressure during climb is 2.1 psf at maximum payload (214 passengers) and design mission range of 3500 nautical miles. This version has a ramp gross weight of 520,000 pounds.

The trades of payload versus range for the supersonic cruise case are presented in Fig. 4-3. The fuel capacity has been increased 50,000 pounds for the intercontinental model relative to the basic Model 733-197.

4.2 Sonic Boom Trades

The effect of off-loading fuel on airplane range, gross weight, and sonic boom overpressure is presented in Fig.

4-4. The climb and acceleration schedule has been held constant for these trades and is shown in Fig. B 3-26. It is noted that the overpressure values do not change markedly as range varies. The reduction in climb overpressure is due to reduced weight effects only. The cruise overpressure reduction is more rapid due to the combined effects of both reduced weight and increased cruise altitude.

There is considerable flexibility in the manner in which these airplanes can be operated when sonic boom is a significant factor. For example, Fig. 4-5 illustrates the trades between sonic boom overpressure and range for the domestic version at a constant gross weight of 408,000 lbs. The climb overpressure is a function of the climb schedule used only, while the maximum cruise overpressure is determined by both the initial cruise weight and altitude. With a constant climb schedule and corresponding constant climb overpressure, total range is a function of cruise altitude and corresponding cruise efficiency only. The total range changes with climb overpressure because of different fuel requirements for each climb schedule. Similar trades exist for all gross weight-payload combinations.

4.3 Low Speed Performance and Noise Trades

The takeoff and noise trades are presented in Fig. 4-6. Takeoff performance is presented for sea level, 86 degrees Fahrenheit conditions.

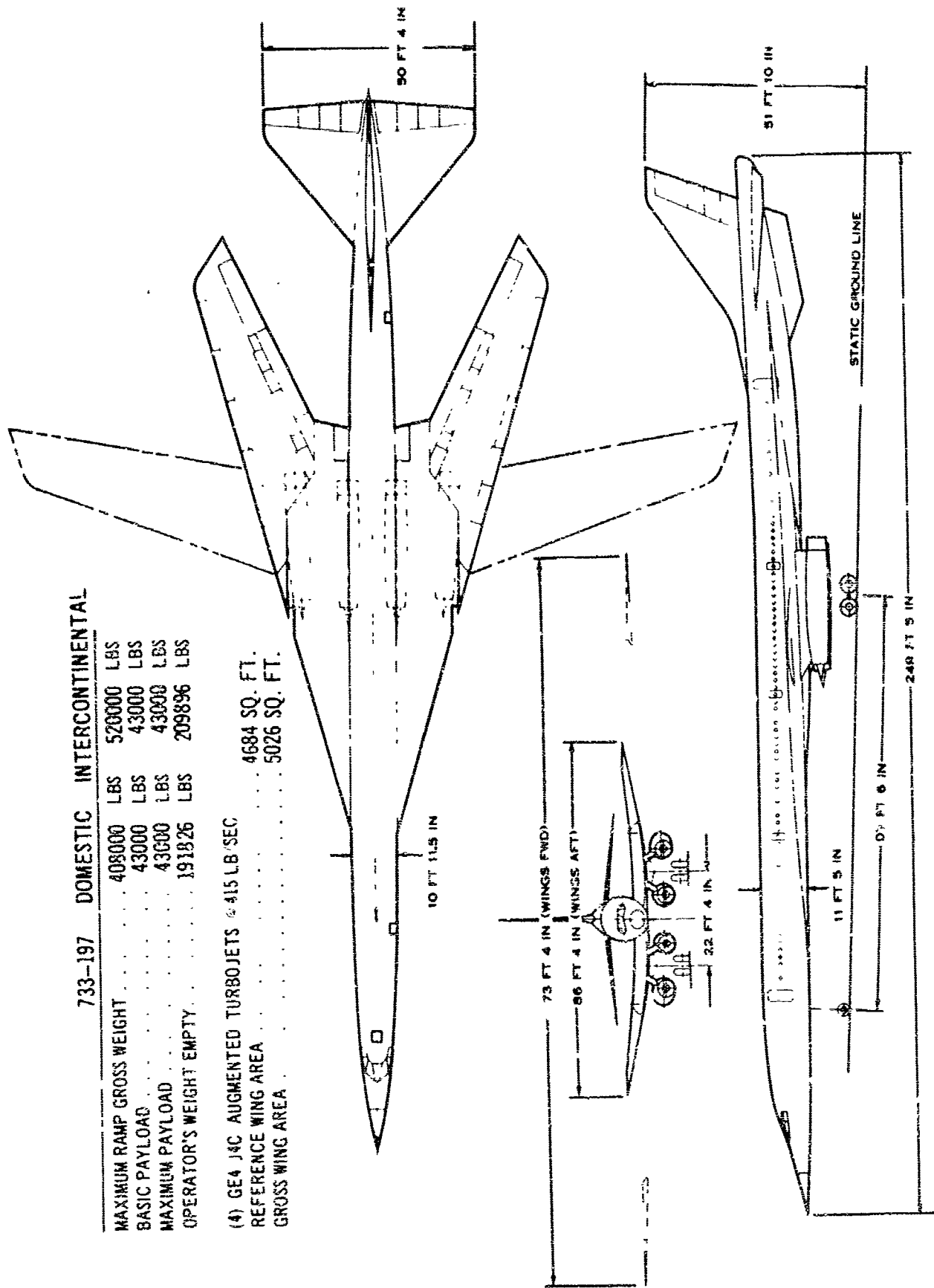
Takeoff field length is not a limiting factor on airplane growth because of the excellent high-lift characteristics and large amount of power available. For the 520,000-pound intercontinental version with maximum augmented thrust, the field length is only 7350 feet, the takeoff speed is 168 knots, the community noise is 112 PNdB, and the airport noise is 126 PNdB.

The CAR landing distance for standard day, sea level conditions is presented in Fig. 4-7. The CAR landing

733-197 DOMESTIC INTERCONTINENTAL

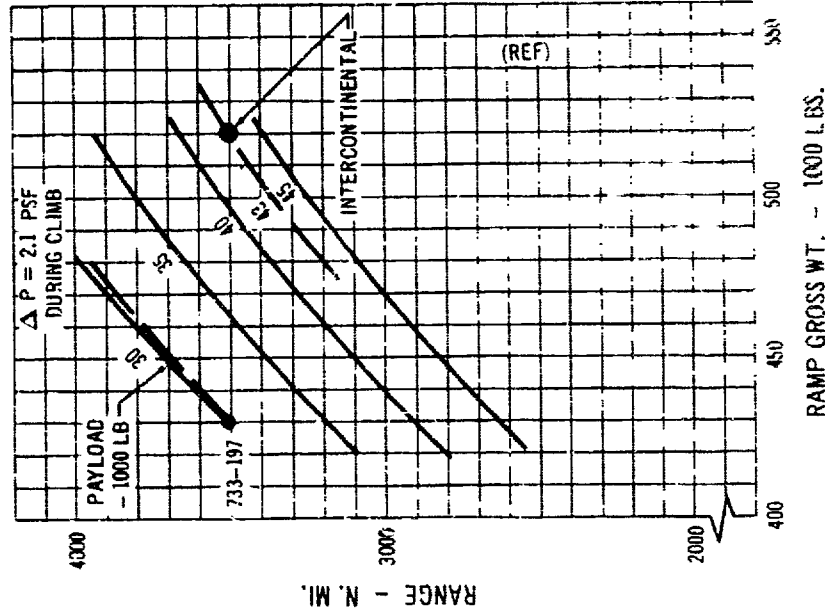
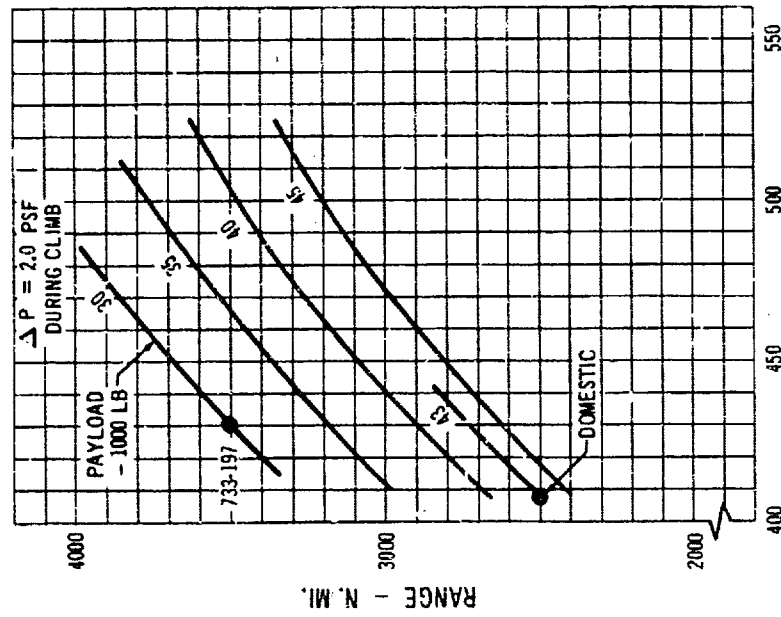
MAXIMUM RAMP GROSS WEIGHT . . .	408000 LBS	520000 LBS
BASIC PAYLOAD . . .	43000 LBS	43000 LBS
MAXIMUM PAYLOAD . . .	43000 LBS	43000 LBS
OPERATOR'S WEIGHT EMPTY . . .	191826 LBS	209896 LBS

(4) GE4 J4C AUGMENTED TURBOJETS @ 415 LB/SEC
 REFERENCE WING AREA . . . 4684 SQ. FT.
 GROSS WING AREA . . . 5026 SQ. FT.

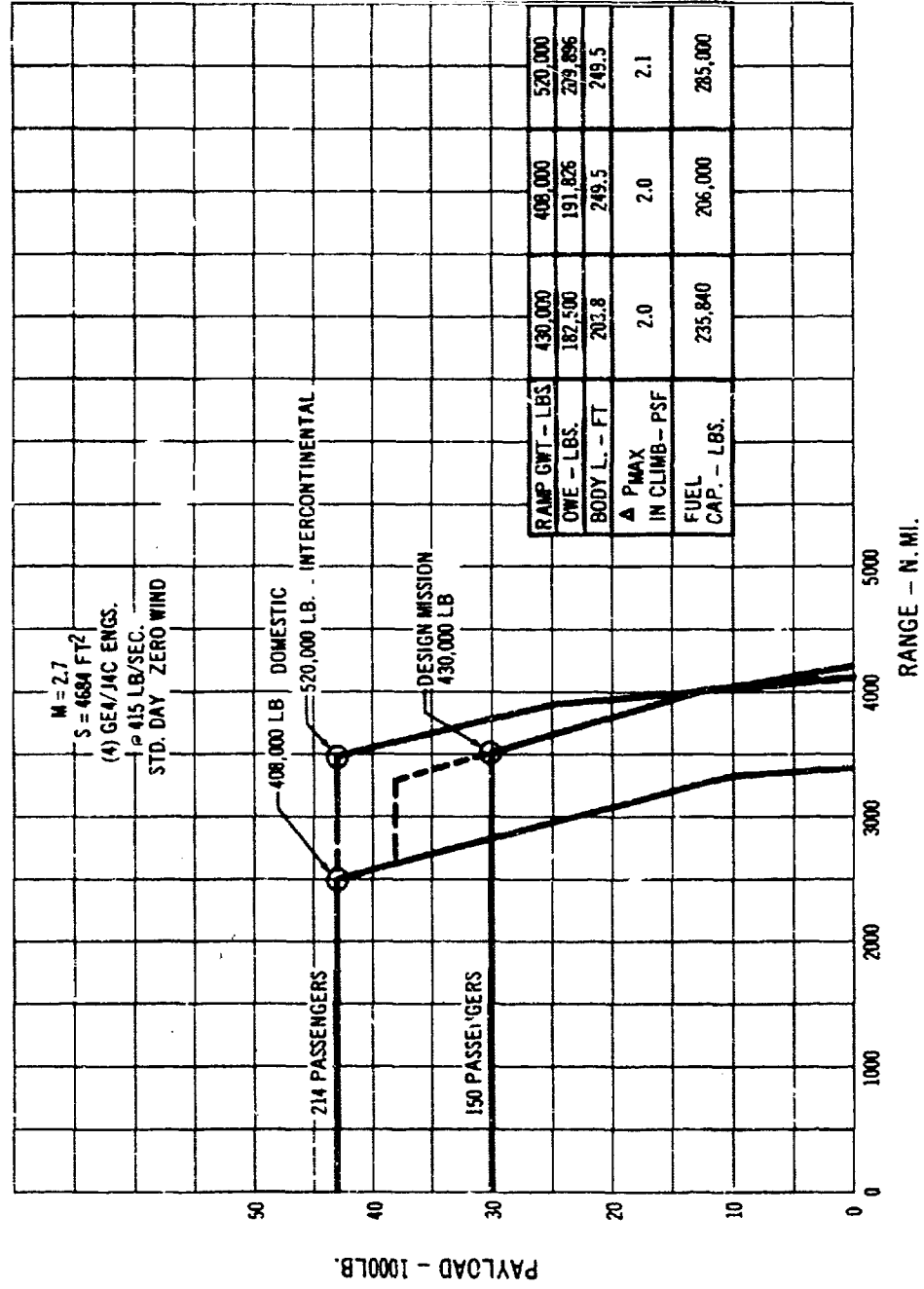


4-1 733-197 Three-View, Growth Model

WING AREA = 4684 FT²
 (4) GE4/J4C ENGS @ 415 LB/SEC
 STD. DAY

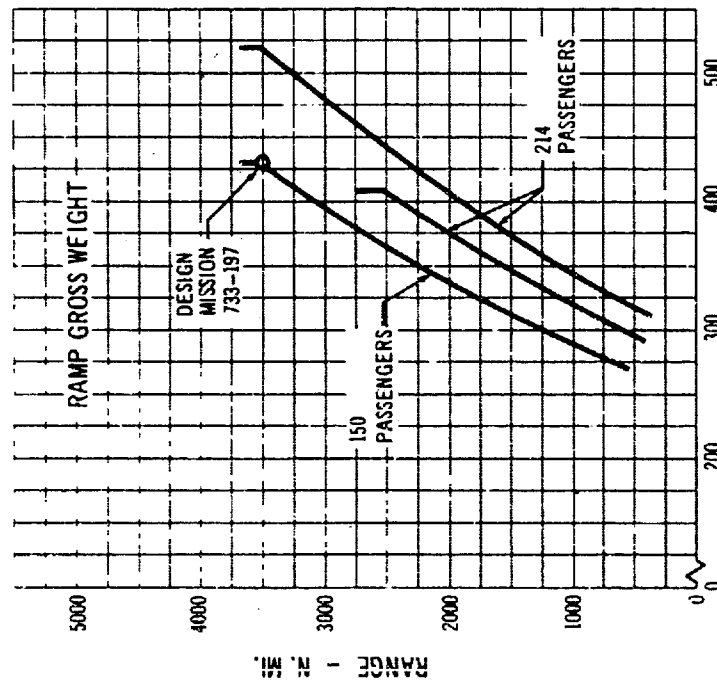


4.2 Extended Body Airplane Growth



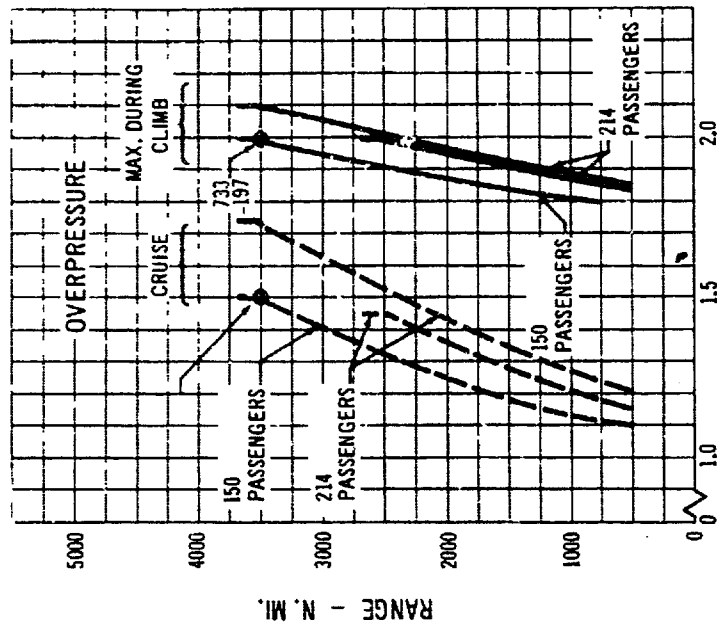
4-3 Growth Payload - Range

CRUISE MACH = 2.7
 $S_W = 4684 \text{ FT}^2$
 (4) GE4/J4C ENGS. @ 415 LB/SEC.
 STANDARD DAY
 ZERO WIND

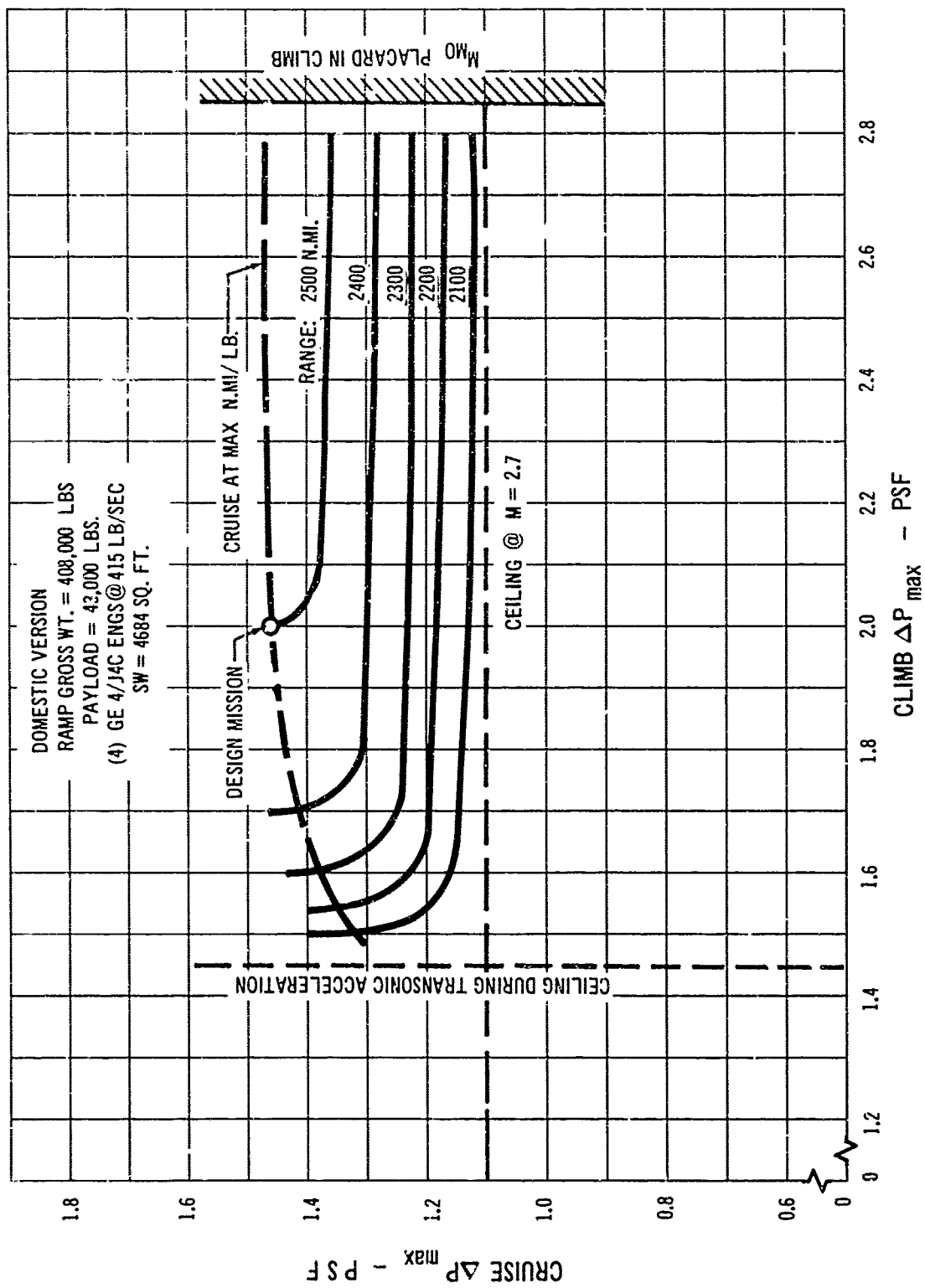


RAMP GROSS WEIGHT - 1000 LB.

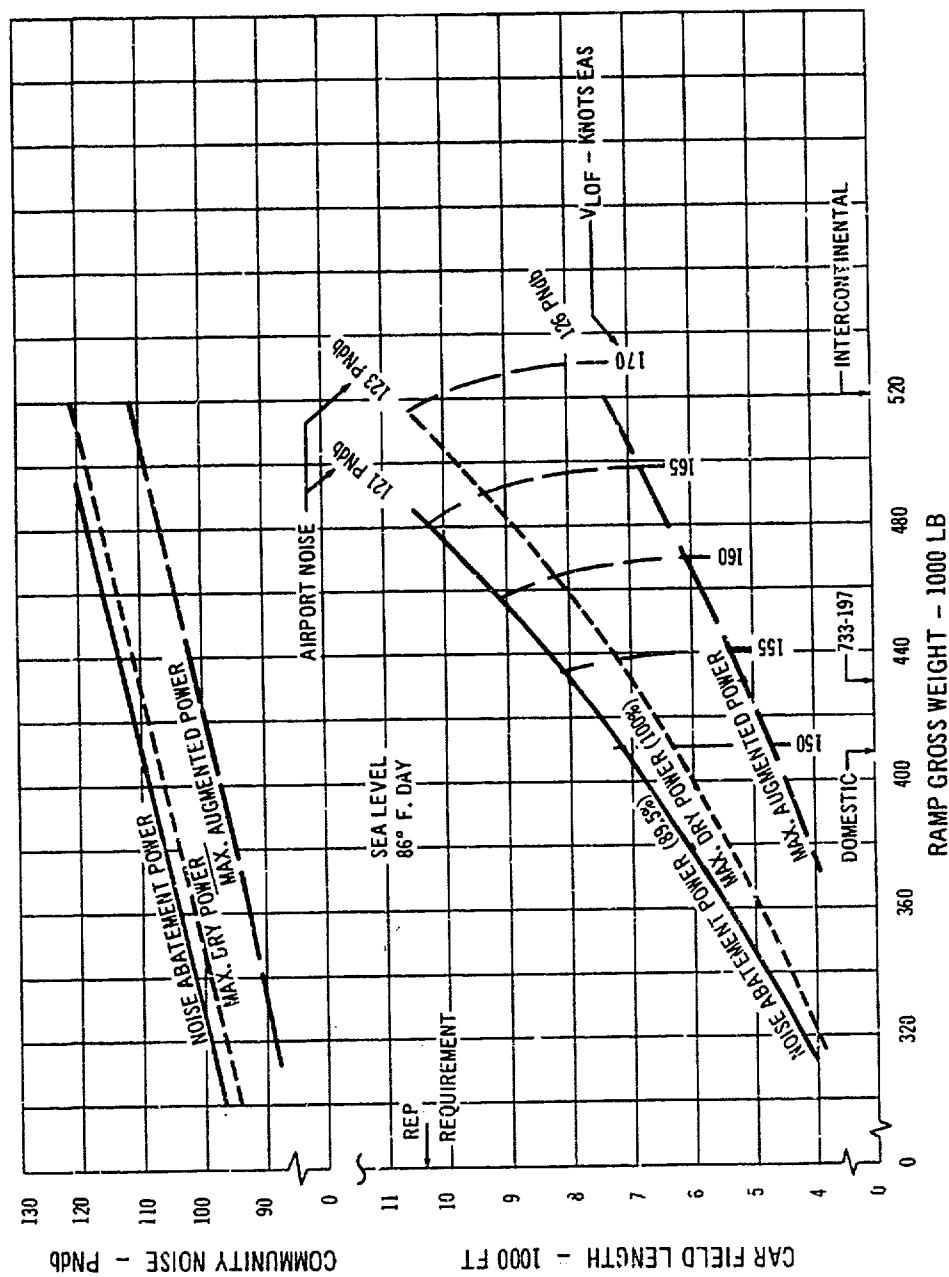
4.4 Gross Weight and ΔP Versus Range - Growth Airplanes



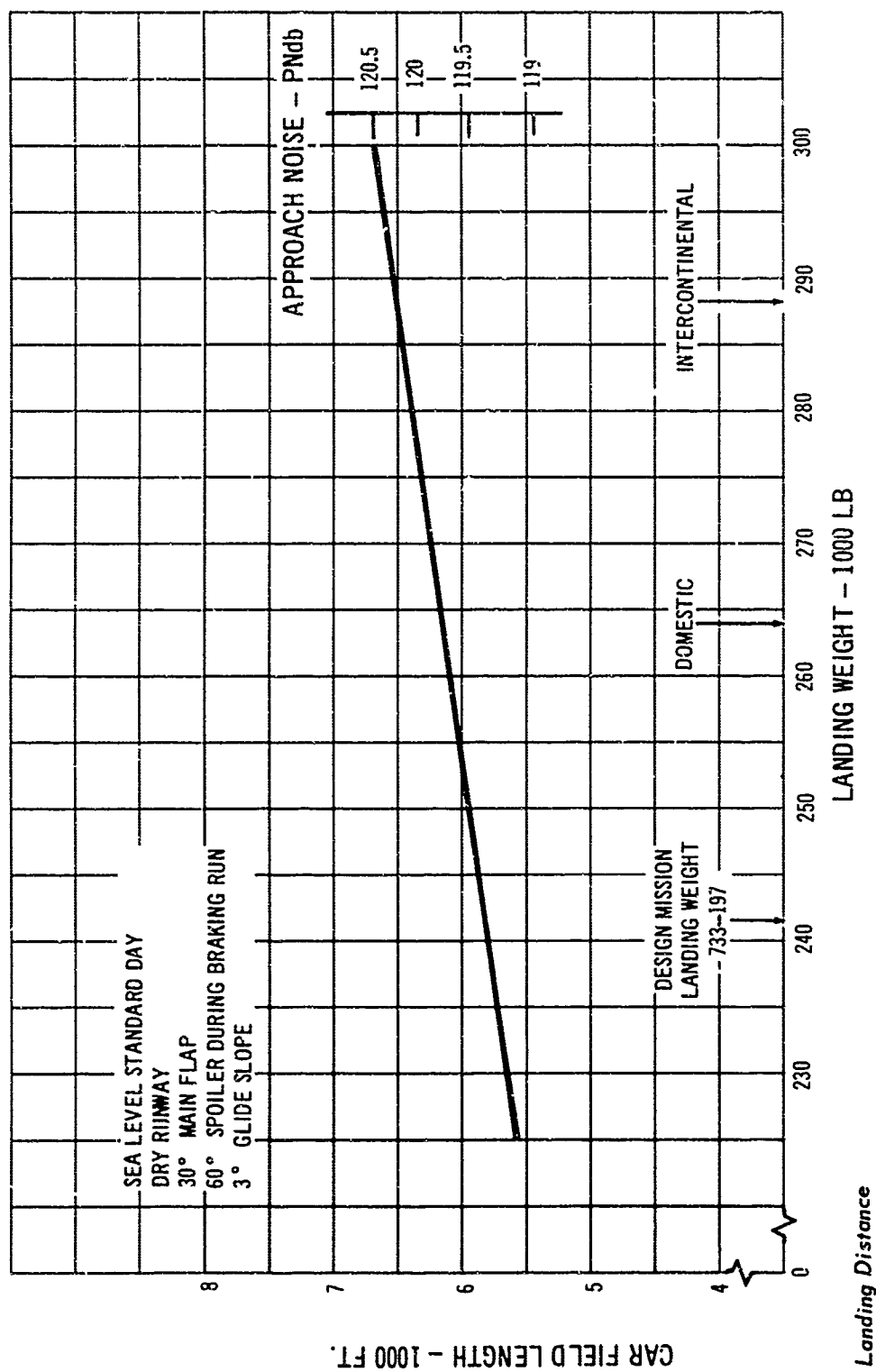
ΔP OVERPRESSURE - P. S. F.



4-5 Sonic Boom Trades



4-6 Take-Off Performance and Noise Trades



4-7 Landing Distance

distance of the intercontinental version, with full payload and maximum range reserves, is 6550 feet for a 289,000-pound landing weight. Relative to the Model 733-197, the approach noise increases less than 1 PNdb. The approach speed is 129 knots using the presently authorized 1.3

(CAR stall speed) criterion.

4.4 Performance Summary

Table 4-A summarizes the performance of the two growth airplanes relative to the Model 733-197.

TABLE 4-A PERFORMANCE SUMMARY

MODEL	733-197	DOMESTIC	INTERCON- TINENTAL
BODY LENGTH - FEET	203.8	249.5	249.5
RAMP GROSS WEIGHT - 1000 LBS	430	408	520
RANGE - NAUTICAL MILES	3500	2500	3500
PASSENGERS (TOURIST)	150	214	214
THRUST MARGIN TRANSONIC ($\frac{T-D}{D}$) MIN.	.54	.52	.30
SONIC BOOM OVERPRESSURE P.S.F.			
CLIMB	2.0	2.0	2.1
CRUISE	1.50	1.45	1.74
TAKEOFF PERF. (86°F, SEA LEVEL)			
CAR T.O.F.L. FT.	7950	7100	7350
POWER SETTING	89.5% MAX DRY	89.5% MAX DRY	MAX. AUGMENTED POWER
APPROACH SPEED - KTS	118	123	129
CAR LANDING FIELD LENGTH - FEET	5850	6150	6550



D6-2400-11

SECTION 5.0
CONFIGURATION DEVELOPMENT

TABLE OF CONTENTS

5.0 CONFIGURATION DEVELOPMENT.....	5/1
5.1 Analytical Configuration Development.....	5/1
5.1.1 Engine-Airframe Matching.....	5/1
5.1.2 Engine Selection.....	5/8
5.1.3 Wing Geometry.....	5/12
5.1.4 Cruise Speed Selection.....	5/12
5.2 Wind Tunnel Research and Development Program.....	5/13
5.2.1 Supersonic Wing Research.....	5/14
5.2.2 Transonic Wing Research.....	5/15
5.2.3 High-Lift System Development.....	5/15
5.2.4 Stability and Control.....	5/17
5.2.5 Propulsion Testing.....	5/17
5.2.6 Configuration Development.....	5/19

5.0 CONFIGURATION DEVELOPMENT

The design of a commercial air transport is based on the following initial factors: (1) design range, (2) payload and body size, (3) cruise speed, and (4) structural material. These factors are used to determine the optimum wing geometry. Following this the best match between engine and airframe must be chosen and the engine to be used must be selected.

Economics are an important part of preliminary design. Growth potential in terms of increased future earning power is determined by wing area, engine size, and the ability to increase body length. Furthermore, airplane growth must not significantly alter the basic efficiency and operational flexibility of the design.

A variable sweep configuration was chosen for the Model 733-197, because it offers the best means of achieving the requirements of a commercial supersonic transport. The excellent supersonic cruise performance obtained with a highly swept arrow planform is combined with the efficiency and favorable handling qualities of an unswept, high span wing in low speed flight. The resulting operational flexibility, compatibility with present transports and air traffic systems, safety, and economic operation provide a desirable airplane for commercial operation. Variable sweep makes it possible to choose a wing area and engine size with excellent growth potential without compromising the performance of the basic airplane.

A detailed discussion of the fundamental choice of a variable sweep configuration may be found in the Summary. Volume M-VI presents the basis for choosing the design range and payload.

The choice of body size was influenced by economics, weight considerations, and growth potential. Five-abreast seating has been chosen because of the favorable compromise between body weight and drag. The six-abreast seating of present subsonic jets would result in a fuselage

with relatively high friction drag and wave drag, and a correspondingly greater ramp gross weight. The high fineness ratio fuselage for four-abreast seating would virtually eliminate the potential for growth by adding body length.

This section is divided into two parts. Par. 5.1 discusses the analytical portion of the configuration development, i.e., engine-airframe matching, engine selection, and wing design and cruise speed selection. Par. 5.2 covers the wind tunnel testing program which has been conducted in support of the configuration development work. This includes supersonic and transonic wing research, high-lift system development, stability and control, powerplant location, and inlet and nozzle performance.

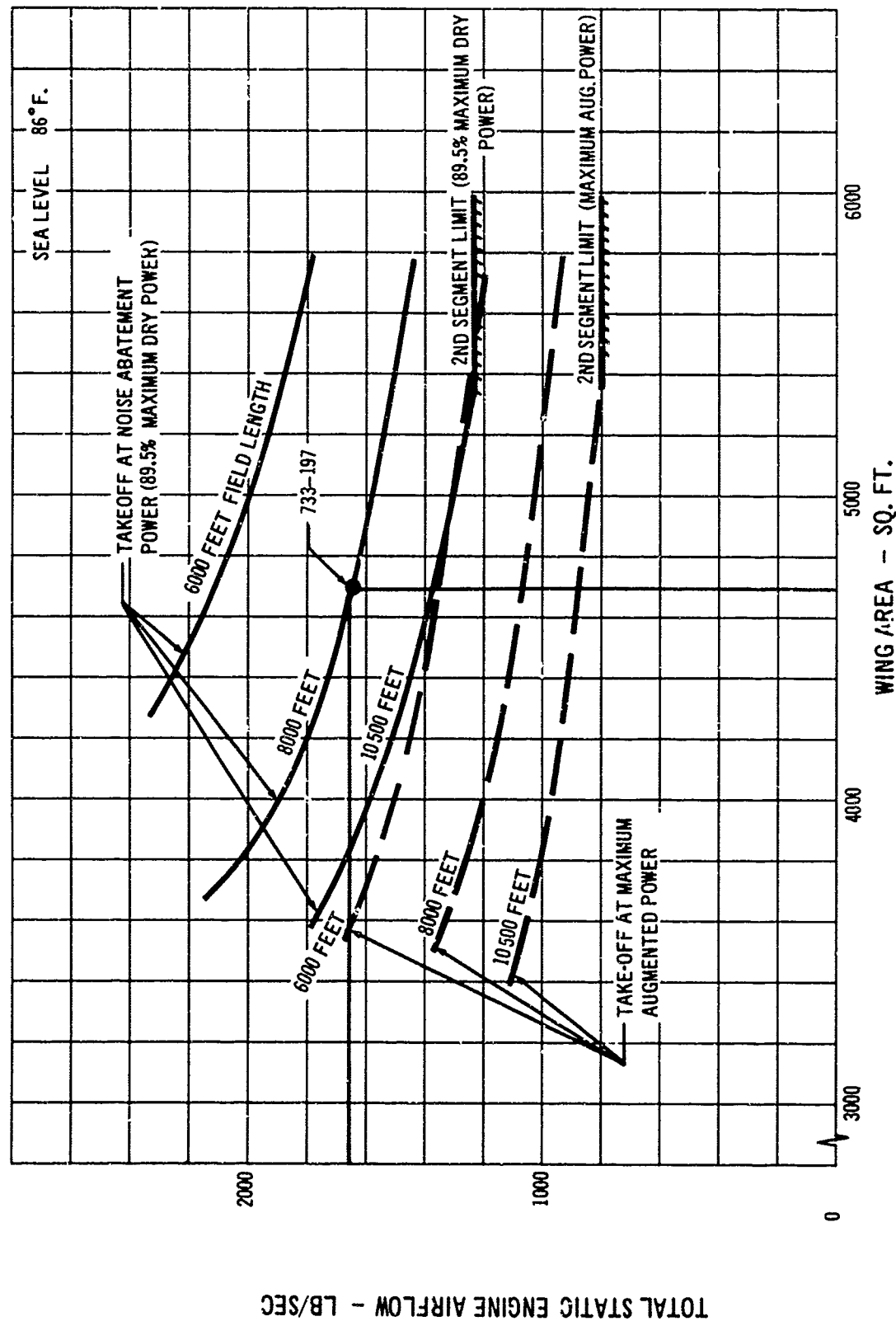
5.1 Analytical Configuration Development

5.1.1 ENGINE-AIRFRAME MATCHING

Because the selection of the wing area and powerplant size are so basic in achieving good operational economics and airplane growth potential, this subject is discussed in depth. The important considerations in the design of an airplane are the takeoff, climb and acceleration, cruise, and landing phases of flight. In addition, community noise and airport and landing restrictions must be considered and met in the initial design stages.

It is most convenient to illustrate the effects of trades between wing area and powerplant size when airplane gross weight is held constant. The ramp gross weight of 430,000 pounds and the GE 4/J4C engine, which has been chosen for the Model 733-197, are used in this discussion to present the various trades.

Takeoff performance trades are presented in Fig. 5-1 for sea level, 96 degrees Fahrenheit conditions. The purpose of these trades is to show the effect of wing area on powerplant size required for a constant takeoff field length. As noted, data for two levels of takeoff thrust are shown.



5-1 Take-Off Performance - Sea Level, 86°F.

The data indicated by solid lines represent trades obtained using the noise abatement takeoff power setting, which is 89.5 percent of maximum dry power Hot Day. This power setting gives a community noise level of 112 PNdB for the model 733-197 configuration. The model 733-197 is noted to have a CAR takeoff field length of 7950 feet for this condition. The corresponding second segment climb gradient is 0.07. Data indicated by dashed lines are trades obtained using maximum augmentation thrust where maximum takeoff performance is desired. The CAR takeoff field length of the model 733-197 would be reduced from 7950 feet to 5200 feet using maximum augmentation. The trades of Fig. 5-1 indicate that there is considerable overload capability in the airplane. (This is discussed in Section 4.0, Growth, where the airplane has an increased ramp gross weight of 520,000 pounds. The CAR takeoff field length of this airplane is 7350 feet using maximum augmentation power.)

These trades show that the powerplant size decreases as wing area increases for a constant takeoff field length requirement. The data show that the maximum wing size which can be utilized in meeting all the takeoff performance requirements is ultimately restricted by the second-segment climb gradient. This gradient is dependent upon the lift-drag ratio of the takeoff configuration. Due to the variable sweep feature of the model 733-197, a high lift-drag ratio is achieved and choice of wing area is not restricted because of second segment climb considerations.

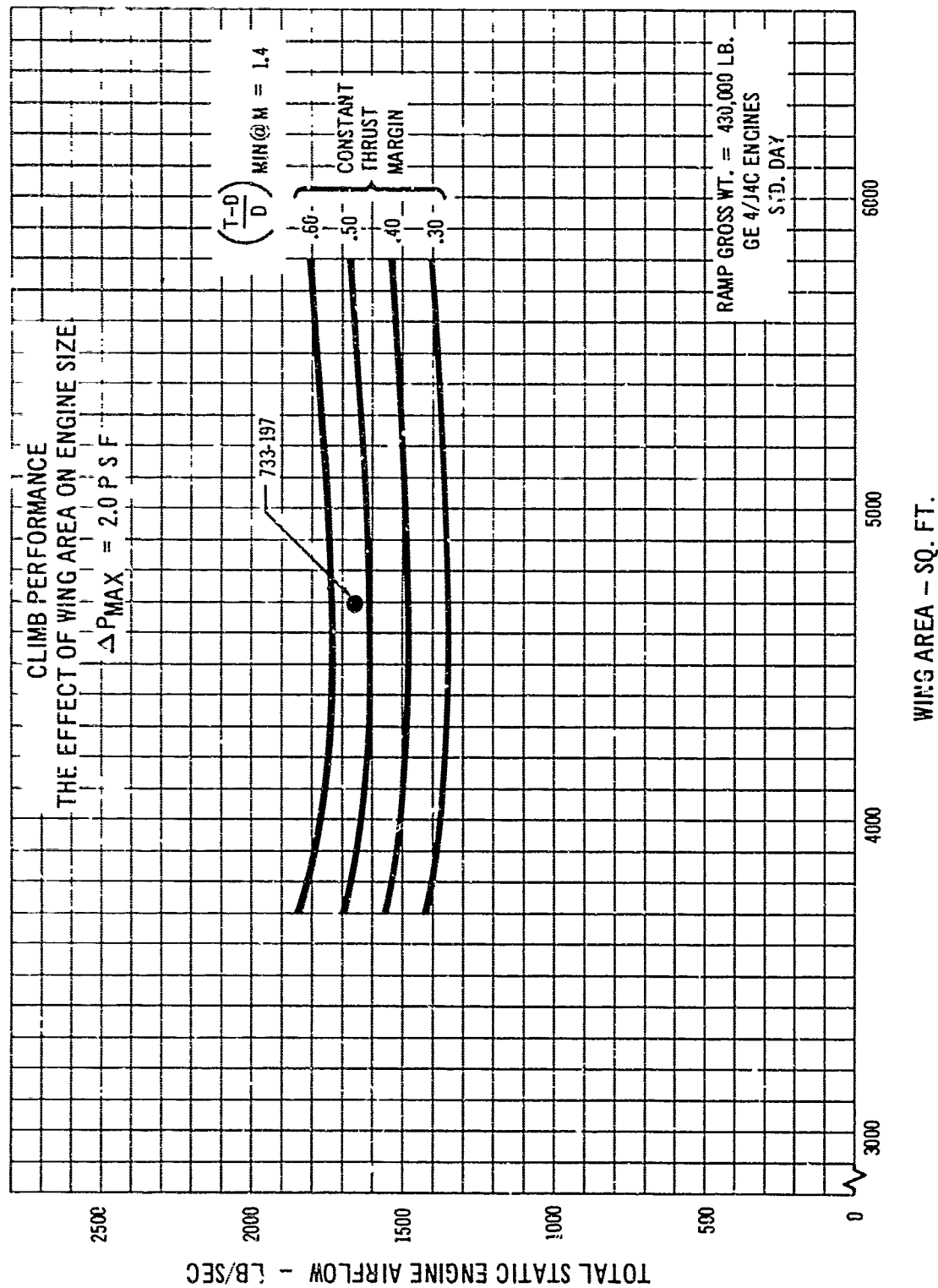
The climb and acceleration performance trades of wing area and powerplant size are presented in Figs. 5-2 and 5-3. Fig. 5-2 shows the effect of wing area on the powerplant size required to achieve various minimum thrust margins during climb, with maximum sonic boom overpressure held constant at 2.0 PSF. Thrust margin has been defined as $\frac{T-D}{D}$ where T is total thrust, and D is the total drag, in level flight. A $\frac{T-D}{D}$ value of 0.54 implies

there is a 54 percent excess of thrust available above that necessary for level flight for the example altitude and Mach number. Fig. 5-2 shows that the acceleration thrust margin does not vary significantly with wing area, for a given engine size.

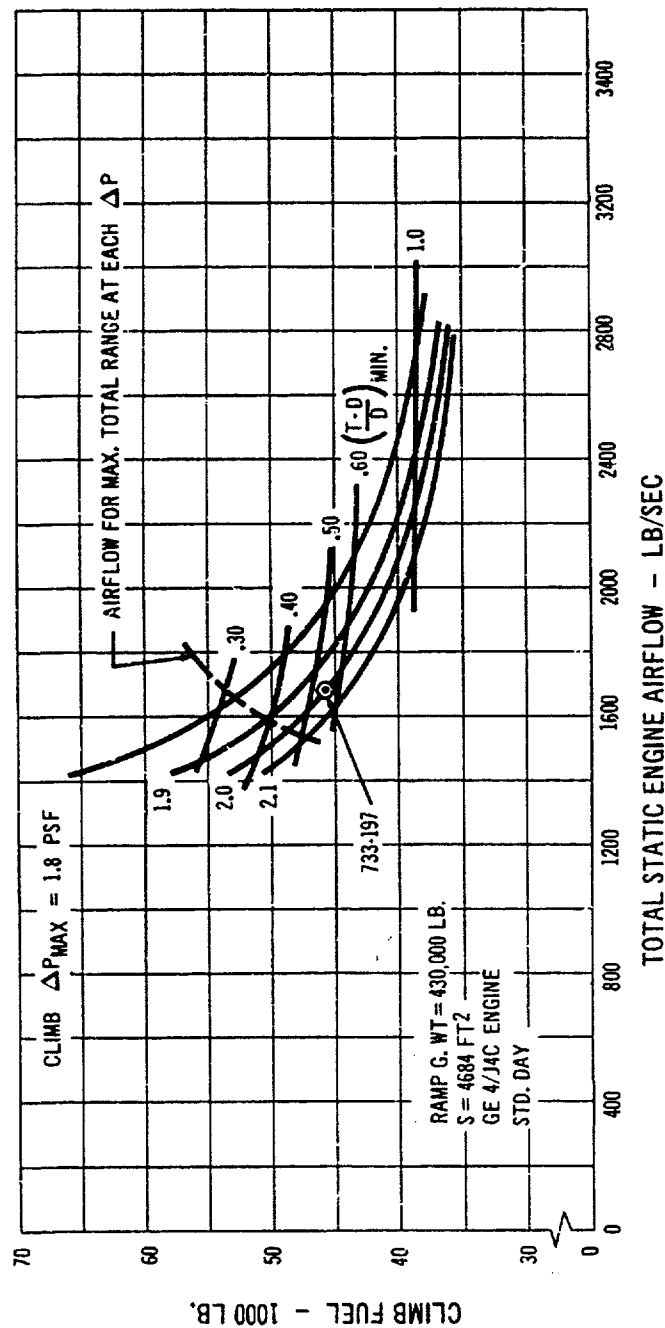
The effect of powerplant size on climb fuel is shown on Fig. 5-3 for several values of both thrust margin and sonic boom overpressure during climb. The ramp gross weight of 430,000 pounds and wing area of 4684 square feet have been held constant. Also shown is the locus of engine sizes for maximum range at each sonic boom overpressure. Fig. 5-3 shows that the powerplant size required for maximum range is considerably lower than that required for minimum climb fuel, regardless of the climb overpressure. Also, the optimum thrust margin for maximum total range is much lower than that required for minimum climb fuel. This occurs because the beneficial effect of increased engine airflow on climb fuel is more than offset by the adverse effect of the added powerplant weight.

A large thrust margin is desirable from an airplane growth standpoint and for this reason the Model 733-197 has a larger engine size than would have been selected for meeting "design point" performance requirements. Oversizing of the powerplant is also desirable for off-design considerations. Fig. 5-3 shows that the penalty in going to a lower sonic boom overpressure is less severe the higher the design engine airflow. The climb overpressure of the Model 733-197 can be reduced to 1.8 PSF with only a 7000 pound penalty in climb fuel.

Cruise considerations of the engine-airframe matching problem are presented in Fig. 5-4. Contours of cruise range factor $\frac{L}{D} \frac{V}{TSFC}$ are shown for combinations of wing area and powerplant sizes. Two crossplots are shown. First, the airplanes which have maximum range factor at each wing area; and second, the airplanes which operate at five percent above minimum TSFC for optimum cruise.



5-2 Climb Performance

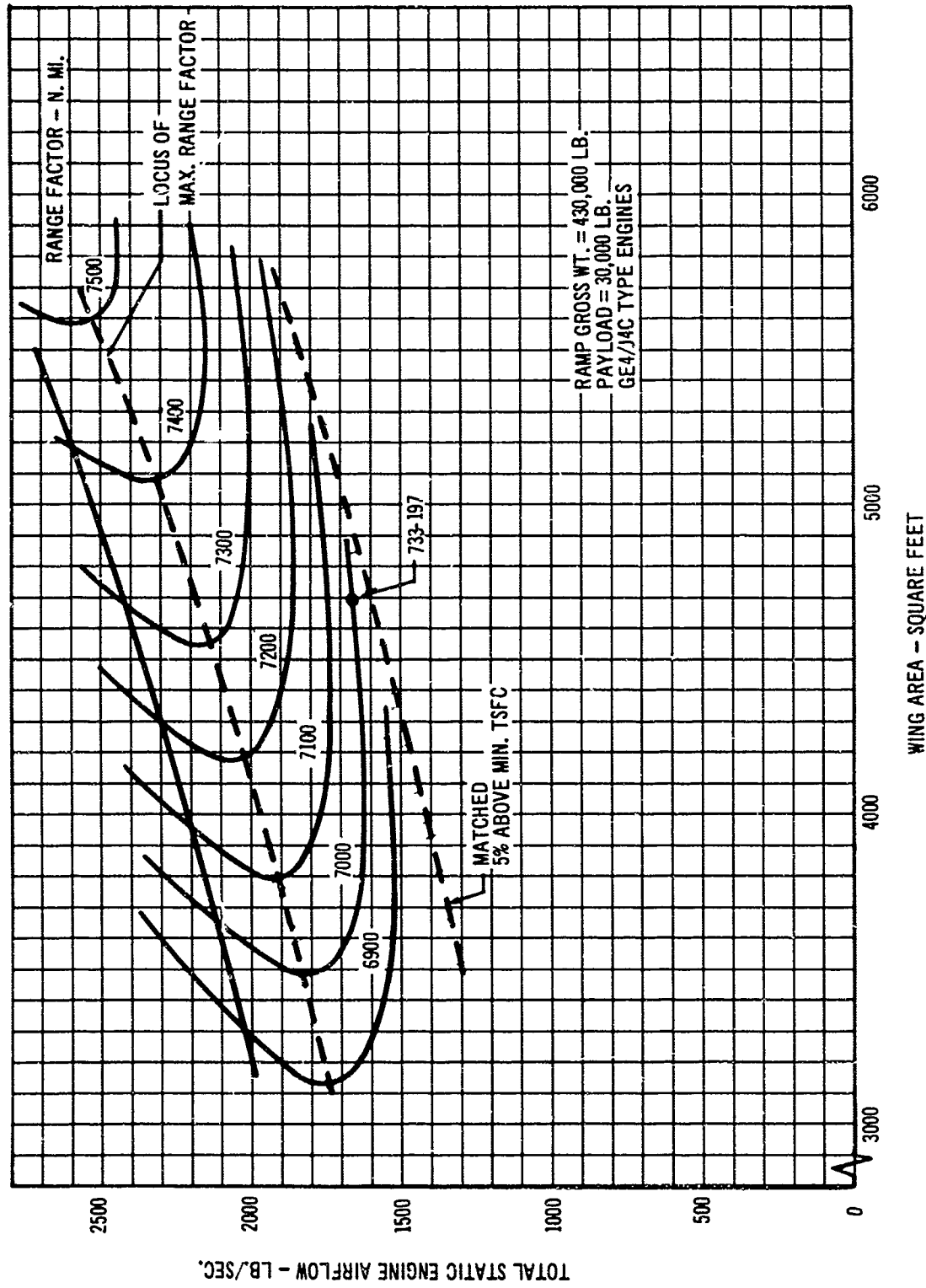


5.3 Climb Performance - The Effect of Engine Airflow on Climb Fuel

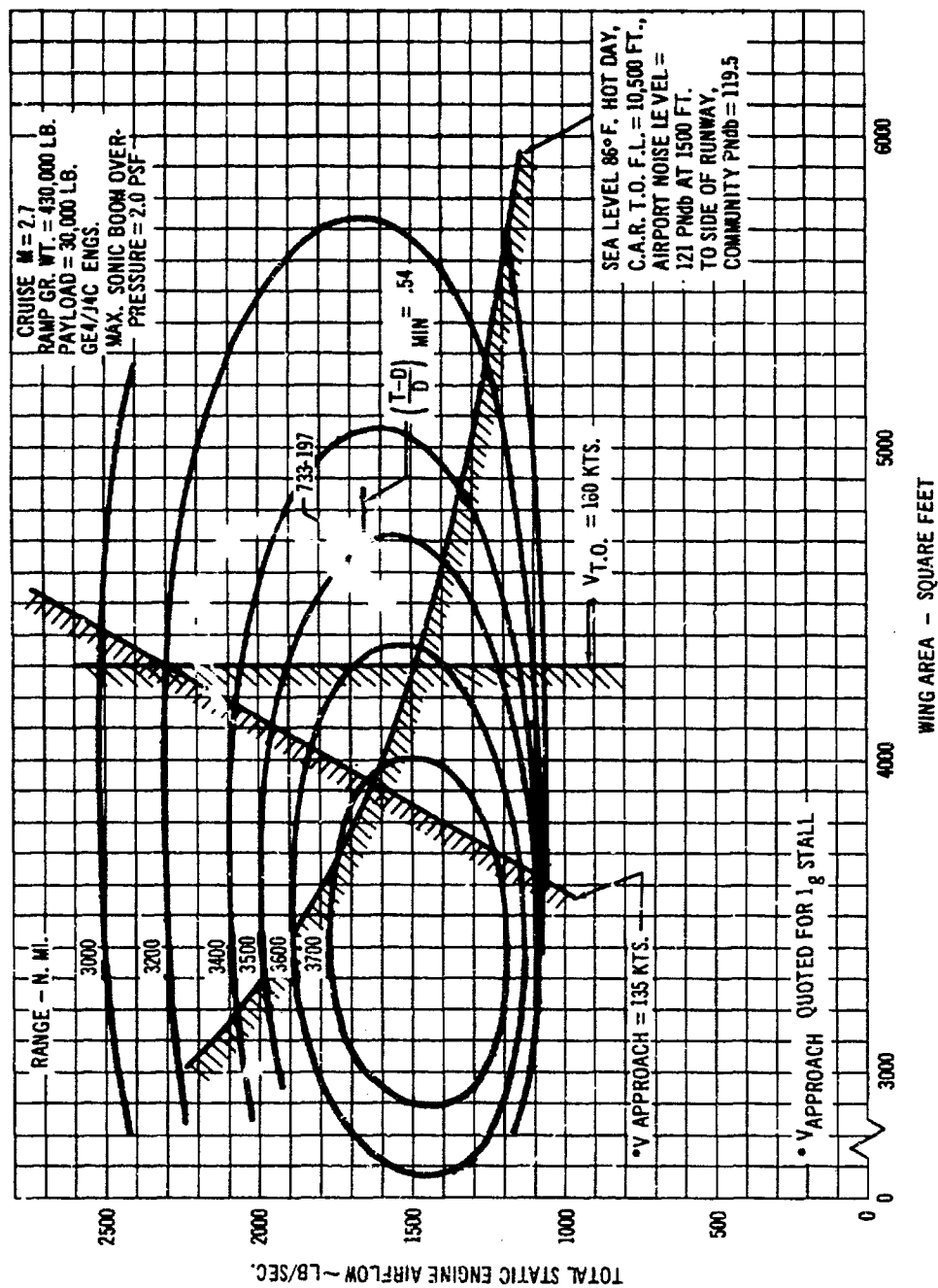
The latter type match results in very nearly the minimum value of engine weight plus fuel required for the design mission range. It represents the type of match which occurs on the Model 733-197.

The complete trades of range performance versus powerplant size and wing area are presented in Fig. 5-5. The effects of wing and powerplant weight, acceleration and climb fuel, cruise match and reserves, are included in this presentation. It is noted that the constant range contours are closed. This is in contrast to Fig. 5-4, the cruise

performance plot, which was open-ended and provided ever-increasing values of range factor with increases in wing area. The range contours in Fig. 5-5 close at the greater wing areas due to wing weight effects. The Model 733-197 engine size and wing area values are shown on Fig. 5-5 with reference to various performance requirement lines. A smaller powerplant size (1550 pounds per second) could have been selected. However, by increasing the size to 1660 pounds per second only an insignificant change in range occurred and the growth potential and



5-4 Cruise Performance $M = 2.7$



5-5 Engine - Airframe Matching

off-design performance capabilities have been enhanced. It is noted that the Model 733-197 exceeds the performance requirements in the areas of landing approach and takeoff speed objectives set by the RFP. The takeoff field length and noise requirements are also shown to be clearly not limiting for the powerplant size and wing area selected for the Model 733-197.

5.1.2 ENGINE SELECTION

The engines offered for the Supersonic Transport are: a Curtiss-Wright nonaugmented turbojet (CWTJ70A-4); a General Electric augmented turbojet (GE4/J4C); and a Whitney turbofan (JT11F-12). Studies were conducted utilizing each of these engines to determine their effect on the design gross weight, wing area, powerplant size, acceleration characteristics, hot day atmospheric effects, and takeoff and landing characteristics.

The gross weights required to meet the RFP requirements with the above engines matched to airframes similar to the 733-197 are shown in Fig. 5-6. These data represent optimum point designs, i.e., minimum gross weight, wing area, and powerplant size without consideration of growth potential or mission flexibility. The purpose of Fig. 5-6 is to show the relative merits of the various engine cycles holding a constant set of ground rules. It can be seen that a gross weight of 413,000 pounds and wing area of 4130 square feet will meet the 2.0 PSF overpressure requirements for the General Electric augmented turbojet, GE4/J4C. However, in order to provide greater off-design flexibility and growth potential the 733-197 configuration was sized with a wing area of 4684 square feet and GE4/J4C engine airflow of 1660 pounds per second, which resulted in a ramp gross weight of 430,000 pounds.

A takeoff wing loading of 100 PSF was held constant for the engine selection studies. This results in a takeoff speed of 160 knots, an RFP requirement. Also, the engine size was selected for either maximum range or a mini-

mum transonic thrust margin of 0.30, whichever condition resulted in the greater airflow.

The range-payload capabilities of the various engines matched to the 733-197 airframe with a gross weight of 430,000 pounds and wing area of 4684 square feet are presented in Fig. 5-7. The results show that the nonaugmented turbojet, CWTJ70A-4, gives the greatest range when matched to the Model 733-197 configuration.

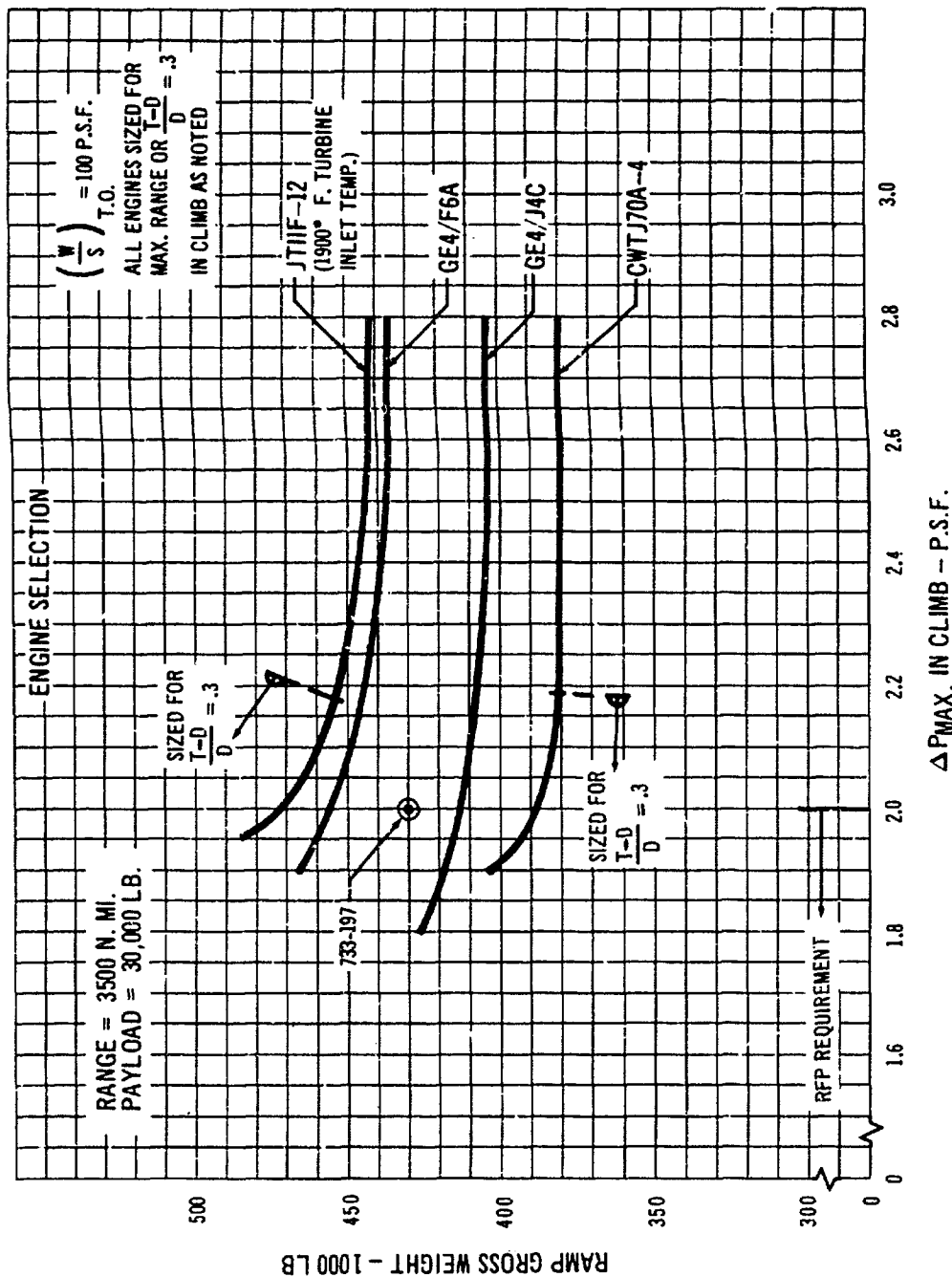
The CWTJ70A-4 engine has a higher thrust-to-weight ratio and lower TSFC's over the entire flight range. This results in about 5 percent less climb fuel than the augmented turbojet GE4/J4C engine, and a 2½ percent higher range factor in cruise. These effects account for the 5 percent greater range relative to the GE4/J4C. (The reserves and the installed engine weight values for the CWTJ70A-4 and the GE4/J4C are about the same.)

The GE4/F6A fan engine has a 10 percent lower supersonic range factor than the augmented turbojet GE4/J4C and uses 40 percent more fuel in climb. Installed engine weight is 12 percent less than the GE4/J4C. Also, the reserve fuel is 10 percent less due to lower TSFC's in holding and subsonic cruise. However, these favorable effects are not sufficient to overcome the cruise range factor and climb fuel penalties and the resulting range is about 6 percent less than for the augmented turbojet powered airplanes at ΔP of 2.0 PSF.

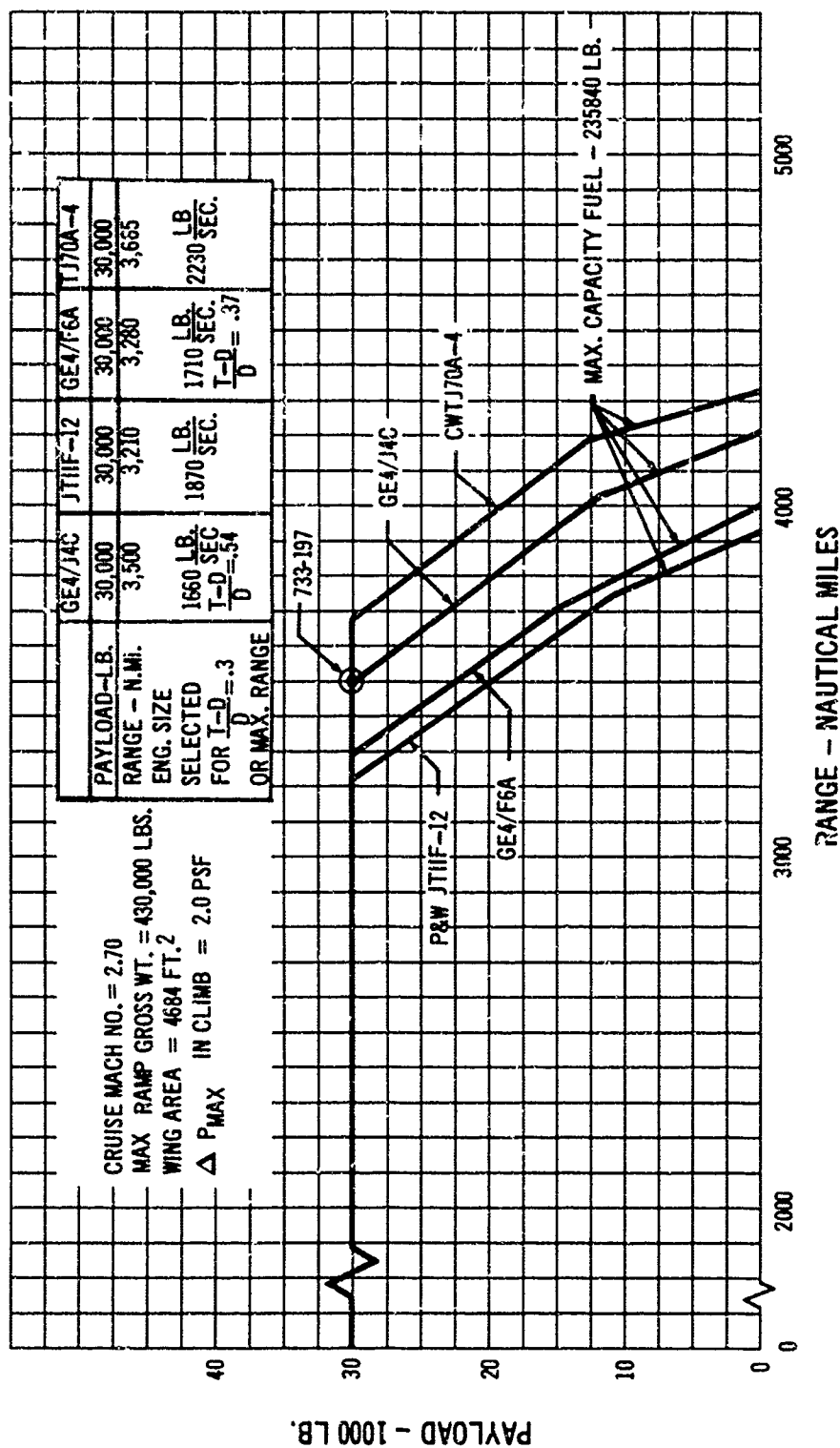
The installed weight of the Pratt & Whitney JT11F-12 turbofan is about the same as for the GE4/J4C. However, climb fuel is 25 percent greater and the supersonic range factor is 10 percent lower. Reserve fuel is 10 percent less due to lower subsonic TSFC's. The net result is an 8 percent range loss as compared to the GE4/J4C.

A summary of the engine selection studies, presented in Table 5-A, compares the two types of engine-airframe matching which have been discussed above.

The GE4/J4C engine was selected on the basis of relatively less risk in development (compared to the CWTJ70A-4) while achieving the best performance. (The



5-6 Engine Selection



5.7 Range Comparison

TABLE 5-A ENGINE SELECTION SUMMARY
MACH 2.7 CRUISE

I CONSTANT GROSS WEIGHT - WING AREA MATCHED

RAMP GROSS WEIGHT = 430,000 LB.

WING AREA = 4684 FT²

PAYLOAD = 30,000 LB

V_{T.O.} < 160 KNOTS

ΔP_{MAX.} = 2.0 P.S.F.

ENGINE TYPE	RANGE - N.MI.	ENGINE AIRFLOW	LB SEC
GE4/J4C	3500		1660
CWTJ-70A-4	3665		2230
GE4/F6A	3280		1710
P&WJT 11F-12	3210		1870

II CONSTANT RANGE - PAYLOAD MATCH

RANGE = 3500 N. MI.

PAYLOAD = 30,000 LB.

V_{T.O.} = 160 KNOTS

ΔP_{MAX.} = 2.0 P.S.F.

ENGINE TYPE	RAMP GROSS WT - LBS.	WING AREA - FT ²	ENGINE LB AIRFLOW - SEC
GE4/J4C	413,000	4130	1470
CWTJ-70A-4	387,500	3875	1950
GE4/F6A	456,500	4565	1760
P&WJT 11F-12	472,000	4720	2110

details of the engine selection are covered in Vol. A-VI.) However, any of the offered engines could be fitted to the basic model 733-197 if desired.

5.1.3 WING GEOMETRY, DESIGN AND SELECTION

The Model 733-197 wing was selected to provide high aerodynamic efficiency, with good stability and control characteristics, throughout the entire flight range. (See Section 2.0 for wing geometry drawings.) The planform evolved from theoretical studies and wind tunnel tests on arrow wings with subsonic leading edges and zero taper ratio. According to theory, this wing planform has the highest supersonic lift-drag ratio potential. Wind tunnel tests showed, however, that taper ratios of about 0.2 resulted in no loss in lift-drag ratio relative to the zero taper ratio case. Further wind tunnel testing demonstrated a need for moderate wing taper to provide good stability by preventing nonlinearities in the pitching moment versus lift characteristics at low speeds with the wings at high sweep positions. As a result of trade studies encompassing structural weight, performance, and stability considerations, a wing taper ratio of .354 was selected for the Model 733-197. Further changes to the wing planform were necessitated for installation of the landing gear, and the wing pivot carry-through structure. This required that the wing cutout at the trailing edge be filled-in near the body.

The wing leading edge sweep angles, although influenced by weight considerations, were primarily dictated by a balance between aerodynamic drag, and stability considerations. The leading edge sweep angle for supersonic cruise at a Mach number of 2.7 is 74 degrees. The subsonic leading edge condition results in low wave drag and permits the use of camber and twist for low drag-due-to-lift. The leading edge is swept 42 degrees for high subsonic cruise at a Mach number of 0.85. The leading edge sweep angle for takeoff and landing is 20 degrees. Use of

this low sweep angle permits takeoff and landing speeds comparable to present day commercial jet aircraft. The wing aspect ratios for the leading edge sweeps of 74, 42 and 20 degrees are 1.59, 6.04 and 9.06, respectively. (Section 2.0.)

The wing pivot is located at 46 percent of the local chord at the 38 percent semi-span station. This location permits a large subsonic span (173 feet), with adequate provisions for mounting the nacelles and landing gear. The pivot axis is oriented to minimize changes to the desired camber and twist distribution as the wing sweep is varied. The design of the wing camber and twist distribution and thickness distribution is discussed in Appendix C. The resulting maximum camber is about 1 percent of the local chord over the entire span. The maximum wing twist is 4.3 degrees between 12 percent semi-span station and the wing tip. The wing root chord plane at the side of the body is -0.7 degrees referenced to the body centerline. The wing thickness ratios vary from 4.1 percent near the side of the body to 2.5 percent at 65 percent semi-span and to the wing tip.

5.1.4 CRUISE SPEED SELECTION

The design cruise speed of Mach 2.7 has been selected with consideration of productivity, technology and direct operating cost. The use of titanium as a structural material provides a basic airframe structure which, with relatively minor changes, will be capable of operating at a speed of Mach 3 or above.

However, engine manufacturers and component vendors indicate that developmental costs will be substantially greater as speeds go to Mach 3 or above. The non-metallic materials such as insulation, fuel tank backing board and transparent structures are affected to a greater extent with the increased temperature gradients at the higher speed. For example, the increase in heat load on environmental control and fuel systems markedly increases their weight. At the higher temperatures, an increasing

amount of fuel tank insulation is required; and at speeds much in excess of Mach 2.7, fuel inerting becomes a requirement.

Selection of the Mach 2.7 cruise speed makes possible a design with maximum consideration for safety, operational reliability and operating economics because it is within the temperature technology expected in the 1970 time period.

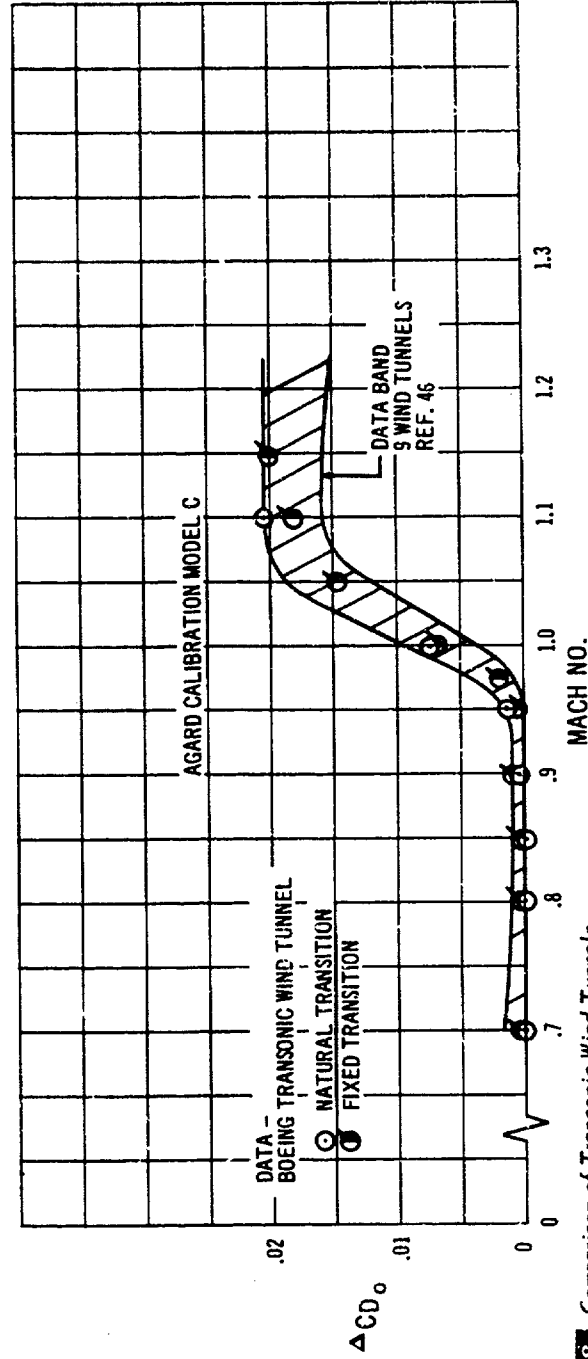
5.2 Wind Tunnel Research and Development Program

The Boeing Model 733-197 configuration is based on the results of an extensive wind tunnel test program carried out over the past five years. This program has spanned the entire spectrum of flight speeds for the supersonic

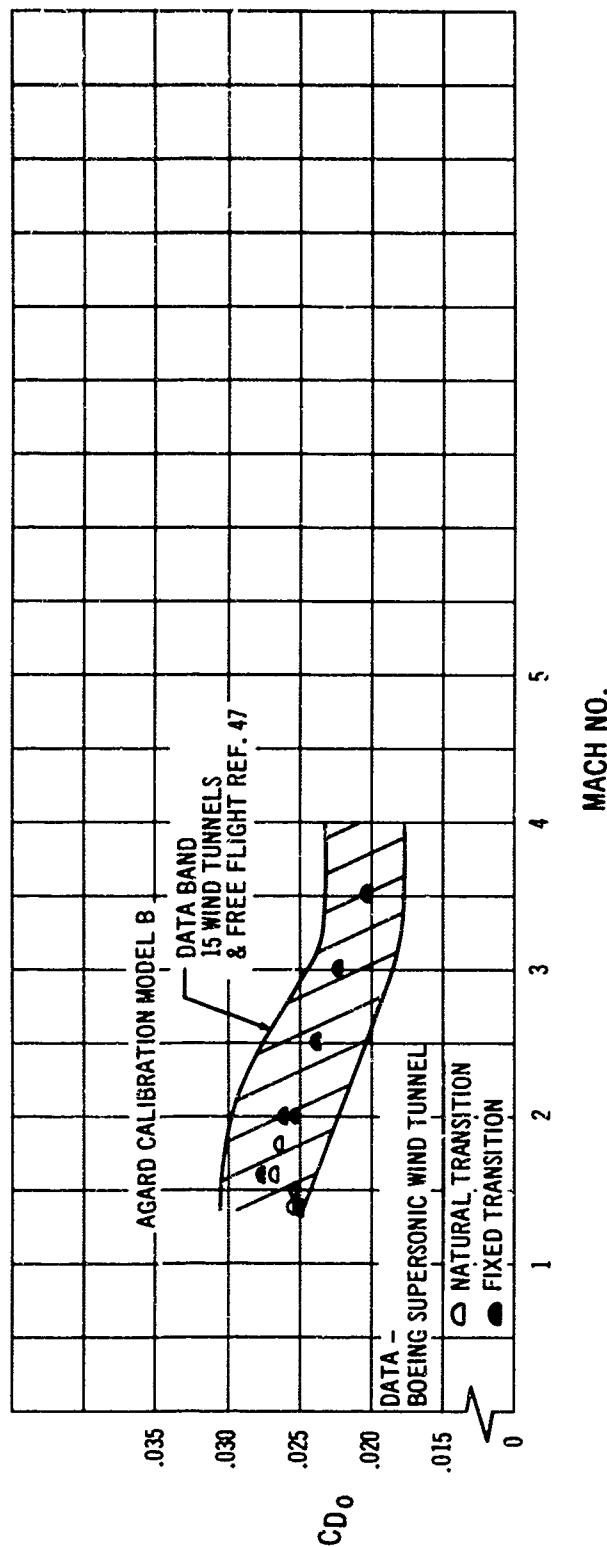
transport and has included both research and configuration development testing. Over 5000 hours of wind tunnel testing specifically related to the supersonic transport have been completed. Including other programs, the Boeing Company has invested more than 11,000 hours of wind tunnel testing in variable-sweep configurations.

Low speed testing has been conducted in the 8 foot by 12 foot wind tunnel at the University of Washington Aeronautical Laboratory which makes 75 percent of its testing time available to Boeing. The Boeing Company's privately owned 8 foot by 12 foot transonic wind tunnel and 4 foot by 4 foot supersonic wind tunnel have been used for testing at Mach numbers between 0.5 and 4.0.

The data for the standard AGARD models shown in Figs. 5-8 and 5-9 illustrate that experimental results



5-8 Comparison of Transonic Wind Tunnels



5-9 Comparison of Supersonic Wind Tunnels

obtained in the Boeing Wind Tunnels are in good agreement with those obtained in the other major wind tunnels in the world.

All of the models tested during this program have been constructed in the company owned model shop which is one of the most complete and modern facilities of this type in the world. A description of the wind tunnels and shop is given in Volume A-IX.

The development of a complex airplane, such as the supersonic transport, requires that these facilities be available on short notice to evaluate new design ideas quickly and accurately. Extended periods of wind tunnel test time must be available to accomplish the tailoring and refinement of a configuration which are necessary to develop its full potential. The Boeing complex of wind tunnels and

ments, as has been demonstrated in previous airplane development programs.

5.2.1 SUPERSONIC WING RESEARCH

A major research program has been directed toward achieving the low drag-due-to-lift values that are predicted theoretically for cambered and twisted arrow wings. In this effort, 43 separate arrow wings with numerous variations have been tested. Considerable progress has been made in developing an understanding of the practical limitations to theoretical design through detailed pressure and flow visualization studies. For example, techniques have been evolved to design for low drag-due-to-lift with tailored lifting and thickness pressure distributions which

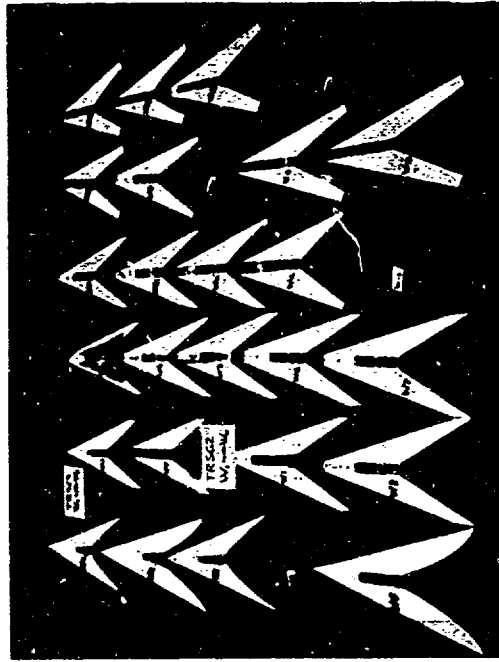
avoid premature flow separation. A typical wing-body model, installed in the Boeing supersonic wind tunnel is shown in Fig. 5-10. Others of the arrow wings tested are shown in Fig. 5-11.



5-10 Typical Supersonic Research Model

5.2.2 TRANSONIC WING RESEARCH

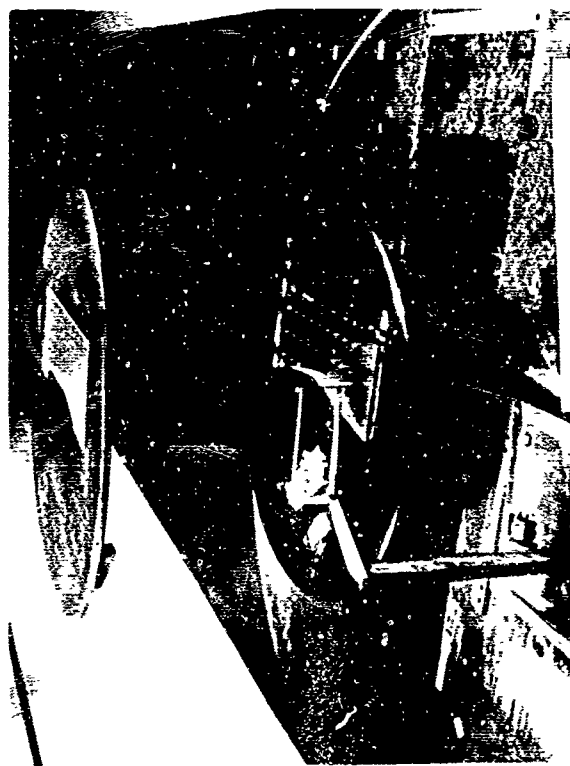
A separate wing research effort has been directed toward understanding the problems of transonic airfoils, wings and bodies. It included work on the development of new transonic airfoil sections, designed by advanced aerodynamic analysis and evaluated in the Boeing transonic wind tunnel. The quasi-two dimensional test setup used is shown in Fig. 5-12. Experimental results show that these airfoils have significantly greater drag divergence Mach numbers than the commonly used high Mach number airfoils. Further tests, using these new airfoils on wings with contoured bodies, have shown the airfoils to be effective three-dimensionally (Fig. 5-13). Results of this work are incorporated into the SST to provide significant improvements in transonic aerodynamic performance as indicated in Fig. 5-14.



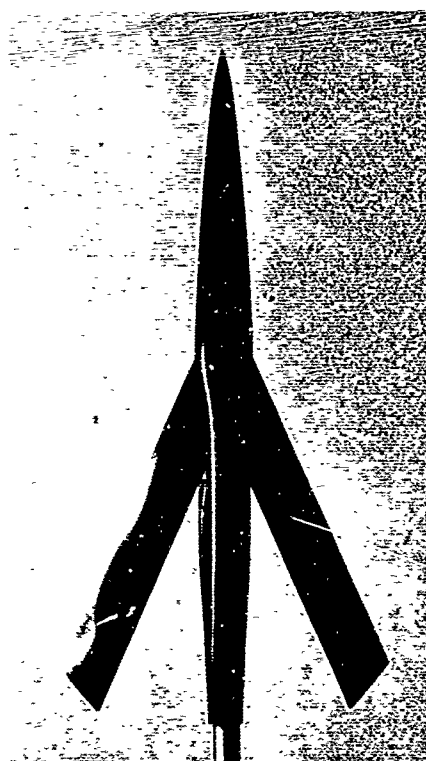
5-11 Supersonic Arrow Wing Models

5.2.3 HIGH LIFT SYSTEM DEVELOPMENT

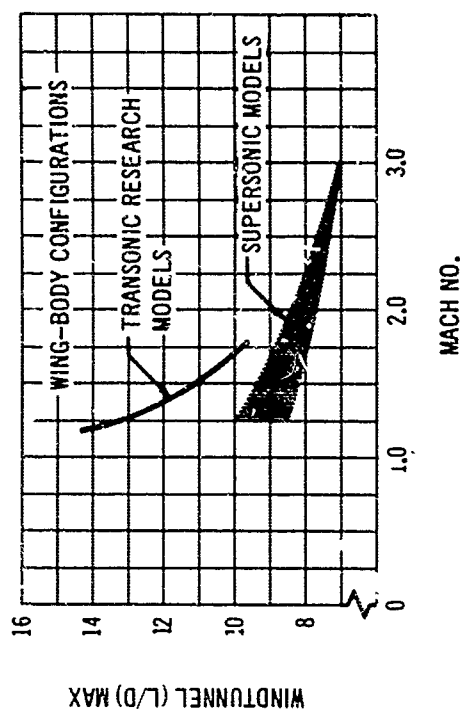
Low-speed wind tunnel testing of high-lift systems has emphasized full exploitation of the potential of the variable sweep wing. One of the wind tunnel models is shown in Fig. 5-15. Single and double slotted trailing edge flaps with various amounts of Fowler action have been tested. Leading edge devices tested have included Krueger and slotted flaps. The effects of wing geometry have been explored in conjunction with testing high lift devices. These have included pivot location and wing sweepback angle, tested with various planforms. Results of these studies have been supplemented and guided by flight tests of advanced high lift systems on the Model 367-80 Jet Transport prototype.



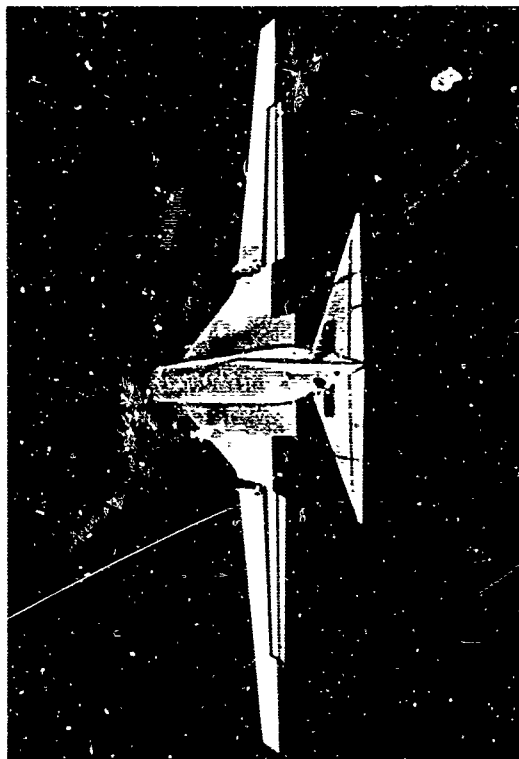
5-12 Two-Dimensional Airfoil Test Model



5-13 Typical Transonic Research Model



5-14 Benefit of Transonic Research



5-15 Typical High Lift Model

5.2.4 STABILITY AND CONTROL

Stability and control testing of variable-sweep configurations has emphasized the evaluation of various wing pivot locations over the complete range of wing sweep angles to ensure good stability and control characteristics. This work has also included extensive testing of wing geometry effects on longitudinal stability.

Canard and horizontal tail configurations, as well as arrangements using both of these surfaces together, have been studied for longitudinal stability and control. Fig. 5-16 shows a model under test for stability and control considerations, in the transonic tunnel.

The rapid deterioration of directional stability at high attitudes and high speeds has required testing of numerous vertical and ventral tail configurations in conjunction with horizontal tail dihedral and anhedral angles. Wind tunnel tests have been run to evaluate the control characteristics



5-16 Transonic Stability And Control Model

of promising configurations and to establish control power levels about all three axes. Fig. 5-17 shows one of the configurations tested.

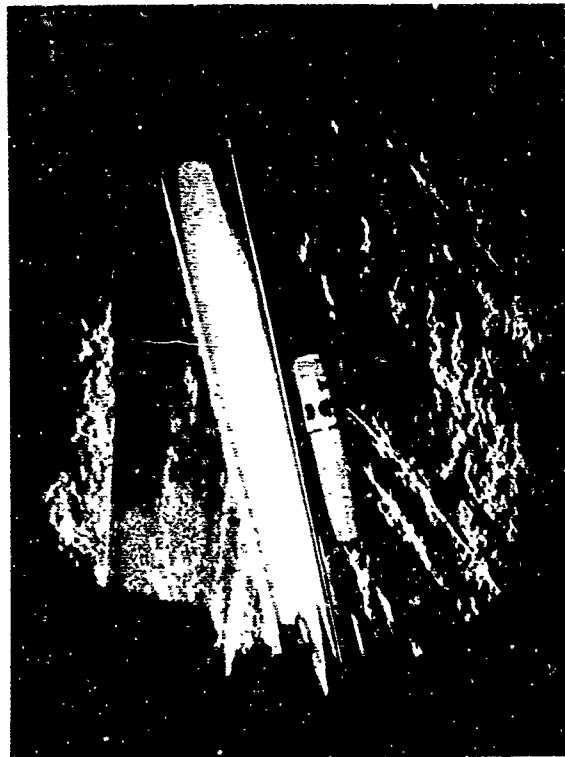
The effects of undesirable forces and moments resulting from an engine or inlet system failure at supersonic speeds have been evaluated with scale models which simulate the flow conditions caused by various types of failure. The Schlieren photograph in Fig. 5-18 shows the shock pattern formed following an inlet unstart and after the bypass doors have opened.



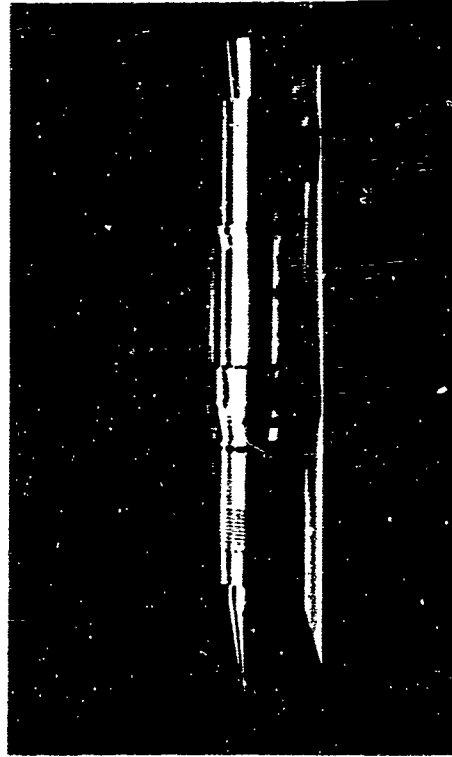
5-17 Supersonic Lateral Control Test

5.2.5 PROPULSION TESTING

Isolated inlet tests have been conducted to improve inlet performance and stability and to evaluate new design approaches. A one-fifth scale inlet with its support and mass-flow measuring tube is shown in Fig. 5-19 as it was tested in the supersonic wind tunnel.



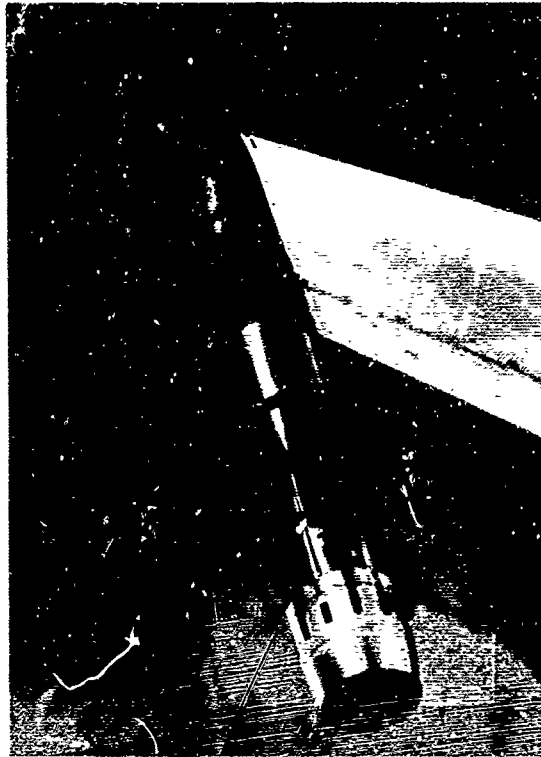
5-18 Simulated Engine Failure Test



5-19 Inlet and Flow Tube Model

Exhaust nozzle testing is also carried out in the supersonic and transonic wind tunnels with the test rig shown in Fig. 5-20. Nozzle high pressure air is supplied through a strut which contains instrumentation for measuring mass flow and forces. Additional information on inlet and nozzle testing is included in Volume A-VI.

As part of a study to determine the best locations for engines, investigations have been carried out to determine the character of the local flow fields in which the supersonic inlet must operate. Local Mach number, sidewash, and downwash in regions considered for engine installations have been measured on wing-body configurations. Fig. 5-21 shows a test configuration with the flow field probes used.



5-20 Exhaust Nozzle Model



5-21 Supersonic Flow Survey Model

Nonuniform flow field effects on the supersonic inlet performance have also been studied. Inlets are tested in the flow fields of wings as shown in Fig. 5-22. Here a scale model axisymmetric, external-internal compression inlet is shown in a test configuration as used for testing from subsonic to high supersonic Mach numbers.

Tests to determine inlet interference are run with the model shown in Fig. 5-23. Two inlets are shown mounted side-by-side, in the supersonic wind tunnel, in a test to determine the region of interference during started and unstirated conditions and also to determine the effect of operating an inlet inside this region.

5.2.6 CONFIGURATION TESTING

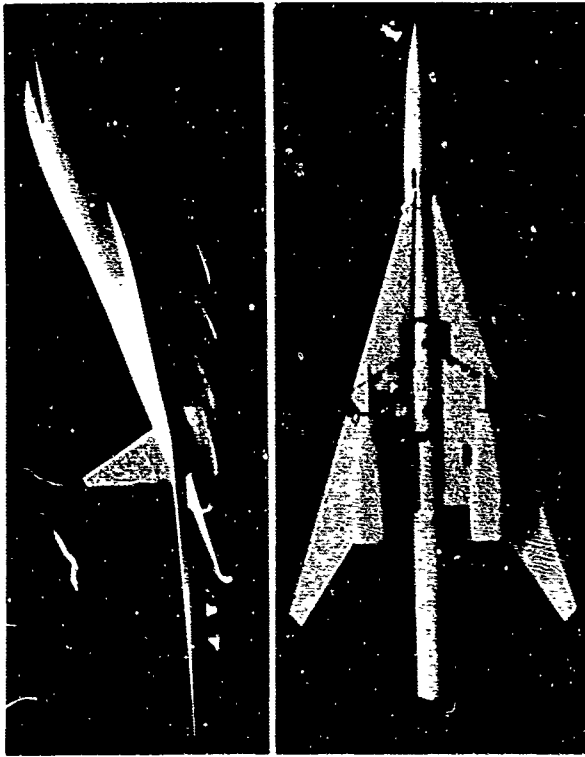
Complete SST configurations have been tested concurrent with research efforts in order to assess overall aerodynamic characteristics. Recent tests of variable-sweep



5-22 Inlet Model in Presence of a Wing



5-23 Inlet Interference Model

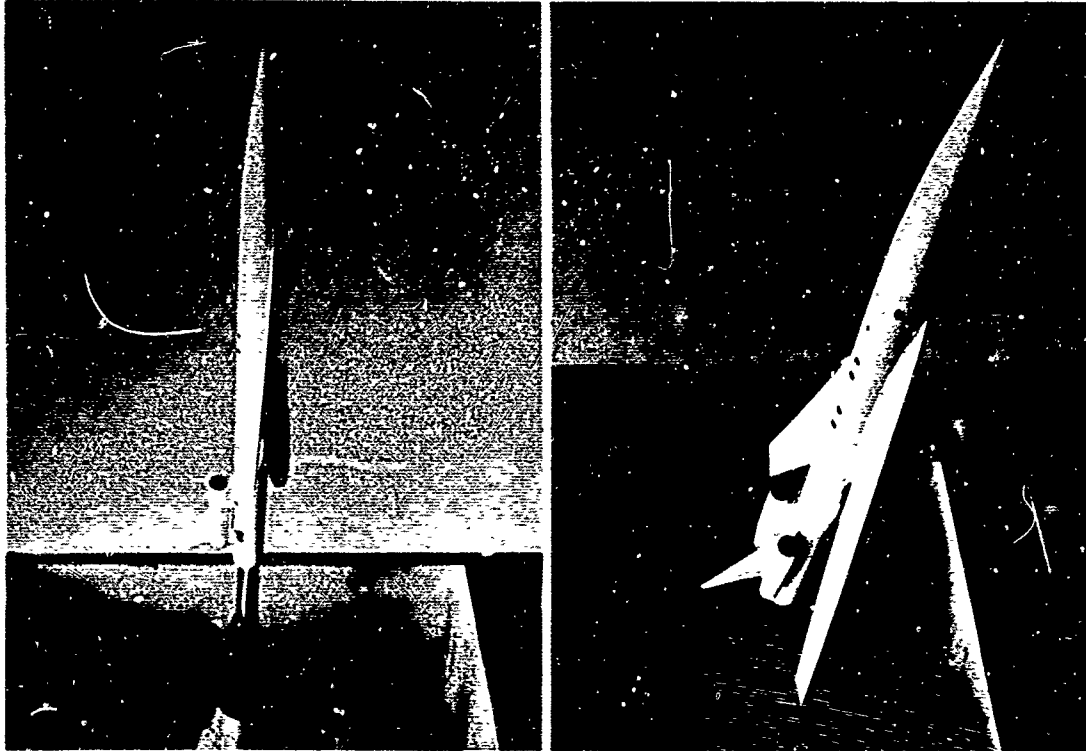


5-24 Podded Engine Configurations

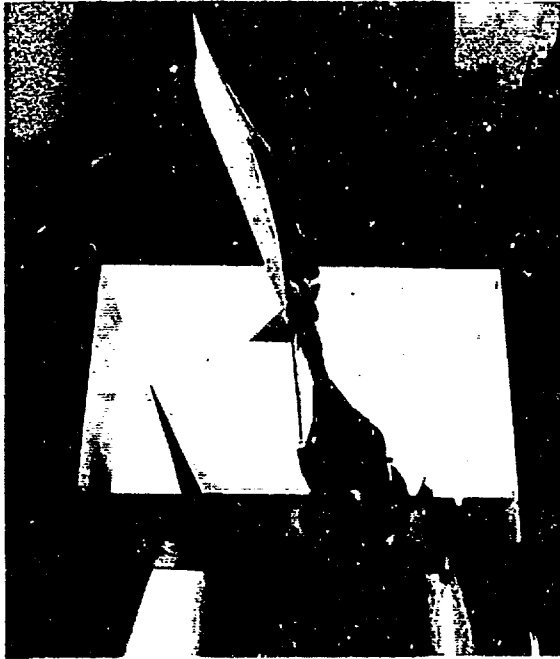
configurations have investigated the use of both single and double podded nacelles mounted in various locations on struts below the wing, as shown in Fig. 5-24. Movable wing models, with possible wing sweeps from 20 to 75 degrees, have assured consistent data at all sweep angles and Mach numbers.

Earlier designs of three and four-engine configurations, with either one or two engines mounted aft by the tail and two more mounted on struts under the body, are shown as tested in the supersonic wind tunnel in Fig. 5-25. These configurations had an inboard wing pivot hidden in the body.

Buried engine designs have also been tested, as illustrated in Fig. 5-26. For these configurations, the nacelles were integrated into the wing, on each side of the body, and an outboard wing pivot location was used.



5-25 Three And Four Engine Configurations



5-26 Buried Engine Configuration



SECTION 6

PERFORMANCE SUBSTANTIATION

TABLE OF CONTENTS

6.0 PERFORMANCE SUBSTANTIATION	6/1
6.1 Cruise Configuration	6/1
6.1.1 Drag Buildup	6/1
6.1.2 Minimum Drag Coefficient	6/3
6.1.3 Drag Due to Lift	6/9
6.1.4 Trim Drag	6/13
6.2 Takeoff and Landing Configuration	6/14
6.2.1 Lift Curves	6/14
6.2.2 Lift to Drag Ratios	6/15
6.2.3 Wings at 74 DEGREES Sweep	6/17
6.3 Sonic Boom	6/19

C6.0 APPENDIX C

C/1

6.0 PERFORMANCE SUBSTANTIATION (RFP 3.2.7.4)

The aerodynamic characteristics of the Model 733-197 are based on experimental results obtained with both fixed and variable sweep wing models in Boeing wind tunnels. Extensive use has also been made of data developed in NASA basic research programs and in the NASA studies of the supersonic transport. Well established methods have been used to extrapolate wind tunnel results to the full scale airplane, including the use of flight test data where applicable.

Substantiation of the aerodynamic characteristics is presented in three sections:

- 6.1 Cruise Configuration
- 6.2 Takeoff and Landing Configuration
- 6.3 Sonic Boom

6.1 Cruise Configuration

In this section the external aerodynamic efficiency of the 733-197 is substantiated. The drag evaluation of the cruise configuration is discussed in the following paragraphs:

- 6.1.1 Drag Buildup
- 6.1.2 Minimum Drag Coefficient
 - 6.1.2.1 Skin Friction
 - 6.1.2.2 Pressure Drag
- 6.1.3 Drag Due to Lift
- 6.1.4 Trim Drag

Discussion of each of the drag items is presented under the appropriate subject heading and detailed substantiation data are given in Appendix C of this volume.

6.1.1 DRAG BUILDUP

All of the coefficient data presented in this section for the 733-197 airplane are based on a reference wing area of 4684 square feet and mean aerodynamic chord of 64.52 feet. The reference dimensions are based on a "theoretical arrow wing" planform which corresponds to the fully swept wing with a leading edge sweep of 74 degrees, as

defined in Section 2.0. The gross wing area in this configuration is 5026 square feet.

The drag buildup may be examined by means of the following equation:

$$C_D = C_{D_{min}} + K (C_L - \Delta C_L)^2$$

$$\text{where } K = \frac{\Delta C_D}{(C_L - \Delta C_L)^2} = \text{drag due to lift factor}$$

$$\text{and } C_{D_{min}} = C_{D_{friction}} + \Delta C_{Dr}$$

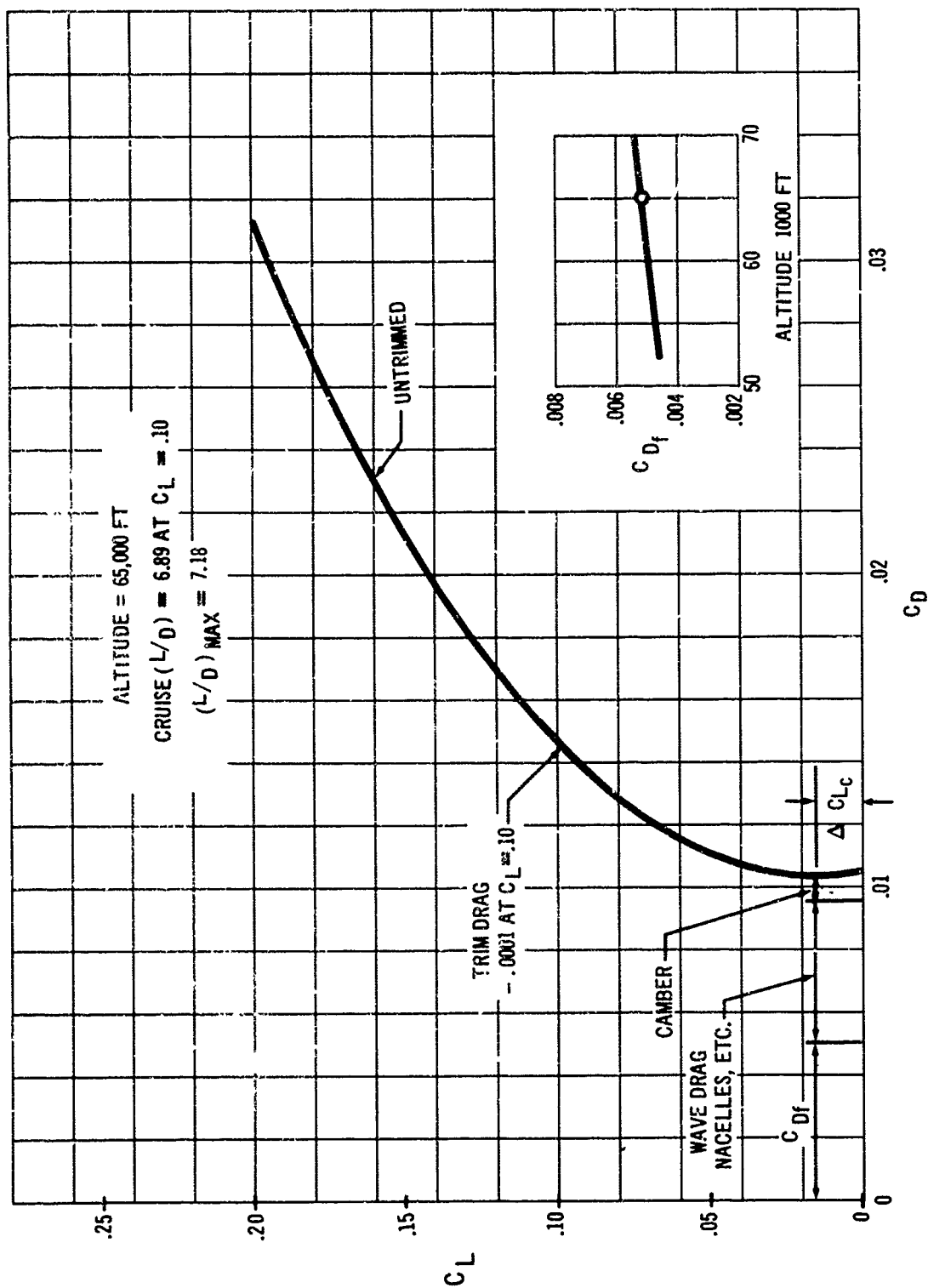
$$\Delta C_{Lc} = \text{camber lift increment}$$

$$\Delta C_{Dr} = \text{pressure drag}$$

The zero load drag of the tail surface is included in $C_{D_{min}}$. Thus, trim drag is defined as an increment from the zero tail load condition. In accordance with the common definition of net thrust (gross thrust less free stream ram drag), the drag due to the inlet off-design air spillage, bleed, overboard discharge, and due to the nozzle is included as part of the external drag in the pressure drag term of $C_{D_{min}}$.

The cruise polar at Mach 2.7 is shown in Fig. 6-1 for an altitude of 65,000 feet. At that altitude the airplane cruises at a lift coefficient of 0.1 with a trimmed lift-drag ratio (L/D) of 6.89. The minimum drag coefficient is .0104 and includes the above mentioned powerplant associated drags as part of the external drag. It also includes a substantiated increment of .00013 for surface roughness, as well as a general allowance for contingencies. The total allowance for roughness and contingencies is about eight percent of the skin friction drag. The effect of center of gravity position on trimmed cruise L/D is shown in Fig. 6-2.

Fig. 6-3 shows the variation of L/D at constant sweep angles with Mach number. The variation of L/D with Mach number, for the basic mission, is shown in Fig. 6-4,

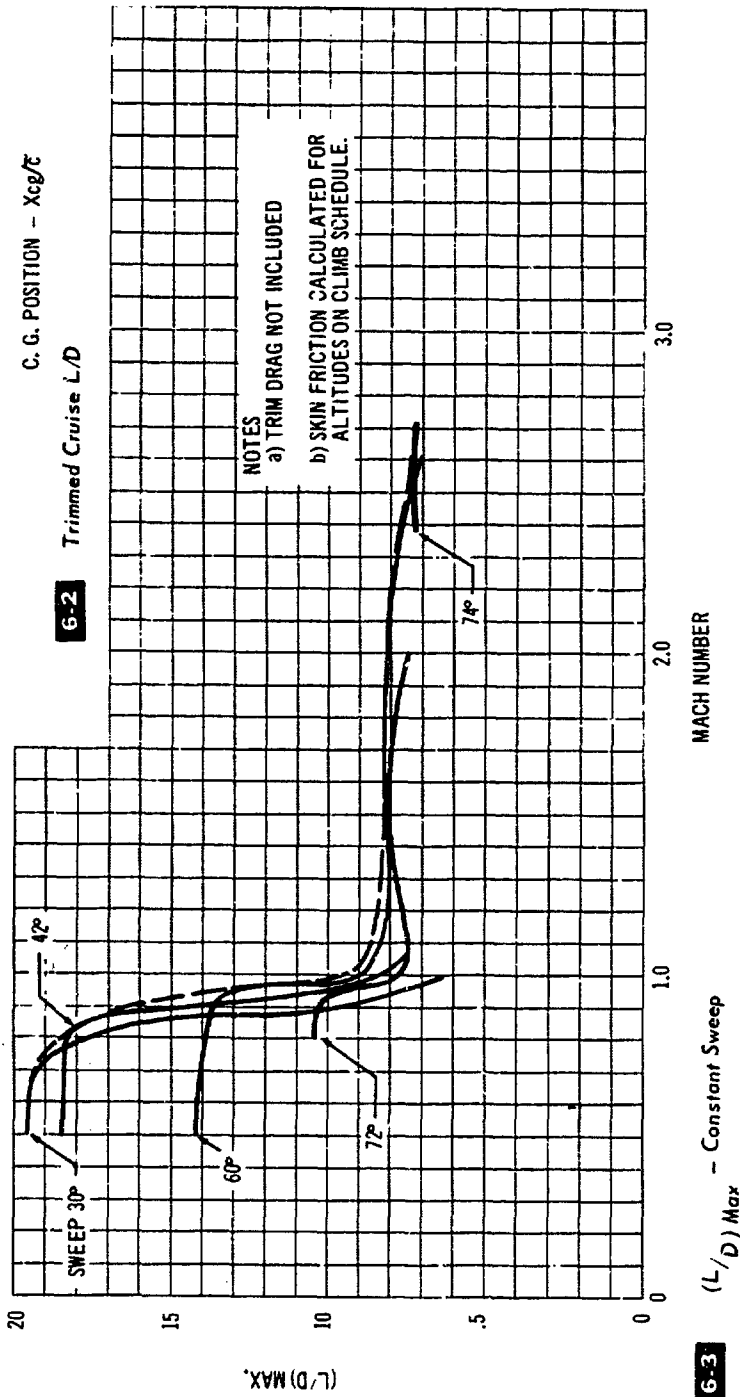
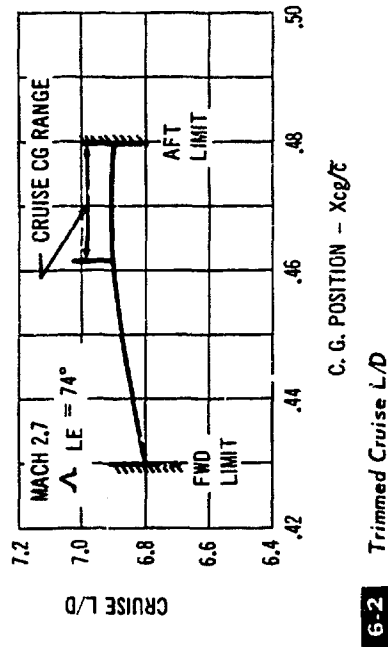


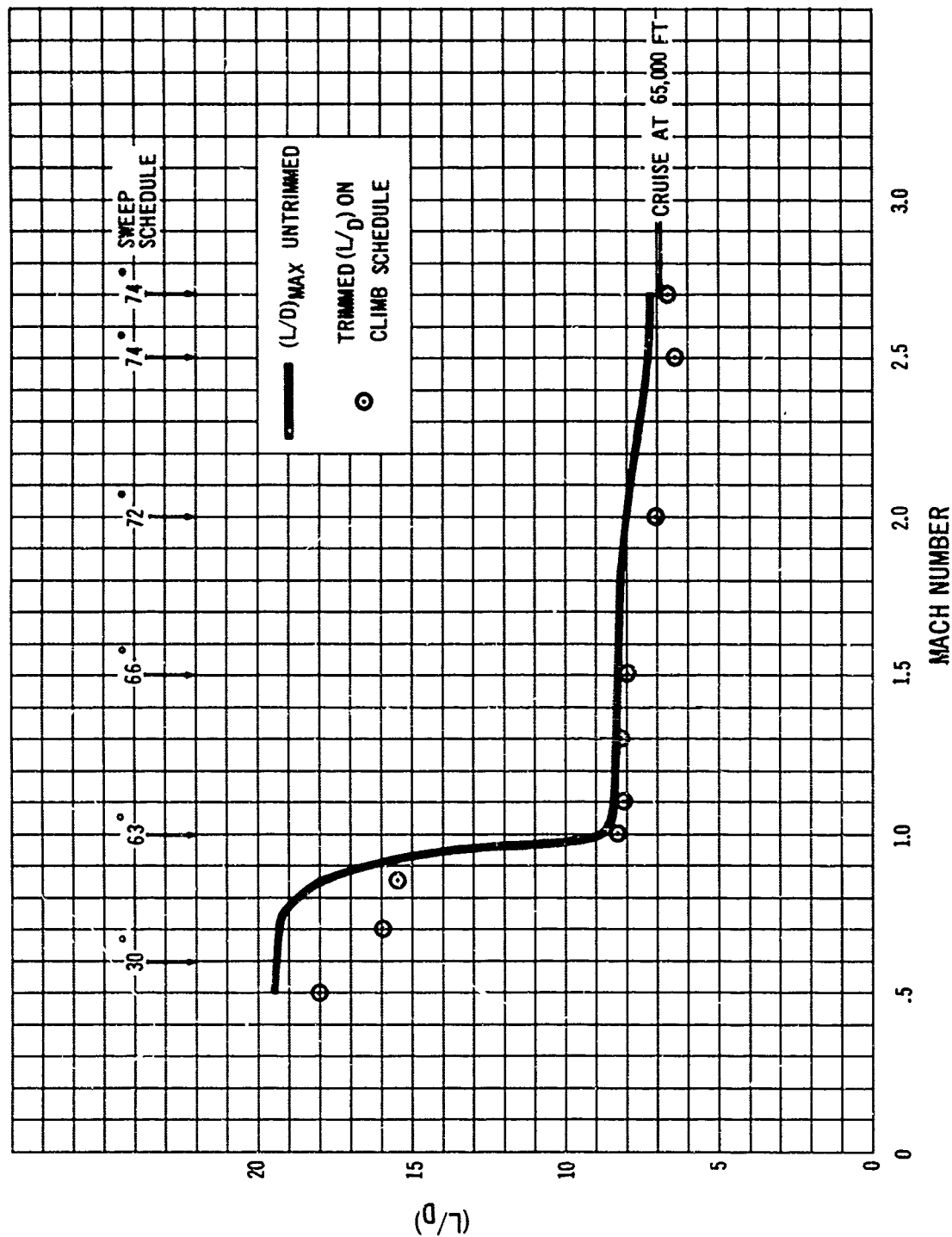
6-1 $M = 2.7$ Cruise Drag Polar

corresponding to the climb sweep schedule. The lift coefficients for the basic mission are presented as a function of Mach number in Fig. 6-5, and drag polars for several Mach numbers are presented in Fig. 6-6.

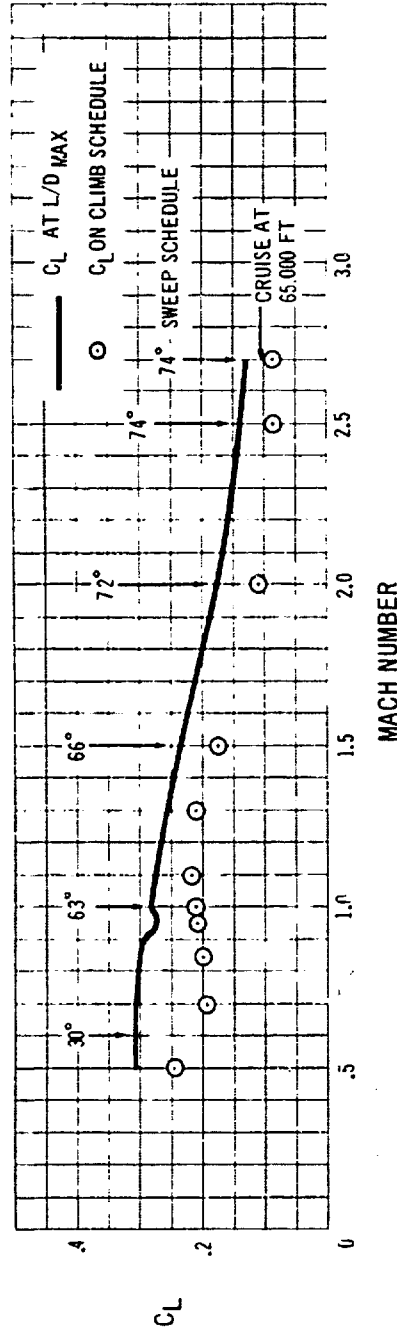
6.1.2 MINIMUM DRAG COEFFICIENT

The minimum drag coefficient is made up of skin friction drag and pressure drag. The latter is further subdivided into wave drag and camber drag. Fig. 6-7 shows the total minimum drag of the 733-197 for the climb and acceleration schedule.





6-4 Lift - Drag Ratio on Climb Schedule.



6-5 Lift Coefficients on Climb Schedule

6.1.2.1 Skin Friction Drag

The calculation of skin friction drag, as well as the extrapolation of wind tunnel model drag to full scale flight conditions, is based on the mean enthalpy method. This method of calculating turbulent skin friction drag is substantiated by NASA and Boeing test-theory comparisons. Although not shown as part of the skin friction, an allowance in drag has been made for skin roughness, taking into account surface waviness, and the protuberances due to manufacturing that will be present on the airplane. The derivation of this is described in the Appendix to this section (C). Although discussed under skin friction, this drag is at least partially pressure drag and is shown as part of ΔC_{Dp} in the drag buildup, Fig. 6-9.

At cruise flight conditions the airplane will have some amount of laminar flow. Calculations have shown this to be equivalent to a reduction of about 1.5 percent in wetted area, but no credit is taken for this reduction in drag level. It is considered as part of an allowance for contingencies.

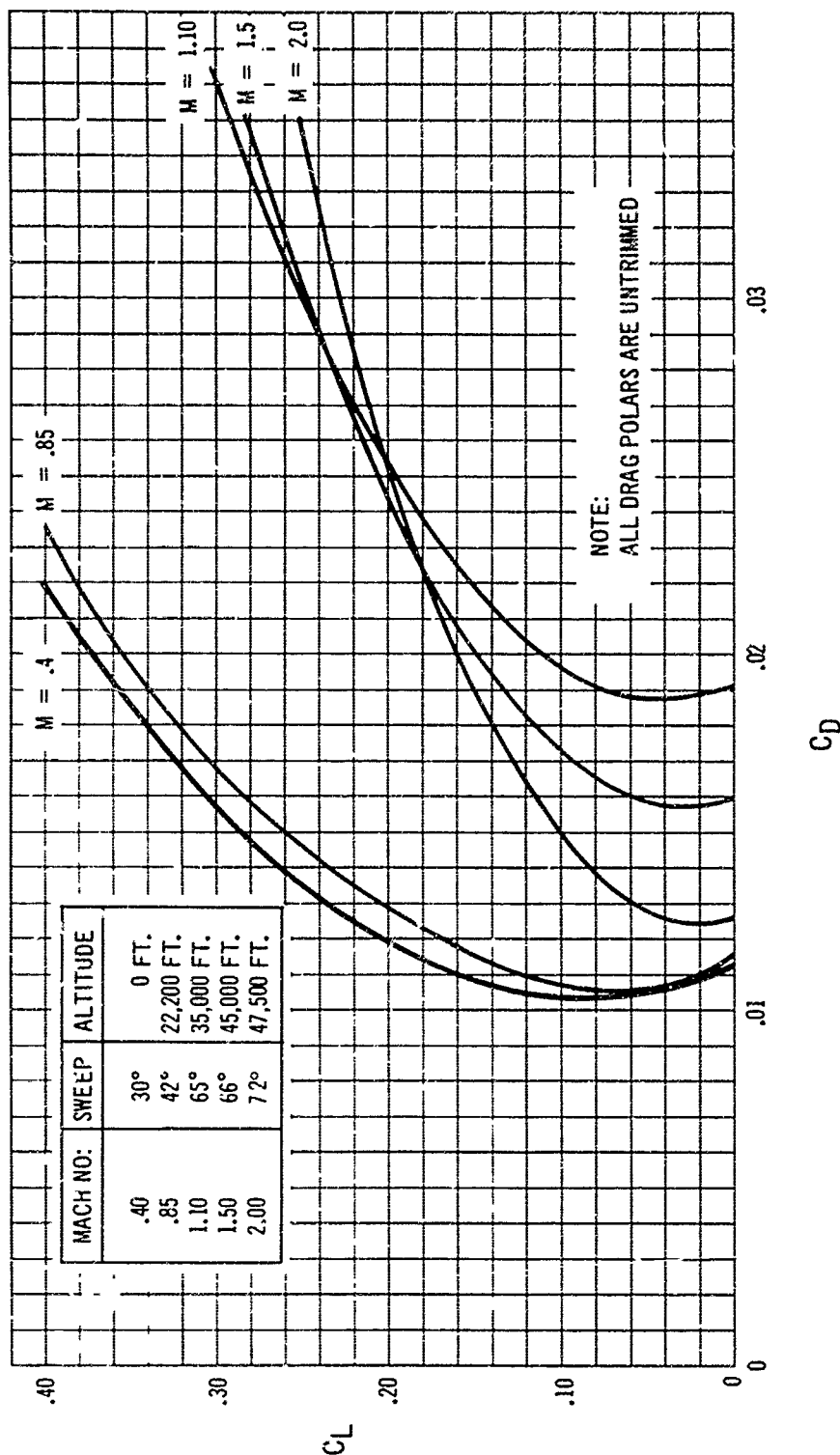
All skin friction data was thus assumed extrapolated to fully turbulent flow conditions.

Skin friction calculations were carried out by analyzing each component separately. Table 6-A illustrates the procedure and gives the skin friction drag breakdown at Mach 2.7, 65,000 feet altitude.

6.1.2.2 Pressure Drag

Pressure drag is defined as the difference between the measured wind tunnel model minimum drag, and the estimated model skin friction drag. There are inevitable differences between the wind tunnel models and the airplane, such as the closure of the body, and the pressure drag of the 733-197 has been corrected for these differences.

Well-proven analytical methods have been used to apply corrections to the wind tunnel data. These are described in Section C6.1 of the Appendix, where correlations of the methods with experimental data are shown.

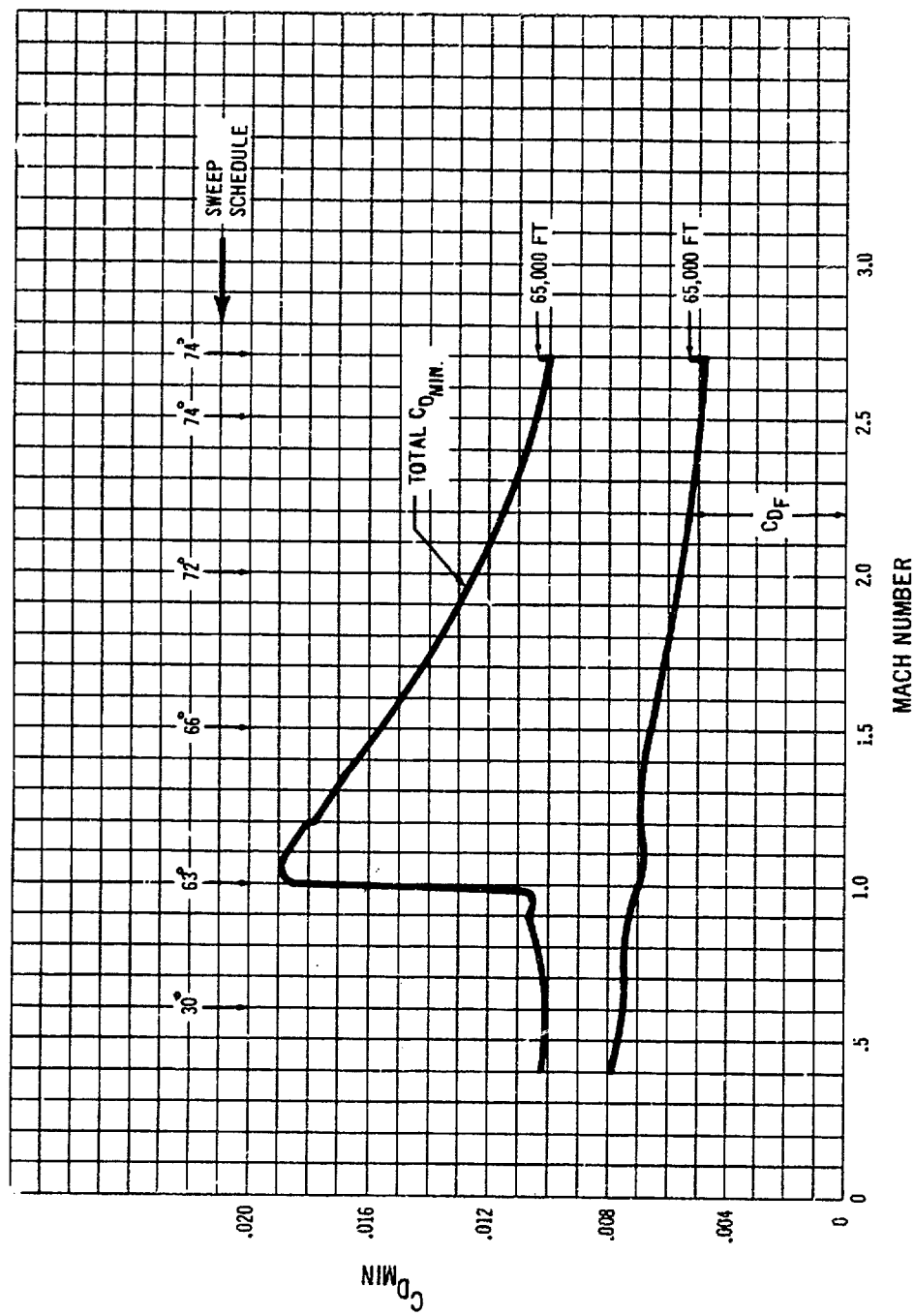


6-6 Drag Polars

Part of the pressure drag is defined as the thickness wave drag. The thickness wave drag includes the wave drag of the body, wing, empennage, nacelles, struts and landing gear fairings, as well as the interference drag between these components. Fig. 6-8 shows this drag as a function of Mach number, for the configuration with the wings swept to 74 degrees. The canopy drag is shown as

a separate item since it was obtained from special model tests of the 733-197 forebody. Detailed analysis of these tests and further discussion of the thickness wave drag, including relevant area plots, are given in Appendix C.

The remainder of the pressure drag consists of measured camber drag and powerplant associated drag. The latter consists of spillage drag, excess engine bleed and



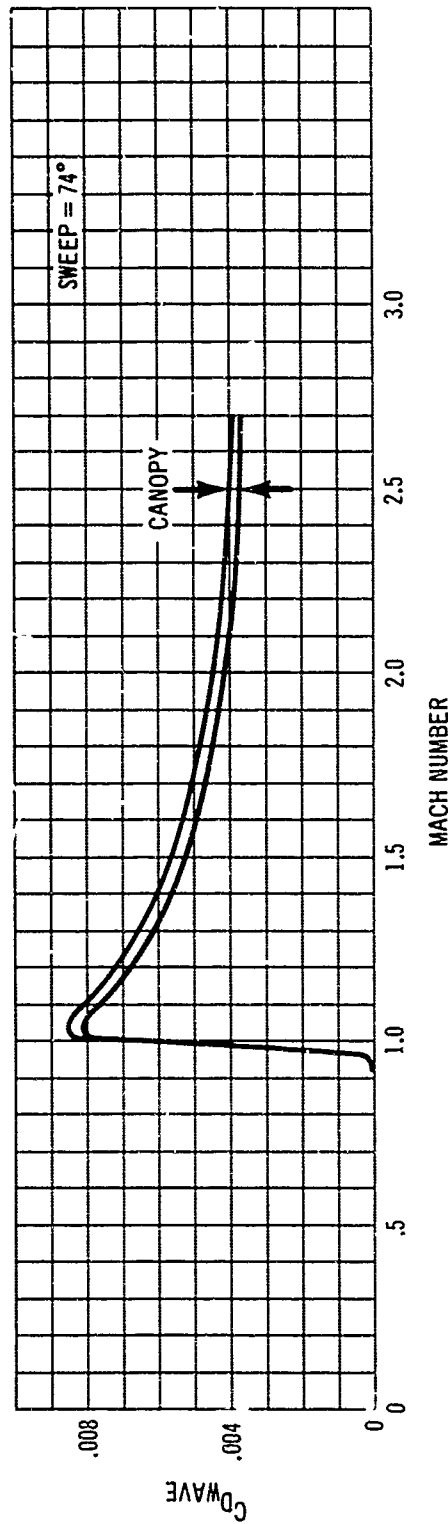
6-7 Minimum Drag Coefficient on Climb Schedule

TABLE 6-A Skin Friction Breakdown

ALTITUDE = 65,000 FT. MACH NO. = 2.7 REF. AREA = 4684 SQ. FEET

COMPONENT	A WET. SQ. FT.	$A_w/S_{REF.}$	REF. FT. L	$R_e \times 10^{-6}$	C_F	C_{DF}
BODY	5339	1.140	203.83	315.9	.00108	.001231
WING	8144	1.739	DONE BY STRIPS		.00132 *	.002295
NACELLES	1769	.378	29.5	45.7	.00146	.000552
HORIZONTAL TAIL	1900	.406	21.5	33.3	.00153	.000621
VERTICAL TAIL	906	.193	20.6	32.0	.00154	.000298
VENTRAL	250	.053			.00108	.000057
STRUTS	400	.085	30.8	47.8	.00145	.000123
TOTALS	18708	3.994 **				.005177

* AVERAGE FOR THE STRIPS ** WETTED AREA RATIO = 3.722 BASED ON GROSS WING AREA



6-8 733-197 Thickness Wave Drag

bypass drag, and pressure drag associated with off-design operation of the nozzle.

The total pressure drag of the 733-197 airplane is presented in Fig. 6-9. Each of the components discussed previously is shown.

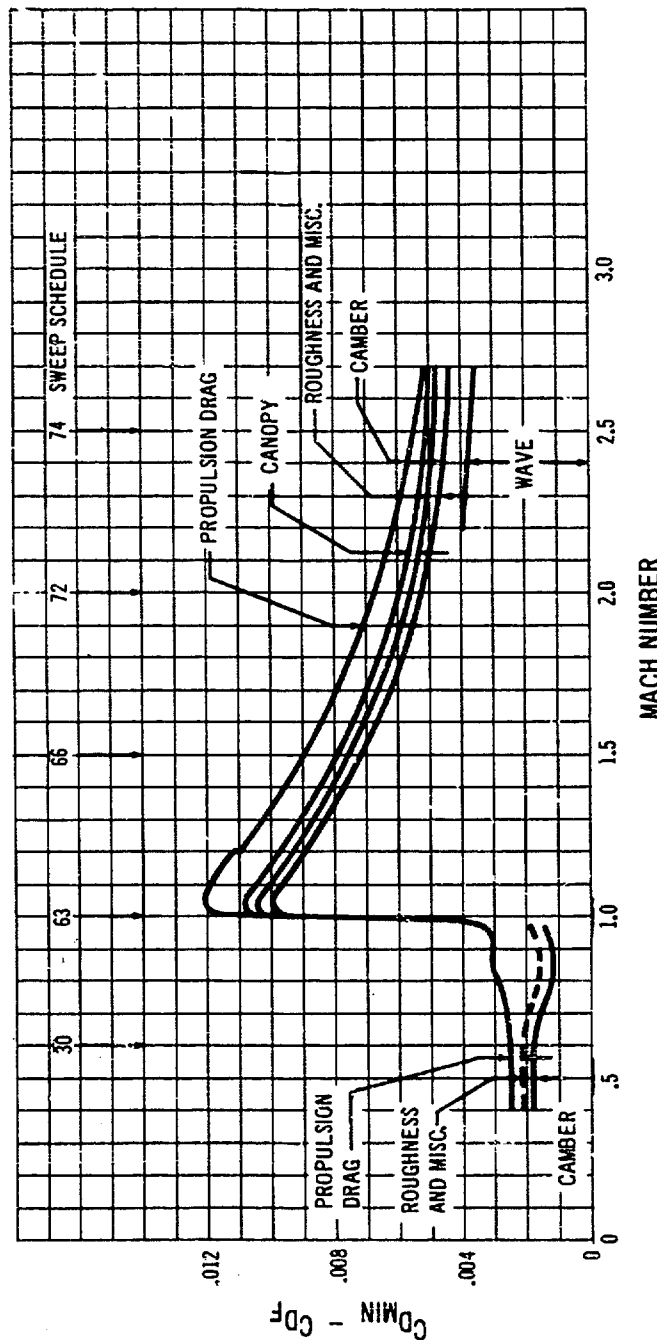
6.1.3 DRAG DUE TO LIFT

The drag due to lift of the 733-197 is based on Boeing wind tunnel test results. Discussion is divided into two sections:

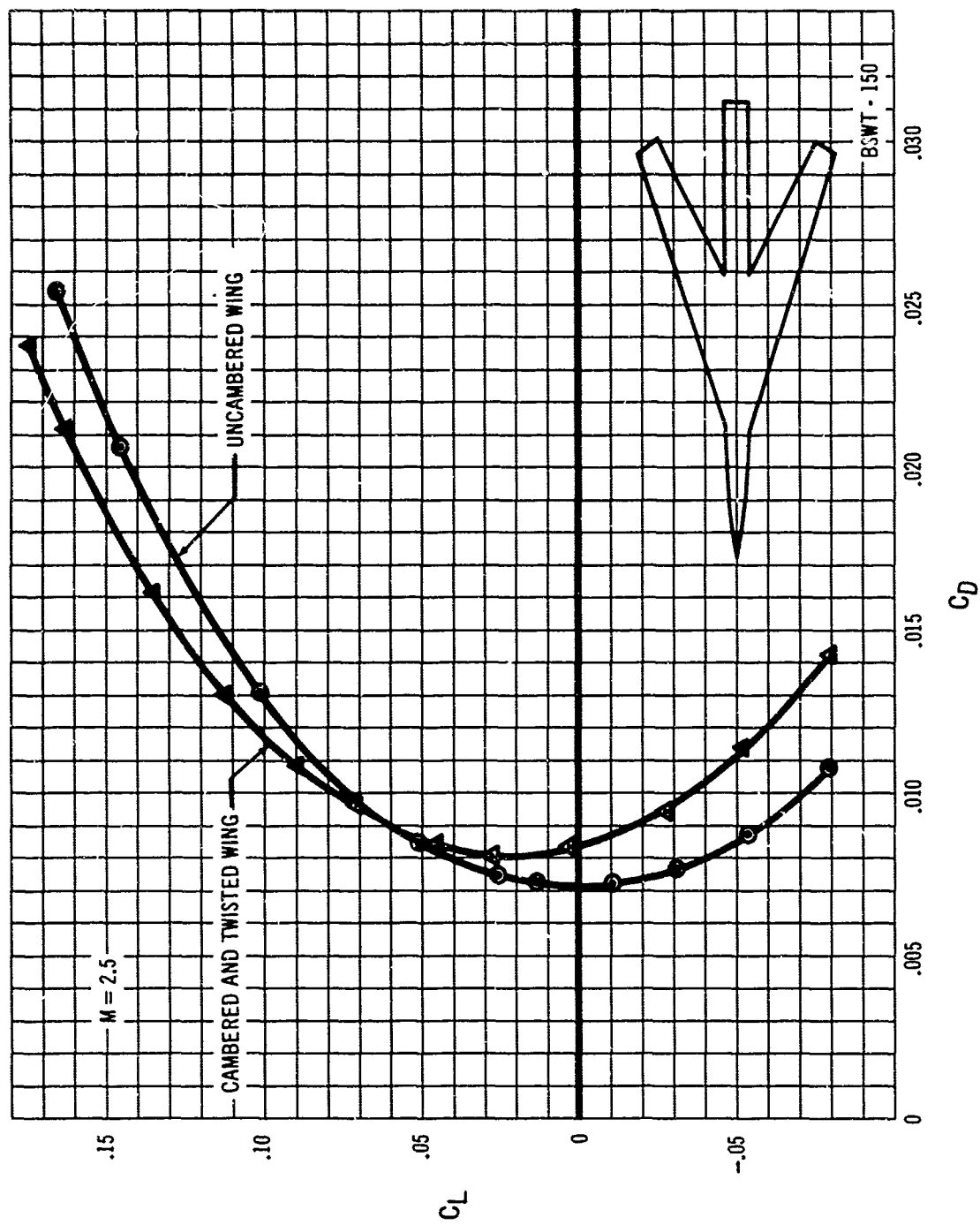
Drag Due To Lift At Supersonic Cruise
Drag Due To Lift At Mach 0.4 to 2.5

6.1.3.1 Drag Due to Lift at Supersonic Cruise

The cambered and twisted arrow wing of the 733-197 provides excellent supersonic drag due to lift. This capability has been derived from the results of Boeing's substantial wind tunnel research program on arrow wings, as well as



6-9 733-197 Pressure Drag



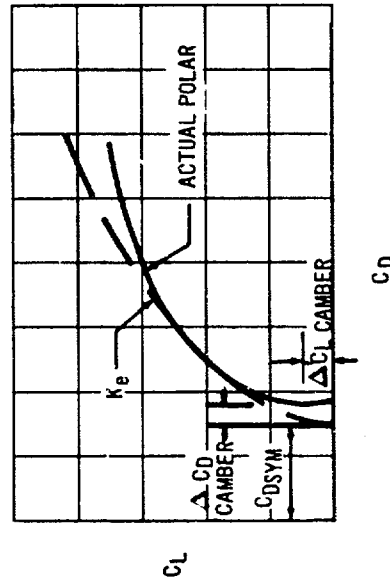
6-10 Flat and Cambered Wing Polars

from NASA research. Typical wind tunnel test results in Fig. 6-10 compare a flat wing with a cambered and twisted wing, illustrating the improved drag due to lift of cambered wings.

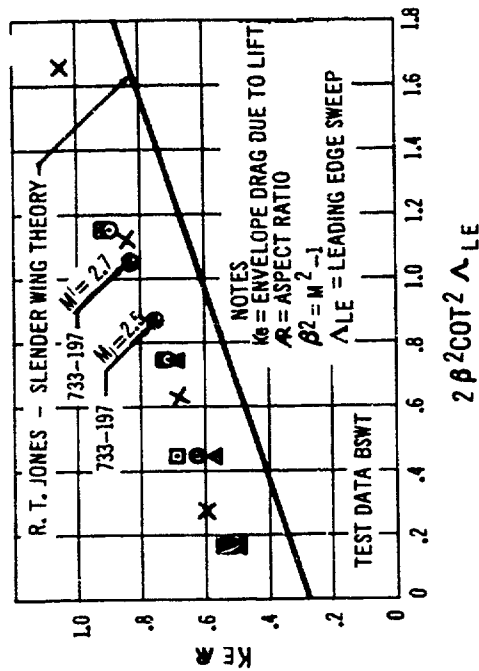
A convenient way to compare test results for many different wing designs is on the basis of envelope drag due to lift factor K_e . Fig. 6-11 defines K_e . As shown, K_e is related to the zero-lift drag of the unwarped wing.

Test results for several wings with planforms similar to that of the 733-197 have been correlated on the basis of aspect ratio, leading edge sweep, and Mach number as guided by the lower bound formula for slender wings derived by R. T. Jones in Ref. 1. These are shown in Fig. 6-12.

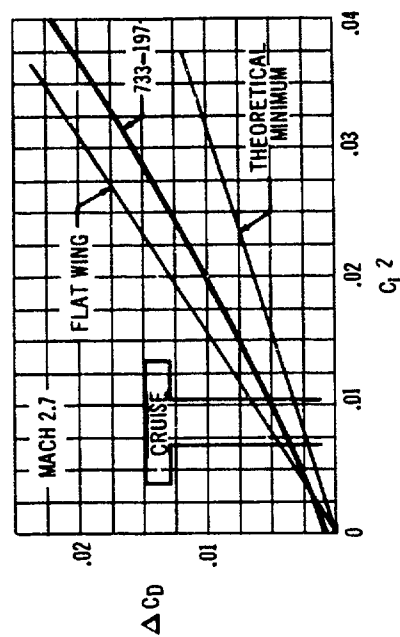
The envelope drag due to lift values for the 733-197 are shown for wing sweep 74 degrees at Mach numbers 2.7 and 2.5. Fig. 6-13 compares the drag due to lift of the 733-197 to that of a flat wing and to the theoretical optimum. It is seen that, although a reasonably low level of drag is achieved, considerable improvement is still



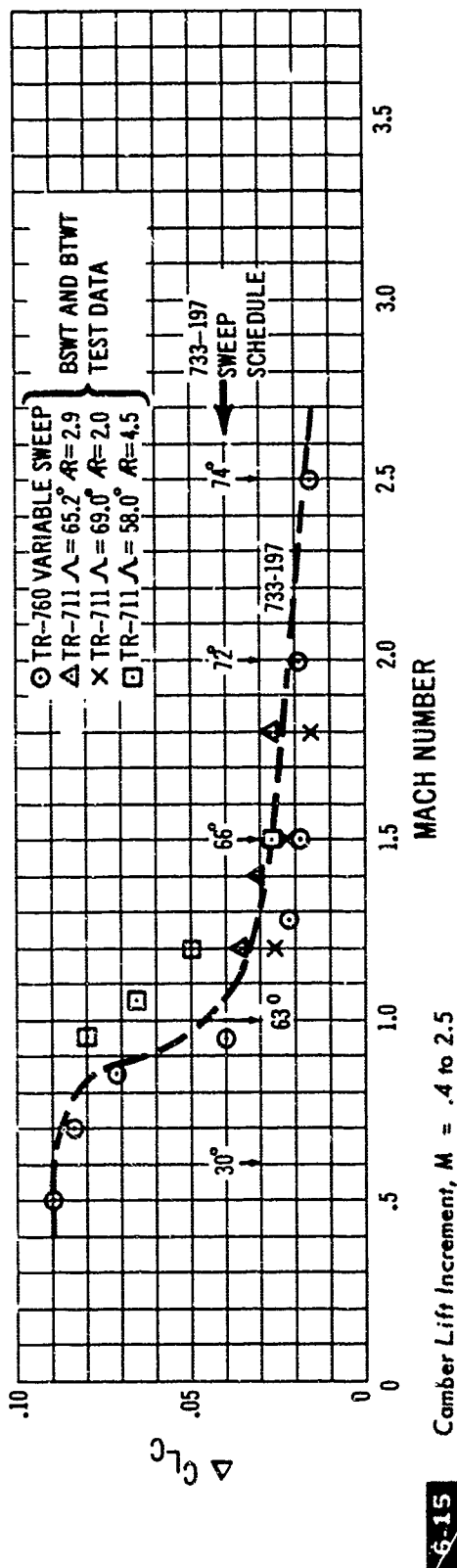
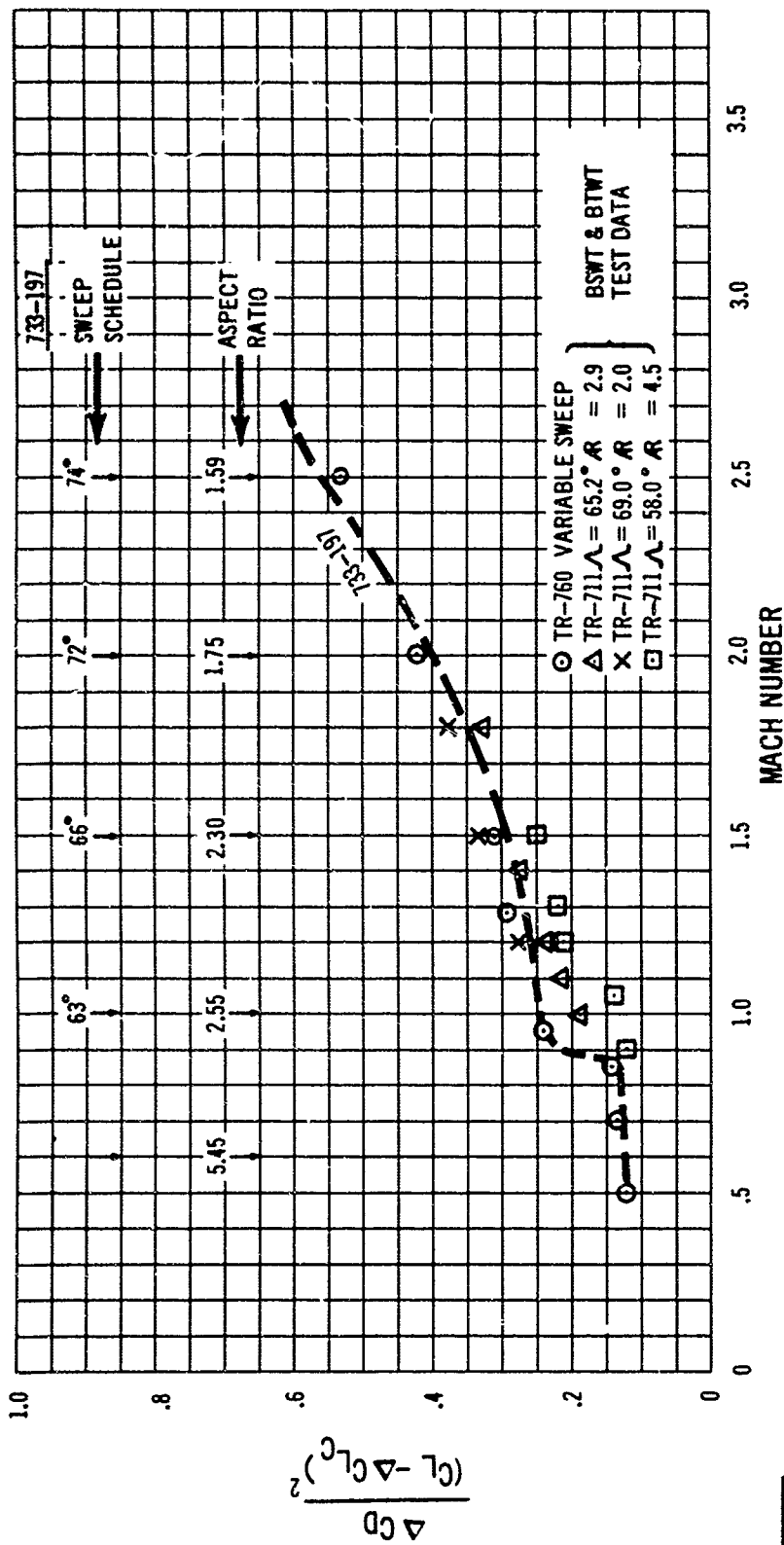
6-11 Envelope Drag Due to Lift



6-12 Correlation of Drag Due to Lift Test Results



6-13 733-197 Drag Due to Lift



possible. Improvement of the drag due to lift from its present value will thus be obtained with the benefit of a continuing wing research and development program. Further improvements due to Reynolds number scale effects are also probable. The 733-197 wing is cambered for a design lift coefficient (C_L) of 0.10 at Mach 2.7. The camber drag increment and camber lift increment are based on test results of wings with varying design C_L and a planform similar to that of the airplane. Substantiating plots are shown in Par. C6.1.4 of Appendix C.

Airplane drag due to lift is also a function of nacelle interference effects and trim moments. Substantiated results pertaining to the 733-197 are discussed in Par. C6.1.3 of Appendix C.

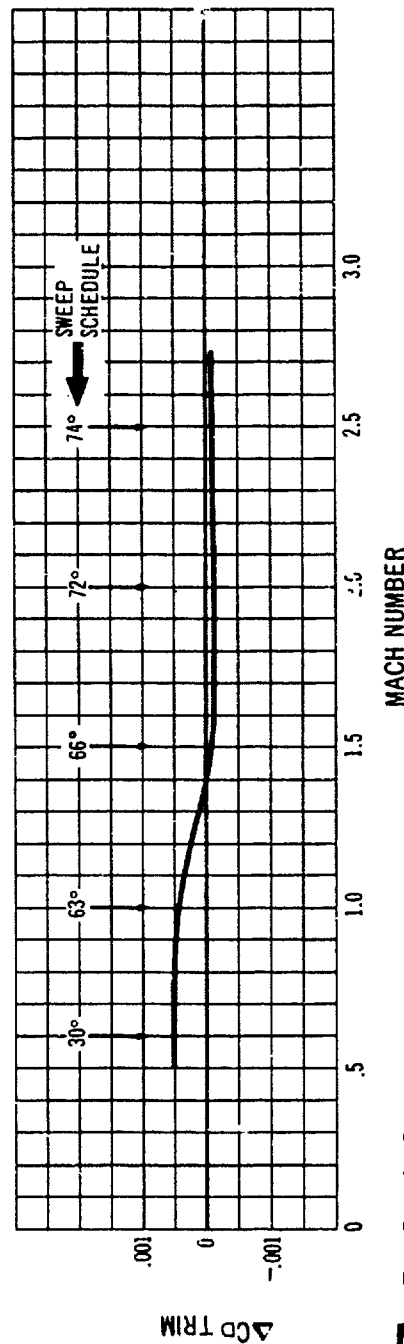
6.1.3.2 Drag Due to Lift at Mach 0.4 to 2.5

The incremental lift due to camber, ΔC_{Lc} , and the basic drag due to lift factor, $\frac{\Delta C_D}{(C_L - \Delta C_{Lc})^2}$ are based on test

results from the variable sweep TR-760 model and other available wing-body data for wings of similar sweep and aspect ratio. These results for drag due to lift and ΔC_{Lc} are plotted in Figs. 6-14 and 6-15 as a function of Mach number. The 733-197 sweep, and aspect ratio, are indicated for the climb and acceleration schedule. As shown, the estimated ΔC_{Lc} and drag due to lift for the 733-197 are bracketed by the wind tunnel data.

6.1.4 TRIM DRAG

The trim drag increments applied to the 733-197 airplane were determined by constructing tail drag polars from wind tunnel data for a geometrically similar model. Trim drag is defined as a drag increment from the airplane zero tail load condition. The zero-load drag of the tail is included in the total airplane $C_{D_{min}}$. Fig. 6-16 presents trim drag increments for the 733-197 along the basic mission climb and acceleration schedule. Additional data and discussion of trim drag are included in the Appendix C6.1.5.



6-16 Trim Drag for Basic Mission

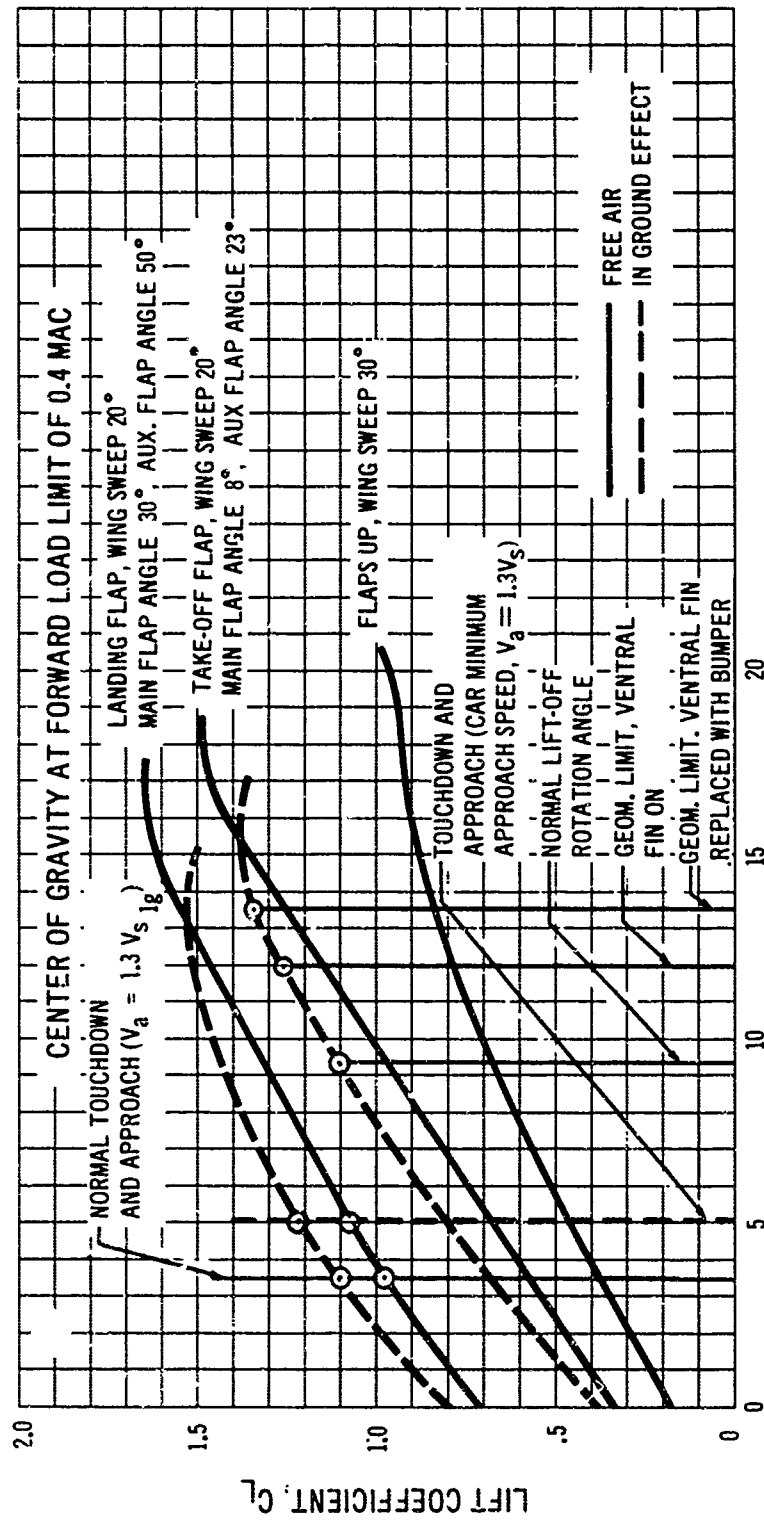
6.2 Takeoff and Landing Configurations

6.2.1 LIFT CURVES

Lift coefficient is shown plotted against body reference angle of attack in Fig. 6-17. The body reference line is parallel to the floor of the forward passenger cabin. The lift curves are shown for landing and takeoff flap angles (wing leading edge sweep of 20 degrees) and for flaps

retracted at the minimum applicable sweep angle of 30 degrees. They apply to the loaded wing under typical 1-g flight conditions (Refer to Section 3.3.1.4 of Volume A-VII for the wing sweep/flap angle schedule).

Body reference line angles of attack at liftoff, climb-out (takeoff safety speed V_2), approach, and touchdown are compared with those of a typical subsonic jet airplane in Table 6-B.



6-17 Trimmed Lift Curves

TABLE 6-B Body Reference Angle with Respect to Flight Path
(Angle of Attack) (Positive, Nose Up)

THRUST WEIGHT RATIO	AIRPLANE		CONDITION
	MODEL 733-197 SUPERSONIC TRANSPORT	MODEL 707-320B SUBSONIC JET	
.25	1.13V _{S1g} , 9.4°	1.2V _S , 9°	LIFT-OFF
	1.2V _{S1g} , 9.5°	1.27V _S , 9.5°	CLIMB AT TAKE-OFF SAFETY SPEED
.25	1.3V _S , 5.2°	1.3V _S , 6°	APPROACH
	1.3V _{S1g} , 3.6°		
	1.22V _S , 5.2°	1.22V _S , 6°	TOUCH-DOWN
	1.22V _{S1g} , 3.5°		

mediate flap setting. The lift-off C_L and flap setting corresponding to a lift-to-drag ratio necessary for requirements such as noise abatement or minimum climb gradient may be obtained from this figure. The curve may be used to make a quick assessment of airplane minimum field length (a simple function of thrust, weight and CL_{LOF}) as limited by second segment climb capability at the speed V_2 . A procedure for this would be as follows:

Use the available thrust with one engine out to determine the L/D required to meet the second segment minimum climb gradient $\gamma = 0.03$: $(L/D)_{required} = \frac{1}{\text{Thrust/Weight}} - 0.03$. Use the CL_{LOF} corresponding to

The body angles of attack for the two airplanes are similar at takeoff, while for approach and landing the 733-197 requires less nose-up attitude. This improves visibility and facilitates landing, especially in adverse weather conditions.

A further discussion on the takeoff and landing speeds is given in Par. C6.2 of Appendix C.

Note on Stall Speeds:

In Table 6-B, V_S is the stall speed as defined in the current FAA regulations of SR 422B and used as the reference stall speed at this time. It is the minimum speed obtained in a controlled approach to the stall at a deceleration of one knot per second.

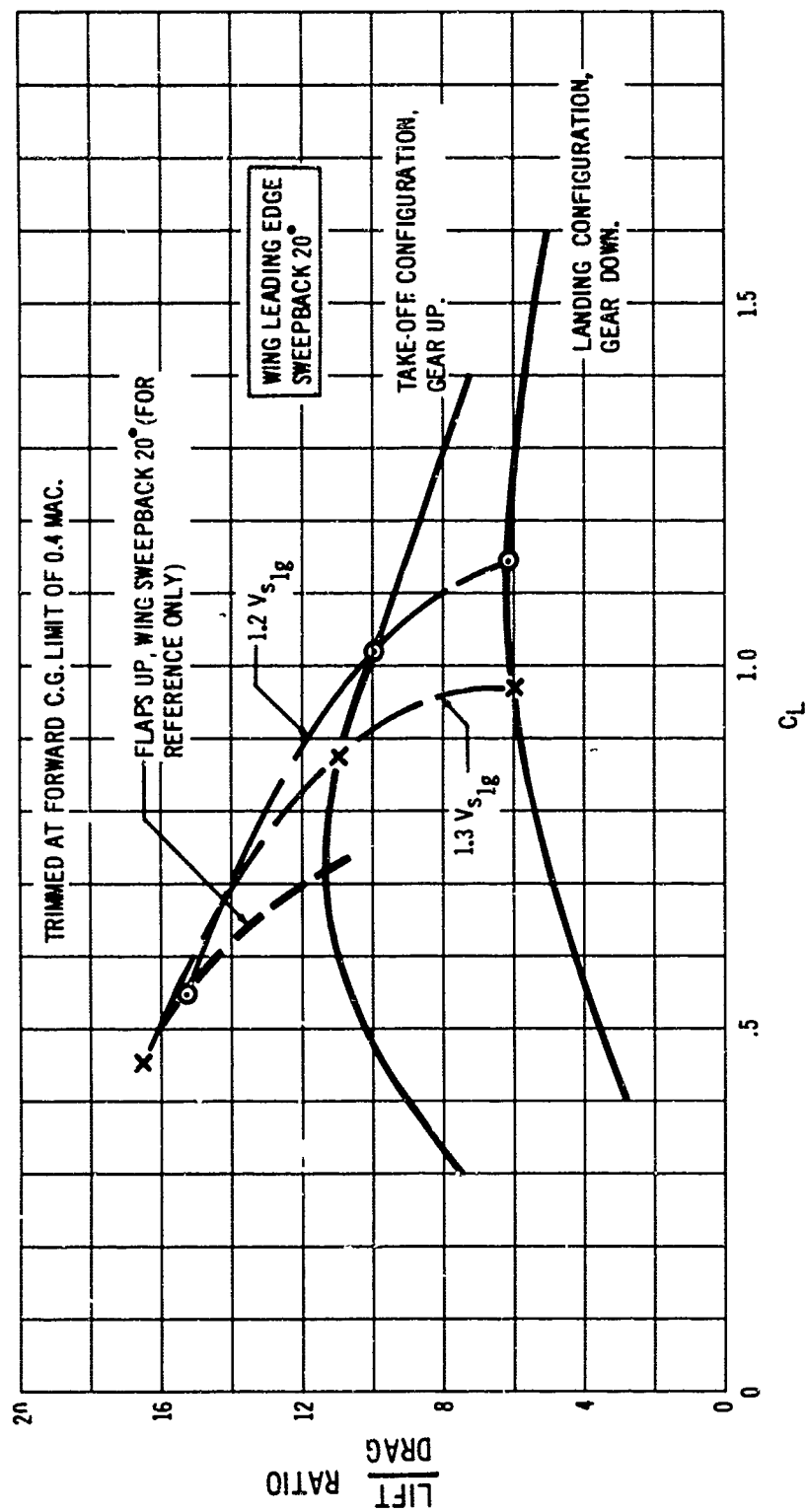
V_{Si} is the minimum speed in flight at which the airplane can develop a lift force (normal to the flight path) equal to the airplane weight. The "Tentative Airworthiness Objectives and Standards for Supersonic Transport Design Proposals," dated August 15, 1963, issued by the Flight Standards Service of the Federal Aviation Agency, proposes the use of V_{Si} as the reference stall speed for the SST.

6.2.2 LIFT-TO-DRAG RATIOS

Lift/drag ratio variation with lift coefficient is shown in Fig. 6-18 for the takeoff and landing configurations. The airplane L/D is 10 at a typical climb condition following noise abatement procedures. Landing approach value, with gear extended, is six.

The high thrust to weight ratios obtainable on this airplane give flexibility in takeoff operations when noise abatement is not a prime consideration. It is possible to take off at any flap setting when using maximum augmented thrust.

An envelope curve of L/D at the minimum takeoff safety speed $V_2 = 1.2V_{Si}$ against lift-off C_L (CL_{LOF}), is shown in Fig. 6-19. This is simply a curve drawn through the appropriate values at each flap angle. Thus, any point on the curve represents a value obtainable at some inter-



6-18 $\frac{\text{Lift}}{\text{Drag}}$ Ratio For Various Flap Settings

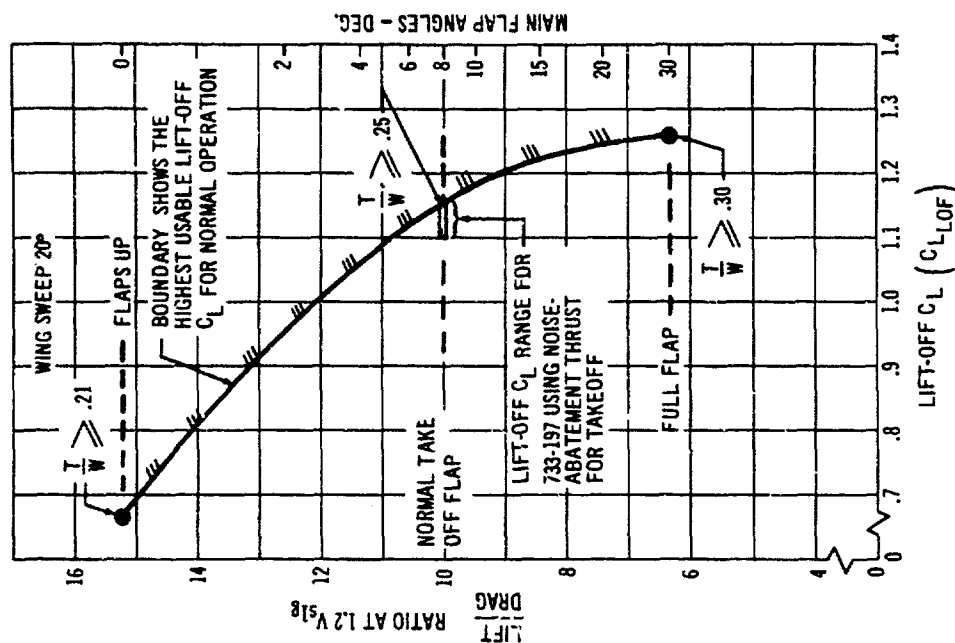
the L/D required to compute minimum takeoff field length; read the takeoff flap setting giving these performance levels from the auxiliary scale of Fig. 6-19.



6.2.3 WINGS AT 74 DEGREES SWEEP

Trimmed lift is shown against body angle of attack for low speed flight conditions with flaps down in Fig. 6-20. The maximum usable C_L , flaps down, is limited to 0.9 at an angle of attack of 20 degrees. A landing approach lift coefficient of 0.45 may be used (body angle of attack = 10 degrees) and touchdown would be at a body angle of attack of 8.5 degrees. These are quite moderate values which would not present any difficulties if a wings-back landing should be necessary.

Low speed lift-to-drag ratio variation with C_L is shown on Fig. 6-20 for the landing configuration. Approach will be made at $C_L = .45$ with an L/D of 3.9, gear down. Climb gradient capability at this condition, with maximum dry power on three engines, will be .128 (Sea level, 86 degrees Fahrenheit at landing weight with fuel for go-around).



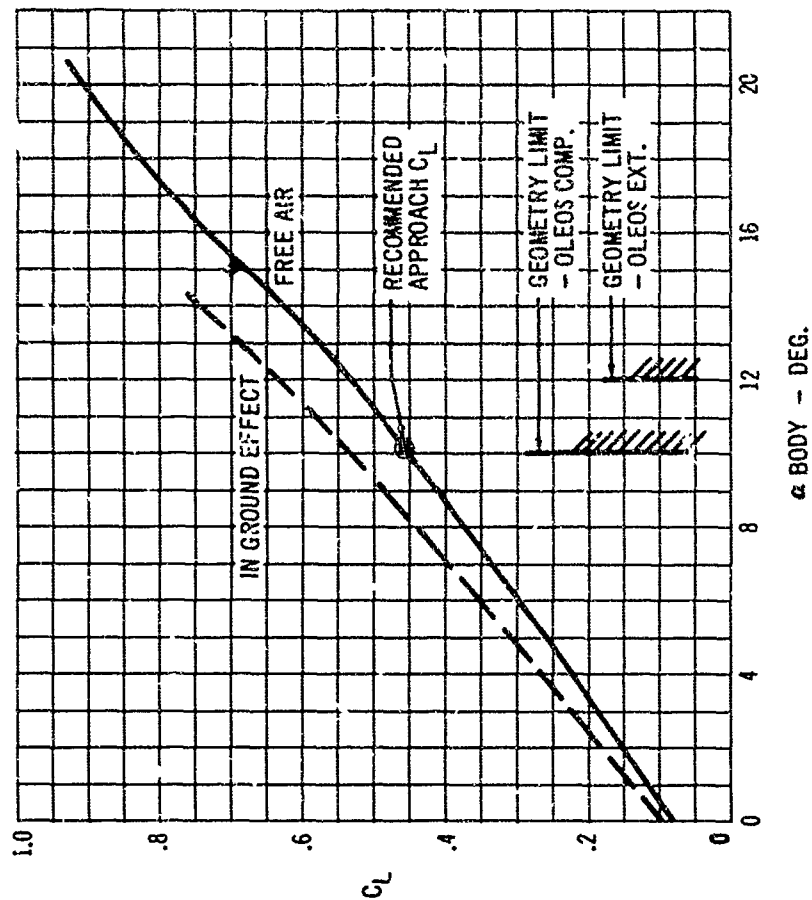
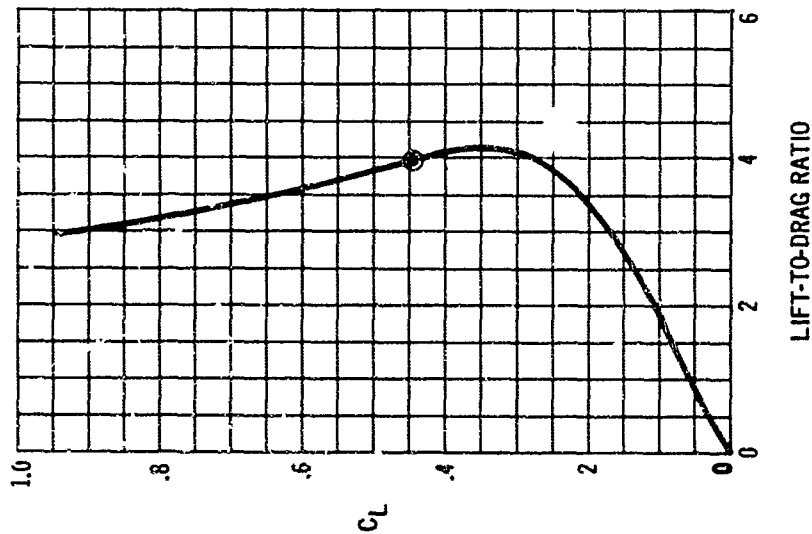
6-19 Lift-Off C_L Variation With L/D In Climb

733-197 FULL SCALE ESTIMATE

$\Delta LE = 7\%$

TRIMMED AT .43 M.A.C.

FLAPS DOWN - GEAR DOWN



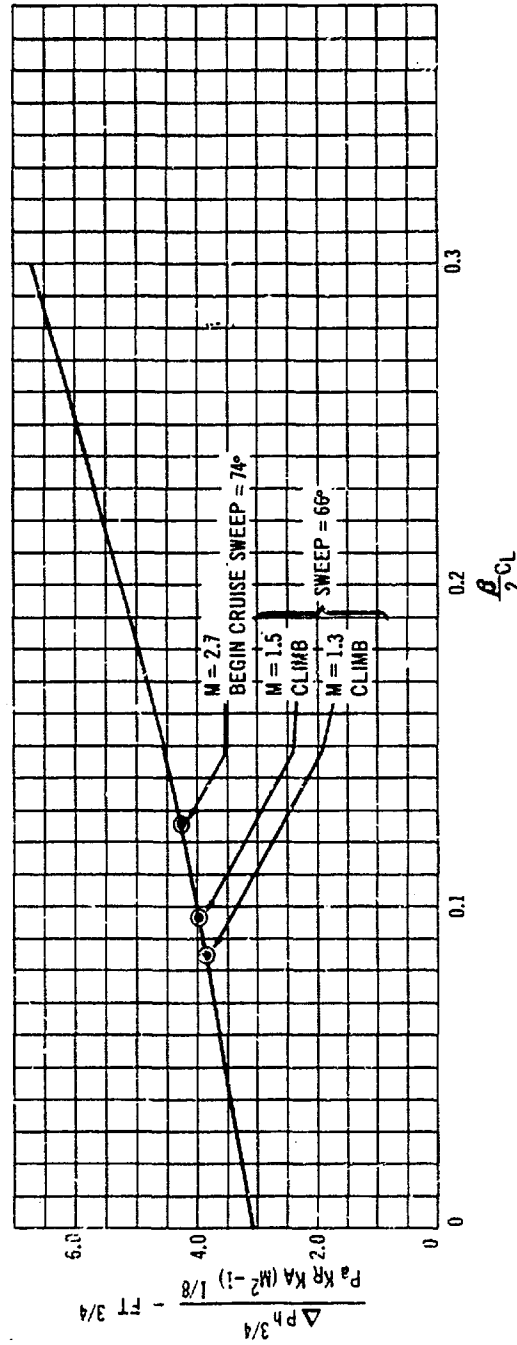
6-20 Trimmed Lift and Drag With Wings Fully Swept

6.3 Sonic Boom

The sonic boom characteristics of the 733-197 were calculated using the most up-to-date methods available. The theory is the same as that in use at the NASA Langley Research Center, as described in Refs. 2 and 3. It is the theory developed by Whitcomb, with allowances for atmospheric effects. Extensive use is made of digital computer facilities in order to analyze, in detail, the interactions among the various components of the airplane, including the interactions between the airplane lift and its volume.

The parametric plot of Fig. 6-21 summarizes the sonic boom characteristics of the 733-197. The factor $\Delta P h^{3/4} / P_a K_R K_A (M^2 - 1)^{1/8}$ is plotted against $\beta_{CL}^2/2$, where:

- ΔP = Peak positive overpressure
- P_a = Ambient pressure at airplane altitude
- K_R = Ground reflectivity factor
- K_A = Atmospheric correction factor
- h = Vertical distance from ground to airplane
- M = Airplane Mach number
- C_L = Lift Coefficient
- β = $(M^2 - 1)^{1/2}$



6-21 733-197 Sonic Boom Characteristics

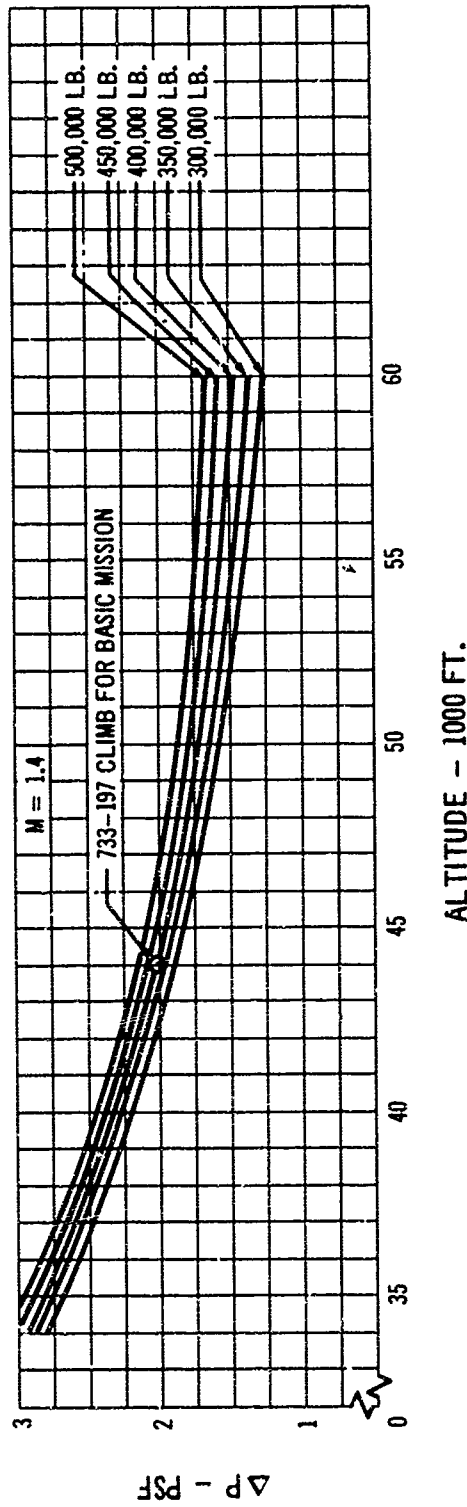
This parametric method of presenting sonic boom results was developed by the NASA (Refs. 4 through 7) and provides a convenient way of describing the sonic boom properties of the airplane for a very wide range of flight conditions. The line on the plot corresponds to a leading edge sweep of 74 degrees. Specific points are shown at the critical climb and cruise conditions. These were individually computed at the appropriate geometry for the sweep schedule. Although the length of the lift distribution is somewhat reduced at the lower Mach numbers, the effects of this are counteracted by improvements in the shape of the lift distribution, as well as lift-volume interactions.

Figs. 6-22 and 6-23 examine, in more detail, the sonic boom of the 733-197 for a typical climb Mach number of 1.4, and the cruise Mach number, 2.7. The plots are for a

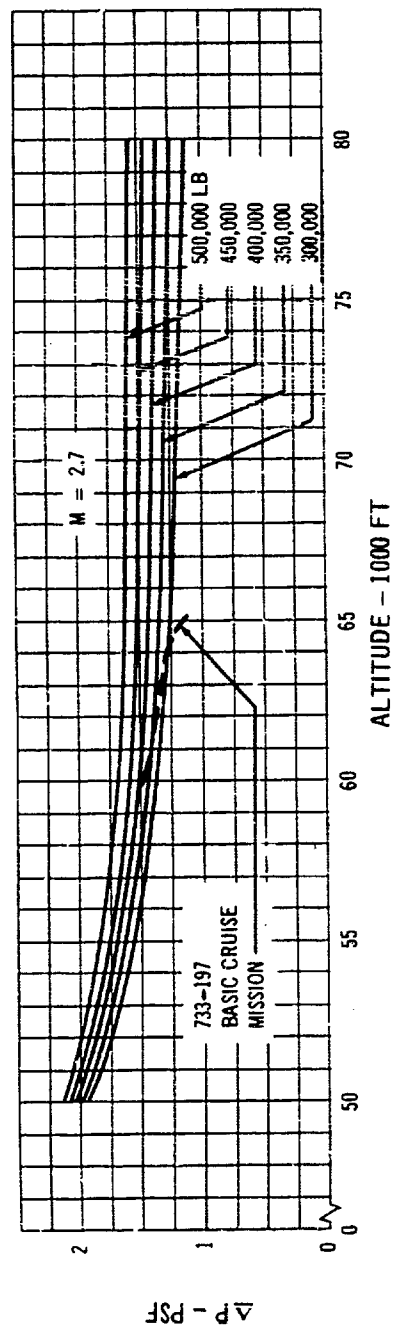
wide range of airplane weights and indicate that, for its basic mission, the airplane does not exceed the levels of 2 psf overpressure in climb and 1.5 psf during cruise. It is seen that such requirements could also be met with substantial increases in the weight of the airplane through small changes in flight altitude.

The relationship of the airplane's sonic boom to the absolute lower bound sonic boom (Ref. 8) is shown in Fig. 6-24. The design of this airplane affords means of approaching this lower bound.

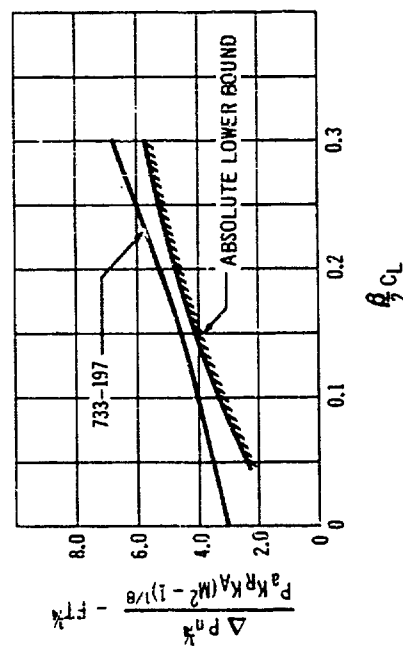
A detailed account describing the methods used and substantiating the results shown is given in Appendix C. Plots of the relevant area and lift distributions as well as plots of the "F(y) functions" for the 733-197 are shown. Comparisons between the analysis method and experiment also are included.



6-22 Sonic Boom at Mach 1.4



6-23 Sonic Boom at Mach 2.7



6-24 733-197 Lower Bound Comparison



SECTION 7

TABLE OF CONTENTS

7.0 STABILITY AND CONTROL	7/1
7.1 Flight Control System	7/1
7.1.1 Longitudinal Controls	7/1
7.1.2 Lateral Controls	7/6
7.1.3 Directional Controls	7/10
7.2 Handling Qualities	7/13
7.2.1 Static and Maneuvering Longitudinal Stability and Control	7/13
7.2.2 Static Directional Stability and Control	7/25
7.2.3 Flight Dynamics	7/26
7.2.3.1 Unaugmented Longitudinal Dynamics	7/29
7.2.3.2 Augmented Longitudinal Dynamics	7/30
7.2.3.3 Unaugmented Lateral-Directional Dynamics	7/34
7.2.3.4 Augmented Lateral-Directional Dynamics	7/37
7.2.3.5 Gain Changing	7/37
7.2.3.6 Lateral Control Characteristics	7/40
7.2.4 Handling Qualities in Case of System Failures	7/41
7.2.4.1 Wing Sweep Failure	7/45
7.2.4.2 Primary Flight Controls	7/45
7.2.4.3 Stability Augmentation	7/46
7.2.4.4 Engine Inlet Shock Expulsion	7/47
D7.0 STABILITY AND CONTROL APPENDIX	
D7.1 Nomenclature	D/1
D7.2 Airplane Geometry	D/4
D7.3 Static Longitudinal Stability and Control Data	D/4
D7.4 Static Lateral-Directional Stability and Control	D/40
D7.5 Engine Inlet Shock Expulsion Data	D/58
D7.6 Dynamic Stability Parameters	D/65

7.0 STABILITY AND CONTROL (RFP 2.7, 2.8.1, 2.8.2, 2.8.3, 2.8.7, 3.2.7.2, 3.2.7.3, 3.2.7.4, 3.2.8, 3.2.11)

7.1 Flight Control System

An exceptional degree of safety and reliability has been designed into the primary flight control system of the Boeing supersonic transport. The system is hydraulic powered and sized to provide ample control power throughout the entire flight envelope. Major emphasis has been placed on system redundancy to ensure safe flight with single or multiple control system failures. All controls have independent, triplicated aerodynamic surfaces, and independent, triplicated hydraulic power systems. This degree of system redundancy combined with the sizing of the segmented control surfaces provides safe flight and landing capability with only one of the three systems operating about any one, or all three, control axes.

The stability augmentation system is dual channel about the pitch and roll axes, and triplicated for yaw damping. However, it should be noted that stability augmentation is not a safety-of-flight consideration. The variable-sweep feature makes stability augmentation unnecessary for all subsonic operation, and only a simple yaw damper will be operating at these conditions to optimize handling qualities. The airplane can be flown quite safely at all supersonic speeds without stability augmentation; and pitch, roll, and yaw damping are required only to provide excellent handling qualities.

A detailed discussion of the flight control systems is contained in Volume A-VII, The Systems Report.

7.1.1 LONGITUDINAL CONTROLS

The longitudinal control system is shown schematically in Fig. 7-1 and a functional block diagram is shown in Fig. 7-2.

Longitudinal stability and aerodynamic balance con-

siderations result in the selection of a conventional horizontal tail configuration for the variable-sweep airplane. Tail sizing and planform selection for the Boeing SST are dictated by the requirement for a satisfactory stability margin for the flexible airplane at the critical maximum Mach number (M_D) condition with a light weight, low-drag tail structure. The selected tail planform provides a stiff structure which permits the use of conventional, but large, elevator control surfaces, and assignment of the trim function to the horizontal stabilizer. A large degree of control redundancy is thus possible through segmenting the elevator into eight independent surfaces backed up by the trimmable stabilizer.

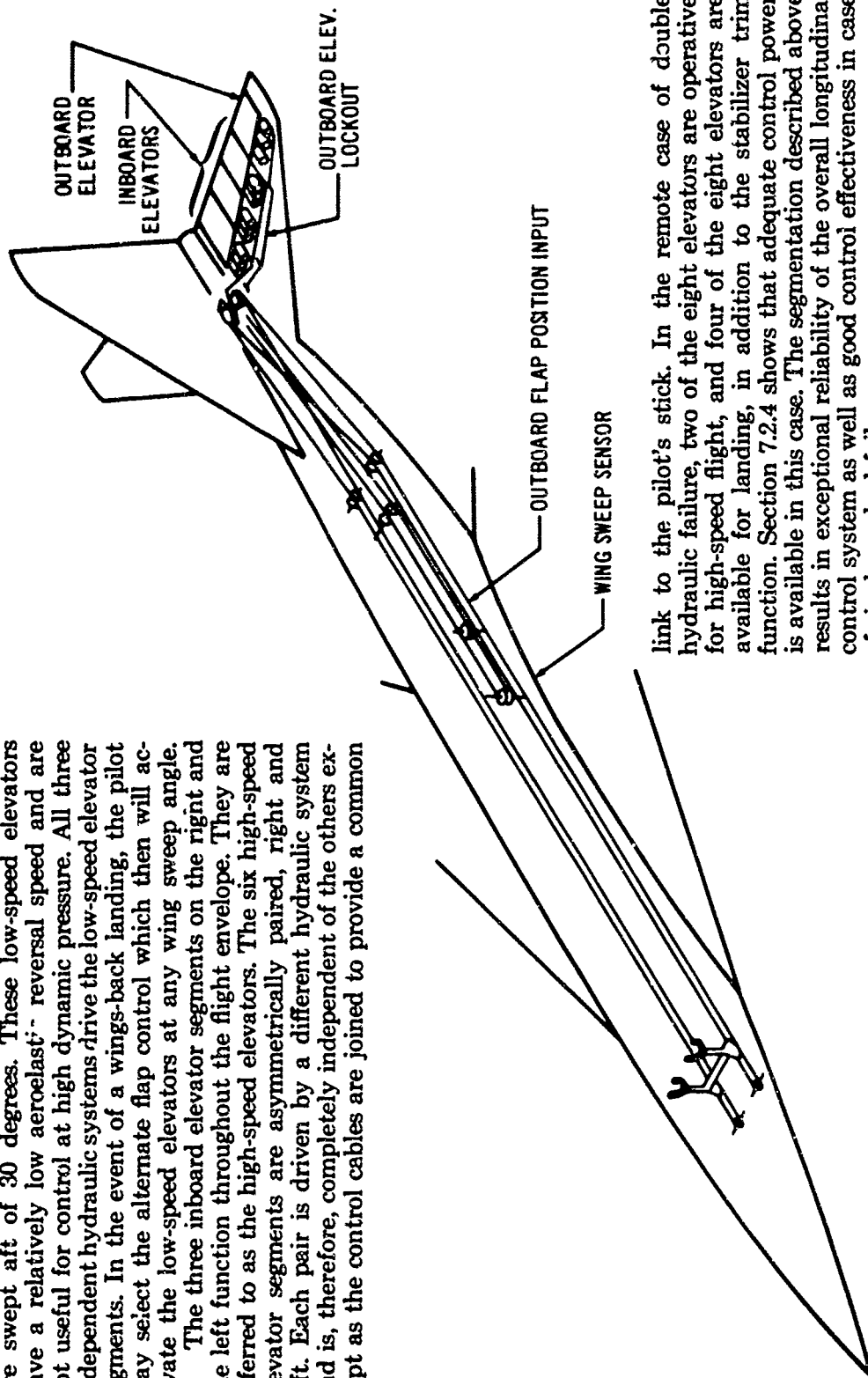
The stabilizer incidence is positioned by a triple-powered, irreversible, hydraulically operated, jackscrew. Trim changing is accomplished with trim switches on the control stick hand grips and with manual longitudinal trim wheels. Fig. 7-3 shows a block diagram of this system. The additional functions of flap trim compensation and wing sweep angle trim compensation could be added to this system with ease if a requirement should develop for these features. At the present time these features are thought to be unnecessary.

The elevators are operated directly from the control sticks and are sized to provide good control power throughout the operating flight envelope. They are capable of maneuvering the airplane to the structural limit load factor or to stall at most flight conditions within the envelope bounded by M_D and V_A . Elevator control power available yields a takeoff rotation speed capability which in no way restricts airplane takeoff performance. In the landing configuration, control power available in excess of trim requirements is sufficient to provide pitch response which is somewhat superior to that of the Boeing 707-320 airplane (See Section 7.2).

The most outboard of the eight elevator segments on the right and the left provide increased pitch control during low-speed flight and become inoperative as the wings

are swept aft of 30 degrees. These low-speed elevators have a relatively low aeroelastic reversal speed and are not useful for control at high dynamic pressure. All three independent hydraulic systems drive the low-speed elevator segments. In the event of a wings-back landing, the pilot may select the alternate flap control which then will activate the low-speed elevators at any wing sweep angle.

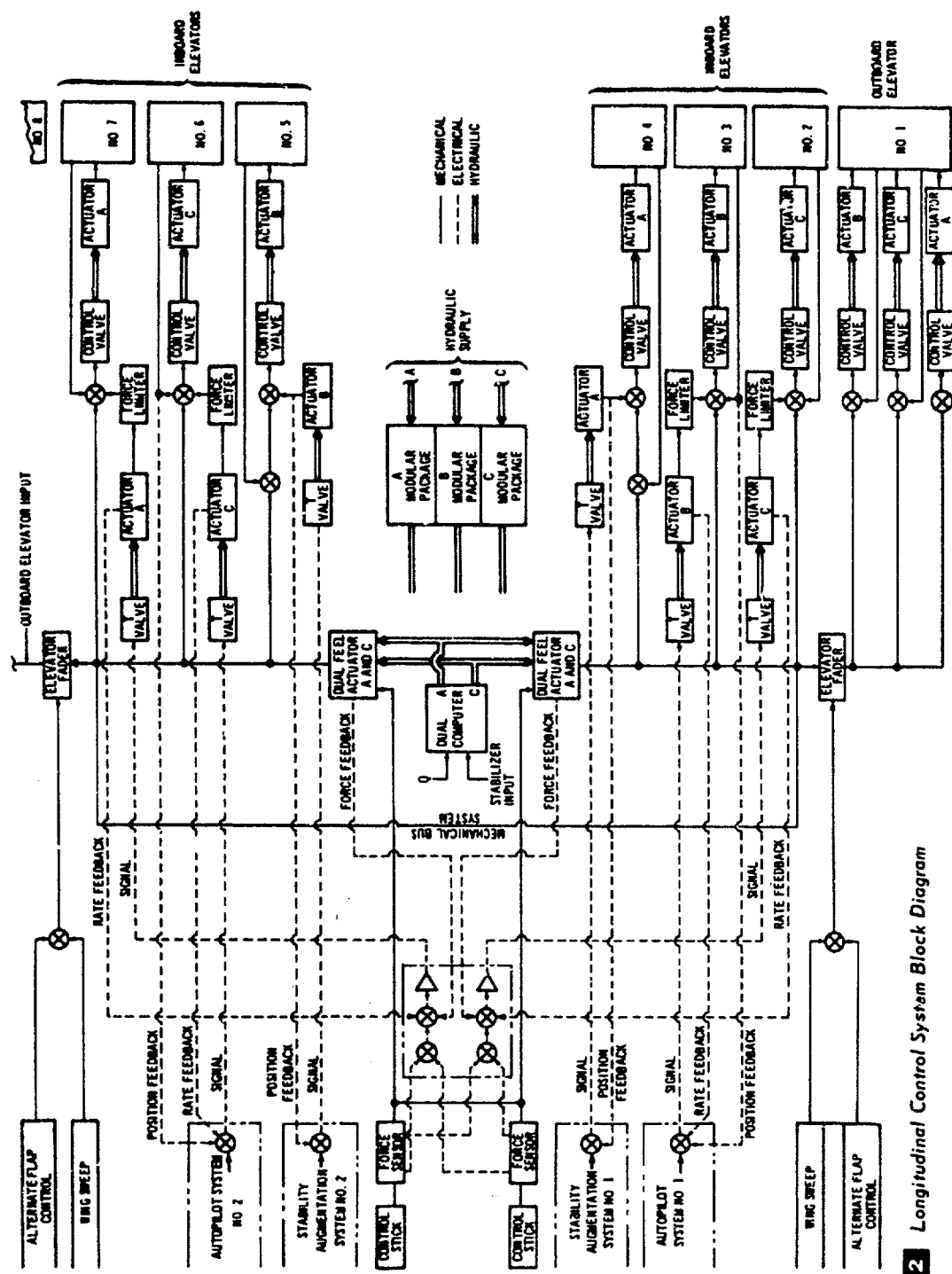
The three inboard elevator segments on the right and the left function throughout the flight envelope. They are referred to as the high-speed elevators. The six high-speed elevator segments are asymmetrically paired, right and left. Each pair is driven by a different hydraulic system and is, therefore, completely independent of the others except as the control cables are joined to provide a common



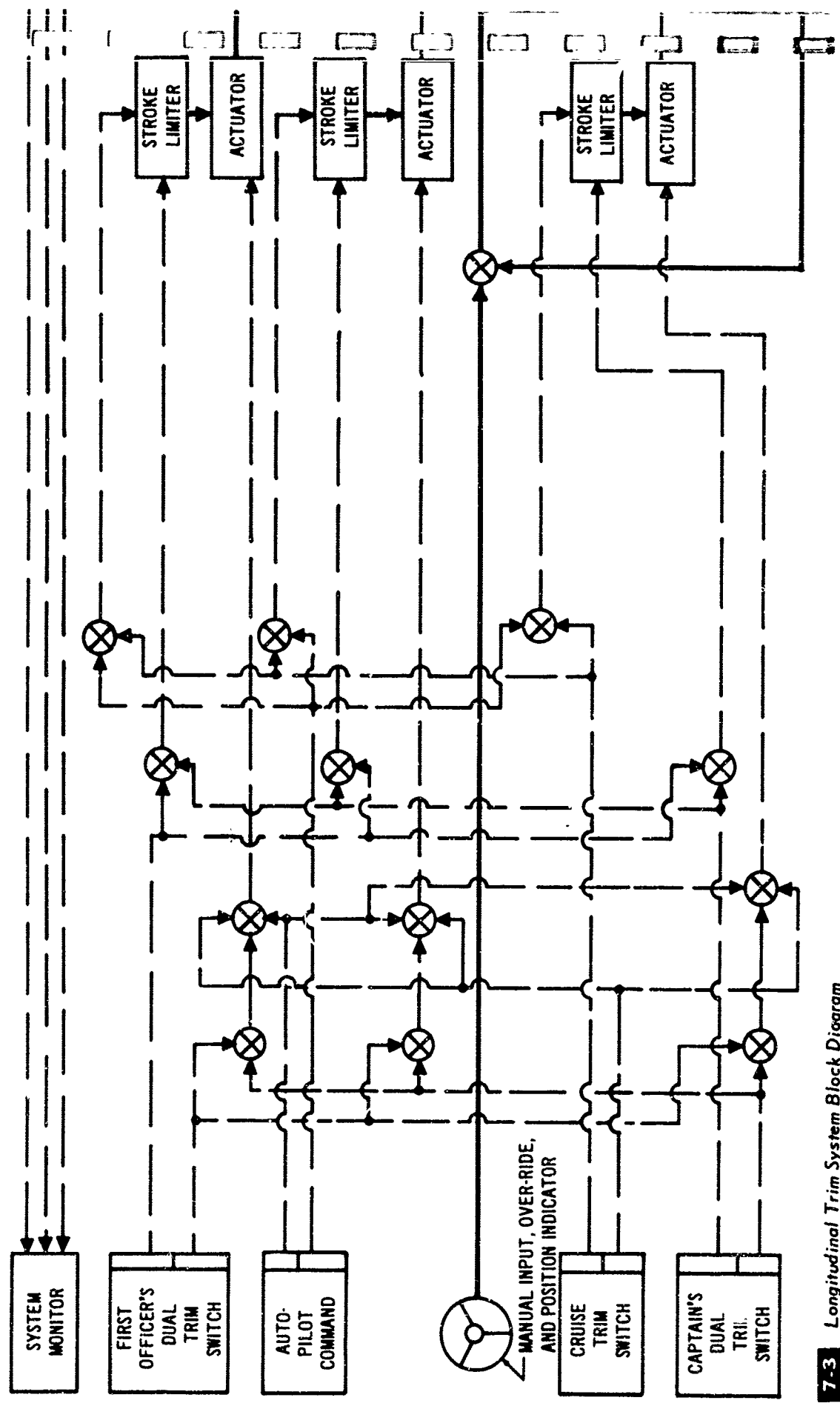
link to the pilot's stick. In the remote case of double hydraulic failure, two of the eight elevators are operative for high-speed flight, and four of the eight elevators are available for landing, in addition to the stabilizer trim function. Section 7.2.4 shows that adequate control power is available in this case. The segmentation described above results in exceptional reliability of the overall longitudinal control system as well as good control effectiveness in case of single or dual failures.

Artificial feel is controlled by a feel computer which responds to stabilizer angle, Mach number, and dynamic pressure. The feel units are located near the elevator power control packages and servos to provide positive centering. Friction and breakout forces are controlled

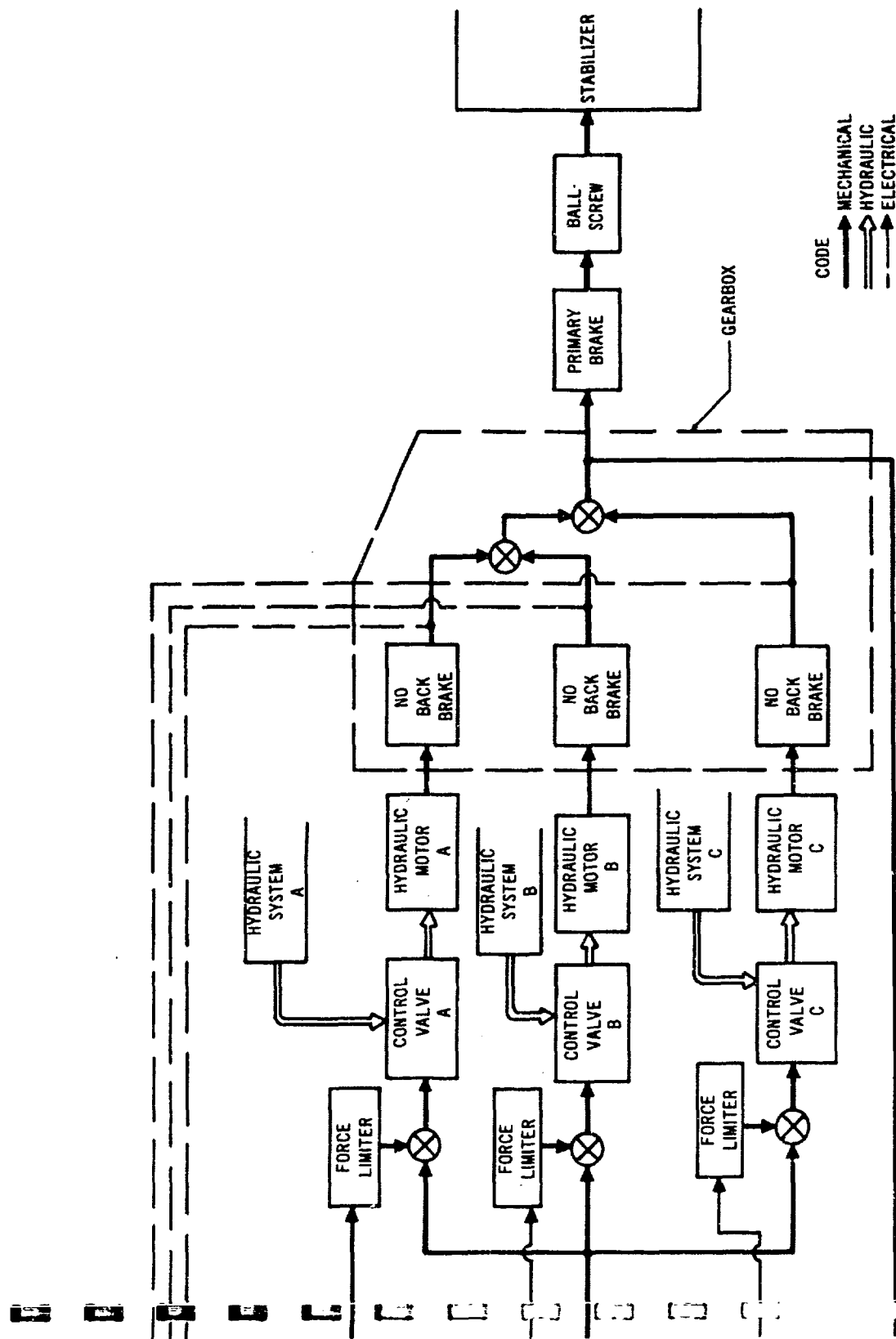
7-1 Longitudinal Control System Schematic Diagram



7-2 Longitudinal Control System Block Diagram



7-3 Longitudinal Trim System Block Diagram



at a low level by means of force sensors on the control sticks which control hydraulic servos on the elevators. In this electrical-command system, the pilot's control forces are artificially maintained at the level determined by the feel computer. A conventional cable system connects the control sticks to the elevator servos and, in the event of failure, the pilot can override the electrical-command system and control the elevator servos manually. This system combines the tailor-made control force qualities of the electrical-command system with the high degree of reliability of a mechanical control system.

The feel system is duplicated. Single mechanical failure halves the control forces felt by the pilot. Single hydraulic failure does not affect pilots' feel. Upon dual hydraulic failure the feel system reverts to a mechanical spring feel.

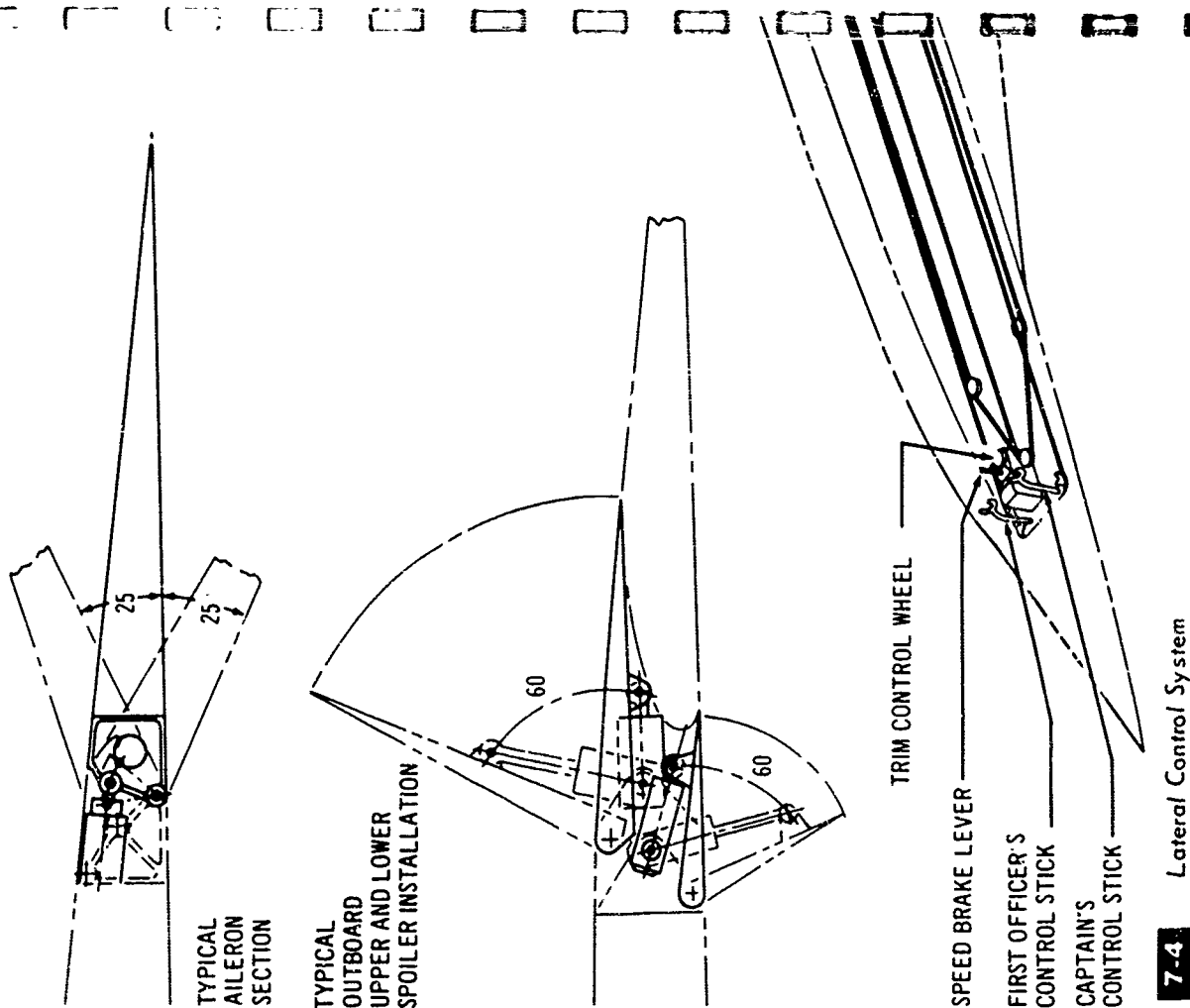
A duplicated stability augmentation system drives the inboard pair of elevators in series with the pilot's commands. The duplicated autopilot signals are added in parallel so that the stick moves in response to auto-pilot signals.

7.1.2 LATERAL CONTROLS

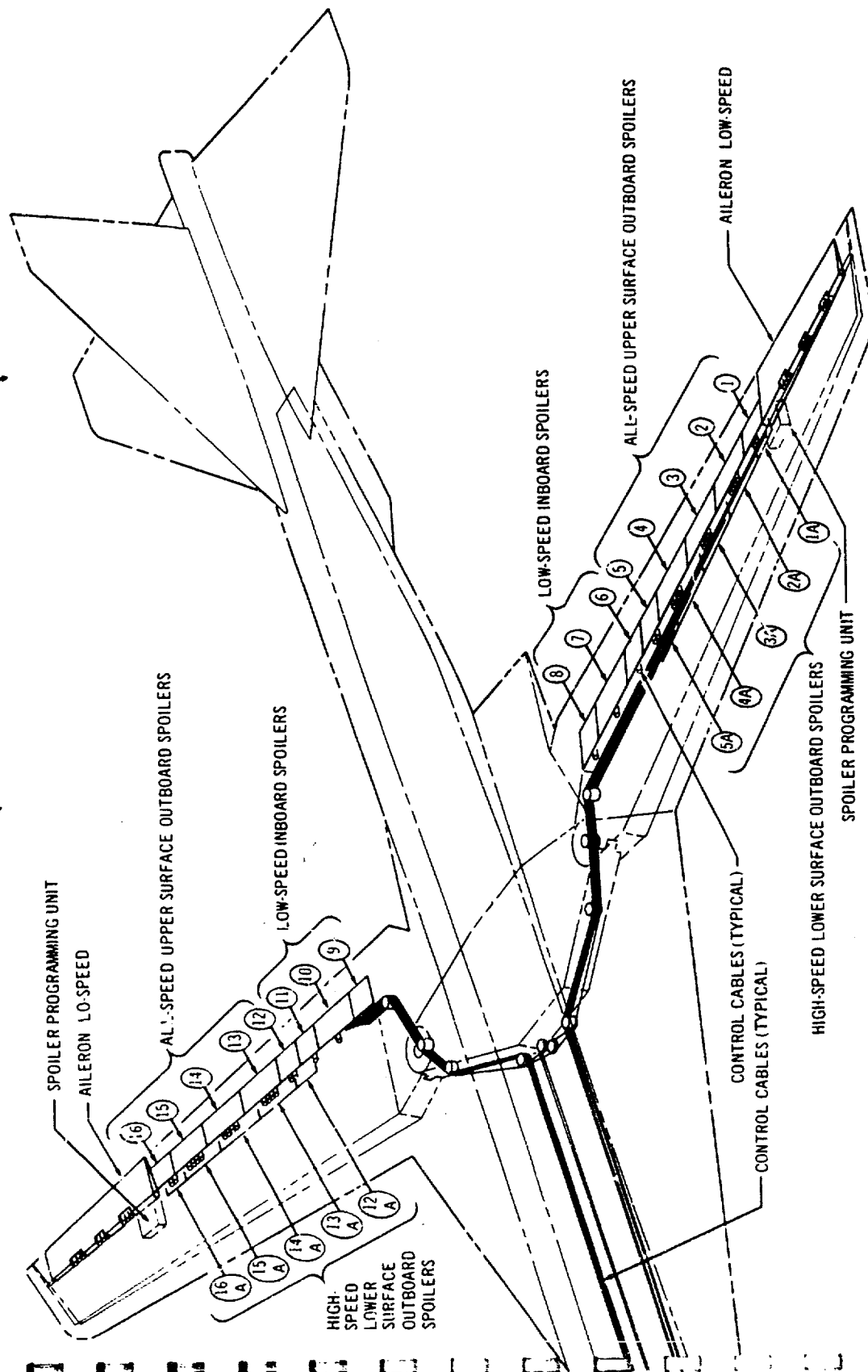
The lateral control system is shown schematically in Fig. 7-4, and in block diagram in Fig. 7-5.

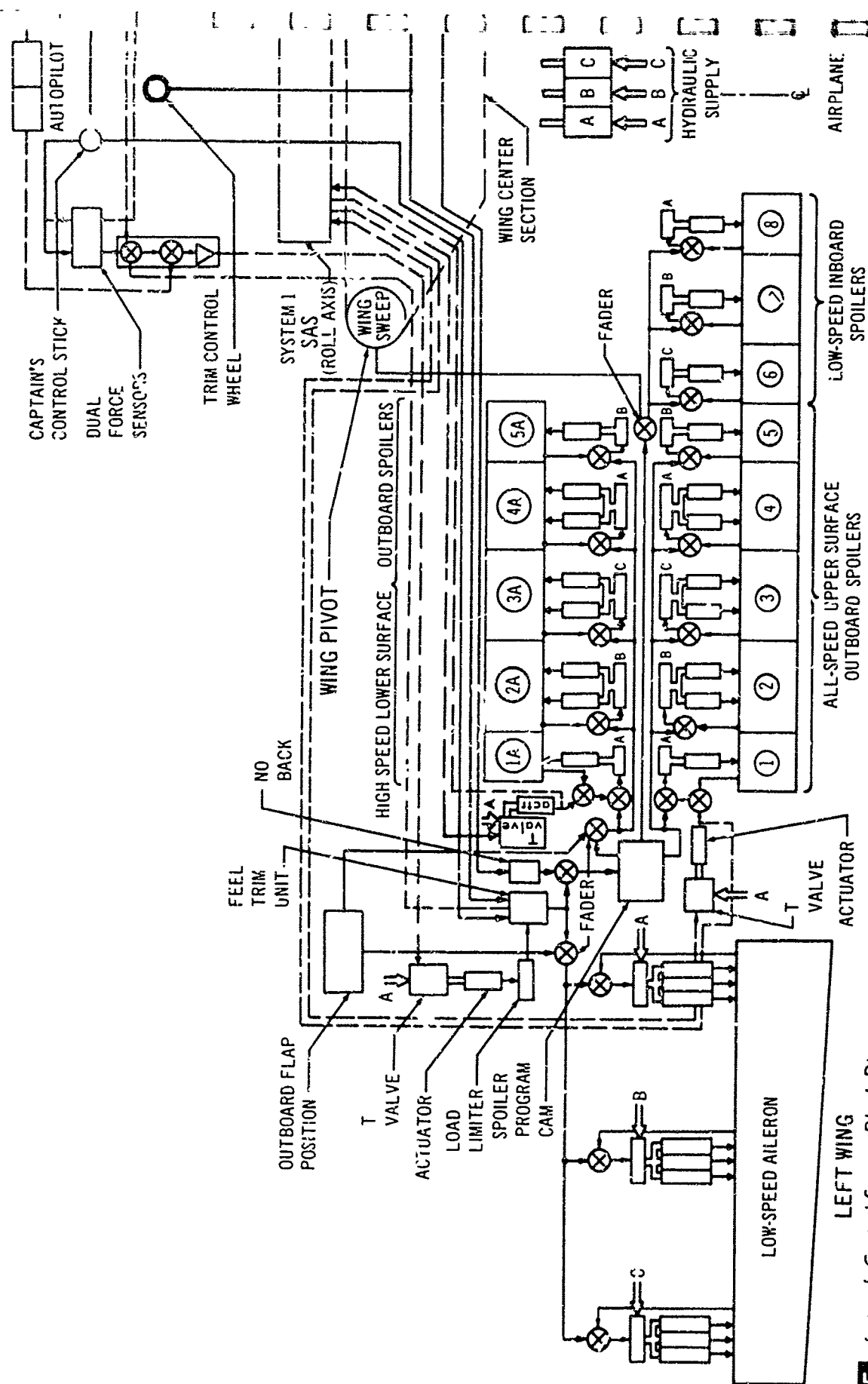
Lateral control is provided by a combination of multi-segment wing spoilers and outboard trailing-edge ailerons. During low-speed flight with wings forward of 30 degrees all upper-wing-surface spoilers and the ailerons operate. As the wings sweep aft, the inboard spoilers become inoperative. The ailerons, due to their outboard location, have a low aeroelastic reversal speed and are, therefore, locked at neutral when the wing flaps fully retract. This is the case for sweep angles larger than 30 degrees.

The wing upper-surface outboard spoilers function throughout the flight envelope. When the trailing edge flaps are up, these spoilers are augmented by wing lower-

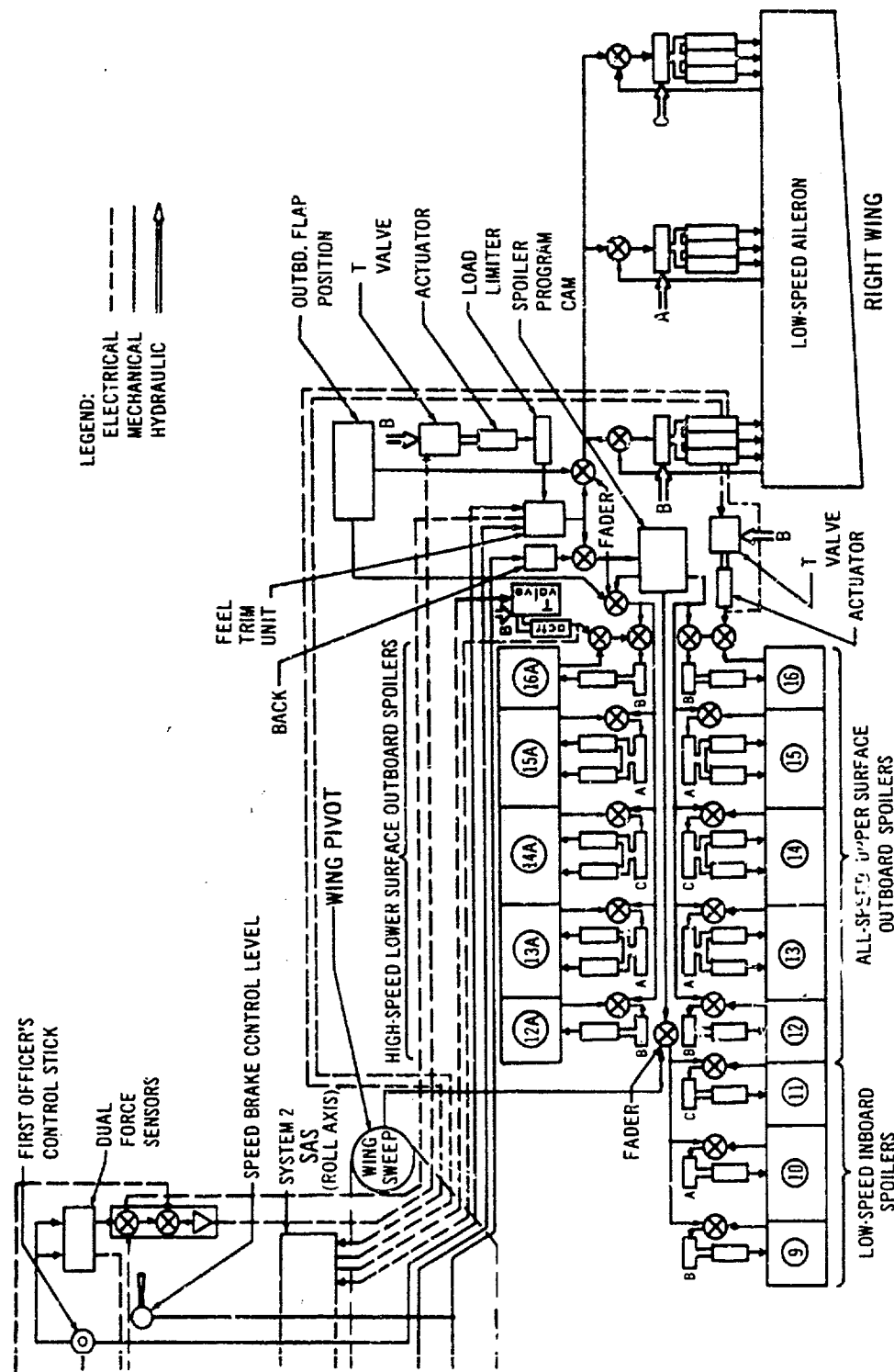


7-4 Lateral Control System





7-5 Lateral Control System Block Diagram



surface spoilers that not only serve to increase roll authority during high-speed flight but also reduce yaw-due-to-lateral-control to a very low value, thereby improving high-speed roll coordination and reducing Dutch roll excitation from this source. In addition, they reduce pitch interactions introduced by the upper spoilers.

The high-speed part of the lateral control system is sized to yield a roll rate of at least 30 degrees per second within the normal flight envelope. The low-speed part is sized to provide excellent roll control in the approach configuration using a minimum bank angle of 10 degrees in one second as a design criterion. The system as proposed yields good lateral control over the angle of attack and Mach number range.

The proposed system has several advantages over alternatives, such as the rolling-stabilizer concept. The latter results in undesirable yaw-to-roll ratios due to lateral control, similar to the problems posed by elevon controls on tailless airplanes. Also, the rolling-tail presents serious reliability problems because of its integration with the longitudinal control system.

In the event of a wings-back landing, the pilot will be able to select the alternate flap control which then will activate the ailerons at any wing sweep angle. The lower surface spoilers (normally operative when the wings are aft of 30 degrees) become inoperative when flaps are extended. It is recommended that the pilot shut off the roll damper in this case.

The lateral control feel units are located in the wings in order to have a short path between the control valves and the centering signal. Friction and breakout force are controlled, as in the longitudinal axis, by means of control stick force sensors and actuators in the wings. The dynamic stick forces are thereby maintained at an optimum level. A conventional cable system continuously maintains a mechanical connection between the control stick and the hydraulic servos on the surfaces and allows the pilot to override the electrical-command system in emergencies.

A duplicated stability augmentation system operates in series with the pilot's commands to actuate the outermost upper-surface, and lower-surface spoiler panels. The duplicated autopilot operates the lateral control surfaces in parallel with pilot inputs through the electrical-command system, in order to have sufficient authority in all conditions of flight.

Lateral trim is provided by a mechanical system with a control wheel in the cockpit which controls the null position of the spring feel units in each wing.

The lateral control system is highly redundant with triple independent hydraulic systems and duplicated autopilot and stability augmentation. Adequate control power is available in the remote case of double hydraulic failure. This is shown in Section 7.2.4.

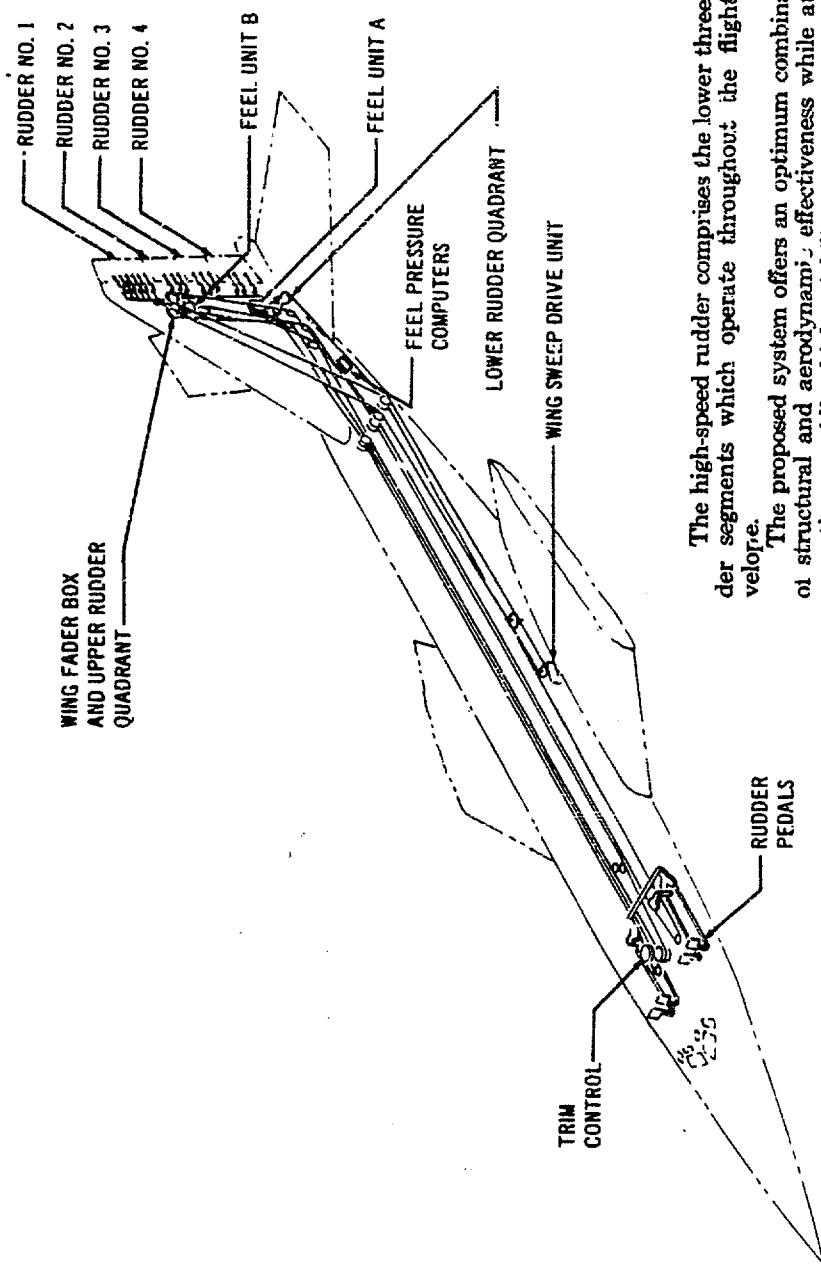
7.1.3 DIRECTIONAL CONTROLS

The directional control system schematic is shown on Fig. 7-6 and its block diagram appears on Fig. 7-7.

A conventional fixed vertical fin provides directional stability and is augmented by a ventral fin for maintaining stability at high angle of attack at high Mach numbers. Four trailing-edge rudders provide directional control and trim.

Vertical and ventral tail surfaces are sized in combination to yield a satisfactory level of directional stability at the highest angle of attack attainable at the most critical maximum Mach number condition. Rudder size is governed by the requirement to be able to land under crosswind conditions of 30 knots at 90 degrees, as well as to control engine-out conditions.

The operation of the four independent rudder segments is scheduled to maintain a high level of control throughout the large flight envelope of this airplane. The top segment, the low-speed rudder, provides increased directional control during low-speed flight. It is locked when the wings sweep aft of 30 degrees because of its poor effectiveness due to aeroelastic reversal at high speed.



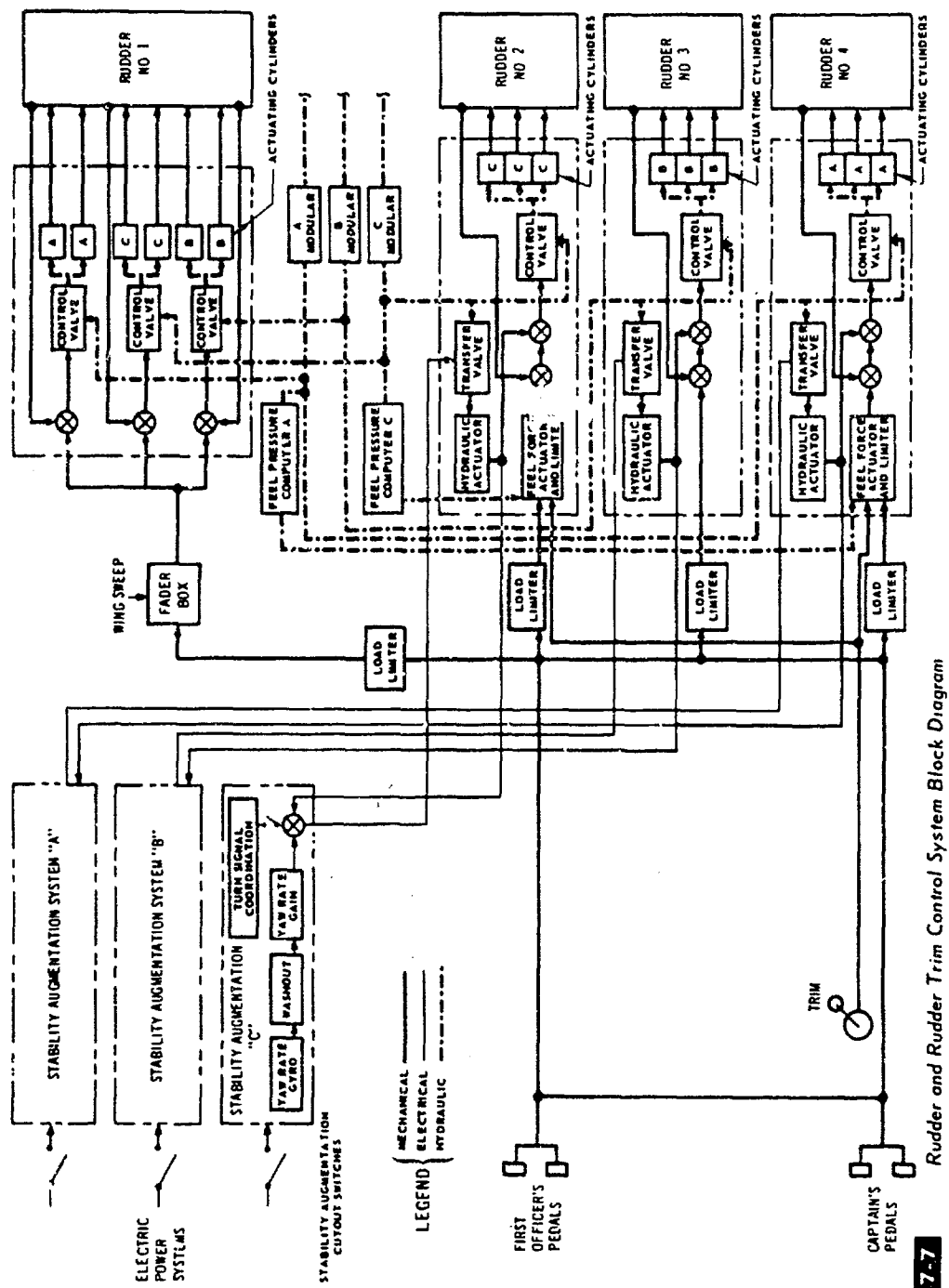
The high-speed rudder comprises the lower three rudder segments which operate throughout the flight envelope.

The proposed system offers an optimum combination of structural and aerodynamic effectiveness while at the same time providing high reliability.

The feel system includes a deflection restraint responding to dynamic pressure which serves to limit deflection at high speed for structural reasons.

The rudder actuator hydraulic servos are connected directly to the rudder pedals with the only interruption

7-6 Directional Control System



Rudder and Rudder Trim Control System Block Diagram

caused by the mechanical low-speed rudder fader which is driven by a signal derived from wing sweep angle.

Because of the desirability of Dutch roll damping during cruise and during a wings-back landing, the directional stability augmentation system is triply redundant. Three independent, series-connected stability augmentation systems drive the three high-speed rudders, so that each of the damper-rudder combinations is electrically, mechanically, and hydraulically independent of the others.

The autopilot does not have a mode requiring rudder deflection.

In the remote case of double hydraulic failure, two of the four rudders still remain in operation at low speed, and one remains operable at high speed. Section 7.2.4 shows that adequate control power is available in this case.

7.2 Handling Qualities

The Boeing variable-sweep SST will provide handling qualities which are similar or superior to those of current jet transports. This is largely attributable to the excellent stability and the control characteristics inherent in the variable-sweep design. This feature avoids the many design compromises to stability and control enforced by a fixed-wing concept optimized for supersonic cruise. The low-wing-sweep, high-aspect-ratio configurations available for subsonic operation provide good handling qualities without the need for stability augmentation. Only a simple yaw damper is required to provide the pilot precise flight path control. The structural flexibility characteristics of the arrow wing counter the effects of sweep transition and Mach number, resulting in extremely small changes in static margin and trim during the design mission. No fuel pumping nor geometry changes are necessary to maintain safe stability margins anywhere in the flight envelope, either for normal or emergency descent operations. An added benefit of the flexible arrow wing is the relieving effect it has on the problem of load factor

sensitivity to small attitude perturbations incurred with operation in the high-altitude, high-air-speed, SST environment. As a result the airplane is safely controllable in supersonic flight with no stability augmentation. A three-axis augmentation system is provided to minimize pilot work load and to ensure passenger comfort. Augmentation gain is a simple function of wing sweep, without requiring an air data system.

Tail sizes and structural stiffness requirements for satisfactory stability margins at maximum dive Mach number conditions permit the use of conventional, but large, elevator and rudder control surfaces. These powerful surfaces place in the pilot's hands greater control authority, regardless of flight condition, than is the current standard. This control authority is matched in the lateral axis by employment of ailerons and large, multi-segmented upper and lower wing spoilers. The combination of triplicated, independent aerodynamic surfaces and triplicated, independent hydraulic power systems provides a level of safety and reliability superior to that of current jet transports.

7.2.1 STATIC AND MANEUVERING LONGITUDINAL STABILITY AND CONTROL

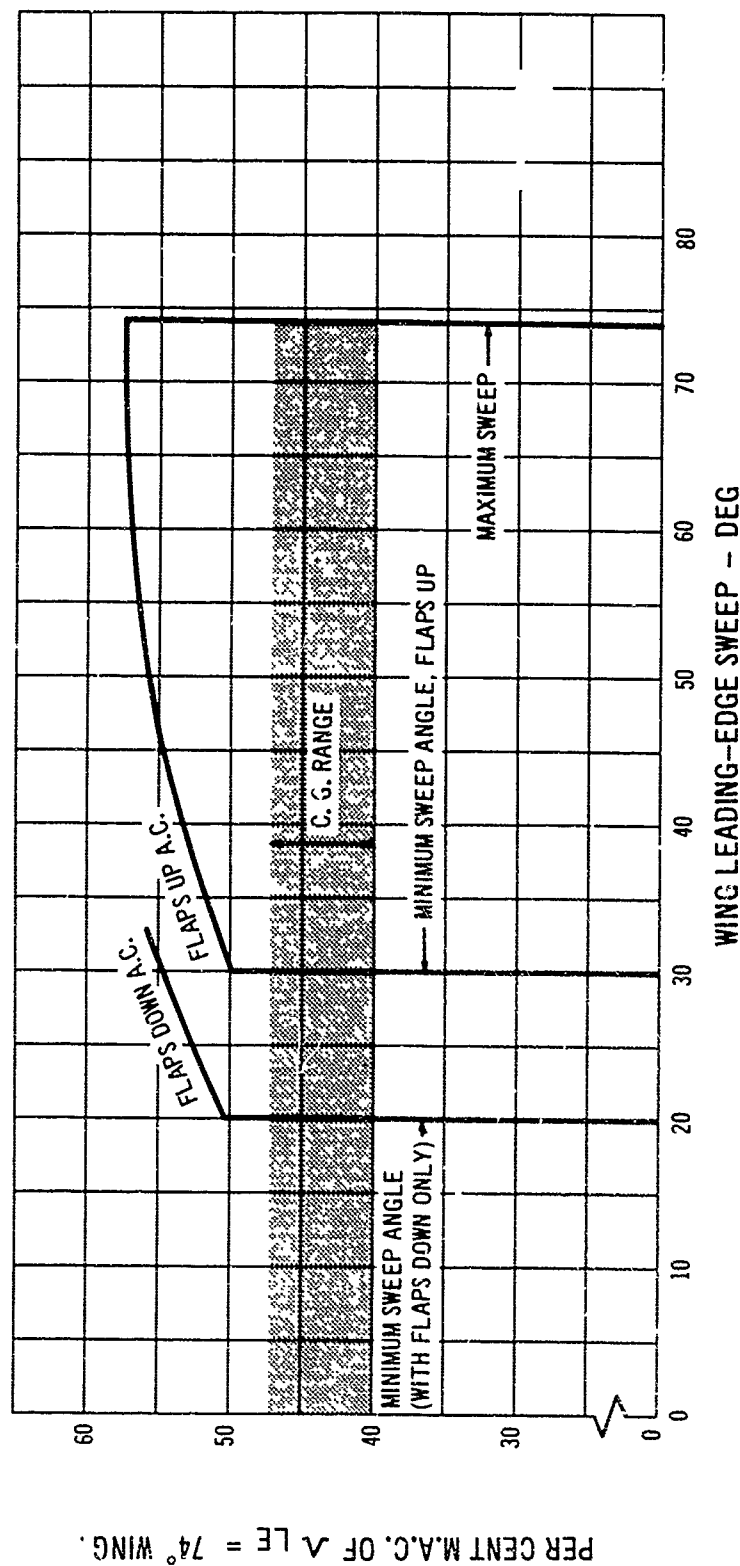
The proposal airplane provides good stability and control characteristics over the entire operating range of sweep angle, Mach number, altitude, and angle of attack. The configuration has no pitch-up tendencies anywhere in the flight envelope, including angles of attack through and well beyond the stall, and experiences no significant nonlinearities in static stability characteristics. These excellent flight characteristics are the result of extensive variable-sweep research conducted by The Boeing Company over the past several years. Wind tunnel test substantiation data and a detailed discussion of the stability and control development are presented in Par. D7.3 of the Appendix.

7.2.1.1 Stability

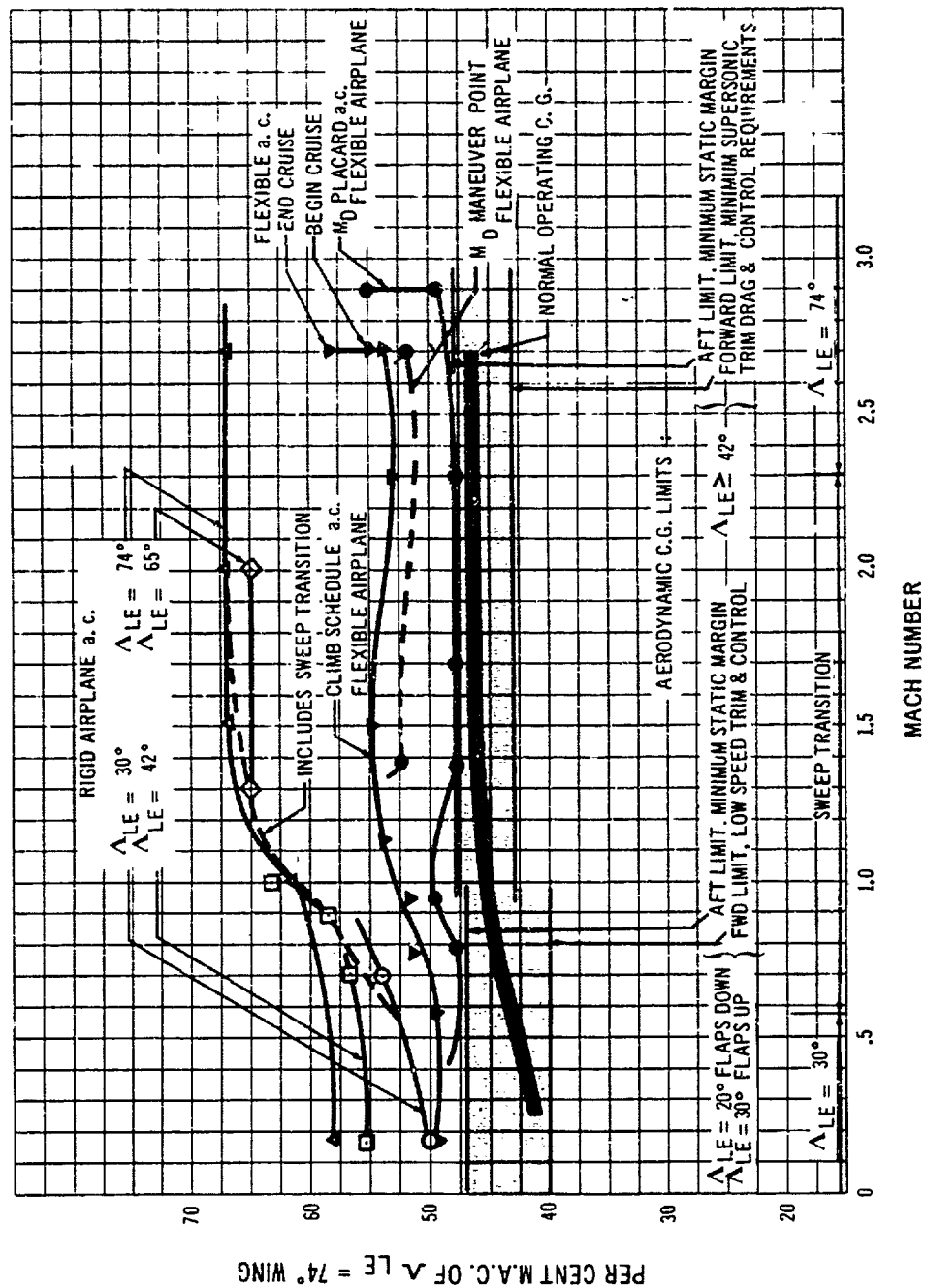
Figs 7-8 and 7-9 present a comprehensive summary of the aerodynamic center (a.c.) and center-of-gravity relationships throughout the flight envelope. The effects of wing sweep and flap position on a.c. (or static neutral point) are shown in Fig. 7-8 for the rigid airplane at low speed. The flaps-up neutral point moves aft from 50 percent m.a.c. to 58 percent m.a.c. as the wings are swept from the minimum flaps-up sweep angle, 30 degrees, to

the maximum 74 degree sweep angle. The reference m.a.c. is that of the 74 degree sweep wing. Lowering the wing flaps moves the neutral point back 5 percent m.a.c. and permits a further reduction in sweep angle to 20 degrees, for improved takeoff and landing performance.

Fig. 7-9 shows static neutral point variation with wing sweep angle and Mach number for the rigid airplane as obtained from wind tunnel test data (see Appendix D7.3). Also shown is the flexible airplane neutral point variation with Mach number and sweep transition along



7-8 Variation of Aerodynamic Center with Wing Sweep, Low Speed



7-9 Aerodynamic Center and Center of Gravity Relationships, Complete Airplane

the climb schedule, during cruise, and at maximum dive Mach number conditions. It is readily apparent that, *when aeroelastic effects are neglected*, large transitions in aerodynamic center occur with the compounding of sweep change and Mach effects. However, *when aeroelastic effects are applied to the rigid test data*, it is seen that the flexible airplane static neutral point variations are reduced to extremely small values. This is simply due to the fact that the high structural-aspect ratio arrow wing is quite flexible, and the incremental aerodynamic center shift forward caused by wing flexure overcompensates for the aft a.c. shift with increasing wing sweep. Figs. D7-22, thru-25 in Appendix D7.3 detail the magnitude of the aeroelastic a.c. shifts on the wing with Mach number and altitude for several wing sweeps.

The aft center-of-gravity limits have been selected for the proposal airplane by a careful matching of the most critical flight conditions from the standpoint of static stability margin. These conditions are: (1) low-speed operation with minimum wing sweep position (desired for good low-speed, flaps-down, and flaps-up performance), and (2) maximum dive Mach numbers where aeroelastic effects shift the neutral point forward. The horizontal tail is structurally designed and sized to provide zero-static margin at the most critical M_D conditions with the most aft center-of-gravity limit attainable, consistent with maintaining a $2\frac{1}{2}$ percent static margin at the desired minimum wing sweep angle of 30 degrees flaps up, and 20 degrees flaps down. The selection of zero static margin at M_D is considered reasonably conservative since sufficient positive maneuvering stability is retained with positive maneuver margins of 3 percent or better as shown in Fig. 7-9. Maneuver points are calculated for various flight conditions using the information presented in Fig. D7-34 in Appendix D7.3.

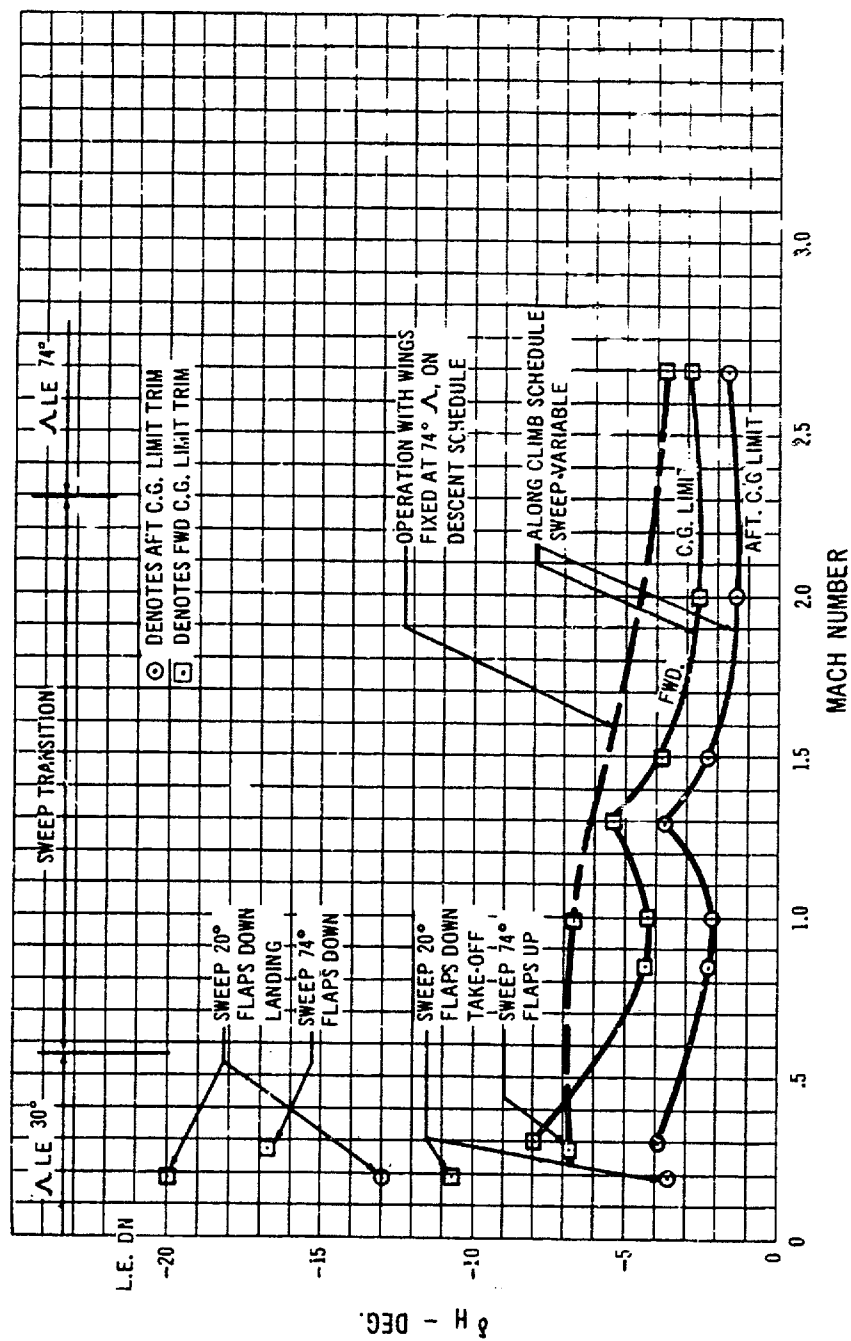
The most aft CG limit possible is desired to permit locating the wing on the body as far forward as possible in order to minimize tail sizes and trim drag, and to min-

imize the forebody length with its associated weight and stability penalties.

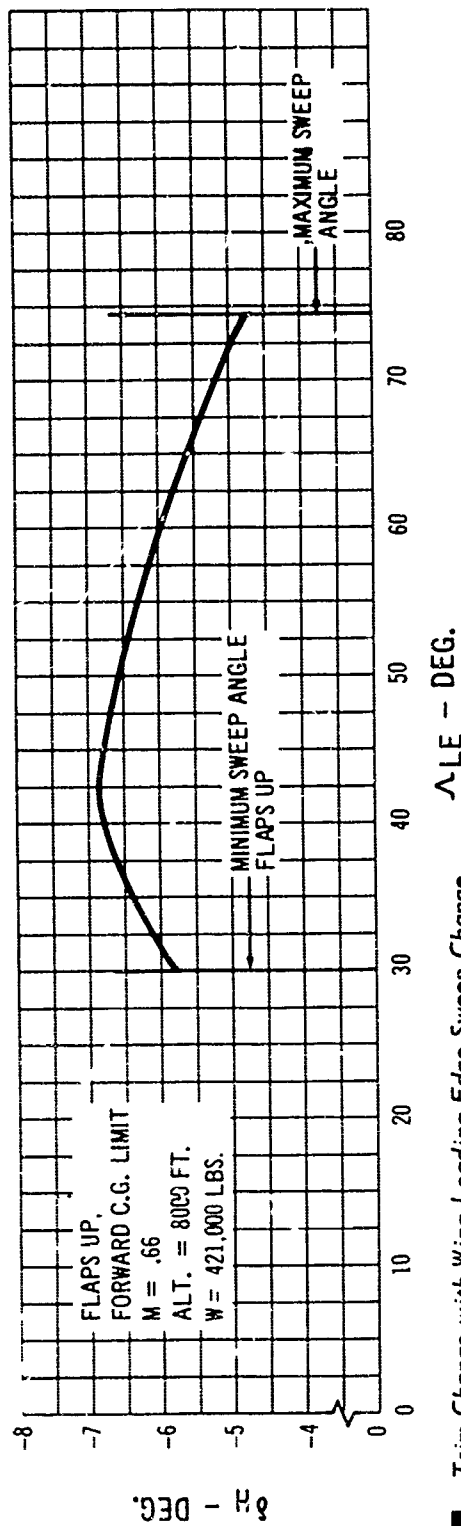
The aerodynamic aft CG and forward CG limits, as shown in Fig. 7-9, for the 733-197 are 47 percent m.a.c. and 40 percent m.a.c. for low speed, low wing sweep operation, and 48 percent m.a.c. and 43 percent m.a.c. for wing sweeps of 42 degrees to 74 degrees. It must be emphasized that the operational CG limits, as defined in Fig. 16-13 of Volume A-IV, The Structures Report, are in all cases within the aerodynamic limits. Therefore, all data which are functions of these aerodynamic limits, such as stability margins, stabilizer trim angles, and elevator per g, are conservative values. No fuel pumping or restrictive wing sweep procedures are necessary to maintain safe stability margins anywhere in the flight envelope, either for normal operations or for emergency operations, such as emergency descent or failure of wing sweep mechanism. Fuel programming is provided only to maintain nearly constant static margins or eliminate trim drag and trim changes.

The range of stabilizer deflections required to trim steady flight conditions throughout the normal mission of the airplane is shown in Fig. 7-10 for forward and aft CG limits. It is seen that the effects of wing sweep, transonic trim shift, and aeroelastic deformations produce very small and gradual changes in trim. As in the case of current jet transports, the largest trim changes occur during flap cycling. Due to the moderate trim variations, neither automatic flap trim compensation nor automatic wing sweep compensation is provided. (The trim system could readily accept these signals if such complexity were necessary.)

Fig. 7-10 also shows the stabilizer angle required for trim when flying the descent placard and landing with the wings fixed at 74 degrees sweep. As previously discussed, no special operating procedures are required, and the trim changes with Mach number are seen to be extremely small.



7-10 (A-V) Stabilizer Angle Required to Trim, Flexible Airplane



7-11 Trim Change with Wing Leading Edge Sweep Change

The longitudinal trim change with wing sweep actualion while holding speed constant is shown in Fig. 7-11. The condition shown is 0.66 Mach number at 8000 feet with the airplane loaded to the forward CG limit at a high gross weight. As the wings sweep aft from 30 degrees, a one degree increase in airplane nose-up trim is required up to 42 degrees of wing sweep; beyond this sweep angle decreasing nose-up trim is required until, at maximum wing sweep (74 degrees), the stabilizer trim angle required is one degree less than that required at 30-degrees sweep. This extremely small trim change and slight reversal in trim direction result from the fact that wing aeroelastic characteristics counter the aft aerodynamic center shift with sweep.

Figs. 7-12 through 7-15 show stick-fixed stability characteristics at forward and aft CG limits at several flight conditions. Elevator versus speed was calculated from the basic longitudinal stability wind tunnel test data and the aeroelastic effects presented in Par. D7.3 of the Appendix. Fig. 7-12 shows good static stability up to

stall initiation for the normal landing configuration with flaps full down, wing sweep at 20 degrees. Wind tunnel testing has shown that the actual stall characteristics are quite similar to those of 707 airplanes. This is shown graphically in the stability data presented in Fig. D7-6 in the Appendix.

Static longitudinal stability characteristics for a low-speed, flaps-up, 30-degree wing sweep condition are shown in Fig. 7-13 with the airplane trimmed at 1.3 Vs. A reversal in elevator gradient is seen to occur as the stall is approached. Since the effective stall speed is considerably above the minimum speed attainable in flight for this configuration, (unlike the flaps-down case previously discussed), elevator to hold 1-g flight is shown down to speeds well below the effective stall speed. At speeds below stall, the elevator gradient is seen to break strongly stable. The effective stall speed for this configuration is discussed in Appendix D7.3. This speed corresponds to the lift coefficient at which the 30-degree-sweep wing stalls. At this attitude, which is a typical stall angle of attack for con-

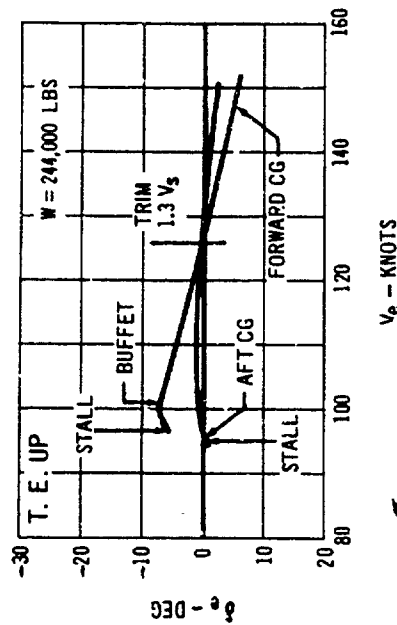
ventional wings of this sweep and aspect ratio, the airplane will be in heavy buffet. As the angle of attack is increased beyond this point, the wing strike will continue to produce higher lift, and, as shown in Fig. 7-13, the airplane will become increasingly more stable. Lower speeds will be attainable with increasing pull forces by the pilot. The above discussed characteristics are not considered to present a serious problem, since the airplane develops strong pitch-down tendencies as the angle of attack is increased beyond the stall. The moderate reversal in elevator gradient entering the stall can either be masked by providing stable stick force gradients with the control feel system, or can be eliminated completely with minor configuration modifications. An increase in tail aspect ratio, for example, is seen to remove almost completely the pitch excursion during the stall (Figs. 7-13 and D7-8). This and other configuration improvements will be investigated in further wind tunnel testing.

Fig. 7-14 shows elevator versus speed characteristics for the airplane trimmed at 2.7 Mach number at 64,000 feet. Elevator gradients are seen to be stable and essentially linear.

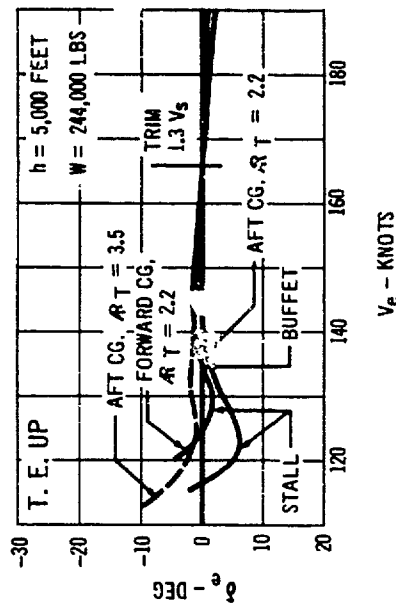
Static stability in the wings-aft landing condition is shown in Fig. 7-15 for the airplane trimmed at the approach speed of 180 knots. Elevator versus speed gradients are strongly stable and nearly linear.

7.2.1.2 Elevator Control Power

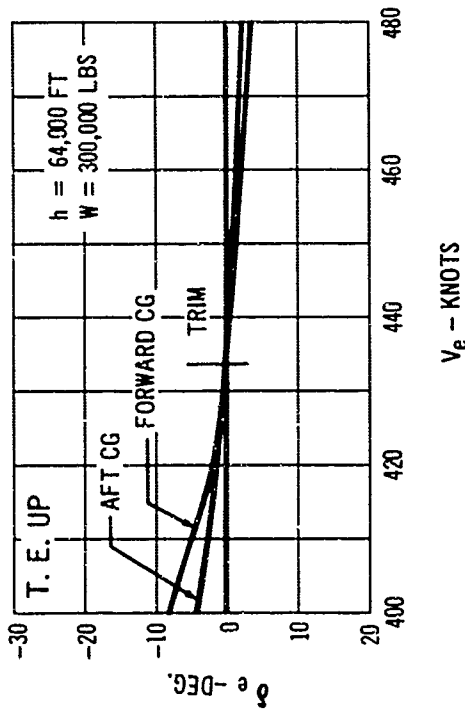
The large, 8-segment elevators provide a powerful longitudinal control system giving the airplane greater maneuver capability and responsiveness than is currently experienced in jet transports. The maneuvering power provided by the elevator is shown in Fig. 7-16 in the plots of elevator angle required-per-g versus Mach number. Elevator-per-g is shown along the climb and descent schedules, and on the dive, and V_A placards. The maximum load factor attainable may be determined



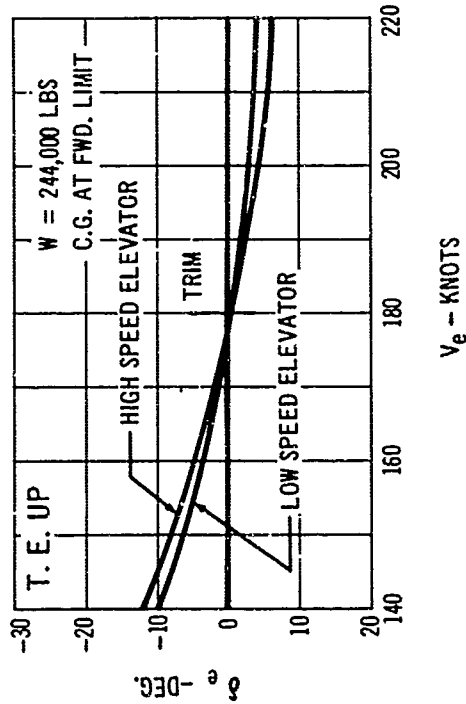
7-12 Static Longitudinal Stability, Landing Configuration



7-13 Static Longitudinal Stability, $\Delta LE = 30^\circ$
Flaps - Up, Low Speed



7-14 Static Longitudinal Stability, Mach = 2.7 Cruise



7-15 Static Longitudinal Stability, Wings - Aft Landing

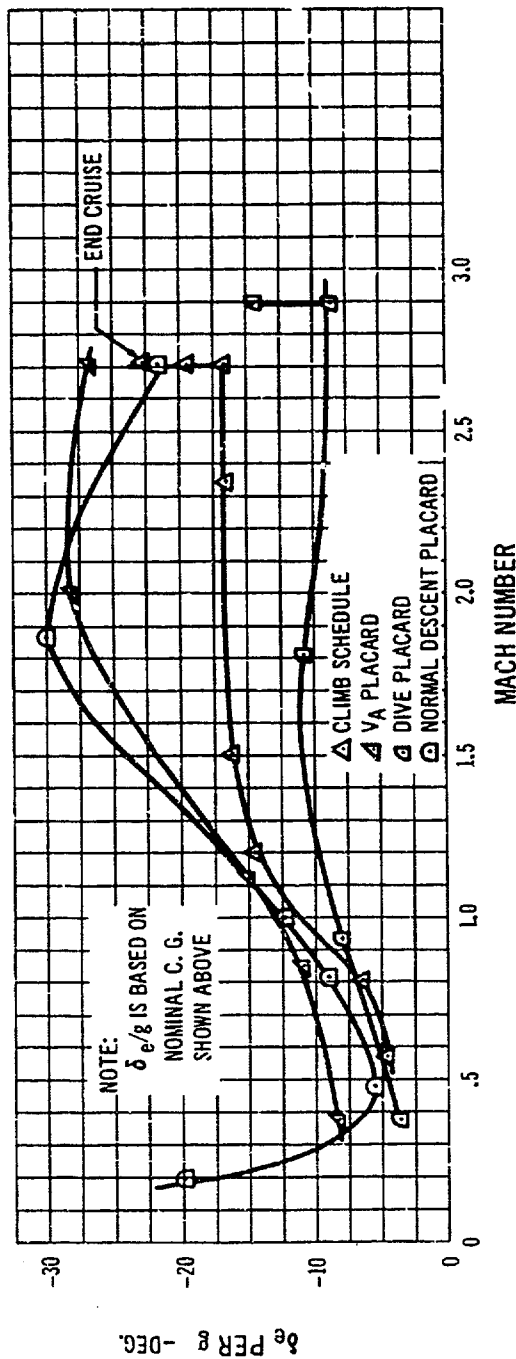
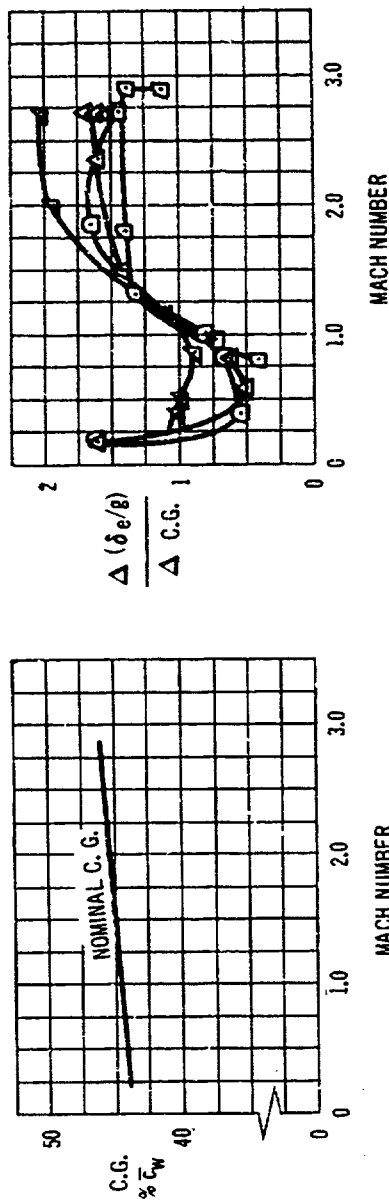
the use of this figure together with Fig. 7-17 which shows the maximum elevator angle available at various flight conditions. It is seen, for example, that at M_D at 1.5 Mach number, 11 degrees of elevator deflection will produce 1-g normal acceleration from trim. The 17.5 degrees of elevator deflection available at this condition (Fig. 7-17) will thus yield a maneuver capability of 17.5/11 or 1.6 g's from trim; providing a total load factor of 2.6 g's.

The takeoff rotation capability provided by the elevators is shown in Figs. 7-18, 7-19, and 7-20. The rotation analysis was made for the airplane loaded to the most forward CG attainable at the maximum and minimum possible gross weights, and with one engine out. The analysis shows that the takeoff rotation capability of the elevator is more than adequate to qualify the airplane for the 1.08 V_{MU} minimum permissible liftoff speed for geometry-limited airplanes. The proposal configuration is seen to provide rapid rotation capability, approximately 2.4 seconds, and to meet easily the requirement to be tail-dragged at .96 V_{MU} for the V_{MU} demonstration test.

Fig. 7-21 shows the elevator deflection required to counter the pitching moment due to flap cycling when the stabilizer trim is inoperative. Approximately half of the 30 degrees of full elevator deflection available is required to trim out the flap moments for either a flap retraction or flap extension.

Sufficient elevator control power must be provided to give the pilot the capability to flare the airplane quickly during landing. This is necessary for rapid recovery from gust upsets or other conditions which place the airplane in danger of contacting the runway at excessive nose-down attitudes or sink rates. Current transports inherit fairly good flare capabilities from meeting the control system design requirement to stall the airplane at the most critical forward CG loading condition. SST configurations, however, inherently tend to possess considerably greater inertia about the pitch axis, and will suffer in control response unless care is exercised in the design. The

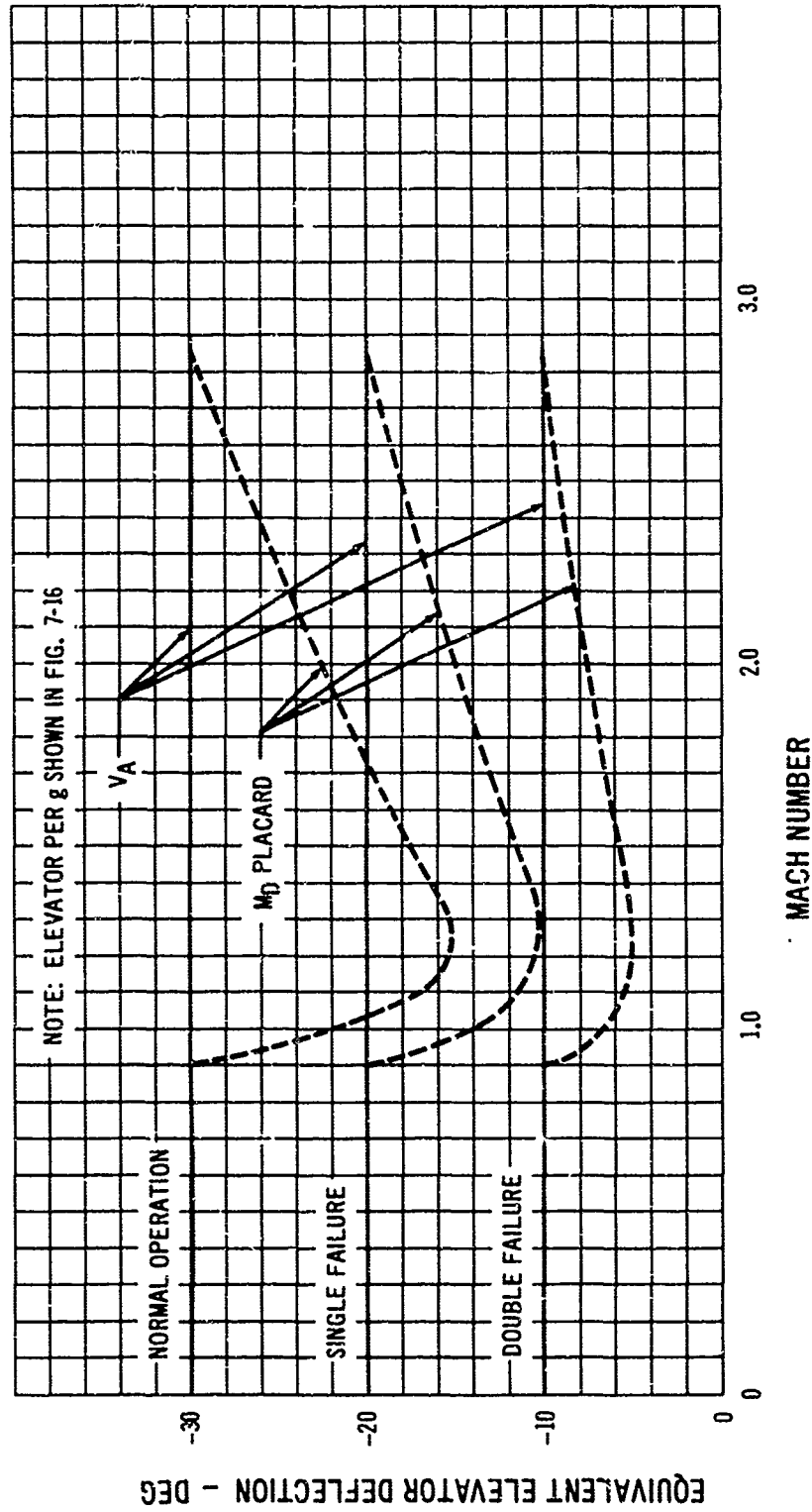
LOAD FACTOR = 1 + $\frac{\text{MAX. } \delta_e}{\delta_e/g}$ WHERE MAX δ_e AVAILABLE
 ATTAINABLE IS SHOWN IN FIG. 7-17 AND 7-39



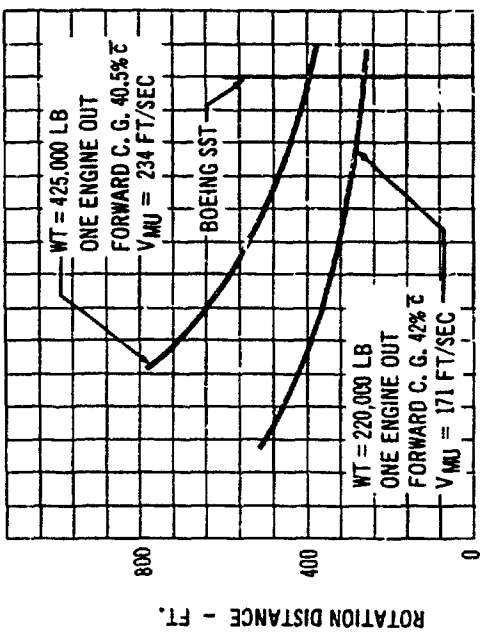
7.16 Elevator Deflection Required During Maneuvering, Flexible Airplane

time history presented in Fig. 7-22 shows the good response characteristics developed by the powerful elevator controls of the Boeing SST. It is seen that for a landing speed of 125 knots at design landing weight, a ramp input of maximum available elevator deflection at maximum rate provides a maximum pitch acceleration of 8.5 deg/sec².

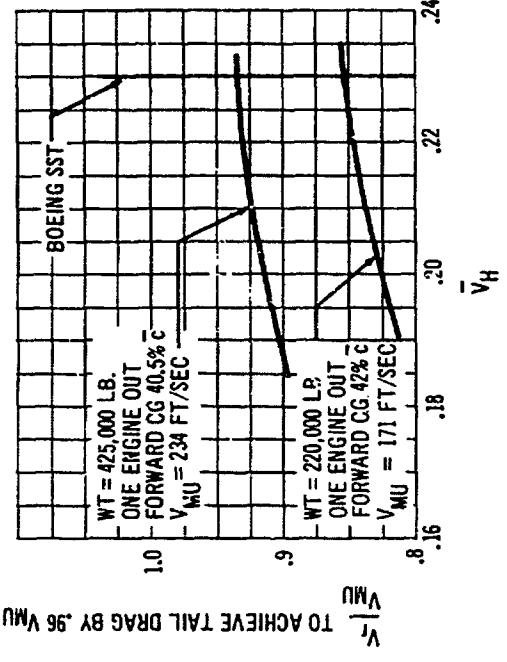
within one second of control initiation. Two seconds after control initiation the load factor has built up to 1.42 g, and by 2.4 seconds the airplane has reached stall. This response is somewhat better than that of the 707-320, which at comparable conditions can develop a maximum pitch acceleration of 5.0 deg/sec².



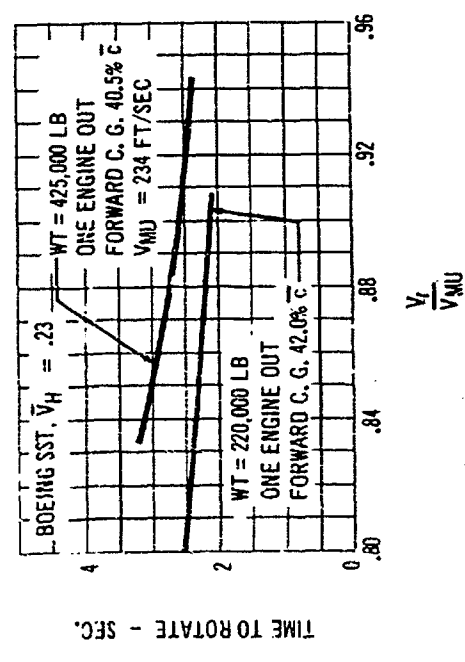
7-17 Longitudinal Control System High-Speed Failure Characteristics



7-18 Effect of Rotation Velocity on Rotation Capability



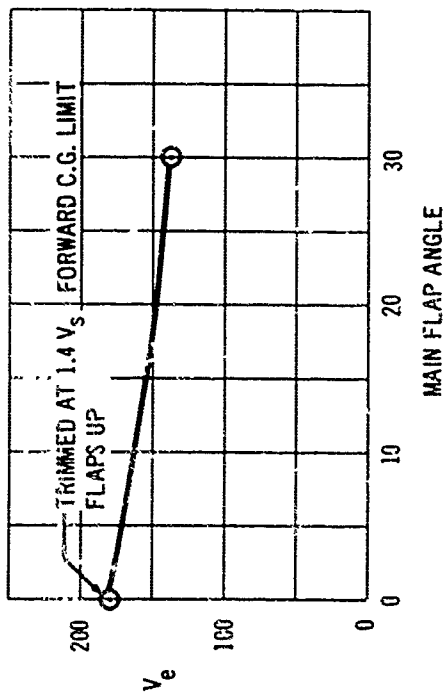
7-19 Effect of Rotation Velocity on Rotation Capability



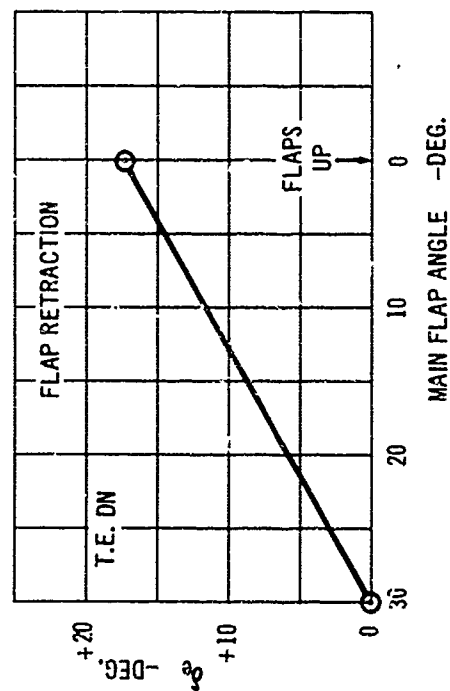
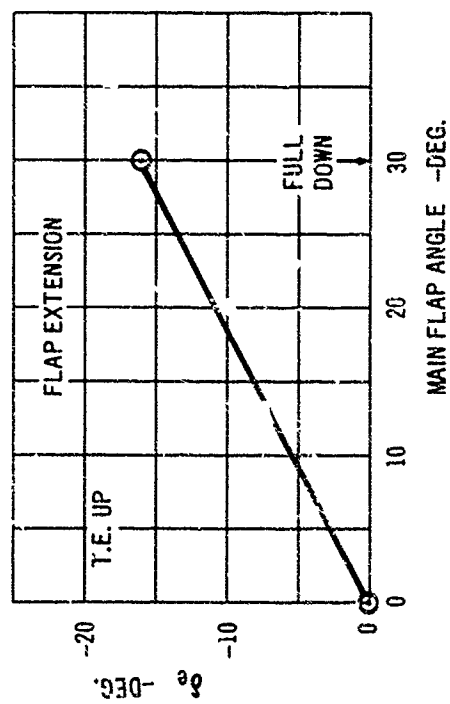
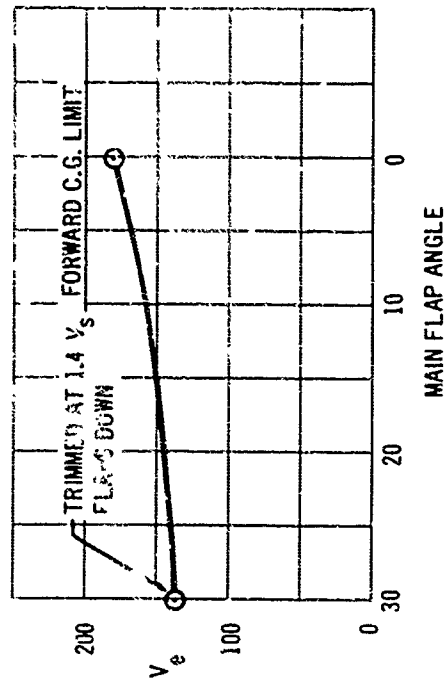
7-20 Effect of Horizontal Tail Volume Coefficient on Rotation Capability

TO ACHIEVE TAIL DRAG BY .96 VMU

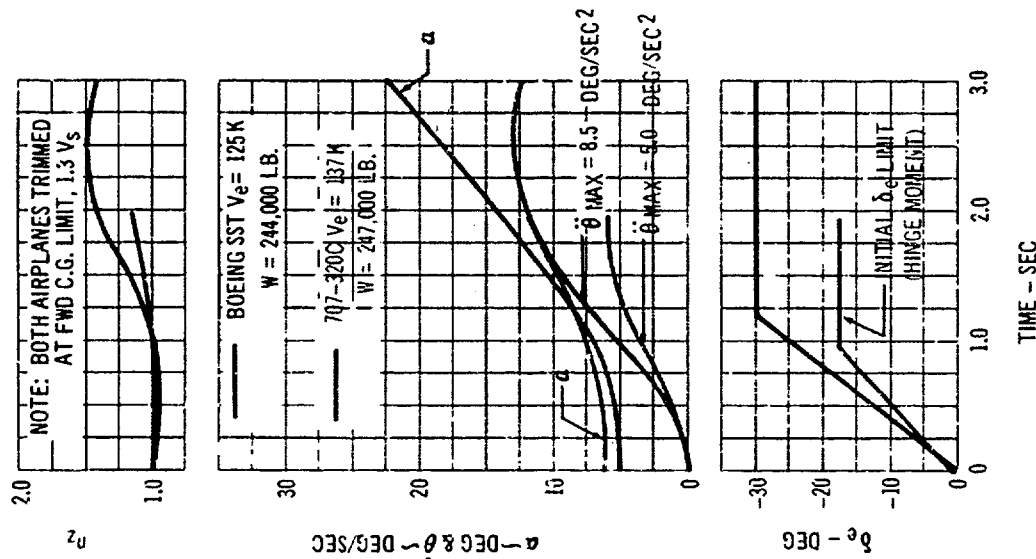
FLAP EXTENSION



FLAP RETRACTION



7-21 Elevator Control Required During Flap Cycle, Without Retraining



7-22 Response to Full Elevator Control, Landing Configuration

7.2.1.3 Control Force Characteristics

No data are presented in this proposal describing the control force characteristics of the Boeing SST. Elevator feel in this airplane will be determined by a computer sufficiently flexible to allow a very arbitrary schedule. Although force characteristics are the classical measure of handling qualities (since they best describe the pilot's experience), their use in the description of the Boeing SST is not significant due to the artificial nature of the feel system.

It must be emphasized that the quality and reliability of the SST longitudinal control system is independent of the feel schedule that will be selected at a more convenient date. A direct, mechanical cable connection is provided between the pilot's column and the control actuator so that ultimate authority over the position of the controls is always in the pilot's hands.

The feel computer will be arranged so that speed stability will be positive throughout the flight envelope including the transonic conditions. Stick force gradient will be relatively independent of static margin and reasonable values of stick gradient will be maintained regardless of the physical effects of Mach number, aeroelasticity, or high dynamic pressure.

A novel electrical-command system will remove virtually all friction and breakout force with no compromise to the integrity of the pilot's mechanical authority over control position (see Volume A-VII).

7.2.2 STATIC DIRECTIONAL STABILITY AND CONTROL

The large vertical tail and ventral fin incorporated in the 733-197 yield a high level of directional stability for all flight conditions. The tail and ventral fin sizing were dictated by the requirement to retain satisfactory stability at the highest angles of attack attainable at maximum Mach numbers. As a result, an exceptional degree of directional stability is available throughout the rest of the

flight envelope, contributing greatly to the good dynamic handling qualities.

Fig. 7-23 shows directional stability, $C_{n\beta}$, versus Mach number for the flexible airplane operating at design climb and descent conditions and on the dive placard at high supersonic Mach numbers. Also shown is the $C_{n\beta}$ for the rigid airplane as obtained from wind tunnel testing. The test data and aeroelastic corrections employed are presented and discussed in Par. D7.4 of the Appendix.

The effect of angle of attack on directional stability is shown in Fig. 7-24 for both the rigid and flexible airplane at the most critical flight condition: supersonic cruise Mach number. This is more critical than the maximum M_0 condition since considerably higher angles of attack are attainable within structural limits when maneuvering from the higher cruise trim lift coefficient. The typical deterioration of $C_{n\beta}$ with increasing α is seen in Fig. 7-24. However, a high level of directional stability is maintained well beyond the α for structural limit load factor, which corresponds to the highest load factor attainable at this condition with full elevator control. It is also shown that $C_{n\beta}$ increases with increasing sideslip angle at the critical higher angle-of-attack conditions. At 13 degrees α , for example, $C_{n\beta}$ is seen to double as the sideslip angle increases from 0 degrees to 5 degrees. These stability characteristics are considered good and require no further improvement.

The ability of the rudder to control the yawing moment imposed by the failure of an outboard engine during the takeoff is shown in Fig. 7-25. The large, 4-segment rudder system provides the capability of maintaining zero sideslip at speeds down to 96 knots. This is well below the V_1 speed of 137 knots for the design mission gross weight. Section 7.2-4 discusses the system failure conditions shown in Fig. 7-25.

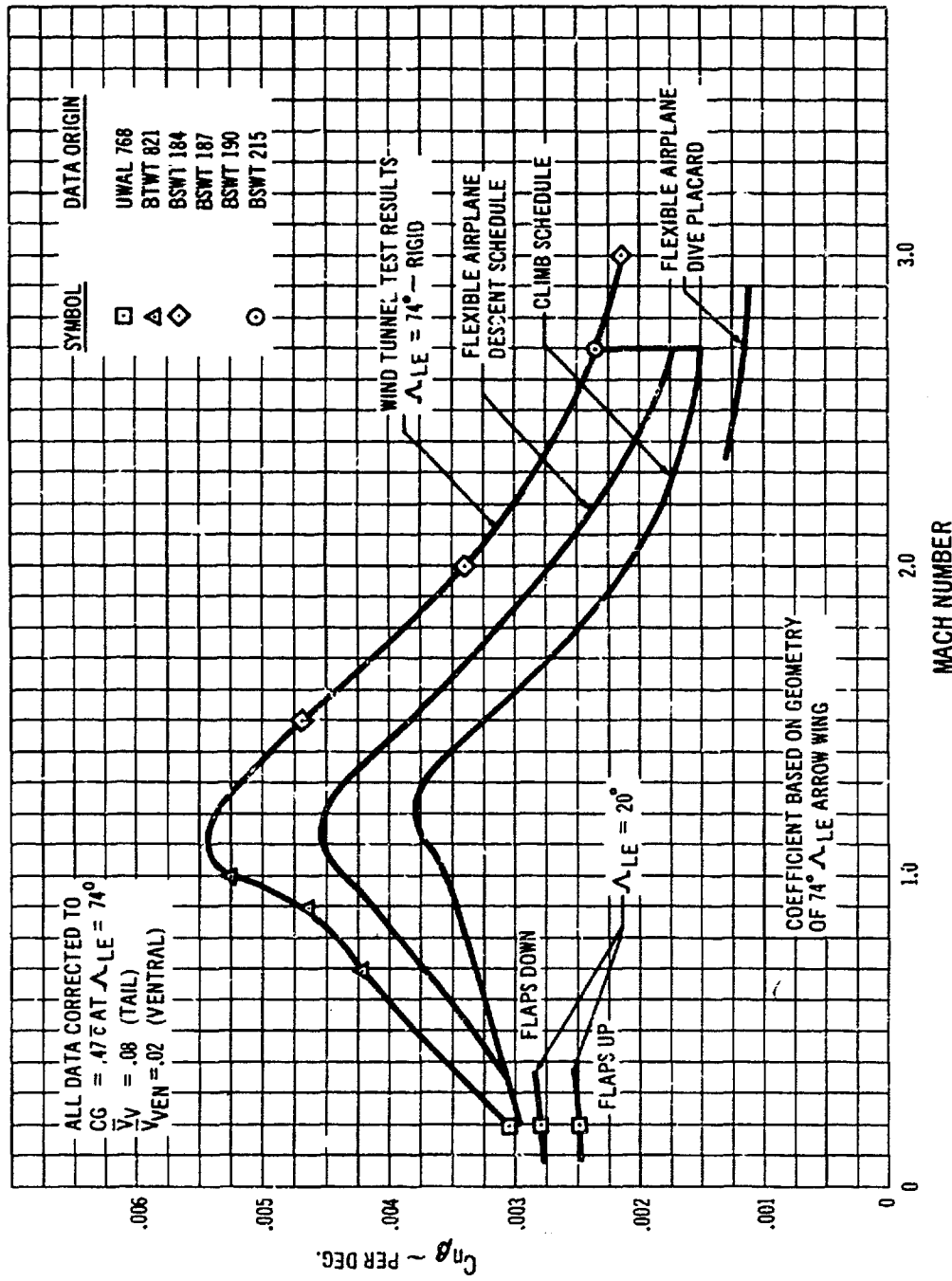
Fig. 7-26 shows the lateral and directional control required in a steady sideslip in the landing approach con-

dition. Maximum rudder control develops 15 degrees of sideslip, and the lateral control required at this condition is only 12% of the available control. This level of control power provides the capability to land in 90 degree crosswinds exceeding 30 knots. Operation with system failures as shown on the figure is discussed in Section 7.2.4.

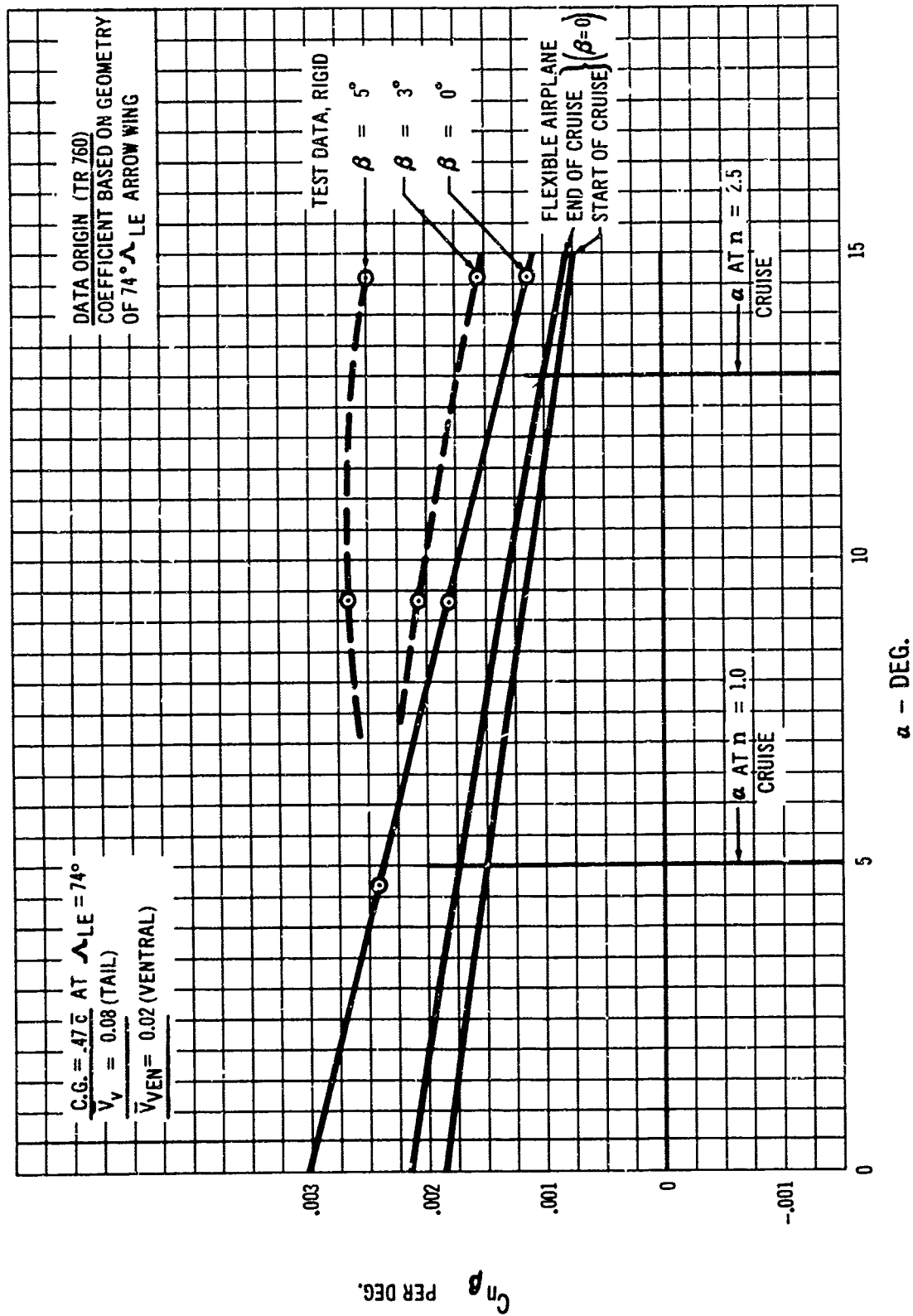
The rudder deflection available and the deflection required to maintain zero sideslip with an outboard engine failed is shown in Fig. 7-27 for operation along the climb schedule where engine thrust is high. The rudder control available is seen to be more than adequate to balance the asymmetric thrust.

7.2.3 FLIGHT DYNAMICS

The variable-sweep wing feature of the Boeing SST provides exceptionally good dynamic handling qualities in all areas of the flight envelope. The capability of operating with moderate-to-low wing sweep at subsonic speeds results in good stability characteristics for the basic, unaugmented airplane. Stability augmentation about the pitch and roll axes is not required at subsonic speeds, and only a simple yaw damper is provided to optimize the configuration. The resulting dynamic characteristics are equivalent to and in many cases superior to those of current jet transports. At supersonic speeds the dynamic characteristics of the unaugmented airplane are such that stability augmentation is not required for safe flight. Boeing flight simulator investigations have shown the airplane to be quite tractable without augmentation. This is in spite of the low damping ratios of the longitudinal short period mode inherent with any SST configuration operating in a high true airspeed and high altitude environment. A three-axis augmentation system is provided to ensure the excellent handling qualities required to maintain precise flight path control and maximum passenger comfort throughout the mission profile. System gain levels are a simple function of wing sweep.



7-23 Directional Stability - $C_{n\beta}$ - Along Normal Operating Schedule

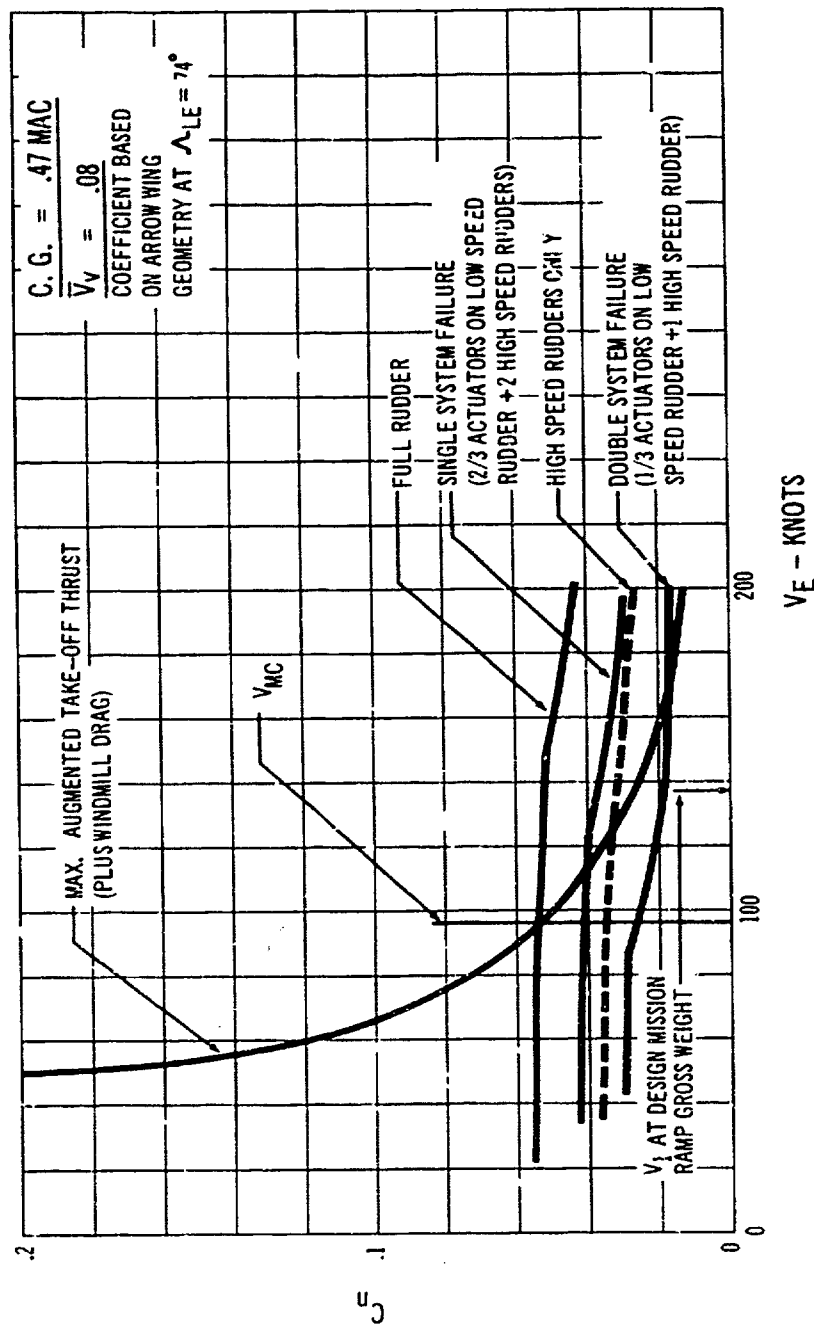


7-24 Directional Stability $C_{n\beta}$ - at $M = 2.7$ Cruise - Flexible

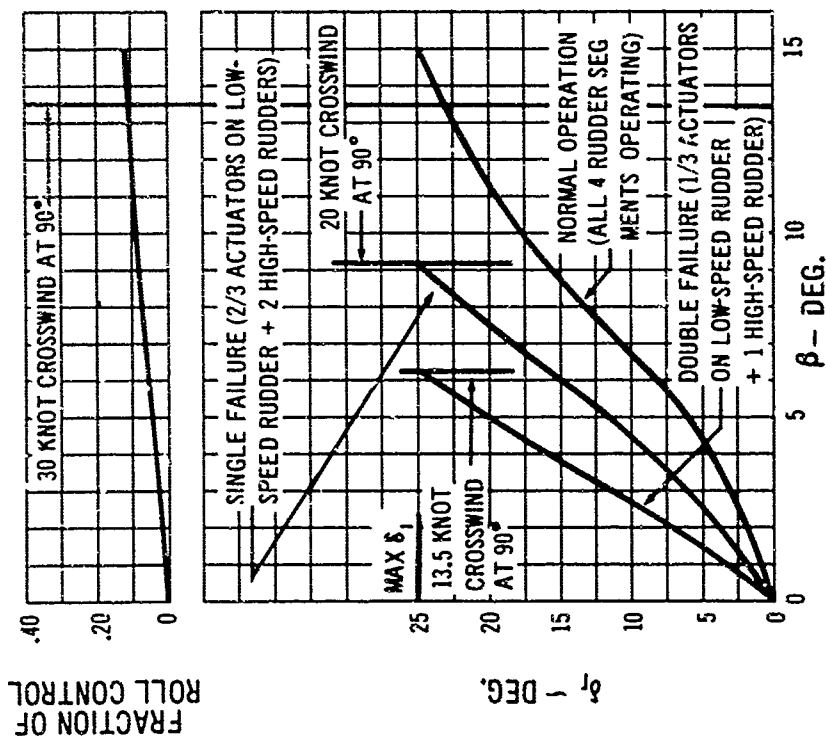
7.2.3.1 Unaugmented Longitudinal Dynamics

The basic unaugmented longitudinal short-period characteristics are presented in Fig. 7-28. Long-period (phugoid) results, and the stability parameters for each flight

Eight significant flight conditions were selected for analysis of dynamic behavior. Airplane characteristics, inertial parameters, and aerodynamic derivatives are tabulated for each of the eight conditions in Section D7.6 of the Appendix.



7-25 Effect of Critical Engine - Out During Takeoff



7-26 Steady Sideslip, Landing Configuration, $V = 125$ Knots
condition discussed are compiled in the Appendix, Section D7.6.

At cruise Mach number the short-period damping ratios are low. A Boeing flight simulator evaluation has shown this flight condition to be safely flyable and the oscillatory tendencies to be easily controllable. The short-period frequencies experienced with the variable sweep design were found to be an aid to controllability in this flight condition.

At transonic speeds the short period damping ratios are similar to the minimum levels that a 707-320 experiences in some areas of its flight envelope. Thus, no undue problems without augmentation are expected for the Boeing SST at these flight conditions. Augmentation is provided to ensure optimum handling qualities as required for precise control of flight path along the climb schedule.

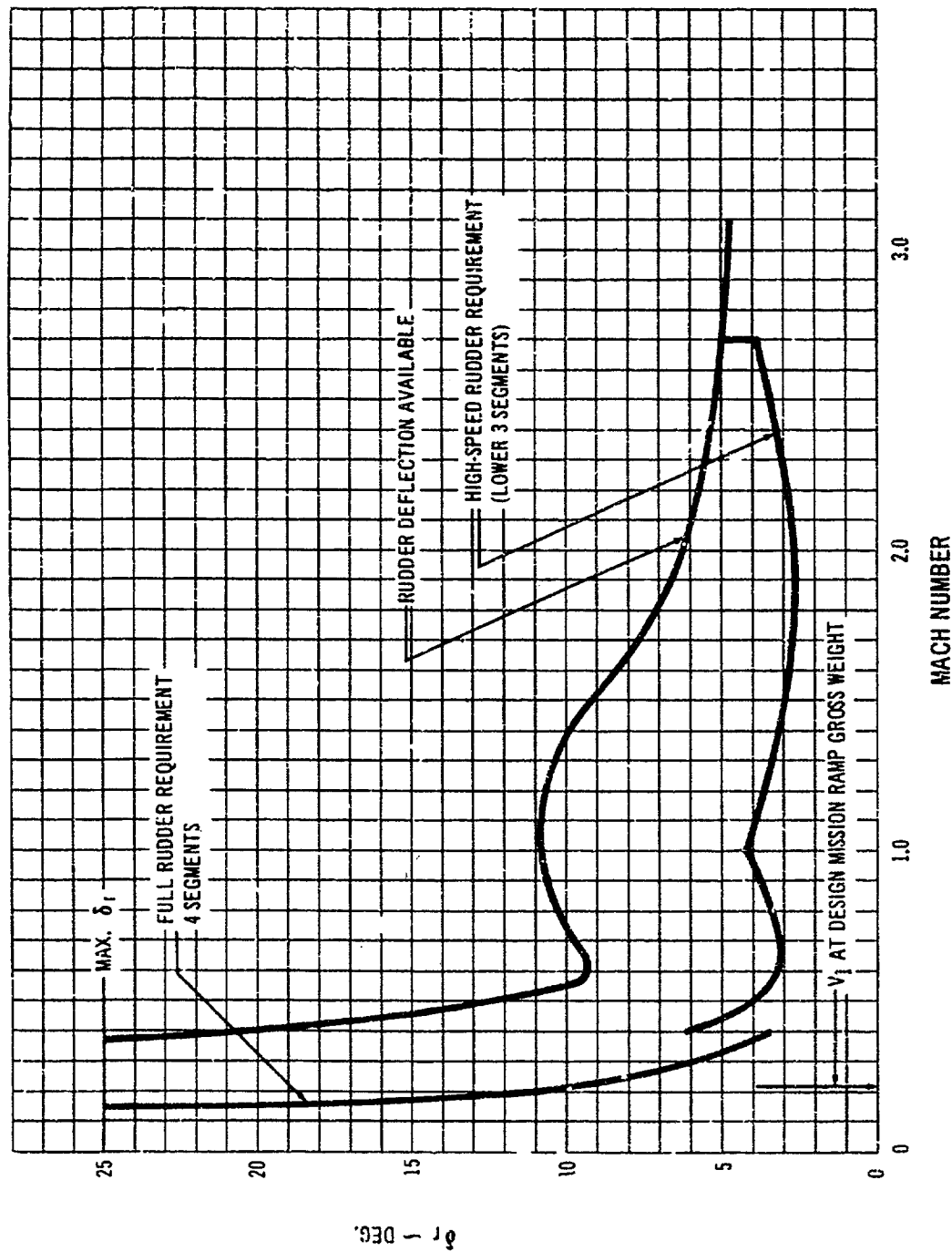
At subsonic speeds the pitch damper is not required. Fig. 7-28 shows that the subsonic characteristics are similar to the 707-320 except during landing approach where the SST damping level is much higher.

Loss of the pitch damper does not result in a hazardous situation at any flight condition. Since the pitch damper is a dual channel system operating on separate surfaces, at least two failures have to occur before the system is totally disabled.

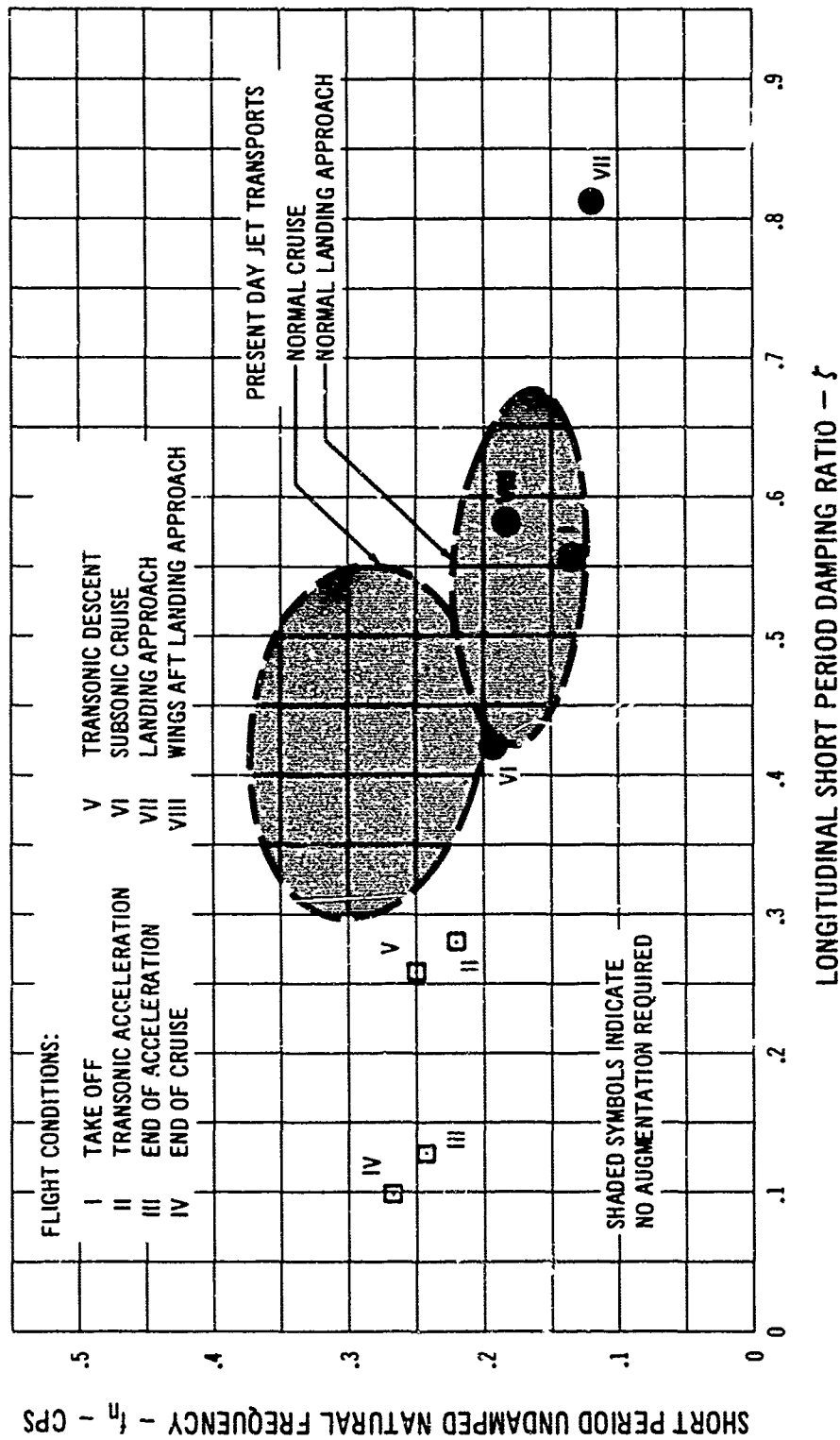
7.2.3.2 Augmented Longitudinal Dynamics

The augmented longitudinal characteristics are predicted to be excellent. The short period is always well damped. The phugoid periods range from 38 to 380 seconds and are damped. Stability parameters, SAS surface effectiveness, and gain levels for the flight conditions discussed are compiled in Appendix D7.6. Fig. 7-29 presents the short period results in the natural frequency and damping ratio plane. Phugoid results are presented in the table of stability derivatives for the individual flight conditions, Appendix, Section D7-6. As shown in Fig. 7-29 the short period is well damped at all flight conditions and airplane characteristics are similar to those of the 707-320.

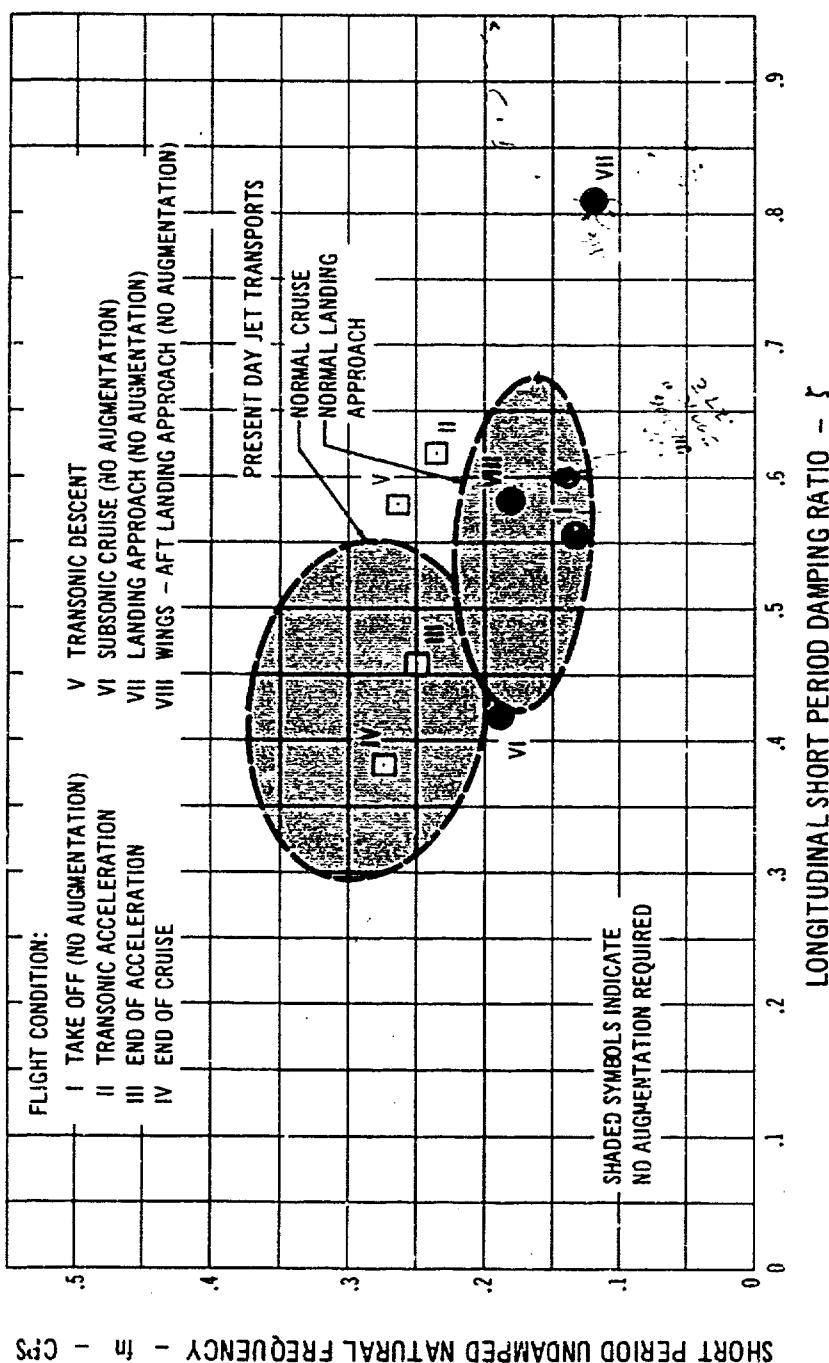
Although the short period characteristics are excellent, a possibility of high sensitivity of load factor to airplane attitude changes exists as it does for all airplanes flying at high true airspeeds. Analysis of Model 733-197 has shown that it does not suffer from pitch sensitivity at high speeds due to its unique combination of high wing loading, high wing sweep, and low wing rigidity.



7-27 Rudder Required to Trim Critical Engine-Out Along Climb Schedule, Flexible



7-28 Longitudinal Short Period Characteristics - Unaugmented



7-29 Longitudinal Short Period Characteristics - Augmented

If pitch sensitivity is high, small and often imperceptible attitude changes result in significant changes in load factor and a resultant difficulty in maintaining constant altitude and preventing unpleasant oscillations. A measure of this load factor sensitivity is $n_{\dot{\alpha}}$, a parameter including airplane lift characteristics and dynamic pressure. This parameter is defined in Fig. 7-30 with a comparison of the Boeing SST and several other contemporary airplanes. Values for the 707-320 are shown at Mach .8 and altitudes of 20,000 and 30,000 feet. Experience has shown that the 707-320 is much more sensitive to small attitude changes at the lower altitude, high airspeed condition. The same is true for the F-104B flying at two different altitudes and constant Mach number. A comparison of two types of SST's, a fixed delta and a variable sweep, shows that the variable sweep is less sensitive because of its higher wing loading, lower aspect ratio, and greater wing structural flexibility. Flight simulator analyses of the Model 733-197 have shown it to be similar to a 707-320 in short period response when each airplane is at its normal cruise airspeed.

The handling qualities situation is quite different at landing approach. As shown in Fig. 7-29, the short period is well-damped and has a natural frequency of .12 cycles per second. The phugoid has a period of 38 seconds and is also well damped. This results in a configuration with characteristics somewhat like a 707-320 on landing approach at high weight. One difference is that the 707-320 has an approach speed about 15 knots higher than the Boeing SST.

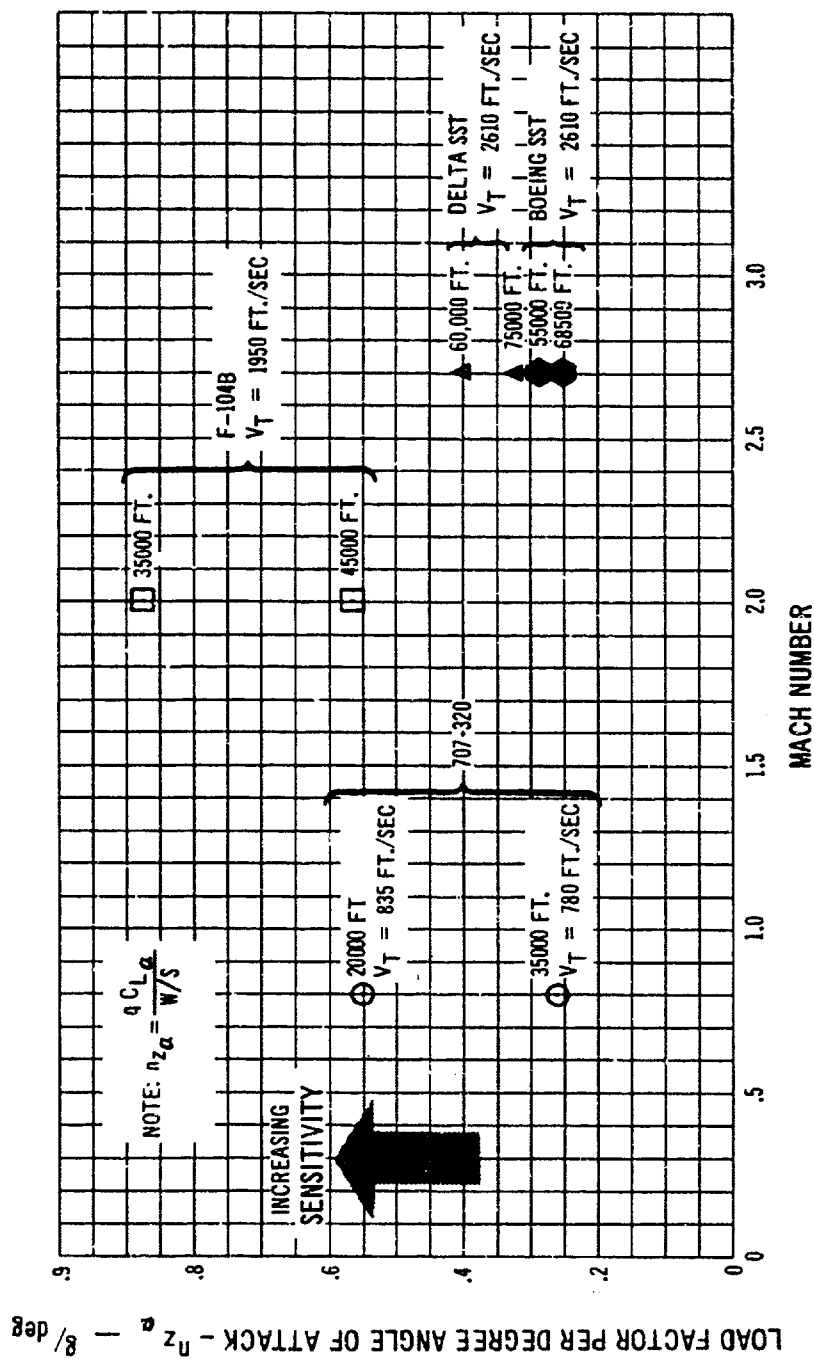
Longitudinal short period frequency augmentation ("stiffening") has been suggested as a possibility for improving the handling characteristics during landing approach. Boeing flight simulator research presented in Fig. 7-31 shows that relatively low short-period natural frequencies are desirable for large transport type airplanes. Fig. 7-31 also shows that short-period natural frequencies on the order of .7 cycles per second give completely un-

acceptable characteristics. For smaller airplanes, such as fighter types, a frequency of about .7 cycles per second is ideal. These results are reasonable since the short-period frequency and damping ratio govern airplane attitude response to elevator input, while the quantity $n_{\dot{\alpha}}$ (defined in Fig. 7-30) determines airplane flight path response to attitude changes. Airplanes that have low values of this quantity on landing approach (present day jet transports, variable geometry or delta wing SST's) require relatively low values of short period natural frequency for best handling qualities. This provides a good match of airplane attitude response and flight path response. A frequency augmentation system (lagged pitch rate in this case) was evaluated on the flight simulator and the result is shown as a point in Fig. 7-31. Since this system provided the very beneficial side effect of making the phugoid much more heavily damped, the pilot rating was higher than the case where pure frequency augmentation was used. A system of this type will be considered in detailed Phase II simulator evaluations indicate a requirement in this area for the Boeing SST.

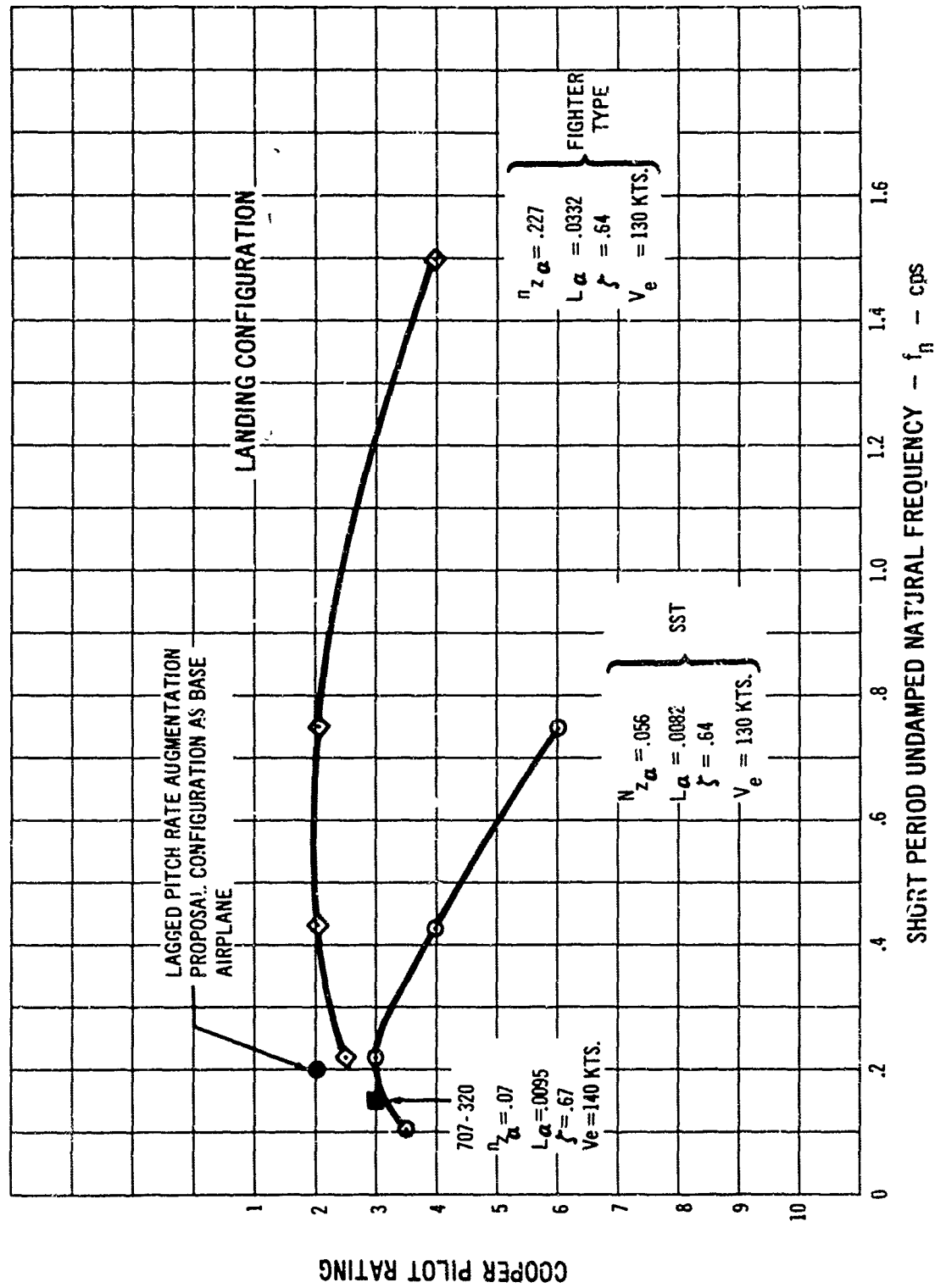
Fig. 7-28 shows that the 733-197, during a wings-aft landing approach, has characteristics somewhat like a 707-320 on landing approach at forward CG's. This, plus the well damped phugoid mode, results in good handling qualities at low speed with wings aft.

7.2.3.3 Unaugmented Lateral-Directional Dynamics

Analyses of the lateral-directional dynamics have shown that the 733-197 airplane provides acceptable characteristics at most flight conditions without stability augmentation. Fig. 7-32 shows the unaugmented Dutch roll characteristics expressed in terms of "reciprocal of cycles to damp to half amplitude" and the "ratio of bank angle-to-equivalent lateral velocity." The unaugmented airplane is seen to satisfy the requirements of MIL-F-8785 for minimum damping without augmentation. Comparison with



7-30. Load Factor Sensitivity to Angle of Attack Change



7-31 Effect of Short Period Natural Frequency on Pilot Rating

the 707-320 unaugmented Dutch roll characteristics shows that the Boeing SST provides improved damping at most of the flight conditions investigated.

The wings-aft landing condition has received special attention in the development of the proposal configuration. As a result of the large degree of directional stability provided in the airplane, the lateral-directional dynamics do not pose a serious problem in this condition. This is indicated by the Dutch roll characteristics presented in Fig. 7-32 for the unaugmented airplane. Flight simulator evaluations of wings-aft handling characteristics during the landing approach have shown that landings can be performed quite safely with stability augmentation inoperative about all axes.

7.2.3.4 Augmented Lateral-Directional Dynamics

Stability augmentation in the form of simple yaw and roll damping provides the 733-197 with excellent lateral-directional dynamic characteristics at all flight conditions. Fig. 7-33 shows the good Dutch roll characteristics attained, and shows that the Boeing SST Dutch roll damping is considerably superior to that of the 707-320 at most flight conditions. Flight simulator evaluations have shown that good lateral-directional dynamic characteristics are provided for the augmented 733-197 at all flight conditions, including the wings-aft landing.

The Boeing SST provides excellent turn characteristics, evidencing no requirement for automatic turn coordination. Flight simulator evaluations have shown that turn coordination with feet-off-the-pedals is excellent for all flight conditions investigated except the wings-aft landing approach. Here a level of pilot coordination is required which is approximately equivalent to that required for the 707-320 in the landing approach configuration. Evidence of these characteristics is presented in Tables D7-B

through D7-1, where the roll-yaw coupling parameter, ω_ϕ/ω_ψ , is tabulated for each of the eight flight conditions evaluated. The values of ω_ϕ/ω_ψ are seen to be within the optimum band of .85 to 1.05 for all but the wings-aft landing configuration.

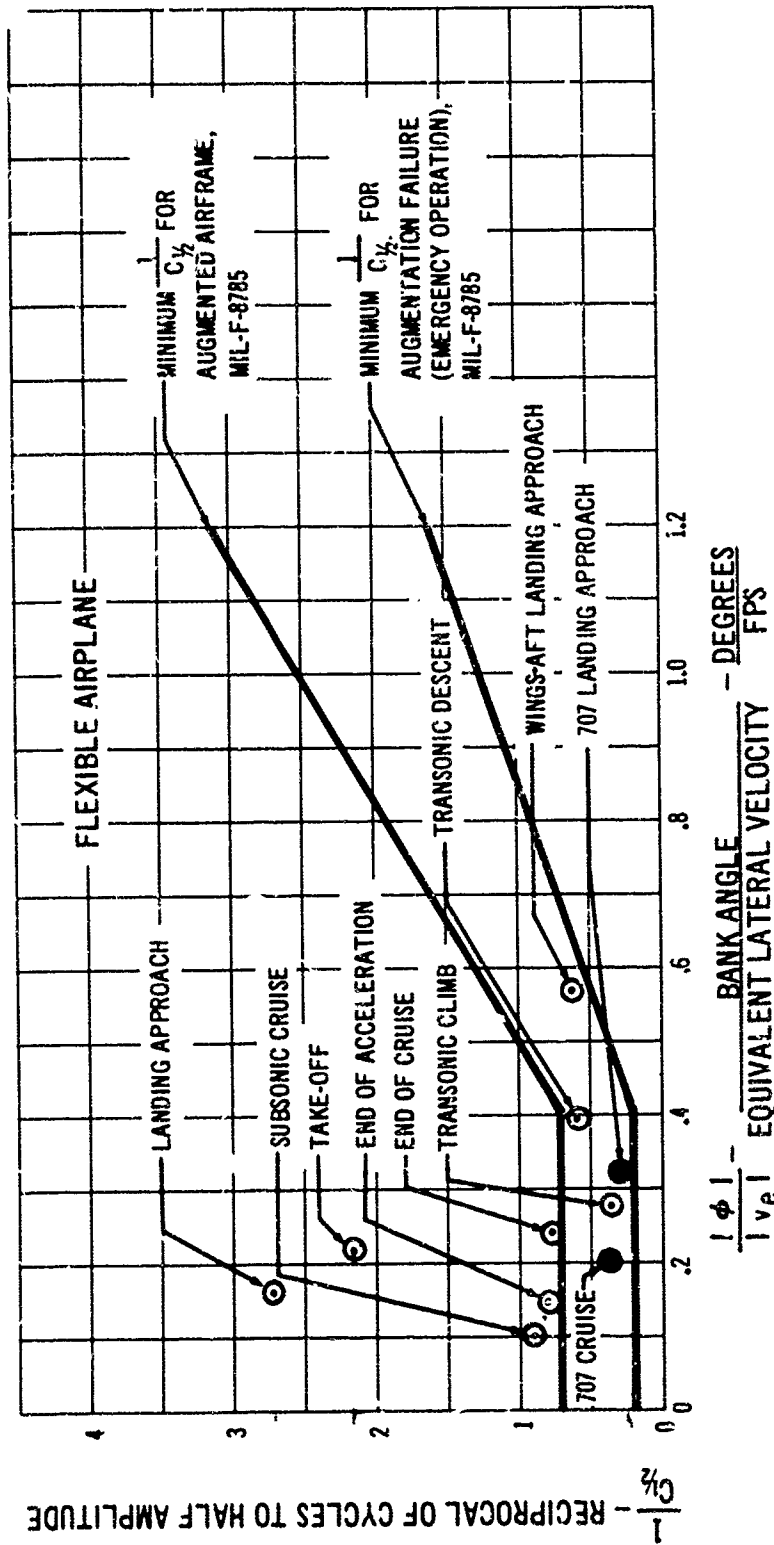
7.2.3.5 Gain Changing

Studies of the longitudinal and lateral-directional dynamic characteristics of the 733-197 have pointed out that stability augmentation is not required for safety of flight. However, during normal flight, stability augmentation in the form of pitch, yaw and roll damping serves to reduce the pilot's work load and to optimize the airplane handling qualities. The augmentation gain changes are very simple functions of wing position and are described in detail below. The autopilot gains, on the other hand, are changed using the air data computer. The autopilot requirements are discussed in detail in Volume A-VII.

LATERAL AUGMENTATION REQUIREMENTS

Roll damping augmentation is required only during high speed flight with the wings at 74 degrees of sweep (see Par. 7.2.3.6). Approximately doubling of the roll damping coefficient by artificial means will yield the desired roll response. Since roll damping operates through the outer, upper and lower surface spoiler panels only, a relatively high gain of 5 deg/deg/sec. is used during wings aft flight. As the wings are swept forward, roll damping augmentation is automatically reduced to the level required for autopilot inner loop damping. In the wings-aft landing case it will be recommended that the pilot switch off the roll damping augmentation.

Full augmentation is maintained for roll rates up to 12 degrees per second. If future studies indicate that more damping authority is required, this can be accomplished by adding the next inboard spoiler panels to the augmentation circuit.



7-32 Boeing SST Dutch Roll Damping Characteristics, No Augmentation

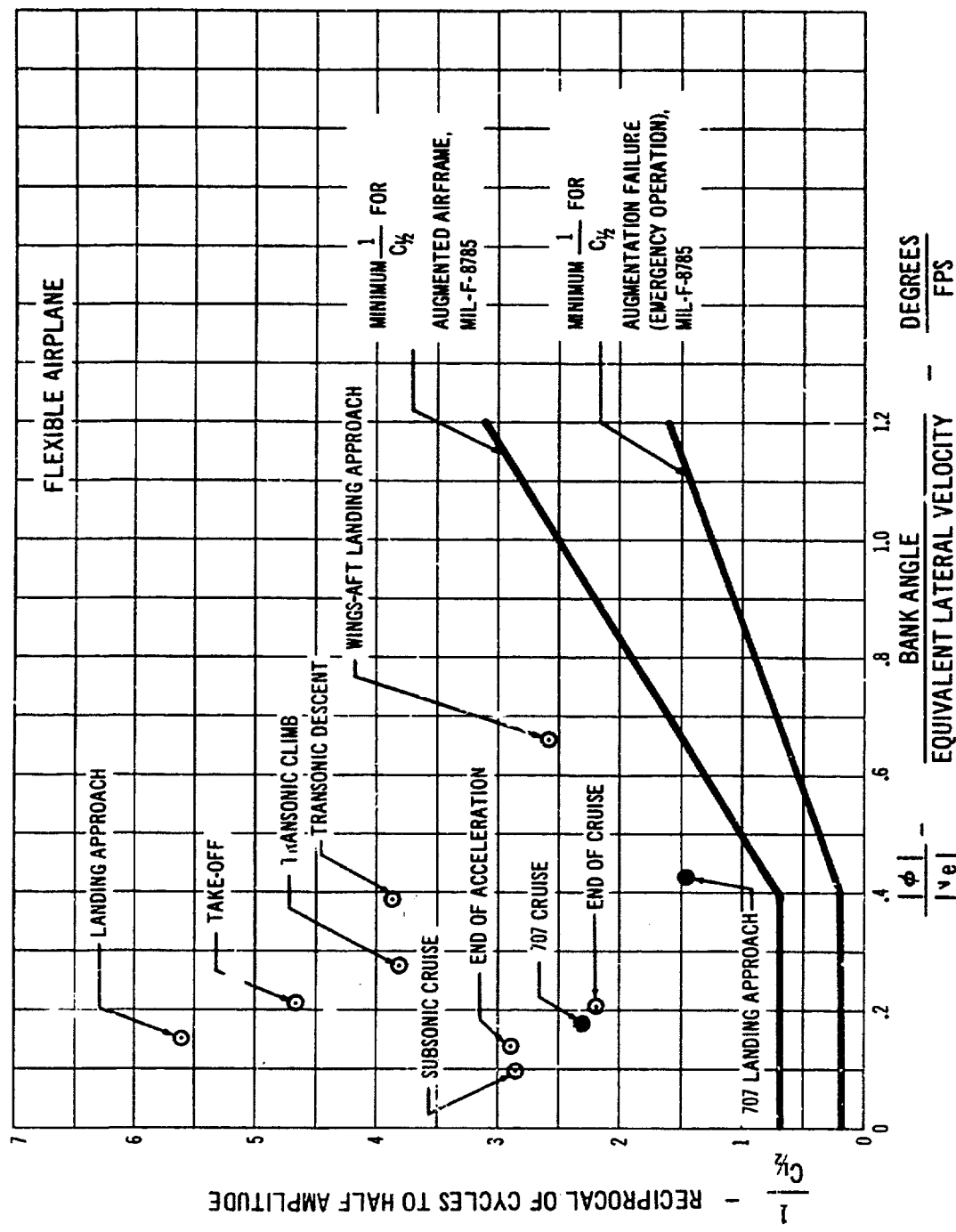
LONGITUDINAL AUGMENTATION REQUIREMENTS

Pitch damping augmentation is required only during high speed flight. No pitch damping augmentation is required with sweep angles less than 50 degrees. A constant gain of 3 deg/deg/sec is recommended for transonic flight, and at 74 degrees of sweep a constant gain of 5 deg/deg/sec yields optimum longitudinal dynamics for high-speed flight. It will be recommended that the pilot switch

off the pitch damping augmentation for the wings-aft landing to ensure maximum control authority.

DIRECTIONAL AUGMENTATION REQUIREMENTS

Full time yaw damping augmentation is used to improve handling qualities. It is stressed however that the airplane is safely flyable anywhere in the proposed flight envelope with no augmentation about any axis.



7-33 Boeing SST Dutch Roll Damping Characteristics, Augmented Airframe

Two gain levels as a simple function of wing sweep are used. For wing sweeps greater than 50 degrees a gain level of 1.9 deg/deg/sec is required, and a gain level of 1.5 deg/deg/sec is used for wing sweeps below 50 degrees.

7.2.3.6 Lateral Control Characteristics

The Boeing SST provides the pilot with a high degree of lateral control authority through the employment of large ailerons and large multi-segment, upper and lower surface wing spoilers. All upper-surface spoilers and the ailerons operate for low-speed roll control at wing sweeps forward of 30 degrees. At sweep angles greater than 30 degrees, the inboard spoilers are inoperable (due to interference with the fixed wing center-section), and the ailerons are locked at neutral (due to their low aeroelastic reversal speed). The upper-surface outboard spoilers function at all speeds, and are supplemented by lower-surface spoilers at wing sweeps aft of 30 degrees.

The maximum roll-rate capability throughout the flight envelope is shown in Fig. 7-34 for coordinated (single degree of freedom) rolls. It is seen that very high roll rates are available to the pilot at all normal operating conditions. Fig. 7-35 presents the bank angles attainable in one second and the roll time constants associated with the maximum roll rates available for several important flight conditions. At takeoff and landing conditions, the lateral response is exceptionally good. For example, on the landing approach it is possible to develop a 22 degree bank angle in one second, with a maximum roll rate of 33 degrees per second and a roll time constant of 0.35 seconds. At supersonic cruise conditions the time constants of the unaugmented roll response are higher than desirable and the unaugmented roll rates are higher than necessary. Moderate roll damping is therefore incorporated to yield time constants near 1.5 seconds, roll rates in excess of 30 degrees per second, and a bank angle in one second of approximately 9 degrees. Flight simulator studies have shown that this improvement in the roll time

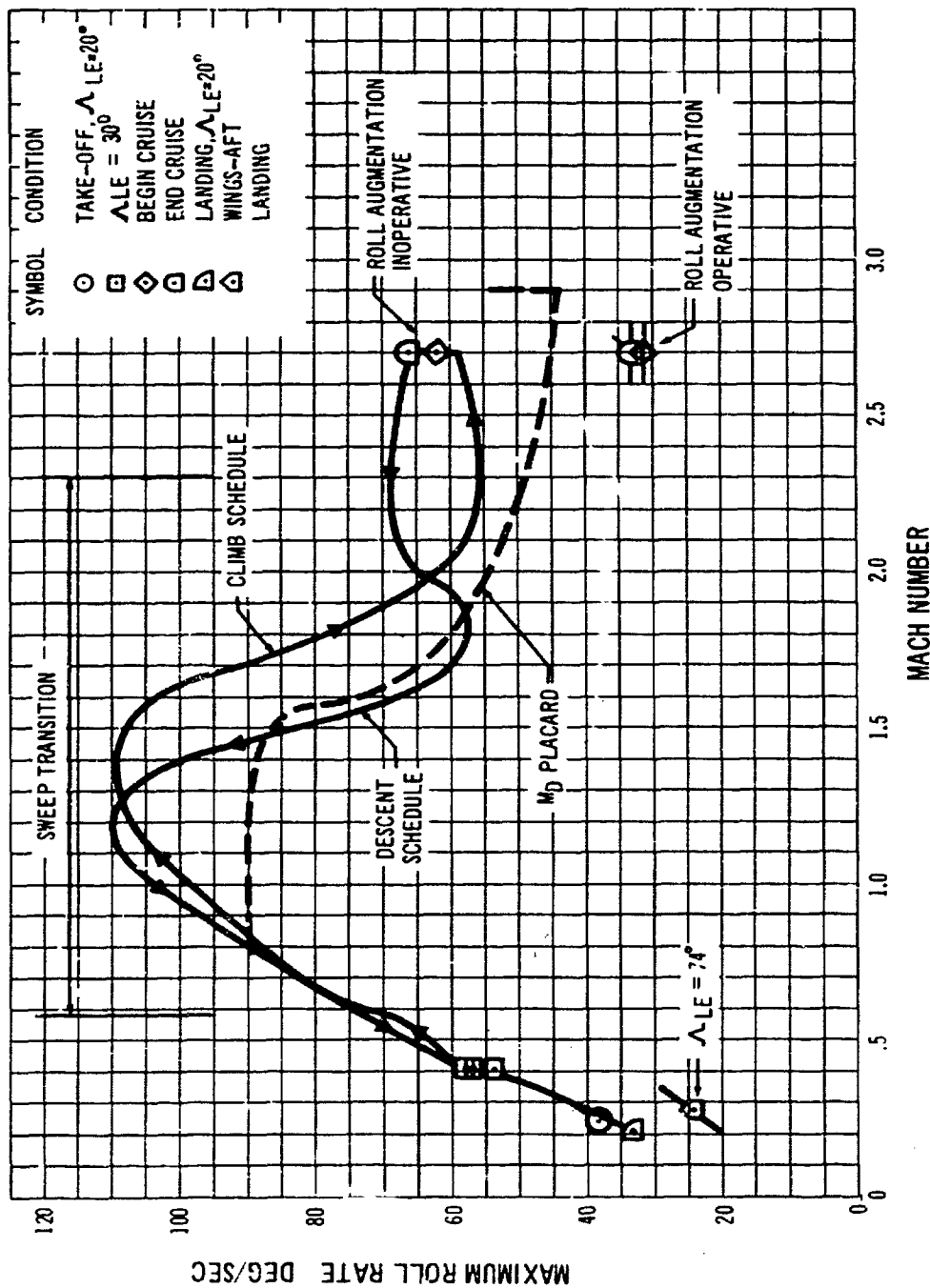
constants through roll damping provides good lateral handling qualities.

As discussed in Section 7.2.3.4, automatic turn coordination will probably not be required for the Boeing SST. The basic lateral-directional, dynamic stability characteristics of the airplane, combined with the low yawing moment-to-rolling moment characteristics of the lateral control system provide excellent turn coordination without rudder inputs. This has been confirmed during flight simulator evaluations of the proposal airplane.

Fig. 7-36 presents a more detailed analysis of the critical low-speed flight regime. The effects of airspeed and gross weight on roll performance are shown for the normal landing and takeoff conditions. The lateral control power available for the wings-aft landing is shown as affected by airspeed and roll damping. As discussed in Section 7.1.2, the roll damper is shut off for this flight condition. The reason for this is apparent in the figure, where maximum roll rate decreases with roll damping. The wings-aft landing lateral control power provides roll rates of approximately 25 degrees per second, roll time constants of approximately 1.1 seconds, and bank angle of eight degrees attainable in one second. Boeing flight simulator studies of this flight condition have shown these roll response characteristics to be satisfactory.

Roll performance with single and double hydraulic system failures is shown in Fig. 7-37. It is seen that good roll performance is still provided in the case of a single failure. Roll rates of 22 to 28 degrees per second are available at both supersonic cruise and low-speed conditions. For the extremely remote case of a double hydraulic system failure, roll performance is greatly reduced but remains adequate for safe handling qualities.

Wind tunnel testing is currently scheduled to evaluate additional lateral control devices, such as spoiler-slot-deflector arrangements, which are expected to provide substantial increases in control power at high angles of attack.

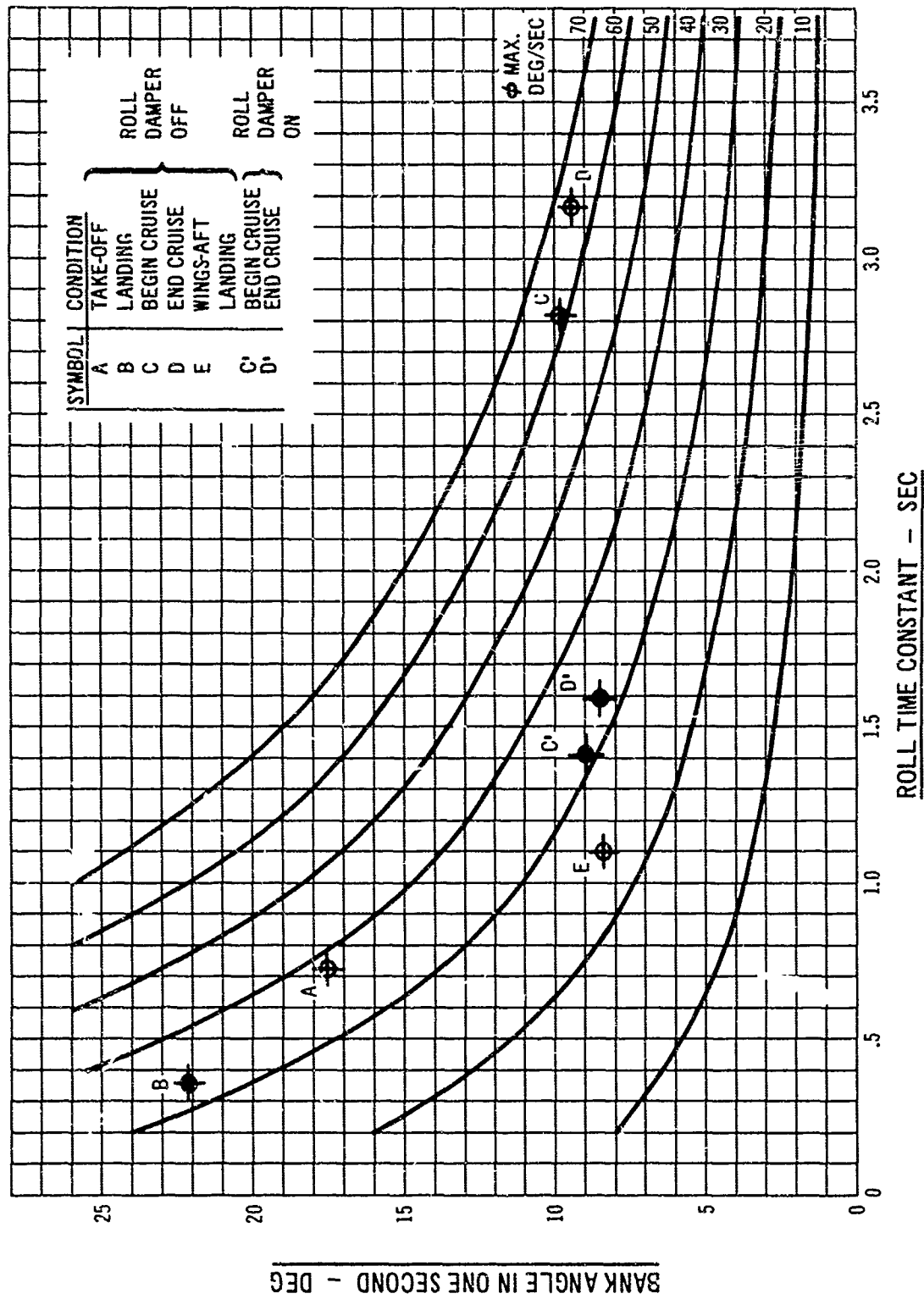


7-34 Maximum Roll Rates Available, Flexible Airplane

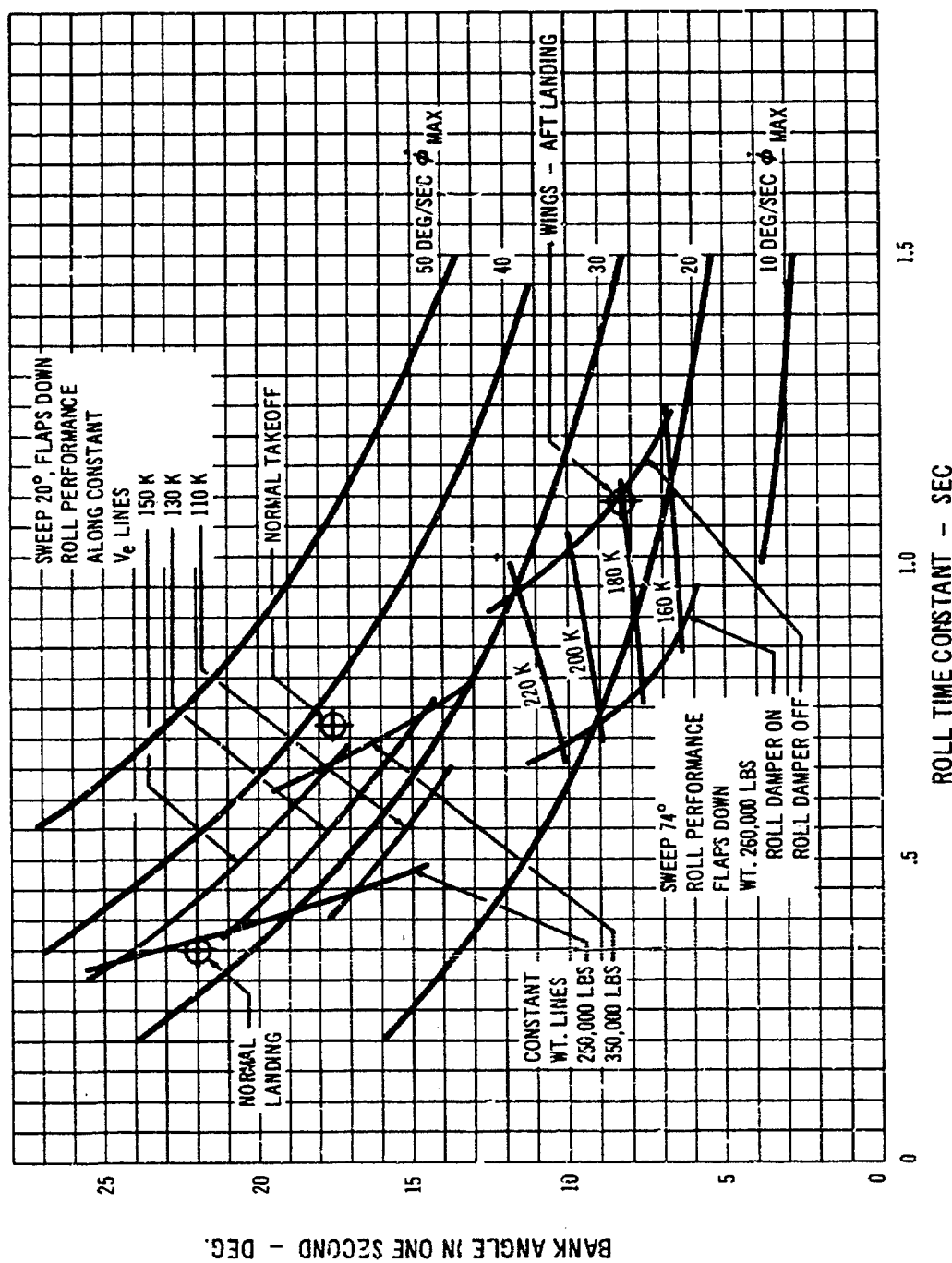
Inertial roll-yaw-pitch coupling is nowhere divergent in the flight envelope of the 733-197, either for the augmented or unaugmented airplane.

7.2.4 HANDLING QUALITIES IN CASE OF SYSTEM FAILURES

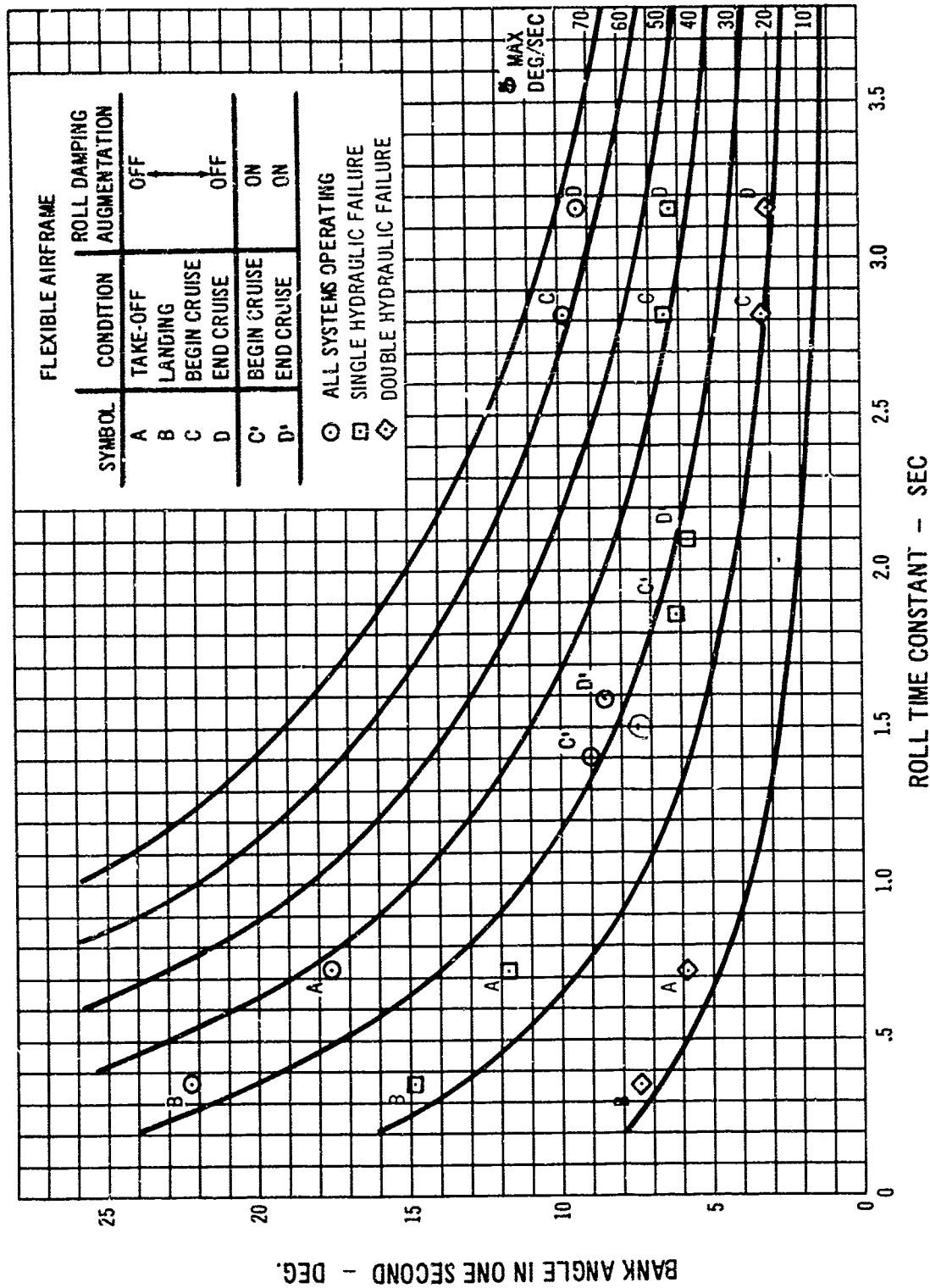
The Boeing SST achieves a high level of safety and reli-



7-35 Typical Roll Performance Parameters, Flexible Airplane



7-36 Low-Speed Roll Performance, Flexible Airplane



7-37 Roll Performance With Hydraulic Failures

ability by means of using proven components, by means of placing ultimate authority on mechanical systems, and by means of redundant design. The redundancy features allow multiple modes of operation which are described in detail in the Flight Controls Section of the Systems Report, Volume A-VII. The aerodynamic stability and control of the airplane, when operating with failures of the wing sweep mechanism, flight controls, or engines are discussed here.

7.2.4.1 Wing Sweep Failure

The wing sweep mechanism is triple redundant and complete loss of the ability to position sweep angle is extremely remote. Nevertheless in the following discussion this possibility is assumed to have occurred.

a. WING SWEEP IRREVERSIBILITY

Upon failure of the mechanism, the wing will remain at its existing sweep angle. It is noted that the aerodynamic forces on the wing are such as to tend to reduce wing sweep angle.

b. FAILURE OF THE WING TO SWEEP AFT AFTER TAKEOFF

In this event, the pilot will have the choice of continuing the flight at low subsonic speeds or returning and making a normal landing.

c. FAILURE OF THE WING TO SWEEP FORWARD FROM THE CRUISE POSITION

Figs. 7-10 and 7-15 show that the pilot has adequate control to perform the deceleration, descent and landing procedures with the wing at the most critical maximum sweep angle. Actuation of the alternate flap control will engage the low-speed controls (excepting the low-speed rudder) regardless of wing sweep angle. Compound failures will not prevent a safe landing. Fig. 7-38 shows that the elevator provides sufficient control without retrimming.

the stabilizer to perform a landing for the compound failure of a jammed stabilizer and the wing fixed at cruise sweep. Longitudinal trim required in a wings-back landing is actually somewhat less than required in a normal landing. The effect on elevator authority of one or two hydraulic system failures will not prevent a successful landing with the wings aft. The stability augmentation system is not essential during a wings-aft landing (see Section 7.2.3).

7.2.4.2 Flight Controls

a. STABILIZER ACTUATOR FAILURE

Stabilizer actuation failure is an extremely remote possibility due to the high degree of redundancy incorporated in the system. Partial power failure will reduce trim rate only, and will not affect trim authority. Complete power failure will impose out-of-trim-stick forces. It should be noted that stabilizer torque limits have been set to assure that a jack-knifed elevator-stabilizer combination cannot overpower the system.

Runaway trim is easily handled by the pilot since only light force application at the rim of the trim wheel will overpower the low-power electrical system and stop wheel rotation. The pilot can then switch off the electrical system and trim manually. A detailed discussion of the stabilizer system operation is presented in Section 3.2.2.2 of Volume A-VII.

The ability of the elevator to maneuver the airplane throughout the flight envelope without stabilizer trim adjustments is shown in Figs. 7-38 and 7-16. Takeoff, flap and gear retraction and extension, pattern maneuvering and a normal landing can be performed without retrimming.

b. ELEVATOR FAILURE

The loss of a single hydraulic system will deactivate two of the six high speed elevators and will reduce the hinge

moment capability of the low-speed elevator by one third. The remaining hinge moment capability is sufficient to move the low-speed elevator to 30 degrees at takeoff rotation speed. The loss of the two hydraulic systems will deactivate four of the six high-speed elevators and reduce the low-speed elevator hinge moment capability by two thirds. Since the stabilizer provides a backup to the elevators as a longitudinal control system, the pilot is provided with pitch authority of unparallelled redundancy, and therefore, reliability.

Figs 7-17 and 7-39 show the equivalent elevator authority remaining after one and two hydraulic failures for low and high speed flight respectively. The remaining authority can be translated into maneuvering and control capability by reference to Fig. 7-13. Even with the elevator system totally inoperative, the stabilizer provides a potential for longitudinal control.

c. RUDDER FAILURES

The rudder system is similar in redundancy to the elevator system. Ultimate directional control after complete failure of the rudder system is available from differential thrust. As in most airplanes the lateral control system backs up the directional control system in extreme emergencies.

Fig. 7-26 shows the crosswind landing capability of the airplane with single and double failures in the rudder control. Since the airplane may be landed in a crosswind while moderately misaligned with the runway, a single hydraulic failure will still allow landing in the required 30 knot crosswind.

The ability of the partially failed rudder to hold an onboard engine failure during takeoff is shown in Fig. 7-25. It is seen that rudder control power is still adequate to balance the thrust asymmetry with a single rudder failure. With a double hydraulic failure on the rudder, the pilot must throttle the balancing engine. Since considerable reserve thrust is available due to noise limits, this is a safe procedure.

d. LATERAL CONTROL FAILURES

The aileron-spoiler system has redundancy similar to the elevator and rudder. Fig. 7-37 shows the roll rates available after single and double hydraulic failures. It is seen that reasonable control is available even in the remote emergency of a double hydraulic failure.

7.2.4.3 Stability Augmentation

The stability augmentation system is dualized and each independent half operates through one section of the segmented control surfaces. As a result, the worst effect of a hard-over SAS signal is equal to or less than a surface deflection equivalent to one-third of the rudder authority, one-sixth of elevator authority, and an even smaller fraction of roll authority. These effects are further reduced during landing and takeoff operations when the low speed controls are operating.

a. LATERAL AUGMENTATION FAILURES

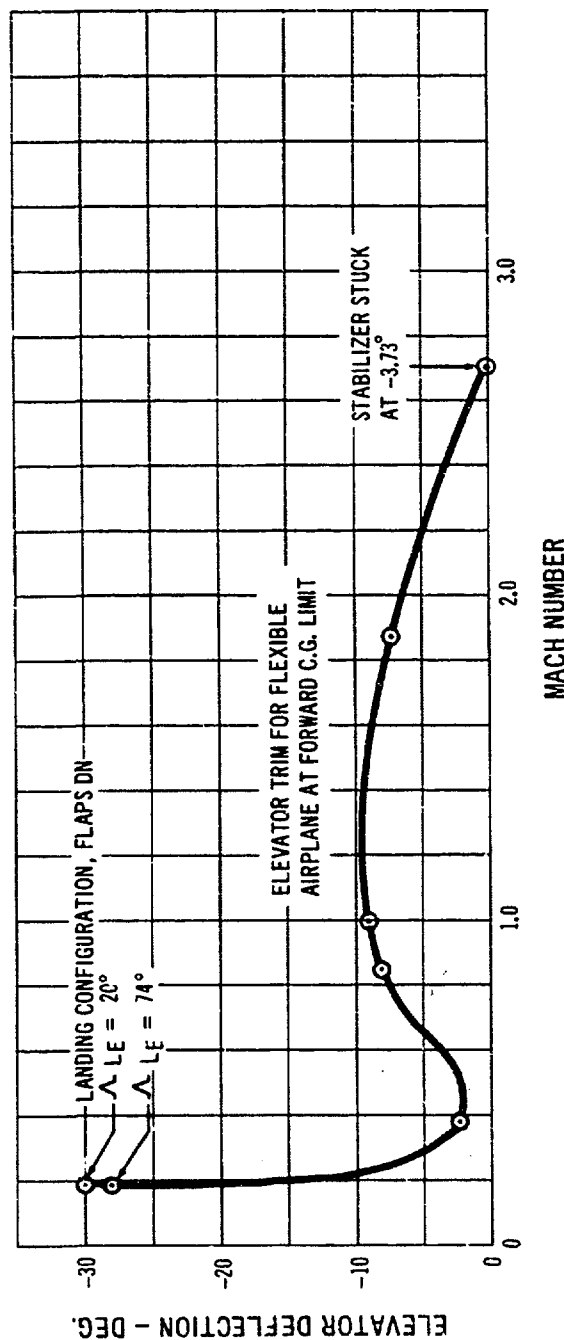
Since the roll damper's only reason for existence is the improvement of roll time constants (Figs. 7-35, 7-36), a failure will only make turn entries and other rolling motions mildly unpleasant.

b. LONGITUDINAL AUGMENTATION FAILURES

Complete failure of the longitudinal augmentation system still yields safe frequency-damping relations for the short period mode at all flight conditions. This is shown in Section 7.2.3.

c. DIRECTIONAL AUGMENTATION FAILURES

Although the yaw augmentation system is triplicated, it is not a safety of flight item. Triplication was adopted to make the extremely remote case of wings-aft landing as easy as possible for the pilot to handle. It has been shown in Section 7.2.3 that even in the case of wing sweep



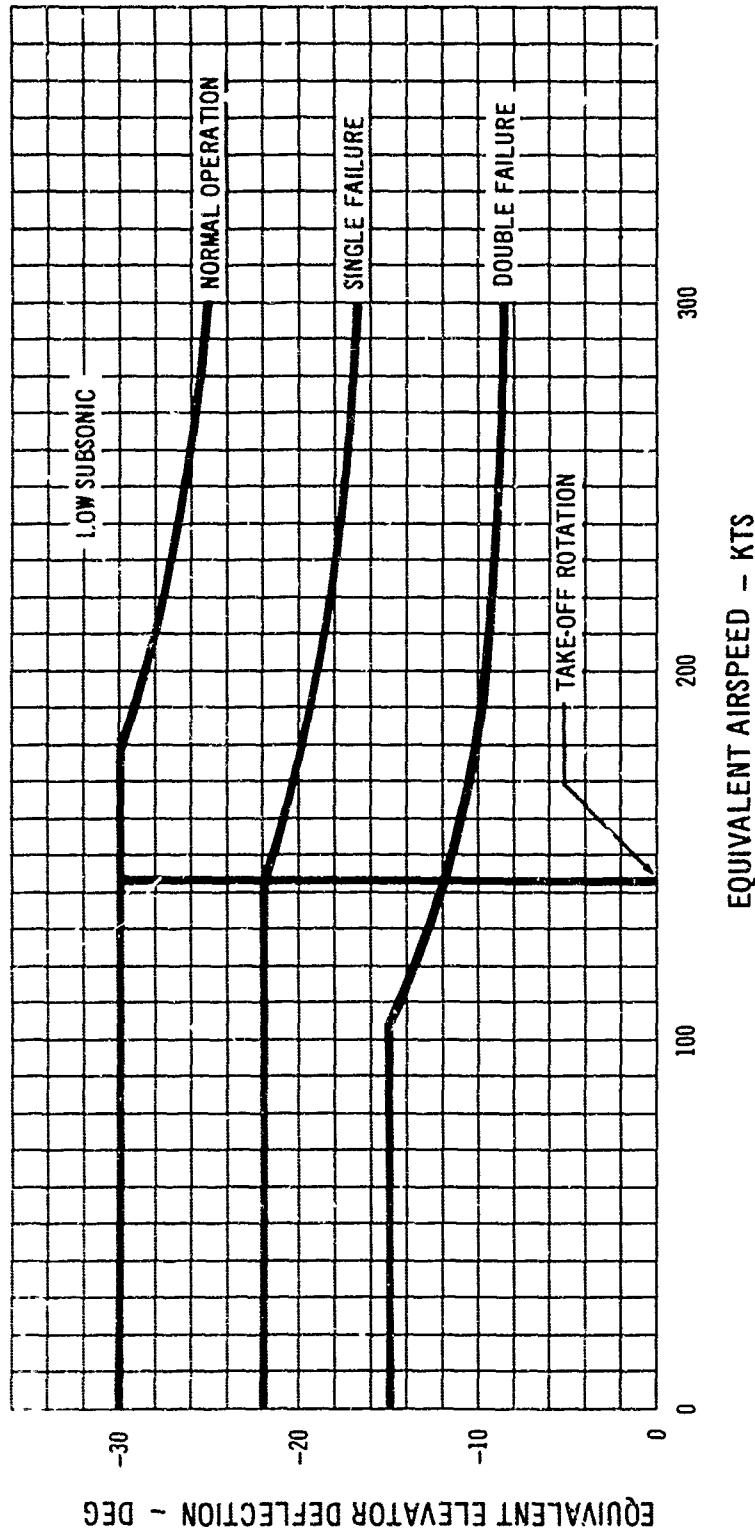
7-38 Elevator Trim Capability Along Normal Descent Schedule with Stabilizer Angle Stuck at Cruise Setting

mechanism failure and accumulated triple failures in the yaw augmentation system, an acceptable flight configuration remains.

7.2.4.4 Engine Inlet Shock Expulsion

The inboard engine placement selected for the proposal airplane minimizes the asymmetric forces and moments on the airplane following an engine failure. At supersonic speeds the shock-induced forces and moments are sensitive to both lateral and fore and aft locations of the engines. Analyses of wind tunnel tests simulating unstalled inlets and predictions of the resulting aircraft motion have shown that a sudden engine failure does not present a dangerous control problem to the pilot or a hazard to the airplane structure.

There are three regimes of flow possible in the 733-197 inlet during supersonic flight, as shown in Fig. 7-40. Condition I, shown for cruise Mach number, is that for a started inlet with the spike shock just impinging on the inlet lip. This is the normal condition of flow. An engine failure or compressor surge momentarily produces Condition II. The strong shock pattern is unstable, and will oscillate from just forward of the inlet face to a point near the spike tip. As the normal shock in the inlet moves forward of the throat, the automatically controlled by-pass doors and the spring-loaded secondary air doors open, establishing flow condition III a fraction of a second following inlet unstart. Condition III is stable, with an oblique shock pattern off the spike, and the normal shock stabilized at the lip.



7-39 Longitudinal Control System Low-Speed Failure Characteristics

The inlet is capable of by-passing sufficient air to stabilize the shocks as in flow Condition III after the windmilling brake has been applied and the engine has decelerated during an engine shutdown. A complete discussion of engine inlet mechanism and characteristics is presented in Volume A-VI, Section 3.4 "Inlet Performance."

Wind tunnel tests were conducted with models of the Boeing proposal airplane to evaluate the aerodynamic

moments and forces on the airplane with the abnormal flow conditions II, and III in the inlet. The tests were conducted with nacelles in several fore and aft and lateral locations, and are discussed in Paragraph D7.5 of the Appendix.

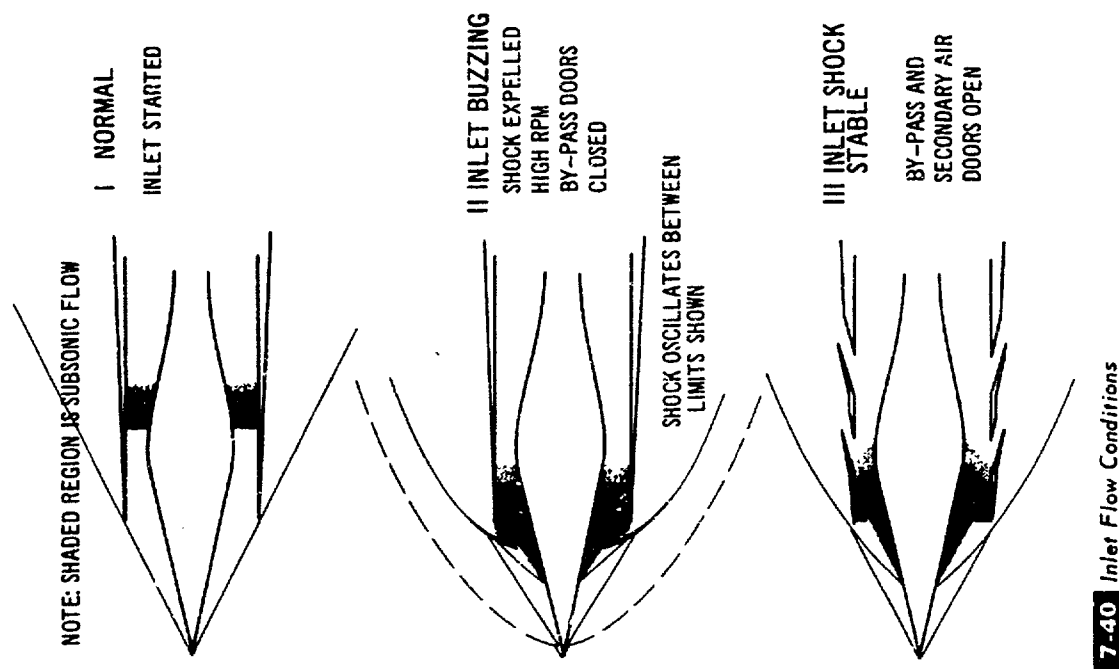
Figures 7-41 and 7-42 present time histories of the airplane motions, without corrective control, following abrupt failure of an engine at 2.7 Mach number. The flight conditions shown are the most critical of the many condi-

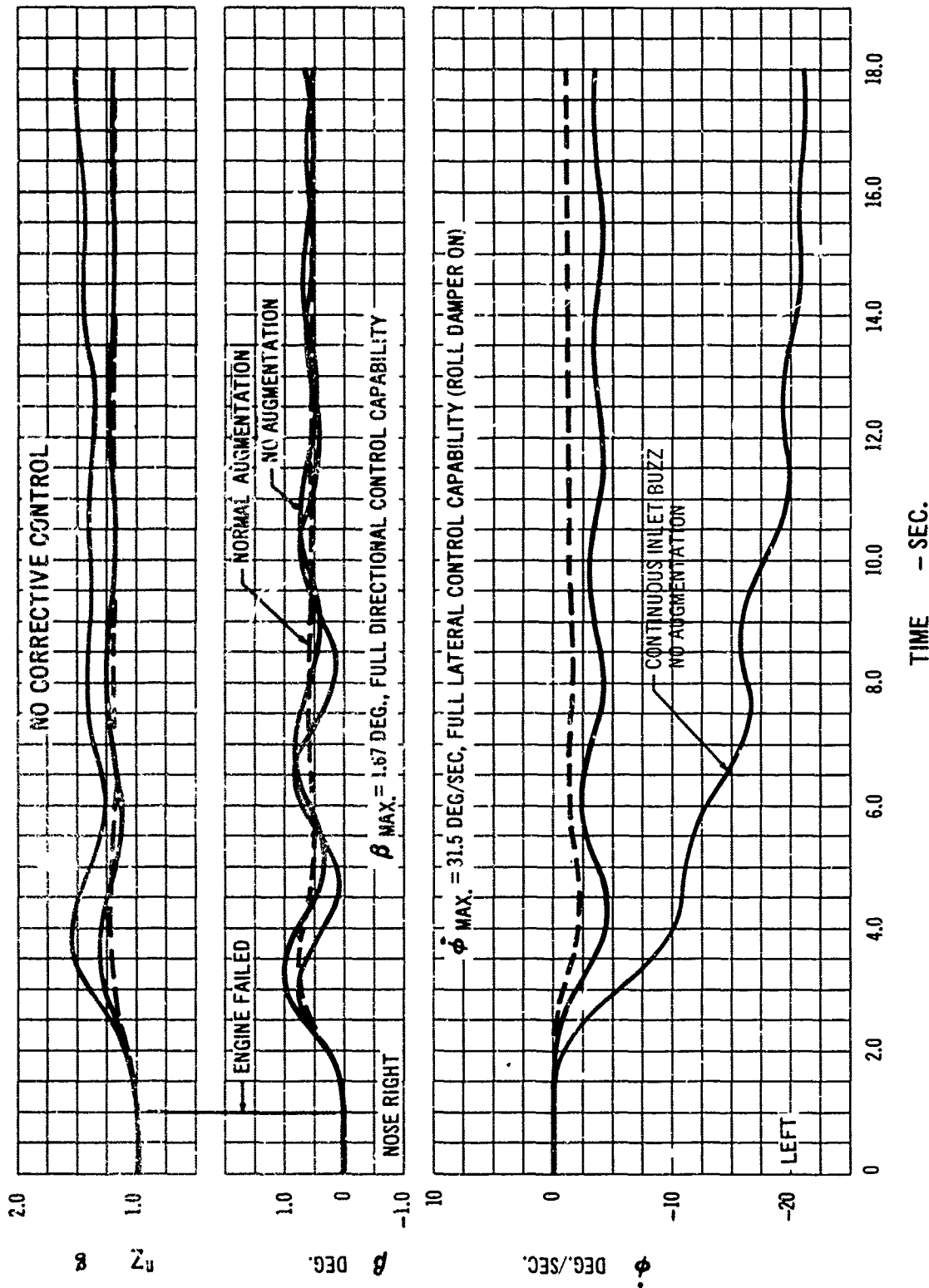
tions analyzed. These are: (1) the failure of an outboard engine at Mach 2.7 at the end of acceleration and climb; and (2) the failure of an inboard engine at the end of cruise. The aerodynamic forces and moments due to the expelled shock pattern used in these analyses are presented in Paragraph D7.5 of the Appendix.

The failure of an outboard engine at the end of acceleration is the more critical of the two conditions. The moments introduced by asymmetric thrust, with the engines operating at acceleration thrust level, are very large compared to the aerodynamic forces and moments resulting from inlet unstart. Figure 7-41 presents time histories of the airplane motions following engine failures without corrective control.

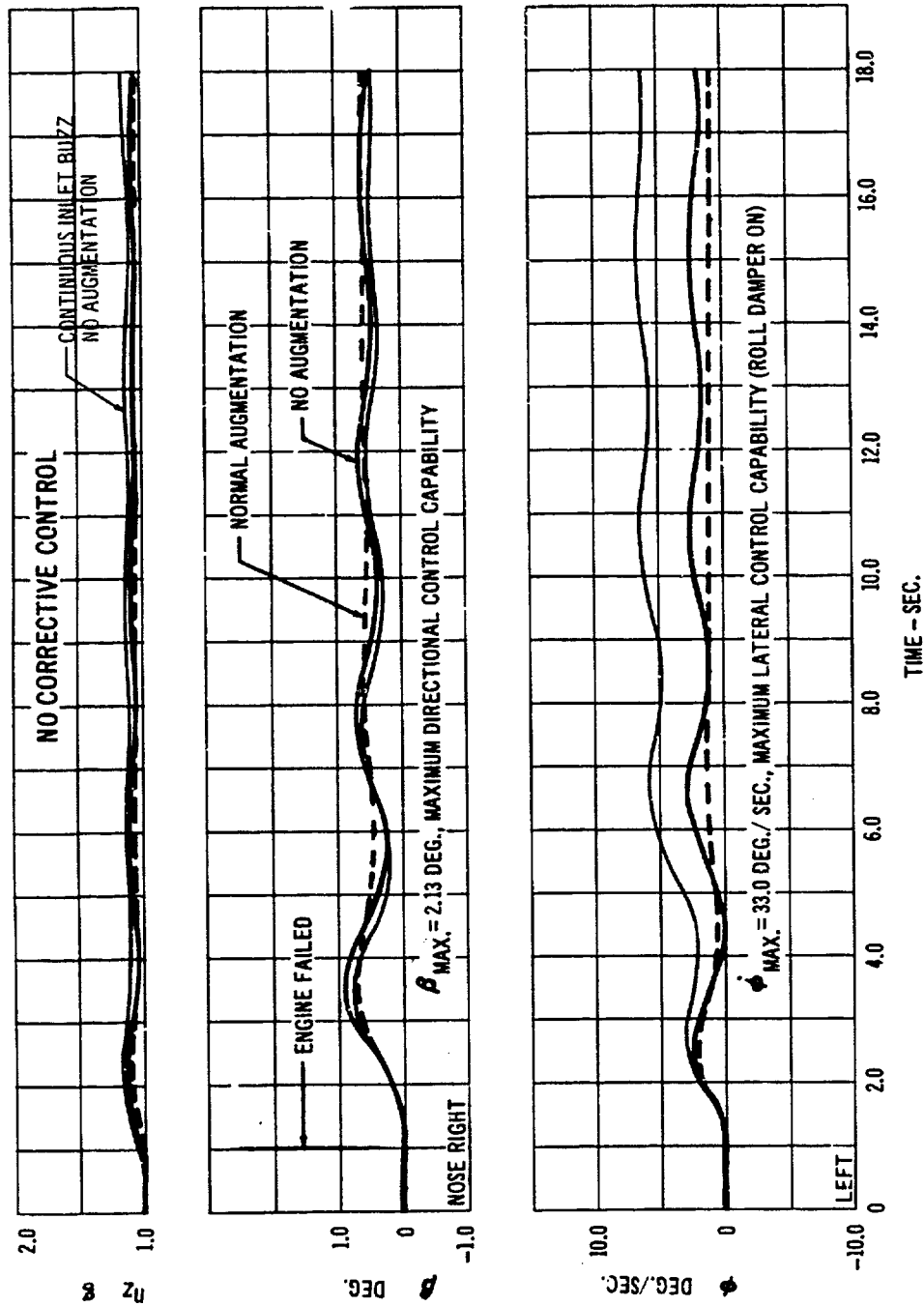
The engines are operating at lower thrust levels at the end of cruise than at the end of acceleration, and the aerodynamic forces and moments due to inlet unstart are more important relative to the asymmetric thrust moments. An inboard engine failure is the more critical at this condition, and the resultant airplane motions are shown in Fig. 7-42. The disturbances are smaller than those present at the end of acceleration and are readily controllable with or without stability augmentation.

As discussed previously, both spring loaded secondary air doors and automatically controlled (powered) by-pass doors are provided. The spring loaded doors are independently capable of establishing flow condition III in case the powered doors fail to open. In a design which might use powered doors only, a failure of the door power would produce condition II (continuous buzz) during the interval between shock expulsion and commencement of the restart cycle. Airplane motion during this condition is also shown on Figs. 7-41 and 7-42. The disturbances to the airplane flight path are seen to be only slightly larger than for the case using by-pass doors, and the airplane is readily controllable.





7-41
 Airplane Dynamics Following Failure of Left Outboard Engine
 (End of Acceleration, Mach = 2.7, h = 55,200 Ft.)



7.42 Airplane Dynamics Following Failure of Left Inboard Engine
(End of Cruise, Mach = 2.7, $h = 68,500$ Ft)

SECTION 8

FLIGHT CRITERIA

TABLE OF CONTENTS

8.0 FLIGHT CRITERIA.....	8/1
8.1 Design Weights.....	8/1
8.2 Flight Load Factors.....	8/2
8.2.1 Maneuver Load Factor.....	8/2
8.2.2 Gust Load Factor.....	8/2
8.3 Center of Gravity Limits.....	8/3
8.4 Mission Profiles.....	8/4
8.5 Design Airspeed.....	8/4
8.5.1 Flap Speeds— V_i	8/5
8.5.2 Maneuvering Speeds— V_A	8/5
8.5.3 Speed for Maximum Intensity Gust— V_B	8/5
8.5.4 Cruising Speed— V_C	8/6
8.5.5 Maximum Operating Speed— V_{MO} , M_{MO}	8/6
8.5.6 Dive Speed— V_D , M_D	8/6
8.5.7 Wing Sweep Placard Speeds.....	8/6
8.5.8 Landing Gear Placard Speeds.....	8/9
8.5.9 Aileron Operating Speeds.....	8/9
8.5.10 Spoiler Operating Speeds.....	8/9
8.6 V-n Diagrams.....	8/9
8.7 Fatigue Load Spectra.....	8/13

9.0 FLIGHT CRITERIA (RFP 3.2.6)

The design criteria for the proposal airplane comply with the requirements of Civil Aeronautics Manual 4b (CAM 4b) (Ref. 9) including the current amendments and appendices. In addition, special criteria are applied as necessary to assure structural integrity, with careful attention to special problem areas of the supersonic transport.

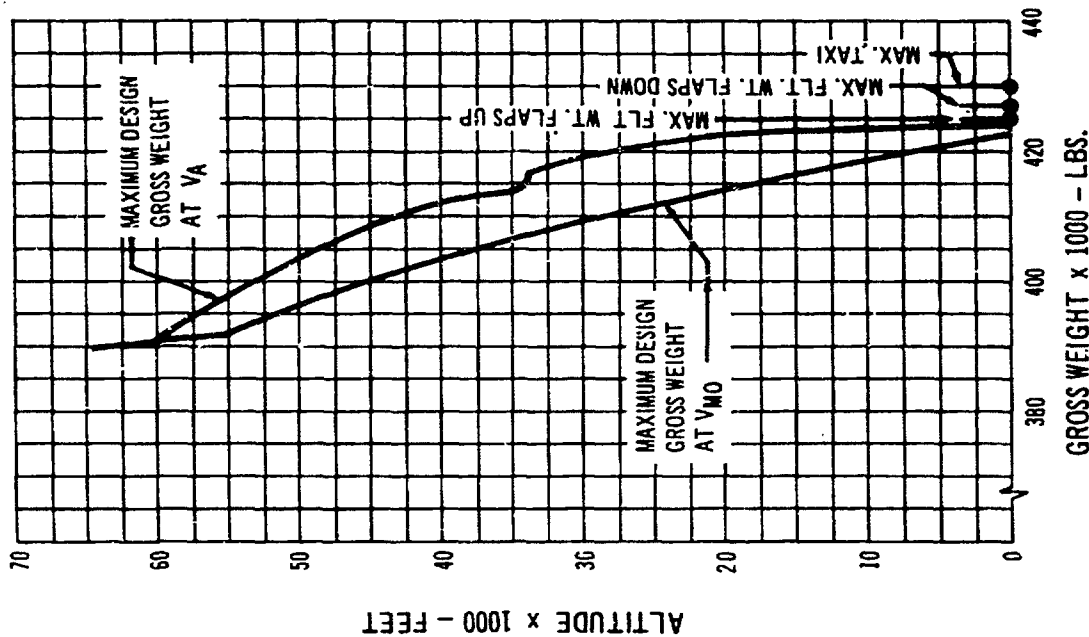
Aerodynamic and inertia load distributions are obtained from analyses which place the airplane in equilibrium with regard to vertical forces and pitching moments. Consideration is given to center of gravity location, mass distribution, wing sweep position, and thermal environment effects. The design loads and methods used in obtaining these loads are presented and discussed in Volume A-IV, "Structural Report."

8.1 Design Weights

Airplane gross weights for structural design are consistent with the CAM 4b.210. The maximum flight design weights consider fuel usage during acceleration and climb. The reserve fuel for minimum flying weight is based on the requirements of CAM 4b.210(c). Design gross weights are as follows:

Maximum Ramp Weight	430,000 pounds
Operator's Weight Empty	182,500 pounds
Minimum Flying Weight	195,000 pounds
Maximum Flight Weight	427,000 pounds
Flaps Down	425,000 pounds
Flaps Up	
Design GW with Zero Outboard Wing Fuel	360,000 pounds
Maximum Landing Weight	260,000 pounds
Beginning of Cruise Max Weight	390,000 pounds

The maximum design gross weight versus altitude which is used for structural design is shown in Fig. 8-1.



8-1 Maximum Design Gross Weight



8.2 Flight Load Factors

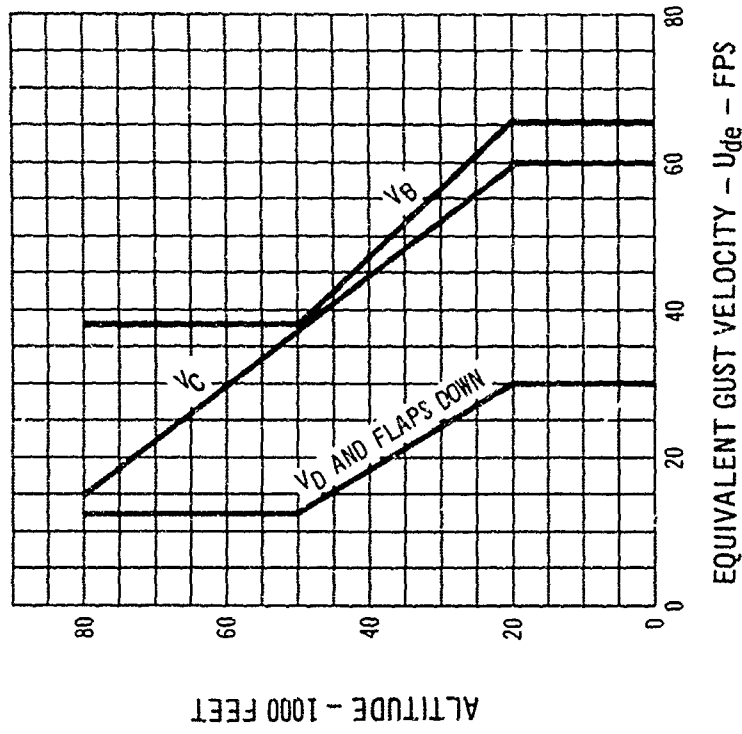
Criteria for design limit load factors are presented for both maneuver and gust conditions. An ultimate factor of safety of 1.5 is applied to all limit conditions.

8.2.1 MANEUVER LOAD FACTOR

In general, the requirements of CAM 4b.211 (a) and CAM 4b.212 are applicable. Symmetric flap-up maneuvers to a limit positive load factor of 2.5 and a limit negative load factor of 1.0 are considered between the design maneuvering speeds V_A and V_D/M_D .

At the operator's weight empty, a maneuver load factor of 2.25 is used; whereas, at the minimum flying weight, a maneuver load factor of 2.5 is used. For the takeoff and landing configurations, with both leading edge and trailing edge flaps deflected, maneuvers are restricted to a positive load factor of 2.0 and a negative load factor of 0.0.

From V_A to V_{SO} the ultimate fail-safe maneuver load factor is 2.0 combined with a factor of 1.15 to account for dynamic effects of failure under static load.

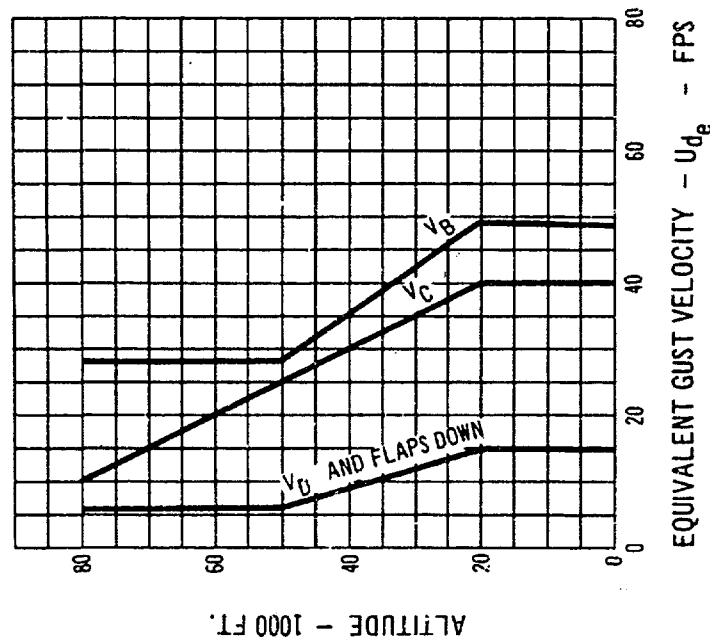


8-2 Design Gust Velocities

8.2.2 GUST LOAD FACTOR

The gust loadings are defined by the sharp edge gust concept. During Phase II, additional analyses will be made based on discrete gust and power spectral methods.

When using the sharp edge gust method, the requirements of CAM 4b.211 (b) apply except that, for cruise conditions, the cruise gust velocity as defined in CAM 4b.211 (b) (2) is increased to 60fps at all altitudes be-

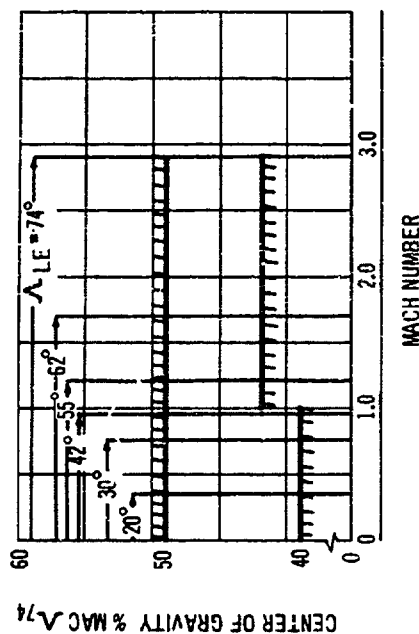


8-3 Fail Safe Design Gust Velocities

tween sea level and 20,000 feet, decreasing linearly to 15 fps at 80,000 feet. Gust velocities for V_n and V_o are assumed constant above 50,000 feet.

Design gust velocities are shown in Fig. 8-2 and the fail-safe gust velocities are shown in Fig. 8-3. The airplane rigid lift curve slope is used in the analysis.

Details of the power spectral analyses to be conducted in Phase II are presented in Volume A-IV, "Structural

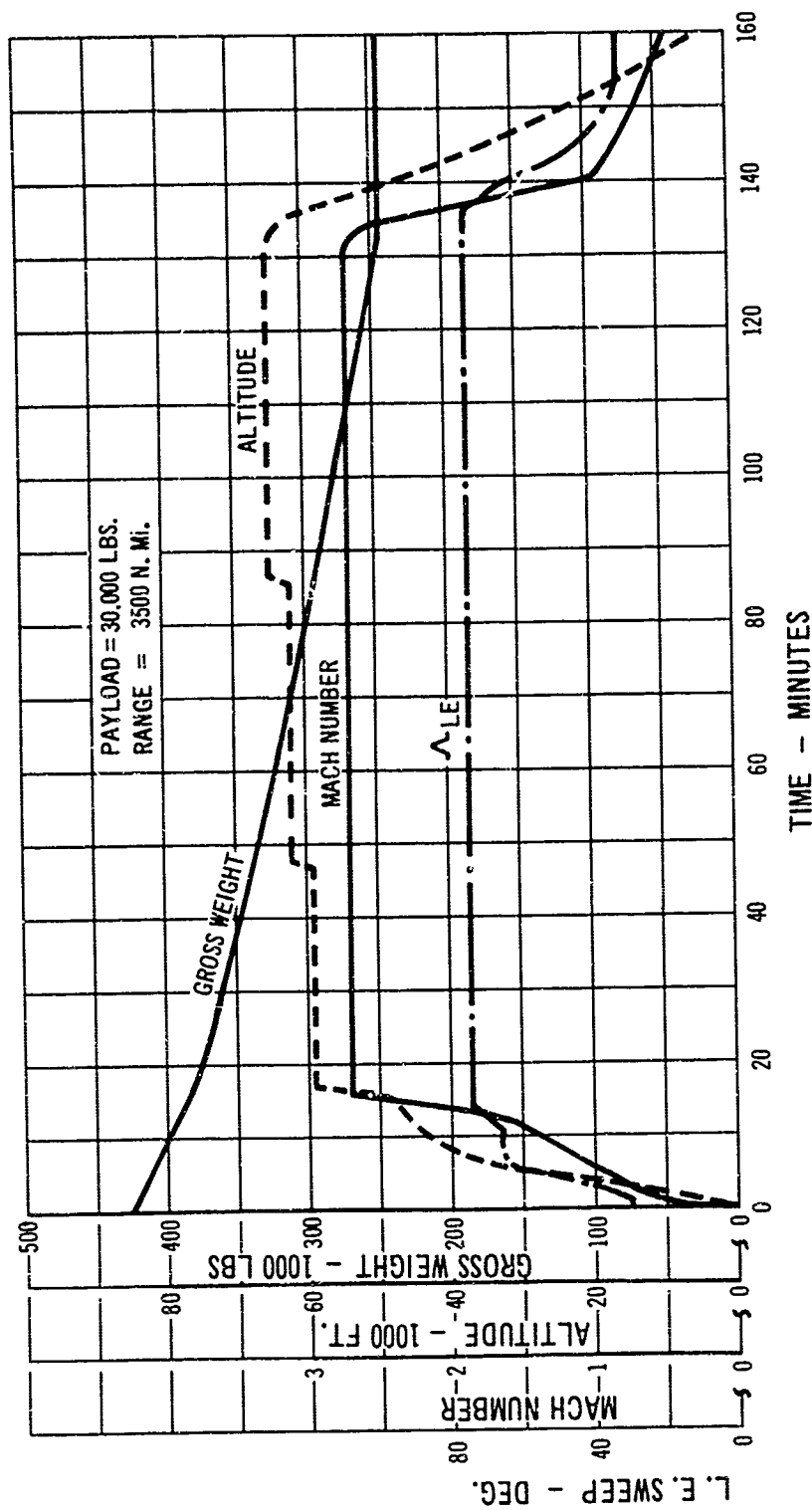


8-4 Structural Design - C. G. Limits

Report." This analysis will be used as a supplemental study and will assist in the establishment of structural design loads. Design by sharp edge gust methods will be continued, and dynamic amplification allowances will be determined from comparisons with power spectral analyses.

8.3 Center of Gravity Limits

Structural design center of gravity limits allow for unrestricted loading of passengers. Fuel movement due to flight attitude is considered. The structural design limits are one percent MAC outside the operational limits to allow for CG movements due to fuel shift during extreme attitude conditions. The design center of gravity envelope is shown in Fig. 8-4.



8-5 Basic Mission Profile

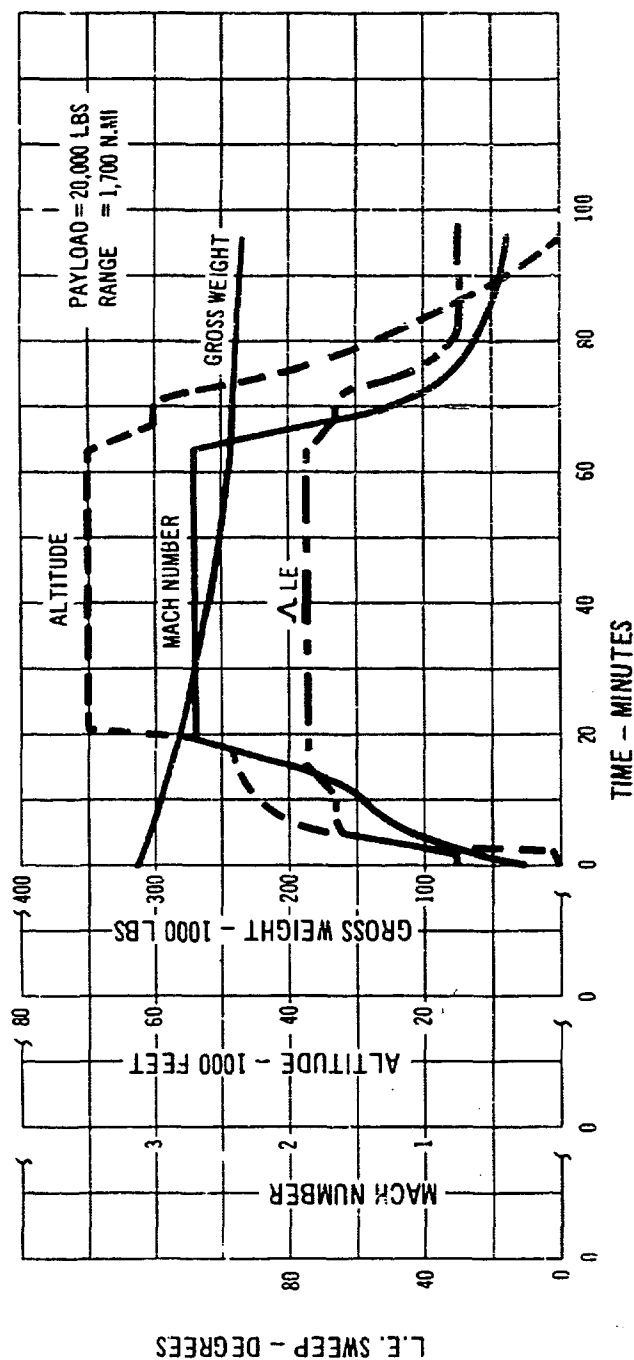
8.4 Mission Profiles

The changes in airplane gross weight, speed, altitude, and wing sweep with flight time for the basic 3500 nautical mile design mission are illustrated in Fig. 8-5. The basic mission profile is used to determine the temperature spectra for calculations of thermal effects presented in Section 6.0 of Volume A-IV, "Structural Report." Both this basic design mission and a shorter mission of 1700 nautical

miles are considered in the fatigue analysis. The length of the shorter mission is a weighted average based on projected SST usage. The profile for this mission is shown in Fig. 8-6.

8.5 Design Airspeeds

Except for special considerations used in establishing maximum design dive speeds is noted in Section 8.5.6 structural design air speeds comply with CAM 4b.210(b). Wing



8.6 1700 Nautical Mile Mission Profile

sweep position design limit versus flight Mach number and altitude are shown in Figs. 8-7a, 8-7b, and 8-7c.

8.5.1 FLAP SPEEDS— V_r

Flap placard speeds for takeoff and landing configurations are set to give the recommended margins on the stall speeds as specified in CAM 4b. The flap placard speeds are shown in Fig. 8-9.

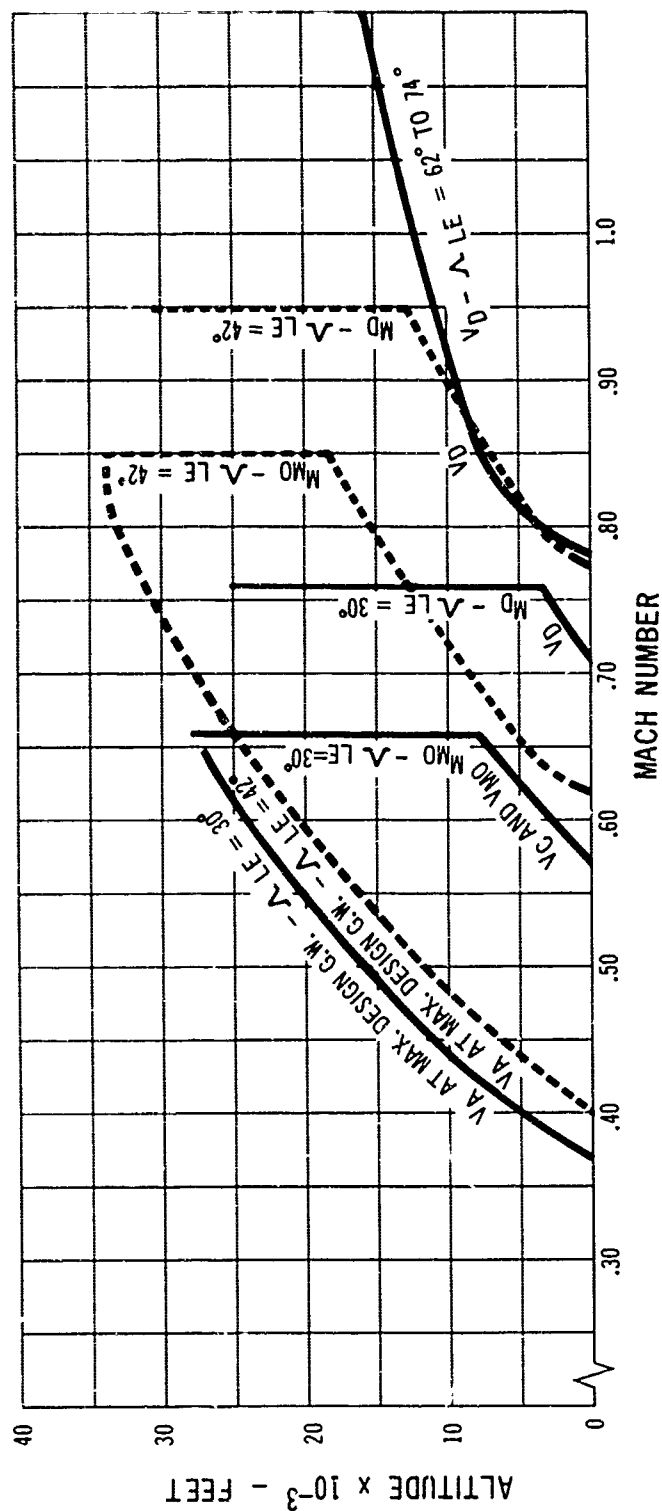
8.5.2 MANEUVERING SPEEDS— V_A

Design maneuvering speeds for all applicable wing sweep

positions are selected where the positive C_N max curve intersects the positive maneuver load factor line. In establishing V_A , consideration is given to the maximum static lift coefficient as well as the maximum lift coefficient based on airplane control limits. The V_A speed versus altitude is shown on Fig. 8-8.

8.5.3 SPEED FOR MAXIMUM INTENSITY GUST— V_B

For subsonic flight, maximum intensity gust penetration speeds comply with the requirements of CAM 4b.210 (b) (3),



8-7 a Design Speed-Altitude Envelopes - Low Sweep Range

and are consistent with airplane slowdown capability. Wing sweep position is considered in establishing V_B speeds. V_B is not considered at supersonic speeds.

8.5.4 CRUISING SPEED— V_C

The design cruising speed conforms with CAM 4b.210(b) (4). The maximum operating speed V_{MO} , Section 8.5.5, is equal to V_C .

8.5.5 MAXIMUM OPERATING SPEED— V_{MO} , M_{MO}

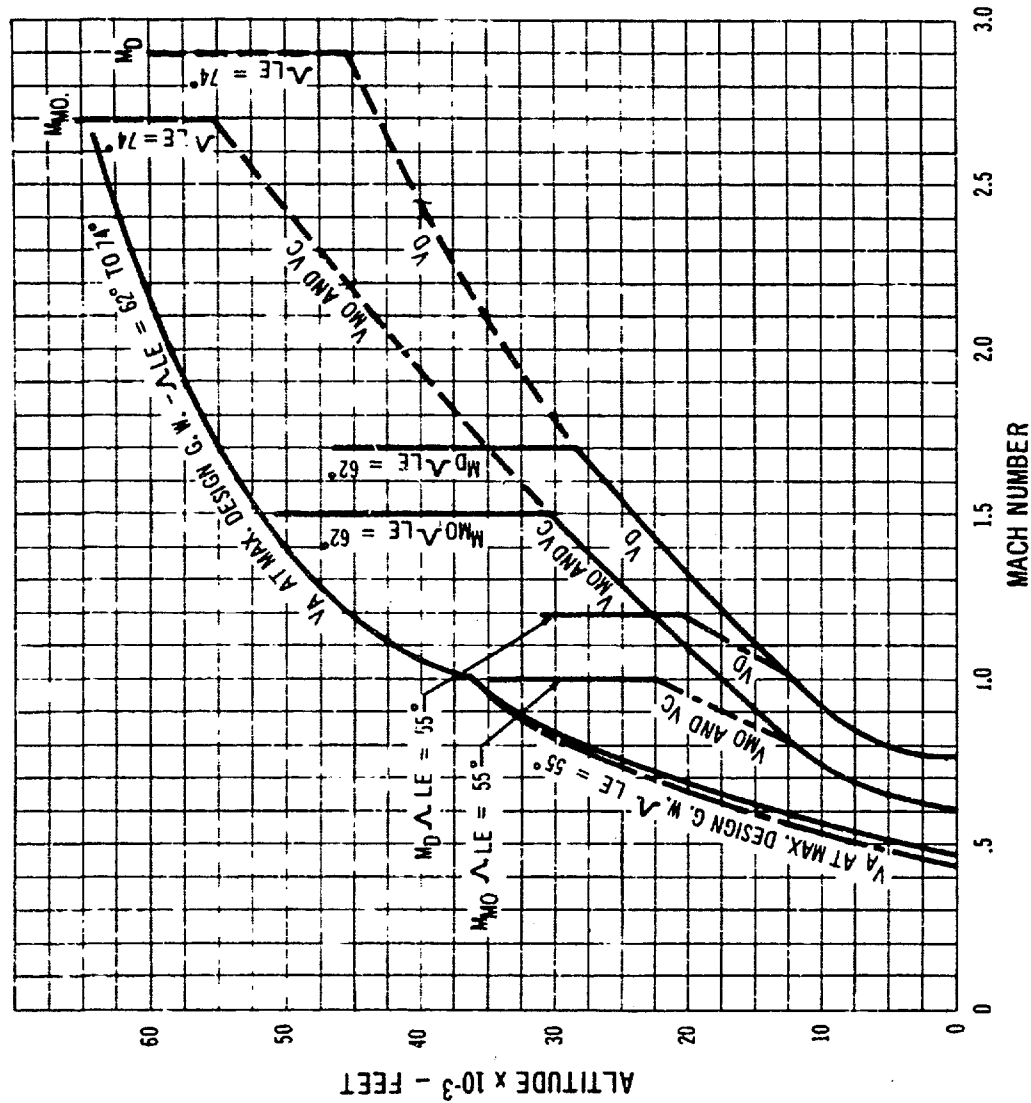
The maximum operating speed boundary, V_{MO} , is set by gust and engine pressure limitations. M_{MO} is set by a stagnation temperature of 500° F, but does not exceed Mach 2.7. See Figs. 8-8, 8-7a, and 8-7b.

8.5.6 DIVE SPEED— V_D , M_D

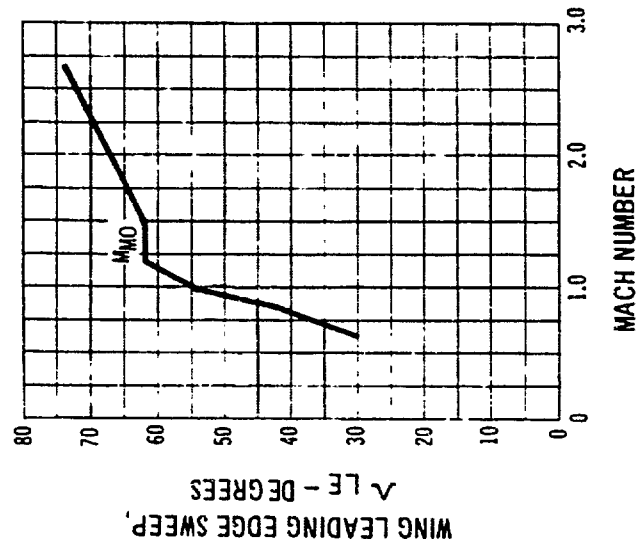
The dive speed V_D , is determined as 1.25 V_{MO} at subsonic speeds and at supersonic speeds, by a 7½ degree nose down upset with cruise thrust for twenty seconds followed by a .5g pullout maneuver. In addition, V_D/M_D has a margin of at least .2M over V_{MO}/M_{MO} at all supersonic speeds (Figs. 8-7a and 8-7b).

8.5.7 WING SWEEP PLACARD SPEEDS

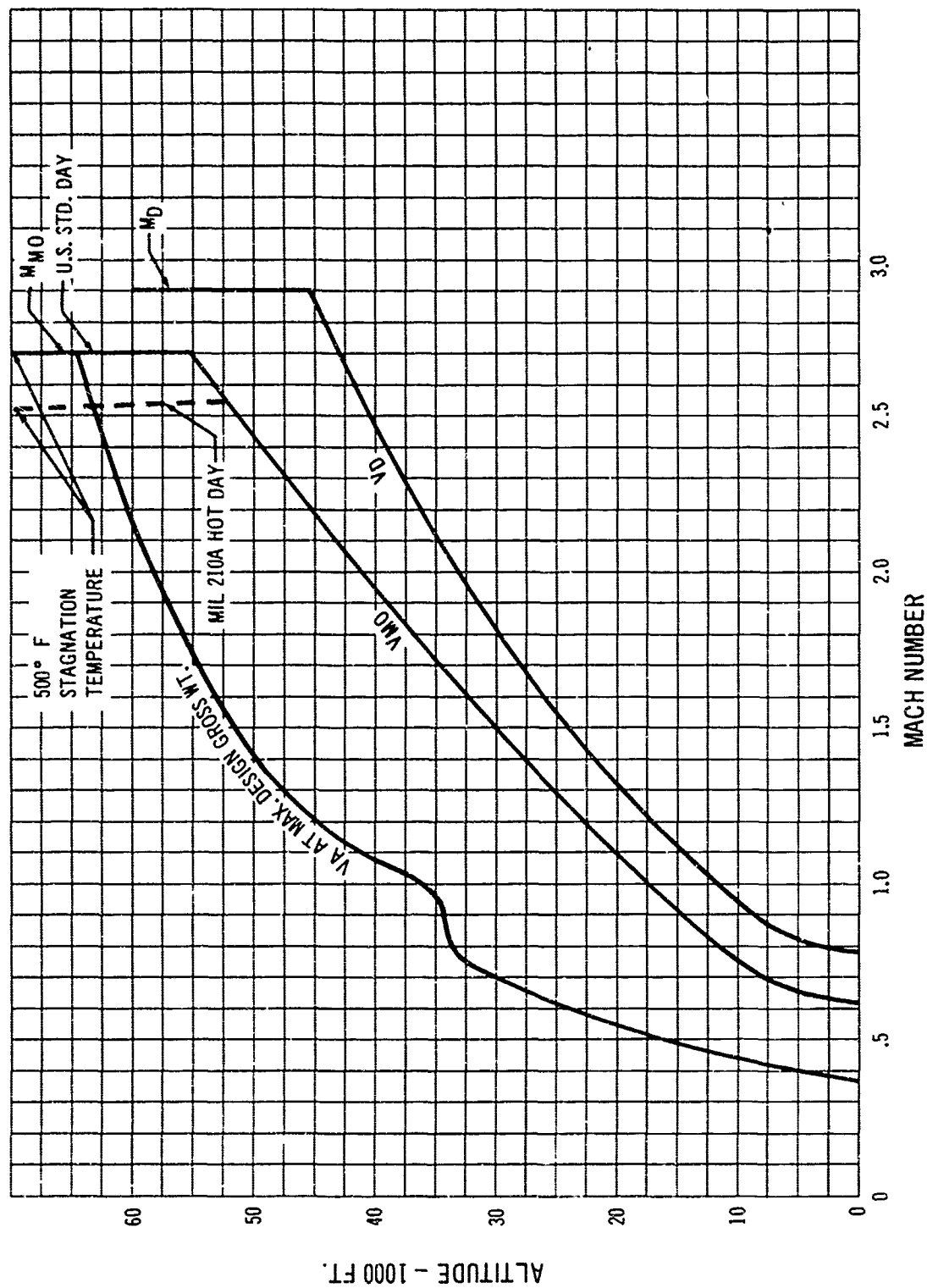
The operational wing speed schedule is selected on the basis of performance and pilot technique. However, the structural design of the wing allows a tolerance on sweep position to allow for inadvertent overspeeds. The structural limits on wing sweep position are noted on Figs. 8-7a through 8-7c.



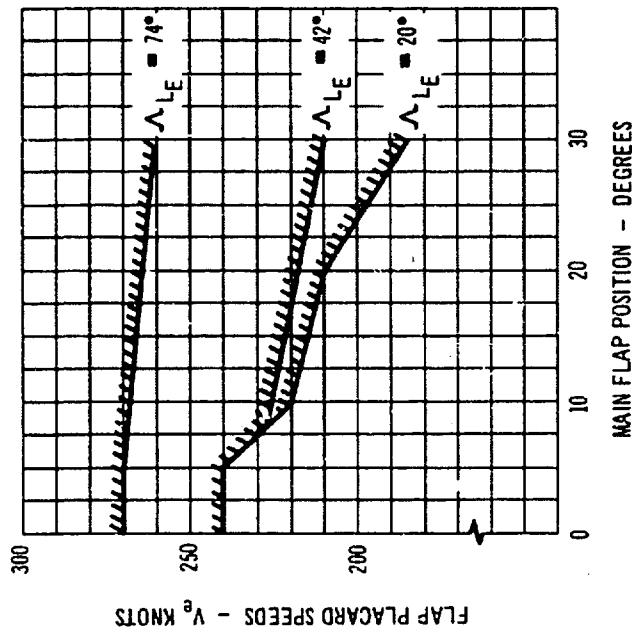
8-7 b Design Speed - Altitude Envelopes - High Sweep Range



8-7 c Wing Sweep Placard



8-8 Speed Altitude Diagram



8.9 Flap Placard Speeds

8.5.8 LANDING GEAR PLACARD SPEEDS

The landing gear placard speeds are established to be compatible with the landing and takeoff procedures of the airplane, and are similar to those of the Boeing Model 707 airplanes, as shown below:

Operating Speed, V_{LO}	270 knots EAS or $M = .90$ (extending)
Extended Speed, V_{LE}	270 knots EAS or $M = .83$ (retracting)
	320 knots EAS or $M = .90$



8.5.9AILERON OPERATING SPEEDS

For normal operations, the ailerons are used for roll control in the low speed regime only and will be locked out when the wing is swept aft of 30°. For all landing conditions, the operating speed placard is consistent with the flap placard speeds of Fig. 8-9.

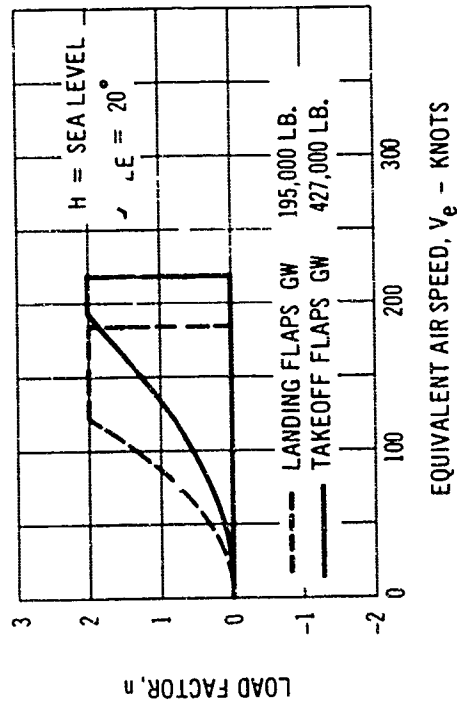
8.5.10 SPOILER OPERATING SPEEDS

There are two banks of spoilers, one inboard and one outboard. The outboard bank is used at all speeds and consists of both upper and lower surface spoilers. Use of inboard spoilers and outboard lower surface spoilers is limited to sweep angles of 30° or less.

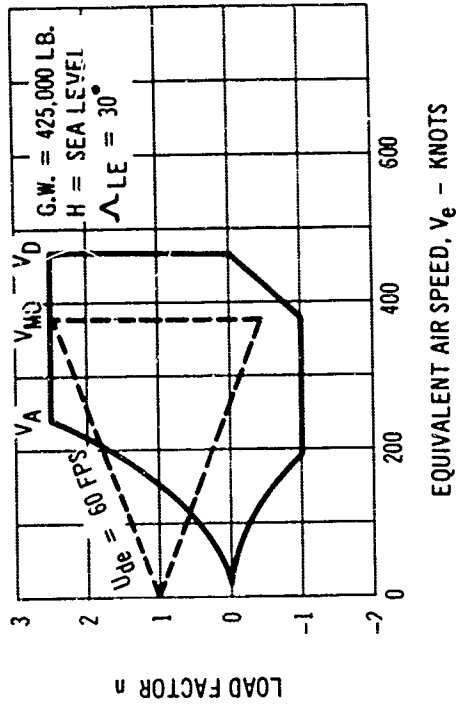
The operating speed placard for each bank of spoilers is consistent with the wing sweep placard speeds of Figs. 8-7a and 8-7b.

8.6 V-n Diagrams

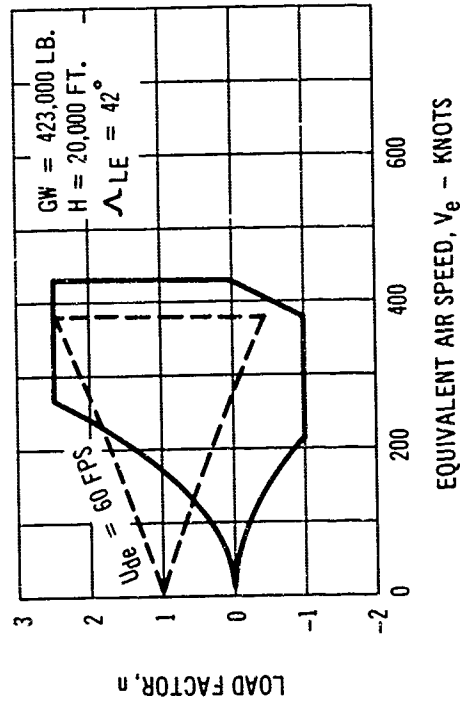
Maneuvering and gust envelopes illustrated in Figs. 8-10a through 8-10h show combinations of gross weight, speed, and load factor at constant altitude for both the clean and the high-lift configurations. The V-n diagrams are presented for individual wing sweep positions consistent with the operation of the airplane.



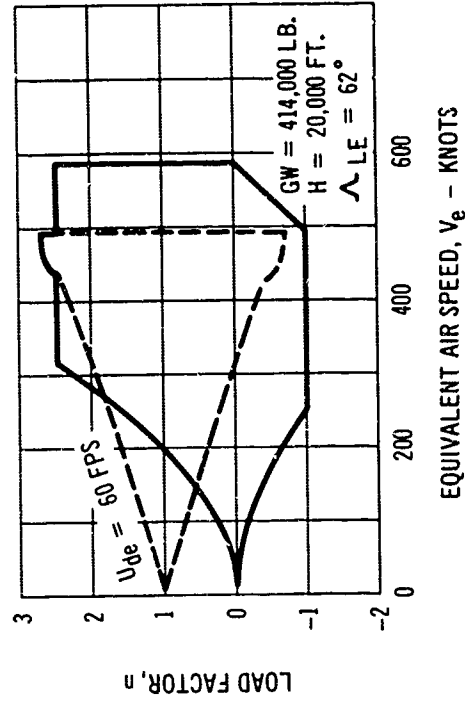
8-10 a V-n Diagram Flaps Down



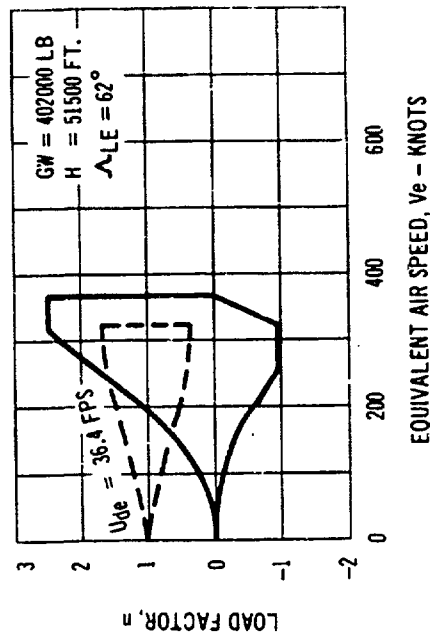
8-10 b V-n Diagram, Maximum Flight Weight



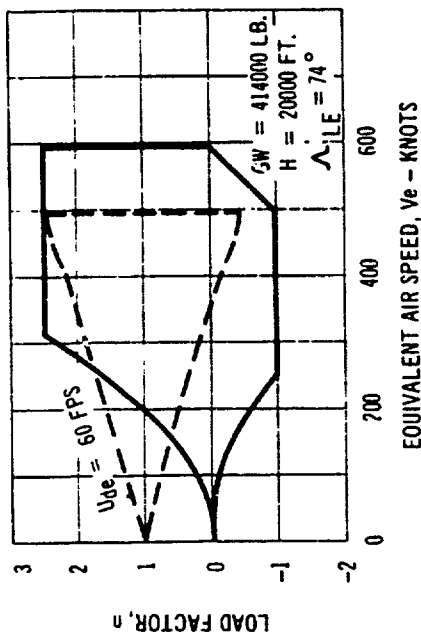
8-10 c V-n Diagram, Maximum V_A Climb Weight



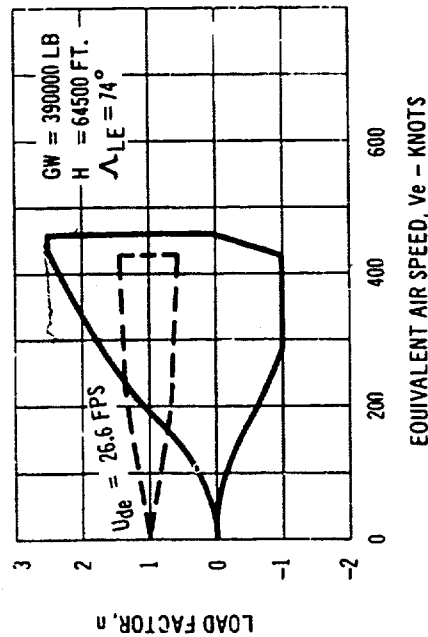
8-10 d V-n Diagram, Maximum V_{MO} Climb Weight



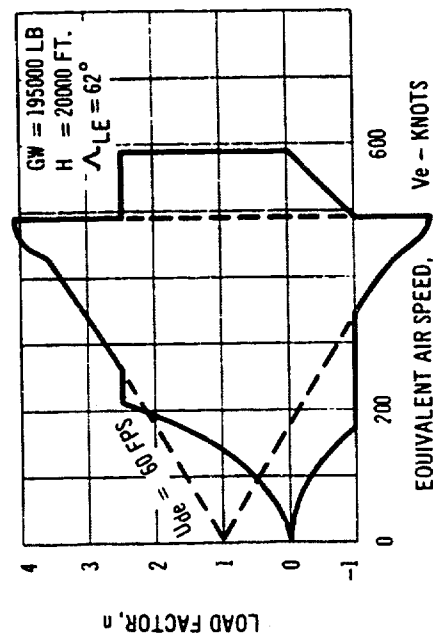
8-10 e V-n Diagram, Maximum V_A Climb Weight



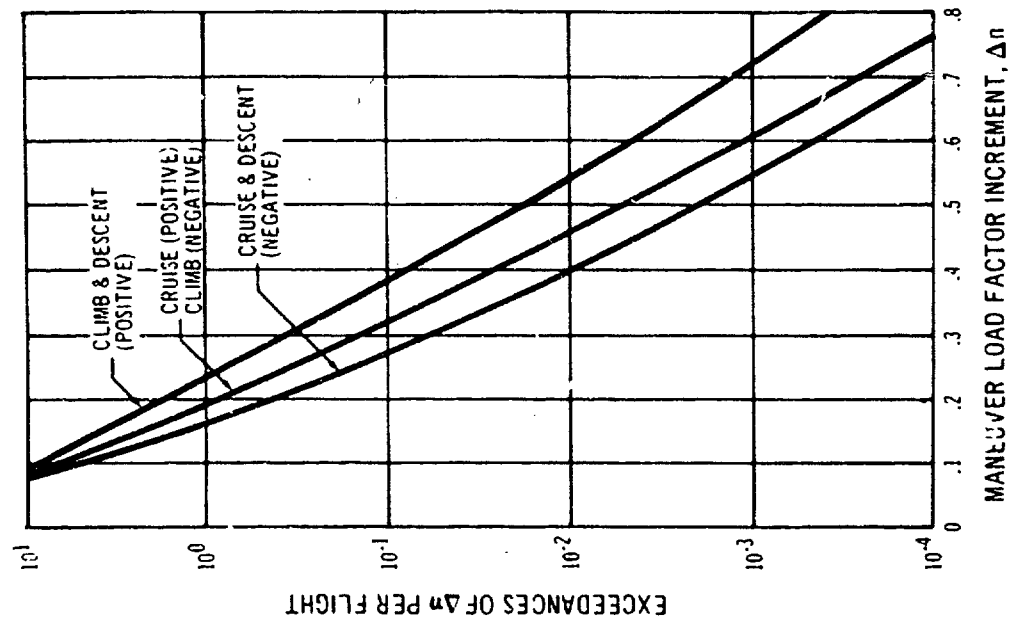
8-10 f V-n Diagram, Maximum V_{MO} Climb Weight



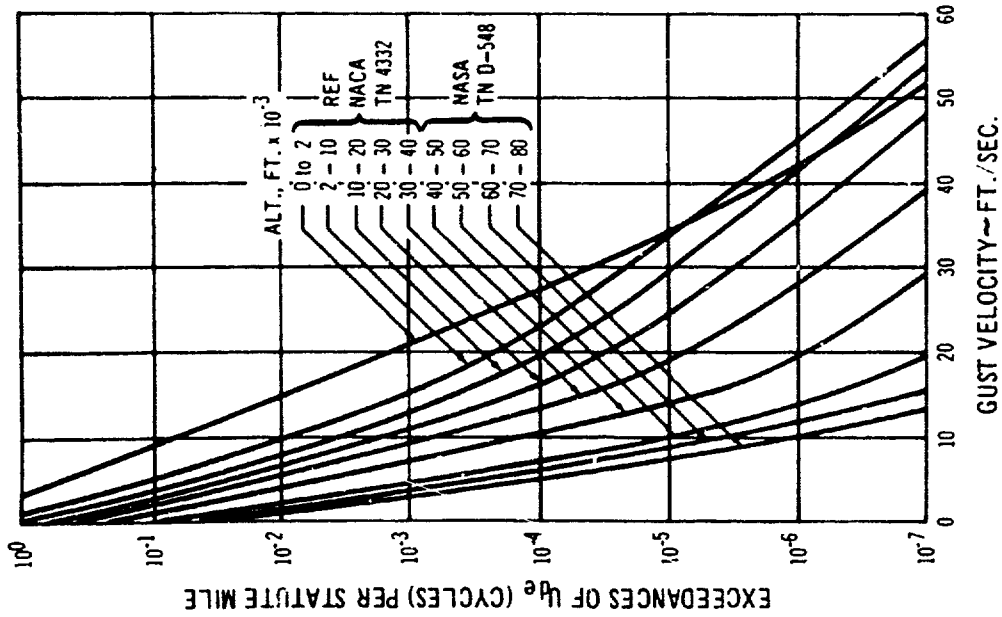
8-10 g V-n Diagram, Maximum V_{MO} Climb Weight



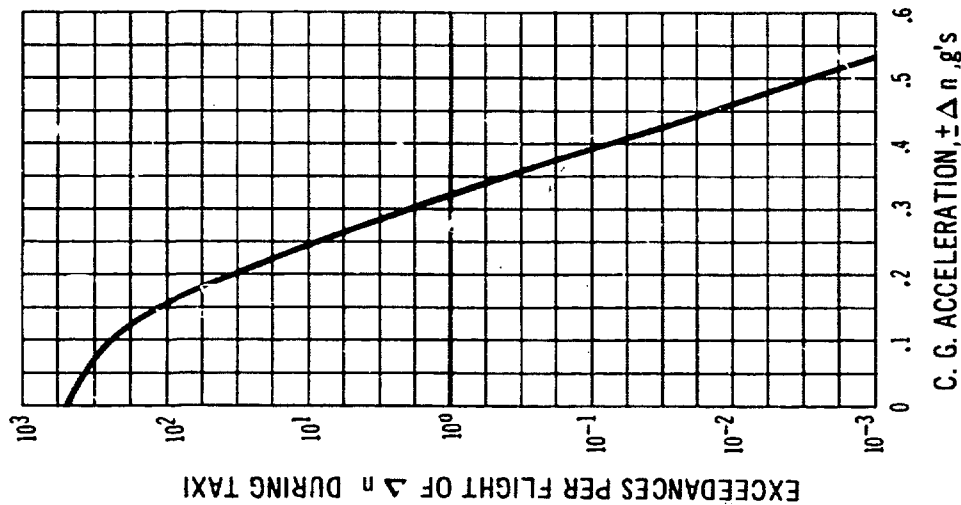
8-10 h V-n Diagram, Minimum Flying Weight



8-11 Maneuver Load Factor Spectra



8-12 Gust Spectra



8-13

Taxi Load Factor Spectrum

8.7 Fatigue Load Spectra

The loading spectra on which the fatigue life evaluation is based are derived from established environmental data, subsonic transport operational experience, and projected SST usage. The types of loadings considered for the preliminary fatigue analysis, presented in Section 9.1 of Volume A-IV, are those resulting from gusts, maneuvers, runway roughness, body pressurization, and temperature gradients. Spectra will be developed during Phase II for loads resulting from buffet, landing impact, braking, pivoting, turning, and slowing.

The gust environment is taken from Ref. 10, and is shown in Fig. 8-12. Reliance on discrete gust methods will be continued until sufficient operating experience on large supersonic airplanes has been established and adequate power spectral design methods are available.

The maneuver load spectra are based on the data received from the Airworthiness Branch, ASMD, NASA Langley Research Center (letter dated May 15, 1963). Exceedance curves, faired through the plotted data points, are shown in Fig. 8-11 for operational flights. Similar data are available for training flights and will be incorporated into the fatigue analysis during Phase II.

Runway roughness data are taken from Ref. 11. Of the several runway definitions presented in the reference, the one designated "airline experience" was selected, and is shown in Fig. 8-13. For application, half of the load factor increments per flight are assumed to occur during taxi-out at the takeoff gross weight and half during taxi-in at the landing gross weight.



REFERENCES

D6-2400-11

REFERENCES

Copies of the following referenced data may be obtained by making a request to either:

The Boeing Company
Suite 120 Commonwealth Building
1625 K Street
Washington 6, D.C.

or

The Boeing Company, Airplane Division
P.O. Box 707
Renton, Washington
Attn: M. L. Pennell
Organization 6-2000
Mail Stop 73-60

1. Jones, R. T., and Doris Cohen, Aerodynamics of Wings at High Speeds, Sec. A in "Aerodynamic Components of Aircraft at High Speeds," Vol. VII of "High-Speed Aerodynamics and Jet Propulsion," Princeton University Press, Princeton, 1957.
2. Carlson, H. W., "The Influence of Airplane Configuration on Sonic Boom Characteristics." Paper presented at AIAA-ASD Vehicle Design and Propulsion Meeting, 1963.
3. Maglieri, D. J. Ritchie, V. S. and Bryant, John F., "In Flight Shock-Wave Measurements Above and Below a Bomber Airplane at Mach Numbers from 1.42 to 1.69." NASA TN D-1968, 1963.
4. Carlson, H. W., "An Investigation of the Influence of Lift on Sonic Boom Intensity by Means of Wind Tunnel Measurements of the Pressure Fields of Sev-

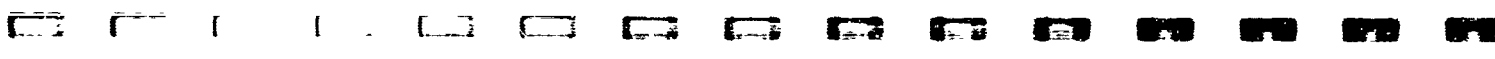
- eral Wing-Body Combinations at a Mach number of 2.01." NASA TN D-881, 1961.
5. Hubbard, H. H., et al, "Ground Measurements of Sonic Boom Overpressures for the Altitude Range of 10,000 feet to 75,000 feet." NASA TM X-633, 1962.
6. Carlson, H. W., "The Lower Bound of Attainable Sonic Boom Overpressure and Design Methods of Approaching This Limit." NASA TN D-1494, 1962.
7. Carlson, H. W., and Morris, Odell A., "Wind Tunnel Investigation of the Sonic Boom Characteristics of a Large Supersonic Bomber Configuration." NASA TM X-898, 1963.
8. Jones, L. B., "Lower Bounds for Sonic Bangs." Journal of the Royal Aeronautical Society, Volume 65, 433-436, 1961.
9. CAM 4b Airplane Airworthiness Transport Categories, September, 1962.
10. Coleman, T. and Stickley, J., "Turbulence Environment for Supersonic Transports." Society of Experimental Test Pilots, Quarterly Review - Supersonic Transport Symposium, Volume V, Number 4, 1961.
11. Milwitsky, B., "Study of Taxiing Problems Associated with Runway Roughness." NASA Memo 2-21-59L, February, 1959.
12. Omitted.
13. Tien, C. and Blegen, K., "Substantiation of IBM Program (TA-08-II) for Calculation of Take-Off and Landing Performance." Boeing Document D6-6431.
14. Kulfan, R. M., "Turbulent Boundary Layer Flow Past a Smooth Adiabatic Flat Plate." Boeing Docu-

- ment D6-7161, May, 1961.
- *15. Czarnicki, K. R., Jackson, M. W., and Monta, W. J., "Studies of Skin Friction at Supersonic Speeds, in 'Proceedings of NASA Conference on Supersonic Transport Feasibility Studies and Supporting Research.' Pages 177 to 190, 1963.
 16. Chapman, D. R., and Kester, R. H., "Turbulent Boundary Layer and Skin Friction Measurements in Axial Flow Along Cylinders at Mach Numbers Between 0.5 and 3.6." NASA Technical Note 3097, 1955.
 17. Matting, F. W., Nyholm, D. R., Thomas, J. R., and Thomas, A. G., "Turbulent Skin Friction at High Mach Numbers and Reynolds Numbers in Air and Helium." NASA R-82, 1961.
 18. Shutts, W. H., Hartwig, W. H., Weiler, J. E., "Final Report on Turbulent Boundary Layer and Skin Friction Measurements on a Smooth, Thermally Insulated Flat Plate at Supersonic Speeds." Defense Research Laboratory Report, D.R.L.-364, C.M.-823, 1960.
 19. Horton, E. A., and Tetervin, N., "Measured Surface Defects on Transonic Airplanes and Analysis of Their Drag Contribution." NASA Technical Note 1024.
 20. Czarnicki, K. R., Sevier, J. R., and Carmel, M. M., "Effects of Fabrication-Type Roughness on Turbulent Skin Friction at Supersonic Speeds." NASA Technical Note 4299, 1958.
 21. Czarnicki, K. R., Monta, W. J., "Pressure Distributions and Wave Drag Due to Two-Dimensional Fabrication-Type Surface Roughness on an Ogive Cylinder at Mach Numbers of 1.61 and 2.01." NASA Technical Note D-835, 1961.
 22. Hopko, R. N., "The Effect of Some Surface Roughness Elements on the Drag of a Body of Revolution at Supersonic Speeds." NASA Research Memo L 54121, 1954.
 23. Lomax, H., and Heaslet, M. A., "Recent Developments in the Theory of Wing-Body Drag." Institute of Aeronautical Sciences Preprint No. 617, 1956.
 24. Kane, E. J., "The Application of Symmetric Area Rule for the Prediction of Transonic Drag Rise Due to Nacelles." Boeing Document D6-8046, 1962.
 25. Sheppard, L. M., "Methods for Determining the Wave Drag of Non-Lifting Wing-Body Combinations." RAE Report and Memoranda No. 3077, 1957.
 26. Koh, B., and Solvang, O., "Pressure on Bodies of Revolution at Supersonic Speeds." Boeing Document D6-7842, 1963.
 27. Lighthill, M. J., "Higher Approximations, Sec. E in General Theory of High Speed Aerodynamics, Vol. VI of High Speed Aerodynamics and Jet Propulsion." Princeton University Press, Princeton, 1954.
 - *28. Harris, R. V., Analysis and Correlation of Aircraft Wave Drag, in "Proceedings of NASA Conference on Supersonic Transport Feasibility Studies and Supporting Research." Pages 153 to 164, 1963.
 29. Sigalla, A., "A Note on the Calculation of Supersonic Inlet Drag." Boeing Document D6-5513, 1962.



30. Whitham, G. B., "The Flow Pattern of a Supersonic Projectile in Communications on Pure and Applied Mathematics," Vol. V, pages 301 to 348, 1952.
31. Kane, E. J., "Sonic Boom—State of the Art (1961)." Boeing Document D6-8965, 1962.
32. Hasel, L. E., "An Experimental Pressure-Distribution Investigation of Interference Effects Produced at a Mach Number of 3.11 by Wedge-Shaped Bodies Located Under a Triangular Wing." NASA Technical Memo X-76, 1959.
33. Carlson, H. W., "Aerodynamic Characteristics at Mach Number 2.05 of a Series of Highly Swept Arrow Wings Employing Various Degrees of Twist and Camber." NASA Technical Memo X-332, 1960.
- *34. McLean, F. E., and Carlson, H. W., Application of Wing Warp and Aerodynamic Interference to Improve Supersonic Performance, in "Proceedings of NASA Conference on Supersonic Transport Feasibility Studies and Supporting Research," pages 165 to 176, 1963.
- *35. Whitcomb, R. T., "An Approach to Obtaining Increased Supersonic Lift-Drage Ratios and Reduced Sonic Boom." NASA Technical Memo X-799, 1963.
36. Young, A. D., "The Induced Drag of Flapped Elliptic Wings with Cut-Out and with Flaps that Extend the Local Chord." A.R.C. Technical Report R & M No. 2544 (Ministry of Supply) 1951.
37. Young, A. D., "The Aerodynamic Characteristics of Flaps." A.R.C. Technical Report, R & M No. 2622 (Ministry of Supply), 1947.
38. Thwaites, B. (Editor), "Incompressible Aerodynamics." Oxford Clarendon Press, 1960.
39. Solvang, O., "Zero Lift Wave Drag." Boeing Document D6-7749, 1961.
40. Woodward, F., "A Method of Aerodynamic Influence Coefficients with Application to the Analysis and Design of Supersonic Wings," Boeing Document D6-8178, 1962.
41. Irving, O., "Influence of Non-Smooth Geometries on Sonic Boom." Boeing Document D6-7942, 1961.
42. USAF Stability and Control Handbook.
43. AF Report 33-1-24, Part 2.
44. Etkin, B., "Dynamics of Flight." John Wiley and Sons, 1959.
- *45. NASA Report 51-41, Vol. 6, Section 6.4.
46. H. Valk, "A Review of Measurements on AGARD Calibration Model C in the Transonic Speed Range." National Aero and Astronautical Research Institute Report M. P. 203, August, 1961.
47. J. P. Hartzuiker, "A Review of Measurements on AGARD Calibration Model B in the Mach Number Range from 1.4 to 8." National Aero and Astronautical Research Institute Report M. P. 200, March, 1961.
48. Horne, Walter B. and Leland, Trafford J. W. "Runway Slipperiness and Slush." Journal of the Royal Aeronautical Society, September, 1963.

*These references should be obtained from the NASA.



APPENDIX A
APPENDIX TO SECTION 2
CONFIGURATION DESCRIPTION

TABLE OF CONTENTS

A2.1	Geometric Data.....	A/1
A2.1.1	Wing.....	A/1
A2.1.2	Wing Definition.....	A/1
A2.1.3	Lateral Control Surfaces.....	A/1
A2.1.4	High Lift Devices.....	A/5
A2.1.5	Horizontal Stabilizer.....	A/5
A2.1.6	Vertical Tail.....	A/6
A2.1.7	Wetted Areas.....	A/6
A2.2	Design Weights.....	A/10
A2.3	Center of Gravity Data.....	A/10
A2.4	Moments of Inertia.....	A/10

A2.0 CONFIGURATION DESCRIPTION

The data presented in this appendix consists of a detailed tabulation of the geometric dimensions and areas for the wing, horizontal and vertical tails, and the control surfaces. Centerline diagrams are included to correlate the tabulation and the physical shape of the surface. Basic weight, balance, and moment of inertia information are included with a brief definition of the data presented.

A 2.1 Geometric Data

The following data set forth the dimensional characteristics of the wing, horizontal tail, vertical tail, and control surfaces of each.

The Model 733 dimensional data will be used to mathematically develop the complete airframe envelope, using a Boeing dimension system specifically designed for this purpose. The IBM 7094 program output is used for engineering, tooling, and manufacturing applications to ensure dimensional control in the design and fabrication of the airframe.

A2.1.1 WING (Fig. A2-1)

Gross Wing Area, ft ²	5026
Reference Wing Area, ft ²	4684
Reference MAC, ft	64.52
Aspect Ratio @ $\Lambda_{LE} = 74^\circ$	1.59 (Sw = 4684 ft ²)
@ $\Lambda_{LE} = 42^\circ$	6.04 (Sw = 3390 ft ²)
@ $\Lambda_{LE} = 20^\circ$	9.06 (Sw = 3315 ft ²)
Taper Ratio (Ref. Area = 4684 ft ²)	.354
Sweep @ .25 chord,	
Wing Aft, degrees	72.24
Wing Fwd., degrees	17.52
Dihedral, degrees	0
Angle of Incidence of Root Chord to Fuselage Ref. Line (Wing Aft), degrees	-1
Angle of Incidence of Chord @ 90% semispan to Fuselage Ref. Line (Wing Aft), deg.	- 5.174

A2.1.2 WING DEFINITION

The wing airfoil sections are defined streamwise @ leading edge sweep of 74° . The thickness ratios and ordinates are given in percent of local chord. A modified biconvex thickness distribution is used for the inboard wing sections (B-733-1). Other sections are derived from the NACA 63 series airfoils (B-733-2 and -3). The airfoil ordinates are noted in Table A2-A. The wing twist distribution is given in Fig. A2-2.

A2.1.3 LATERAL CONTROL SURFACES

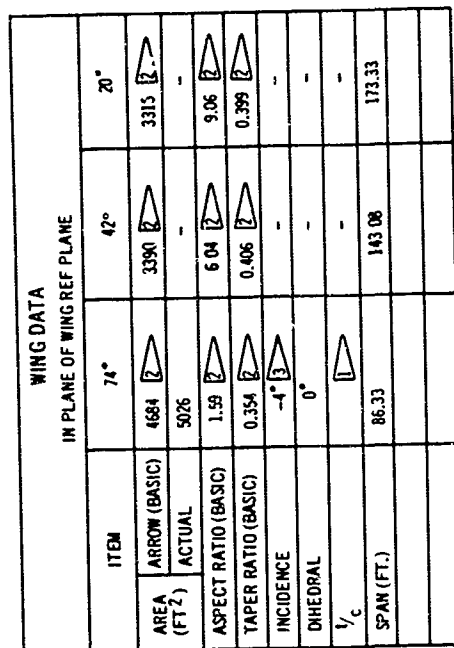
The lateral control surfaces are defined at a wing sweep angle of 20 degrees as shown in Fig. A2-3.

AILERON

Area, ft. ² (total)	168
Span, ft.	19
Spanwise Loc. from ζ Airplane:	
Inboard edge, ft.	63
Outboard edge, ft.	82
Chord, % Wing Chord	34

SPOILERS

Type	Low & High Speed (upper & lower) Segmented	Low Speed Only Segmented
Area, ft. ² (total)	320	87.5
Span, ft.	29.6	15
Spanwise Loc. from ζ Airplane:		
Inboard edge, ft.	34.4	20
Outboard edge, ft.	63	34.4
Chord, % Wing Chord	15	15



 SEE 1/2 IN CONTROL AIRFOIL DATA TABLE.

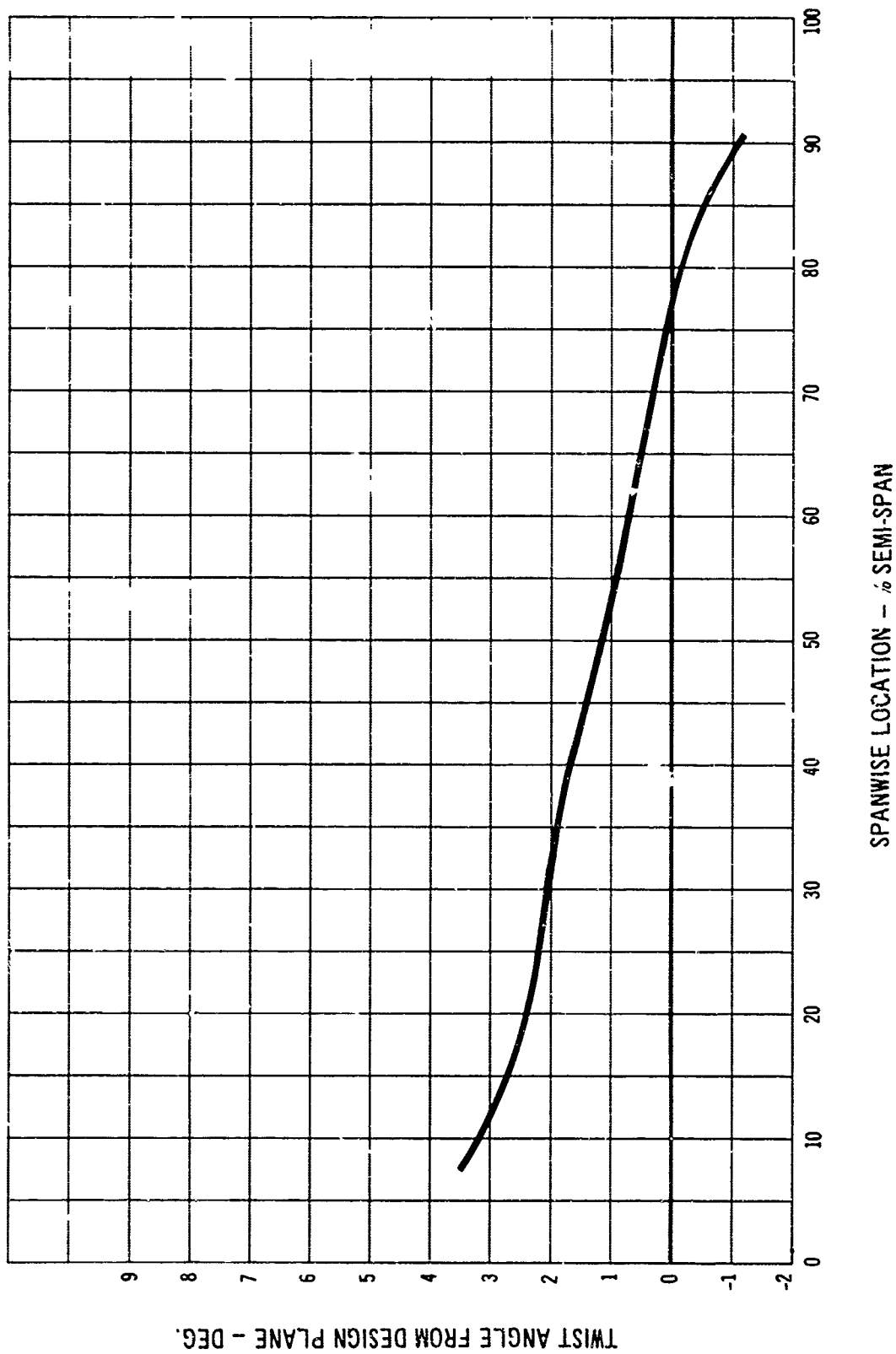
THIS WING DATA IS BASED ON ARROW (BASIC) WING AS SHOWN IN DETAIL 1 & DO NOT APPLY TO ACTUAL WING. SEE WING PARAMETER TABLE.

3 ANGLE BETWEEN WING DESIGN PLANE
AND HORIZONTAL REFERENCE PLANE

A 2-1 Wing & Diagram

TABLE A2-A AIRFOIL SECTIONS

X/C (PERCENT)	B-733-1		B-733-2		B-733-3	
	11.6% SEMI-SPAN t/c MAX = .0410		37.8% SEMI-SPAN t/c MAX = .0506		65% → 100% SEMI-SPAN t/c MAX = .0250	
	UPPER ORDINATE	LOWER ORDINATE	UPPER ORDINATE	LOWER ORDINATE	UPPER ORDINATE	LOWER ORDINATE
0.00	0.000	-0.000	0.000	0.000	0.000	0.000
0.50	0.071	-0.020	0.264	-0.205	0.146	-0.097
0.75	0.106	-0.029	0.304	-0.220	0.171	-0.099
1.25	0.176	-0.049	0.383	-0.248	0.220	-0.104
2.50	0.351	-0.097	0.577	-0.319	0.339	-0.114
5.00	0.694	-0.193	0.946	-0.452	0.566	-0.133
7.50	1.020	-0.286	1.289	-0.578	0.778	-0.152
10.00	1.320	-0.375	1.608	-0.695	0.973	-0.171
15.00	1.825	-0.536	2.170	-0.907	1.317	-0.207
20.00	2.220	-0.677	2.634	-1.092	1.598	-0.244
25.00	2.527	-0.802	3.002	-1.252	1.818	-0.285
30.00	2.751	-0.910	3.274	-1.390	1.975	-0.329
35.00	2.896	-1.004	3.449	-1.502	2.070	-0.376
40.00	2.965	-1.082	3.510	-1.550	2.099	-0.401
45.00	2.959	-1.141	3.446	-1.506	2.061	-0.386
50.00	2.881	-1.181	3.286	-1.393	1.971	-0.341
55.00	2.729	-1.209	3.061	-1.248	1.842	-0.286
60.00	2.507	-1.230	2.791	-1.087	1.688	-0.228
65.00	2.234	-1.232	2.493	-0.922	1.514	-0.173
70.00	1.932	-1.199	2.171	-0.760	1.325	-0.123
75.00	1.609	-1.125	1.831	-0.603	1.123	-0.079
80.00	1.271	-1.002	1.479	-0.456	0.912	-0.044
85.00	0.934	-0.823	1.123	-0.326	-0.696	-0.020
90.00	0.612	-0.584	0.759	-0.209	0.472	-0.006
95.00	0.303	-0.393	0.383	-0.102	0.239	-0.001
100.00	0.000	0.000	0.000	0.000	0.000	0.000
L.E. RADIUS	0		.002C		.001C	



A 2-2 Wing Twist Distribution Model 733-197

A2.1.4 HIGH LIFT DEVICES

The high lift devices are defined at a sweep angle of 20 degrees as shown in Fig. A2-3.

OUTBOARD FLAPS:

Double Slotted Flaps with 30% Fowler Action

Distance from ξ Airplane To Inboard Edge, ft.	19.50
To Outboard Edge, ft.	63.0
Maximum Deflection (Main/Auxiliary) Takeoff Deflection	30°/50° 8°/23°
Chord, % Wing Chord	30%/10%
Percent Wing Area Affected	6
Area, ft. ² (Total)	516

INBOARD FLAPS

	Wing Plain Flap	Body Split Flap
Distance from ξ Airplane		
To Inboard Edge, ft.	3.75	0
To Outboard Edge, ft.	9.0	3.75
Maximum Deflection, degrees	40	40
Area, ft. ² (Total)	71	46
Ground Clearance, ft.	...	2.67

LEADING EDGE SLATS (OUTBOARD WING)

	Inboard	Outboard
Distance from ξ Airplane		
To Inboard Edge, ft.	25.8	43
To Outboard Edge, ft.	43	84
Chord, ft.	3.0	2.25
Area, ft. ² (Total)	110	167

A2.1.5 HORIZONTAL STABILIZER

The horizontal stabilizer is shown as Fig. A2-4.

Area (Exposed), ft. ²	950
Span (Total), ft.	50.35
Aspect Ratio	2.086
Taper Ratio	.20
Incidence of Fuselage Ref. Line, Degrees	+10 to -20
Airfoil Section	Bi-convex
Sweep @ .25c, degrees	41.09
MAC, ft.	24.52
Location of LEMAC	
From L. E. Root, ft.	10.316
From Thrust Line, ft.	6 (above)
Anhedral, degrees	5½
Tail Arm (Measured from .40 MAC Wing to .25 MAC Tail, ft.	73.16
Tail Volume Coefficient (Ref. Wing & MAC)	.230

ELEVATOR

Area ft. ² (Total)	264
Span (one side) ft.	23.55
Chord, % Stabil. Chord	21.5 Inboard
Distance from ξ Airplane	49.8 Outside
To Inboard Edge, ft.	1.65
To Outboard Edge, ft.	25.2



A2.1.6 VERTICAL TAIL

The vertical tail is shown as Fig. A2-5

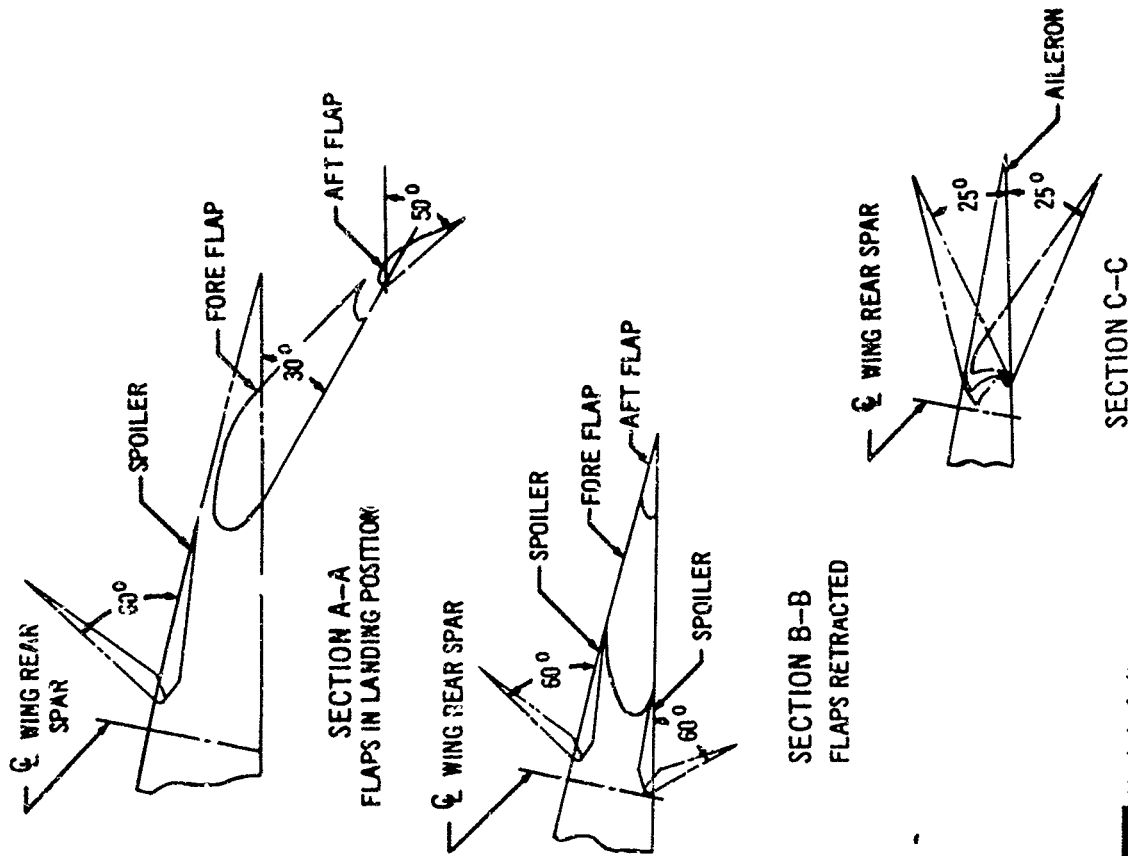
Area, ft. ²	471.70
Span, ft.	22.92
Taper Ratio	.254
Aspect Ratio	1.113
Sweep @ .25c degrees	50.84
MAC, ft.	23.05
Location of LEMAC	13.118
From LE Root, ft.	20.00
From Thrust Line, ft. (of outboard engine)	20.00
Airfoil Section	Bi-convex
Tail Arm (Measured from 0.40 MAC)	70.58
Wing to .25 MAC Tail, ft.)	.082
Tail Volume Coefficient (Ref. Wing Area & MAC)	

RUDDER

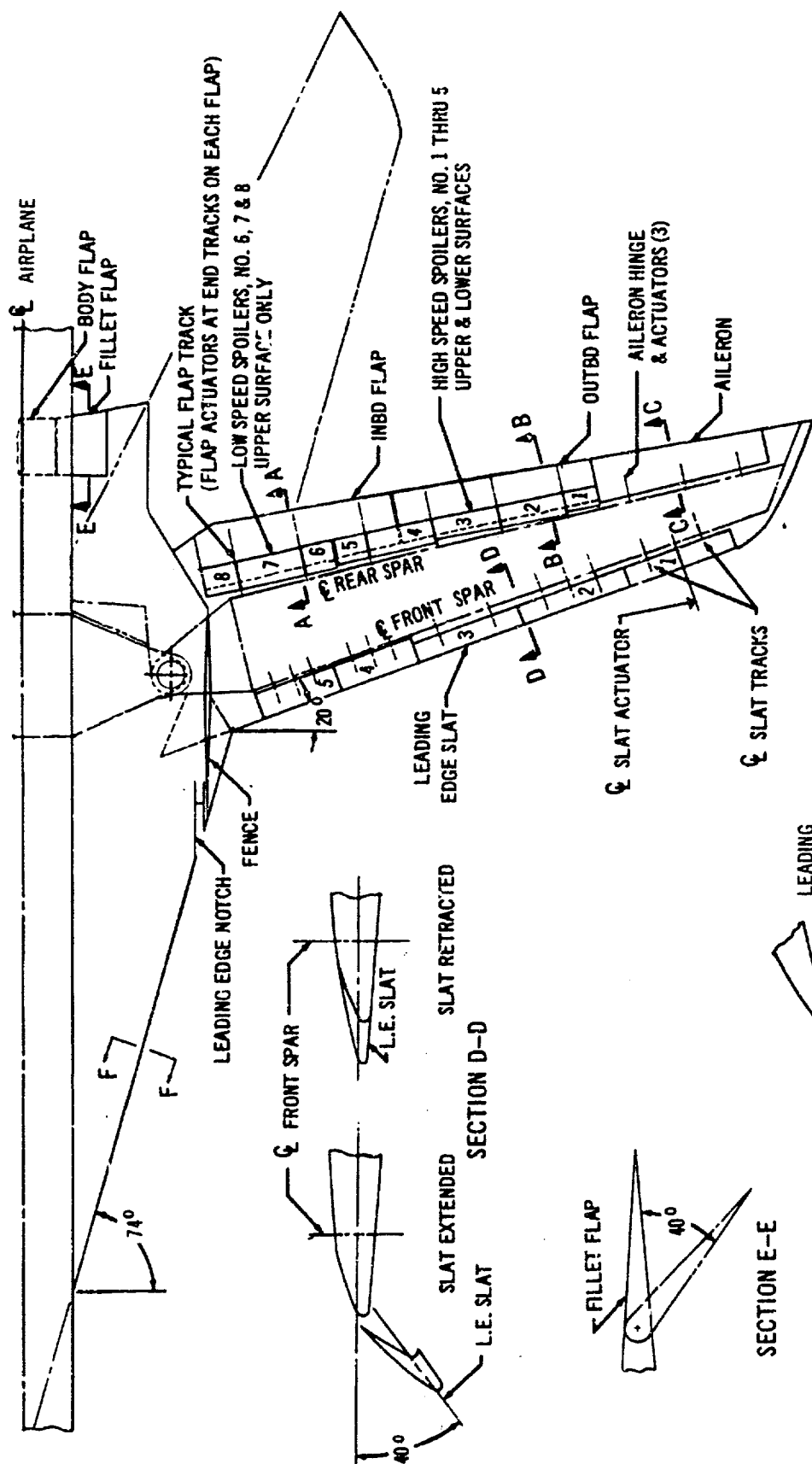
	Low Speed Only	Low & High Speed
Area, ft. ²	48.75	83.80
Span, ft.	7.75	11.75
Chord, Avg. ft.	6.3	7.16

A2.1.7 WETTED AREAS

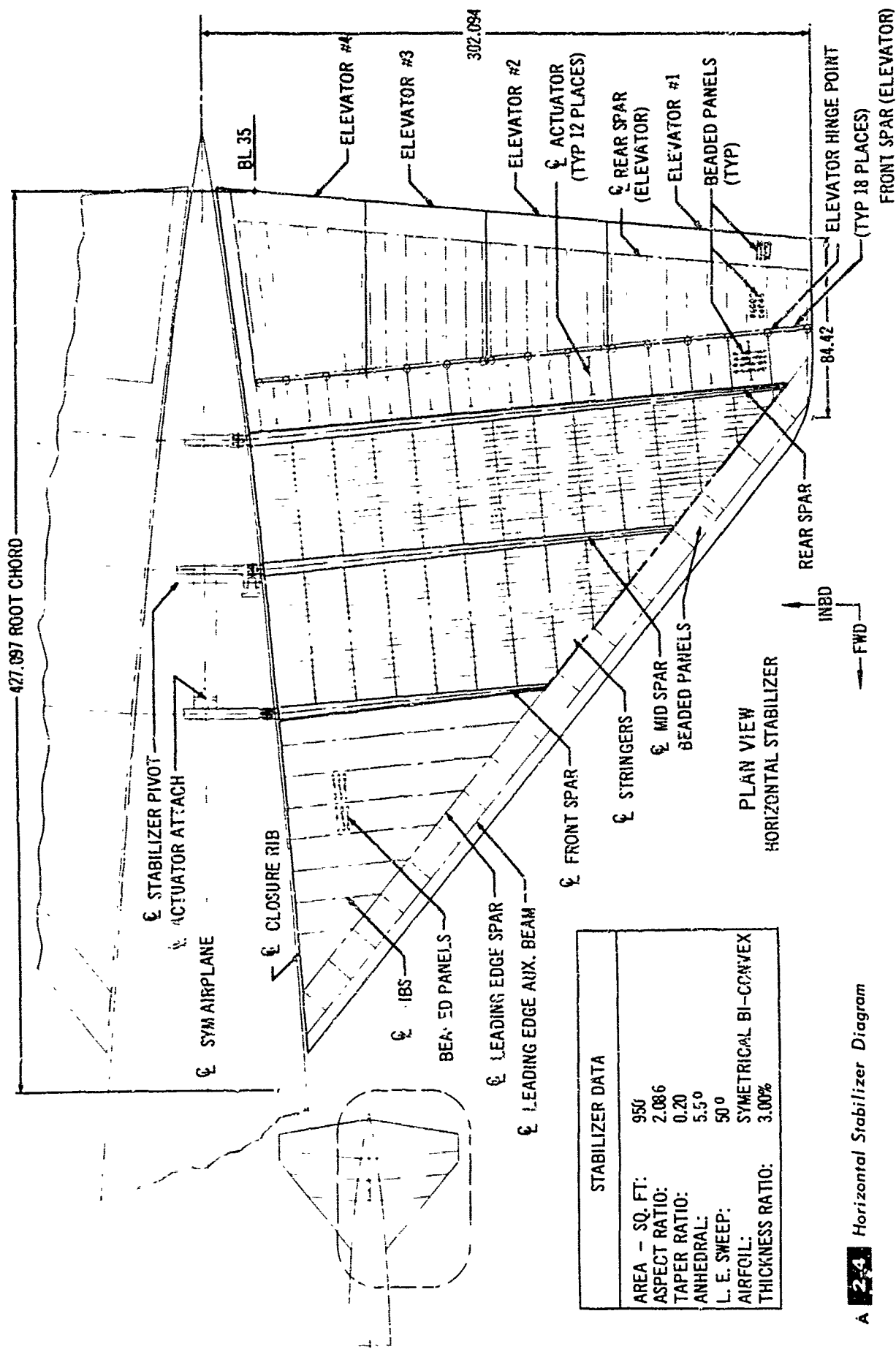
	(Ft. ²)
Fuselage	5339
Wing	8144
Horizontal Tail	1900
Vertical Tail	906
Ventral	250
Nacelles	1769
Struts	400
TOTAL	18,708 Ft. ²



A 2.3 High Lift Devices



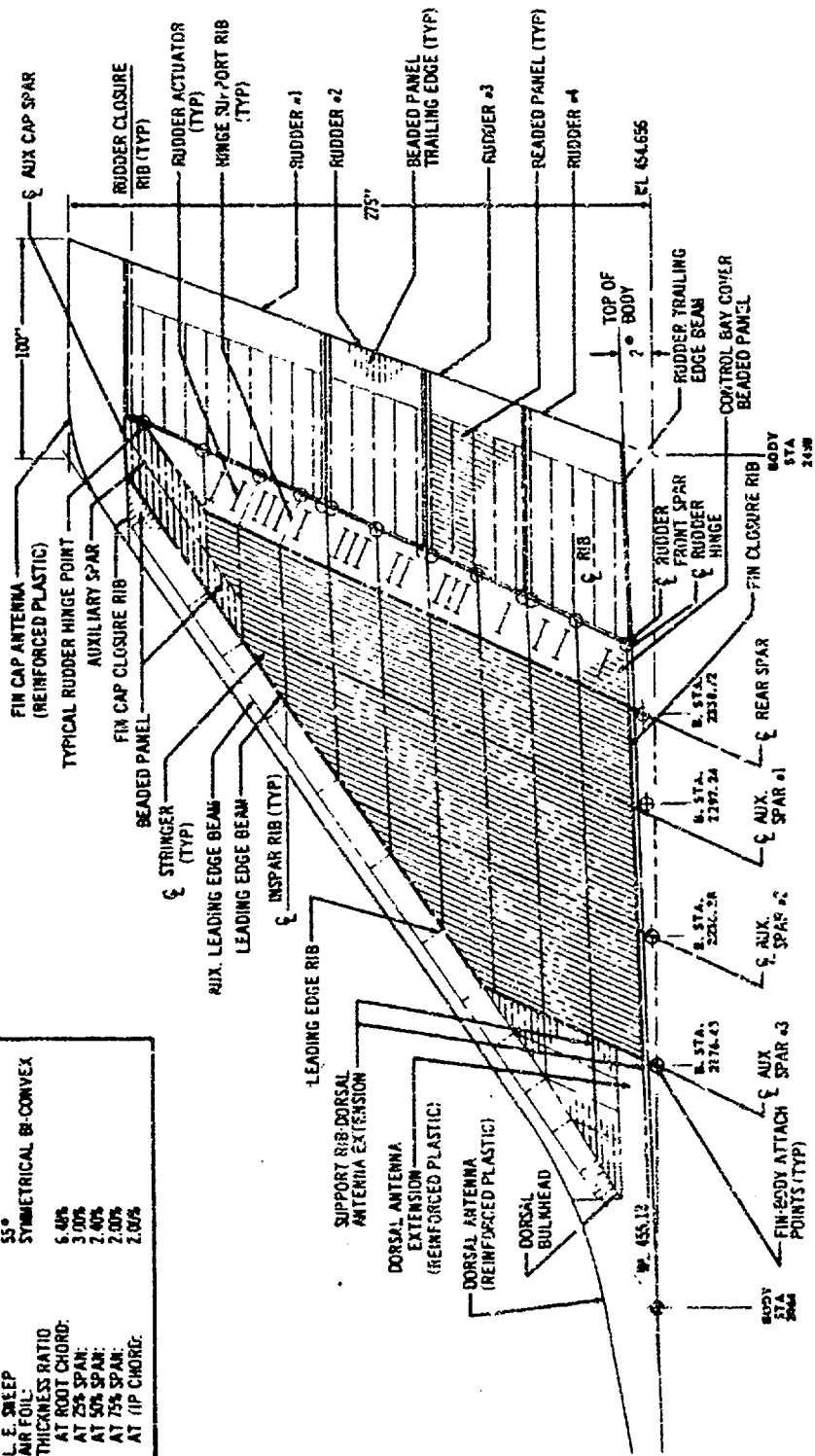
PLAN VIEW - WING



STABILIZER DATA	
AREA - SQ. FT:	950
ASPECT RATIO:	2.086
TAPER RATIO:	0.20
ANHEDRAL:	5.5°
L. E. SWEEP:	50°
AIRFOIL:	SYMMETRICAL BI-CONVEX
THICKNESS RATIO:	3.00%

A 2-4 Horizontal Stabilizer Diagram

FIN DATA	471.70	SYMMETRICAL BE-CONVEX
ASPECT RATIO:	1.113	
TAPER RATIO:	0.254	
L.E. SLEEP	55°	
AIR FOIL:		
THICKNESS RATIO	5.40%	
AT ROOT CHORD:	3.00%	
AT 25% SPAN:	2.40%	
AT 50% SPAN:	2.00%	
AT 75% SPAN:	2.00%	
AT TIP CHORD:		



A 2-5 Fin & Rudder Structural Arrangement Diagram

A.2.2 Design Weights

(Pounds)	
Gross Weight (Maximum Taxi)	430,000
Maximum Ramp Weight	430,000
Minimum Takeoff Weight (Flaps Down)	427,000
Maximum Design Flight Weight (Flaps Up)	425,000
Maximum Design Fuel Usage Weight	405,000
Maximum Gross Weight with	
Zero Outboard Wing Fuel	360,000
Maximum Landing Weight	260,000
Maximum Zero Fuel Weight	220,500
Minimum Flying Weight	195,000
Operator's Weight Empty	182,500
Manufacturer's Weight Empty	176,940
Maximum Fuel Capacity	235,840
(5,200 Gallons @ 6.7 lbs. gallon)	

A.2.3 Center of Gravity Data

Operator's weight Empty CG	
(Wings Fwd. Gear Down)	45.5% MAC
Operator's Weight Empty CG	
(Wings Fwd. Gear Up)	44.4% MAC

A \pm 0.5 MAC tolerance is allowed about the above centered of gravity locations to account for manufacturing variations. The center of gravity (including tolerances for

manufacturing variations, passenger seating variations, and allowances for in-flight movement) must fall within the following center of gravity limits for all design weight conditions, as shown in Fig. A2-6.

For commercial airplanes, due to the large variations possible in loading payload, it is assumed the airplane center of gravity can reach these limits at the design weights, unless specifically restricted. The limits used for structural analysis are tabulated below.

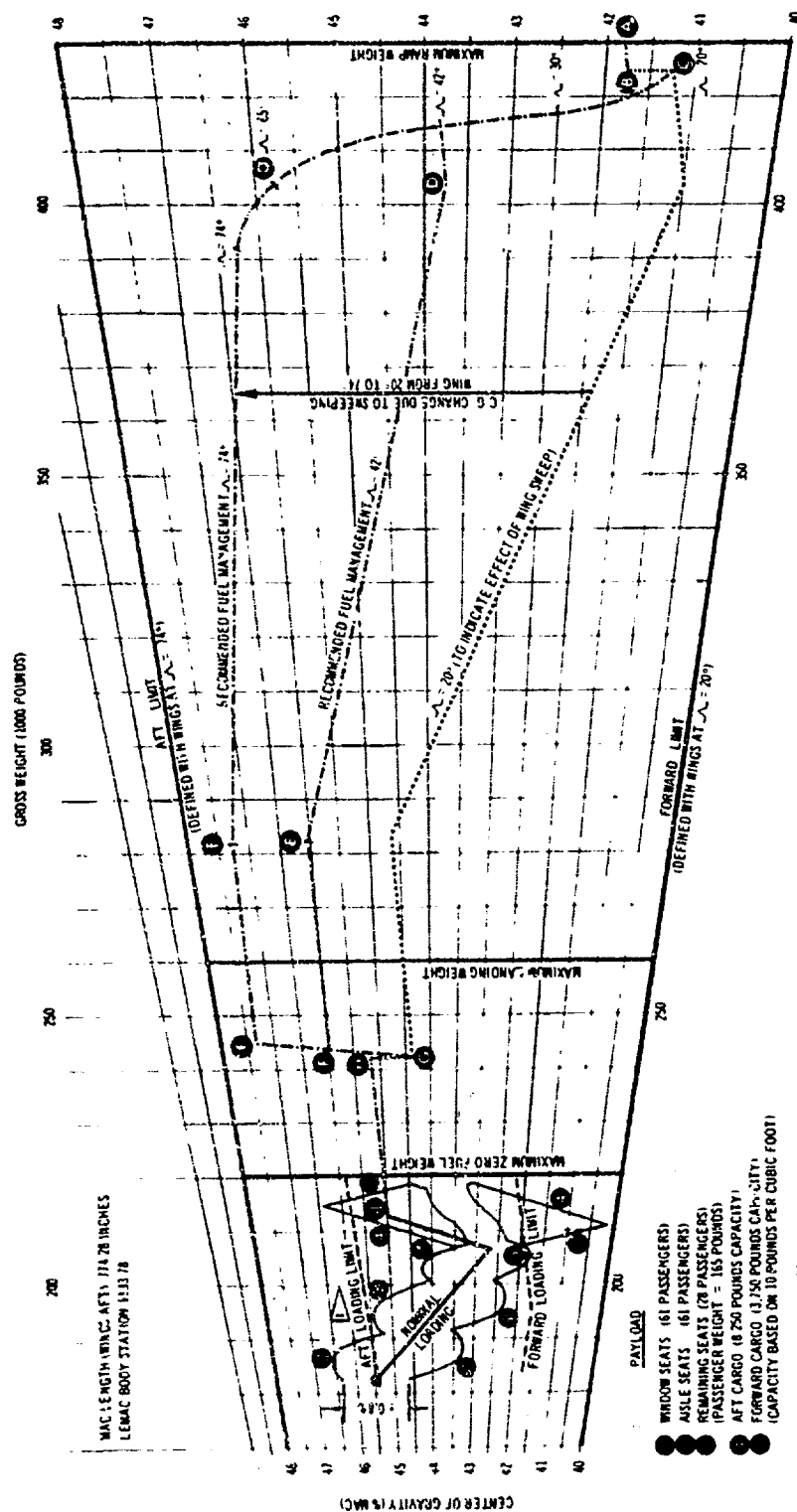
	Subsonic	Supersonic
Forward	39% MAC	42% MAC
Aft	49% MAC	49% MAC

A.2.4 Moments of Inertia

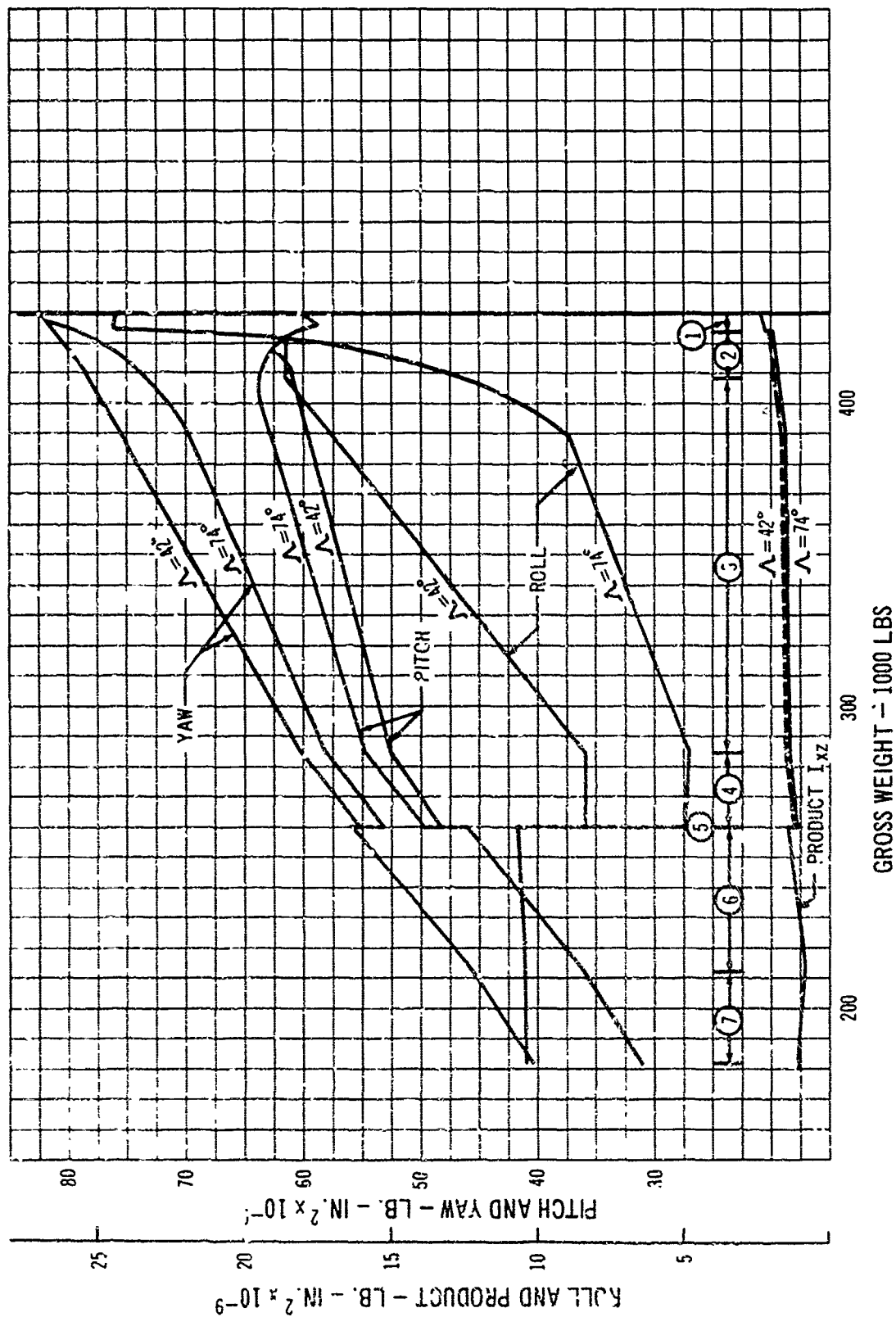
The moment of inertia vs. gross weight is shown in Fig. A2-7 is based on a 30,000-pound payload mission. A description of the flight conditions analyzed is tabulated in Table A2-B.

The roll axis is parallel to the airplane reference waterline. As shown by the small product of inertia term, this corresponds very closely to the airplane principal axis. The angle between the reference waterline and the principal axis varies from 1.5° to 2.3°. The moments of inertia about the principal axis differ 0.5% at most from the values shown, and were, therefore, not shown separately.





A 2-6 Balance and Loading Chart



A 2-7 Moment of Inertia versus Gross Weight

TABLE A 2-B MOMENT OF INERTIA CONDITIONS

CONDITION	GEAR	NORMAL MISSION	WING LEADING EDGE SWEEP	FUEL USED
(1) TAKE-OFF	DOWN	ALL	20°	BODY MAIN TANKS EQUALLY
(2) CLIMB	UP	SUPERSONIC SUBSONIC	20° to 65° 20° to 42°	BODY MAIN TANKS EQUALLY
(3) CRUISE	UP	SUPERSONIC SUBSONIC	65° to 74° 42°	FORWARD BODY AND OUTBOARD WING EQUALLY
(4) CRUISE	UP	SUPERSONIC SUBSONIC	74° 42°	BODY MAIN TANKS EQUALLY
(5) DESCENT AND LANDING	DOWN	SUPERSONIC SUBSONIC	74° to 20° 42° to 20°	BODY MAIN TANKS EQUALLY
(6) RESERVE FUEL				BODY MAIN TANKS EQUALLY
(7) PAYLOAD (30,000 POUNDS)				



APPENDIX B
APPENDIX TO SECTION 3
AIRPLANE PERFORMANCE
TABLE OF CONTENTS

B.3.1 RANGE CAPABILITY	B/1	B.3.3 TAKEOFF	B/13
B.3.1.1 Effect of Temperature on Supersonic Range.	B/1	B.3.3.1 CAR Takeoff Field Length—Standard Day	B/13
B.3.1.2 Effect of Wind and Altitude on Supersonic Range	B/2	B.3.3.2 CAR Takeoff Speeds	B/15
B.3.1.3 Range After Engine Failure, $M = 0.85$ Cruise	B/2	B.3.3.3 Turning Capability at Takeoff Speeds	B/15
B.3.1.4 Range After Engine Failure, $M = 2.70$ Cruise	B/2	B.3.3.4 CAR Takeoff Field Length, Effect of Headwind	B/17
B.3.1.5 Range After Pressurization Failure	B/4	B.3.3.5 CAR Takeoff Field Length, Effect of Slush on Runway	B/18
B.3.1.6 Alternate Airport Range With Wing Sweep at 74 Degrees	B/4	B.3.3.6 Takeoff Fuel Variation with Thrust	B/18
B.3.1.7 Effect of OWE Changes on Design Gross Weight	B/5	B.3.3.7 Airport Noise Profiles at Takeoff Power	B/18
B.3.1.8 Effect of Cruise Range Factor Changes on Design Gross Weight	B/5	B.3.3.8 Noise Profiles in Climbout	B/19
B.3.1.9 Subsonic Payload-Range	B/6	B.3.3.9 Takeoff Fuel Allowance	B/19
B.3.1.10 Subsonic Cruise Flight Profile	B/8		
B.3.1.11 Effect of Wind and Altitude on Subsonic Range	B/8	B.3.4 CLIMB	B/19
		B.3.4.1 Climb and Acceleration Schedule	B/19
		B.3.4.2 Climb and Acceleration Performance, Standard Day	B/21
B.3.2 FLIGHT LIMITS	B/10	B.3.4.3 Climb and Acceleration Performance, Standard + 20 Degrees Fahrenheit Day	B/21
B.3.2.1 Service Ceiling	B/10	B.3.4.4 Climb and Acceleration Performance, Standard 20 Degree Fahrenheit Day	B/22
B.3.2.2 Wing Sweep Schedule	B/10	B.3.4.5 Sonic Boom Overpressures in Climb	B/22
B.3.2.3 Stall Speeds and Minimum Level Flight Speeds	B/10	B.3.4.6 Rate of Climb	B/26
B.3.2.4 Minimum Usable Flight Speed. Wing Sweep—74 Degrees	B/13	B.3.4.7 Subsonic Climb and Acceleration Performance, Standard Day	B/26

B.3.5 CRUISE	B/26	B.3.7 HOLDING	B/35
B.3.5.1 Optimum Cruise Fuel Mileage.....	B/26	B.3.7.1 Subsonic Holding Fuel Flow.....	B/35
B.3.5.2 Fuel Mileage at $M = 2.7$, Standard Day.....	B/27		
B.3.5.3 Fuel Mileage at $M = 2.6$, Standard + 20 Degrees Fahrenheit Day.....	B/29	B.3.8 LANDING	B/35
B.3.5.4 Fuel Mileage at $M = 2.7$, Standard - 20 Degrees Fahrenheit Day.....	B/30	B.3.8.1 CAR Landing Field Length.....	B/35
B.3.5.5 Wing Sweep Selection for Subsonic Cruise.....	B/31	B.3.8.2 CAR Landing Speeds.....	B/35
B.3.5.6 Subsonic Cruise Fuel Mileage, Wing Sweep = 30 Degrees.....	B/32	B.3.8.3 Effect of Runway Braking Coefficient.....	B/35
B.3.5.7 Subsonic Cruise Fuel Mileage, Wing Sweep = 42 Degrees.....	B/32	B.3.8.4 Effect of All Braking Devices.....	B/37
B.3.5.8 Sonic Boom Overpressure in Cruise.....	B/33	B.3.8.5 Thrust for Level Flight, Approach Speed Stability.....	B/37
		B.3.8.6 Landing Field Length with Wings Swept 74 Degrees.....	B/37
B.3.6 DESCENT	B/33	B.3.8.7 Thrust Required and Approach Speed Stability with Wings Swept 74 Degrees.....	B/45
B.3.6.1 Descent Schedules.....	B/33	B.3.8.8 Landing Noise, Lateral Spread.....	B/45
B.3.6.2 Normal Descent—Maximum Range.....	B/33	B.3.8.9 Approach and Landing Fuel Allowance.....	B/45
B.3.6.3 Normal Descent—Minimum Time.....	B/33		
B.3.6.4 Emergency Descent.....	B/35	B.3.9 PERFORMANCE CALCULATION METHODS	B/49
B.3.6.5 Sonic Boom Overpressures in Descent.....	B/35	B.3.9.1 Mission Calculations.....	B/49
		B.3.9.2 Takeoff and Landing Distances.....	B/51

B.3.0 PERFORMANCE

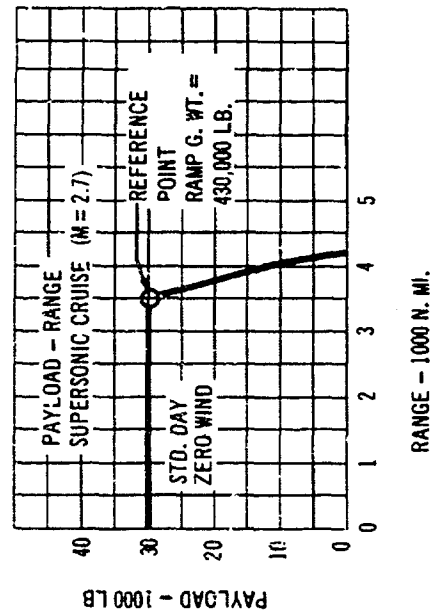
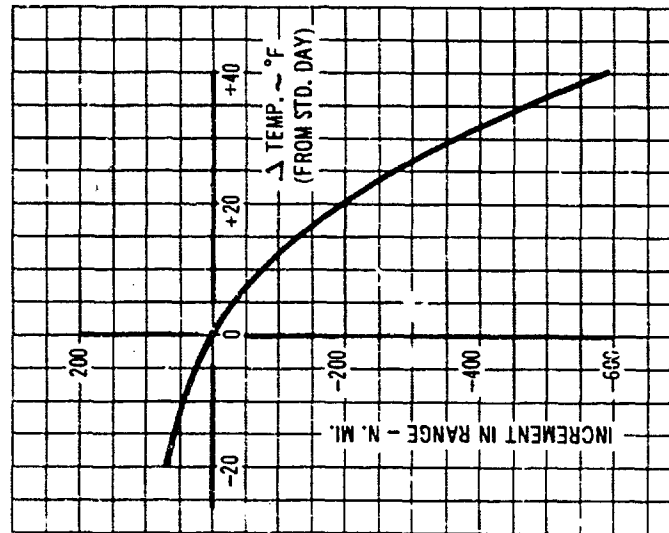
B.3.1 Range Capability

B.3.1.1 EFFECT OF TEMPERATURE ON SUPERSONIC RANGE

The effect of temperature changes on supersonic range is shown in Fig. B 3-1. The design mission was used as the reference point. These data show increases in temperature

have a much larger effect than decreases in temperature; at standard temperature - 20 degrees Fahrenheit a range increase of about 70 n.mi. occurs while at standard + 20 degrees Fahrenheit a range loss of about 200 n.mi. occurs. This is due to the fact that cruise fuel mileage decreases significantly on hot days while it improves only slightly on cold days as shown in Figs. B 3-34, B 3-35, and B 3-36. The increased range on a cold day is due to a more rapid climb to cruise speed. The decrease in range on a hot day

MAX. CLIMB $\Delta P = 2.0$ PSF



NOTES:

- 1) FOR TEMP. ABOVE STD. 500° F
STAGNATION TEMP. HELD CONSTANT
- 2) FOR TEMP. BELOW STD.
MACH 2.7 HELD CONSTANT
- 3) STD. DAY RESERVES USED

B 3-1 Effect of Temperature on Total Range

is due to a slower climb to cruise speed and a lower cruise fuel mileage.

B.3.1.2. EFFECT OF WIND AND ALTITUDE ON SUPERSONIC RANGE

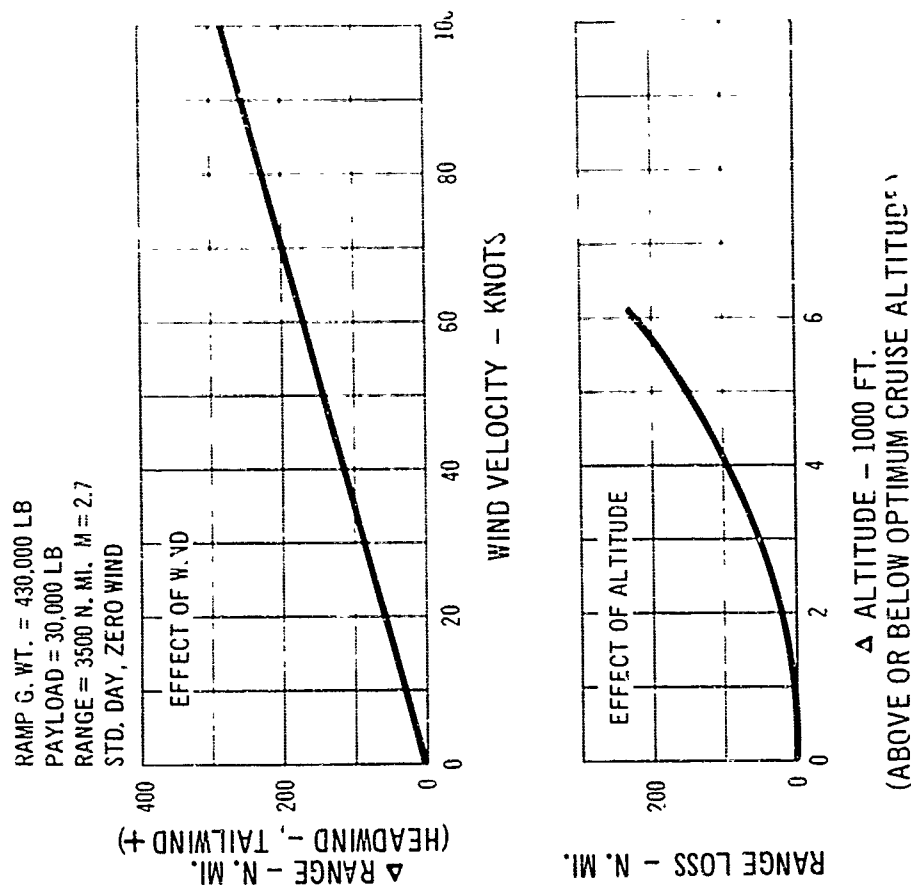
Fig. B 3-2 shows the effect of wind and cruise altitude on the design range capabilities of the airplane. These data show that a 50-knot headwind will lower the design cruise range from 3500 n.mi. to 3360 n.mi. while cruising 4000 feet below the optimum cruise altitude will lower the range from 3500 n.mi. to 3400 n.mi.

B.3.1.3 RANGE AFTER ENGINE FAILURE, CONTINUE AT SUBSONIC CRUISE

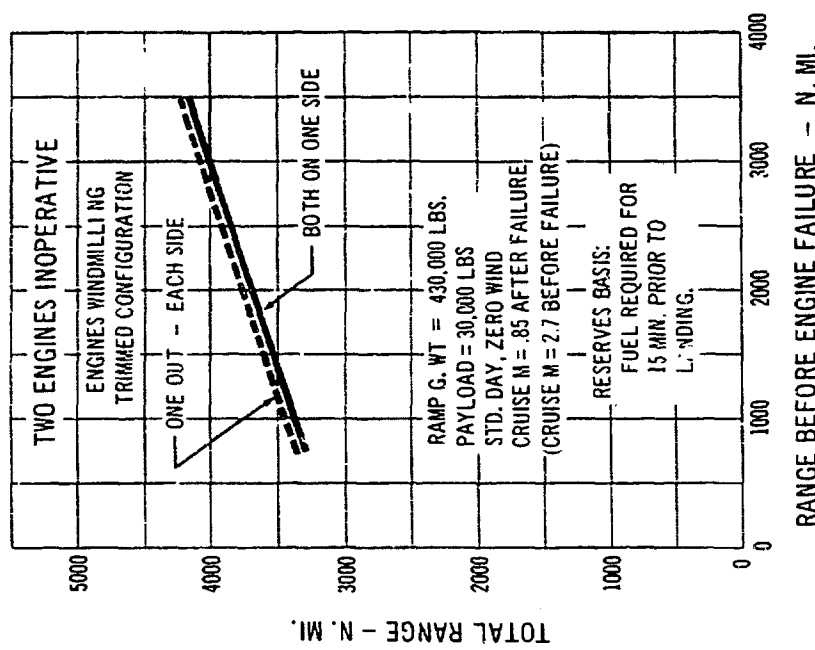
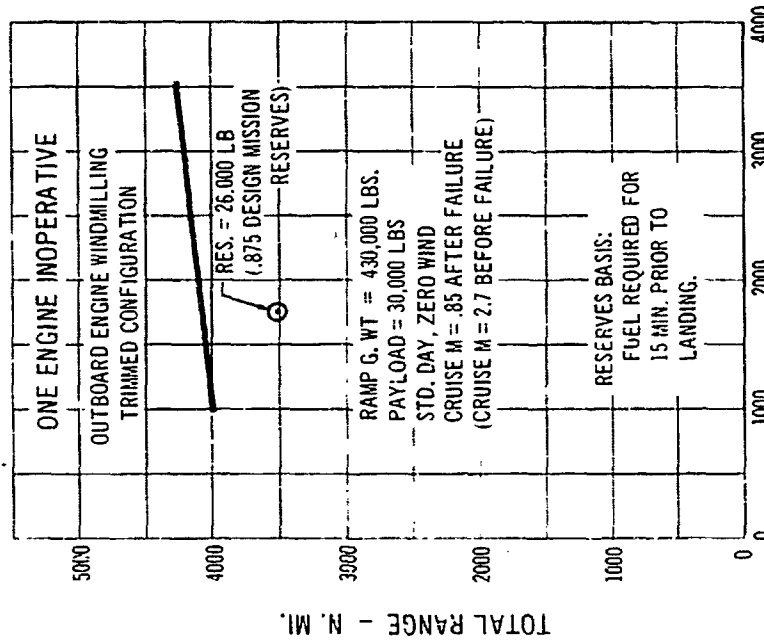
Fig. B 3-3 shows the range available for both the one- and two-engine inoperative cases, at $M = 0.85$ cruise and 42-degree wing sweep for the design mission. The asymmetric drag is balanced with aerodynamic controls only. Reserve fuel is that sufficient for a 15 minute hold prior to landing. These data show that for the most critical case, two engines failing at mid-range, the design mission can be completed with 100 n.mi. to spare (about 16 percent of the normal reserve fuel in addition to the 15-minute hold and normal landing fuel allowance). For the one-engine inoperative case, the design mission can be completed with 550 n.mi. to spare (about 87 percent of the normal fuel reserves in addition to the 15-minute hold and normal landing fuel allowance). This is due to the excellent subsonic performance available with the variable sweep wing in the 42-degree sweep position.

B.3.1.4 RANGE AFTER ENGINE FAILURE, CONTINUE AT SUPERSONIC CRUISE

Fig. B 3-4 shows the range available for the one-engine inoperative case at $M = 2.7$ cruise for the design mission. The asymmetric drag is balanced with aerodynamic controls only. Reserve fuel is that sufficient for a 15-minute hold prior to landing. These data show that for the most



B 3-2 Effect of Wind and Altitude on Supersonic Range



B-3-3

RANGE BEFORE ENGINE FAILURE -- N. MI.
Range After Engine Failure -- Continue at M = .85

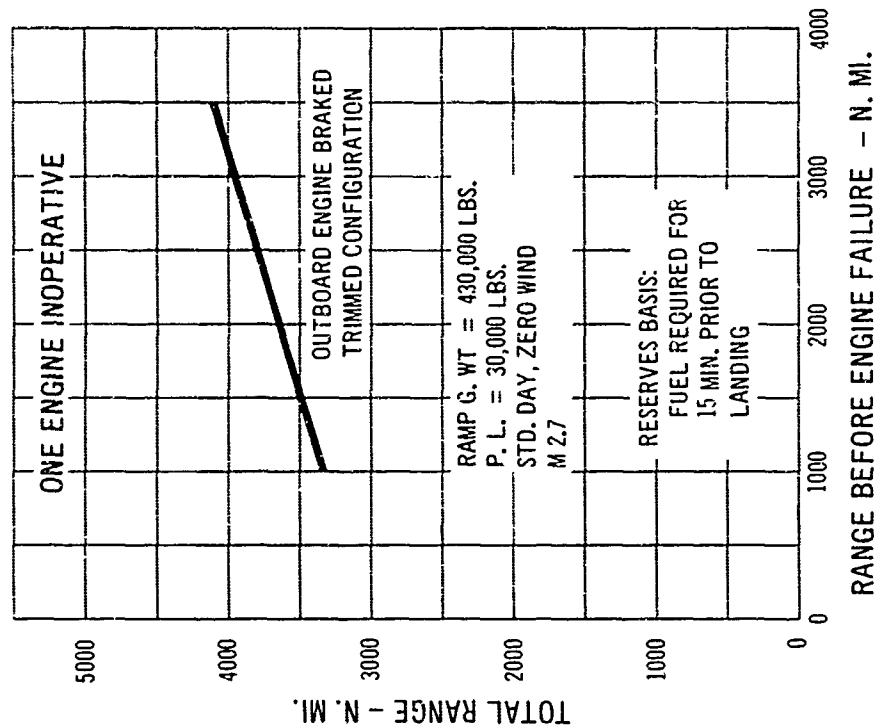
critical case, engine failure at mid-range, the design mission can be completed with 60 n.mi. to spare (about 10 percent of the normal reserve fuel in addition to the 15-minute hold and normal holding fuel allowance). With two engines inoperative M = 2.7 cruise is impractical due to the high drag.

B.3.1.5 RANGE AFTER PRESSURIZATION FAILURE

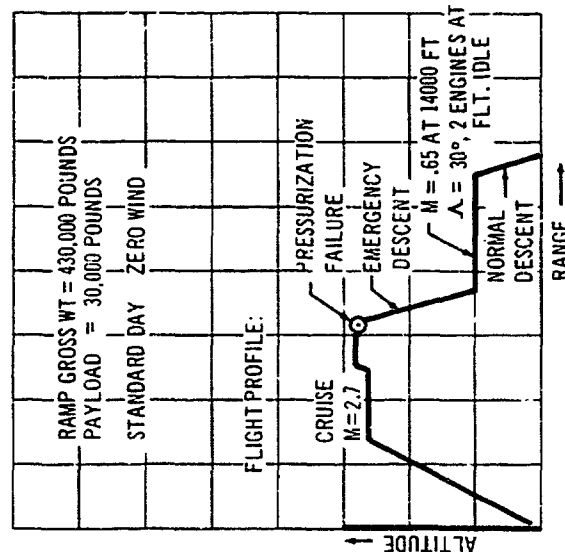
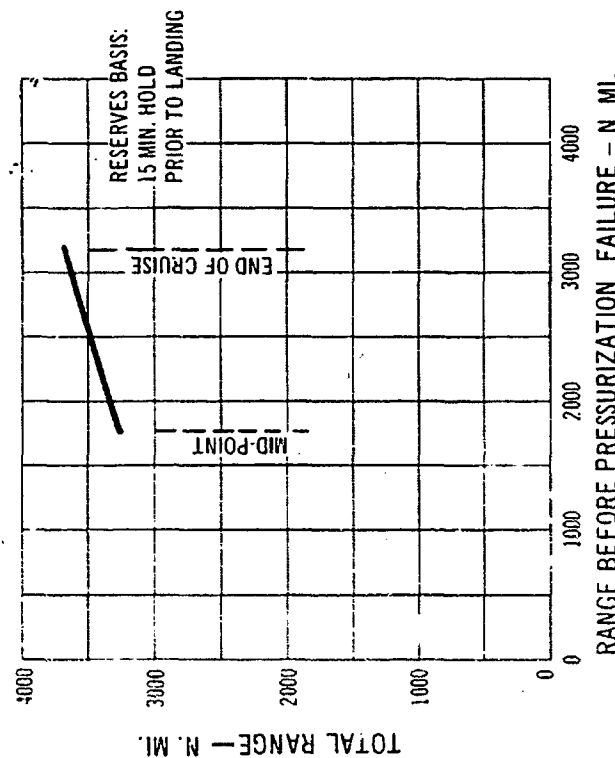
Fig. B 3-5 shows the range available after a pressurization failure at cruise altitude for the design mission case. The range shown is based upon an emergency descent to 14,000 feet with the remainder of the flight carried out at this altitude at a Mach number of 0.65 and a wing sweep of 30 degrees (max. n.mi./lb. for these conditions). Reserve fuel is that sufficient for a 15-minute hold prior to landing. These data show that for the critical case of pressurization failure at mid-point the airplane has a range capability of 3230 n.mi., or an alternate radius of 1480 n.mi., sufficient to get to the nearest alternate on virtually all routes. For example, on the New York-to-Paris route Gander or Shannon are only 850 n.mi. away at the mid-range point.

B.3.1.6 ALTERNATE AIRPORT RANGE WITH WING SWEEP AT 74 DEGREES

Fig. B 3-6 shows the alternate airport range available with wing sweep at 74 degrees for the design mission. The distance shown versus reserve fuel assumes the descent and cruise to alternate are done with wings at 74 degrees. Reserve fuel is that sufficient for a 15-minute hold prior to landing. These data show that using the normal reserves, on arrival at the 500 statute-mile alternate, sufficient fuel is remaining for 2 1/4 minutes' holding (including the required 15 minutes).



B 3-4 Range After Engine Failure - Continue at M = 2.7



B 3-5 Range After Pressurization Failure

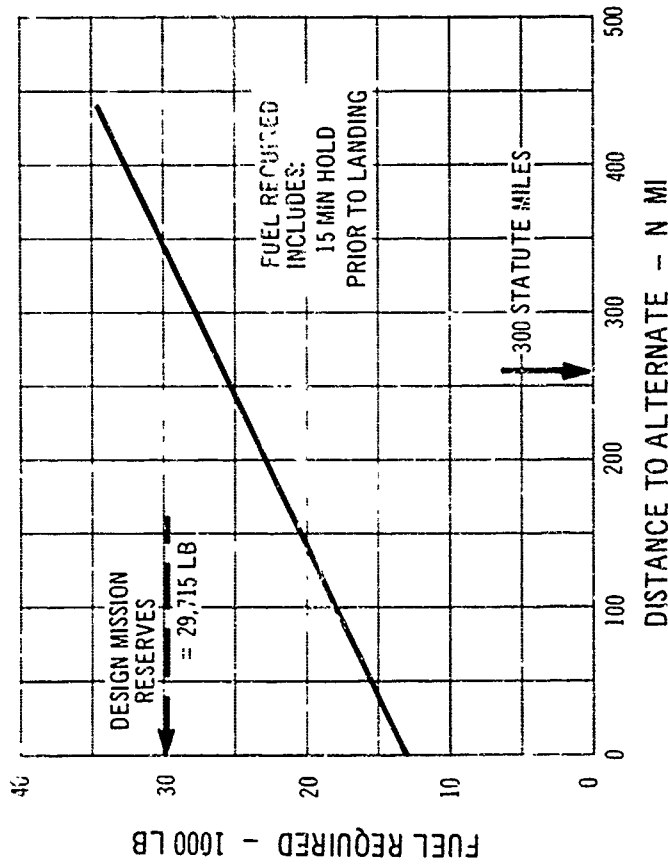
B.3.1.7 EFFECT OF OWE CHANGES ON DESIGN GROSS WEIGHT

The effects of small changes in operators' weight empty (OWE) on the design gross weight of the Model 733-197 to maintain the design mission range of 3500 n.mi. is presented in Fig. B 3-7.

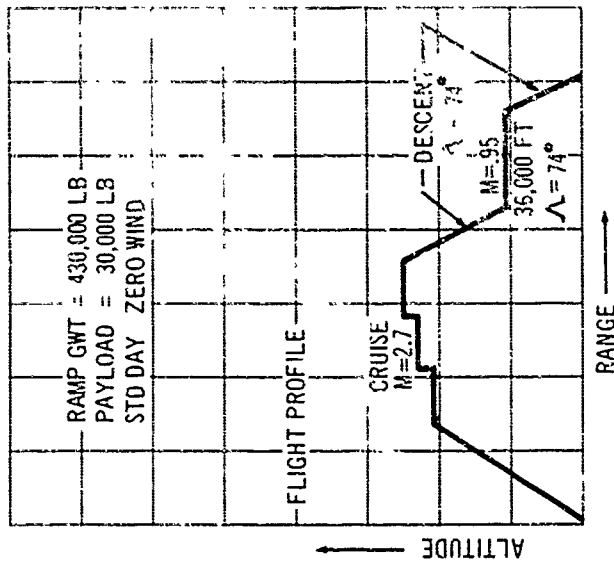
A 1 percent reduction in OWE (1825 pounds) results in a 5000-pound decrease in gross weight to 425,000 pounds.

B.3.1.8 EFFECT OF CRUISE RANGE FACTOR CHANGES ON DESIGN GROSS WEIGHT

The effects of incremental changes in cruise L/D and TSFC on the Model 733-197 are shown in Fig. B 3-8. A 1 percent improvement in L/D (or TSFC) results in a decrease in gross weight of about 4000 pounds to maintain the design mission range of 3500 n.mi.



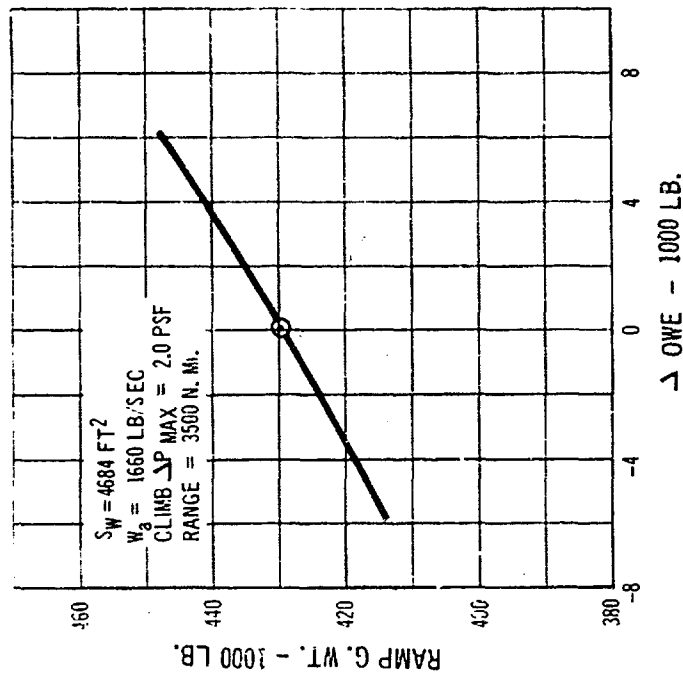
B 3-6 Range to Alternate with Wing Sweep 74 Degrees



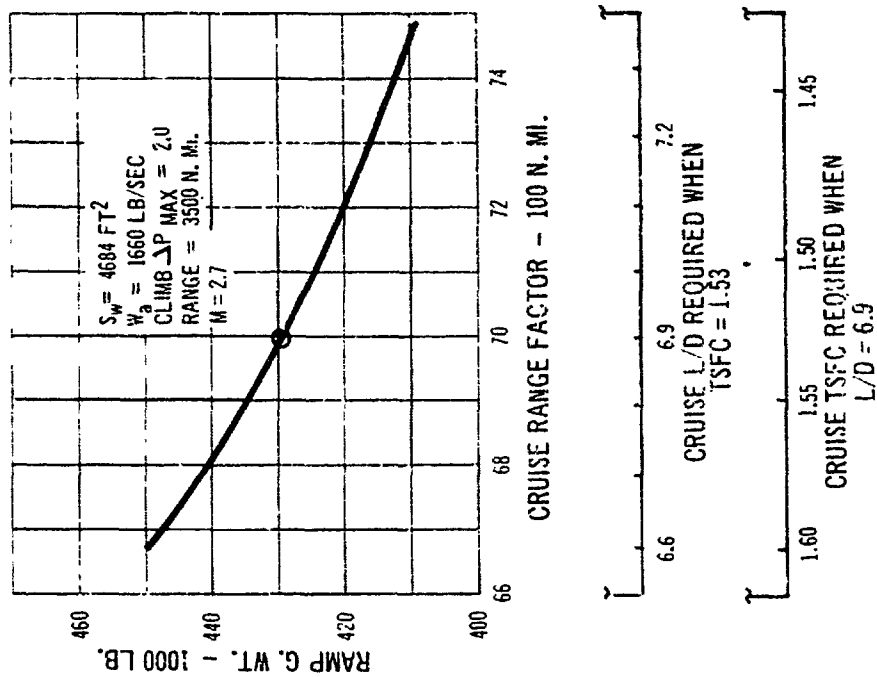
B.3.1.9 SUBSONIC PAYLOAD--RANGE

Fig. B 3-9 shows the payload-range capability of the Model 733-137 for standard day, zero wind conditions at the normal subsonic cruise speed of $M = 0.85$ and wing sweep of 42 degrees. A range of 3850 n.mi. is possible with the design payload of 150 passengers (30,000 pounds). A range

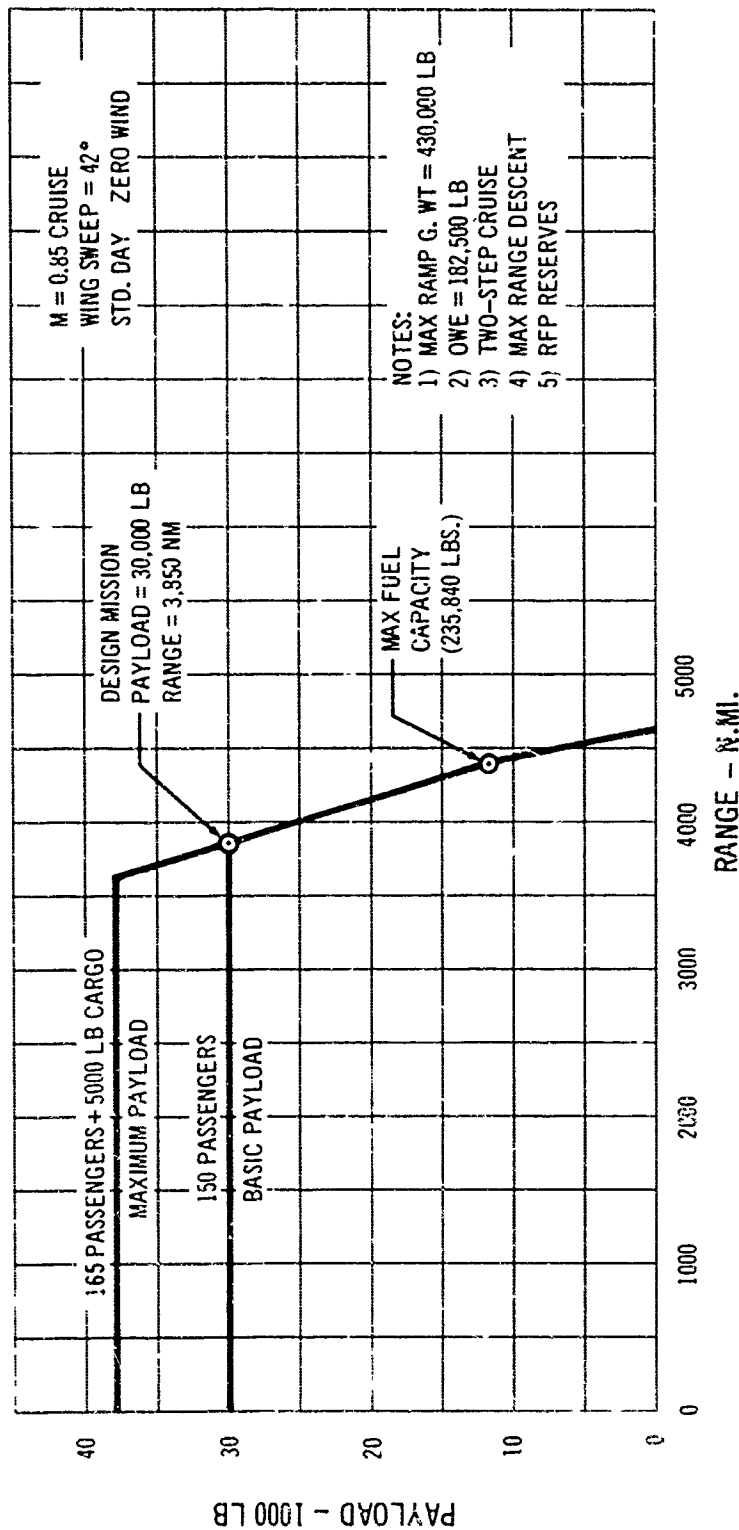
of 3620 n.mi. is possible with the maximum payload of 165 passengers plus 5000 pounds cargo (38,000 pounds) while at maximum fuel capacity and zero payload a maximum range of 4610 n.mi. is possible. These data are based upon a constant altitude two-step climb cruise technique and maximum range descent.



B 3-7 Operators' Weight Empty Trade



B 3-8 Range Factor Trade



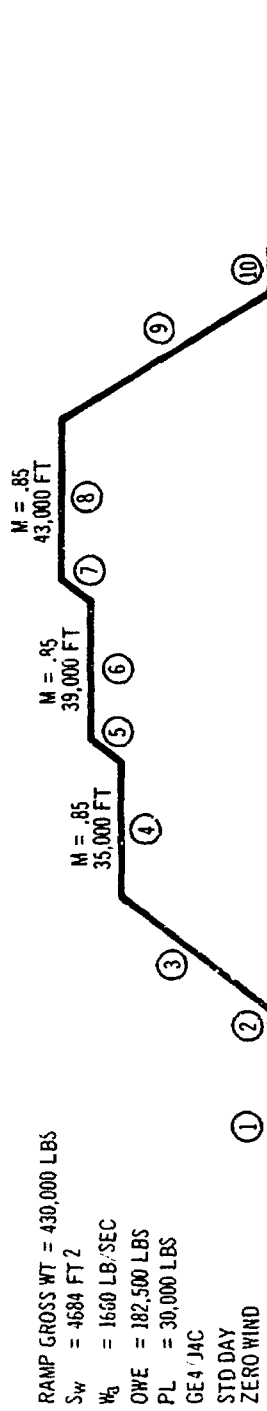
B 3-9. Payload - Range, Subsonic Cruise

B.3.1.10 SUBSONIC CRUISE FLIGHT PROFILE

A detailed breakdown of the subsonic cruise mission is presented in Fig. B 3-10. The fuel used, weight, time, and distance for each segment of the mission is given. The total range is 3850 n.mi. with a ramp gross weight of 430,000 pounds. The significant increase in subsonic over supersonic cruise range is the result of (1) less climb fuel required, (2) higher cruise lift-to-drag ratio, and (3) lower specific fuel consumption. Variable sweep contributes significantly to the excellent subsonic cruise capabilities of the airplane.

B.3.1.11 EFFECT OF WIND AND ALTITUDE ON SUBSONIC RANGE

Fig. B 3-11 shows the effect of wind and cruise altitude on the maximum range, full payload capabilities of the airplane. These data show that a 50-knot headwind will lower the design cruise range from 3850 n.mi. to 3450 n.mi., while cruising 4000 feet below the optimum altitude will lower the range from 3850 n.mi. to 3770 n.mi. These data are based on a practical two-step climb constant altitude cruise technique.



	FUEL USED - LB	FUEL REMAINING - LB	WEIGHT AT END OF OPER. - LB	TIME - HR	DISTANCE - N. MI.
1. Take-Off Taxi (10 MIN.) Take-Off Run	3,290 1,640	214,210 212,570	426,710 425,070	0 0	0 0
2. S.L. Acceleration	2,240	210,330	422,830	.013	4
3. Climb and Acceleration	12,460	197,870	410,370	.087	40
4. M = .85 Cruise at 35,000 ft, $\gamma = 42^\circ$	54,370	143,500	356,000	2.107	1028
5. Climb	1,300	142,200	354,700	.020	6
6. M = .85 Cruise at 39,000 ft, $\gamma = 42^\circ$	54,700	87,500	300,000	2.512	1227
7. Climb	1,100	86,400	298,900	.013	6
8. M = .85 Cruise at 43,000 ft, $\gamma = 42^\circ$	52,065	34,315	246,815	2.828	1379
9. Descent	2,300	32,015	244,515	.475	160
10. Approach and Landing (6 min. at S.L.)	2,300	29,715	242,215	0	0
	187,785			8.055	3850
Reserves:					
a. 7% Trip Fuel	12,915		229,300		
b. 260 N.Mi. Altn. Cruise, M = .85, $\gamma = 42^\circ$	8,000		221,300		
c. 0.5 Hr. Hold at 15,000 Ft, $\gamma = 30^\circ$	8,800		212,500		
TOTAL RESERVES	29,715				
TOTAL FUEL	217,500				

B 3-10 Subsonic Cruise Flight Profile

B.3.2 Flight Limits

B.3.2.1 SERVICE CEILING

The service ceilings (100 feet per minute rate of climb) for the Model 733-197 are given in Fig. B 3-12 where maximum thrust augmentation has been used. Weights of 380,000 and 250,000 pounds have been shown. These values are typical of weights at the beginning and ending of cruise. Service ceilings are also presented for the maximum dry power case.

B.3.2.2 WING SWEEP SCHEDULE

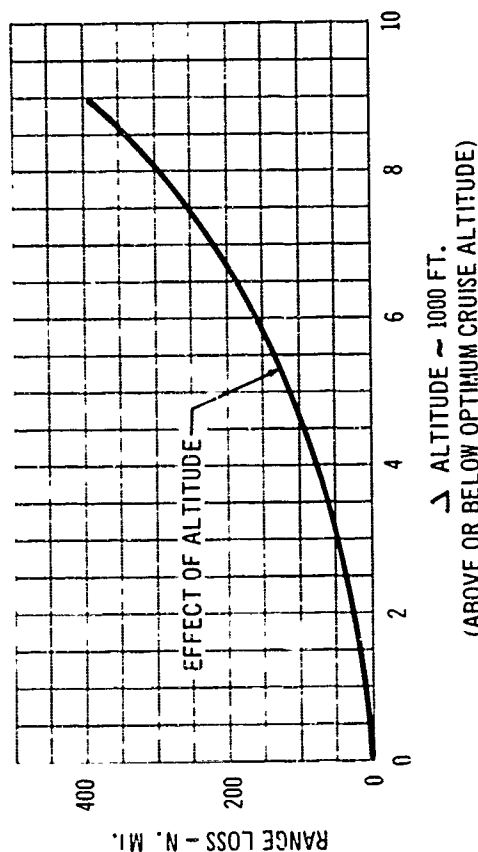
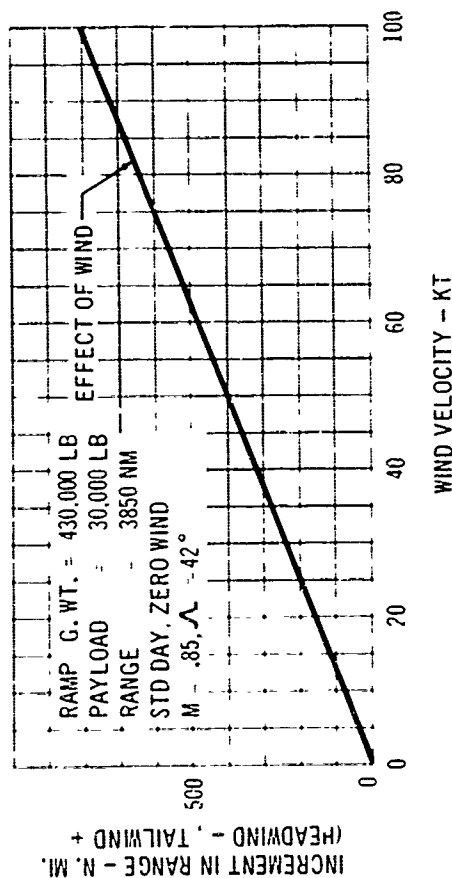
Leading edge sweep position as a function of Mach number is depicted on Fig. B 3-13 for the climb and descent schedules shown in Figs. B 3-26 and B 3-42. This sweep schedule will be accomplished by pilot selection using a constant sweep rate maintaining near-maximum aerodynamic efficiency.

For subsonic cruise a sweep position of 42 degrees will be used at a Mach number of 0.85. Holding will be accomplished at a leading-edge sweep of 30 degrees.

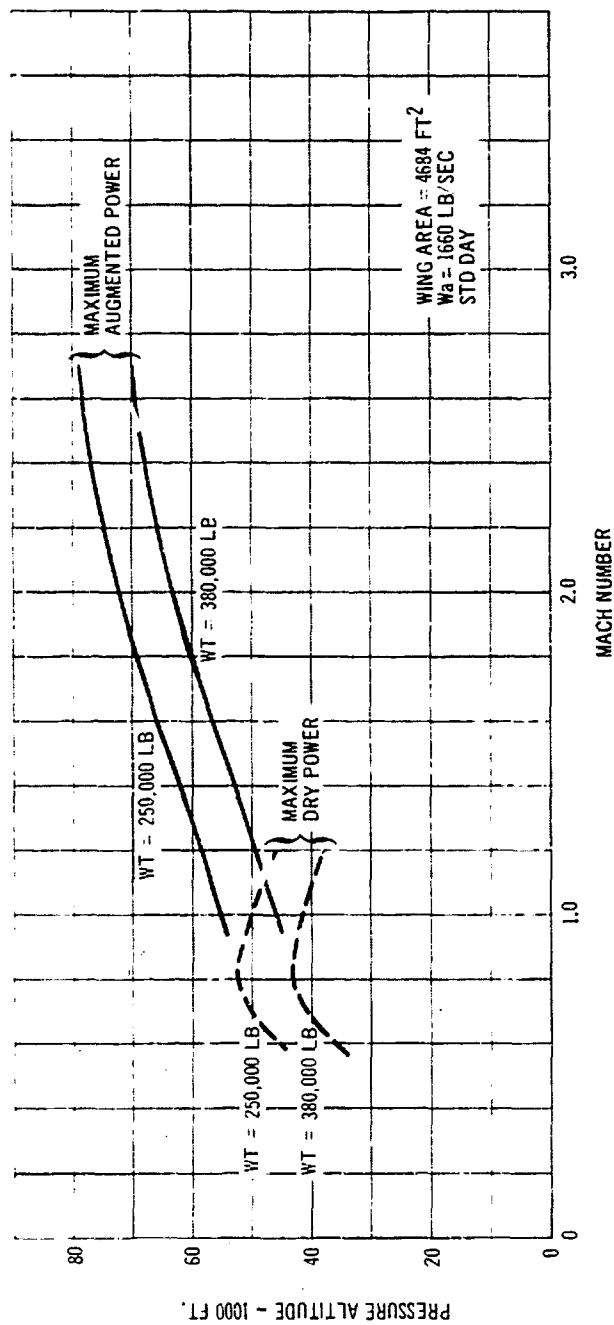
B.3.2.3 STALL SPEEDS AND MINIMUM LEVEL FLIGHT SPEEDS (4T-112 A & B)

Airplane stall speeds (1-g normal acceleration values) are shown in Fig. B 3-14 as a function of weight. The data are for the minimum appropriate wing sweep angles of 30 degrees with flaps up, and 20 degrees at takeoff and landing flap setting. The center of gravity location is at the forward loading limit of 40 percent m.a.c.

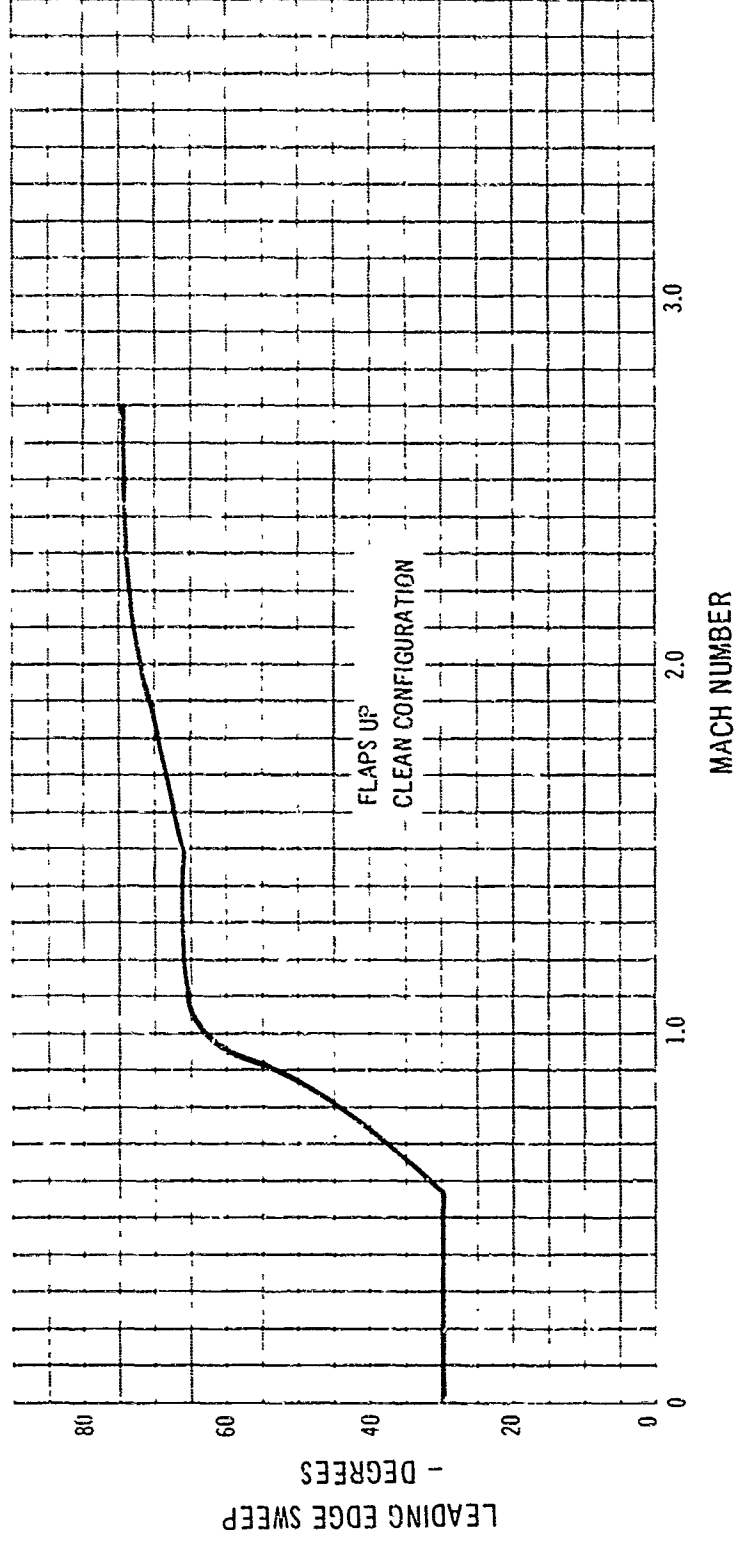
The minimum level flight speed curves shown in Fig. B 3-14 are applicable for two power levels under standard day conditions at sea level; four engines at maximum abatement takeoff thrust and three engines at maximum dry thrust, which are appropriate to takeoff conditions in a normal or one engine out situation. It will be noted that V_{NE} is in every case less than the one g stall speed with zero thrust.



B 3-11. Effect of Wind and Altitude on Subsonic Range



B 3.12 Service Ceiling



B 3-13 Wing Sweep Schedule

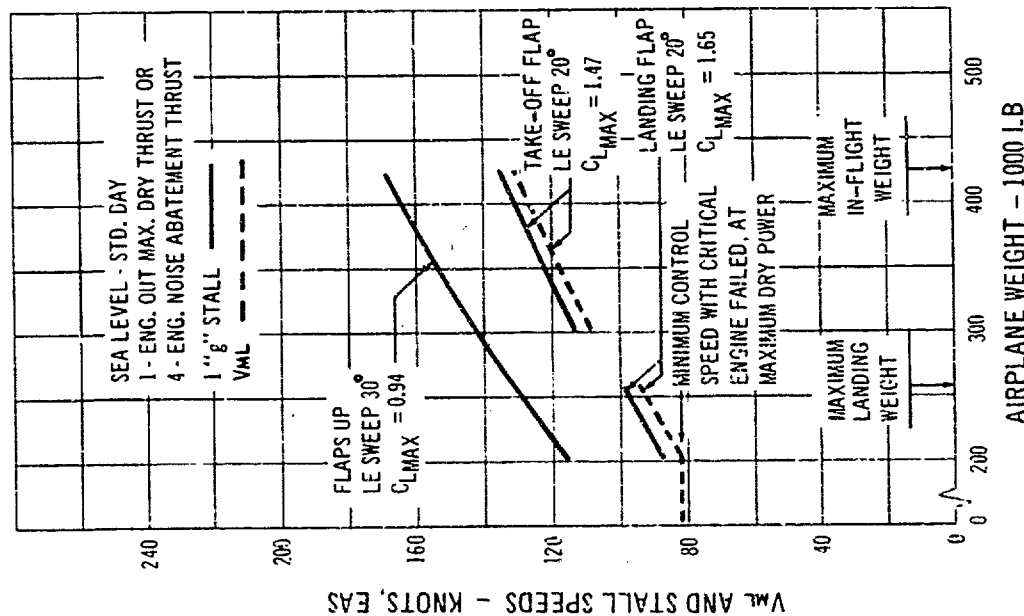
B.3.2.4 MINIMUM USABLE FLIGHT SPEED, WING SWEEP - 74 DEGREES

For a wings-back landing condition, the 74-degree leading-edge sweep case is covered by Fig. B 3-15. Stall speed is no longer considered relevant for this configuration due to the extreme angle of attack at which it is reached. In its place, the "minimum usable" speed has been selected at an angle of attack of 20 degrees; in accordance with this concept, the minimum level flight speeds are also restricted to this angle of attack, or less.

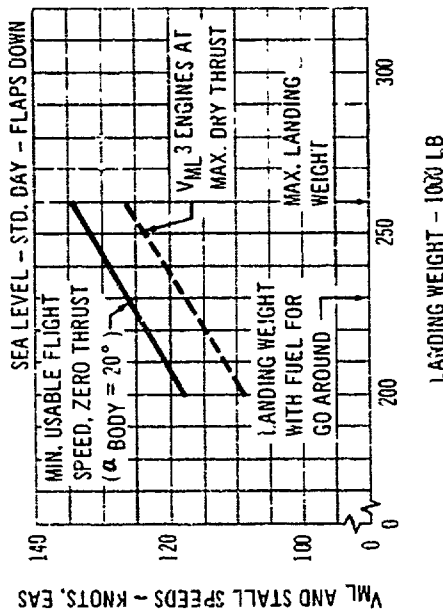
B.3.3 Takeoff

B.3.3.1 CAR TAKEOFF FIELD LENGTH, STANDARD DAY

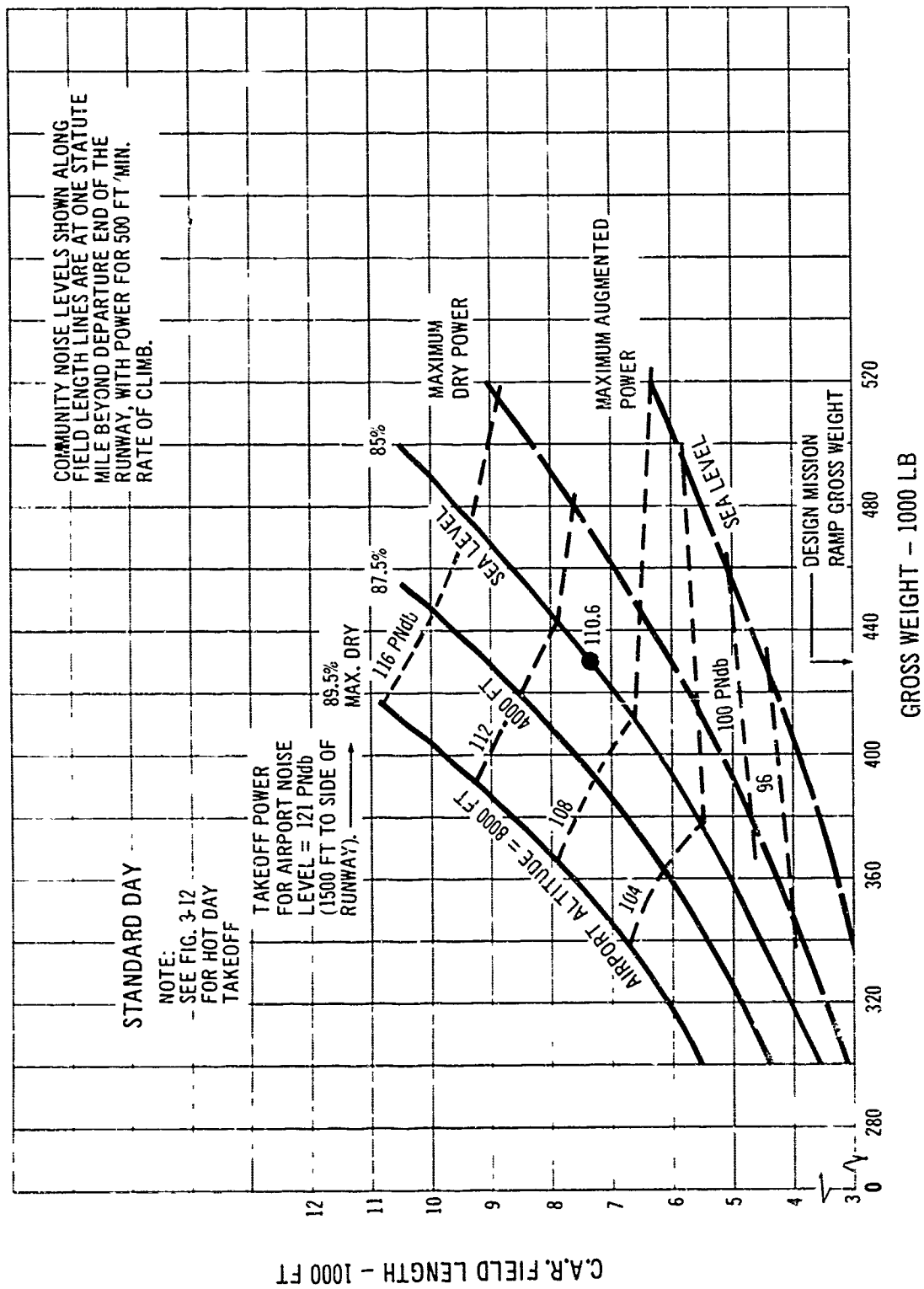
Fig. B 3-16 shows the CAR takeoff field length capability of the Model 733-197 for standard day, zero wind conditions. Data are presented for the normal range of operating weights and altitudes using noise-abatement power.



B 3-14 Stall and Minimum Flight Speeds



B 3-15 Fig. A3.2-4 Minimum Usable Flight Speed, $\alpha_{LE} = 74^\circ$



B 3-16 Take-Off Distance - Standard Day

The corresponding community noise levels are indicated. Data are also shown for the sea level case using maximum dry and maximum augmented power.

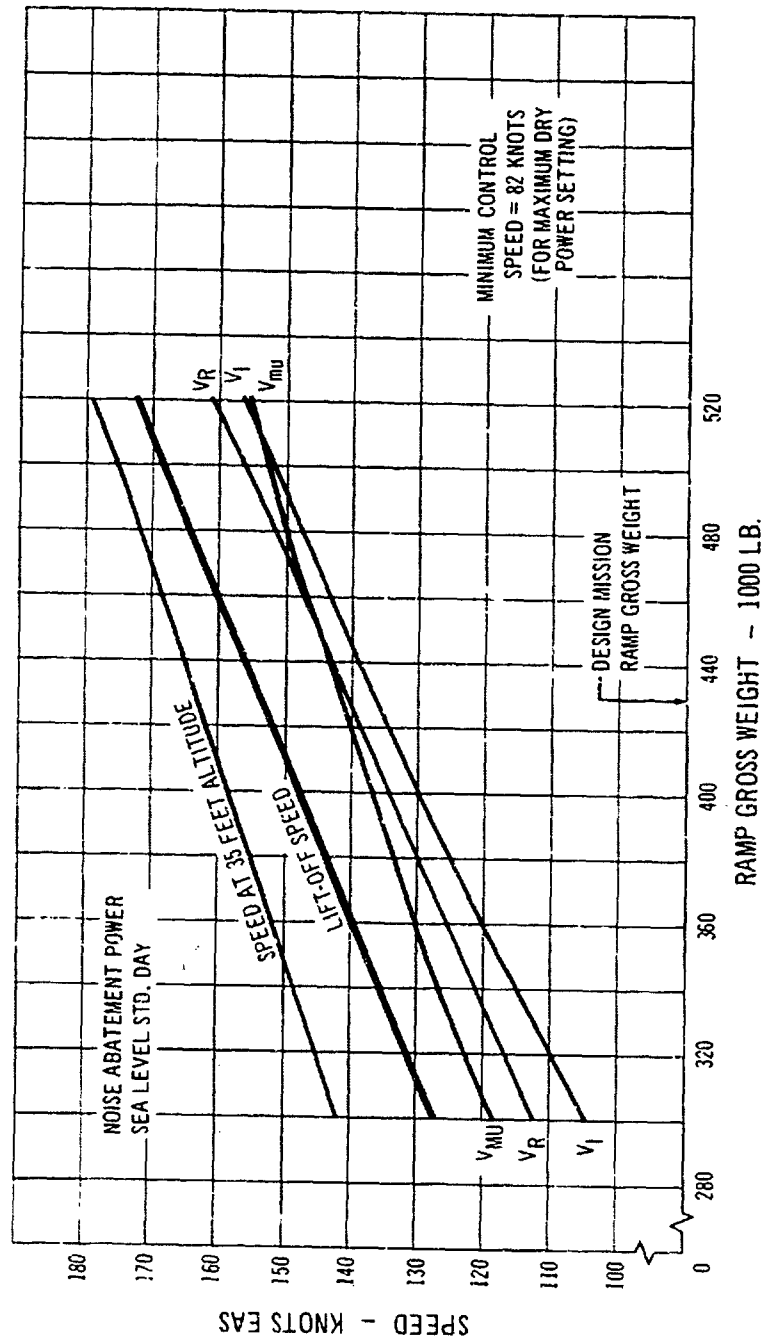
B.3.3.2 C A R TAKEOFF SPEEDS

Fig. B 3-17 shows the CAR takeoff speeds for sea level standard day conditions. These data, together with that of Fig. B 3-18 for the 8000-foot, 86 degrees Fahrenheit case

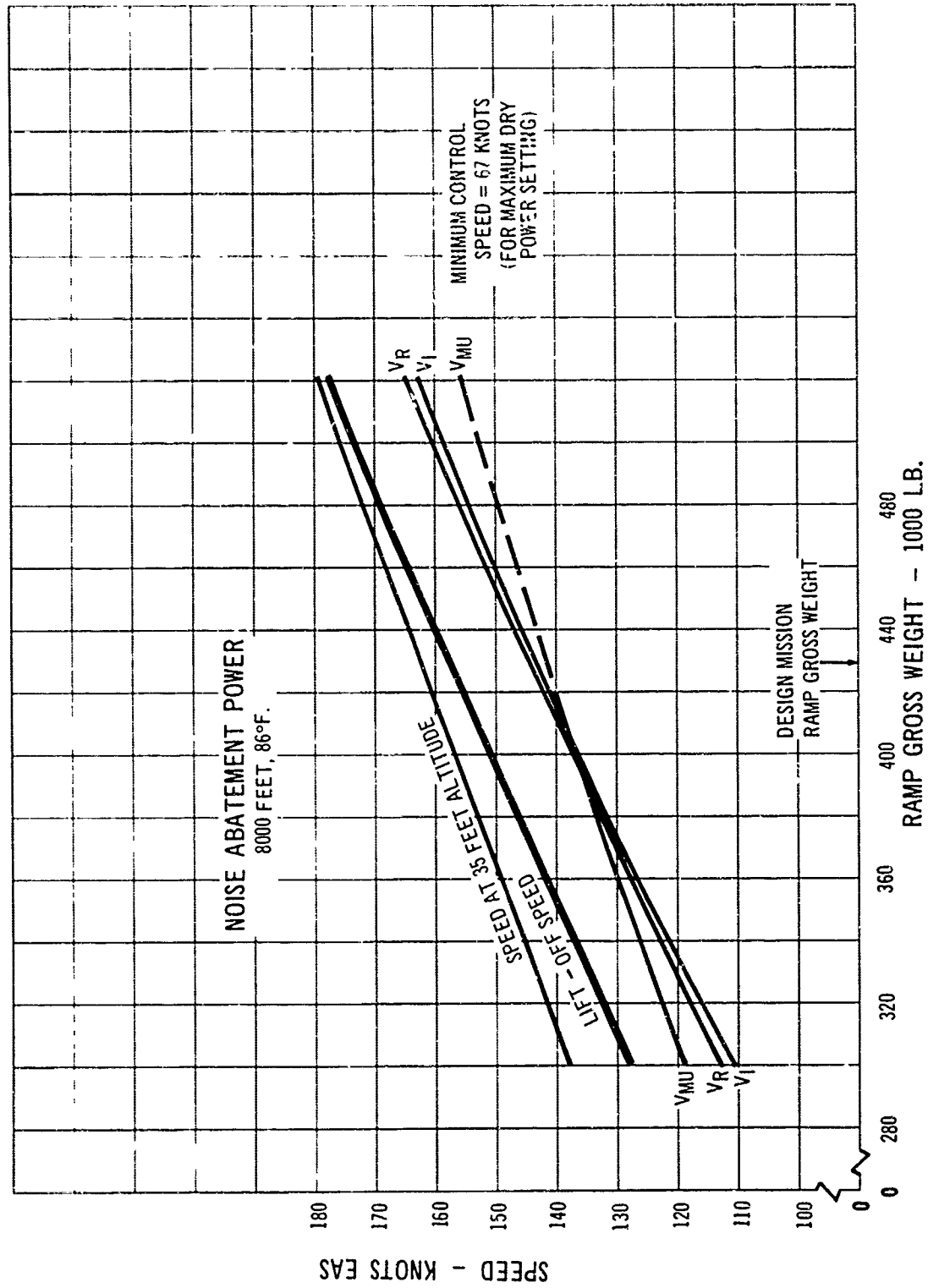
present the extremes in takeoff speeds.

B.3.3.3 TURNING CAPABILITY AT TAKEOFF SPEEDS

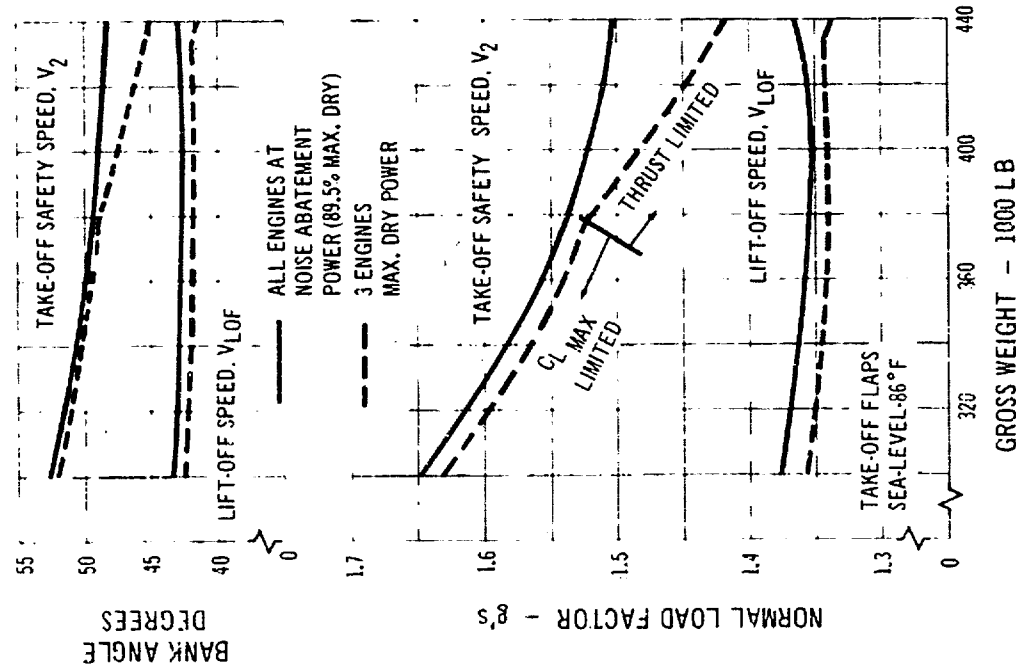
Normal load factor and bank angle obtainable in sustained turns at the liftoff and takeoff safety speeds are shown in Fig. B 3-19. The limiting load factor is reached when either: (a) thrust available equals drag; or (b) $C_L \leq C_{L_{max}}$. Data are shown for a range of flight weights



B 3-17 Take-Off Speeds - Sea Level, Standard Day



B 3-18 Take-Off Speeds - 8000 Feet, 86°F



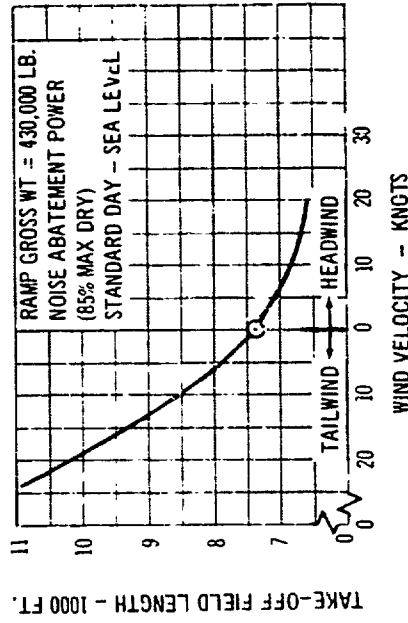
B 3-19 Sustained Turning Capability at Take-off Speeds

in the takeoff configuration, at sea level with an air temperature of 86 degrees Fahrenheit (standard day + 15 degrees Centigrade). Normal takeoff power (four engines) and maximum dry thrust (three engines) have been used for the example figures.

At the design gross weight of 430,000 pounds, the flap-down maximum flight weight is 427,000 pounds; at this weight and with one engine inoperative, the load factors obtainable are 1.34 at V_{LOF} and 1.44 at V_2 ; corresponding bank angles are 42 degrees and 46 degrees, respectively.

B.3.3.4 CAR TAKEOFF FIELD LENGTH, EFFECT OF HEADWIND

Effect of headwind on takeoff field length appears on Fig. B 3-20. This shows data for the design mission ramp gross weight of 430,000 pounds, for sea level, standard day conditions. The usual allowance of CAM 4b for computing wind effects on performance has been made. One hundred and fifty percent of the tailwind was used, while advantage was taken of only 50 percent of the nominal headwind.



B 3-20 Effect of Wind Velocity On Take-off Distance

B.3.3.5 C A R TAKEOFF FIELD LENGTH, EFFECT OF SLUSH ON RUNWAY

Takeoff field length variation with slush depth is shown in Fig. B.3-21. Noise-abatement thrust has been used for comparative purposes, although in practice full power would probably be used. Balanced field lengths become more critical than four-engine takeoff distances due to the retarding effects of the slush during three-engine acceleration above the refusal speed V_1 . Distances were evaluated for a ramp gross weight of 430,000 pounds at a representative air temperature of 40 degrees Fahrenheit, sea level.

B.3.3.6 TAKEOFF FUEL VARIATION WITH THRUST

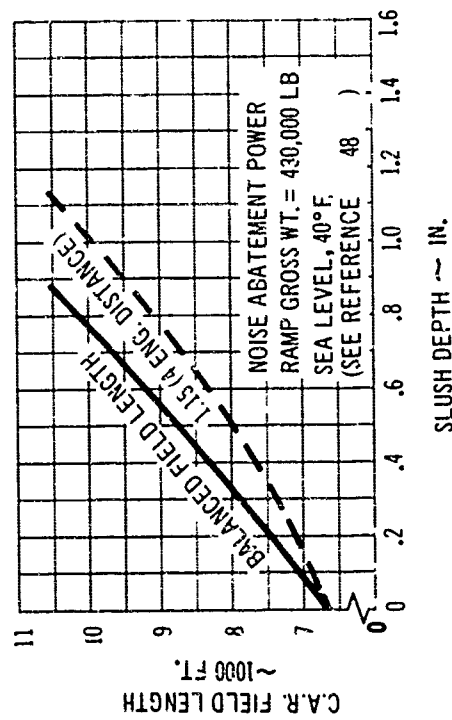
Fuel for taxi, takeoff and acceleration to 180 knots is shown for standard and standard + 15 degrees Centigrade conditions at sea level on Fig. B.3-22 as function of takeoff power. The power settings normally used where low takeoff noise is a criteria are:

85 percent maximum dry on a standard day;
89.5 percent maximum dry on a standard + 15 degrees Centigrade day.

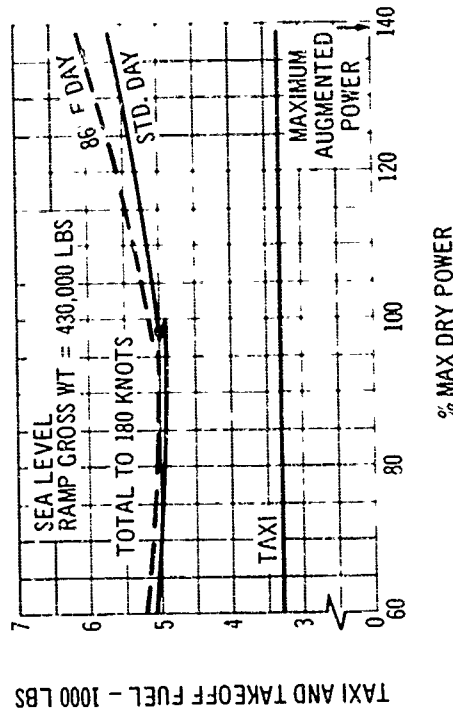
B.3.3.7 AIRPORT NOISE PROFILES AT TAKEOFF POWER

A typical takeoff power used for noise abatement purposes is 85 percent maximum dry thrust on a standard day at sea level. Airport static noise profiles are shown in polar form for this case in Fig. B.3-23. As noted in Volume A-VII these noise levels, as estimated by Boeing, are approximately 3PNdb greater than those supplied by General Electric for the GE4 J4C engine. Also the noise levels shown are for unsuppressed engines. The sound suppressors to be developed during Phase II will result in a reduction of from 2 to 5 PNdb, according to present estimates.

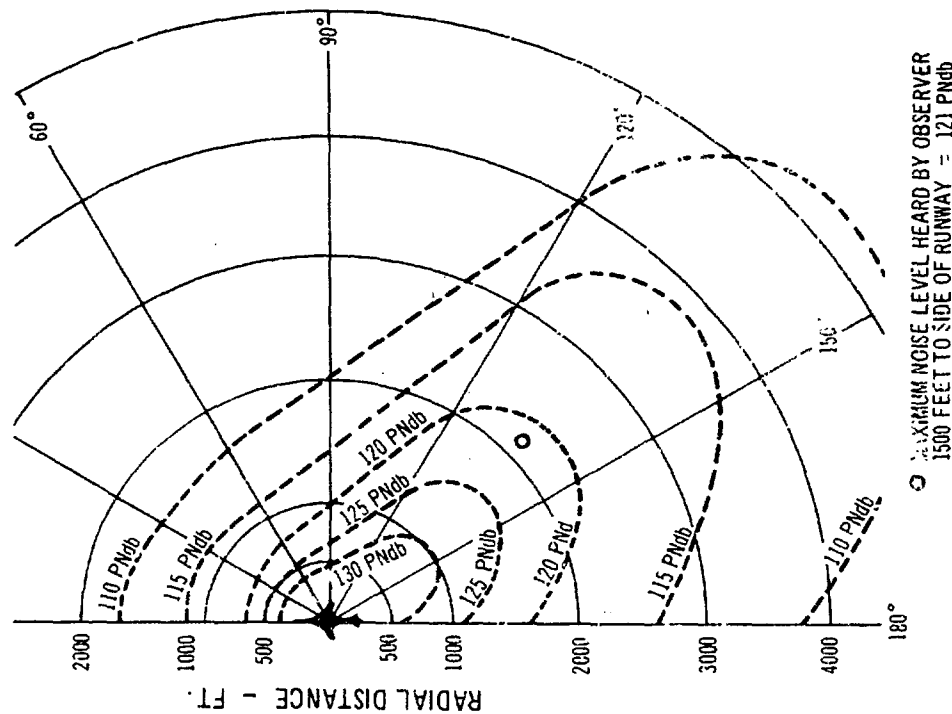
The highest noise level perceived by an observer standing 1500 feet to the side of the takeoff path, as the airplane passes on its takeoff run, is shown on the



B.3-21 Effect of Slush on Take-Off Field Length



B.3-22 Effect of Power Setting on Take-Off Fuel



B 3-25 Airport Noise for Static Take-Off Engine Thrust (85% Maximum Dry), Standard Day, Sea Level.

diagram. It will not exceed 121 PNdb.

These noise data, together with those of Section B 3.3.8, have been evaluated by the methods described in Section 8.0 of proposal document, Volume A-VII, Systems.

B.3.3.8 NOISE PROFILES IN CLIMB-OUT

Noise levels below and to the side of the airplane takeoff path are shown in Fig. B 3-24. After liftoff, the airplane climbs at takeoff power and the noise levels are shown by the solid lines. At a point one statute mile beyond the runway departure end, perceived noise would reach a maximum of 123 PNdb. By throttling back the engines to give a climb rate of 500 ft./min. over the community area, noise levels are reduced to only 110.6 PNdb. This large reduction is made possible by the high lift/drag ratio obtainable with the variable sweep airplane.

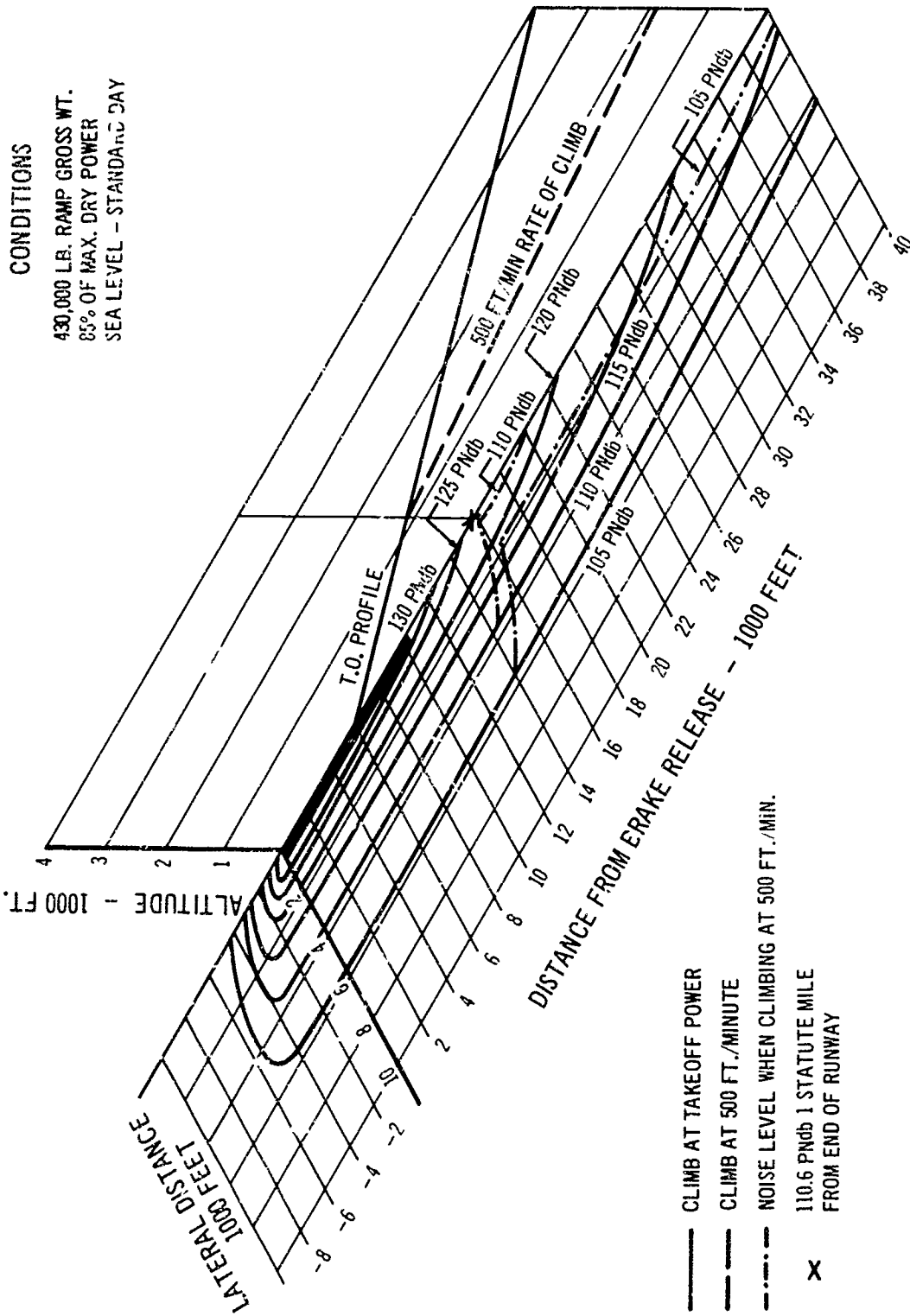
B.3.3.9 TAKEOFF FUEL ALLOWANCE

Fig. B 3-25 shows the takeoff fuel allowance used in the basic design mission calculations. Data are shown for a range of takeoff weights and operating temperatures. The allowance consists of 10 minutes at taxi thrust plus the fuel required for the actual takeoff and acceleration to 180 knots.

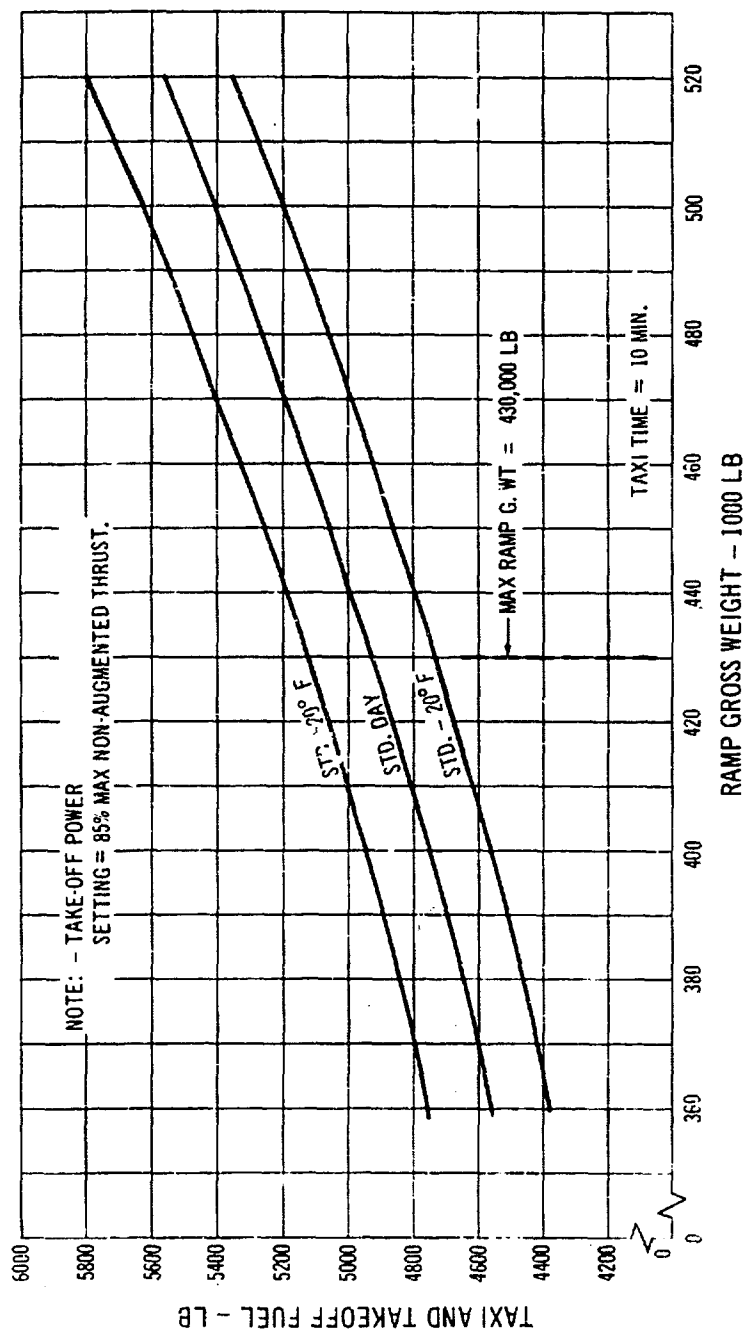
B.3.4 Climb

B.3.4.1 CLIMB AND ACCELERATION SCHEDULES

Climb and acceleration schedules for the range of operating temperatures are shown in Fig. B 3-26. The normal climb schedules are those which result in a maximum sonic boom overpressure in climb of 2.0 psf for the maximum gross weight airplane. Acceleration along the structural design placard (M_{wo}) would result in sonic boom overpressures greater than 3.0 psf. The cruise speed limits are included in this figure and are those M_{ch} numbers



P 3-24 Noise Profile for Take-off



B 3-25 Taxi And Take-Off Fuel

which result in a stagnation temperature of 500 degrees Fahrenheit.

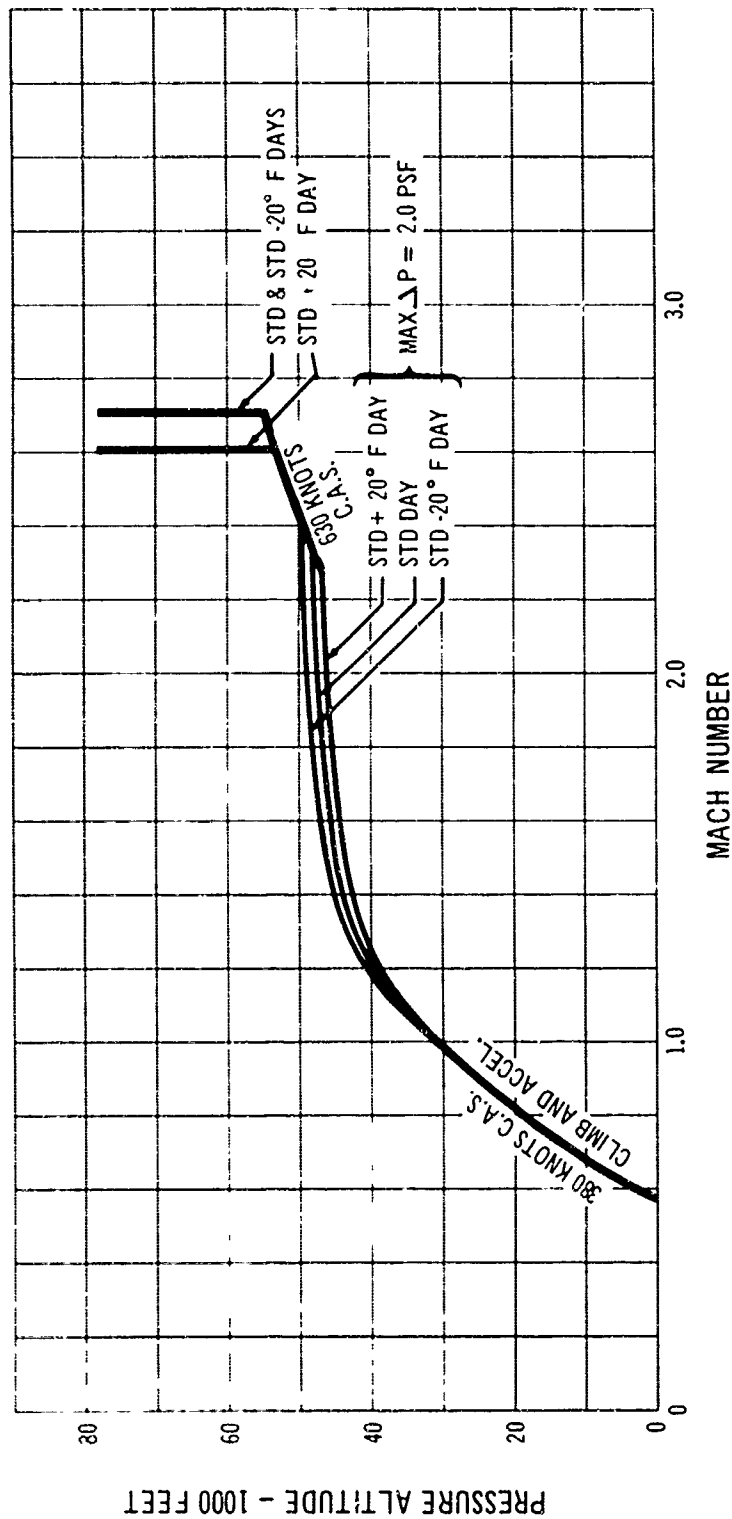
on the sweep schedule given in Fig. B 3-13 and climb and acceleration schedule given in Fig. B 3-26.

B.3.4.2 CLIMB AND ACCELERATION PERFORMANCE (STANDARD DAY)

Fig. B 3-27 shows time, fuel, and distance required versus altitude for climb and acceleration to cruise speed (M = 2.7) and altitude on a standard day for the normal range of operating weights. These data are based

B.3.4.3 CLIMB AND ACCELERATION PERFORMANCE (STANDARD + 20 DEGREE FAHRENHEIT DAY)

Fig. B 3-28 shows time, fuel, and distance required versus altitude for climb and acceleration to cruise speed (M = 2.6) and altitude on a standard plus 20 degrees



B 3-26 Climb and Acceleration Schedule

Fahrenheit day for the normal range of operating weights. These data are based on the sweep schedule given in Fig. B 3-13 and climb and acceleration schedule given in Fig. B 3-26.

B.3.4.4 CLIMB AND ACCELERATION — 20 DEGREE FAHRENHEIT DAY

Fig. B 3-29 shows time, fuel, and distance required versus altitude for climb and acceleration to cruise speed ($M = 2.7$) and altitude on a standard minus 20 degrees

Fahrenheit day for the normal range of operating weights. These data are based on the sweep schedule given in Fig. B 3-13 and climb and acceleration schedule given in Fig. B 3-26.

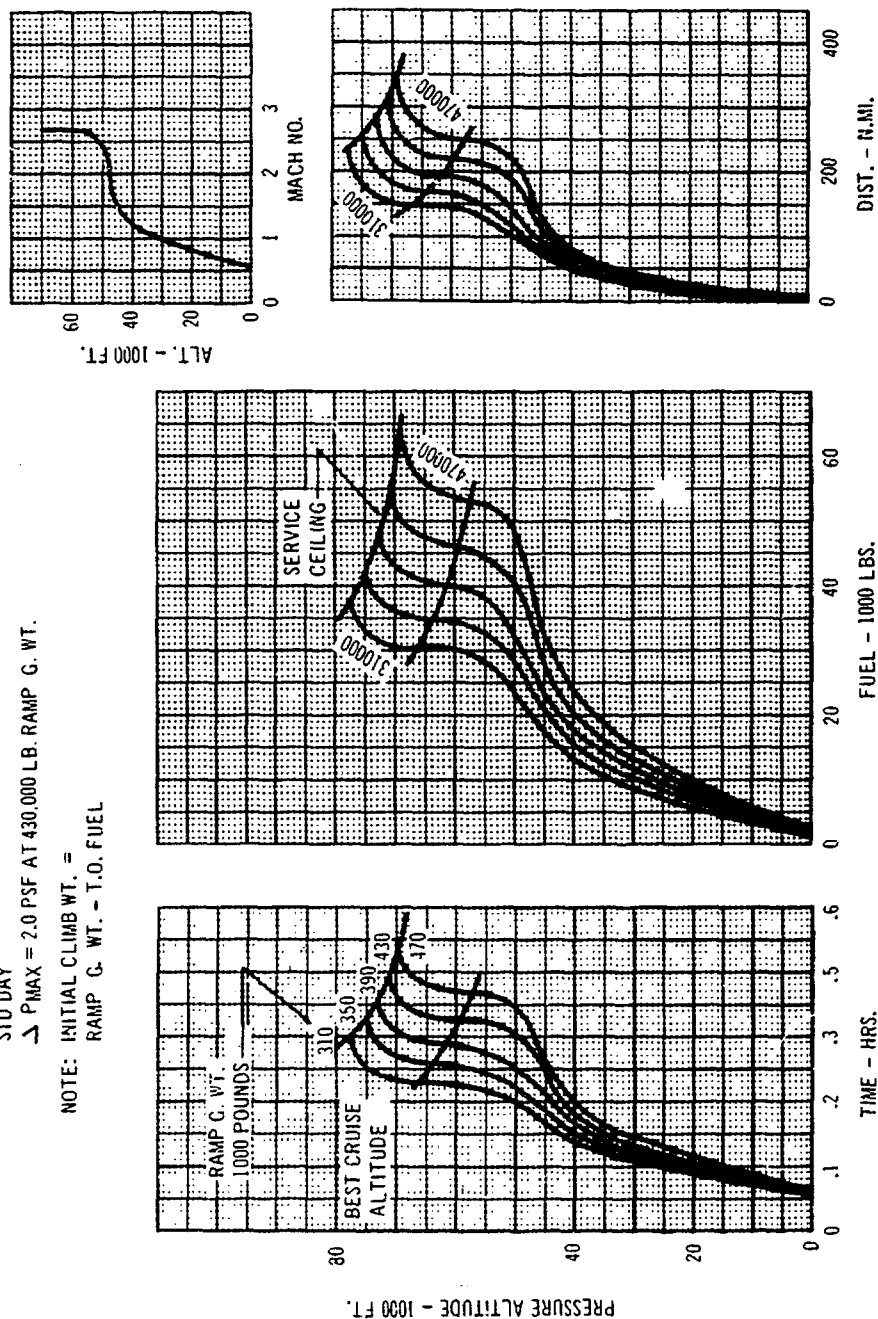
B.3.4.5 SONIC BOOM OVERPRESSURES IN CLIMB

Fig. B 3-30 shows the sonic boom overpressures in climb versus altitude for the normal range of operating weights and temperatures. These data correspond to the climb data shown in Figs. B 3-27, B 3-28, and B 3-29, and are

$\Delta P_{MAX} = 2.0 \text{ PSF AT } 430,000 \text{ LB. RAMP G. WT.}$

NOTE: INITIAL CLIMB WT. =

RAMP G. WT. - T.O. FUEL

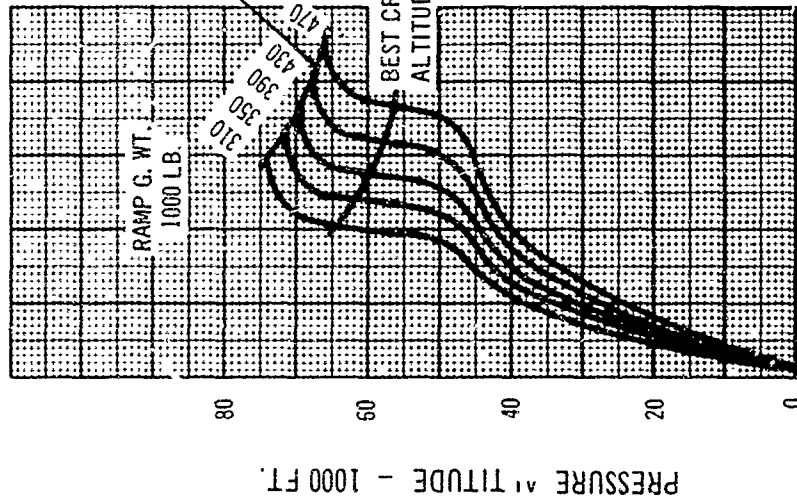


B 3-27 *Climb and Acceleration, Standard Day*

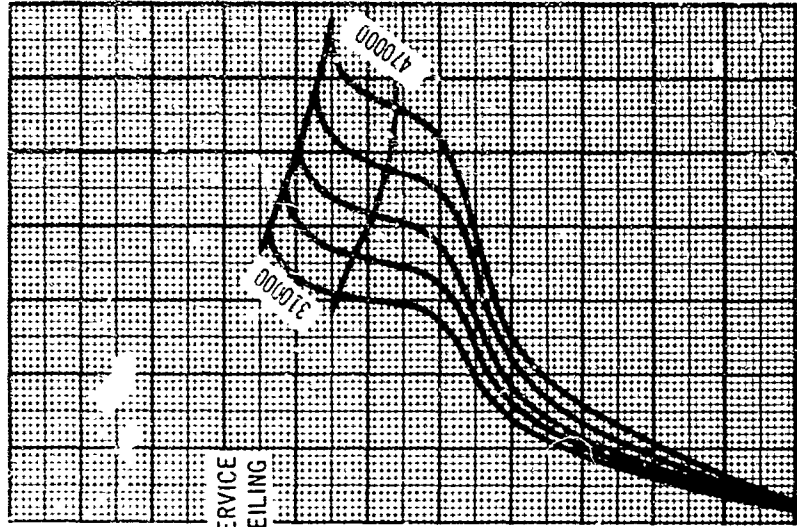
STD DAY + 20-F

$\Delta P_{MAX} = 2.0$ PSF AT 430,000 LB. RAMP G. WT.

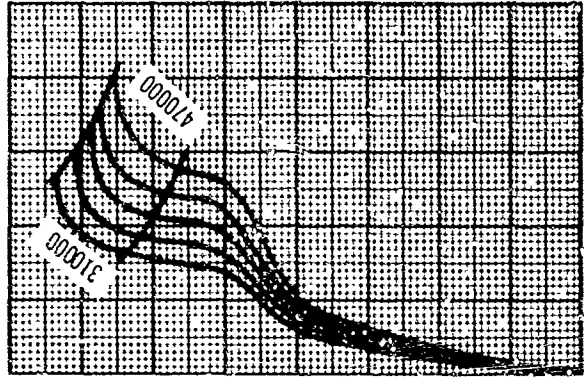
NOTE INITIAL CLIMB W.F. =
RAMP G.WT. - T.O. FUEL



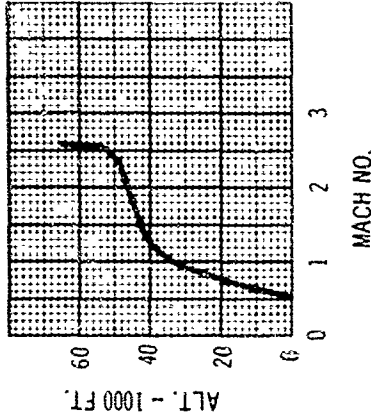
TIME - HRS.



FUEL - 1000 LBS

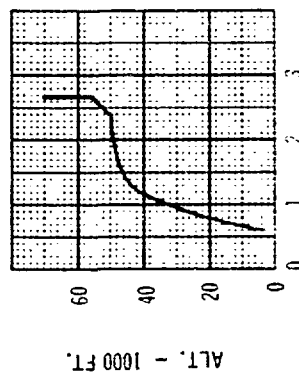


DISTANCE - N.MI.

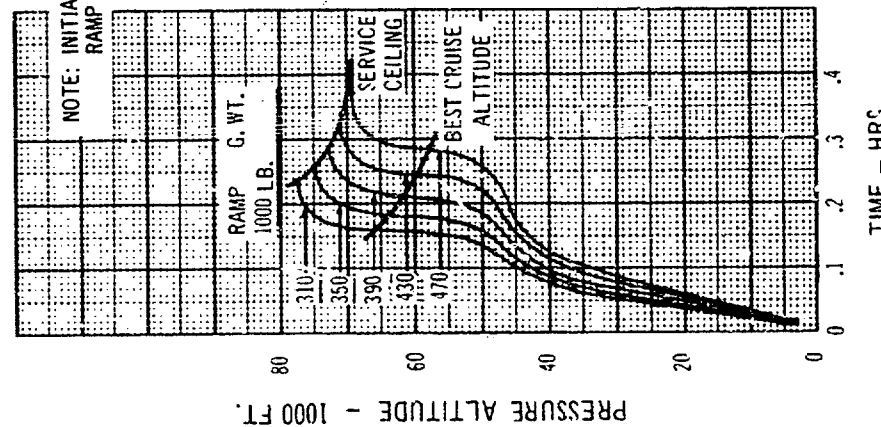
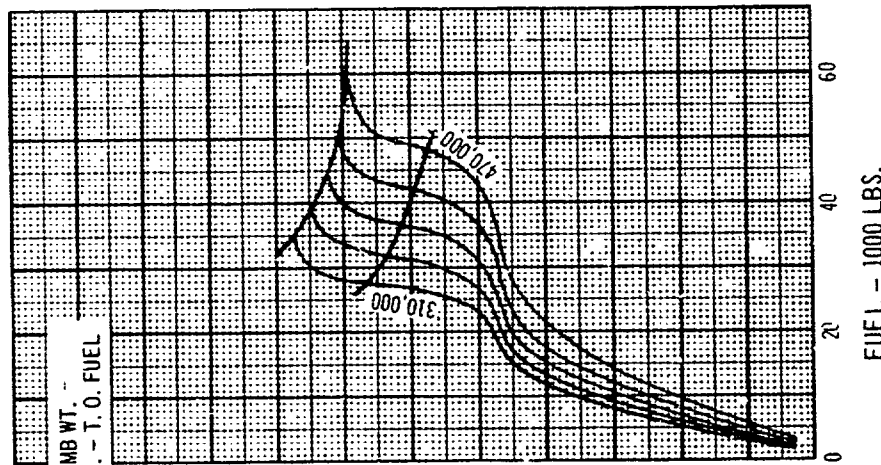
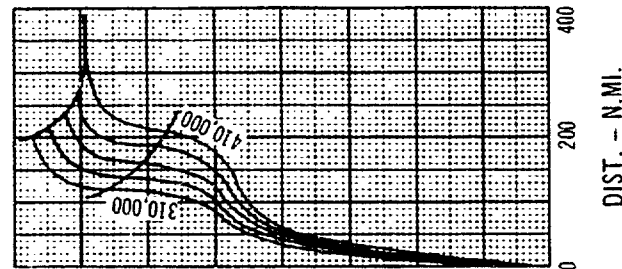


B 3-28 *Climb and Acceleration, Std Day +20 F.*

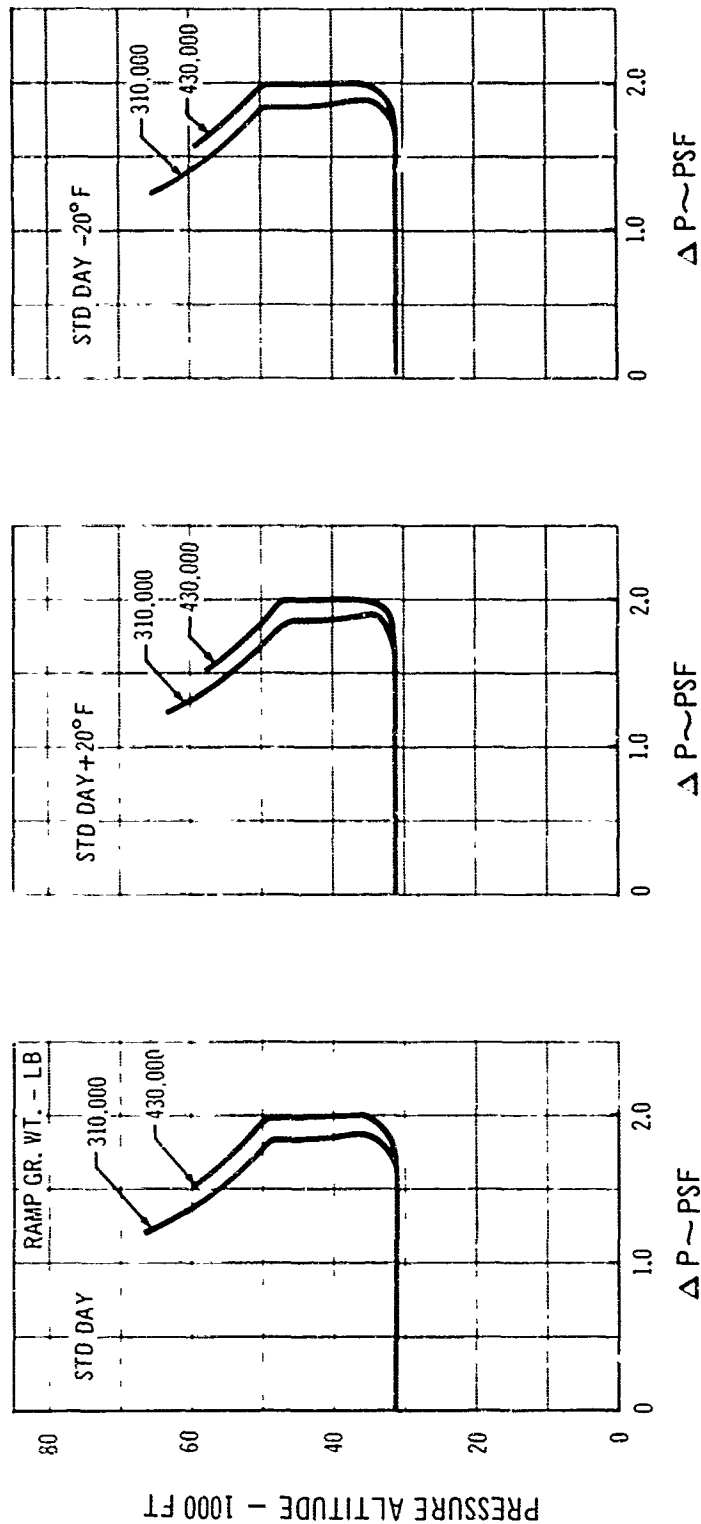
STD DAY - 20° F
 $\Delta P_{MAX} = 2.0 \text{ PSF}$ @ 430,000 LB. RAMP G. WT.



MACH NO.



B 3-29 Climb and Acceleration (Std. Day - 20° F)



B 3-30 Sonic Boom Overpressures in Climb

in compliance with the overpressure requirements specified in the RFP.

B 3.4.6 RATE OF CLIMB

Fig. B 3-31 shows typical standard day rate of climb versus altitude data for three Mach numbers (0.85, 1.4, and 2.7) for the normal range of operating weights.

B 3.4.7 SUBSONIC CLIMB AND ACCELERATION PERFORMANCE (STANDARD DAY)

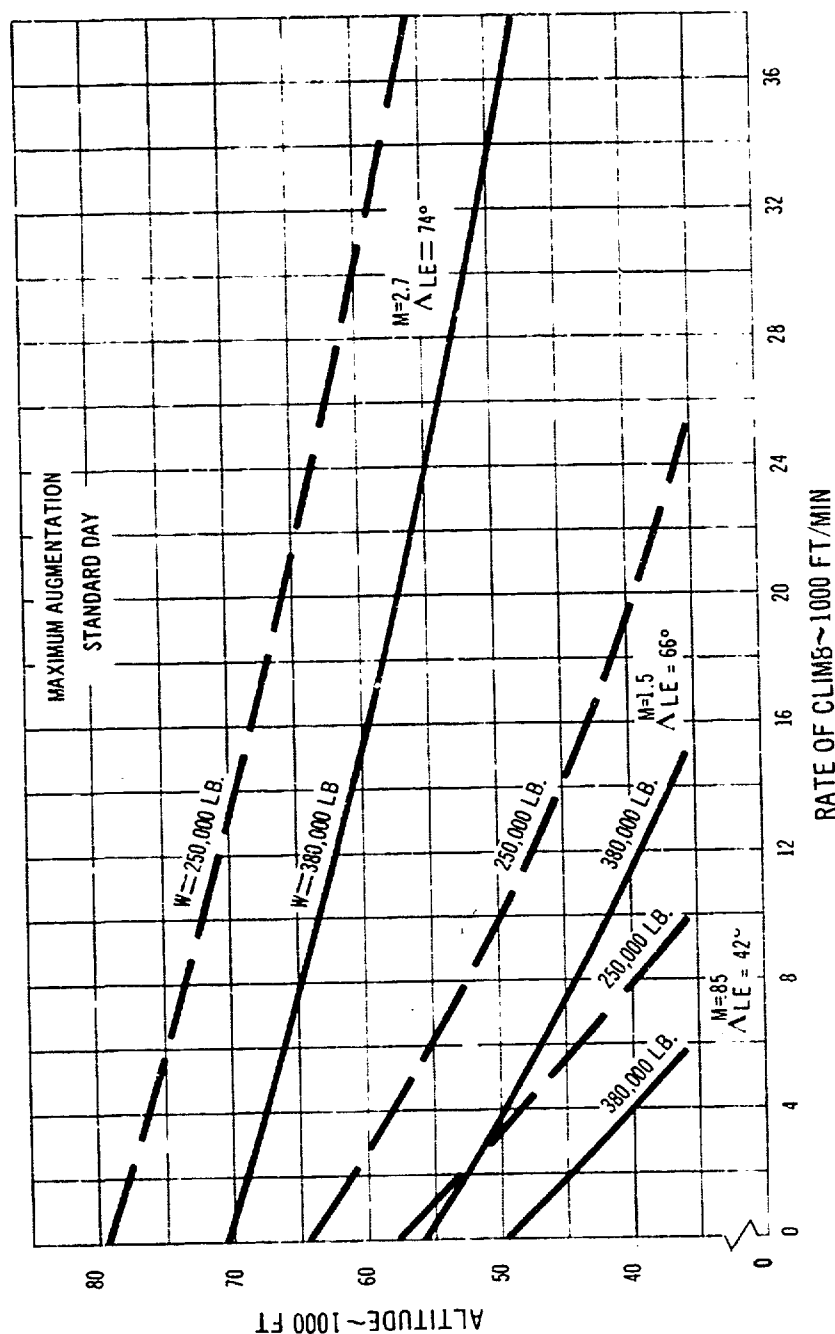
Fig. B 3-32 shows the time, fuel and distance required

versus altitude for climb and acceleration to a subsonic cruise speed ($M = 0.85$) and altitude on a standard day for the normal range of operating weights. These data are based on use of the wing sweep schedule given in Fig. B 3-13 and climb and acceleration schedule given in Fig. B 3-26 up to the cruise wing sweep angle of 42 degrees and cruise Mach number of 0.85.

B 3.5 Cruise

B 3.5.1 OPTIMUM CRUISE FUEL MILEAGE

Fig. B 3-33 shows the optimum fuel mileage capability of

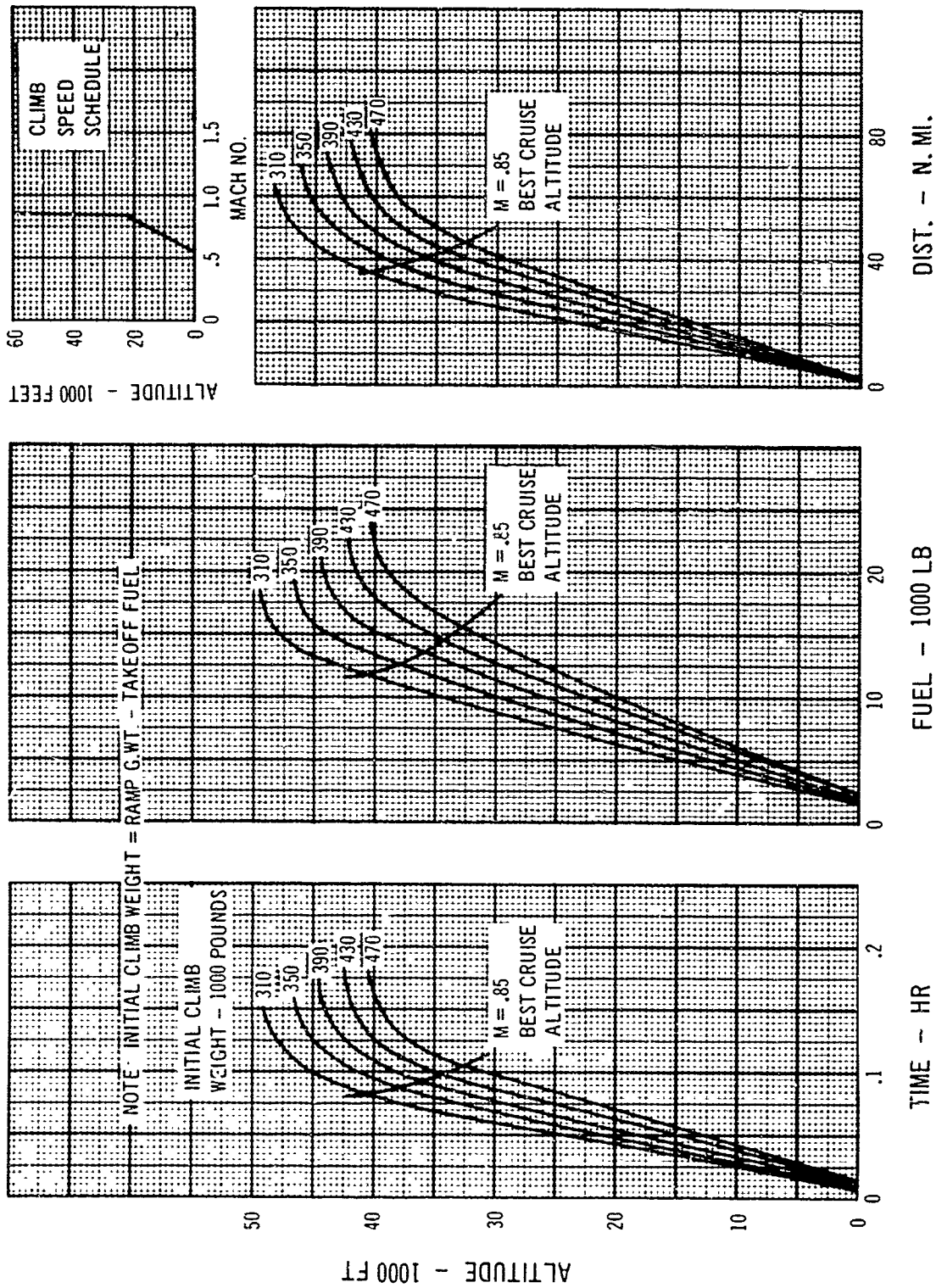


B 3-31 Rate Of Climb

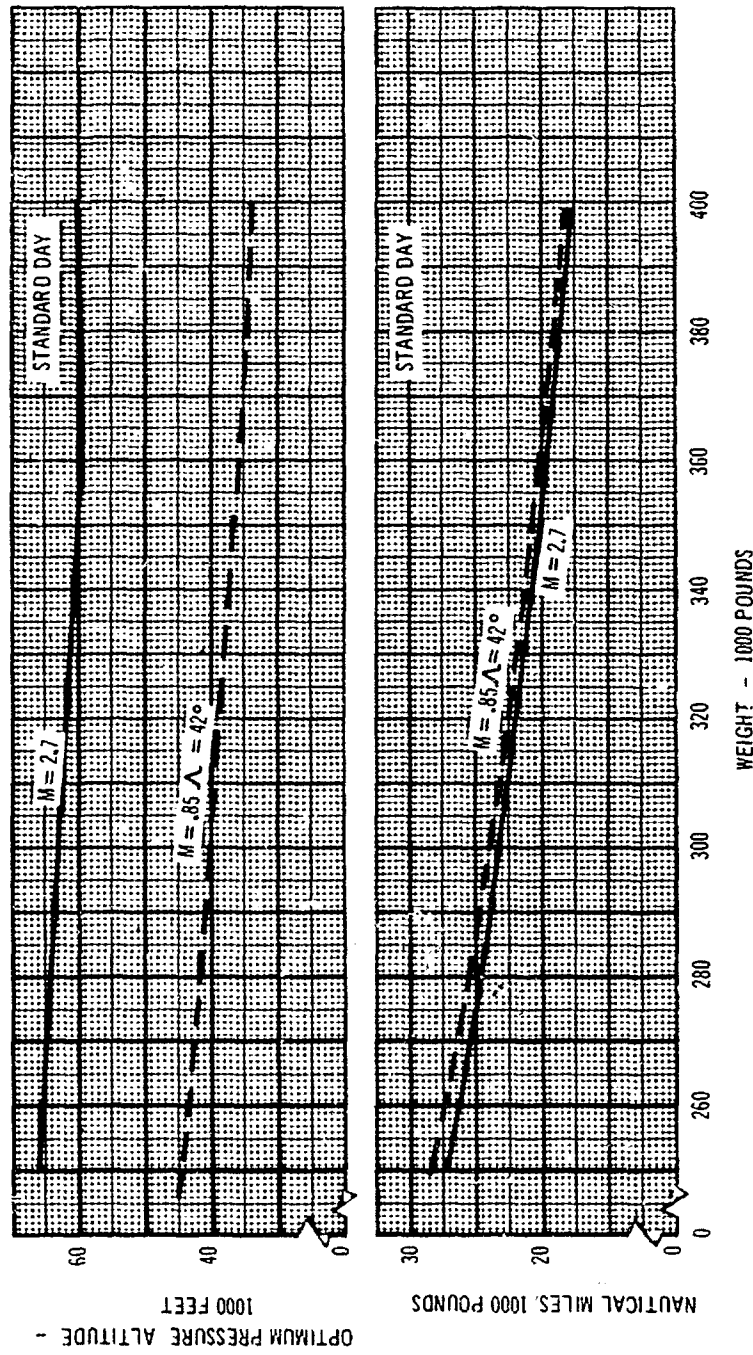
B 3.5.2 FUEL MILEAGE AT $M=2.7$ (STANDARD DAY)

the airplane at both supersonic ($M=2.7$) and subsonic ($M=0.85$) cruise speeds together with the cruise altitude required. In the case of supersonic cruise it should be noted that the cruise altitude at high gross weights is that required to meet the RFP 1.5-psf sonic boom over-pressure requirement.

Fig. B 3-34 shows the fuel mileage capability of the airplane on a standard day at the maximum cruise speed of $M=2.7$ for the normal range of operating weights and altitudes. The altitude for maximum range is shown



B-3-32 Climb and Acceleration - Subsonic Climb - Standard Day



B 3-33 Optimum Cruise Fuel Mileage - Standard Day

as well as the altitude at which the sonic boom overpressure is 1.5 psf in accordance with the RFP requirements.

B.3.5.3 FUEL MILEAGE AT $M=2.6$ (STANDARD DAY +20 DEGREES FAHRENHEIT)

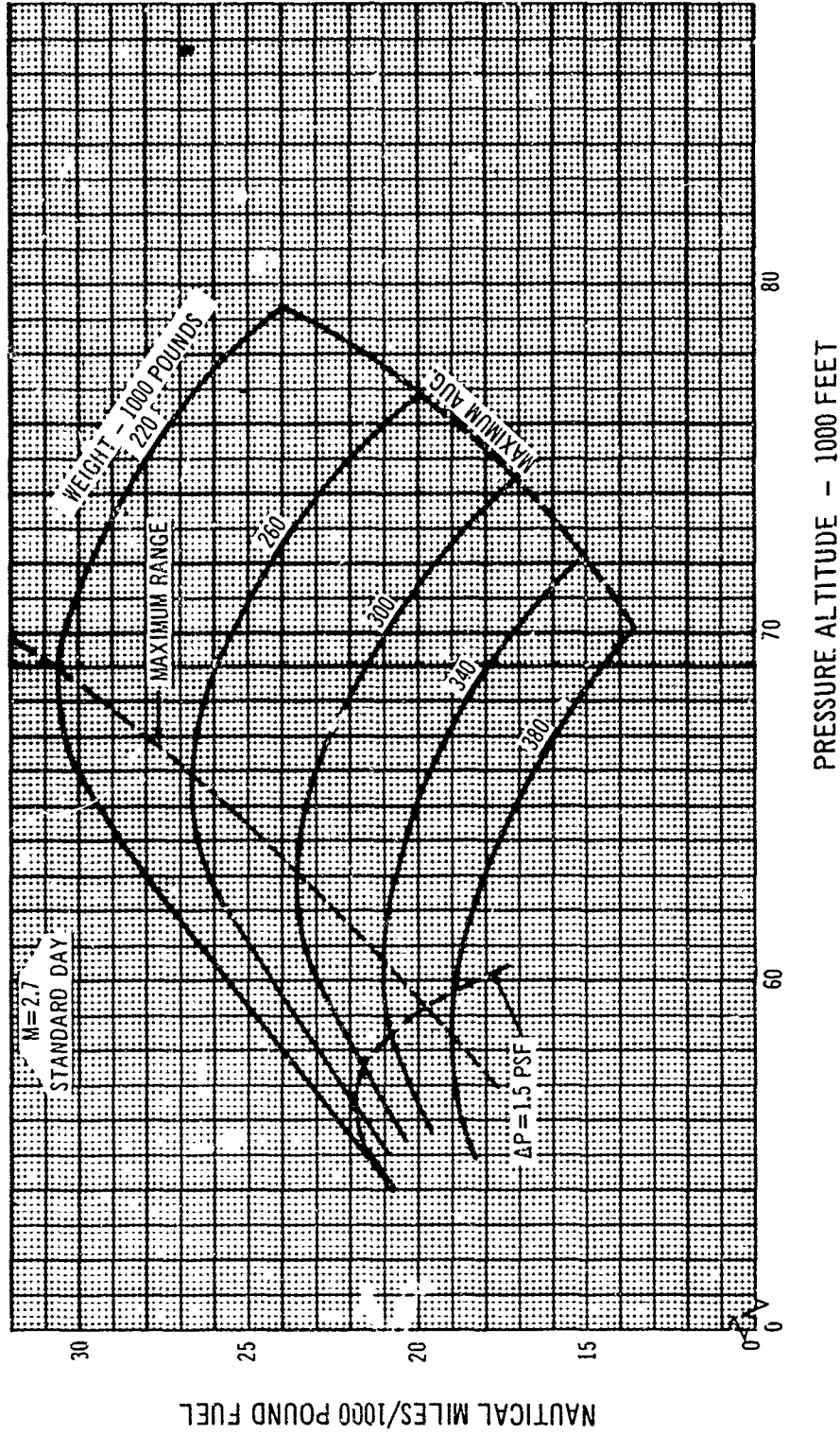
Fig. B 3-35 shows the fuel mileage capability of the air-

plane on a standard plus 20-degree Fahrenheit day at the maximum cruise speed of $M = 2.6$ for the normal range of operating weights and altitudes. The altitude for maximum range is shown as well as the altitude at which the sonic boom overpressure is 1.5 psf in accordance with the RFP requirements.

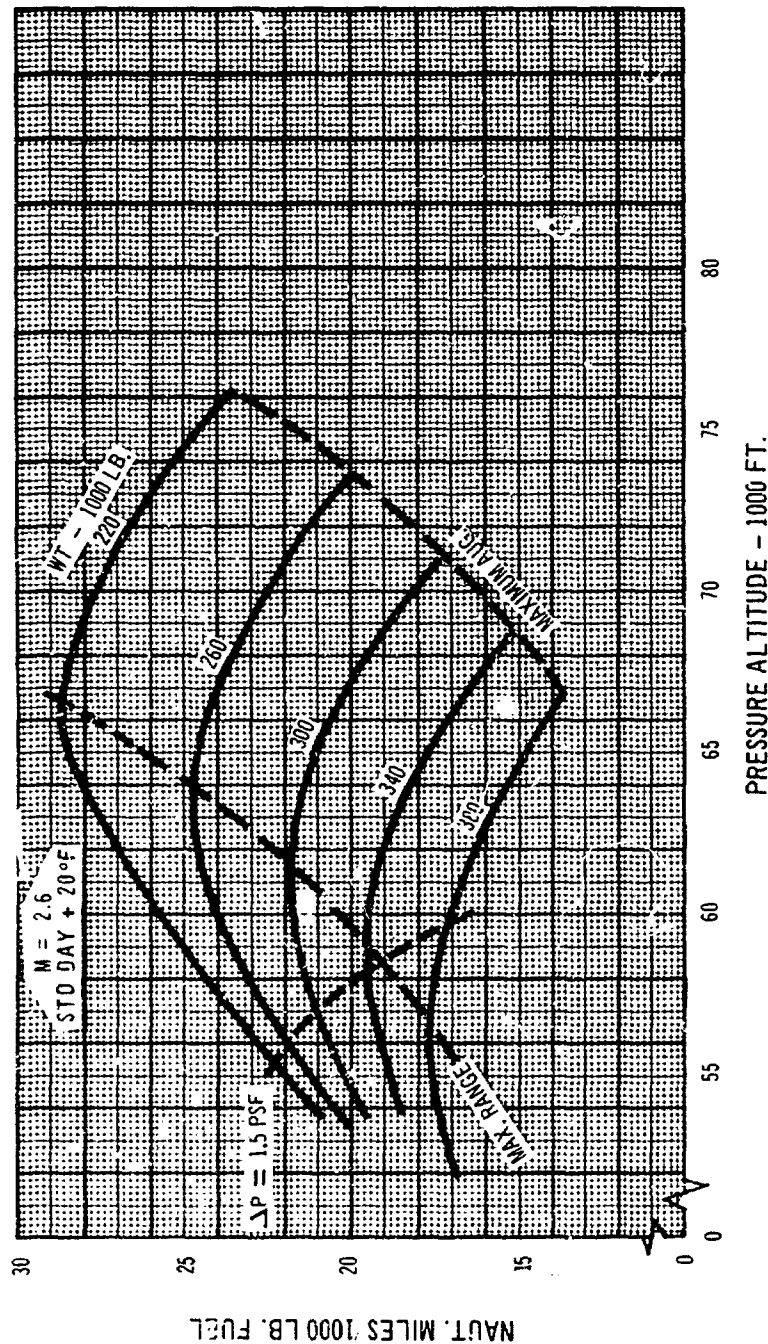
B.3.5.4 FUEL MILEAGE AT M = 2.7 (STANDARD DAY 20 DEGREES FAHRENHEIT)

Fig. B 3-36 shows the fuel mileage capability of the airplane on a standard minus 20-degrees Fahrenheit day

at the maximum cruise speed of $M = 2.7$ for the normal range of operating weights and altitudes. The altitude for maximum range is shown as well as the altitude at which the sonic boom overpressure is 1.5 psf in accordance with the RFP requirements.



B 3-34 Supersonic Cruise Fuel Mileage (Std. Day)



B-3-35 Supersonic Cruise Fuel Mileage (STD Day + 20°F.)

B.3.5.5 WING SWEEP SELECTION FOR SUBSONIC CRUISE

An outstanding feature of the variable sweep wing of the Model 733-197 is its high aerodynamic efficiency at subsonic Mach numbers. Fig. B-3-37 shows the aerodynamic cruise efficiency ($M L/D$) versus Mach number for wing sweep angles of 30 degrees, 42 degrees, and 50 de-

grees. Based on these data, a wing sweep angle of 42 degrees and a Mach number of 0.85 have been selected for best subsonic cruise. For Mach numbers below about 0.75 a wing sweep angle of 30 degrees is best. Cruise fuel mileage is therefore presented in the following sections for both wing sweep angles.

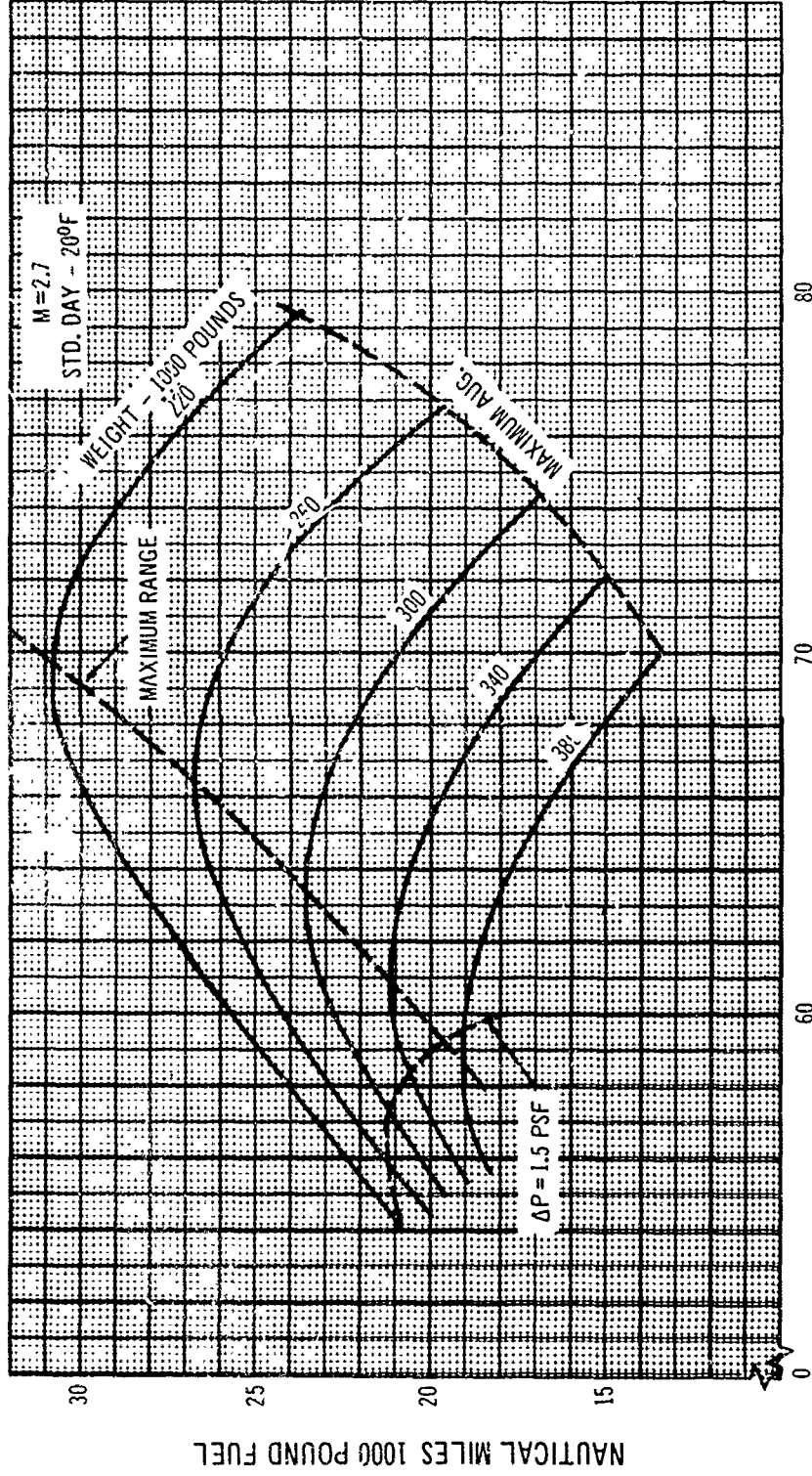
B.3.5.6 SUBSONIC CRUISE FUEL MILEAGE, WING SWEEP 30 DEGREES

Fig. B 3-38 shows the subsonic cruise fuel mileage capability of the airplane with the wings forward at a leading-edge sweep angle of 30 degrees. Data are presented at four altitudes over the normal range of operating weights on a standard day. The effect of nonstandard tempera-

tures on the fuel mileage is negligible.

B.3.5.7 SUBSONIC CRUISE FUEL MILEAGE, WING SWEEP 42 DEGREES

Figs. B 3-39 and B 3-40 show the subsonic cruise fuel mileage capability of the airplane with the wings swept forward at a leading-edge sweep angle of 42 degrees. Data



B 3-36 Supersonic Cruise Fuel Mileage (Std. Day - 20° F)

are presented at five altitudes over the normal range of operating weights on a standard day. The effect of nonstandard temperatures on the fuel mileage is negligible. These data are recommended for use in all normal subsonic cruise missions as the best compromise between speed and range capability.

B.3.5.8 SONIC BOOM OVERPRESSURE IN CRUISE

Fig. B 3-41 shows the sonic boom overpressure in cruise versus aircraft weight over the normal range of operating altitudes. The optimum cruise altitude line is shown and is limited above weights of 365,000 pounds by the RFP requirement of 1.5 psf maximum sonic boom overpressure in cruise.

B.3.6 Descent

B.3.6.1 DESCENT SCHEDULES

Fig. B 3-42 shows the normal and emergency descent schedules for all operating temperatures.

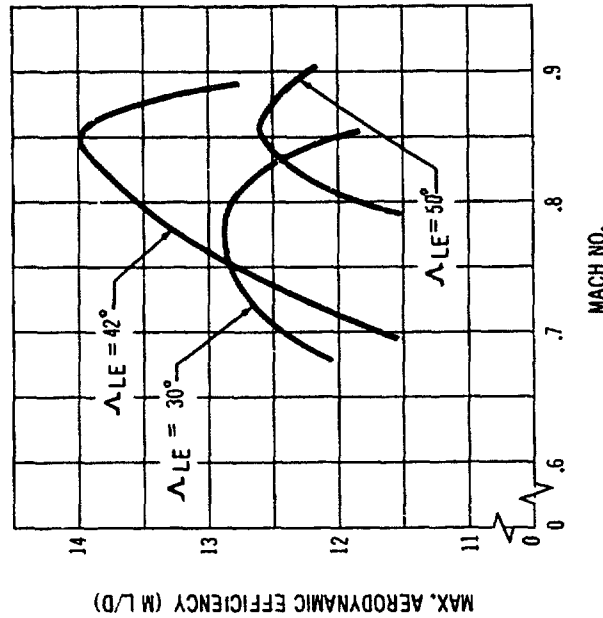
Two normal descents are shown, one which results in maximum range and the other in minimum time within the restriction of cabin pressure altitude not exceeding a rate of descent of 300 feet per minute. These descents use the same optimum wing sweep schedule as given for climb in Section B.3.2.2. The supersonic portion of the descent was chosen to approximate the maximum lift drag ratio vs. Mach number. The resulting maximum overpressure of 1.4 psf occurring at $M = 1.27$ is below the RFP requirement of 1.5 psf. The maximum overpressure could be lowered to 1.3 or 1.2 psf with a very small penalty in range.

The emergency descent schedule shown was selected to give minimum time to 30,000 feet and then to 14,000 feet within the structural placard limitations.

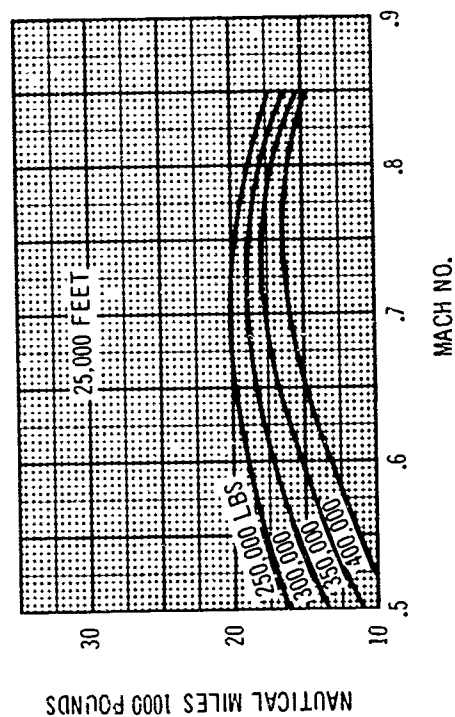
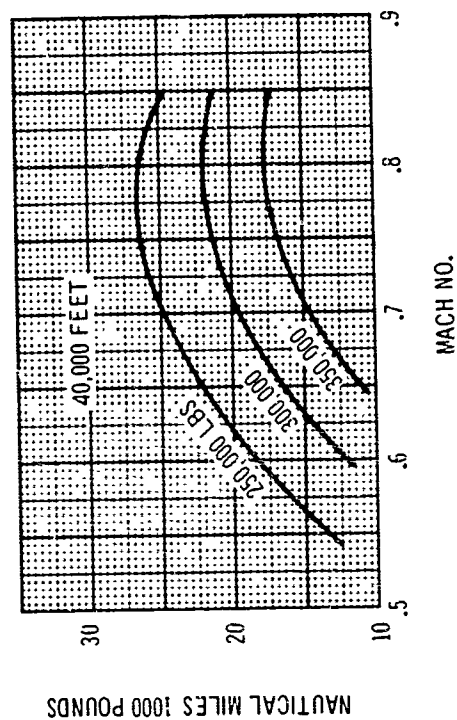
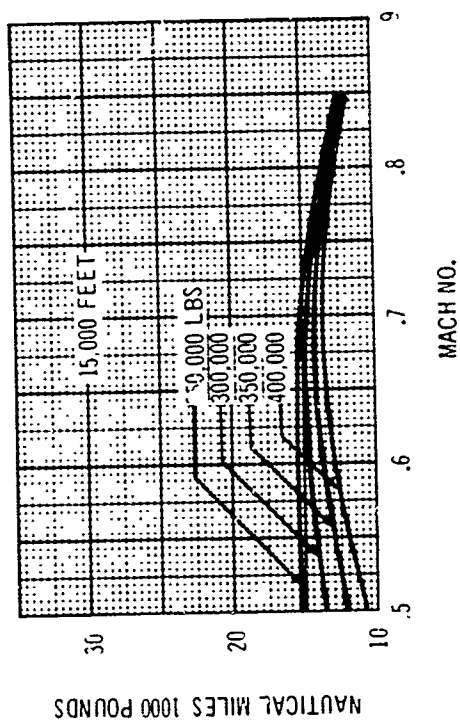
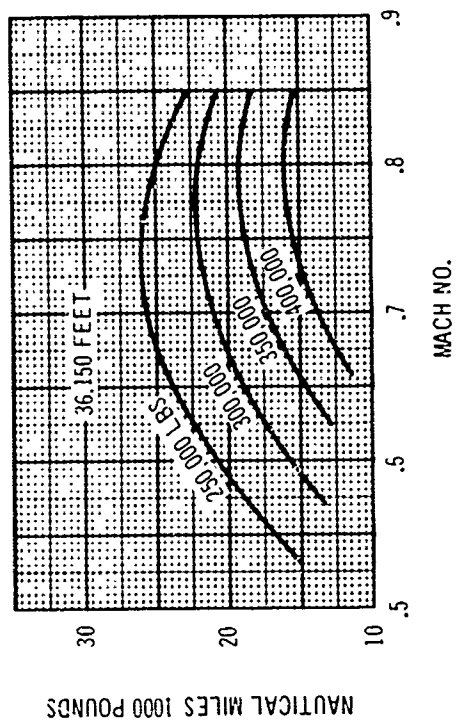
B.3.6.2 NORMAL DESCENT—MAXIMUM RANGE

Fig. B 3-43 shows time, fuel, and distance versus altitude for normal maximum range descents. The wing sweep schedule given in Section B.3.2.2 is used with the airplane in the clean configuration.

Fig. B 3-44 shows time, fuel, and distance versus altitude for normal minimum time descents. The wing sweep schedule given in Section B.3.2.2 is used with the airplane in the clean configuration. This schedule results in a cabin



B 3-37 Wing Sweep Selection for Subsonic Cruise



Subsonic Cruise Fuel Mileage—Standard Day ($\Lambda = 30^\circ$)

B 3.38

rate of descent just under 300 feet per minute regarded as maximum under normal conditions.

B.3.6.4 EMERGENCY DESCENT

Fig. B 3-45 shows time, fuel, and distance versus altitude for emergency descents. These data are based on the use of wing spoilers at 60 degrees during the descent to 14,000 feet pressure altitude and engines at flight idle. The wings are maintained full aft at 74-degrees sweep.

B.3.6.5 SONIC BOOM OVERPRESSURES IN DESCENT

Fig. B 3-46 shows the maximum sonic boom overpressures occurring in both normal and emergency descents over the operating weight range of the airplane.

B.3.7 Holding

B.3.7.1 SUBSONIC HOLDING FUEL FLOW

Fig. B 3-47 shows the subsonic holding fuel flow for three altitudes over the range of normal operating weights. The wing leading-edge sweep is 30 degrees. The present CAR holding speed limits are shown and indicate the compatibility of this airplane with present holding procedures.

B.3.8 Landing

B.3.8.1 CAR LANDING FIELD LENGTH

Fig. B 3-48 shows the CAR landing field length capability of the Model 733-197 for the normal range of operating weights and altitudes. These data are based upon approach speeds 30 percent greater than 1-g stalling speeds and a runway braking coefficient of 0.35.

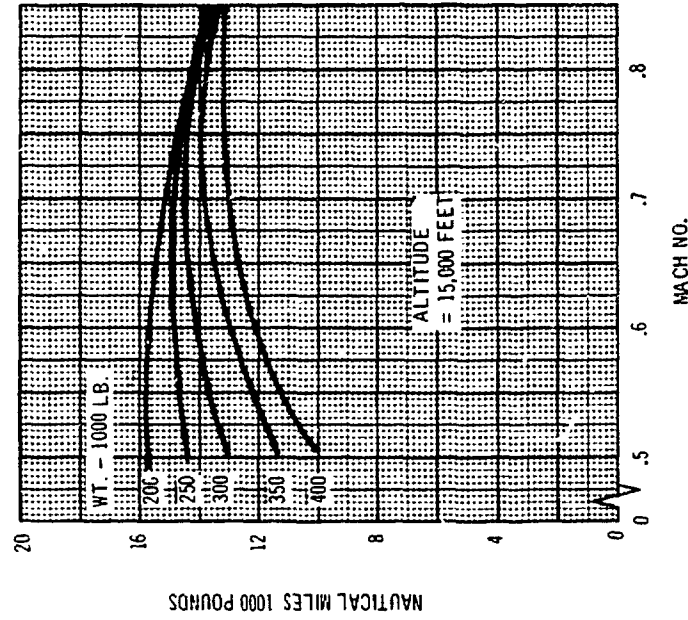
B.3.8.2 CAR LANDING SPEEDS

Fig. B 3-49 shows the CAR landing approach speeds for the Model 733-197 for the normal range of operating weights. These data are based upon a 30 percent margin

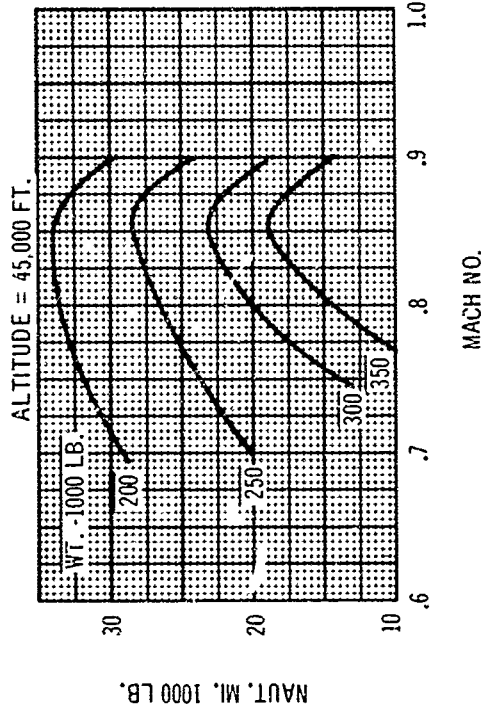
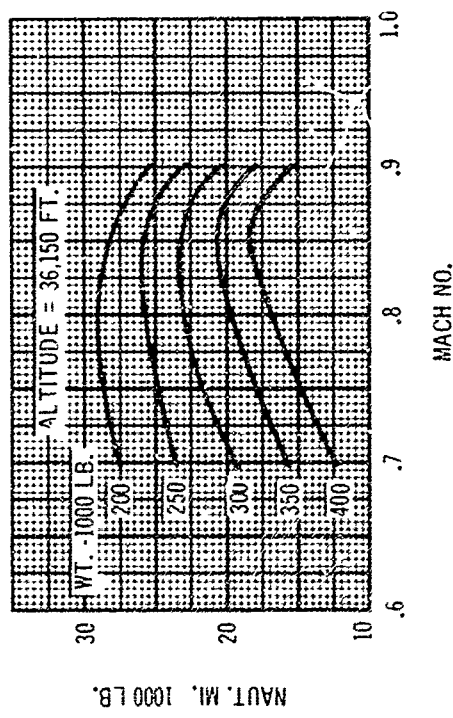
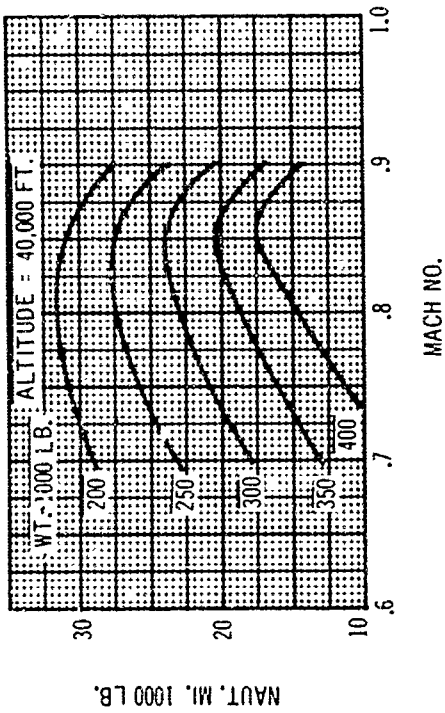
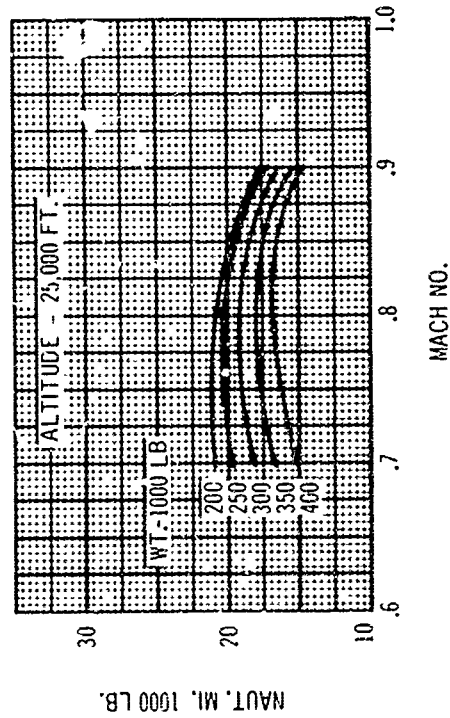
over 1-g stalling speeds.

B.3.8.3 EFFECT OF RUNWAY BRAKING FRICTION

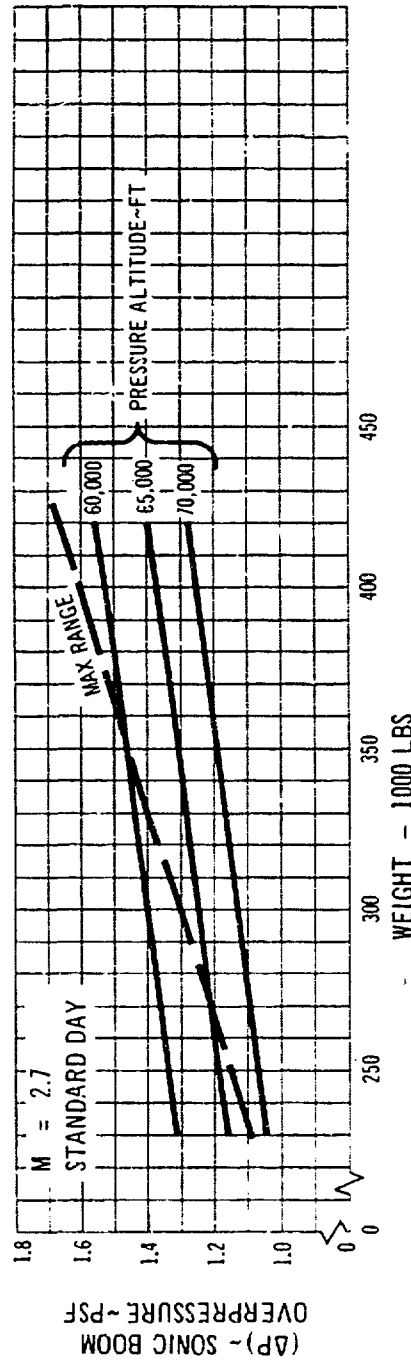
A normal braking friction coefficient of $\mu = 0.35$ is obtainable on dry runway surfaces through the use of individual antiskid devices on each wheel. The effect of



B 3-39 Subsonic Cruise Fuel Mileage Standard Day $\Lambda = 42^\circ$



B 3-40 Subsonic Cruise Fuel Mileage Standard Day $\Lambda = 42^\circ$



B 3-41. Sonic Boom Overpressures in Cruise

variations in friction coefficient on the CAR landing field length is shown in Fig. B.3-50 for a landing weight of 250,000 pounds. Field length increases from 6000 feet at $\mu_{0.35}$ to 7660 feet at $\mu_{0.2}$; this latter value is appropriate for either wet runway or dry ice conditions.

Field length required increases sharply for $\mu_{0.1}$ less than 0.2, but the use of reverse thrust reduces these values materially. (Reverse thrust effects have also been shown in Sections A3.8.2 and 3.8.2).

B.3.8.4 EFFECT OF ALL BRAKING DEVICES

The separate effects on landing field length of wing lift spoilers and reverse engine thrust are shown in Fig. B.3-51 for a range of landing weights. The braking coefficient for this study was the standard dry runway value of 0.35.

B.3.8.5 THRUST FOR LEVEL FLIGHT, APPROACH SPEED STABILITY

Thrust required for level flight in the landing configura-

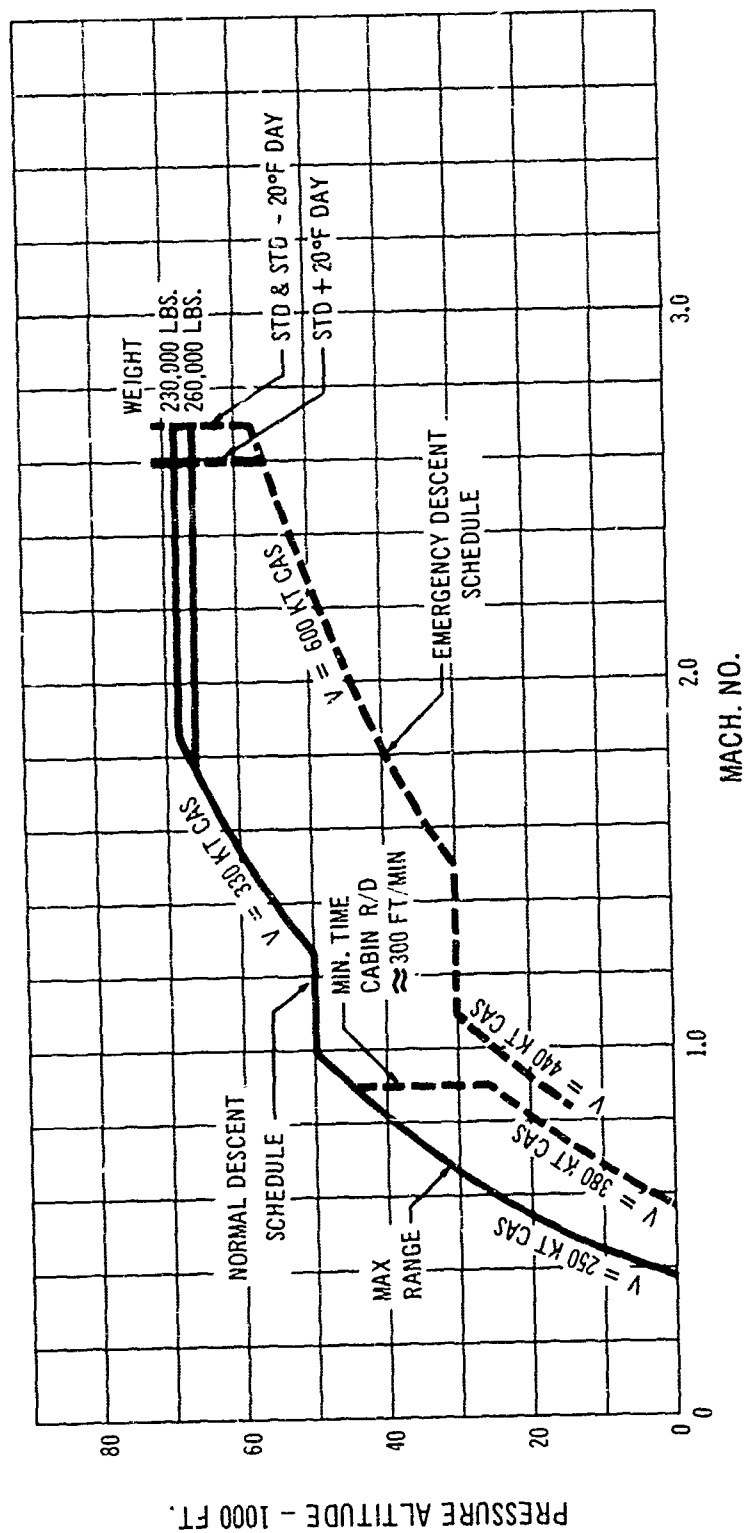
tion, with gear down, is shown versus airspeed for maximum design landing weight and for the design mission landing weight in Fig. B.3-52.

Recommended approach speeds, at $1.3 V_{S_{04}}$ are plotted on the curves and are above the minimum drag speeds. A criterion for minimum acceptable approach speed stability used by NASA in the SCAT studies, (d/dV) (thrust required/weight) = .0012 per knot, is also located on the curves. The Model 733-197 airplane has positive inherent speed stability during approaches.

Climb gradient capability for three engines at maximum dry power is extremely good, 0.187 being available at approach speed at 260,000 pounds weight compared to the minimum required gradient of 0.027.

B.3.8.6 LANDING FIELD LENGTH WITH WINGS SWEEP 74 DEGREES

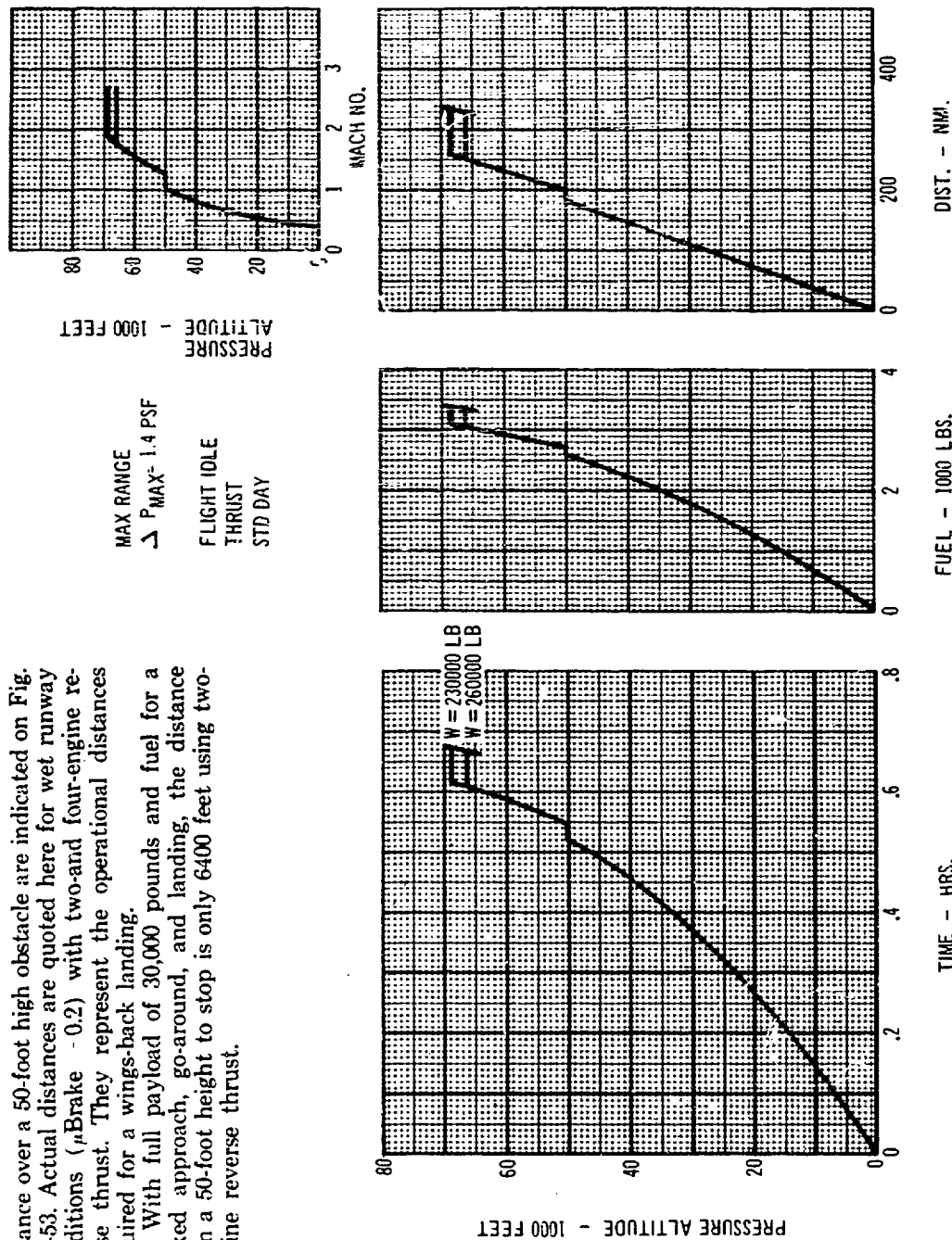
Stopping distances (from touchdown) and total landing



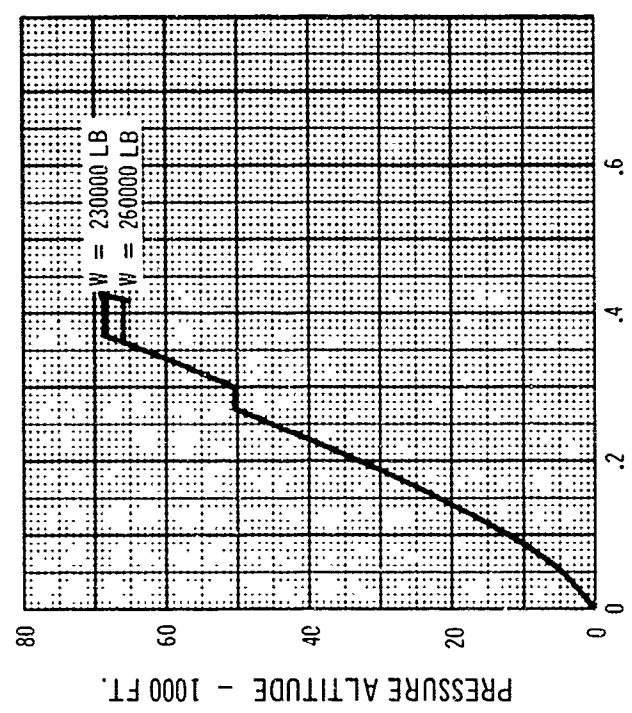
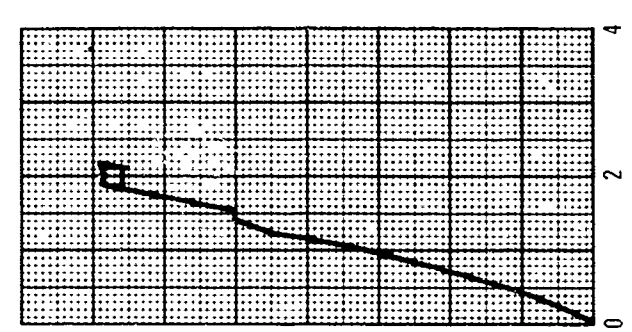
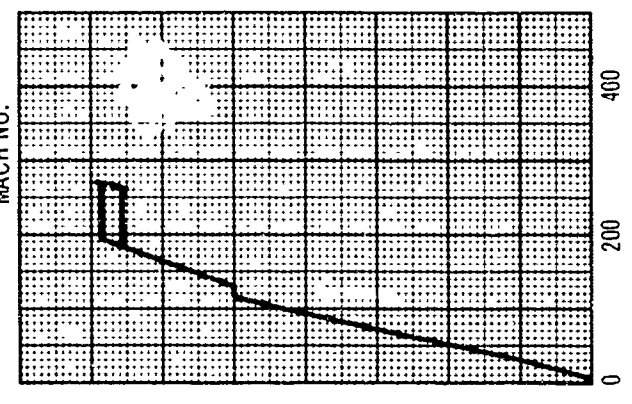
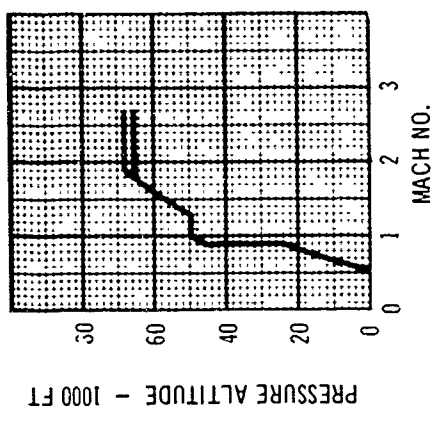
B 3-42 Descent Schedules

distance over a 50-foot high obstacle are indicated on Fig. B 3-53. Actual distances are quoted here for wet runway conditions (μ Brake = 0.2) with two- and four-engine reverse thrust. They represent the operational distances required for a wings-back landing.

With full payload of 30,000 pounds and fuel for a balked approach, go-around, and landing, the distance from a 50-foot height to stop is only 6400 feet using two-engine reverse thrust.



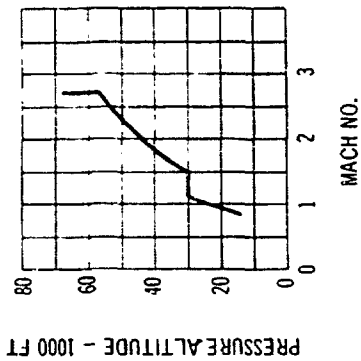
B 3-43 Normal Descent - Max. Range



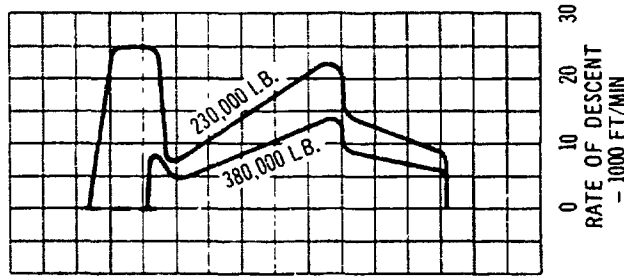
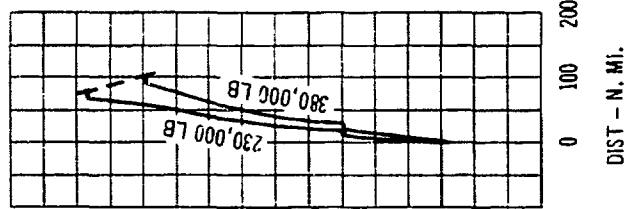
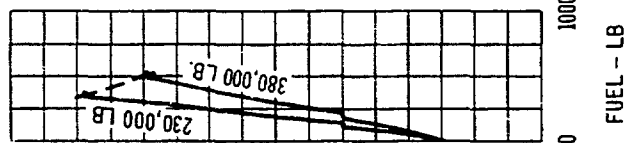
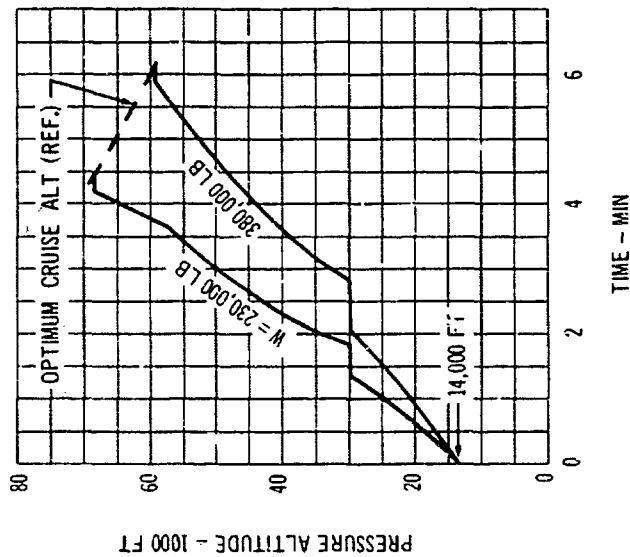
MINIMUM TIME
 MAX ΔP = 1.4 PSF
 FLIGHT IDLE THRUST
 CABIN RATE
 OF DESCENT
 = 300 FT MIN
 STD. DAY

W = 230000 LB
 W = 260000 LB

B 3-44 Normal Descent - Minimum Time



SPOILERS 60°
 FLAPS UP
 GEAR UP
 A = 74°
 FLIGHT IDLE THRUST
 STD DAY



B 3-45 Emergency Descent (to 14,000 Feet Altitude)

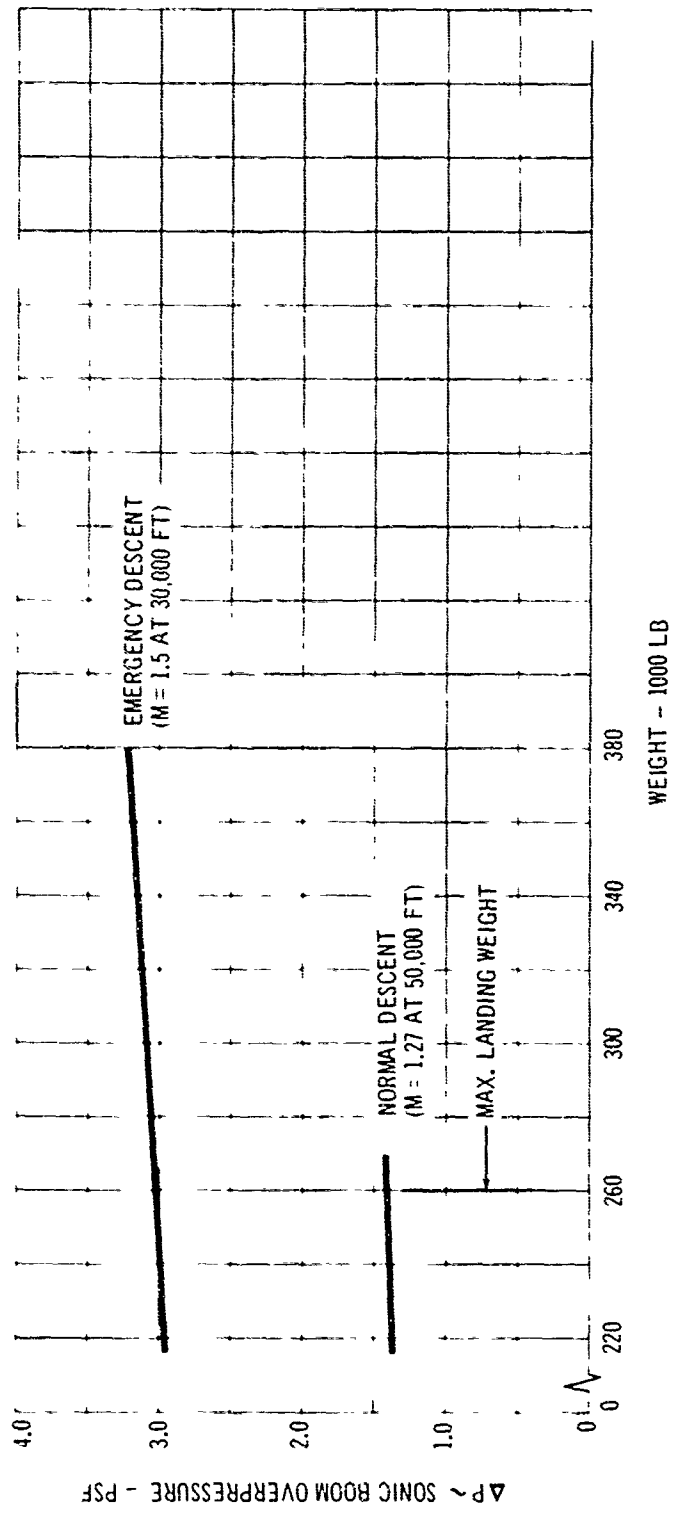
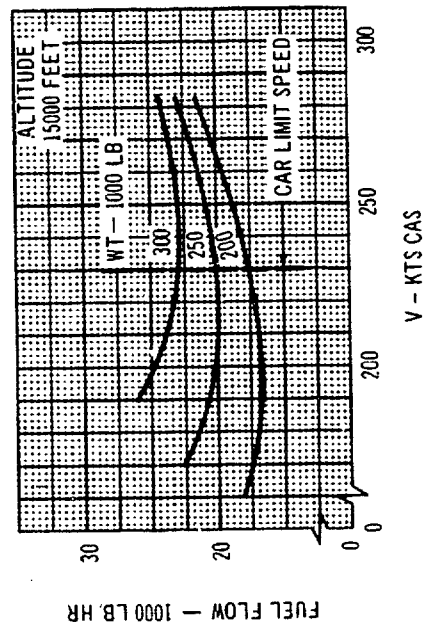
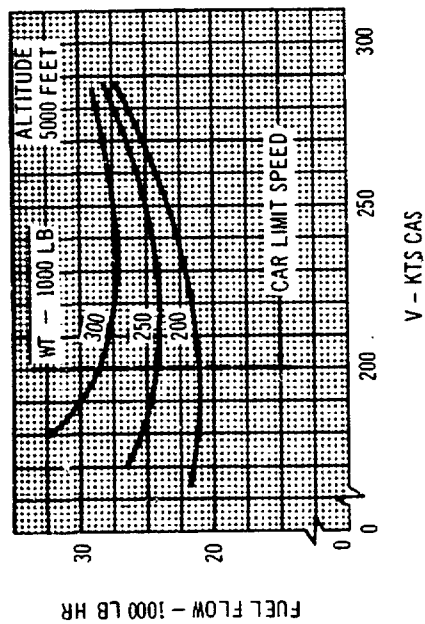
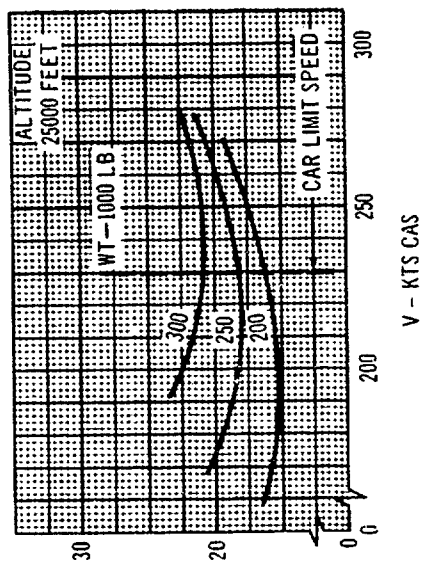


Fig. A4.6-5 (A-V)

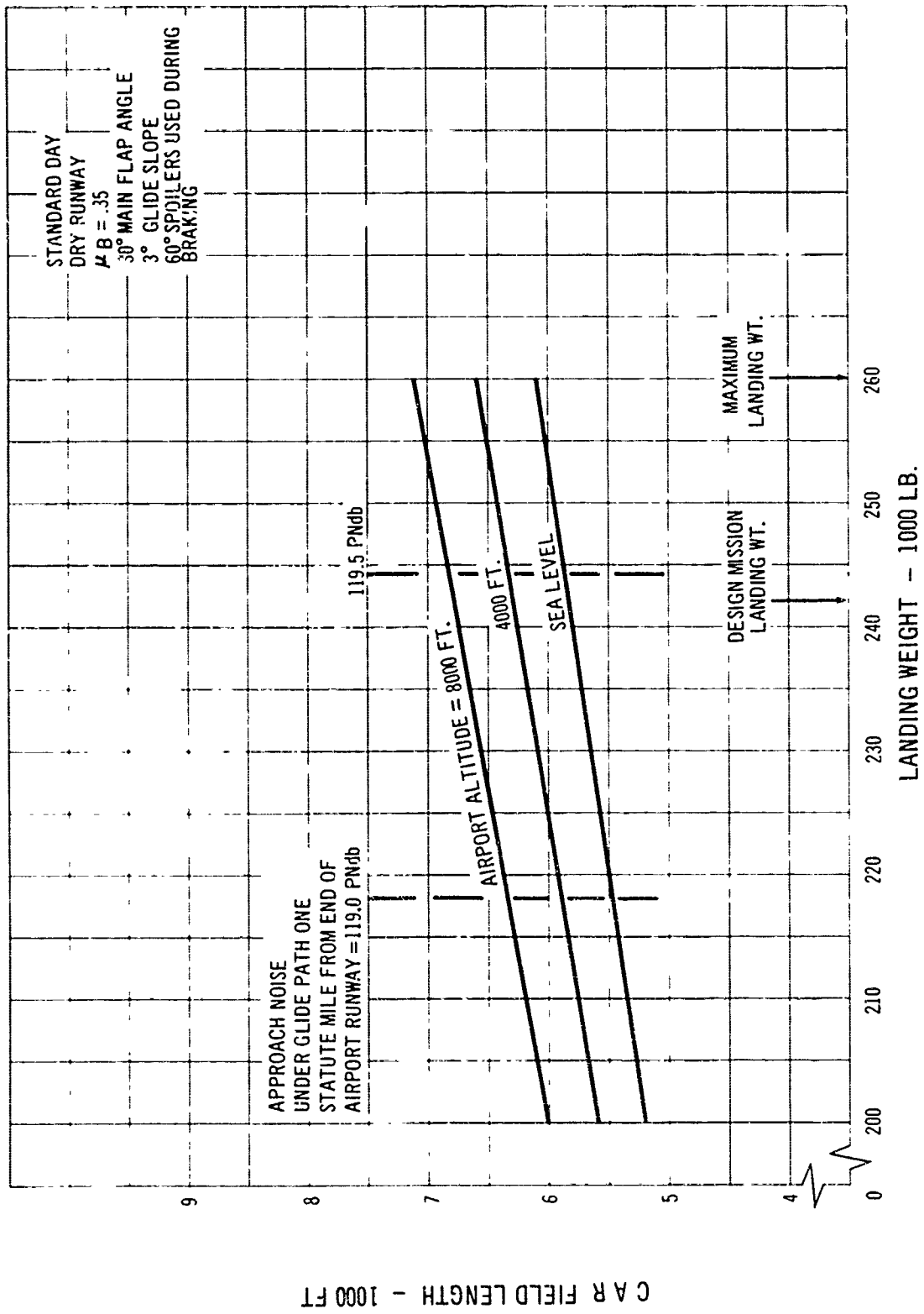
B-3-46 Maximum Sonic Boom Overpressure in Descent



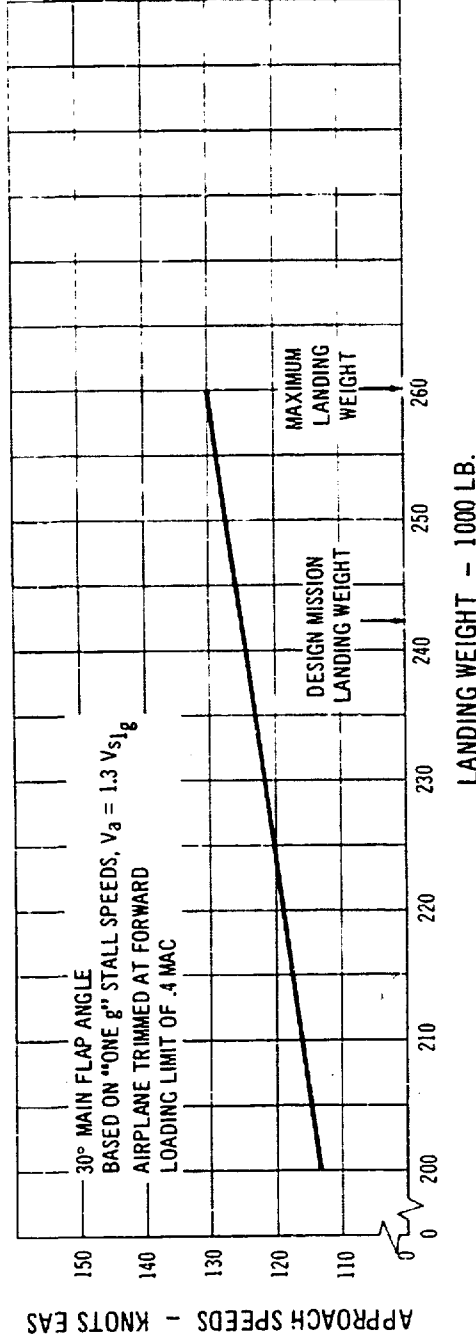
FUEL FLOW - 1000 LB HR



E 3-47 Subsonic Holding Fuel Flow Standard Day $\gamma_{LE} = 30^\circ$



B 3-48 Landing Distance



B 3-49 Landing Speeds

The landing approach speed is 180 knots EAS with a body angle of attack of 10 degrees, which was chosen to give good visibility from the flight deck. The approach speed is at 1.41 times minimum usable flight speed.

B.3.8.7 THRUST REQUIRED AND APPROACH SPEED STABILITY WITH WINGS SWEPT 74 DEGREES

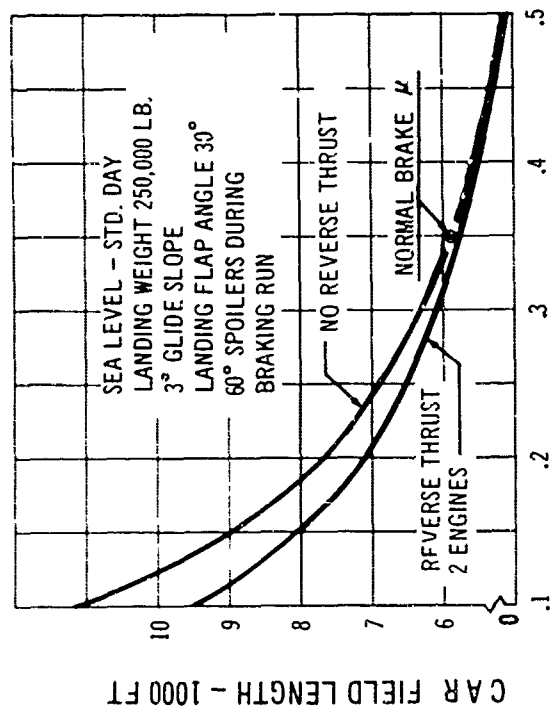
Thrust required for level flight with landing flap, gear down, is shown in Fig. B 3-54. Airplane speed stability is good, the recommended approach speed is 20 knots above that for acceptable speed stability (where (dV/dV) (thrust required weight) = .0012 per knot). Climb capability, on three engines at maximum dry thrust is excellent. A gradient of .128 is achieved in the landing configuration.

B.3.8.8 LANDING NOISE—LATERAL SPREAD

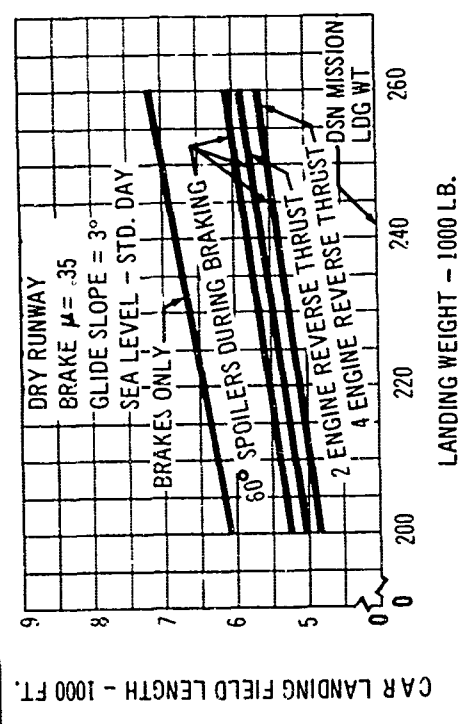
Fig. B 3-55 shows the engine generated noise levels under the airplane glide path for an approach at 250,000 pounds weight. (Design mission landing weight is 242,215 pounds, giving slightly lower noise levels.) The high airplane lift drag ratio makes possible a perceived noise level of less than 120 PNdB.

B.3.8.9 APPROACH AND LANDING FUEL ALLOWANCE

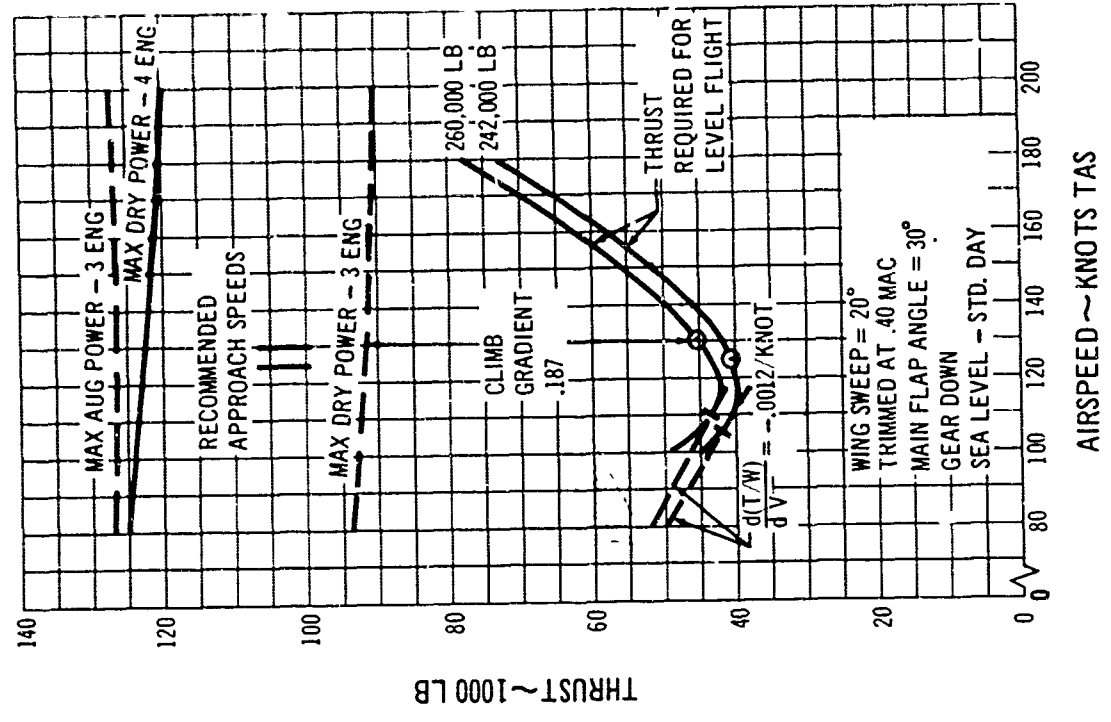
Fig. B 3-56 shows the approach and landing fuel allowance used in the basic design mission calculations. It consists of six minutes holding time at sea level at a speed of 200 knots CAS and amounts to 2300 pounds fuel at the design mission landing weight.



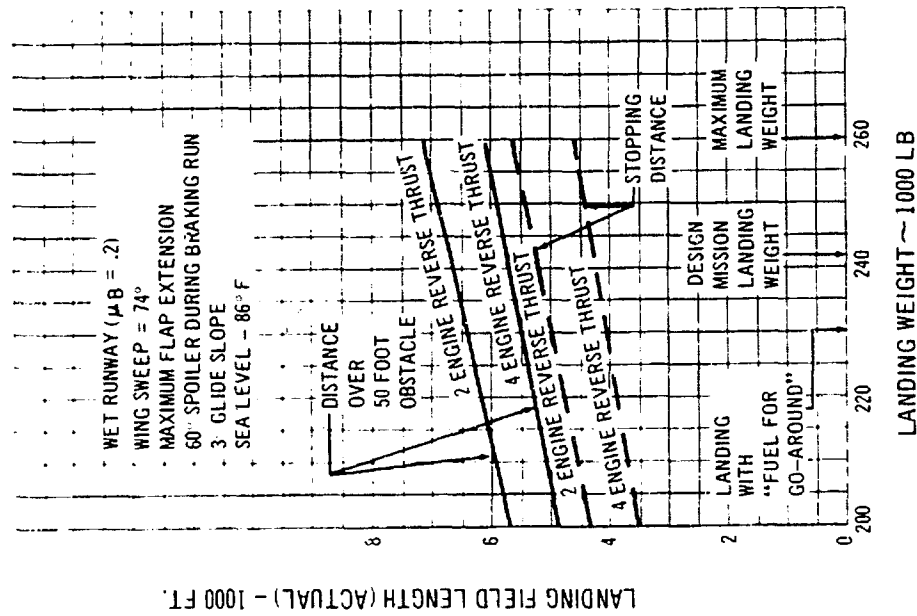
B 3-50 Effect of Runway Braking Friction



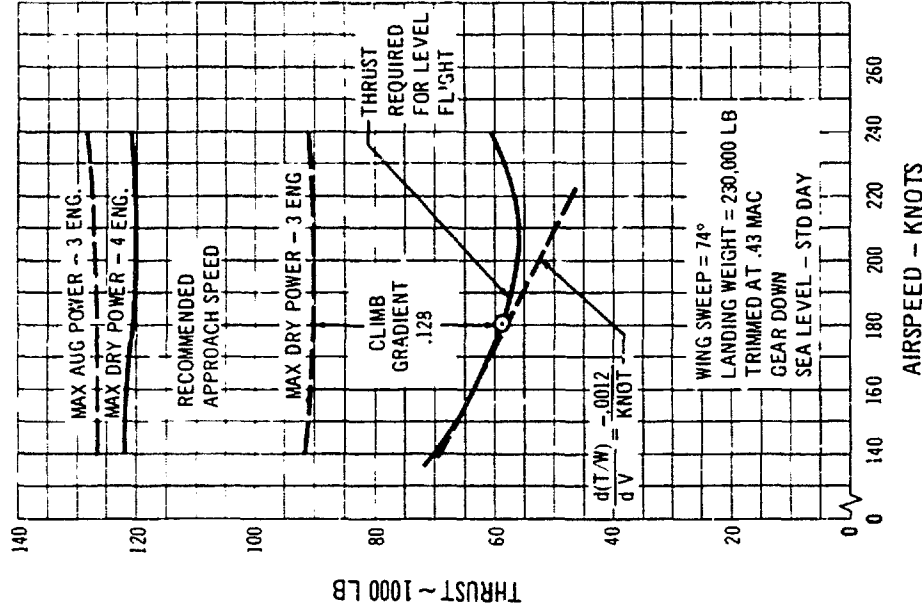
B 3-51 Effect of All Braking Devices on Landing Distance



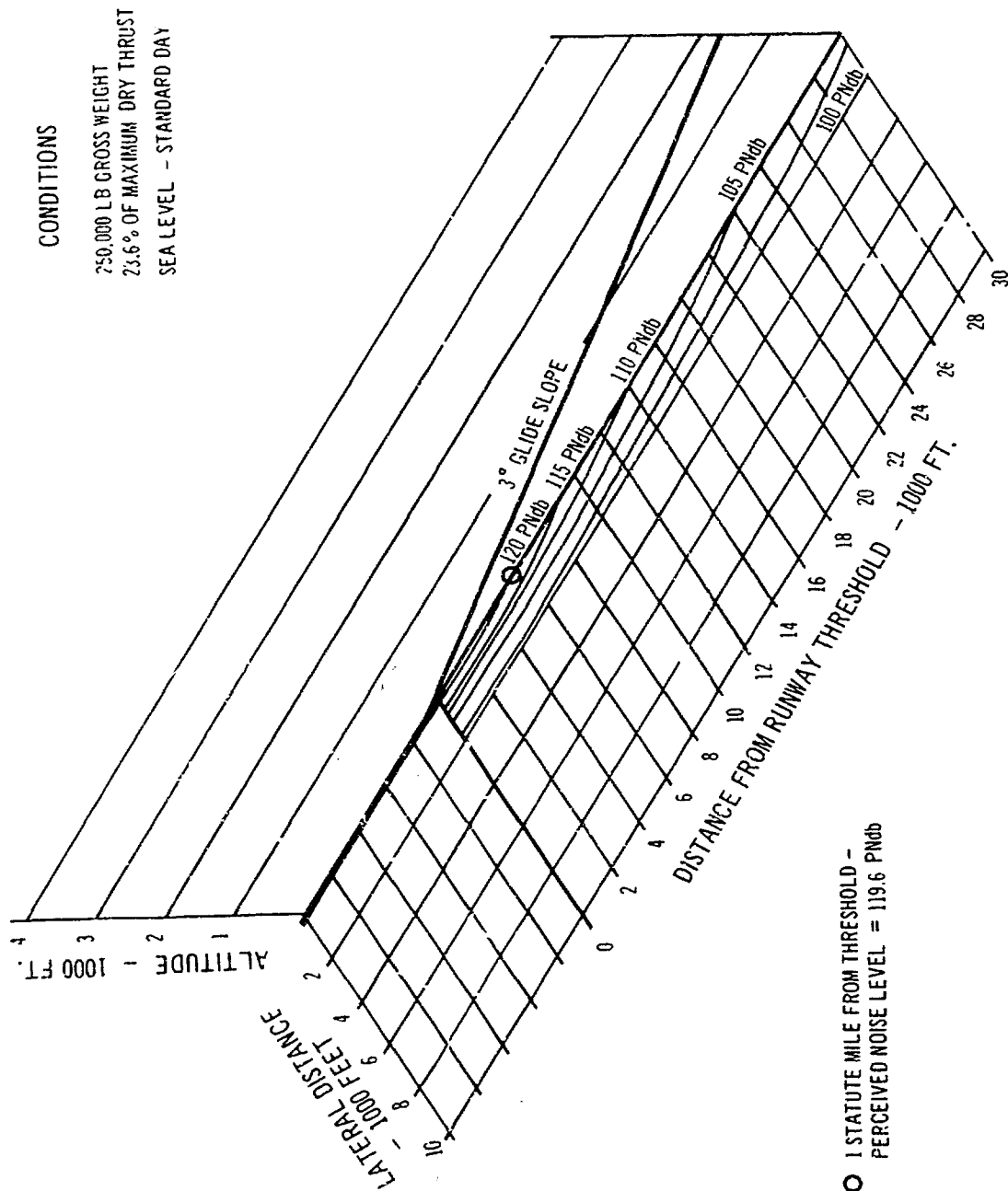
B 3-52 Approach Speed Stability



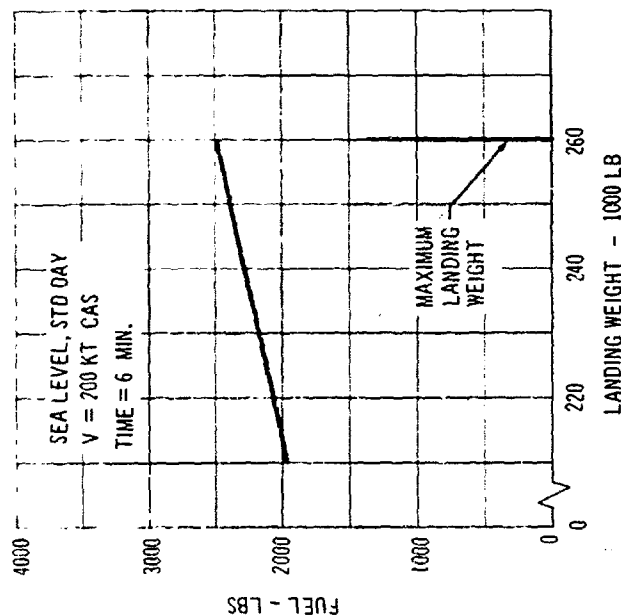
B 3-53 Wet Runway Landing Field Length, Wings Aft



B 3-54 Approach Speed Stability, Wings Aft Landing



B 3-55 Noise Profile for Landing Approach



B 3-56 Approach and Landing Fuel Allowance

B.3.9 Performance Calculation Methods

B.3.9.1 MISSION CALCULATIONS

The methods used in calculating the basic missions presented in this report are presented in the following steps.

B.3.9.1.1 Takeoff Fuel Allowance

The takeoff fuel allowance consists of ten minutes at taxi thrust, plus the fuel required for the actual takeoff.

$$\text{Taxi fuel} = W(\mu_r) \text{ SFC } (\Delta t)$$

Where $\mu_r = .025$ is the rolling friction coefficient of the airplane and $\Delta t = .167$ hours (10 minutes).

The takeoff computation gives the total time for

takeoff to the end of the second segment climb segment.

Takeoff fuel is then:

$$\text{Takeoff fuel} = T(\text{SFC}) (\Delta t_{ro})$$

where T and SFC correspond to the takeoff power setting.

B.3.9.1.2 Climb and Acceleration Time, Fuel and Distance

The flight path for climb and acceleration is defined in terms of a Mach number-altitude schedule. The power setting schedule is predetermined as a function of Mach number.

Climb begins at the end of the second segment climb-out portion of the takeoff calculation.

Climb time, distance, and fuel are computed in discrete Mach number steps along the schedule. The climb continues until cruise Mach number is reached, after which the climb proceeds at constant Mach number in discrete altitude steps until cruise altitude is reached.

The equations used are:

$$\text{TIME} = \Delta t = \left(\frac{\bar{W}}{T \cdot D} \right) \left(\frac{\Delta V}{g} + \frac{\Delta h}{V + \frac{\Delta V}{2}} \right)$$

$$\text{FUEL} = -\Delta W = \bar{T} (\text{SFC}) (\Delta t)$$

$$\text{DIST.} = \Delta R = \left(V + \frac{\Delta V}{2} \right) \Delta t$$

A bar indicates the average of a quantity during the step. The average is obtained by iteration.

B.3.9.1.3 Cruise Time, Fuel and Distance

Cruise range is calculated in increments using the Breguet range formula:

$$\Delta \text{RANGE} = \frac{L}{D} \left(\frac{V}{\text{SFC}} \right) \ln \left(\frac{W_i}{W_f} \right)$$

An energy correction is applied when climbing cruise is calculated. Cruise time is given by:

$$\Delta \text{TIME} = \frac{\Delta \text{Range}}{V}$$

Cruise Mach number is constant, thus V is constant throughout cruise. Skin friction drag is increased as altitude is increased.

Gross weight at start of cruise is equal to the gross weight at end of climb. Gross weight at end of cruise is determined by computing the mission in reverse to the end of cruise (start of descent). Cruise fuel is the difference between gross weight at the start and end of cruise.

B.3.9.1.4 Descent and Deceleration Time, Fuel and Distance

The descent and deceleration is defined in terms of a Mach number-altitude schedule. The engines are normally set at idle thrust.

This segment is generally computed in reverse, beginning with the start of landing and ending at cruise altitude and Mach number.

The computation is made in discrete Mach number steps along the schedule.

The equations used are:

$$\text{TIME } \Delta t = \left(\frac{\bar{W}}{T-D} \right) \left(\frac{\Delta V}{g} + \frac{\Delta h}{V + \frac{\Delta V}{2}} \right)$$

$$\text{FUEL } \Delta W = \bar{T} (\overline{\text{SFC}}) (\Delta t)$$

$$\text{DIST. } \Delta R = \left(V + \frac{\Delta V}{2} \right) \Delta t$$

B.3.1.9.5 Approach and Landing Fuel Allowance

The approach and landing fuel allowance consists of 6 minutes' holding at sea level at 200 knots at the landing weight.

$$\text{FUEL} = \bar{T} (\overline{\text{SFC}}) \Delta t$$

Where Δt .10 hours (6 minutes)

And T Thrust Drag

B.3.9.1.6 Reserve Fuel

HOLDING RESERVE

Holding is calculated in one step using average quantities obtained by iteration. The holding altitude is 15,000 feet. The Mach number is selected which results in minimum holding fuel providing it does not exceed the CAR requirement of 230 knots CAS. The gross weight at the end of the hold is equal to the payload plus OWE.

$$\text{FUEL } \bar{T} (\overline{\text{SFC}}) \Delta t \quad W_{\text{hold}}$$

Where Δt 0.5 hr.

And T Thrust Drag

ALTERNATE CRUISE RESERVE

Alternate cruise is computed in one step using average quantities obtained by iteration. Altitude and Mach number are chosen such that alternate cruise fuel is minimized. Alternate cruise range is 300 statute miles. Gross weight at the end of alternate cruise is:

$$\text{Owe} + \text{payload} + W_{\text{hold}}$$

$$\text{FUEL } \bar{T} (\overline{\text{SFC}}) \Delta t \quad W_{\text{alt}}$$

$$\text{Where } \Delta t = \frac{\Delta \text{Range}}{V}$$

And T Thrust Drag

MISSION RESERVE

The mission reserve fuel, $W_{\text{M.R.}}$ is equal to seven percent of the fuel burned from take-off through landing.

$$\text{FUEL} = \frac{.07}{1.07} \left[(\text{RAMP G.W.} + \text{TAXI FUEL}) - \right.$$

$$\left. \left(\text{OWE} + \text{payload} + W_{\text{hold}} + W_{\text{ALT}} \right) \right] \quad W_{\text{M.R.}}$$

B.3.9.2 TAKEOFF AND LANDING DISTANCES

Takeoff and landing field lengths were calculated by the Flight Manual Performance methods used for certification of present Boeing jet transports (Ref. 13). The following time delays and reverse thrust decay factors were used for the refused takeoff and landing distance calculations.

	TIME DELAY (SEC)	THRUST
Takeoff		
Engine failure recognition to brakes on.	.4	98%
Brakes on to throttles back.	1.4	90%
Throttles back to spoilers up.	2.0	50%
Landing		
Touchdown to brakes on, and spoilers up.	2.0	Idle
Brakes on to reverse thrust (when used).	6.0	20% max. dry
Reverse thrust to 50 knots.	...	40% max. dry
Reverse thrust at end of ground roll.		17% max. dry

For takeoff noise considerations, the airplane height one statute mile from the end of a 10,500 foot runway was calculated by a step by step integration along the flight path using the relations:

$$s = \int \left(\frac{v}{a_t} \right) dv$$

$$\gamma = \int \left(\frac{a_n}{v} \right) dt$$

$$h = \int (v \sin \gamma) dt$$

Where:

s == horizontal distance
v == airplane velocity
a_t == acceleration along the flight path
a_n == acceleration normal to the flight path
t == time
γ == flight path angle
h == height above runway

Accelerations were determined from the force equations:

$$a_n = \frac{g}{W} (L - W \cos \gamma F_L \sin \alpha)$$

$$a_t = \frac{g}{W} (F_L \cos \alpha - W \sin \gamma)$$

Where:

g = acceleration due to gravity
W = airplane gross weight
L = airplane lift
F_L = airplane thrust
α = angle between thrust line and airplane flight path

The flight path was considered to begin at a height of 35 feet above the takeoff surface at the end of the takeoff distance as determined by the Flight Manual Performance method above. Airspeed was allowed to increase from the takeoff safety speed, V₀, to the steady state climb speed.

For landing noise calculations, the airplane height was determined one statute mile from the end of the runway using a 3 degree glide slope. Approach power is the power for steady state glide with the appropriate landing flap configuration.

APPENDIX C

APPENDIX TO SECTION 6 PERFORMANCE SUBSTANTIATION TABLE OF CONTENTS

C6.1	Cruise Configuration	C/1
C6.1.1	Skin Friction Drag	C/1
C6.1.2	Pressure Drag	C/1
C6.1.2.1	Thickness Wave Drag	C/1
C6.1.2.2	Camber Drag	C 5
C6.1.2.3	Additional Propulsion Drag	C/9
C6.1.3	Nacelle Interference Effects	C 10
C6.1.4	Drag Due to Lift	C 12
C6.1.5	Trim Drag	C 20
C6.2	Takeoff and Landing Configuration	C 23
C6.2.1	Configuration Description	C 23
C6.2.2	Takeoff and Landing Speeds and Attitudes	C 30
C6.2.3	Stalling Characteristics	C 36
C6.2.4	Wind Tunnel Test Data	C 38
C6.2.5	Corrections Applied to Wind Tunnel Results	C 39
C6.2.6	Comparisons with Flight Test Data	C 40
C6.3	Sonic Boom	C 42
C6.3.1	Methods and Comparisons with Experiment	C 42
C6.3.2	Sonic Boom Properties of the Model 733-197	C 45

C6.0 PERFORMANCE SUBSTANTIATION

C6.1 Cruise Configuration

C6.1.1 SKIN FRICTION DRAG

The method of calculating skin friction coefficients C_f is described in Reference 14. It is based on the intermediate enthalpy concept as developed by Eckert, Sommer and Short, and Monaghan. The starting point is the empirical formula known as the Karman-Schoenherr equation. Compressibility including variation of specific heats with temperature, is allowed for by evaluating the fluid properties at a reference enthalpy. The reference enthalpy is a function of the free stream temperature and the skin temperature of the airplane. It is also dependent on the Prandtl number of the flow and the specific heats. The method takes into account the variation of these with temperature. This method yields results which are in close agreement with the correlated NASA skin friction data of Reference 15.

Turbulent skin friction coefficient levels are shown in Fig. C6-1 and substantiation of these levels with experiment in Fig. C6-2 and C6-3.

All model skin friction data have been assumed extrapolated to fully turbulent flow conditions with no allowance for any laminar flow.

The effects on skin drag of small external protuberances and general manufacturing roughness is difficult to estimate using small scale models. It is therefore necessary to estimate this drag separately. The procedure adopted at Boeing is similar in philosophy to that described and substantiated in Ref. 19. A detailed investigation was made of the approximate number, type, and size of manufacturing excrescences on the airplane skin. Fig. C6-4 indicates the allowable tolerances for typical gaps, surface waves and other manufacturing protuberances. Drag increments at several Mach numbers were associated with the protuberances, using published NASA test data for similar shapes (Refs. 20, 21, 22).

These basic test data are for experiments where h/δ (h roughness height, δ boundary layer height) is much larger than the comparable numbers on the airplane. It follows that the airplane associated drag should really be smaller than that calculated by this method. No attempts have been made to allow for this.

Figs. C6-5a, b, and c show substantiating plots for the drag increments associated with various roughness elements. Fig. C6-6 shows the increment of drag for skin roughness, other miscellaneous items, and contingencies as a function of Mach number. The computed drag increment at cruise Mach number was 0.00013 but as shown in the figure this was increased to 0.0004 to allow for contingencies and errors of estimation.

C6.1.2 PRESSURE DRAG

Pressure drag is defined as the difference between the minimum drag coefficient of the airplane $C_{D_{min}}$ and the skin friction drag C_{D_f} . Pressure drag is discussed under the following headings:

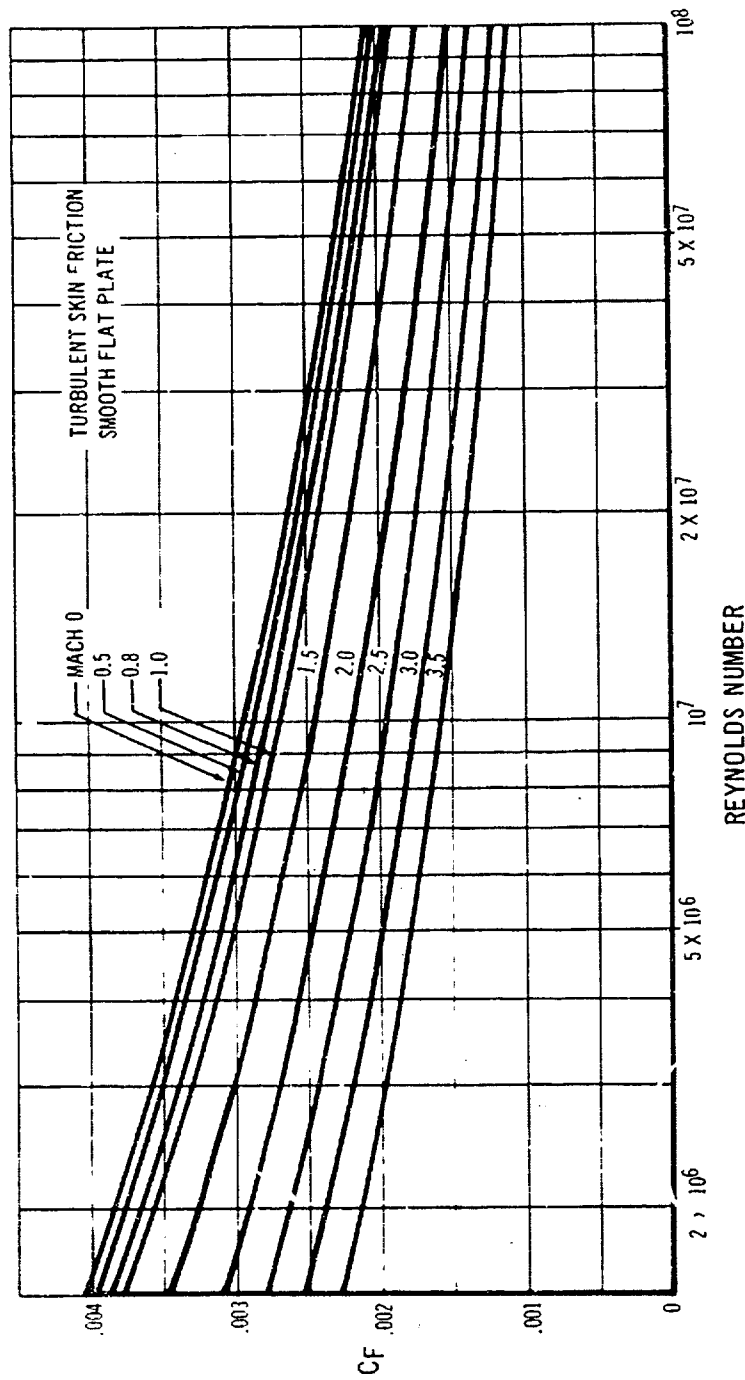
C6.1.2.1 THICKNESS WAVE DRAG

C6.1.2.2 CAMBER DRAG

C6.1.2.3 ADDITIONAL PROPULSION DRAG

C6.1.2.1 THICKNESS WAVE DRAG

Isolation of the thickness wave drag from the rest of the pressure drag serves a dual purpose. It allows corrections to be applied to the model data, such as body closure corrections, or corrections due to minor differences between the airplane and the wind tunnel models. It also allows for comparisons between experiment and analytical methods, and hence leads to better means of designing and optimizing the airframe. In order to make such comparisons meaningful it is necessary to distinguish drag components that are not amenable to theoretical analysis. The drag associated with the canopy is considered to be in this category and therefore the wave drag is analyzed for an airplane defined with an ogive forebody. An allowance



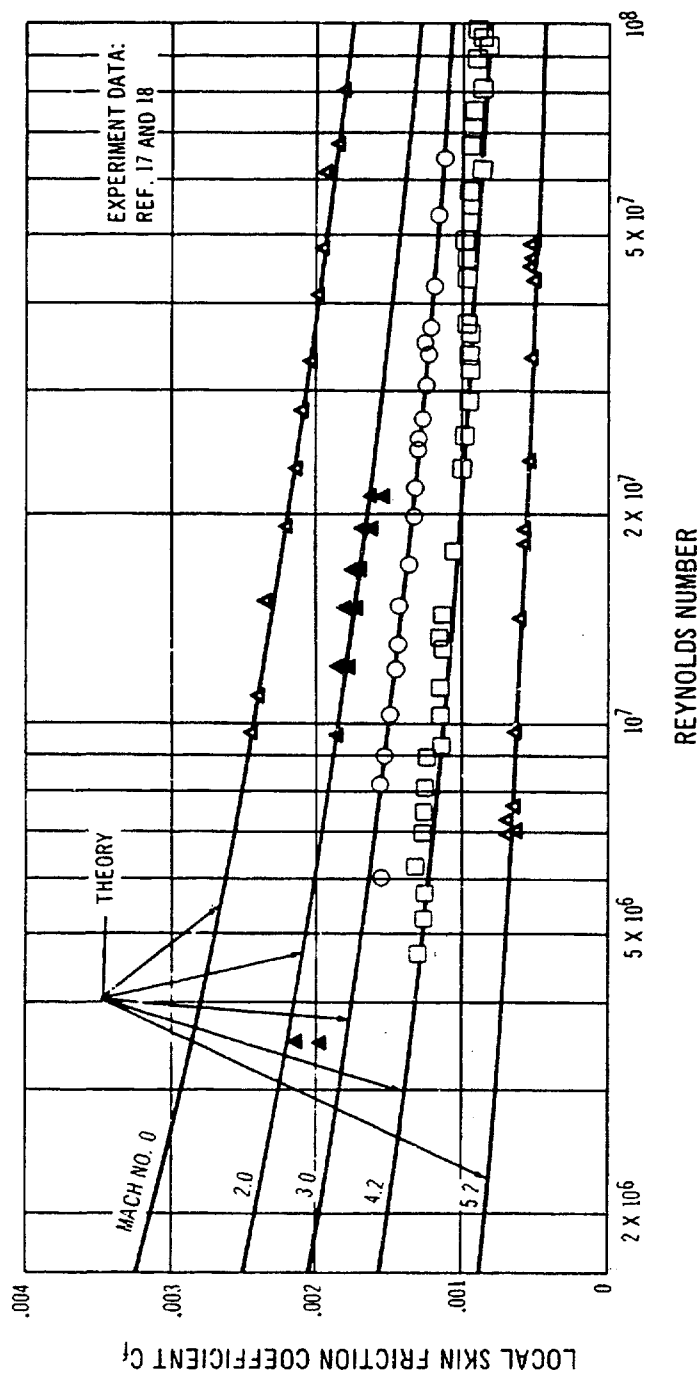
C 6-1 *Turbulent Skin Friction Smooth Flat Plate*

for canopy drag was made based directly on wind tunnel measurements with relatively large scale canopy models that give an accurate evaluation of this drag item.

Bearing in mind the definitions discussed above, the thickness wave drag of the Model 733-197 was evaluated by means of the Supersonic Area Rule. The physical basis of this theory has been well established during the last decade stemming as it does from the pioneering work

of R. T. Whitcomb, R. T. Jones and others; (see Ref. 23). A review of the version of this method used at Boeing can be found in Reference 24.

Justification of this method is ultimately based on comparisons with wind tunnel data as shown in Fig. C6-7 to C6-8. Applications are shown on different configuration arrangements. It will be noted that the comparisons are not restricted to test data obtained in Boeing wind tunnels

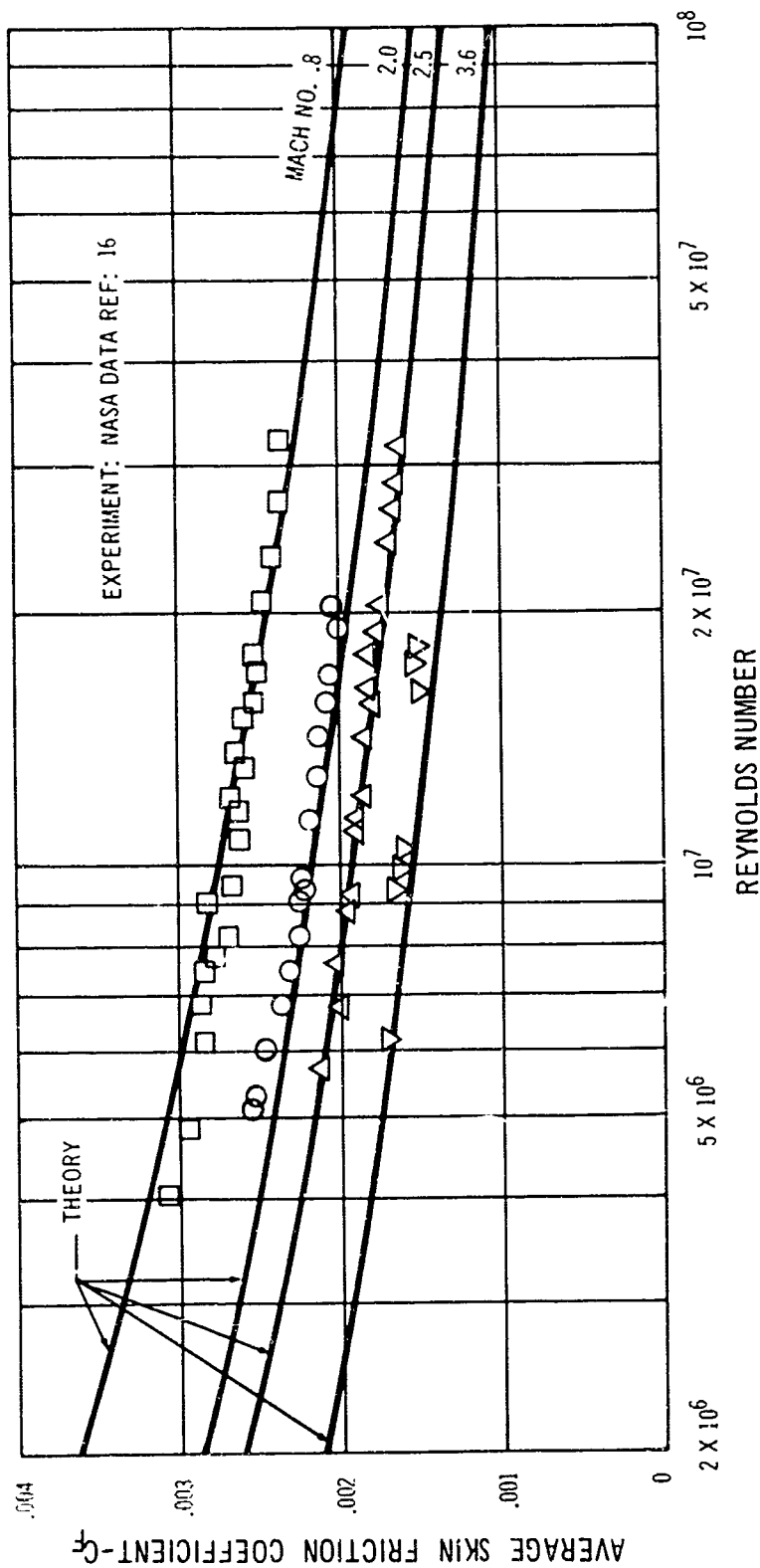


C 6-2 Skin Friction Correlation

but also include data from wind tunnels at the NASA Langley and Ames Research Centers.

The symmetric thickness wave drag of the Model 733-197 is shown in Fig. C6-9 as a function of Mach number for the wings aft configuration. Consistent with the previously discussed definitions it includes only the drag of the wing, body, cowl, struts, empennage and landing gear fairings, as well as interference between these components. Fig. C6-10 shows the Mach 2.7 area plot of the airplane computed in accordance with the Supersonic Transfer Rule, as discussed in Ref. 25.

Fig. C6-10 indicates that a reasonably low wave drag level has been approached. Nevertheless, a detailed breakdown of the drag indicates that a wave drag lower than that used for the performance of the airplane at the time of this writing can be achieved. For instance, at Mach 2.7 the wave drag of the nacelle cowl and landing gear fairings is presently quoted at over 30 percent greater than the estimated isolated component drag. Fig. C6-11 shows calculations indicating improvements in cowl drag due to nacelle relocation and redesign. The improvement at transonic Mach numbers is significant. These calcu-



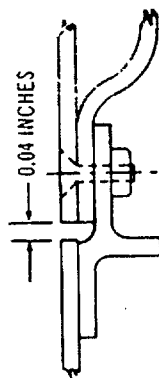
C 6-3 Skin Friction Correlation

lations show configuration refinements which will be explored during Phase II; though no credit for this has been taken in the present drag estimate. A note is required on closure wave drag corrections. It has been found that an improvement in wave drag estimation of boat-tails over and above slender body theory can be obtained by the theory of Ref. 26. It is based on the work of Light-hill on higher approximations in aerodynamics, Ref. 27. Fig. C6-12 shows a comparison between the two theories

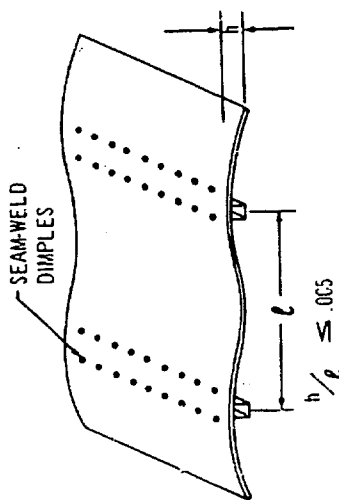
and experiment. The closure drag of the airplane has been evaluated on the basis of that theory. It should be noted, however, that the numerical differences between the two theories as applied to the boat-tail of the Model 733-197 are rather small, of the order of 20 percent of the theoretical wave drag of the isolated afterbody.

Figs. C6-10 and C6-13 show the area plots of the airplane at Mach 2.7 and Mach 1.0 respectively. The Mach 1.0 area plot is of course the normal area distribution of

DOOR OPENINGS

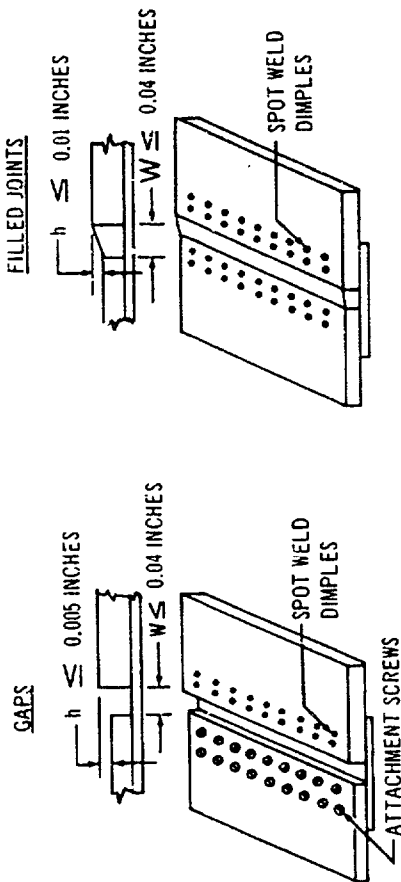


SURFACE WAVES



C 6-4 Surface Roughness Tolerances

the airplane. Fig. C6-14 shows airplane area plots for various "Hayes plane cuts" at Mach 1.1; these are actually more meaningful from a drag point of view. As noted previously the "drag area plots" at Mach 1.1 and 2.7 do not show the canopy. The complicated shape of the canopy is not amenable to linearized theory (basis of area plots). It is more meaningful to measure this drag relative to a smooth ogive and separate it from the basic thickness wave drag. The drag of the Model 733-197 canopy is substantiated below. This discussion on wave drag is con-



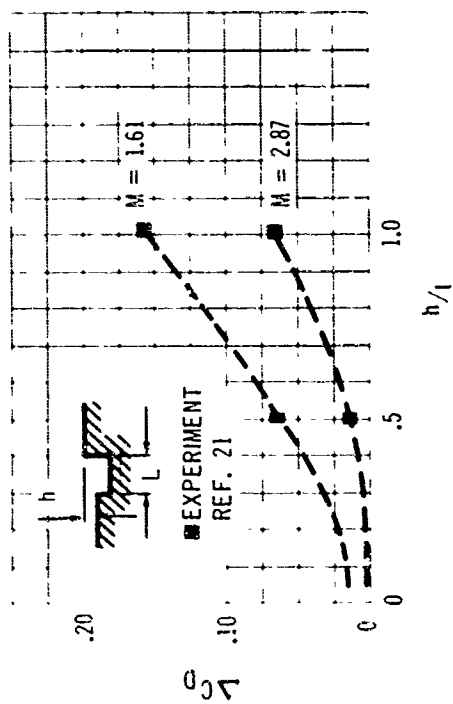
cluded with Table C6-A. It describes the airplane geometry in terms of the NASA wave drag program (Ref. 28).

Supersonic wind tunnel tests have been performed comparing the drag of the Model 733-197 forebody with canopy to that of an axisymmetric ogive. These models were approximately 1/20th scale. A photograph of the Model 733-197 canopy model is given in Fig. C6-15a and a comparison of its area progression to that of the reference ogive is shown in Fig. C6-15b. Typical test results are shown in Fig. C6-15c at $M = 2.7$ comparing drags as a function of body attitude. These results show that the penalty for the canopy reduces rapidly as body attitude is increased.

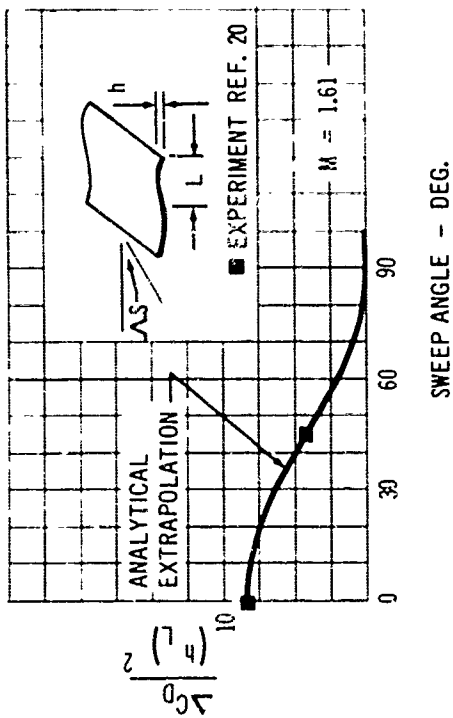
Fig. C6-15d substantiates the canopy drag increment at the approximate flight body attitude of five degrees as a function of Mach number.

C6.1.2.2 Canopy Drag

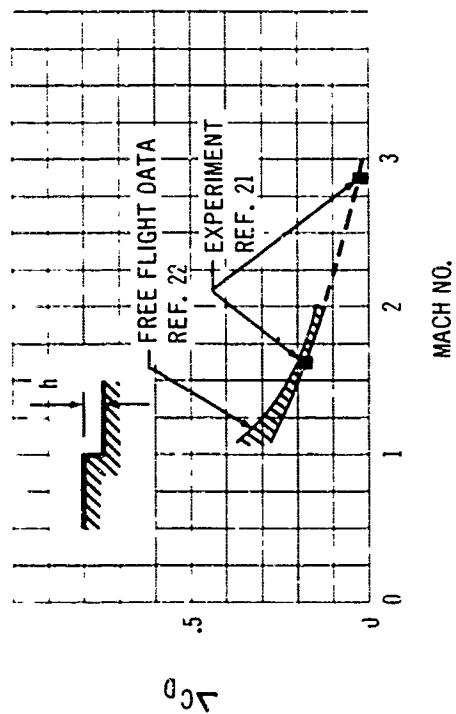
Camber drag is defined as the difference between the measured wind tunnel minimum pressure drag coefficient ($C_{D_{min}}$) and the estimated thickness wave drag (as



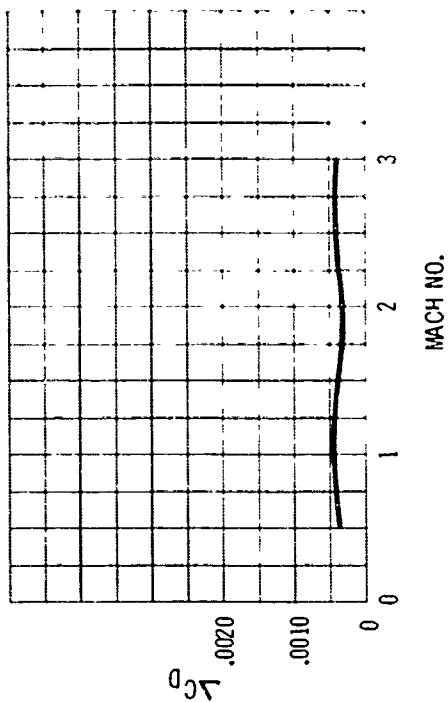
C 6-5 a. Non-Flush Groove Drag-Lip Effect



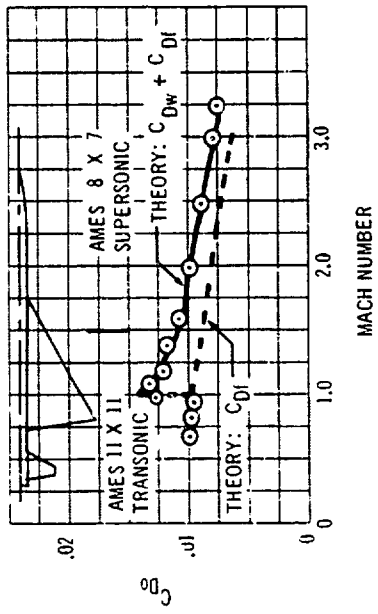
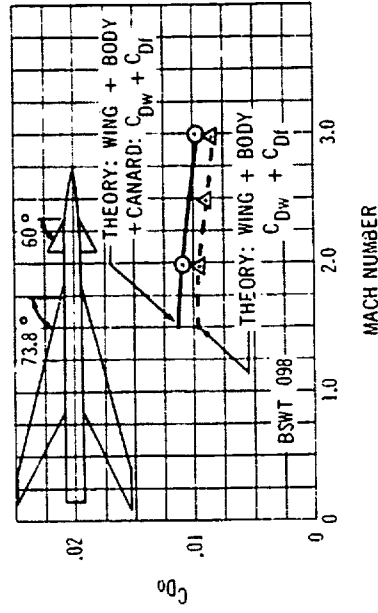
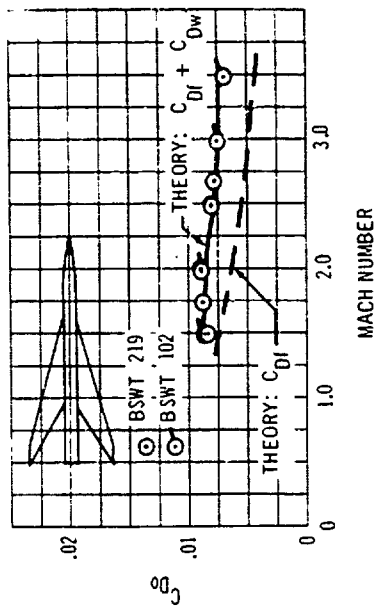
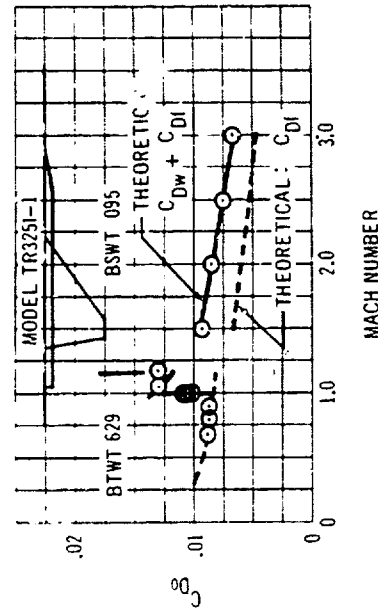
c. Wavy-Surface Drag-Sweep Effect



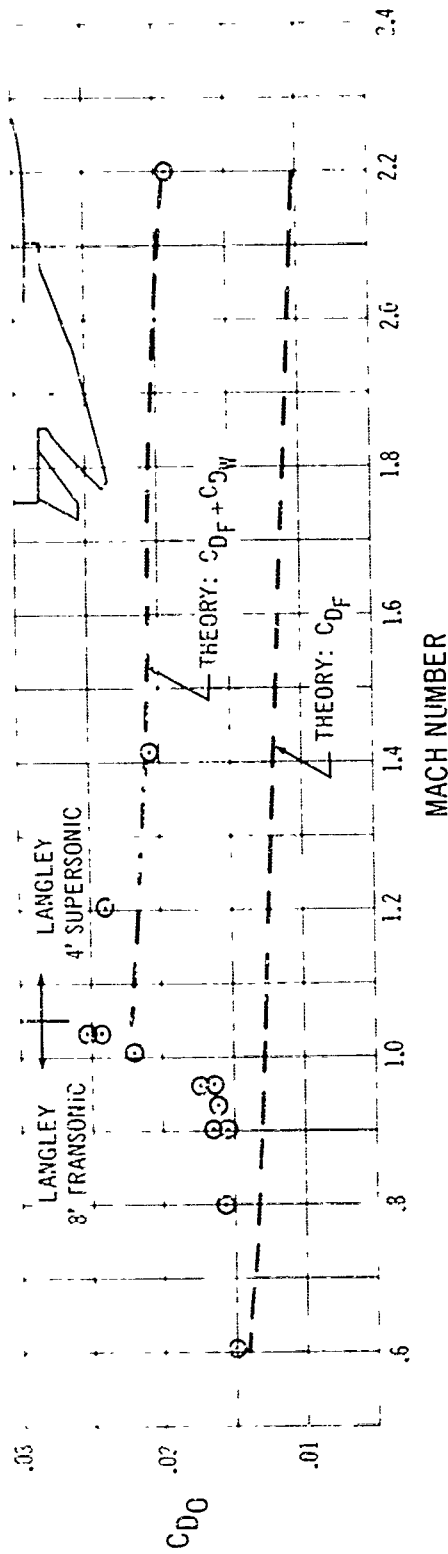
b. Step Drag



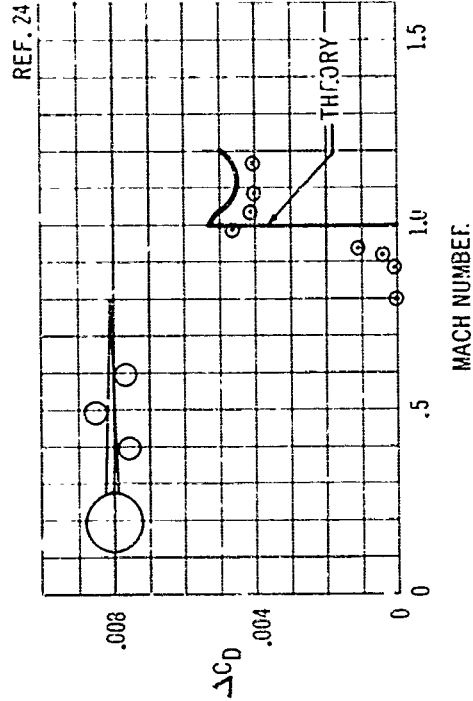
C 6-6 733-197 Surface Roughness and Miscellaneous Drag



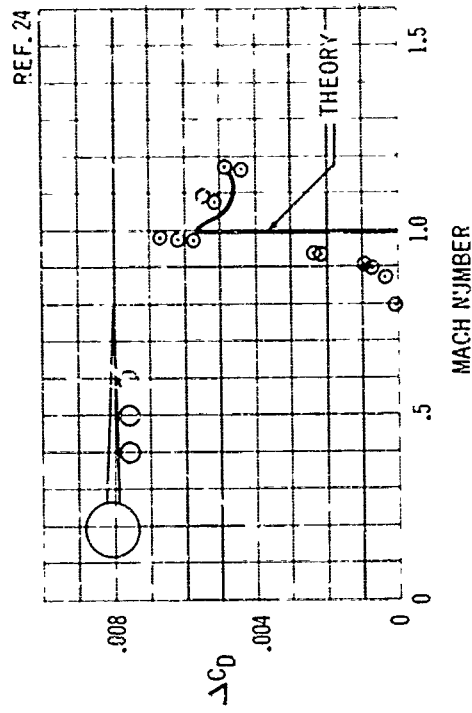
C 6-7 Wave Drag Theory Substantiation



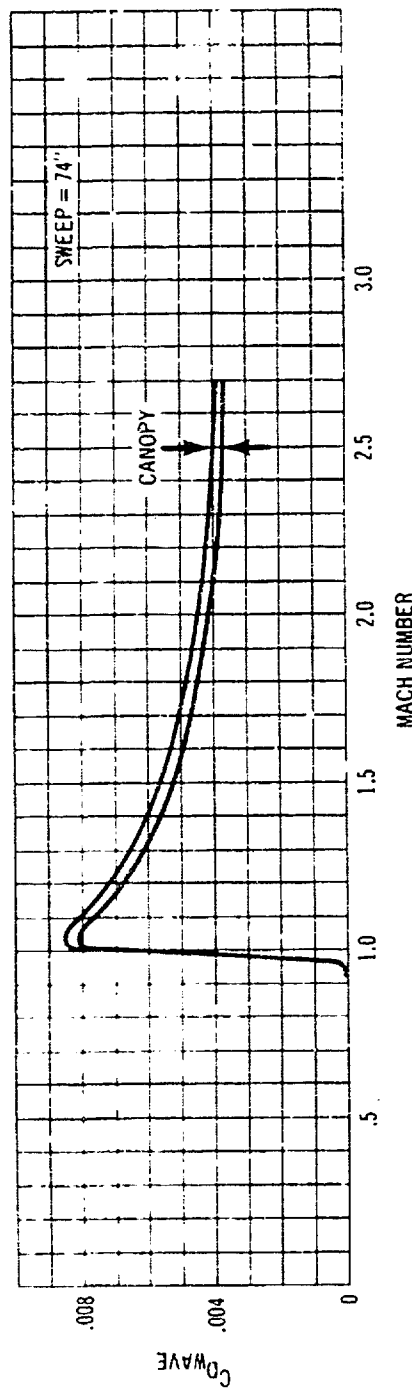
C 6-8 a. Wave Drag Theory Substantiation



c. Transonic Pod Drag Increment



b. Transonic Pod Drag Increment



C 6-9 733-197 Thickness Wave Drag

defined previously) of the wind tunnel model. Essentially it is the difference between the drag measured in the wind tunnel, and that part of the model drag that is amenable to theoretical estimation. It follows that possible errors in the theoretical estimates are included as an increment in the camber drag. The advantage of this procedure is that theory is only used for purposes of extrapolation and for making incremental changes to the wind tunnel data.

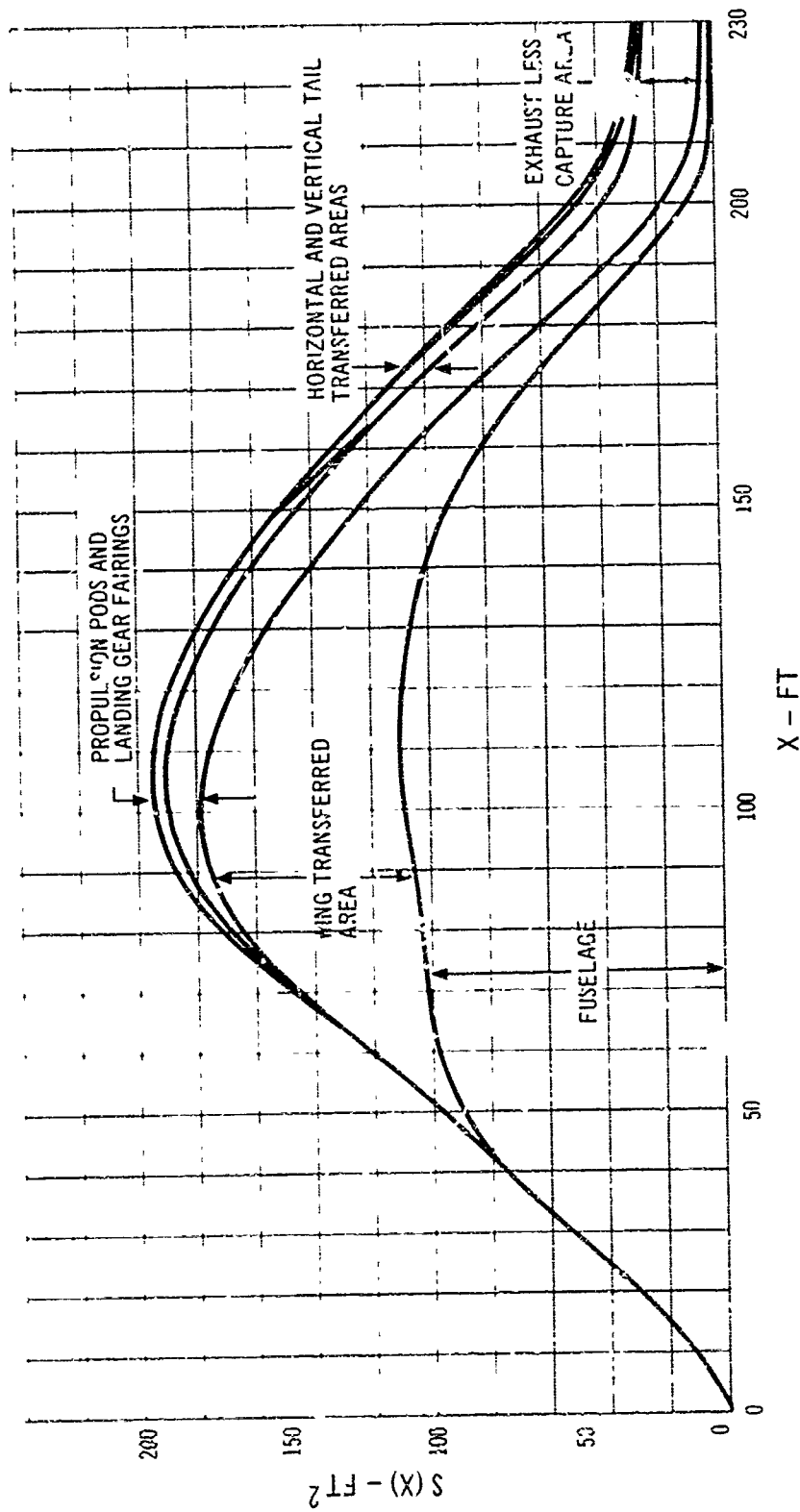
Fig. C6-16 shows wind tunnel results for the Model 733-197 model. The plot shows ($C_{D_{min}} - C_{D_{th}}$) as a function of Mach number for various sweep positions. The theoretical thickness wave drag of the wind tunnel model in the wings-aft configuration is also shown for reference. No attempts were made to analyze the wave drag of the model with the wings partially unswept. At subsonic Mach numbers all the measured difference between the estimated model skin friction and its minimum drag coefficient is attributed to camber drag.

C6.1.2.3 Additional Propulsion Drag

The zero lift wave drag of the struts and nacelles, including interference effects, is included in the previously discussed airplane thickness wave drag. Similarly, the skin friction drag is included in the airplane skin friction estimates.

In order to be consistent with the commonly accepted definition of net engine thrust it is necessary to include in the external drag of the airplane further drag increments associated with the powerplant. An additional drag allowance is therefore made for spillage drag, engine bleed, and bypass drag as well as pressure drag associated with the off-design operation of the nozzle. The drag values attributed to these items are presented in Fig. C6-17.

The basis for these drag estimates is discussed in document A-VI. The spillage drag as shown includes an allowance for the effect of spillage on inlet cowl pressures as discussed and substantiated in Ref. 29.



C 6-10 733-197 Mach 2.7 Area Plot

Other effects associated with nacelle installation are described below.

C6.1.3 NACELLE INTERFERENCE EFFECTS

Location of the nacelles under the wing has an effect on both drag-due-to-lift and pitching moment. Fig. C3-18 shows the pressure drag increment of the nacelles as a

function of C_L at Mach 2.7. The increment at $C_L = 0$ has been accounted as part of the thickness wave drag in Fig. C6-9. The nacelles produce a lift increment of .0047 and a moment increment of .0010 about the center of gravity.

At $C_L = 0.1$, because of the nacelle induced lift, the drag of the airplane is reduced by .00051. This is, however, counterbalanced by an increase in interference drag

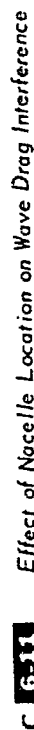
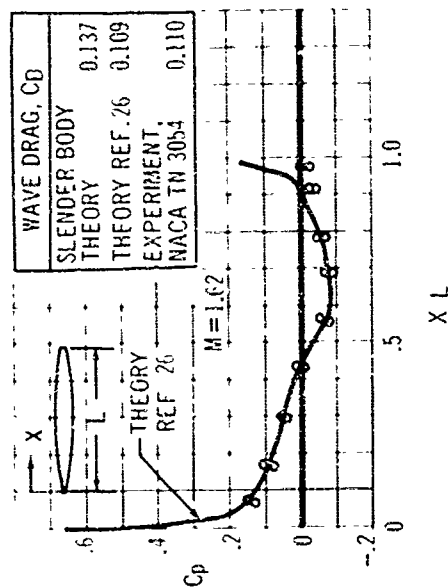


Figure C6-19 shows the computed pressure field due to the racelles on the undersurface of the wing. The calculations are based on the theory of reference 30 and the method of pressure prediction is substantiated in Fig. C6-20. The method of interference calculations is substantiated in Fig. C6-21, using NASA test data.

Further studies have shown that significant improve-



C 6-12 Pressure Drag of Boattailed Body

ments in interference lift can be obtained by rearrangement of the nacelles. Two examples are shown in Fig. C6-22. Fig. C6-23a shows further results obtained in the Boeing supersonic wind tunnel. The corresponding changes in $C_{m_{ac}}$ are indicated in Fig. C6-23b, as this has to be taken into account for a correct analysis of nacelle interference. The investigations shown are part of a continuing study of nacelle interference on the Model 733-197 airplane.

C6.1.4 DRAG DUE TO LIFT

The drag due to lift of the Model 733-197 was obtained from wind tunnel results. Much of the substantiating data are shown in Par. 6.1.3. This Appendix provides further background and discussion on drag due to lift.

The design parameters affecting drag due to lift in subsonic flow are well understood. Aspect ratio is the dominant parameter and the drag due to lift factor is inversely proportional to aspect ratio. In supersonic flow

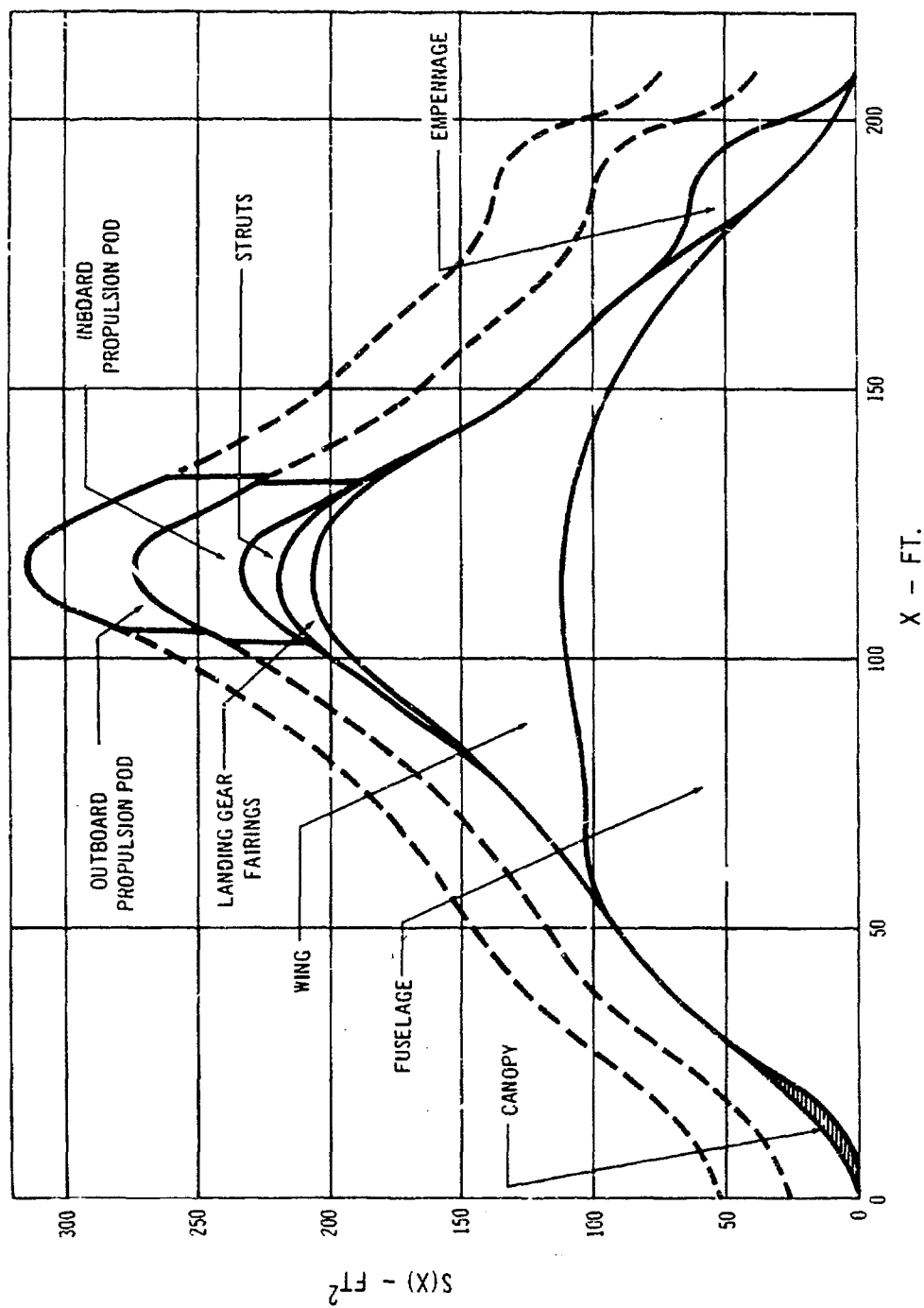
and even in transonic flow, the wing planform as a whole affects the drag due to lift, as do wing thickness ratio and airfoil shape. Considerations of these effects is especially important for the design of arrow wings where high aerodynamic efficiency can be obtained through careful design.

In Fig. C6-24 are shown calculated values of drag due to lift factors K_L . They are plotted versus Mach number for the planform of the Model 733-197. The generally accepted value $(M-1)^{-4}$ for a large class of wings with

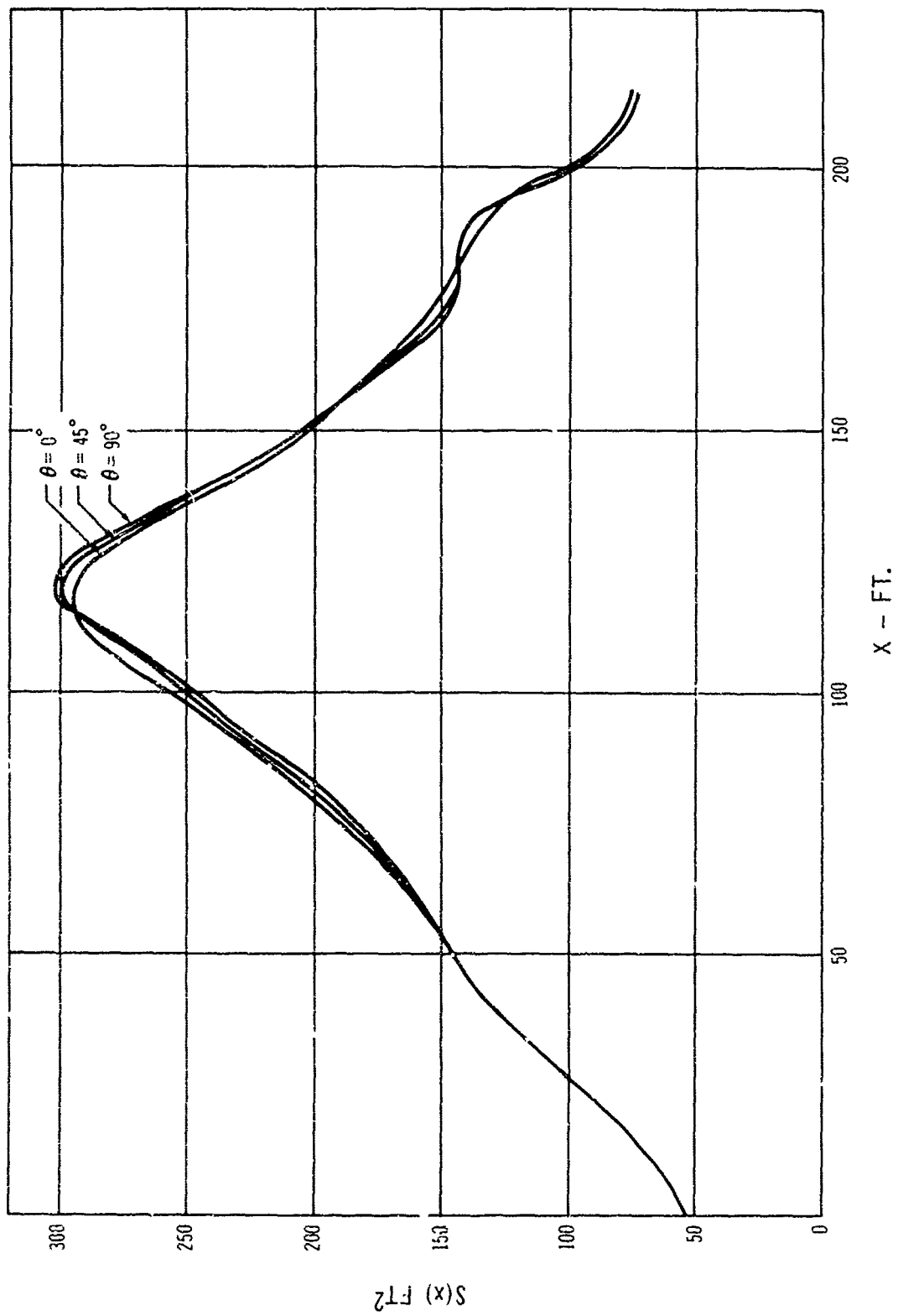
supersonic leading edges is also shown for reference. The great advantage of the arrow wing is clearly shown in the plot (Fig. C6-24). What is also indicated is the penalty associated with the loss of leading edge suction due to separation, a common occurrence with thin highly swept wings. In practice the loss of leading edge suction is not complete (Ref. 33), but despite this, the unwarped arrow wing does not offer too great an advantage in drag due to lift. It is thus necessary, in order to obtain the high aerodynamic efficiency inherent in the arrow wing, to adopt a design approach that will aim for a flow pattern on the wing that will be stable and predictable and will have a low drag. A type of flow which meets these requirements, and which can be obtained on arrow wings, is achieved by cambering and twisting the wing so that the leading edge is an attachment line at, or near, design lift coefficients.

An additional feature of the design is that flow separation takes place only along the trailing edge, so that extensive regions of separated flow on the wing surface itself are avoided, and viscous effects are confined to a relatively thin boundary layer. Furthermore, the flow is smooth everywhere and there are no shock waves on the wing. Fig. C6-25 shows a successful application of this design approach.

The vertical axis, ΔC_{D_L} , is the drag due to lift at lift coefficient C_L . Experimental data of the Boeing arrow wing



C 6-13 733-197 Mach 1.00 Area Plot



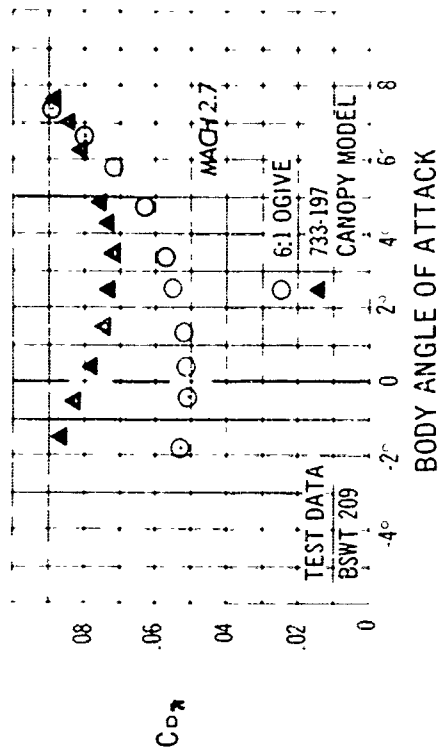
C. 6-14 Mach 1.1 Aerodynamic Area Plots

TABLE C-6-A WAVE DRAG CALCULATION INPUTS

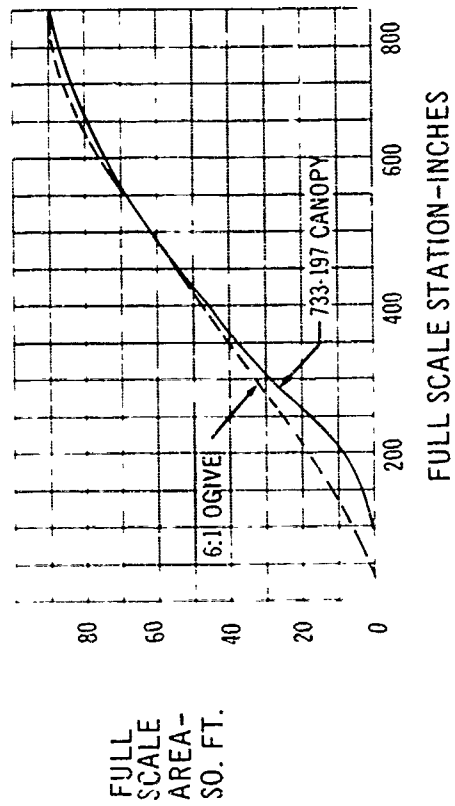
1	2	3	4	5	6	7	8	9	10	11	12	13	14	15	16	17	18	19	20	21	22	23	24	25	26	27	28	29	30	31	32	33	34	35	36	37	38	39	40	41	42	43	44	45	46	47	48	49	50	51	52	53	54	55	56	57	58	59	60	61	62	63	64	65	66	67	68	69	70	71	72	73	74	75	76	77	78	79	80	81	82	83	84	85	86	87	88	89	90	91	92	93	94	95	96	97	98	99	100	101	102	103	104	105	106	107	108	109	110	111	112	113	114	115	116	117	118	119	120	121	122	123	124	125	126	127	128	129	130	131	132	133	134	135	136	137	138	139	140	141	142	143	144	145	146	147	148	149	150	151	152	153	154	155	156	157	158	159	160	161	162	163	164	165	166	167	168	169	170	171	172	173	174	175	176	177	178	179	180	181	182	183	184	185	186	187	188	189	190	191	192	193	194	195	196	197	198	199	200	201	202	203	204	205	206	207	208	209	210	211	212	213	214	215	216	217	218	219	220	221	222	223	224	225	226	227	228	229	230	231	232	233	234	235	236	237	238	239	240	241	242	243	244	245	246	247	248	249	250	251	252	253	254	255	256	257	258	259	260	261	262	263	264	265	266	267	268	269	270	271	272	273	274	275	276	277	278	279	280	281	282	283	284	285	286	287	288	289	290	291	292	293	294	295	296	297	298	299	300	301	302	303	304	305	306	307	308	309	310	311	312	313	314	315	316	317	318	319	320	321	322	323	324	325	326	327	328	329	330	331	332	333	334	335	336	337	338	339	340	341	342	343	344	345	346	347	348	349	350	351	352	353	354	355	356	357	358	359	360	361	362	363	364	365	366	367	368	369	370	371	372	373	374	375	376	377	378	379	380	381	382	383	384	385	386	387	388	389	390	391	392	393	394	395	396	397	398	399	400	401	402	403	404	405	406	407	408	409	410	411	412	413	414	415	416	417	418	419	420	421	422	423	424	425	426	427	428	429	430	431	432	433	434	435	436	437	438	439	440	441	442	443	444	445	446	447	448	449	450	451	452	453	454	455	456	457	458	459	460	461	462	463	464	465	466	467	468	469	470	471	472	473	474	475	476	477	478	479	480	481	482	483	484	485	486	487	488	489	490	491	492	493	494	495	496	497	498	499	500	501	502	503	504	505	506	507	508	509	510	511	512	513	514	515	516	517	518	519	520	521	522	523	524	525	526	527	528	529	530	531	532	533	534	535	536	537	538	539	540	541	542	543	544	545	546	547	548	549	550	551	552	553	554	555	556	557	558	559	560	561	562	563	564	565	566	567	568	569	570	571	572	573	574	575	576	577	578	579	580	581	582	583	584	585	586	587	588	589	590	591	592	593	594	595	596	597	598	599	600	601	602	603	604	605	606	607	608	609	610	611	612	613	614	615	616	617	618	619	620	621	622	623	624	625	626	627	628	629	630	631	632	633	634	635	636	637	638	639	640	641	642	643	644	645	646	647	648	649	650	651	652	653	654	655	656	657	658	659	660	661	662	663	664	665	666	667	668	669	670	671	672	673	674	675	676	677	678	679	680	681	682	683	684	685	686	687	688	689	690	691	692	693	694	695	696	697	698	699	700	701	702	703	704	705	706	707	708	709	710	711	712	713	714	715	716	717	718	719	720	721	722	723	724	725	726	727	728	729	730	731	732	733	734	735	736	737	738	739	740	741	742	743	744	745	746	747	748	749	750	751	752	753	754	755	756	757	758	759	760	761	762	763	764	765	766	767	768	769	770	771	772	773	774	775	776	777	778	779	780	781	782	783	784	785	786	787	788	789	790	791	792	793	794	795	796	797	798	799	800	801	802	803	804	805	806	807	808	809	810	811	812	813	814	815	816	817	818	819	820	821	822	823	824	825	826	827	828	829	830	831	832	833	834	835	836	837	838	839	840	841	842	843	844	845	846	847	848	849	850	851	852	853	854	855	856	857	858	859	860	861	862	863	864	865	866	867	868	869	870	871	872	873	874	875	876	877	878	879	880	881	882	883	884	885	886	887	888	889	890	891	892	893	894	895	896	897	898	899	900	901	902	903	904	905	906	907	908	909	910	911	912	913	914	915	916	917	918	919	920	921	922	923	924	925	926	927	928	929	930	931	932	933	934	935	936	937	938	939	940	941	942	943	944	945	946	947	948	949	950	951	952	953	954	955	956	957	958	959	960	961	962	963	964	965	966	967	968	969	970	971	972	973	974	975	976	977	978	979	980	981	982	983	984	985	986	987	988	989	990	991	992	993	994	995	996	997	998	999	1000	1001	1002	1003	1004	1005	1006	1007	1008	1009	1010	1011	1012	1013	1014	1015	1016	1017	1018	1019	1020	1021	1022	1023	1024	1025	1026	1027	1028	1029	1030	1031	1032	1033	1034	1035	1036	1037	1038	1039	1040	1041	1042	1043	1044	1045	1046	1047	1048	1049	1050	1051	1052	1053	1054	1055	1056	1057	1058	1059	1060	1061	1062	1063	1064	1065	1066	1067	1068	1069	1070	1071	1072	1073	1074	1075	1076	1077	1078	1079	1080	1081	1082	1083	1084	1085	1086	1087	1088	1089	1090	1091	1092	1093	1094	1095	1096	1097	1098	1099	1100	1101	1102	1103	1104	1105	1106	1107	1108	1109	1110	1111	1112	1113	1114	1115	1116	1117	1118	1119	1120	1121	1122	1123	1124	1125	1126	1127	1128	1129	1130	1131	1132	1133	1134	1135	1136	1137	1138	1139	1140	1141	1142	1143	1144	1145	1146	1147	1148	1149	1150	1151	1152	1153	1154	1155	1156	1157	1158	1159	1160	1161	1162	1163	1164	1165	1166	1167	1168	1169	1170	1171	1172	1173	1174	1175	1176	1177	1178	1179	1180	1181	1182	1183	1184	1185	1186	1187	1188	1189	1190	1191	1192	1193	1194	1195	1196	1197	1198	1199	1200	1201	1202	1203	1204	1205	1206	1207	1208	1209	1210	1211	1212	1213	1214	1215	1216	1217	1218	1219	1220	1221	1222	1223	1224	1225	1226	1227	1228	1229	1230	1231	1232	1233	1234	1235	1236	1237	1238	1239	1240	1241	1242	1243	1244	1245	1246	1247	1248	1249	1250	1251	1252	1253	1254	1255	1256	1257	1258	1259	1260	1261	1262	1263	1264	1265	1266	1267	1268	1269	1270	1271	1272	1273	1274	1275	1276	1277	1278	1279	1280	1281	1282	1283	1284	1285	1286	1287	1288	1289	1290	1291	1292	1293	1294	1295	1296	1297	1298	1299	1300	1301	1302	1303	1304	1305	1306	1307	1308	1309	1310	1311	1312	1313	1314	1315	1316	1317	1318	1319	1320	1321	1322	1323	1324	1325	1326	1327	1328	1329	1330	1331	1332	1333	1334	1335	1336	1337	1338	1339	1340	1341	1342	1343	1344	1345	1346	1347	1348	1349	1350	1351	1352	1353	1354	1355	1356	1357	1358	1359	1360	1361	1362	1363	1364	1365	1366	1367	1368	1369	1370	1371	1372	1373	1374	1375	1376	1377	1378	1379	1380	1381	1382	1383	1384	1385	1386	1387	1388	1389	1390	1391	1392	1393	1394	1395	1396	1397	1398	1399	1400	1401	1402	1403	1404	1405	1406	1407	1408	1409	1410	1411	1412	1413	1414	1415	1416	1417	1418	1419	1420	1421	1422	1423	1424	1425	1426	1427	1428	1429	1430	1431	1432	1433	1434	1435	1436	1437	1438	1439	1440	1441	1442	1443	1444	1445	1446	1447	1448	1449	1450	1451	1452	1453	1454	1455	1456	1457	1458	1459	1460	1461	1462	1463	1464	1465	1466	1467	1468	1469	1470	1471	1472	1473	1474	1475	1476	1477	1478	1479	1480	1481	1482	1483	1484	1485	1486	1487	1488	1489	1490	149
---	---	---	---	---	---	---	---	---	----	----	----	----	----	----	----	----	----	----	----	----	----	----	----	----	----	----	----	----	----	----	----	----	----	----	----	----	----	----	----	----	----	----	----	----	----	----	----	----	----	----	----	----	----	----	----	----	----	----	----	----	----	----	----	----	----	----	----	----	----	----	----	----	----	----	----	----	----	----	----	----	----	----	----	----	----	----	----	----	----	----	----	----	----	----	----	----	----	----	-----	-----	-----	-----	-----	-----	-----	-----	-----	-----	-----	-----	-----	-----	-----	-----	-----	-----	-----	-----	-----	-----	-----	-----	-----	-----	-----	-----	-----	-----	-----	-----	-----	-----	-----	-----	-----	-----	-----	-----	-----	-----	-----	-----	-----	-----	-----	-----	-----	-----	-----	-----	-----	-----	-----	-----	-----	-----	-----	-----	-----	-----	-----	-----	-----	-----	-----	-----	-----	-----	-----	-----	-----	-----	-----	-----	-----	-----	-----	-----	-----	-----	-----	-----	-----	-----	-----	-----	-----	-----	-----	-----	-----	-----	-----	-----	-----	-----	-----	-----	-----	-----	-----	-----	-----	-----	-----	-----	-----	-----	-----	-----	-----	-----	-----	-----	-----	-----	-----	-----	-----	-----	-----	-----	-----	-----	-----	-----	-----	-----	-----	-----	-----	-----	-----	-----	-----	-----	-----	-----	-----	-----	-----	-----	-----	-----	-----	-----	-----	-----	-----	-----	-----	-----	-----	-----	-----	-----	-----	-----	-----	-----	-----	-----	-----	-----	-----	-----	-----	-----	-----	-----	-----	-----	-----	-----	-----	-----	-----	-----	-----	-----	-----	-----	-----	-----	-----	-----	-----	-----	-----	-----	-----	-----	-----	-----	-----	-----	-----	-----	-----	-----	-----	-----	-----	-----	-----	-----	-----	-----	-----	-----	-----	-----	-----	-----	-----	-----	-----	-----	-----	-----	-----	-----	-----	-----	-----	-----	-----	-----	-----	-----	-----	-----	-----	-----	-----	-----	-----	-----	-----	-----	-----	-----	-----	-----	-----	-----	-----	-----	-----	-----	-----	-----	-----	-----	-----	-----	-----	-----	-----	-----	-----	-----	-----	-----	-----	-----	-----	-----	-----	-----	-----	-----	-----	-----	-----	-----	-----	-----	-----	-----	-----	-----	-----	-----	-----	-----	-----	-----	-----	-----	-----	-----	-----	-----	-----	-----	-----	-----	-----	-----	-----	-----	-----	-----	-----	-----	-----	-----	-----	-----	-----	-----	-----	-----	-----	-----	-----	-----	-----	-----	-----	-----	-----	-----	-----	-----	-----	-----	-----	-----	-----	-----	-----	-----	-----	-----	-----	-----	-----	-----	-----	-----	-----	-----	-----	-----	-----	-----	-----	-----	-----	-----	-----	-----	-----	-----	-----	-----	-----	-----	-----	-----	-----	-----	-----	-----	-----	-----	-----	-----	-----	-----	-----	-----	-----	-----	-----	-----	-----	-----	-----	-----	-----	-----	-----	-----	-----	-----	-----	-----	-----	-----	-----	-----	-----	-----	-----	-----	-----	-----	-----	-----	-----	-----	-----	-----	-----	-----	-----	-----	-----	-----	-----	-----	-----	-----	-----	-----	-----	-----	-----	-----	-----	-----	-----	-----	-----	-----	-----	-----	-----	-----	-----	-----	-----	-----	-----	-----	-----	-----	-----	-----	-----	-----	-----	-----	-----	-----	-----	-----	-----	-----	-----	-----	-----	-----	-----	-----	-----	-----	-----	-----	-----	-----	-----	-----	-----	-----	-----	-----	-----	-----	-----	-----	-----	-----	-----	-----	-----	-----	-----	-----	-----	-----	-----	-----	-----	-----	-----	-----	-----	-----	-----	-----	-----	-----	-----	-----	-----	-----	-----	-----	-----	-----	-----	-----	-----	-----	-----	-----	-----	-----	-----	-----	-----	-----	-----	-----	-----	-----	-----	-----	-----	-----	-----	-----	-----	-----	-----	-----	-----	-----	-----	-----	-----	-----	-----	-----	-----	-----	-----	-----	-----	-----	-----	-----	-----	-----	-----	-----	-----	-----	-----	-----	-----	-----	-----	-----	-----	-----	-----	-----	-----	-----	-----	-----	-----	-----	-----	-----	-----	-----	-----	-----	-----	-----	-----	-----	-----	-----	-----	-----	-----	-----	-----	-----	-----	-----	-----	-----	-----	-----	-----	-----	-----	-----	-----	-----	-----	-----	-----	-----	-----	-----	-----	-----	-----	-----	-----	-----	-----	-----	-----	-----	-----	-----	-----	-----	-----	-----	-----	-----	-----	-----	-----	-----	-----	-----	-----	-----	-----	-----	-----	-----	-----	-----	-----	-----	-----	-----	-----	-----	-----	-----	-----	-----	-----	-----	-----	-----	-----	-----	-----	-----	-----	-----	-----	-----	-----	-----	-----	-----	-----	-----	-----	-----	-----	-----	-----	-----	-----	-----	-----	-----	-----	-----	-----	-----	-----	-----	-----	-----	-----	-----	-----	-----	-----	-----	-----	-----	-----	-----	-----	-----	-----	-----	-----	-----	-----	-----	-----	-----	-----	-----	-----	-----	-----	-----	-----	-----	-----	-----	-----	-----	-----	-----	-----	-----	-----	-----	-----	-----	-----	-----	-----	-----	-----	-----	-----	-----	-----	-----	-----	-----	-----	-----	-----	-----	-----	-----	-----	-----	-----	-----	-----	-----	-----	-----	-----	-----	-----	-----	-----	-----	-----	-----	-----	-----	-----	-----	-----	-----	-----	-----	-----	-----	-----	-----	-----	-----	-----	-----	-----	-----	-----	-----	-----	-----	-----	-----	-----	-----	-----	-----	-----	-----	-----	-----	-----	-----	-----	-----	-----	-----	-----	-----	-----	-----	-----	-----	-----	-----	-----	-----	-----	-----	-----	-----	-----	-----	-----	-----	-----	-----	-----	-----	-----	-----	-----	-----	-----	-----	-----	-----	-----	-----	-----	-----	-----	-----	-----	-----	-----	-----	-----	-----	-----	-----	-----	-----	-----	-----	-----	-----	-----	-----	-----	-----	-----	-----	-----	-----	-----	-----	-----	-----	-----	-----	-----	-----	-----	-----	-----	-----	-----	-----	-----	-----	-----	-----	-----	-----	-----	-----	-----	-----	-----	-----	-----	-----	-----	-----	-----	-----	-----	-----	-----	-----	-----	-----	-----	-----	-----	-----	-----	-----	-----	-----	------	------	------	------	------	------	------	------	------	------	------	------	------	------	------	------	------	------	------	------	------	------	------	------	------	------	------	------	------	------	------	------	------	------	------	------	------	------	------	------	------	------	------	------	------	------	------	------	------	------	------	------	------	------	------	------	------	------	------	------	------	------	------	------	------	------	------	------	------	------	------	------	------	------	------	------	------	------	------	------	------	------	------	------	------	------	------	------	------	------	------	------	------	------	------	------	------	------	------	------	------	------	------	------	------	------	------	------	------	------	------	------	------	------	------	------	------	------	------	------	------	------	------	------	------	------	------	------	------	------	------	------	------	------	------	------	------	------	------	------	------	------	------	------	------	------	------	------	------	------	------	------	------	------	------	------	------	------	------	------	------	------	------	------	------	------	------	------	------	------	------	------	------	------	------	------	------	------	------	------	------	------	------	------	------	------	------	------	------	------	------	------	------	------	------	------	------	------	------	------	------	------	------	------	------	------	------	------	------	------	------	------	------	------	------	------	------	------	------	------	------	------	------	------	------	------	------	------	------	------	------	------	------	------	------	------	------	------	------	------	------	------	------	------	------	------	------	------	------	------	------	------	------	------	------	------	------	------	------	------	------	------	------	------	------	------	------	------	------	------	------	------	------	------	------	------	------	------	------	------	------	------	------	------	------	------	------	------	------	------	------	------	------	------	------	------	------	------	------	------	------	------	------	------	------	------	------	------	------	------	------	------	------	------	------	------	------	------	------	------	------	------	------	------	------	------	------	------	------	------	------	------	------	------	------	------	------	------	------	------	------	------	------	------	------	------	------	------	------	------	------	------	------	------	------	------	------	------	------	------	------	------	------	------	------	------	------	------	------	------	------	------	------	------	------	------	------	------	------	------	------	------	------	------	------	------	------	------	------	------	------	------	------	------	------	------	------	------	------	------	------	------	------	------	------	------	------	------	------	------	------	------	------	------	------	------	------	------	------	------	------	------	------	------	------	------	------	------	------	------	------	------	------	------	------	------	------	------	------	------	------	------	------	------	------	------	------	------	------	------	------	------	------	------	------	------	------	------	------	------	------	------	------	------	------	------	------	------	------	------	------	------	------	------	------	------	------	------	------	------	------	------	------	------	------	------	------	------	------	------	------	-----



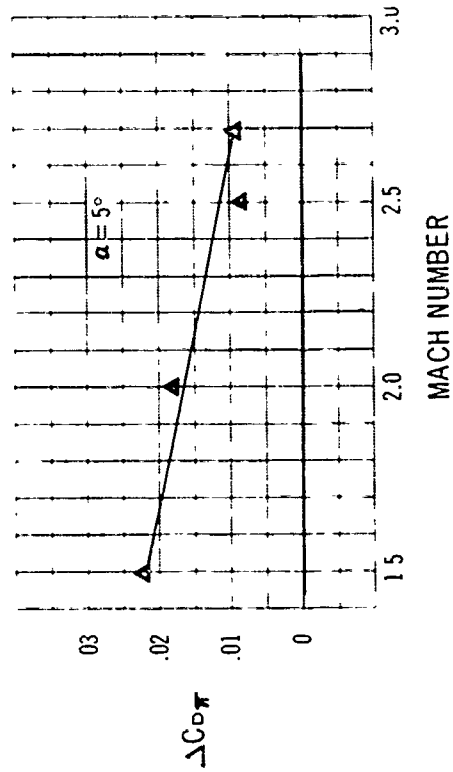
C 6-15 a. Canopy Model



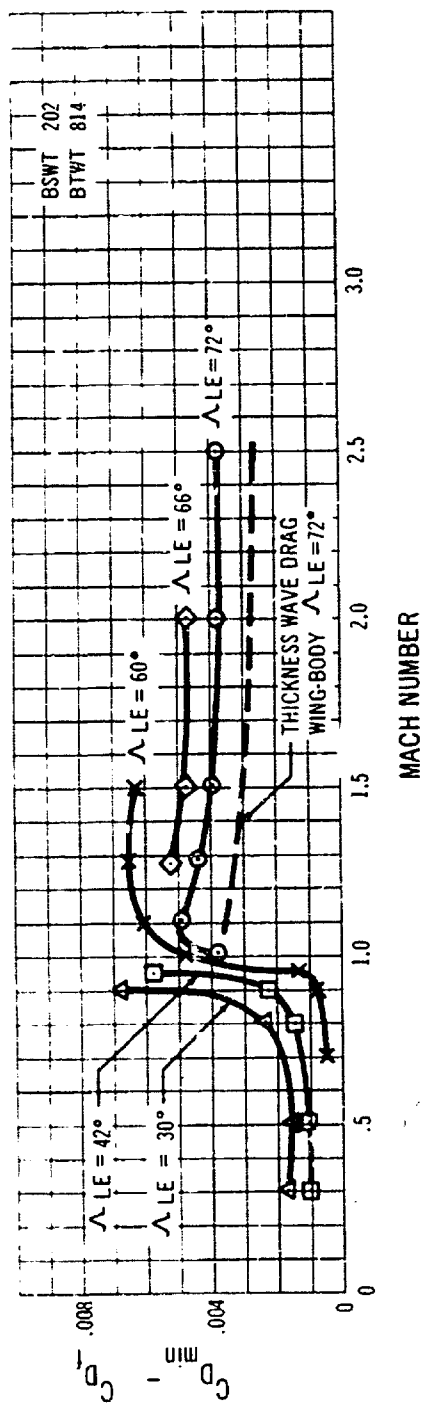
c. Canopy Drag Comparison



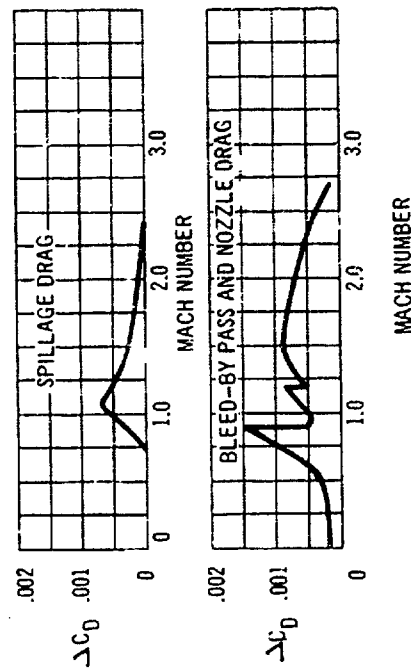
b. Area Plots



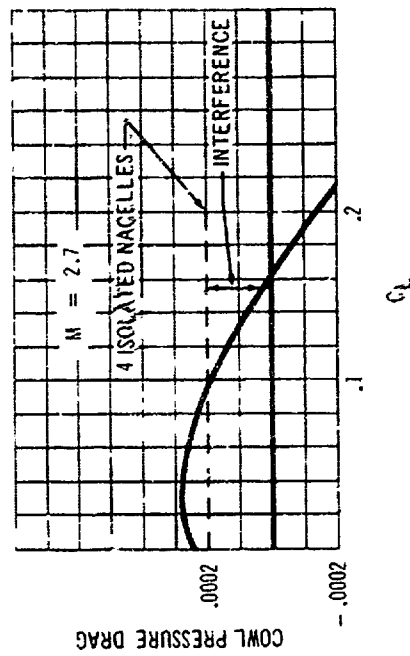
d. Canopy Wave Drag



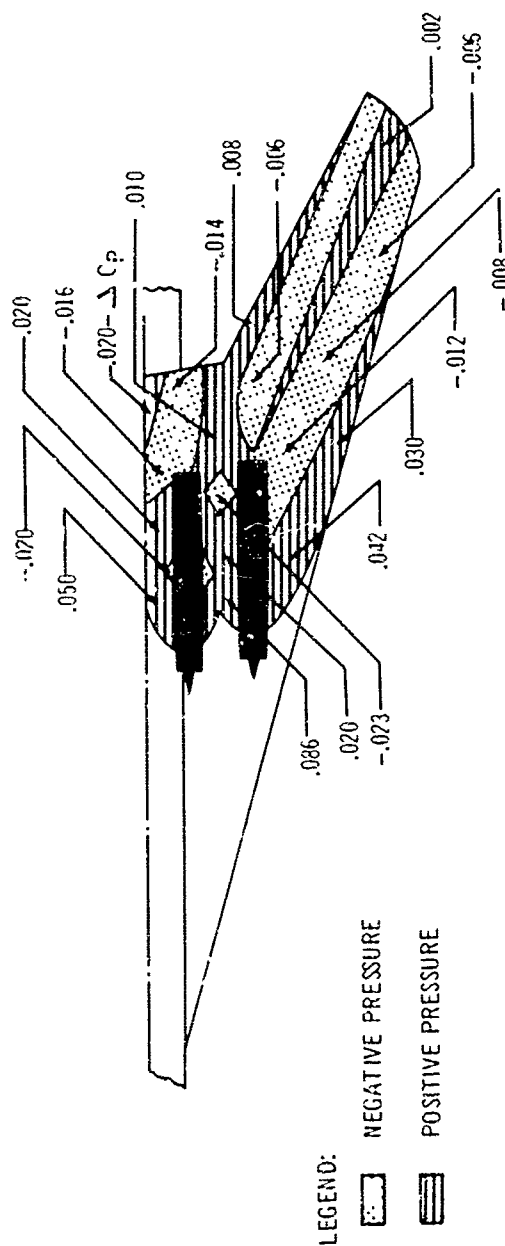
C 6-16 Measured Camber and Thickness Wave Drag



C 6-17 Propulsion Drag Increments



C 6-18 Nacelle Interference Drag



C 6-19 Nacelle Induced Pressures

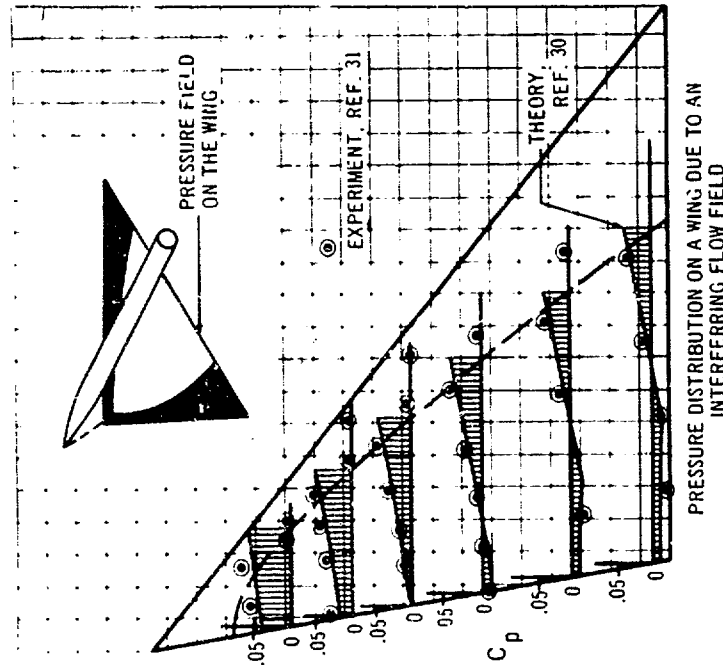
model is shown to provide an efficiency considerably superior to the flat wing without leading edge suction force. Although the measured drag due to lift is larger than the theoretical optimum, it is in reasonable agreement with theory for the more restricted camber and twist utilized on the model. This is particularly true in the C_l range of interest demonstrating the validity of this method of design. As was mentioned, a requirement for the successful design of an arrow wing is a flow situation that is generally free from separation and shock waves over the wing. This requirement can be achieved on combinations of thin wings with slender bodies by controlling the loading over the wing surface and various schemes for achieving this have been devised. On thicker wings, as is discussed in Ref. 34, interactions between thickness and camber

may have a degrading effect on the drag due to lift, compared to very thin wings where such interactions are generally absent. It is therefore necessary, when designing a relatively thick arrow wing, to tailor the thickness distribution both as to section shape, thickness ratio, and the spanwise distribution of section and thickness. Critical areas are the outboard part of the wing where a highly negative pressure coefficient leads to separation and shock waves, and also the leading edge of the wing, near the wing body junction, where a large negative pressure tends to turn the free stream flow inwards towards the body, resulting in the formation of one or more shock waves. It has been found that the flow on the outer parts of the wing can be controlled by keeping a small thickness in this region. The inboard problem is best solved by the selec-

Ref. 35 that tend to pressurize the upper surface of the outboard wing along the trailing edge. A successful application of thickness tailoring as illustrated in Fig. C6-26 utilizing data obtained in the Boeing supersonic wind tunnel.

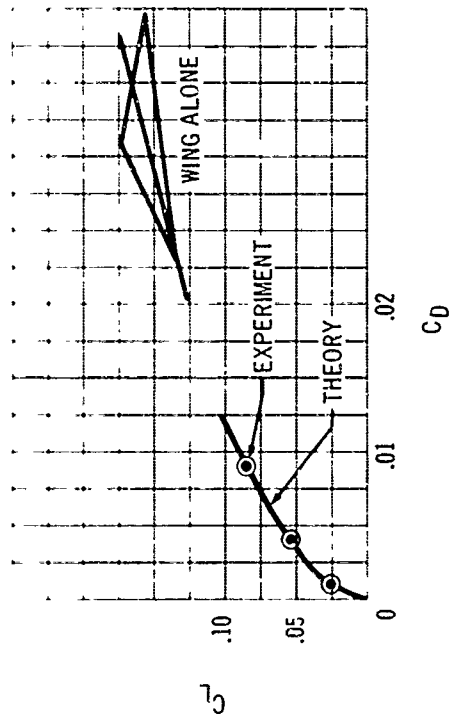
A thin wing W_{10} is compared to a thickened version W_{11} . The basic thin wing has 2.5 percent maximum thickness ratio. The second wing W_{11} had a tailored thickness distribution, 4.15 percent inboard, a 3.5 percent thick section with a round leading edge at 40 percent span and a 2.5 percent thick rounded leading edge profile of the NASA 65-series outboard of 65 percent span. Fig. C6-26a and C6-26b compare calculated upper surface pressures at two critical spanwise stations. It is seen that tailoring the sections on the thicker wing maintains these pressures at roughly the same level as on the thin wing. The justification of this procedure can be seen in Fig. C6-26c and C6-26d where measured drag increments between the two wings are shown. The drag difference is entirely accounted by calculated changes in thickness drag, there being no systematic change in the difference, with lift coefficient. Fig. C6-26d shows that the lack of degradation of drag due to lift factor is maintained over a wide range of Mach number.

Test results from several arrow wing planforms are presented in Fig. C6-27 where envelope drag due to lift is shown as a function of Mach number. These data show that the Model 733-197 cruise drag due to lift has been demonstrated in the wind tunnel on planforms similar to that of the Model 733-197 which has an aspect ratio of 1.3 with 74 degree leading edge sweep. The Model 733-197 camber and twist is selected to give the best possible cruise L/D, consistent with the substantiated envelope drag due to lift, at the airplane matched cruise lift coefficient of 0.10. The camber drag and lift increments for the Model 733-197 cruise polar are based on test results from wings of varying design lift coefficient shown in Fig. C6-28 and C6-29.

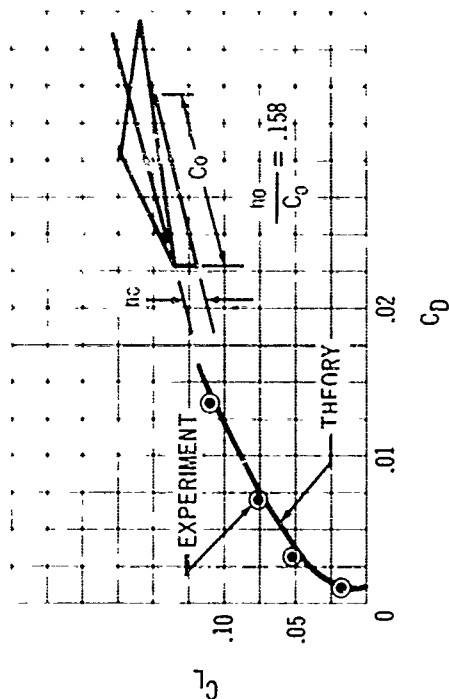


C 6-20 Substantiation of Pressure Field Calculations

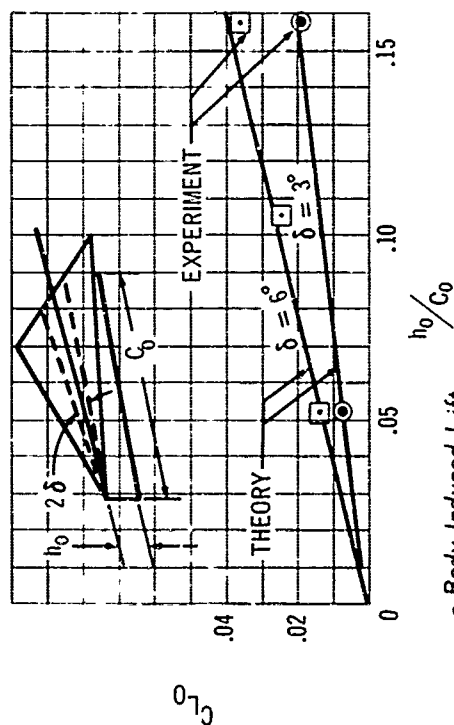
tion of a section shape that produces large positive thickness pressures at the leading edge. These pressures then combine with the large negative loads required by the camber, both for low drag and forward center of pressure condition, to yield a moderate load at the wing apex. The problems associated with increased thickness can also be solved by body contouring as well as "Whitcomb bodies,"



a. Wing Alone Polar



b. Wing-Body Polar



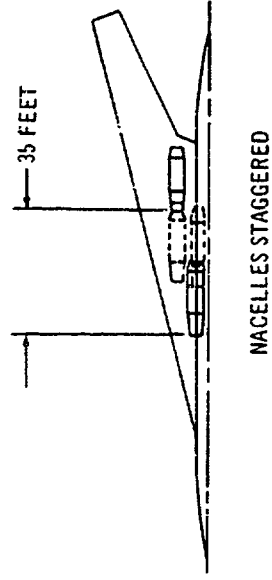
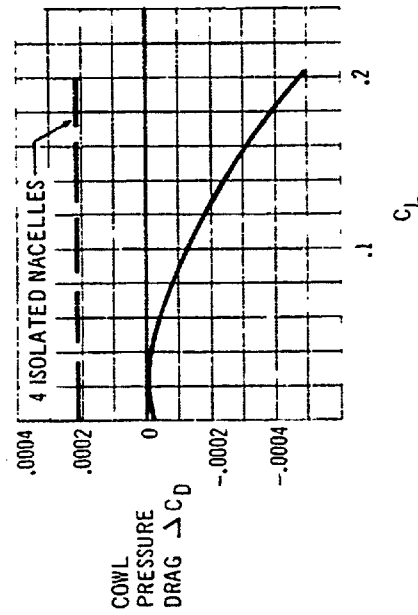
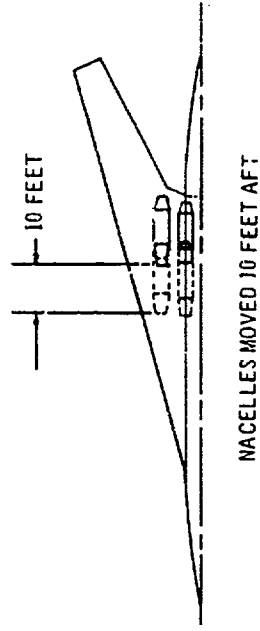
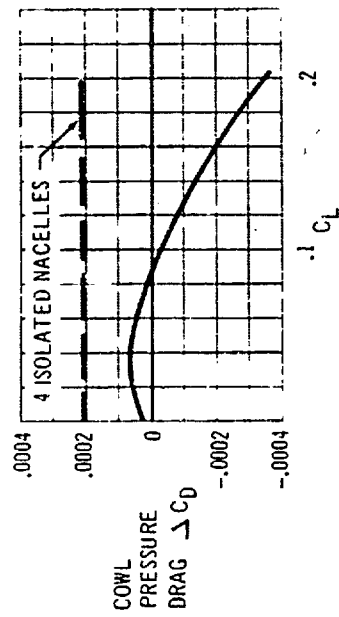
c. Body Induced Lift

C 6-21 Substantiation of Interference Calculations,
Mach 3.11 Experiment Ref. 32

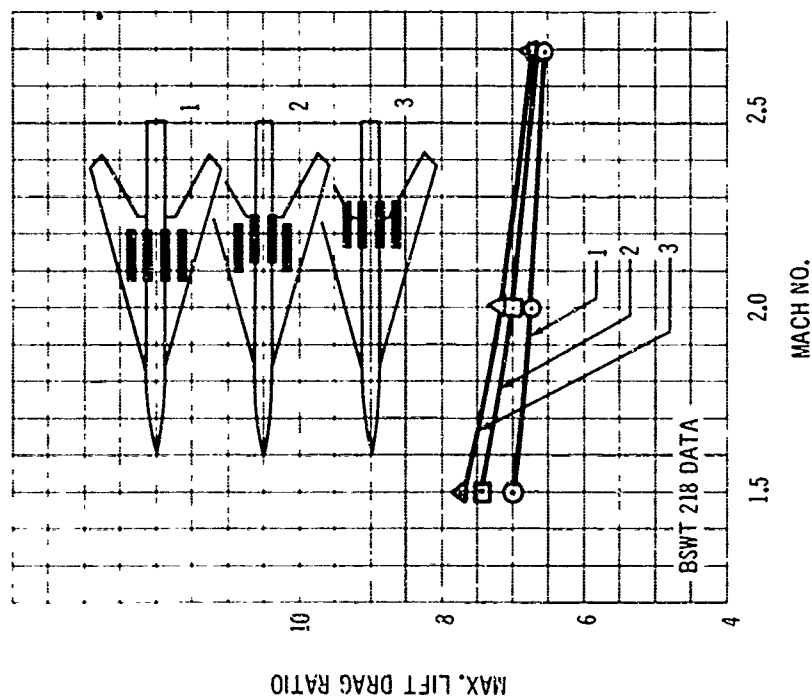
Considerable theoretical and experimental effort has been applied to the problems of transonic airfoils at Boeing. Recently, this work was extended to include application to the wing of a variable sweep model. Although still in its infancy, this effort has already shown that considerable improvement can be made in the transonic region. Fig. C6-30 and C6-31 present test results from an in-board-pivot, variable sweep model and show a significant improvement in L/D_{max} in the critical transonic region.

C6.1.5 TRIM DRAG

Trim drag for the Model 733-197 airplane is calculated as an increment from the zero tail load condition. Small tail up loads therefore result in negative trim drag increments. The increment in airplane lift supplied by the tail in trimming the positive pitching moment of the wing-body combination allows the wing to operate at a slightly lower angle of attack and drag level. When the reduction



C 6-22 Effect of Nacelle Location on Interference Drag

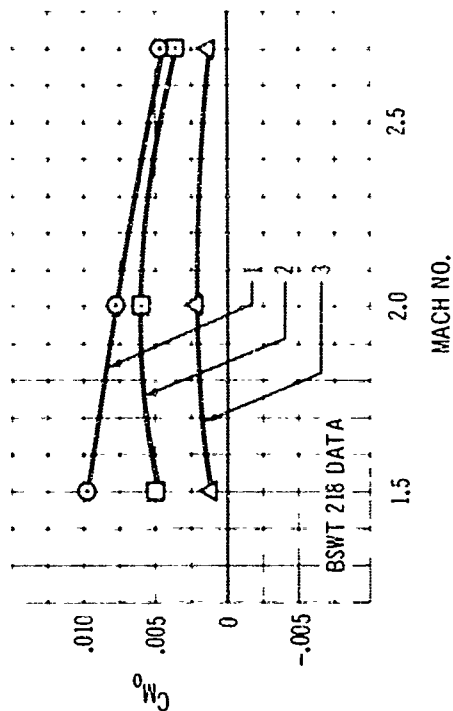


C 6-23. a. Effect of Nacelle Placement on L/D

in wing drag is greater than the increase in tail drag, negative trim drag results.

Fig. C6-32 presents trim drag increments for the Model 733-197 airplane along the basic mission profile.

The trim drag, as applied to the Model 733-197 airplane, was determined from wind tunnel data by constructing tail drag polars from a geometrically similar model.

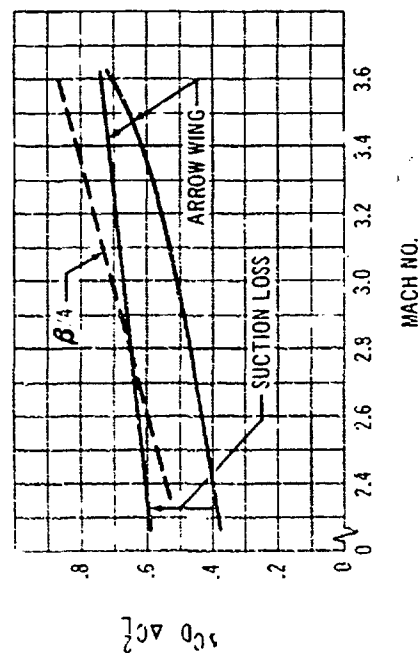


b. Effect of Nacelle Placement on C_{M_0}

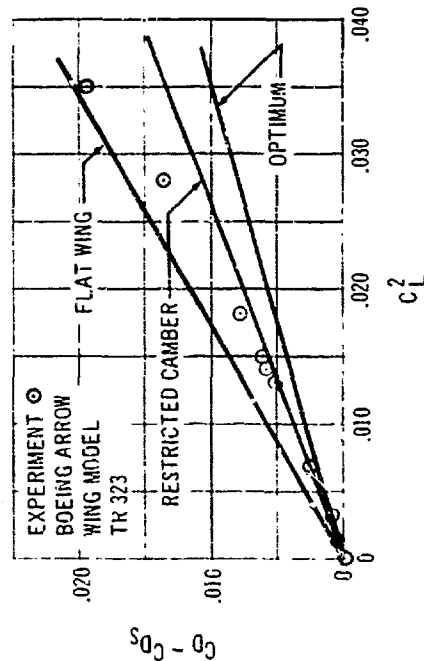
At constant body angle of attack the drag and lift increments of the tail are available from tail on versus tail off data. These polars obtained at various Mach numbers and sweeps were added algebraically to the wing-body-nacelle polars. Fig. C6-33 shows trim drag at a typical Mach number plotted as a function of the moment to be trimmed by the tail.

A representative longitudinal center of gravity location for determining trim drag for the basic mission was obtained by analysis of the airplane balance charts (see Fig. C6-35). This resulted in using 47 percent m.a.c. as an average c.g. location for the supersonic part of the mission. The effect of engine thrust on trim drag was accounted for by an incremental nose up moment, using the thrust minus pod drag for the basic mission.

Fig. C6-34 shows the tail load required to trim as a function of Mach number. It can be seen that this load is generally small. Therefore the trim drag of the airplane is relatively insensitive to small changes in lift coefficient



C 6-24 Drag Due to Lift of Arrow Wings



C 6-25 Effect of Design Method on Drag Due to Lift

and airplane takeoff weight. The latter would be expected to have a small effect on trim because of airplane flexibility. Figs. C6-36 thru C6-38 show trim drag as a function of Mach number, sweep, and lift coefficient for various locations of the center of gravity.

C6.2 Takeoff and Landing Configuration

C6.2.1 CONFIGURATION DESCRIPTION AND EVOLUTION

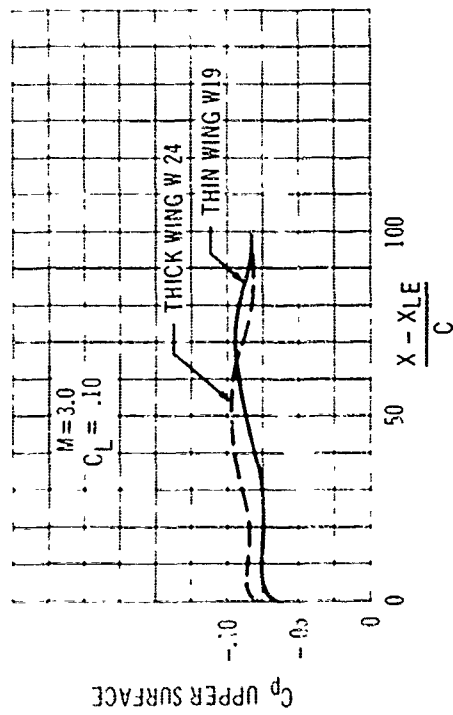
The high lift system used for takeoff and landing is shown in Fig. A2-3 in Appendix A. It consists of:

a. A double slotted flap on the swinging portion of the wing. This has an overall chord length of $0.3c$ (c = local wing chord) and consists of a main and auxiliary flap segment. The two flaps are deflected in sequence to yield the most favorable relationship between the lift-drag ratio and maximum usable lift coefficient.

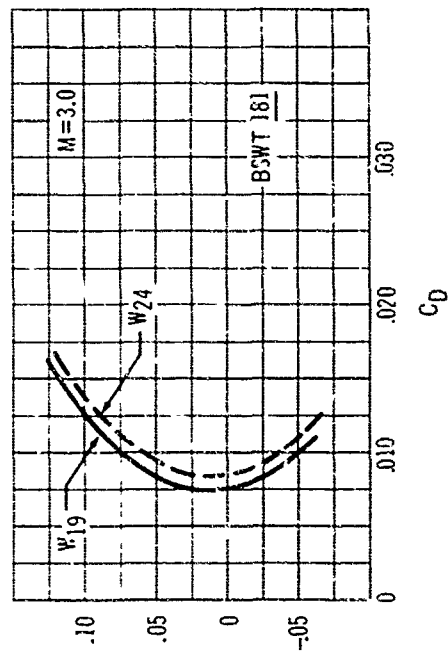
b. Plain center flaps at the wing root and a split flap beneath the fuselage. Plain flaps were chosen for compatibility with the fixed center wing structure. These flaps increase overall efficiency by giving a good span load distribution and contribute appreciably to emergency landing capability with wings back because of their unswept hinge line.

c. Curved leading edge slats along the wing leading edge outboard of the pivot. These suppress outboard wing stalling tendencies due to the thin wing sections, contributing to a high $C_{L_{max}}$ and good lift-drag ratio at climb-out and approach speeds. Additionally, they enhance the airplane lateral control qualities at low airspeeds.

For optimum efficiency of the high lift systems, it is necessary to minimize the influence of the upper-surface vortex (generated by the highly sweptback leading edge of the fixed inner wing) on the outer wing and flaps. Satisfactory performance is obtained with the aid of flow

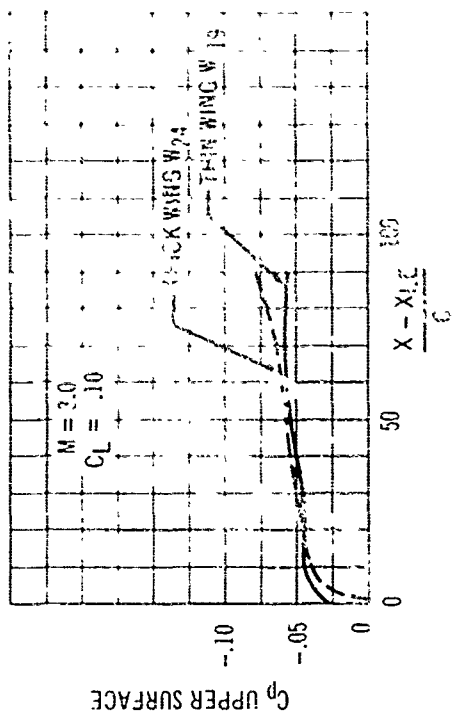


a Upper Surface Pressures at 80% Span

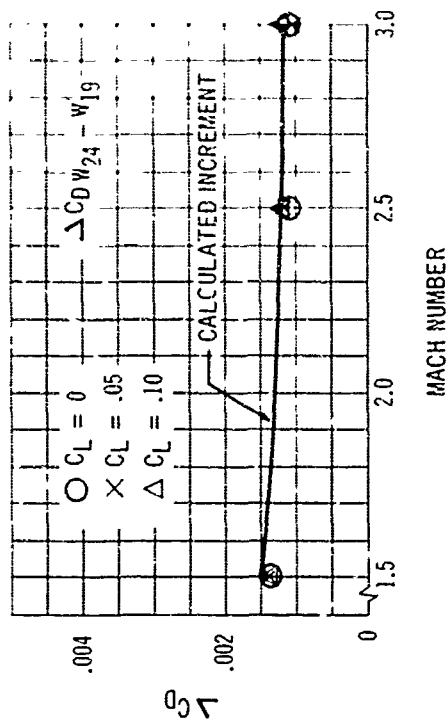


c Comparison of Polars

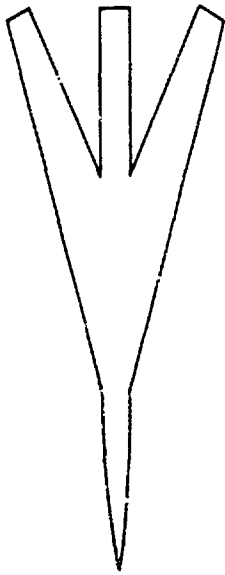
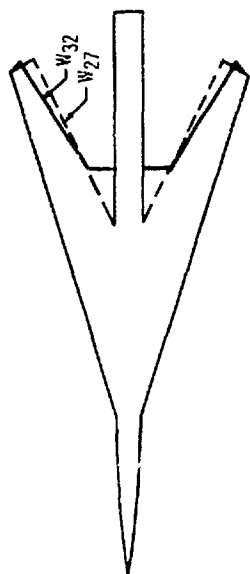
C 6-26 Effect of Thickness Tailoring on Drag Due to Lift



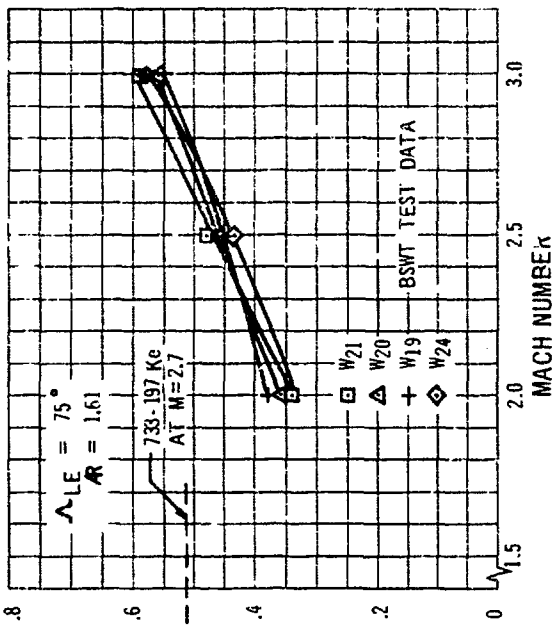
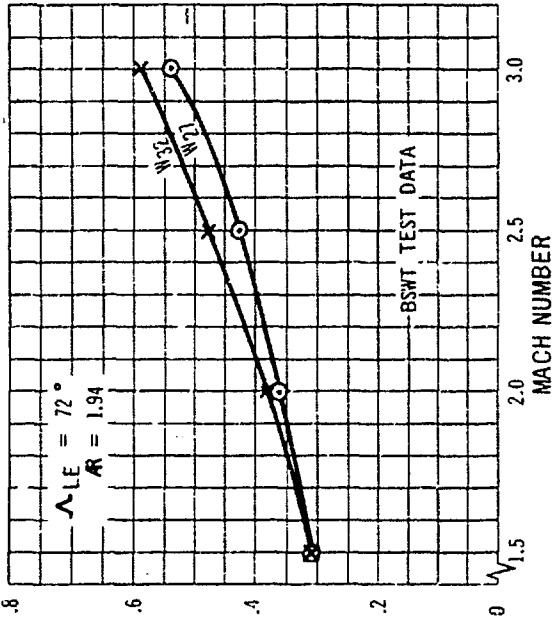
b Upper Surface Pressures at 20% Span



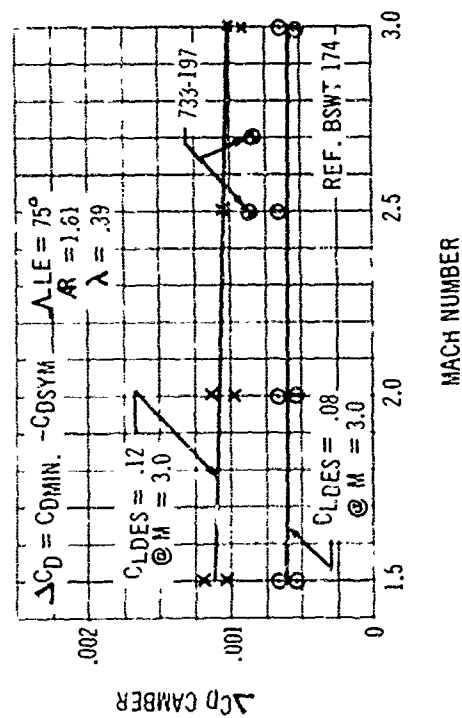
d Effect of Mach Number



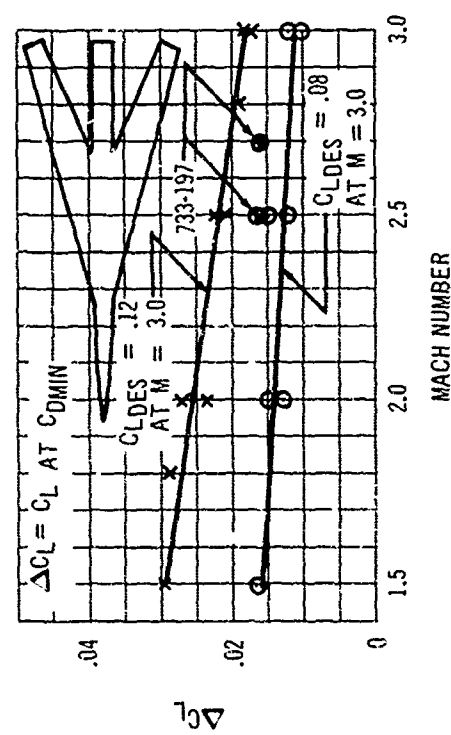
ENVELOPE DRAG DUE TO LIFT (KE)



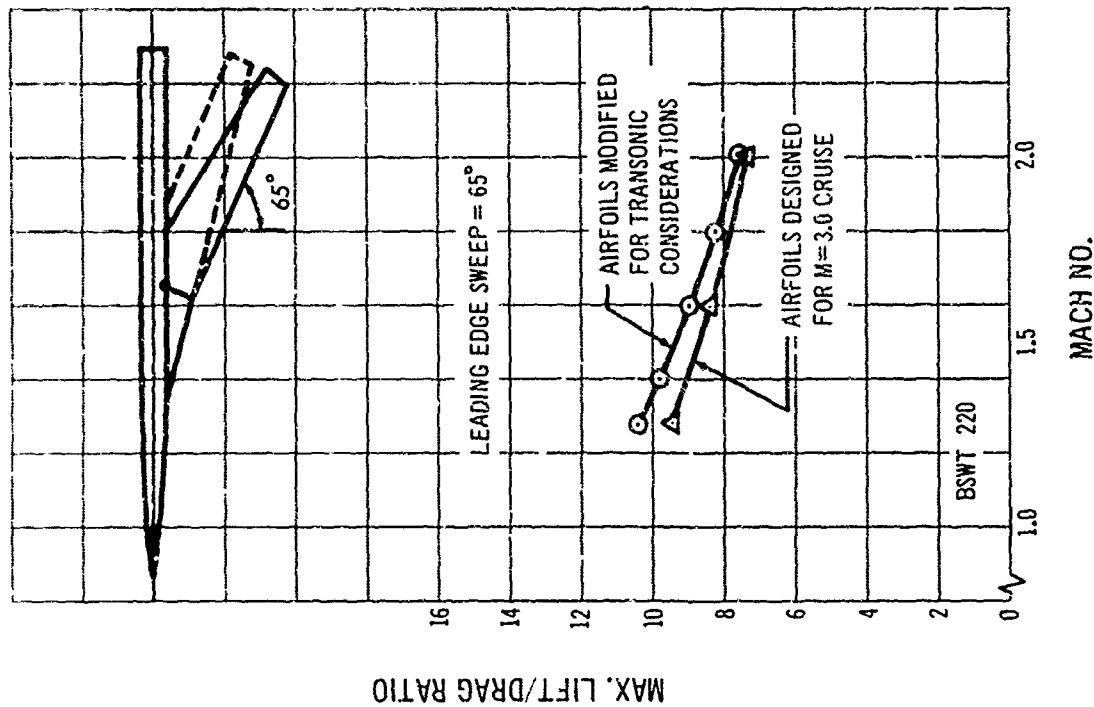
C 6-27 Measured Drag Due to Lift



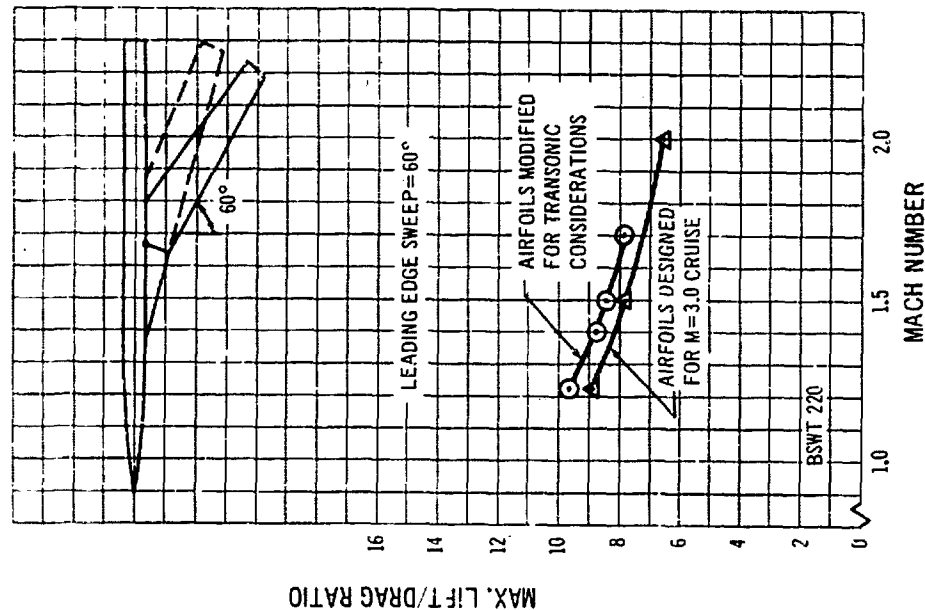
C 6-28 Camber Drag Increment



C 6-29 Camber Lift Increment



C 6-30 Lift/Drag Ratio $\Lambda = 65^\circ$



C 6-31 Lift/Drage Ratio $\Lambda = 60^\circ$

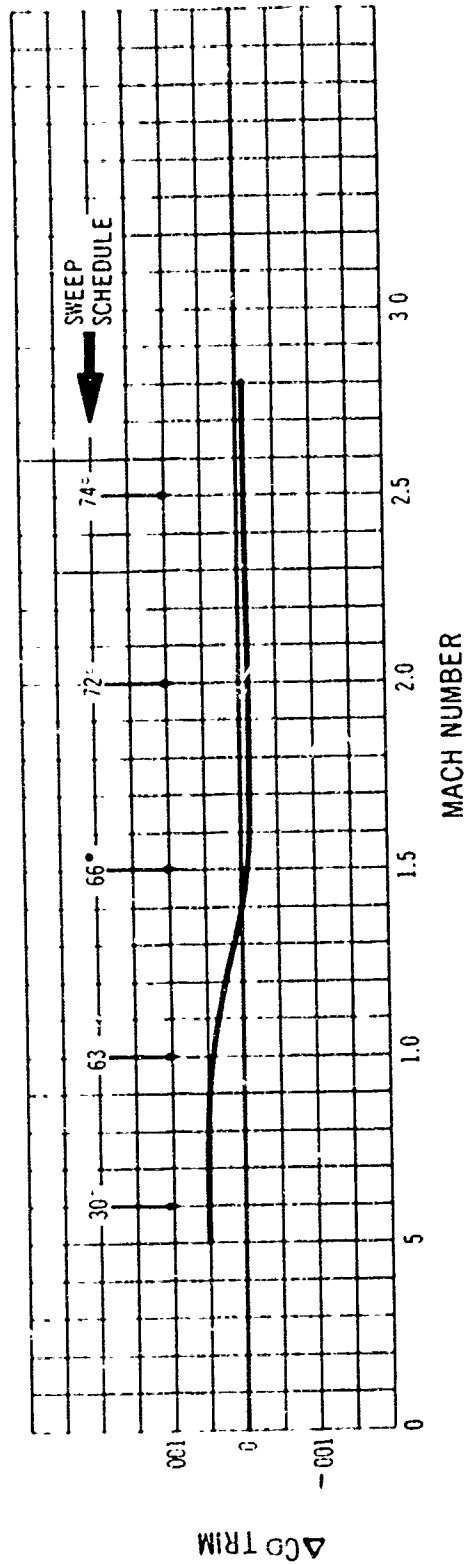
control devices which consist of a means for drooping and rounding the fixed wing leading edge, together with a wing fence and leading edge notch near the intersection of fixed and swing-wing leading edges.

Finally, the most suitable wing planform and spanwise twist distribution commensurate with the high-speed cruise wing design is obtained by the proper choice of taper ratio, wing pivot cant angle and aspect ratio. Within the range of wing sweepback angles of practical interest, namely about 10 degrees to 30 degrees, there is little variation in overall high lift performance. Sweep angle is, therefore, chosen to give an acceptable degree of longitudinal stability, which yields the lowest possible trim drag penalty.

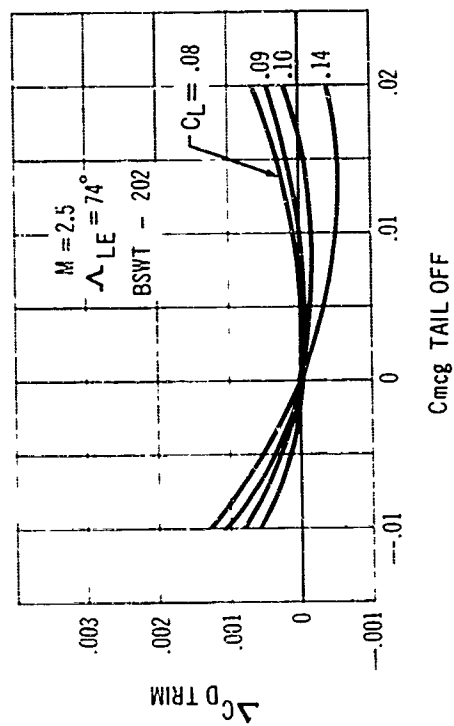
The high lift system of the Model 733-197 configuration proposed by The Boeing Company has been simulated in the wind tunnel to provide the basis for the substantiation of the low-speed performance estimates. The model used for these tests is shown in Figs. C6-39a and C6-39b. Single and double slotted flaps of various span, leading edge slats, and leading edge droop have been included in the testing of this configuration.

The Model 733-197 configuration has the wing hinge located at 37.8 percent semi-span. This outboard location has a favorable effect on wing weight, but care must be taken to ensure that good stability and performance characteristics are retained at low airspeeds. These characteristics have been demonstrated to be excellent in wind tunnel tests of the final Model 733-197 configuration. In addition, tests have shown satisfactory low speed performance with the wings fully swept, with and without flaps deflected, providing the basis for analysis of the landing capability of this aircraft with the wings fully swept. Included in this testing was the effect of the ground plane (see Fig. C6-40).

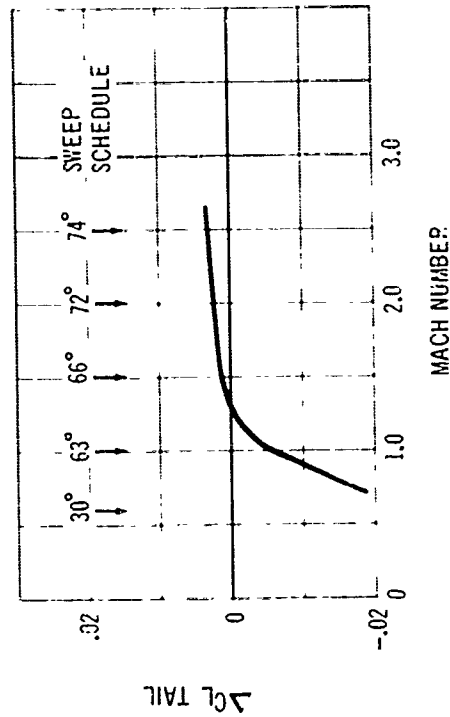
During recent low-speed wind tunnel tests conducted by The Boeing Company emphasis has been placed on visual flow runs using tufts on the upper surfaces of the



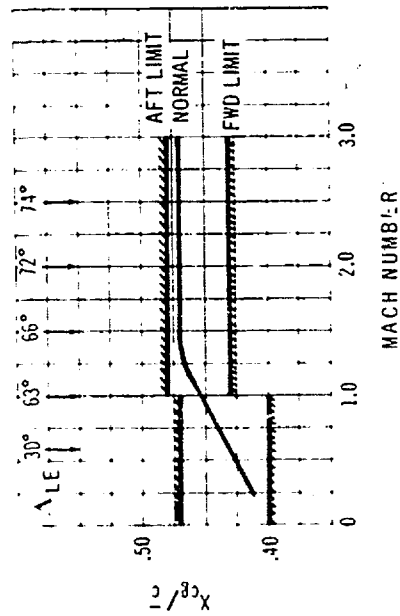
C 6-32 Trim Drag for Basic Mission



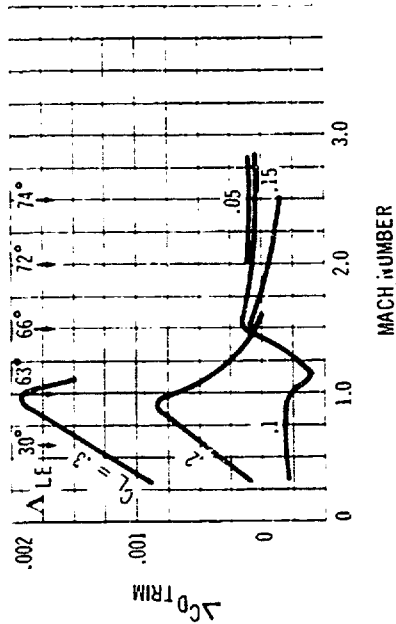
C 6-33 Effect of Pitching Moment on Trim Drag



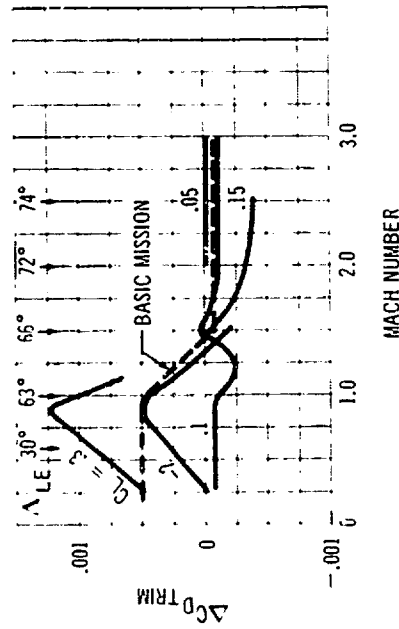
C 6-35 Tail Loads for Basic Mission



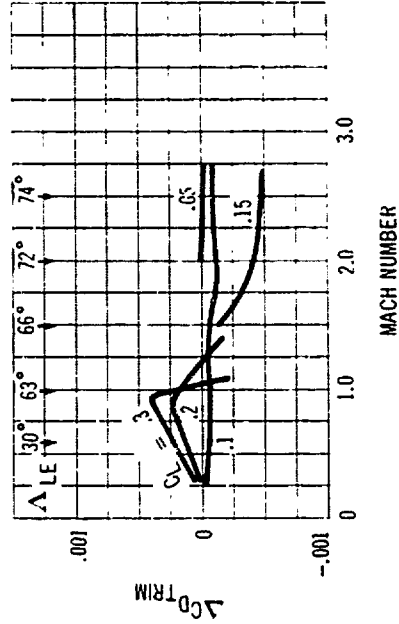
C 6-34 733-197 CG Position



C 6-36 733-197 Trim Drag; CG at Fwd. Limit



C 6-37 733-197 Trim Drag; Normal CG Position



C 6-38 733-197 Trim Drag; CG at Aft Limit

wing and strake (See Fig. C6-41). As a result, considerable progress has been made in the understanding of the flow behavior peculiar to the variable sweep wing planform, and means of reducing unfavorable interference of the strake on the outer wing have been demonstrated.

A strong vortex flow appears under lifting conditions over the upper surface of the strake due to the high sweep angle of the leading edge. Both visual flow runs and force data from wind tunnel tests indicate that the nature of this vortex flow is sensitive to the shape of the strake leading edge. As indicated in Fig. C6-42, a marked improvement in both drag and pitching moment characteristics result from contouring the leading edge on the strake. This effect is present for all flap angles including zero (flaps up). Contouring the strake leading edge does not in itself result in satisfactory behavior to the angle of attack for maximum lift, however, since the spanwise propagation of the flow from the portion of the wing behind the strake to the portion outboard of the strake also has an adverse effect on stability.

The positioning of a wing fence in the region of the wing-strake juncture has been demonstrated to be effective in preventing spanwise flow. As indicated in Fig. C6-43, the combination of the fence with the contoured leading edge on the strake results in an increase in maximum lift and a satisfactory stability behavior through the angle of attack at which the outer wing stalls. This effect is present at all flap angles.

The benefits obtained through positioning of an inboard flap behind the strake have been substantiated by wind tunnel test data. The main attributes of a flap in this region are a high effectiveness due to the flap hinge line being unswept (this is particularly important if a wings-back landing is to be made), a stronger downwash in the vicinity of the tail, which results in a lower trim drag, and a higher maximum lift capability.

A double slotted main flap has been selected for the Model 733-197 configuration to provide a high level of

low speed performance. Wind tunnel test results comparing single and double slotted flaps show a higher lift to drag ratio at $1.2V_s$ for a given maximum lift coefficient and a greater ultimate maximum lift capability for the double slotted flaps (See Fig. C6-44).

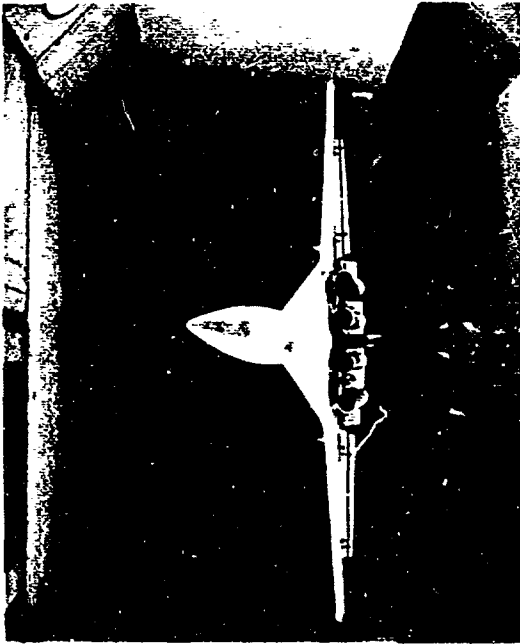
With the aid of simple flow control devices, such as the combination of a contoured strake leading edge and a wing fence, the variable sweep wing can be expected to provide: (1) a low speed performance capability with flaps deflected equivalent to that of present subsonic jet aircraft; (2) satisfactory stability characteristics through an angle of attack at which the outer wing panel stalls; and (3) acceptable pitching behavior at the stall.

C6.2.2 TAKEOFF AND LANDING SPEEDS AND ATTITUDES (3.2.7)

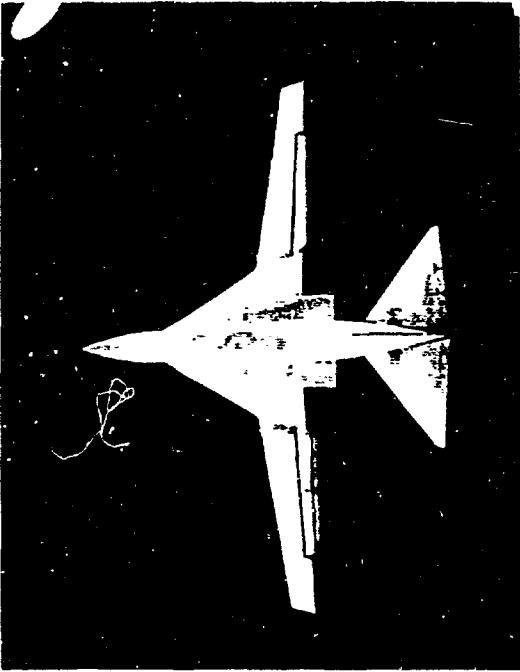
C6.2.2.1 Takeoff Speeds

The critical CAR speeds pertaining to takeoff are shown as functions of airplane thrust to weight ratio in Fig. C6-45. These have been derived to meet the requirements of CAR SR 422B. However, the reference stall speed V_s has been interpreted as $V_{s_{min}}$, the one g minimum level flight speed, power off, to conform with the FAA, Tentative Airworthiness Objectives and Standards for Supersonic Transport Design Proposals. The major impact of the proposed rules change is through its influence on the minimum takeoff safety speed (V_2). If a 0.9 load factor is taken to be an average value at the present CAR stall, then SR 422B would permit a takeoff safety speed (V_2) of $1.2V_s$, about five percent lower than the corresponding value of $1.2V_{s_{min}}$.

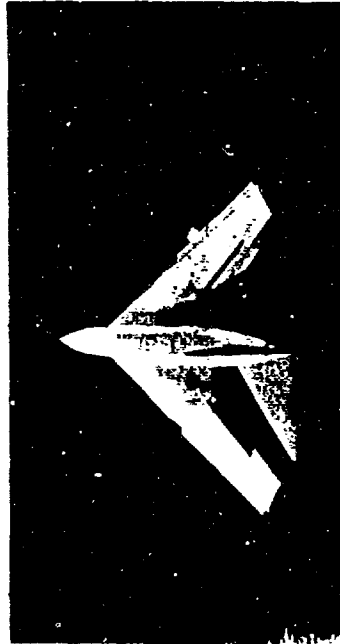
Lift off speeds are dictated by the takeoff safety speed (V_2) at low and medium thrust to weight ratios (T/W). The lift off speed is, therefore, chosen to assure the attainment of the takeoff safety speed V_2 at 35-foot altitude. For takeoff at higher T/W 's, lower liftoff speeds become possible and, since the airplane is geometry-limited, it appears that the $1.08 V_{s_{min}}$ rule will govern the liftoff speed.



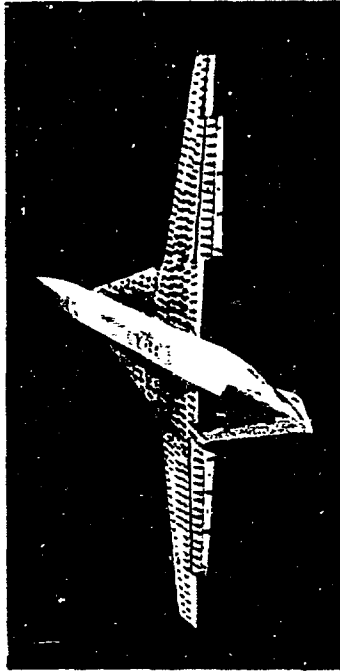
C 6-39 a. Wind Tunnel Model for Low Speed, High-Lift Testing



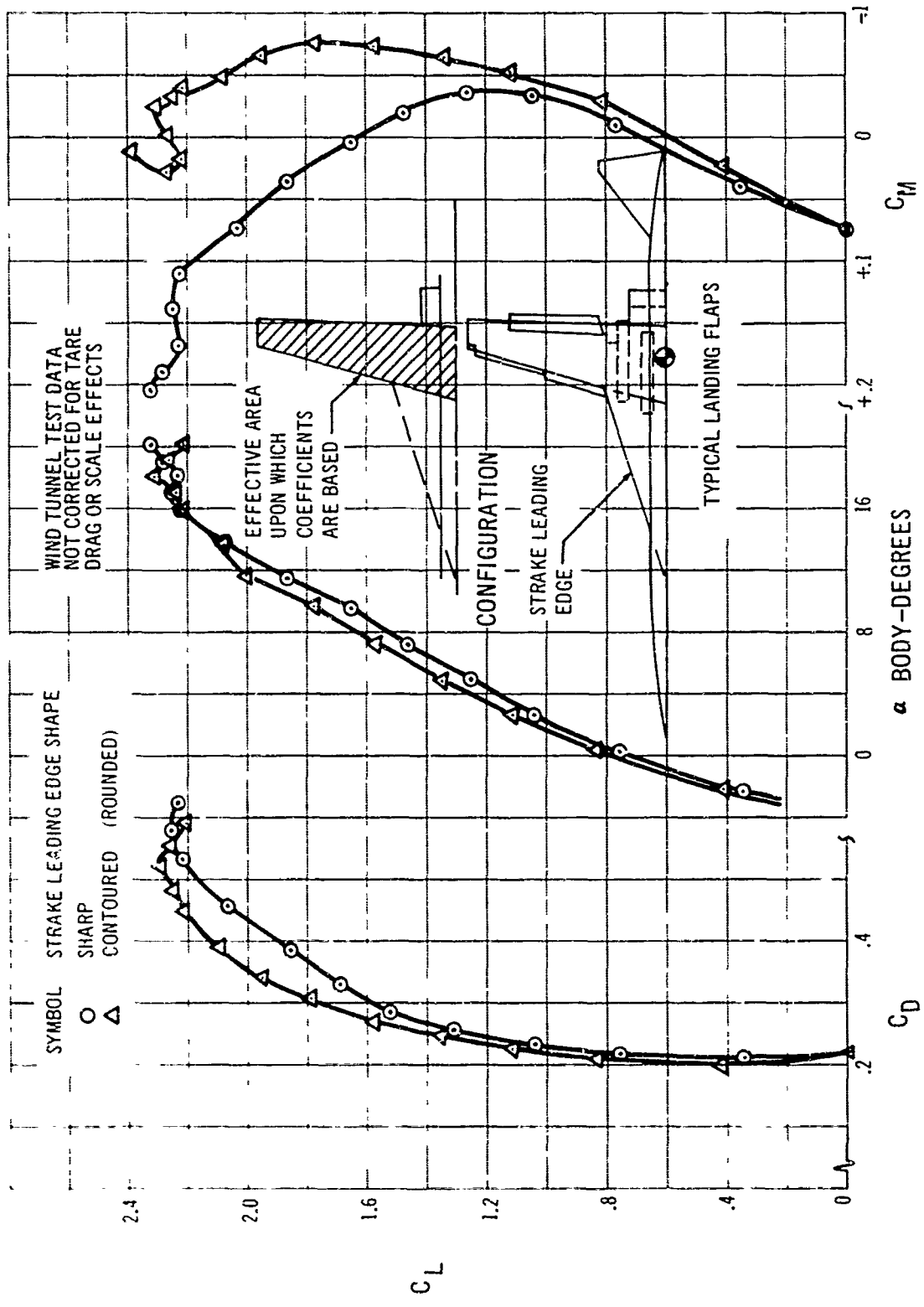
C 6-39 b. Wind Tunnel Model for Low Speed, High-Lift Testing



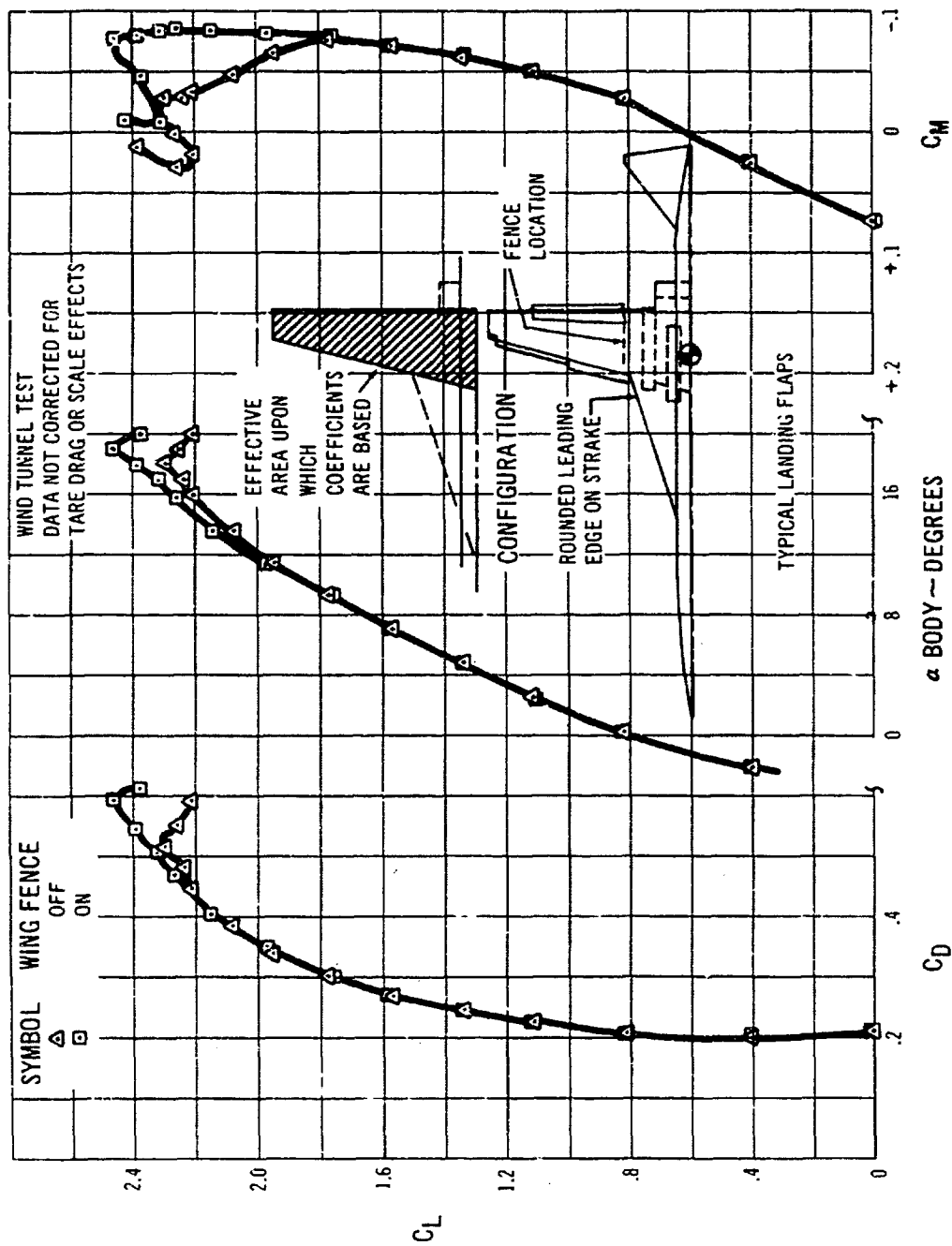
C 6-40 Wind Tunnel Model for Low Speed Testing With Wings Fully Swept



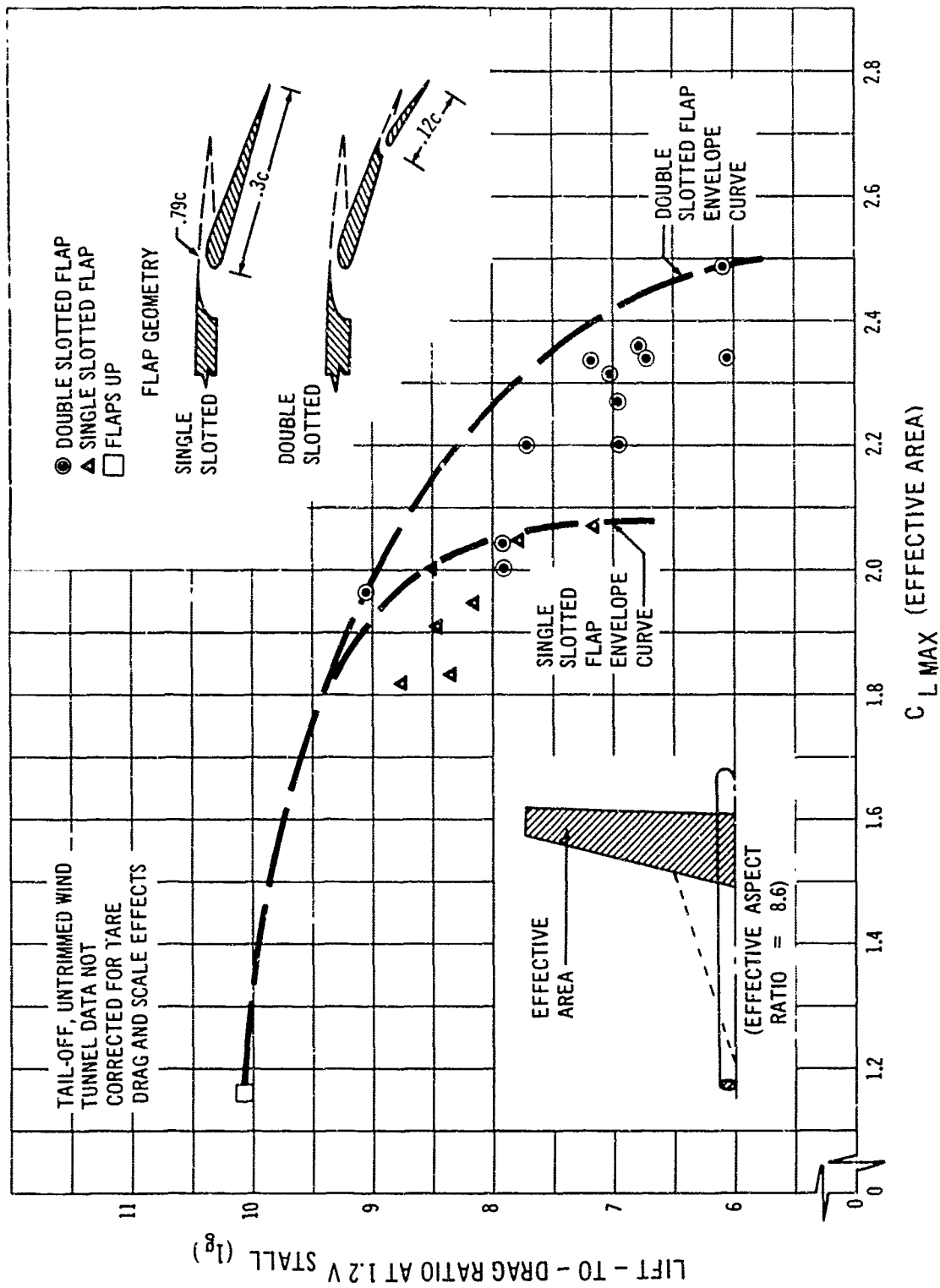
C 6-41 Low-Speed Wind Tunnel Model with Tufts for Visual Flow Runs



C 6-42 Effect of Stroke Leading Edge Shape



C 6-43 Effect of Wing Fence



C 6-44 Double and Single Slotted Flap Performance

Rotation speeds and minimum control speeds have been checked against the relevant criteria of SR 422B. Their derivations are discussed in Section 7.0 of this document. V_1 , the critical engine failure speed, has been determined from balanced field length calculations. It is greater than V_{MC} and less than V_R .

C6.2.2.2 Takeoff Attitudes

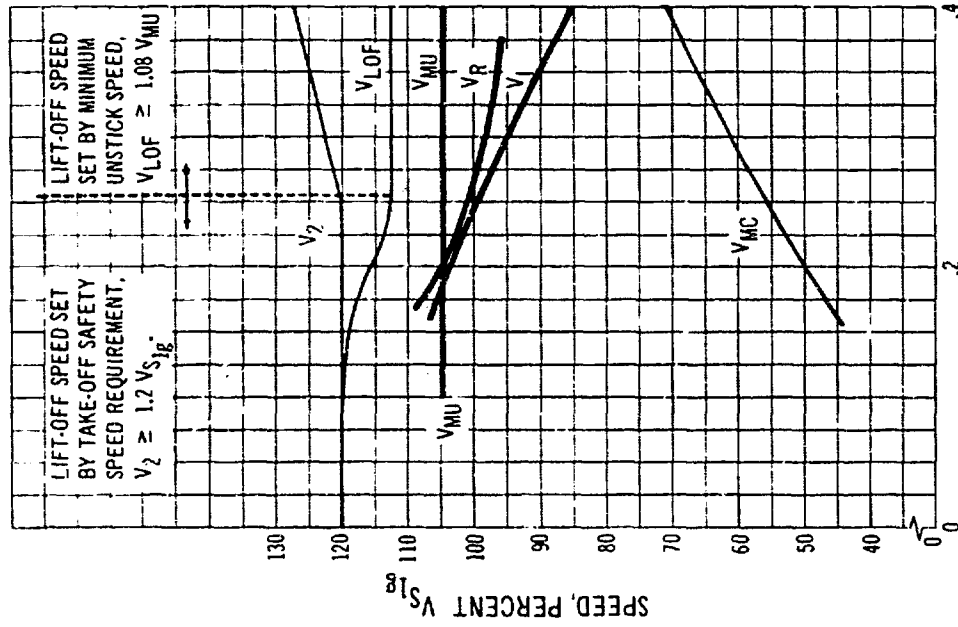
Angle of attack (α_H) is quoted for the airplane body reference line, which is parallel to the forward main cabin floor.

In normal configuration, with its ventral fin on, the maximum possible airplane body attitude for takeoff, with gear oleos fully extended is $\alpha_H = 12$ degrees. Normal lift off will be at $\alpha_H = 9.4$ degrees or less. For demonstration of minimum unstuck speed (V_{MU}), the maximum body angle of attack will be in excess of 13.4 degrees with ventral fin removed and a tail skid fitted.

A comparison of the Model 733-197 supersonic transport liftoff and climb (at 1.2 V_s) body attitudes with the corresponding values for a present-day subsonic jet is shown; no significant differences are found.

TABLE C6-B

Body Attitudes Relative to Horizontal — Takeoff (Nose Up)		
Thrust Weight Ratio	Airplane	
	Supersonic Transport	Subsonic Jet
.25	1.13 V_{st} , 9.4°	1.2 V_s , 9°
.25	1.2 V_{st} , 16.4°	1.27 V_s , 16.5°
		Climb at takeoff safety speed, $\gamma = 7^\circ$



THRUST/WEIGHT RATIO AT LIFT-OFF
(ACTUAL T/W, 3 OR 4 ENGINES OPERATING)

C 6-45 Takeoff Speeds

C6.2.2.3 Landing Speeds

A landing approach speed of $1.3 V_{\infty}$ is permitted by the present CAR SR 422B rules. This is typically about seven knots slower than the target approach speed of $1.3 V_{\infty}$ proposed by the Flight Standards Service of the FAA for the supersonic transport. At either approach speed the airplane handling qualities and flare capability are excellent. Speed stability is good and is covered in Section B.3.8.5.

Speed bleed-off to touchdown is mainly a function of flying technique and this, in turn, is adapted to suit the characteristics of the airplane. The Model 733-197 airplane is very similar in all respects to present day jet transport airplanes in its low speed configuration. It will have essentially the same landing qualities and a touchdown speed of approximately $0.94 V$ approach is predicted on the basis of past experience.

C6.2.2.4 Landing Attitude

Airplane attitudes relative to horizontal are shown for a typical landing in Table C6-C. The airplane pitch angles demanded are always moderate, providing for good visibility at all times. Body attitudes of a typical present-day subsonic jet airplane are also shown for comparison purposes. The supersonic transport has a lower body angle throughout the approach and landing, thus providing improved visibility.

- TABLE C6-C -

Body Attitudes Relative to Horizontal — Landing (Nose Up)		
Airplane		Condition
Supersonic Transport	Subsonic Jet	
$1.3 V_{\infty}$, 0.6°	$1.3 V_{\infty}$, 2.2°	Approach (3° glide slope)
$1.22 V_{\infty}$, 2.6°	$1.22 V_{\infty}$, 4.2°	Touch-down (in ground effect, 1° descent angle)

C6.2.2.5 Landing Speed and Attitude, Wings Swept 74 Degrees

The maximum usable angle of attack for V_{min} is considered to be 20 degrees which corresponds to a lift coefficient of 0.90.

At $1.3 V_{min}$, the lift coefficient would be 0.53, requiring an angle of attack of α_{Total} 12 degrees. This is considered excessive, so an angle of attack of 10 degrees is recommended, giving an approach speed of $1.41 V_{min}$.

Body attitude during approach with a three degree glide slope will be seven degrees nose up (relative to horizontal). At touchdown, with a descent angle of 0.5 degrees ($2.6 \text{ ft./sec. vertical velocity}$), the body attitude will be approximately 8.5 degrees.

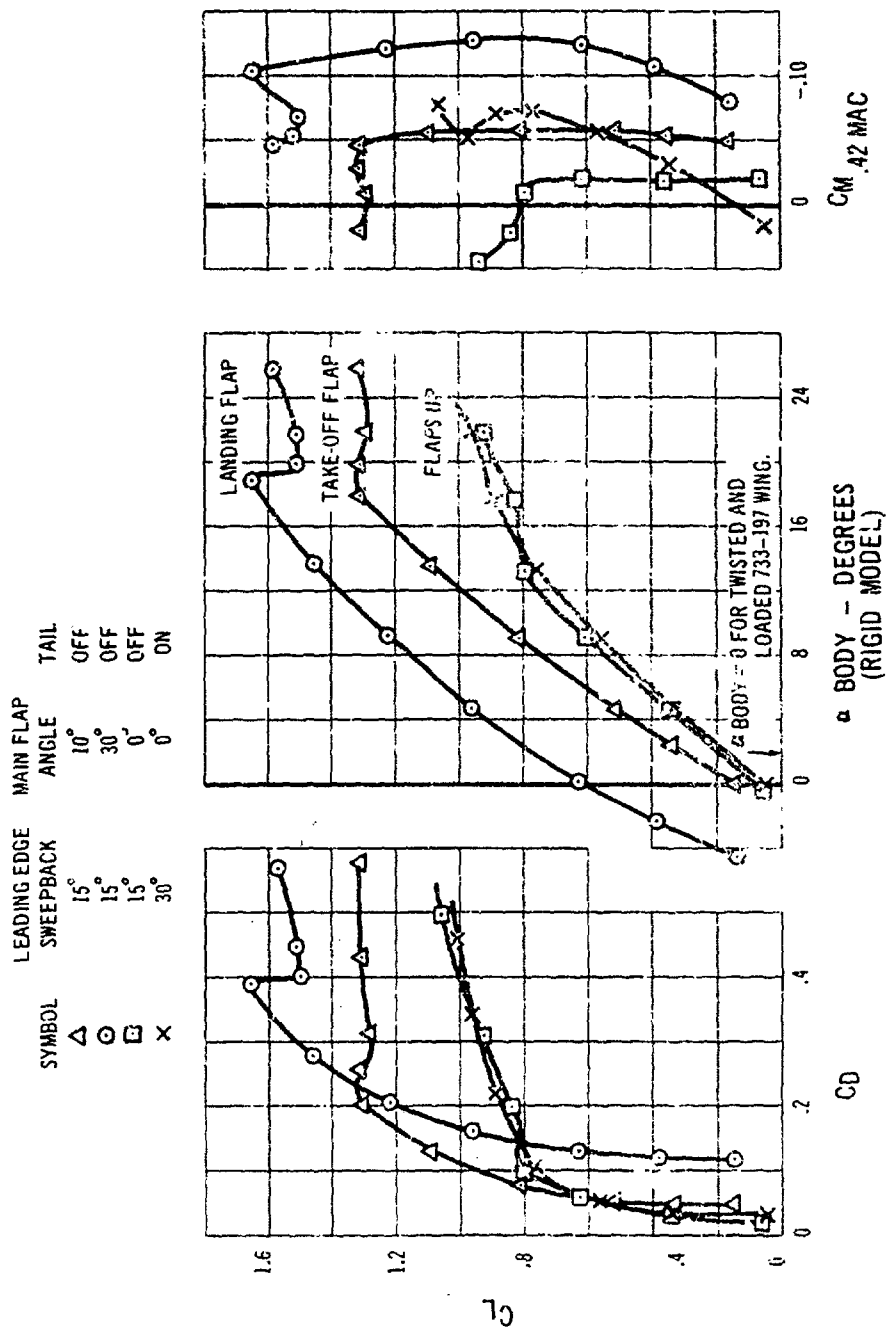
C6.2.3 STALLING CHARACTERISTICS

At takeoff and landing flap settings, the lift curves, drag polars and pitching moment characteristics are conventional, see Fig. C6-46. Stall angles are 19 degrees in both configurations. The lift curves break gently and the lift loss is small; this will ensure good handling qualities with no wing dropping tendencies. Drag shows a normal polar shape right up to the stall.

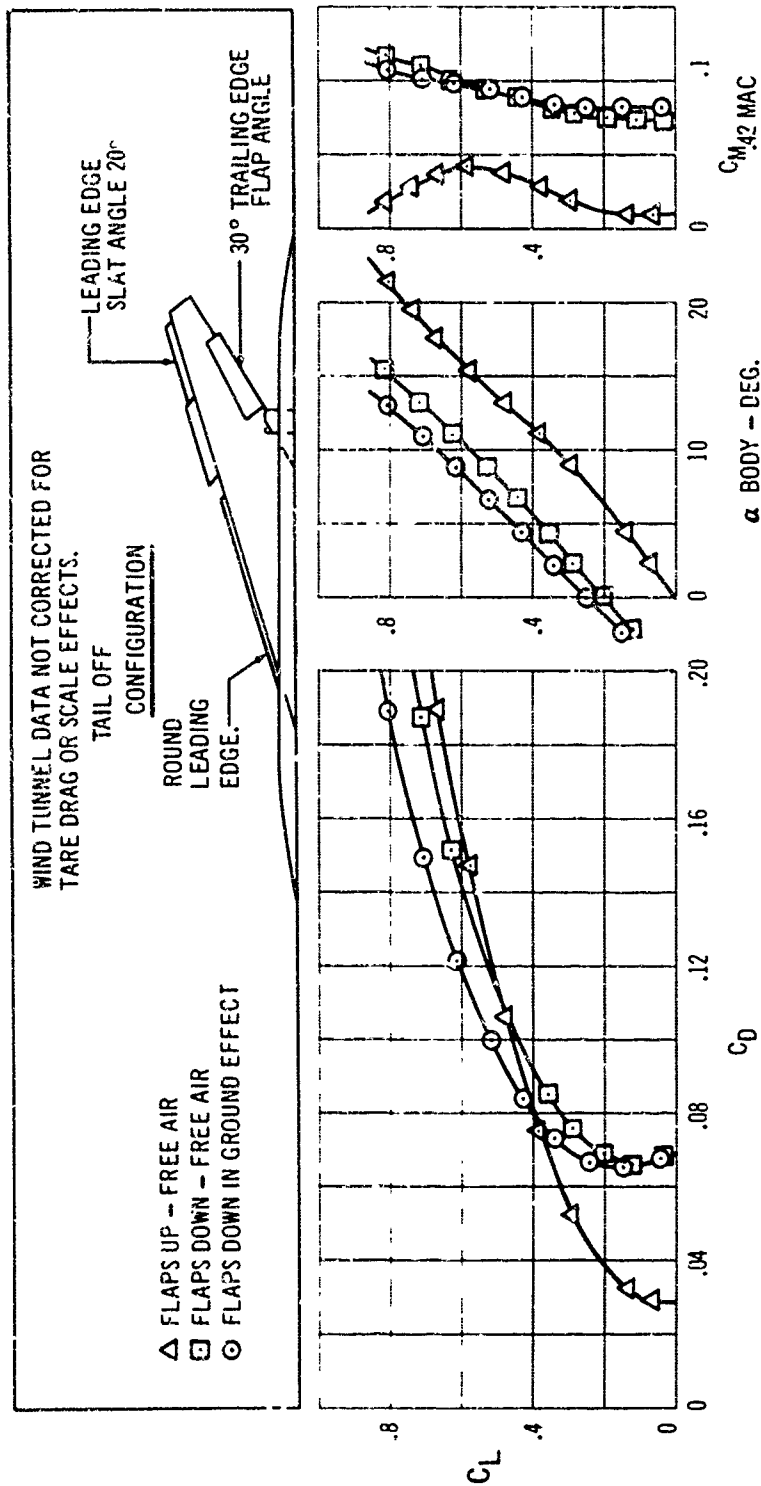
With flaps up, wing swept 30 degrees, the wing does not exhibit a conventional stall pattern. Lift continues to increase up to angles of attack in excess of 30 degrees with a jog in the curve where the outer wing panels become essentially stalled. This occurs at about 18 degrees to 20 degrees angle of attack. Since the appearance of stalled flow on the wing can lead to airframe buffet, deterioration of lateral control, etc. and because the angle of attack is close to the flaps-down stall angle, it is proposed to define the lift in this region as the maximum usable value.

At 74 degrees wing sweep, see Fig. C6-47, a similar situation prevails. Again, the lift continues to increase up to very high angles of attack and an effective maximum usable lift coefficient will be defined at $\alpha_{Total} = 20$ degrees.

MODEL TEST DATA, REYNOLDS NUMBER 2.86×10^6 , NOT CORRECTED FOR TARE OR SCALE EFFECTS



C 6-46 Lift, Drag and Pitching Moment - Low Speed Configuration



C 6-47. Lift, Drag and Pitching Moment, Wing Sweep

C6.2.4 WIND TUNNEL TEST DATA

C6.2.4.1 Lift, Drag and Pitching Moment, Wing Sweep 20 Degrees

Tail-off three component force and moment data are shown for the low speed flight configurations used in takeoff and landing in Fig. C6-46. Model testing was accomplished with wing sweep angles of 15 degrees and 30 degrees, showing a very small influence of this parameter on trimmed $C_{L_{max}}$ and L/D ratio for a fixed level of air-

plane stability. Thus, test data for 15 degrees sweep is considered representative of the Model 733-197 configuration with its flaps-down sweep angle of 20 degrees. This is the data shown.

Other details in which the test configuration differed from the proposed configuration which finally evolved included minor differences in flap span, wing taper and aspect ratio. Standard corrections were applied to allow for these differences in producing the full scale data, as described in Par. C6.2.5.

C6.2.4.2 Lift, Drag and Pitching Moment, Wing Sweep 74 Degrees

Tail-off wind tunnel data is shown in Fig. C6-47 for a low speed model with flaps up and down. Ground effects are included. The tests were made with a wing leading edge sweep angle of 72 degrees, but are representative of the actual 74 degrees sweepback of the Model 733-197 airplane.

The three component data are normal in all respects. A considerable lift increment is obtained from the deflection of the flaps, although the inboard portions of the double slotted flaps cannot be extended at this sweep angle because they are locked in the fixed wing root section. The center plain and split flaps play a large part in producing this lift increment.

C6.2.5 CORRECTIONS APPLIED TO WIND TUNNEL RESULTS

C6.2.5.1 Scale Corrections

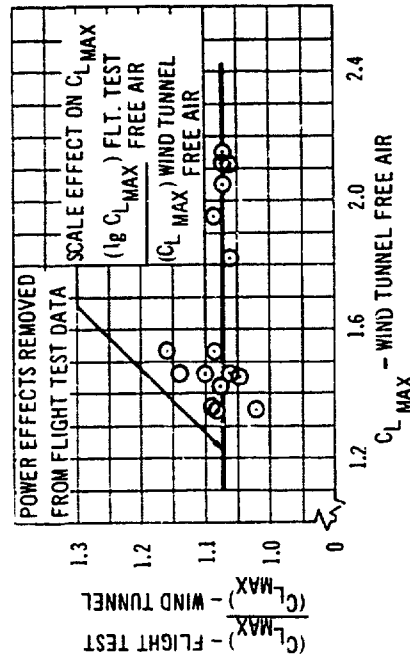
Lift and drag measured in the wind tunnel has been corrected to full scale conditions by well established methods which are the result of correlations between flight measurements and wind tunnel data on models of the same configurations.

a. DRAG — Drag is corrected for model mounting tares and turbulent skin friction drag variation with Reynolds number (transition is fixed on the wind tunnel model by transition strips on all components).

b. LIFT — Lift and $C_{L_{MAX}}$ are corrected to typical flight conditions by applying the empirical factor shown in Fig. C6-48. This factor was derived for $C_{L_{MAX}}$, but has also been applied to lift at all angles of attack since it is smaller than (and hence more conservative than) the calculated theoretical correction to lift from turbulent boundary layer theory.

C6.2.5.2 Other Corrections

Other corrections to the measured wind tunnel data were



C 6-48 Scale Effect on Lift

for:

Flap Span/Wing Span, Refs. 36 and 37

Wing Aspect Ratio, Ref. 36

Ground Effects, Ref. 38

Effect of ground proximity on $C_{L_{MAX}}$ is shown in Fig. C6-49. This has been derived from extensive full scale and model test data by The Boeing Company.

C6.2.5.3 Trim Increments

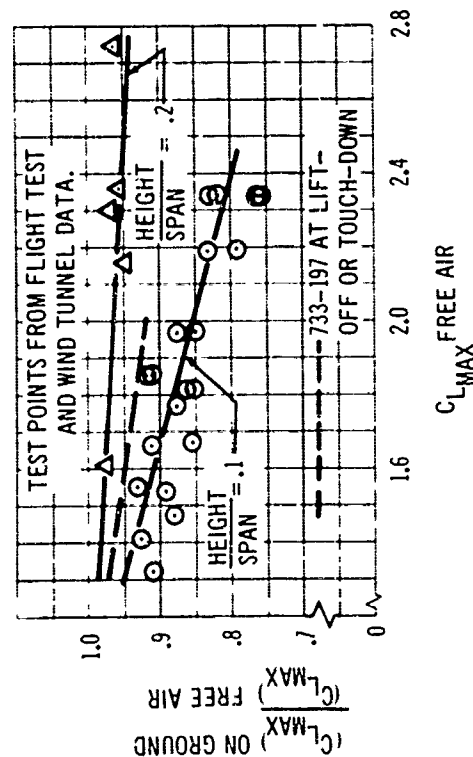
Trimmed aircraft drag polars were derived by adding appropriate increments to lift and drag for the airplane center of gravity location under consideration.

Trimmed lift = tail-off lift + $\frac{\text{pitching moment}}{\text{tail arm}}$

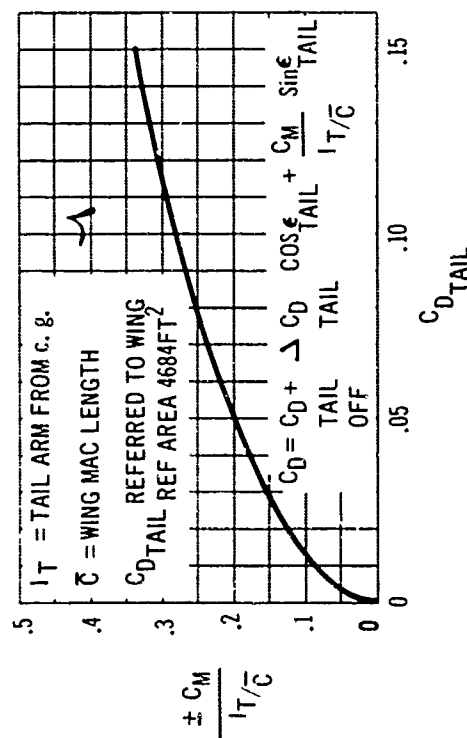
Trimmed Drag = tail-off drag + $\frac{(\text{pitching moment})}{(\text{tail arm})}$

$(\sin \epsilon_{tail}) + (\text{tail drag}) (\cos \epsilon_{tail})$ and,

tail drag = drag of horizontal tail with its lift equal to $\frac{\text{pitching moment}}{\text{tail arm}}$



C 6-49 Ground Effects on C_{LMAX}



C 6-50 Drag of Horizontal Tail

Wind tunnel tests showed that the tail drag coefficient was equal to 80 percent of (C_{LMAX}) . $\tan \alpha_{max}$, a result indicating that less than one-third of the theoretical leading edge suction force was being realized despite the favorable effect of deflecting the elevator for trim at large tail lift coefficients. This is typical of highly sweptback planforms with sharp leading edges. Tail drag coefficient is shown plotted against tail C_L in Fig. C6-50.

Fig. C6-51 shows the tail downwash values obtained from wind tunnel testing. These are quite normal values, changing with lift and flap angle.

C6.2.6 COMPARISONS WITH FLIGHT TEST AND OTHER DATA

The tail-off lift and maximum lift increments obtained on the SST airplane are of a level which is commensurate with those of other flap systems developed over many years of research by The Boeing Company. This may be illustrated in the following manner:

a. **LIFT INCREMENT** — Lift increment due to flaps at constant angle of attack may be written:

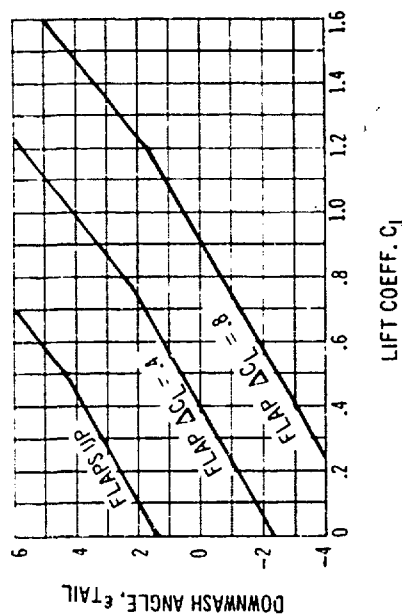
$$\Delta C_L = \frac{dC_L}{d\alpha} \cdot \frac{d\alpha}{d\delta_F} \cdot \delta_F \times \left[\frac{\text{area of flapped part of wing}}{\text{reference area of wing}} \right]$$

$$= \frac{dC_L}{d\alpha} \cdot \frac{d\alpha}{d\delta_F} \cdot \delta_F \cdot \frac{S_{FW}}{S_W}$$

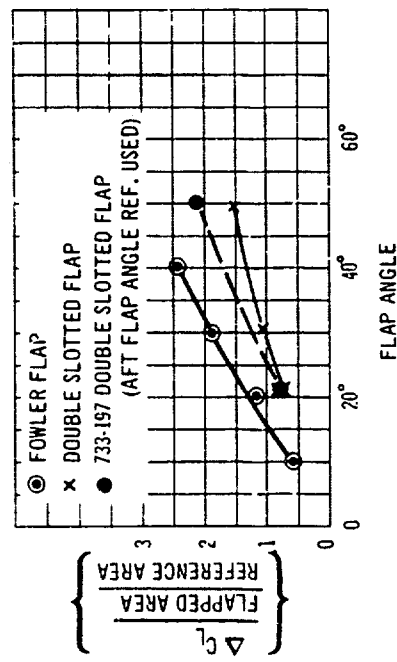
Thus $\frac{\Delta C_L}{\left[\frac{S_{FW}}{S_W} \right]}$, which equals the product $\frac{d\alpha}{d\delta_F} \cdot \delta_F \cdot \frac{dC_L}{d\alpha}$

may be plotted against the effective flap angle δ_F and the resulting curve compared with other flap systems in order to evaluate its lifting efficiency in a relative sense. The Model 733 flap system has been compared with other typical jet airplane systems in Fig. C6-52 from which it can be seen that a high level of efficiency has been obtained.

b. **C_{LMAX} INCREMENT** — The increase in C_{LMAX} from the flaps-up value may also be related to $\frac{\text{reference wing area}}{\text{flapped wing area}}$



C 6-51 Downwash Angle at Horizontal Tail



C 6-52 Flap Lift Comparisons at $\alpha = 4^\circ$

This includes the influence of the wing leading edge and other flow control devices (such as fences, notches, or whatever may be used as a part of the overall high lift configuration).

The Model 733 flap values of $\left[\frac{\Delta C_{L_{max}}}{S_w} \right]$ Flaps Down --- $C_{L_{max}}$ Flaps Up are

plotted against flap angle in Fig. C6-53 for comparison with other proven flap systems. Again, on this basis, the flap is shown to give a reasonable level of efficiency.

C. TRIMMED AIRPLANE LIFT/DRAG RATIOS WITH FLAPS DOWN

A common and satisfactory approximation to an airplane drag curve is of the form,

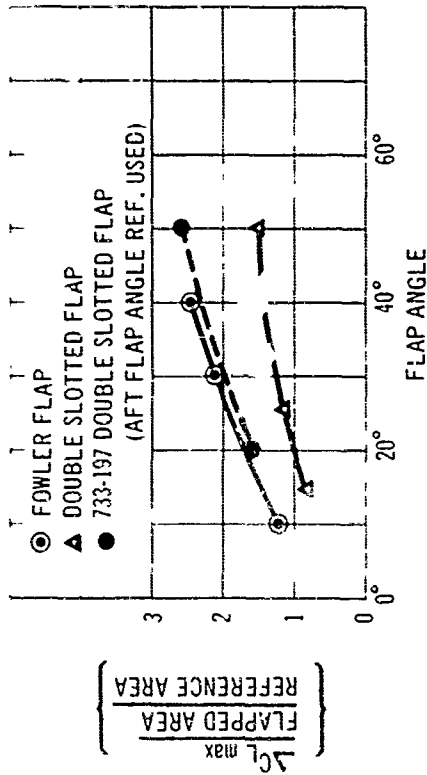
$$C_D = C_{D0} + \frac{C_L^2}{\pi AR} + K \frac{(\Delta C_{L_{max}})^2}{\pi AR}$$

where the first term of the equation is profile drag, the second term is minimum vortex drag with elliptic loading, and the third term is non-elliptic loading vortex drag due to part span flaps. K is constant usually about 1.0.

$$\begin{aligned} \frac{C_D}{C_L} &= \frac{C_{D0}}{C_L} + \frac{C_L}{\pi AR} + K \left[\frac{\Delta C_L}{C_L} \right]^2 \frac{C_L}{\pi AR} \\ &= \frac{C_{D0}}{C_L} + \frac{C_L}{\pi AR} \left[1 + K \left(\frac{\Delta C_{L_{max}}}{C_L} \right)^2 \right] \end{aligned}$$

Lift/drag ratio is the inverse of the foregoing.

It follows that a plot of $\frac{C_D}{C_L}$ or $\left(\frac{C_D}{C_L} \right) = \text{Lift/drag ratio}$ against $\frac{C_L}{\pi AR}$ will shed interesting light on the aerodynamic cleanliness of an airplane when the plot is compared with those for other airplanes. A special significance is achieved if the curve plotted is the envelope of (L/D) at 1.2 V_{st} (the minimum take-off safety speed, a critical condition for takeoff climb) as flap angle changes. This has been



C 6-53 Flap Comparisons at Maximum Lift

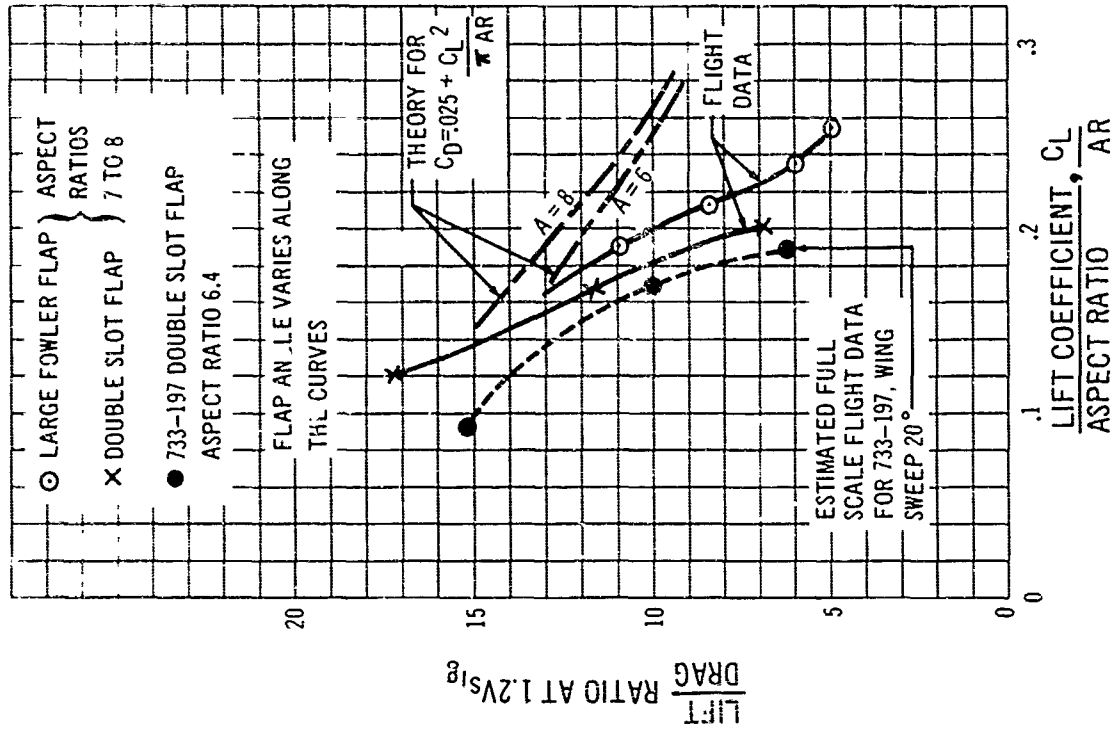
done in Fig. C6-54 where the predicted full scale values for the Model 733-197 are compared with similar values for different airplanes. Theoretical curves are also given for two values of aspect ratio, which has a fairly weak influence in this presentation.

It would appear that the values predicted for the Model 733 are of a good performance level.

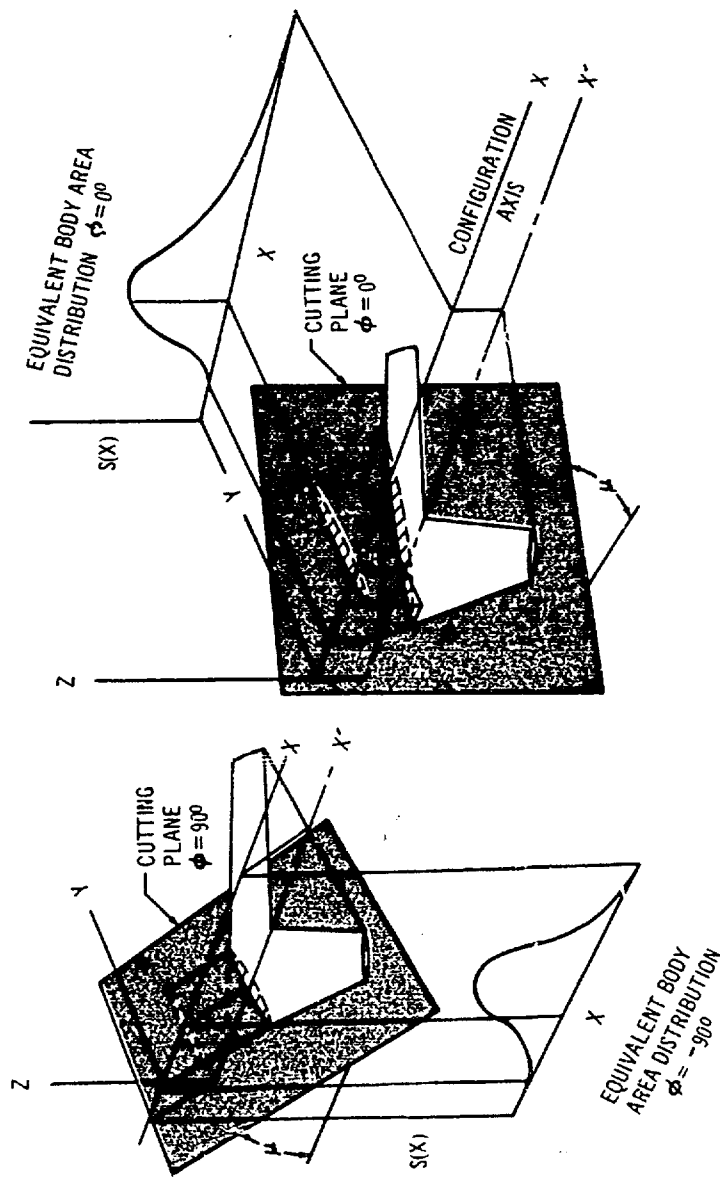
C6.3 Sonic Boom

C6.3.1 METHODS AND SUBSTANTIATION

The sonic boom overpressure produced by an airplane is influenced primarily by the configuration geometry and lift distribution. The contribution of each component of the configuration and the lift is determined by computing its $F(y)$ function. This function was developed by G. B. Whitham and is defined in a paper published in 1952 (Ref. 30). The $F(y)$ function is the key to the computation of sonic boom overpressures. It is defined by Eq. C6-1



C 6-54 Trimmed Lift to Drag Ratio Comparison



C 6-55 "Equivalent Body" Generation by Mach Cutting Planes

$$F(y) = \frac{1}{2\pi} \int_0^y \frac{S''(x) + \frac{(M^2 - 1)^{1/2}}{2} \frac{L'(x)}{q}}{\sqrt{y - x}} dx \quad \text{Eq. C6-1}$$

Here $S(x)$ is the contribution of the volume of the configurations, $L'(x)$ is the contribution of the lift distribution, and M is the Mach number.

Another convenient form of the equation was also

given by Whitham. This is the Stieltjes integral shown below in Eq. C6-2.

$$F(y) = \int_0^y \left(\frac{2}{\beta R(x)} \right)^{\frac{1}{2}} \left(\frac{y-x}{\beta R(x)} \right)^{\frac{1}{2}} \frac{dS'(x)}{2\pi} \quad \text{Eq. C6-2}$$

The function $S(x)$ now represents the contribution of the volume or lift, or both, and $R(x)$ $\left[\frac{S(x)}{\pi} \right]^{\frac{1}{2}}$, and

$\beta = (M-1)^{\frac{1}{2}}$. Although Eq. C6-2 is more difficult to apply analytically than Eq. C6-1, it is readily amenable to digital computer analysis and discontinuities in the integrand can be handled in a straightforward manner.

The method used by The Boeing Company to compute sonic boom intensities for any configuration is outlined in the following paragraphs. The configuration is broken down into its basic components of wing, fuselage, nacelles, horizontal tail (and/or canard), vertical tail (and/or ventral), and lift of each component. Each component is then transferred along the appropriate Mach cutting planes to the axis of the configuration where an "equivalent body of revolution" is generated. The choice of Mach cutting planes is determined by the Mach number of the airplane and an angular location, ϕ . Under the airplane this angle is -90 degrees and to the side the angle is 0 degrees. This is illustrated in Fig. C6-55.

The $F(y)$ function for each "equivalent body" is then computed using Eq. C6-2. The sonic boom for the configuration is determined by summing the $F(y)$ functions for each component and integrating the result according to Eq. C6-3

$$I(y_0) = \int_0^{y_0} F(y) dy \quad \text{Eq. C6-3}$$

The upper limit of this integral is determined by the value of "y" for which $I(y)$ is a positive maximum. The sonic boom overpressure on the ground is determined from eq. C6-4.

$$\Delta P = P_\infty K_R K_A (M^2 - 1)^{\frac{1}{2}} \frac{2^{\frac{1}{2}} \gamma}{(\gamma + 1)^{\frac{1}{2}}} \frac{[I(y_0)]^{\frac{1}{2}}}{(h/\sin \phi)^{\frac{1}{2}}} \quad \text{Eq. C6-4}$$

where:

P_∞ Ambient pressure at airplane altitude
 K_R Ground reflectivity factor (1.9 in this document)
 K_A Atmospheric correction factor (root mean square approximation for standard atmosphere, Ref. 3)

M Airplane Mach number
 h Airplane altitude

γ Ratio of specific heats, 1.4

ϕ Mach cutting plane angle

Some specialized techniques are used in obtaining the appropriate "equivalent bodies" for both the volume and lift contributions to the total sonic boom. The volume contribution of the wing, body, etc. is obtained from the appropriate area distribution determined by a series of Mach cutting planes. These distributions are obtained by submitting each component of the configuration to a digital computer program which is also used to compute the airplane wave drag (Ref. 39). The lift contribution is obtained by first determining the distribution of lift over the configuration. This is done using test data when available, or the method of Ref. 40, or combinations of both. The lift distribution is then transferred along Mach plane cuts to the configuration axis, and is multiplied by $-\sin \phi$. The result is the "equivalent body" for the lift distribution, $B(x)$. The resulting "equivalent bodies" are then submitted to a third digital computer program (Ref. 41, which computes the $F(y)$ function from Eq. C6-2 for each component (including the lift), sums them, and computes the value of $I(y_0)$ according to Eq. C6-3. This value of $I(y_0)$ is then used to compute the sonic boom overpressure on the ground for the airplane according to Eq. C6-4. The method is outlined in more detail in Ref. 31.

The validity of this method has been checked both near to and far from lifting and non-lifting configurations.

Comparisons of the theory with experiment near the configurations are shown in Fig. C6-56. (The data were obtained from Ref. 4.) Figure C6-57 shows the comparison of the theory with flight test data, from Ref. 5.

C6.3.2 SONIC BOOM PROPERTIES OF THE MODEL 733-197

Eq. C6-4 may be rearranged in the form shown below for $\phi = -90$ degrees.

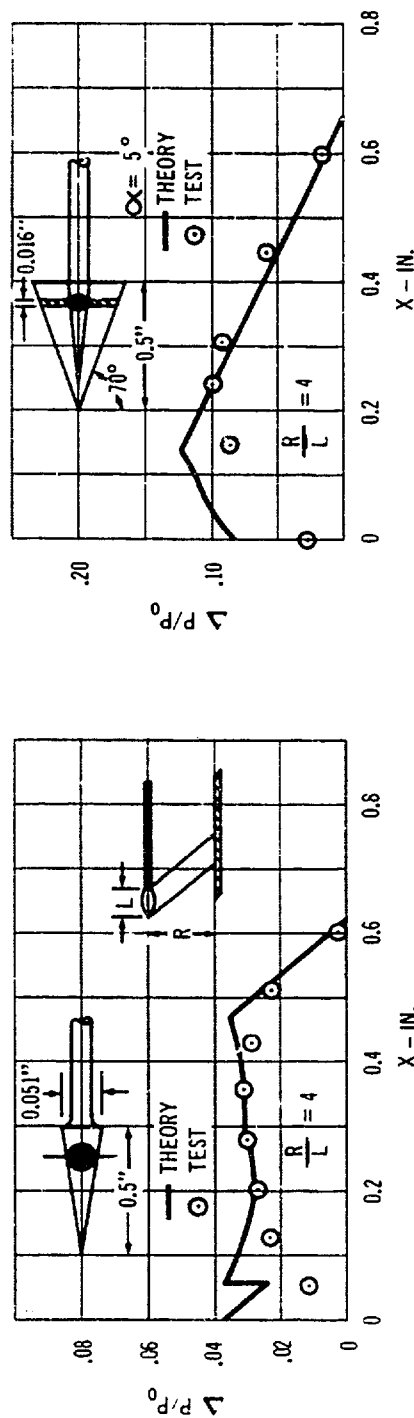
$$\frac{\Delta P_{h1}}{P_{\infty} K_1 (M^2 - 1)^{1/2}} = 1.075 [I(y_0)]^{1/2} \quad \text{Eq. C6-5}$$

The right hand side of the equation is dependent on the configuration arrangement and lift distribution only. It has been found, upon investigation of a number of cases,

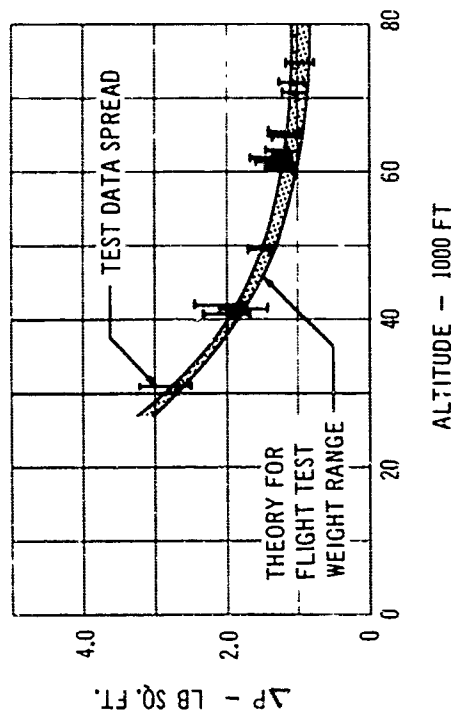
that if the right hand side is plotted against $\beta \frac{C_L}{2}$, the variation with Mach number is not very large. This same result has been found by the NASA (Refs. 2, 6, and 7). Thus the sonic boom characteristics of the airplane are shown in a plot of $1.075 [I(y_0)]^{1/2}$ vs. $\beta \frac{C_L}{2}$ in Fig. C6-58.

Area distributions for the configuration obtained along the appropriate Mach plane cut are shown in Fig. C6-59. The associated lift distributions are shown in Fig. C6-60.

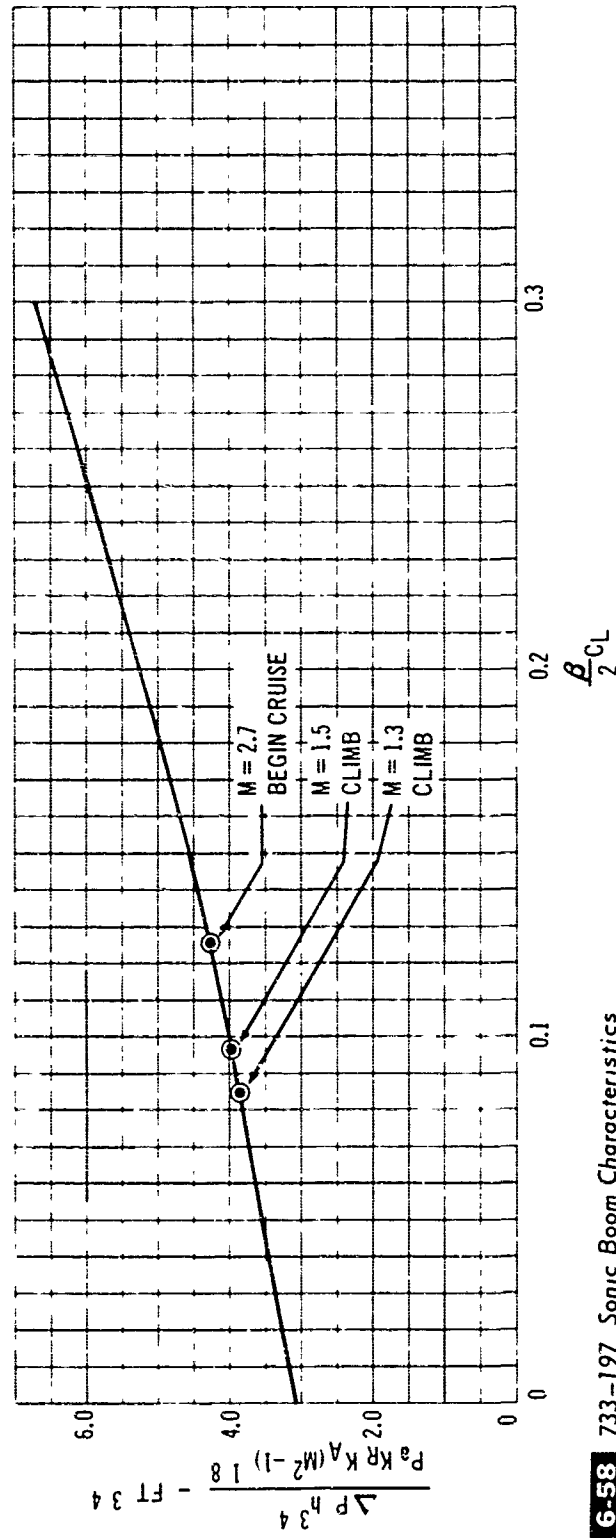
Figs. C6-61 through C6-63 show the resulting $F(y)$ functions for the configuration at $M = 1.3$, and $M = 1.5$ in climb, and $M = 2.7$ at the beginning of cruise. In these plots, the contributions to the $F(y)$ function of the various airplane components are indicated.



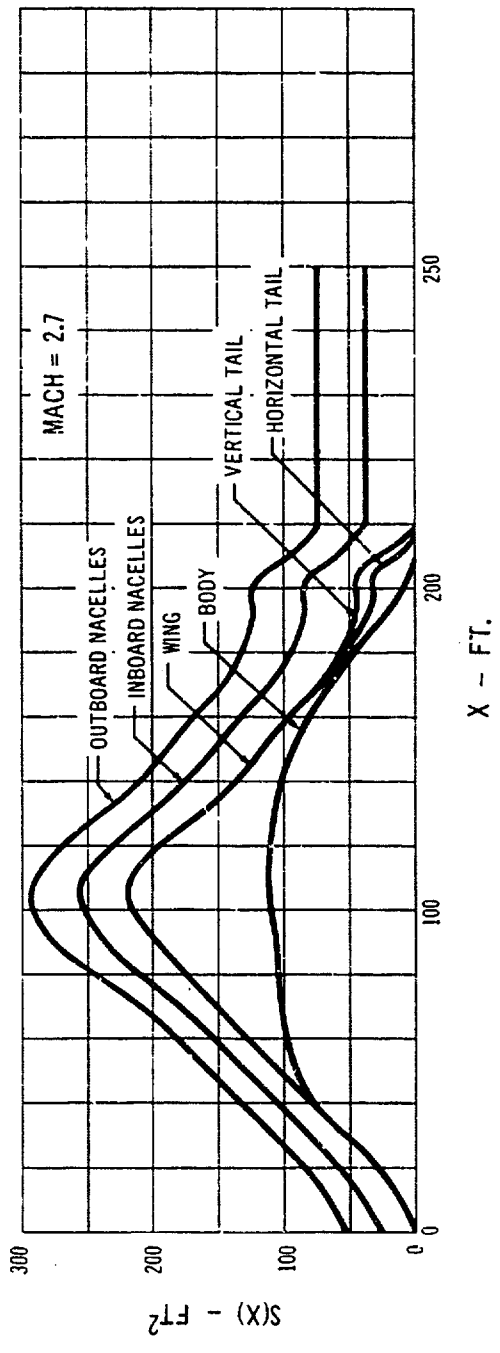
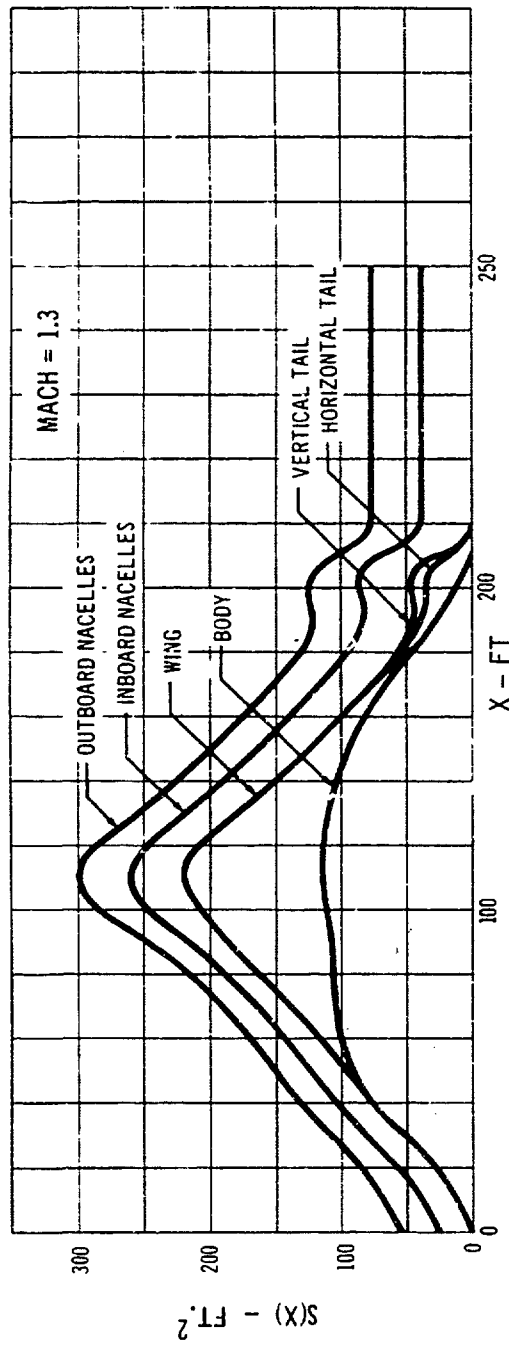
C 6-56 Comparison of Test and Theory Near the Configuration; Mach 2.01



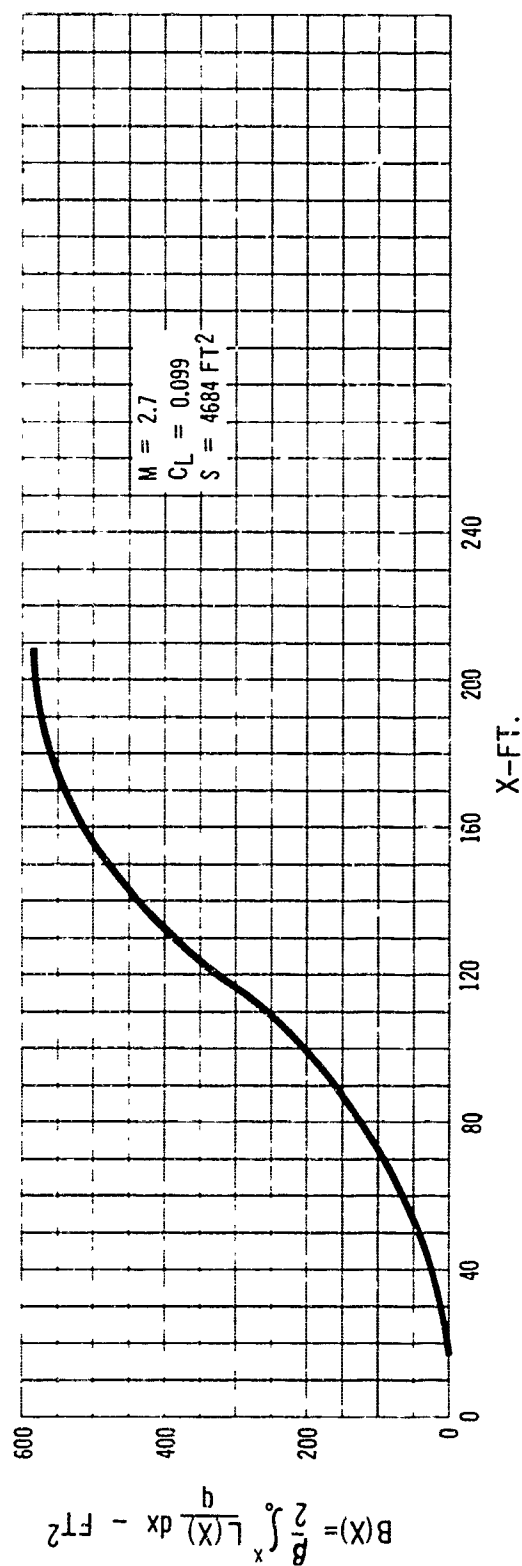
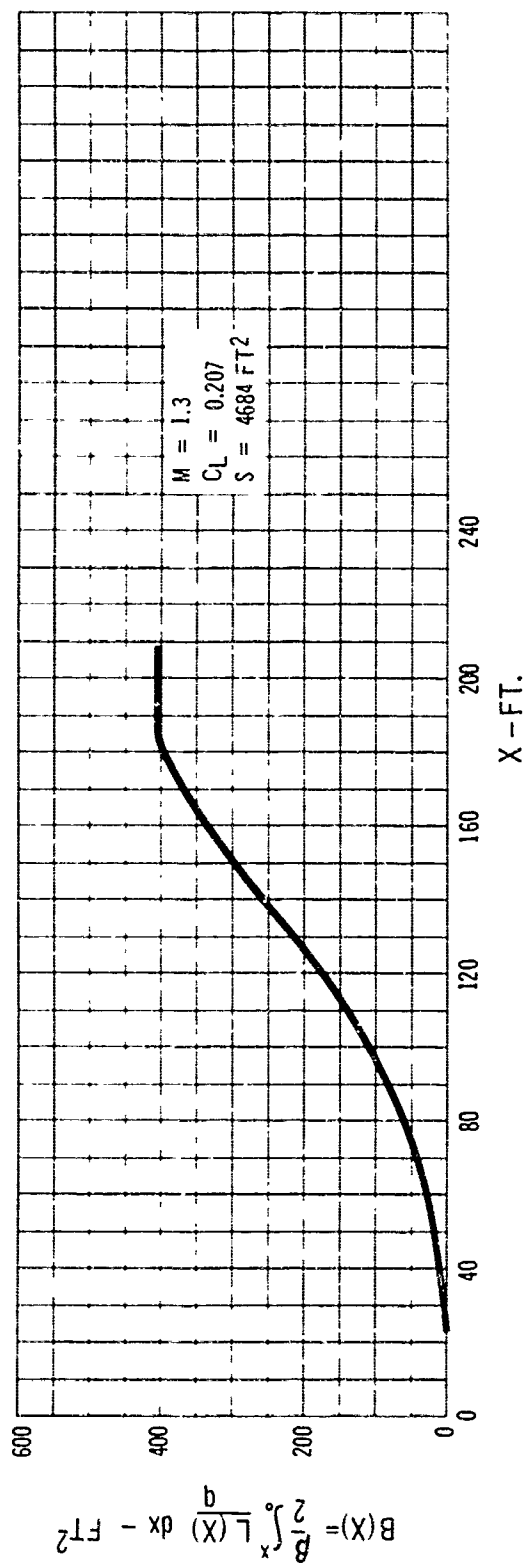
C 6-57 Comparison of Test and Theory
Far From Configuration.



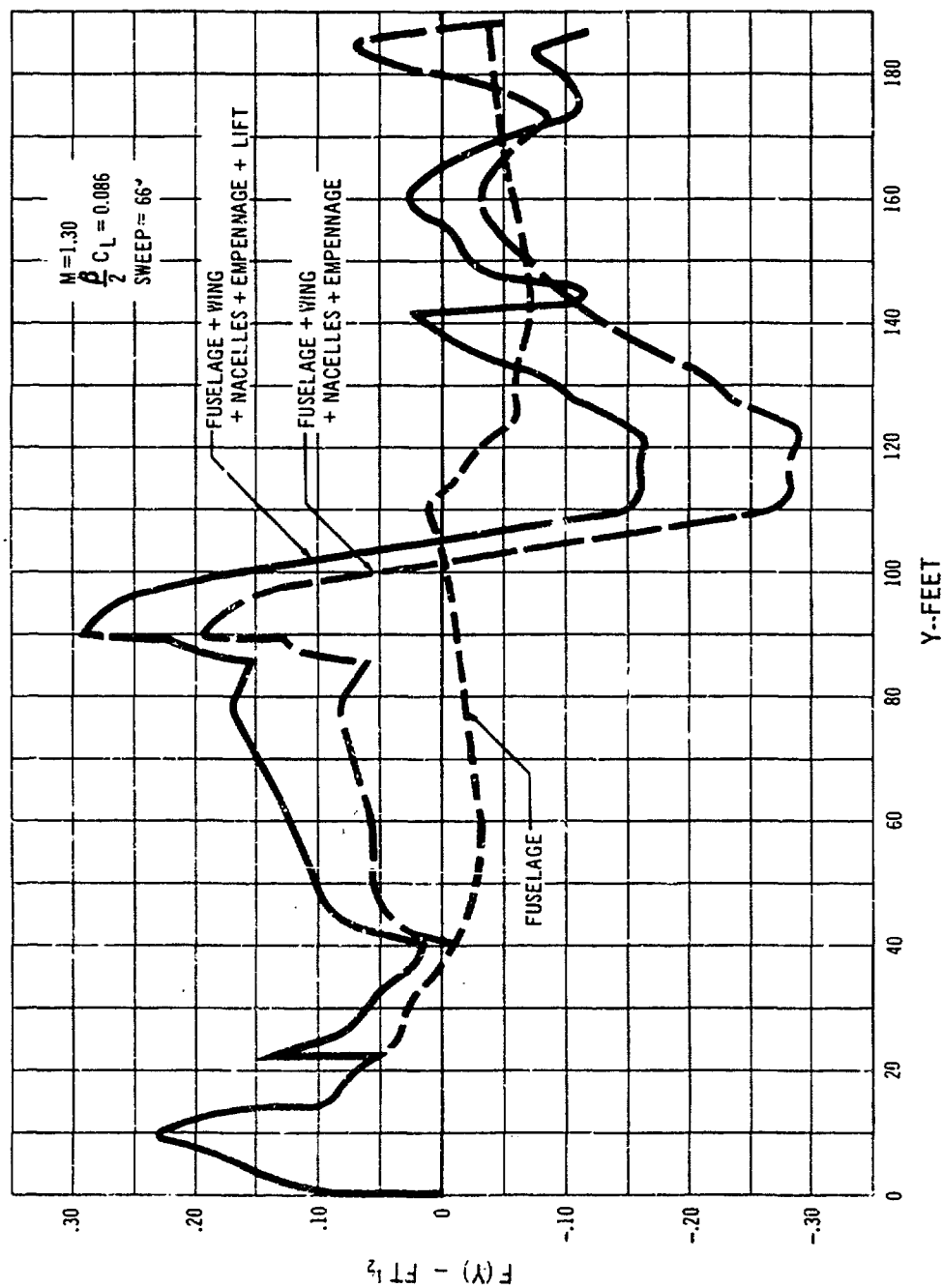
C 6-58 733-197 Sonic Boom Characteristics



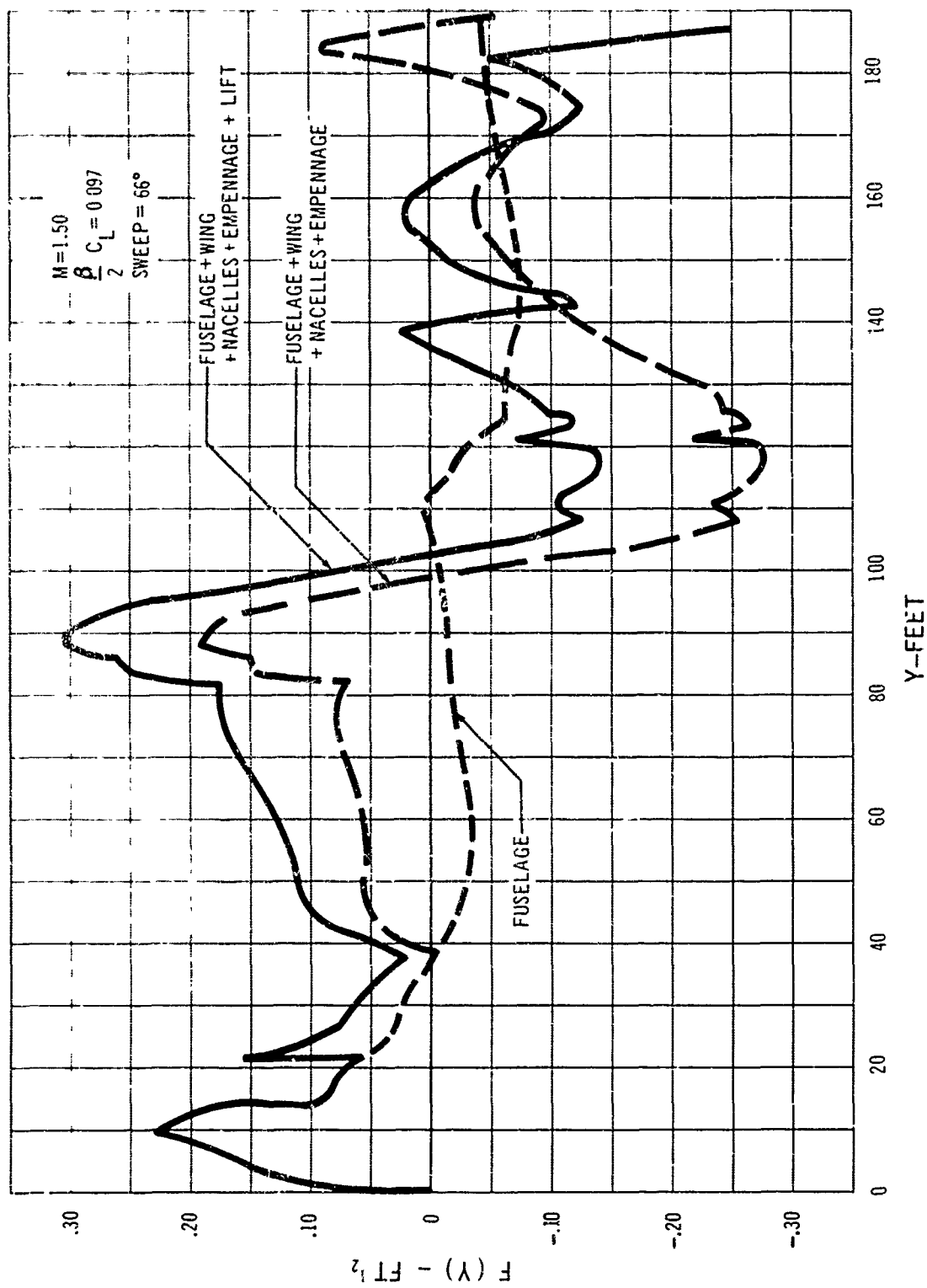
C 6-59 733-197 Area Distributions Used to Estimate Sonic Boom



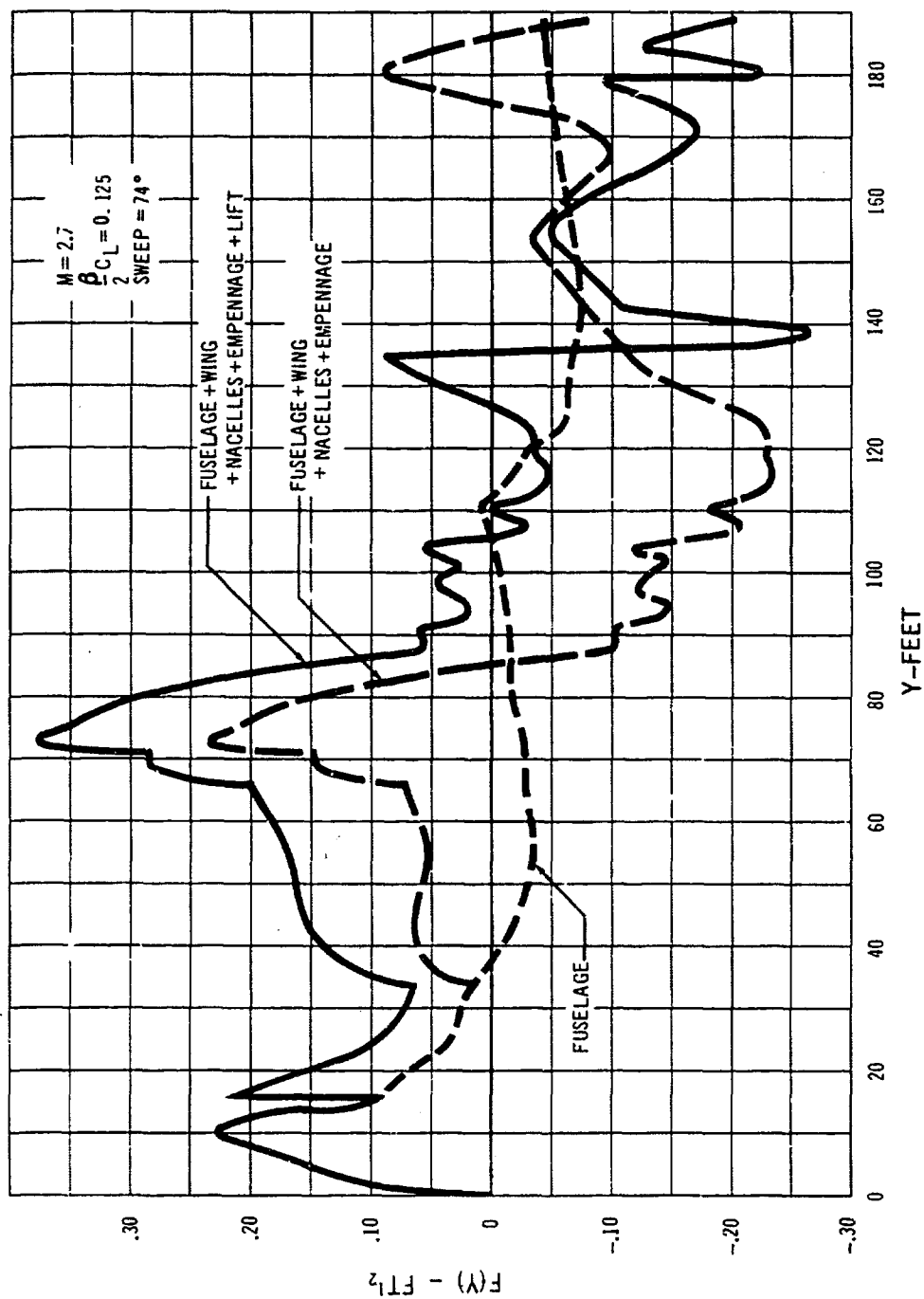
C 6-60 733 - 197 Lift Function, $B(X)$, Distributions



C 6-61 733-197 F (Y) Function at $M = 1.30$



C 6-62 733-197 $F(Y)$ Function at $M = 1.5$



C 6-63 733-197 $F(Y)$ Function at $M = 2.7$

APPENDIX D

APPENDIX TO SECTION 7

STABILITY AND CONTROL

TABLE OF CONTENTS

D7.1 Nomenclature.....	D 1
D7.2 Airplane Geometry.....	D/4
D7.3 Static Longitudinal Stability and Control Data.....	D/4
D7.4 Static Lateral-Directional Stability and Control.....	D/40
D7.5 Engine Inlet Shock Expulsion Data.....	D/58
D7.6 Dynamic Stability Parameters.....	D/65

D7.0 STABILITY AND CONTROL DATA

D7.1 Nomenclature

Coefficients and Derivatives

C_D	Drag Coefficient, Drag qS_x
C_L	Lift Coefficient, Lift qS_x
C_l	Rolling Moment Coefficient, Rolling Moment/ $qS_x b$
C_m	Pitching Moment, Pitching Moment/ $qS_x \bar{c}$
C_n	Yawing Moment, Yawing Moment/ $qS_x b$
C_Y	Side-Force Coefficient, Side Force/ qS_x
$C_{L\alpha}$	Lift-Curve Slope, $\partial C_L / \partial \alpha$
$C_{L\delta}$	Lift Coefficient Due to Surface Deflection, $\partial C_L / \partial \delta$
$C_{L\beta}$	Effective Dihedral Derivative, $\partial C_L / \partial \beta$
$C_{l\delta}$	Roll Control Power Derivative, $\partial C_l / \partial \delta$
$C_{l\dot{\delta}}$	Rolling Moment Coefficient Due to Rolling Velocity, $\partial C_l / \partial (\dot{\delta})$
$C_{l\dot{\delta}}$	Rolling Moment Coefficient Due to Yawing Velocity, $\partial C_l / \partial (\dot{\delta})$
$C_{m\alpha}$	Static Longitudinal Stability Derivative, $\partial C_m / \partial \alpha$
$C_{m\dot{\alpha}}$	Pitching Moment Coefficient Due to Angle-of-Attack Rate, $\partial C_m / \partial (\dot{\alpha})$
$C_{m\delta}$	Pitch Control Power Derivative, $\partial C_m / \partial \delta$
$C_{m\dot{\delta}}$	Pitching Moment Coefficient Due to Pitching Velocity, $\partial C_m / \partial (\dot{\delta})$
$C_{n\alpha}$	Static Directional Stability Derivative, $\partial C_n / \partial \alpha$
$C_{n\delta}$	Yawing Moment Coefficient Due to Surface Deflection, $\partial C_n / \partial \delta$
$C_{n\dot{\delta}}$	Yawing Moment Coefficient Due to Rolling Velocity, $\partial C_n / \partial (\dot{\delta})$
$C_{n\dot{\delta}}$	Yawing Moment Coefficient Due to Yawing Velocity, $\partial C_n / \partial (\dot{\delta})$
$C_{Y\beta}$	Side-Force Derivative, $\partial C_Y / \partial \beta$
$C_{Y\delta}$	Side Force Coefficient due to Surface

$C_{Y\dot{\delta}}$	Deflection, $\partial C_Y / \partial \delta$
$C_{Y\dot{\delta}}$	Side-Force Coefficient Due to Rolling Velocity, $\partial C_Y / \partial (\dot{\delta})$
$C_{Y\dot{\delta}}$	Side-Force Coefficient Due to Yawing Velocity, $\partial C_Y / \partial (\dot{\delta})$
$d\epsilon/d\alpha$	Rate of Change of Downwash With Angle of Attack
$\dot{\psi}$	Roll Rate, $d\psi/dt$
$\dot{\phi}$	Yaw Rate, $d\phi/dt$
$\dot{\theta}$	Pitch Rate, $d\theta/dt$

General

a.c.	Aerodynamic Center
AR	Aspect Ratio b^2/S_w
b	Wing Span
BSWT	Boeing Supersonic Wind Tunnel
BTWT	Boeing Transonic Wind Tunnel
c	Chord
\bar{c}	Mean Aerodynamic Chord of the Basic Airfoil = 74°
C	Cycles to Half Amplitude
$1/C$	Reciprocal of Cycles to Half Amplitude
CG	Center of Gravity
f_n	Undamped Natural Frequency
g	Gravitational Constant, 32.2 feet/second ²
h	Altitude
h_g	Ground Plane Height in Wind Tunnel, Distance from Plane to Model Reference Line
I	Moment of Inertia, Slug-Feet ²
K	Stability Augmentation System Surface Deflection, Degrees per Degree per second of Pitch (Roll, Yaw) Rate
K_{AB}	Body Aeroelastic Factor
LE	Leading Edge

L_{α} L_{α} Aerodynamic Surface Aerodynamic Factor
 l_1 Distance From .25 \bar{c} to C.G.
 l_{10} Distance From .25 \bar{c} to C.G.
 M Mach Number
 MAC Mean Aerodynamic Chord of the Basic Airfoil
or m.a.c. Arrow Wing
 M_{∞} Mach Number, Maximum Operating
 n Load Factor, g's
 n/α Change in Load Factor Per Degree of Angle
of Attack
P.R. Cooper Pilot Rating
 P Damped Period
 p Rolling Velocity
 q Dynamic Pressure, Pitching Velocity
 r Yawing Velocity
 RN Reynolds Number
 R_{α} R_{α} Aerodynamic Surface Aeroelastic Factor
 S Area
SAS Stability Augmentation System
SST Supersonic Transport
TE Trailing Edge
 T_2 Time to Double Amplitude
 $T_{1/2}$ Time to Half Amplitude
 T/W Thrust to Weight Ratio
UWAL University of Washington Aeronautical
Laboratory
 V_A As Defined in Section 3, Volume A-V, Flight
Criteria
 V_{APP} Velocity During Landing Approach
 V_e Equivalent Airspeed
 V_{LNDG} Velocity at Touchdown
 V_{MU} Minimum Unstick Velocity
 V_r Velocity at Start of Rotation

V_s Velocity at Stall
 V_T True Airspeed
 V_i Refused Takeoff Velocity
 V_H Horizontal Tail Volume Coefficient, $\frac{l_H S_H}{\bar{c} S_w}$
 V_v Vertical Tail Volume Coefficient, $\frac{l_v S_v}{b S_w}$
 V_{VTS} Ventral Volume Coefficient, $\frac{l_{VTS} S_{VTS}}{b S_w}$
 W Weight
 W/S Wing Loading, Weight to Wing Area Ratio
 α Angle of Attack of Horizontal Reference Line
 β Sideslip Angle
 Δ Increment
 δ Surface Deflection
 δ_{eq} Equivalent Control Surface Deflection,
 $\left(\frac{\text{Actual Maximum Control Moment Coefficient}}{C_m}$ for Normal Operation $\right)$
 ϵ Inclination of Principal X Axis from Body
Reference X Axis, Positive Nose Down
 ξ Damping Ratio
 η Horizontal Tail Efficiency Factor, $q_1 q_2$
 θ Angle Between the Horizontal Reference Line
and the Horizon
 Λ_{LE} Leading Edge Sweep Angle
 λ Taper Ratio, C_t/C_r
 ρ Air Density
 σ Density Ratio p_0/p_∞
 τ Time Constant
 ϕ Roll Angle
 ψ Yaw Angle
 $|\phi|/|\beta|$ Roll Angle to Sideslip Ratio
 $|\phi|/|v_e|$ Roll Angle to Equivalent Lateral Velocity
Ratio

ω_ϕ Undamped Natural Frequency Derived from
the Numerator of the Bank Angle to Aileron
Transfer Function

ω_d Dutch Roll Undamped Natural Frequency

Subscripts

a Aileron

d Dutch Roll

e Elevator

E Elastic

H Horizontal Stabilizer

MAX Maximum

O Reference, Free Stream

P Phugoid

r Rudder, Root

R Rigid

s Spoiler

S.P. Short Period

t Tip

T Tail

trim Trim Condition

V Vertical

VEN Ventral

w Wing

XX, YY, ZZ, XZ } Moment of Inertia Axis Designation

D7.2 Airplane Geometry

Figure 2-3 shows the general arrangement of the proposal airplane. Since wing sweep is variable, conventional aerodynamic areas and lengths are not constant and the reader must exercise care when interpreting aerodynamic data, especially when the data are in coefficient form.

Unless stated otherwise, aerodynamic data describing the Model 733-197 are referred to the wings-hack, arrow wing, cruise geometry (Reference wing area 4684 Ft²) as shown in Table D7-A. When the wings are forward in the minimum-sweep (20°) configuration the equivalent fixed-wing airplane has a conventional reference area as in Table D7-A. It is seen that the Model 733 reference wing area taken at cruise configuration is about 40 percent larger than that of the equivalent low-speed, fixed-wing airplane. Therefore, the low-speed lift coefficients, as quoted in terms of the arrow wing reference geometry, are correspondingly lower than for more conventional designs. Similarly, the reference mean aerodynamic chord (m.a.c.) is approximately three times as long as the m.a.c. of the equivalent fixed-wing, low-speed airplane, and the minimum safe static margin for the 733 is less than half the value usually seen for conventional designs.

Horizontal and vertical tail geometry is referred to the exposed area of the tails as shown in Table D7-A. Table D7-A also tabulates the important aerodynamic areas and lengths of Model 733 and shows their variation for three important wing sweeps: 20 degrees leading-edge sweep for landing and takeoff; 42 degrees leading-edge sweep for subsonic cruise; and 74 degrees leading-edge sweep for supersonic cruise.

D7.3 Static Longitudinal Stability and Control Substantiation Data

The proposal configuration provides good longitudinal stability and control characteristics over the entire operating range of variable-sweep angle, Mach number, dy-

namic pressure, and angle of attack. No pitch-up nor significant nonlinearities will exist in the pitching moment versus lift characteristics at any flight condition. The longitudinal stability characteristics for representative conditions of sweep, flap setting, and Mach number are discussed in Pars. D7.3.1 and D7.3.2.

D7.3.1 STABILITY DEVELOPMENT OF PIVOT CONFIGURATION

A considerable research effort was required to attain these satisfactory longitudinal stability characteristics for the proposal airplane. Structural and configuration arrangement advantages dictated a wing pivot location which is far enough outboard on the wing to permit location of the engines on the fixed portion of the wing inboard of the pivot. UnswEEPing the wing thus leaves a large area, highly-swept strake (the fixed portion of the wing forward of the pivot). At low-to-moderate out-wing sweep angles, the strong vortex lift generated by the strake tends to produce longitudinal stability problems. If the vortex flow from the strake is allowed to spread onto the outer wing, it will trigger spanwise flow and premature stalling. The outer-wing stall, coupled with the strong lifting capabilities of the strake at high angle of attack, induces a forward shift in the center of lift, thus producing pitch-up. In addition, the downwash ($d\alpha/d\alpha$) generated by the strake vortex system reduces the stability contribution of the horizontal tail which would otherwise oppose the wing-body pitch-up.

The Boeing Company has conducted an intensive aerodynamic research program to investigate many different concepts of variable sweep designs. In the past year alone over 1000 hours of wind tunnel testing have been devoted to the study of stability and control problems. A large portion of this study has been assigned to the solution of the longitudinal problems associated with outboard-wing-pivot designs representative of the proposal airplane. These studies have resulted in the achievement of good stability characteristics through practical,

TABLE D7/A AERODYNAMIC GEOMETRY

REFERENCE GEOMETRY

THE FOLLOWING VALUES DETAIL THE REFERENCE GEOMETRY USED FOR ALL AERODYNAMIC COEFFICIENTS AND DERIVATIVES AT ALL WING SWEEP ANGLES. THIS GEOMETRY IS BASED ON THE 74° SWEEP CONFIGURATION. THE USE OF ANY OTHER GEOMETRIC VALUES IS NOTED SPECIFICALLY FOR EACH PARTICULAR APPLICATION.

	WING	HORIZONTAL TAIL (EXPOSED)	VERTICAL TAIL	VENTRAL
AREA, FT ²	4684.0	950.0	471.7	125.0
SPAN, FT.	86.33	44.51	22.92	4.34
ASPECT RATIO	1.590	2.086	1.113	0.181
C _T C _R	0.354	0.200	0.254	0.662
MAC, IN.	774.278	294.22	276.16	321.82
V (TO .40 MAC WING)		0.230	0.082	0.021

EFFECTIVE GEOMETRY FOR OTHER WING SWEEP ANGLES

WING	$\Lambda_{LE} = 20^\circ$	$\Lambda_{LE} = 42^\circ$	HORIZONTAL TAIL (TOTAL)
AREA, FT ²	3315	3390	AREA, FT ² 1169.0
SPAN, FT	173.33	143.08	SPAN, FT 59.35
ASPECT RATIO	9.06	6.04	ASPECT RATIO 2.170
C _T C _R	0.414	0.406	C _T /C _R 0.180
MAC, IN	259.327	302.759	MAC, IN 323.311

TAIL VOLUME COEFFICIENT (TO .40 MAC WING)	HORIZONTAL TAIL TOTAL	VERTICAL TAIL EXPOSED
$\Lambda_{LE} = 20^\circ$	1.169	0.970
$\Lambda_{LE} = 42^\circ$	0.979	0.813
$\Lambda_{LE} = 74^\circ$	0.277	0.230

minor design modifications. The modifications consist of the incorporation of a notch outboard in the strake leading edge, a wing fence aligned with the notch on the strake, and a strake leading-edge round-nose flap as shown in Fig. 2-3. These aerodynamic fixes are only required for low-speed through subsonic cruise operation (wing sweeps from 20 degrees through 42 degrees) where pitch-up or unacceptable stability deteriorations with angle of attack have been problems. At higher wing sweeps the design selection of wing twist, moderate planform taper, and large tail volume has provided good longitudinal stability characteristics with no modifications required.

Figs. D-1 through D-3 show photographs of the basic low-speed model tested, the notch, fence, and round-nose strake flap leading-edge modifications. Several other pitch-up modifications which proved successful in wind tunnel testing, but which were somewhat less desirable to incorporate in the airplane are shown in Figs. D-4 and D-5. These are:

- a. Chordwise slot along strake root chord at side of body, plus outboard-wing leading edge slats,
- b. M-wing type cutout in strake,
- c. Reduced strake sweep,
- d. Increased tail aspect ratio (from 2.2 to 3.5).

Increased tail aspect ratio, item (d) above, is still under consideration as an over-all design improvement, and may be incorporated during Phase II development. Also, it is considered possible that the round-nose strake may be acceptable as fixed geometry from the standpoint of cruise L/D, with no provision for retraction at high speed.

Fig. D-6 presents wind tunnel test data showing the effectiveness of the stability modifications upon the longitudinal characteristics of the Boeing SST in the landing configuration. The test data are presented for a moment center of 42 percent m.a.c. of the 74 degrees sweep wing, which is 2 percent aft of the forward CG limit. The tail-off pitching moment curve of the unmodified configuration is

seen to be unstable and to break sharply in the pitch-up direction at the moderate C_L of 0.85. The test data show that adding the horizontal tail to this configuration results in no stability improvement for lift coefficients greater than 0.85. The test data for the same configuration modified to include the fence and the round-nose flap on the strake show improved tail input and good stability up through the stall for either the basic Boeing SST low-aspect-ratio-tail configuration, or for the same airplane with the tail aspect ratio increased to 3.5.

At the stall, 18 degrees α , the pitching moment curve breaks slightly in the nose-up direction and then back in the nose-down direction as the stall is explored to extremely high angle of attack. It should be noted that the test data extend for approximately 15 degrees beyond the stall angle of attack. The total excursion in pitching moment coefficient through this range of stalled flight is .04 C_m , which is equivalent to only 6.5 degrees of elevator deflection. This small pitch excursion during the stall is easily controllable and is similar to that experienced in Model 707 transports.

Low-speed longitudinal stability characteristics, flaps up, are shown in Fig. D-7 for 42 degrees of wing sweep (subsonic cruise configuration). The basic Boeing SST with the notch, fence, and round-nose flap on the strake displays good stability.

The pitching moment curve is essentially linear up to 0.8 C_L , which is twice the maximum anticipated trim C_L at 1 g. A mild slope reversal occurs in the pitching moment curve above 0.8 C_L , resulting in a nose-up pitch excursion of about .04 C_m , after which the curve breaks strongly stable. It should be pointed out that the 42 degree sweep wing is stalling during this small pitching moment excursion, as evidenced by the break in the lift curve slope at 20 degrees angle of attack. This is a normal stall α for conventional fixed-wing airplanes of this sweep without inboard strakes. Above this α , buffet will be severe and wing lateral control devices will be ineffective; thus the

continuing stable lift provided by the strake at higher angle of attack will not be useful.

The data shown in Fig. D-7 for the increased aspect ratio tail (AR = 3.5, but same \bar{V}) demonstrate a reduced pitch excursion during the stall near 20-degree angle of attack, and the initial break from linear in the pitching moment curve is delayed until 0.95 Cl.

Fig. D-8 shows similar effects of strake leading-edge notch, and fence treatment for the minimum sweep, flaps-up configuration (leading-edge sweep 30 degrees). Stall of the 30-degree sweep wing initiates near 17 degrees angle of attack for the improved Boeing SST configuration, and is again accompanied by a mild reversal in dC_m/dC_l , followed by a strongly stable pitching moment gradient throughout the stall (data carried 15 degrees beyond stall initiation). Incorporation of the 3.5 aspect ratio tail is seen to provide slightly improved stability at operating Cl.s and to delay the break in the pitching moment curve to 0.95 Cl.

D7.3.2 STABILITY AND CONTROL TEST DATA

Fig. D-9 shows stabilizer and elevator effectiveness available for the landing configuration. The test data shown are for a wing sweep angle of 15 degrees. The stability and control effectiveness characteristics estimated for the 20-degree design sweep position are shown in Fig. D-9 by the colored lines. The stabilizer provides a large trim CG range capability, and the large elevator is a powerful pitch control. An estimated pitching moment curve is shown for stabilizer trimmed to -20 degrees with four of the eight elevators at maximum available deflection (-10 degrees on two low-speed elevators and -30 degrees on two of the six high-speed elevators). This is the landing trim and control available with operation on only one of the three separate hydraulic systems. Adequate control for landing is demonstrated in this emergency condition.

i. Longitudinal stability and control effectiveness are

shown in Fig. D-10 for a takeoff-flap configuration in ground effect. Test data were obtained. 15 degrees wing sweep, and estimated characteristics are shown for the 20-degree design sweep position. The stabilizer and elevator are seen to provide a large degree of trim and control power for takeoff rotation.

Fig. D-11 shows the large degree of stability existing at low speed with the wings in the maximum, 74-degree sweep position. Here the selection of moderate wing taper, wing twist, and the large horizontal tail result in a linear pitching moment curve with a stability margin of approximately 18 percent \bar{c} . Longitudinal trim and control are adequate in this condition, since the control size and travel were designed for the more demanding, low-sweep, flaps full-down condition.

Figs. D-12 through D-16 present representative transonic and supersonic stability characteristics for the proposed airplane. The data shown are from wind tunnel tests in Boeing facilities and contain no corrections for model or airplane aeroelasticity. Photographs of several of the model configurations tested are shown in Figs. D-17 and D-18.

D7.3.3 AERODYNAMIC CENTER

A comprehensive summary of the aerodynamic balance of the proposal airplane is presented in Fig. 7-9 and discussed in detail in Section 7.2. This figure shows the effects of wing sweep, Mach number, and structural aeroelasticity on static neutral and maneuver points. The operating CG and Aerodynamic CG limits throughout the flight envelope are also shown. The tail-off aerodynamic center and center of gravity relationships for various wing sweeps and Mach numbers are shown in Fig. D-19 for the rigid airplane, and for the flexible airplane along the design climb schedule and at beginning and end of cruise. The most significant fact shown in this figure is the extremely small variation in wing-body aerodynamic center (a.c.) experienced by the flexible airframe during the de-

sign mission. Aeroelastic effects hold the a.c. variation to within two percent of the low-speed a.c. throughout climb, acceleration, and supersonic cruise. The points shown for the rigid wing-body were obtained from wind tunnel test data such as presented in the preceding figures. The shaded, flexible airplane points are wind tunnel test data corrected for model and airplane aeroelasticity.

D7.3.4 AEROELASTIC EFFECTS ON STABILITY AND CONTROL

The high speed wind tunnel models of the Model 733 airplane were constructed to represent the full scale airplane as it is deformed aeroelastically at the design cruise condition of $M = 2.7$ and $CL = 0.10$. As a result, corrections to the data are minimized at the important condition of supersonic cruise.

The wind tunnel models have a measurable aeroelastic distortion at the test dynamic pressure and the first step in estimating full scale aeroelastic characteristics was to correct the wind tunnel data to rigid conditions. Fig. D-20 shows the method that was used to make the wind tunnel model flexibility correction. The model was tested at two values of dynamic pressure and the resulting $C_{L,q}$ and a.c. were plotted versus dynamic pressure and extrapolated linearly to zero q . The ratio of the 1500 q and zero q values was used to correct all subsequent tests conducted at 1500 q . A similar method was used to estimate model flexibility effects for tests conducted at other dynamic pressures.

The resulting rigid wind tunnel data are used as an excellent approximation of rigid airplane data.

Rigid airplane aerodynamic centers also include a correction for wind tunnel sting-mount-horizontal-tail interference. Model tail inputs have been reduced 10 percent (approximately a two percent forward a.c. shift) to account for this effect.

A graphic description of the application of aeroelastic

effects to the rigid airplane data is presented in Fig. D-21. As discussed above, the wind tunnel model is an accurate representation of the flexible airplane at standard cruise ($M = 2.7$, $CL = 0.10$). This condition occurs at a 5.7 which is defined as α_{ROT} and used in the following equations. These equations are used to correct rigid airplane data to elastic airplane data:

(1) Moment

(a) Wing-Body

$$C_{m,flex} = C_{m,rigid} + \Delta \frac{dC_m}{d\alpha} (\alpha - \alpha_{ROT})$$

$$\Delta \frac{dC_m}{d\alpha} = \frac{dC_m}{d\alpha} (rigid) - \frac{dC_m}{d\alpha} (flex)$$

$$\frac{dC_m}{d\alpha} = \left(\frac{dC_m}{dC_L} \right) \left(\frac{dC_L}{d\alpha} \right)$$

(b) Tail

$$\Delta C_{m,T}(r_{L,ex}) = \Delta C_{m,T}(rigid) \left(\frac{L}{L_T} \right) (K_{\alpha\alpha})_T$$

(2) Lift

$$C_{L,flex} = C_{L,rigid} - \Delta \frac{dC_L}{d\alpha} (\alpha - \alpha_{ROT})$$

$$\Delta \frac{dC_L}{d\alpha} = \left[1 - \left(\frac{L}{L_T} \right)_{\alpha_T} \right] C_{L,q}(rigid)$$

$$\Delta C_{L,T}(r_{L,ex}) = \Delta C_{L,T}(rigid) \left(\frac{L}{L_T} \right) (K_{\alpha\alpha})_T$$

At conditions other than the standard cruise, α_{ROT} is assumed to occur at one g flight. This simplifying approximation neglects span load variation but is reasonably accurate. α_{ROT} is selected as corresponding to the C_L determined by:

$$C_{L,Mach,alt} = \frac{(C_{L,q})_{Standard\ Cruise}}{(q)_{Mach, alt.}}$$

The following basic aeroelastic parameters were used in the example shown in Fig. D-21

M 2.7 Altitude - 64,000 ft.

$$\Delta \frac{dC_m}{dC_l} = .034$$

$$\left(\frac{L_R}{L_R} \right)_{\alpha_w} = 84 \text{ Airplane}$$

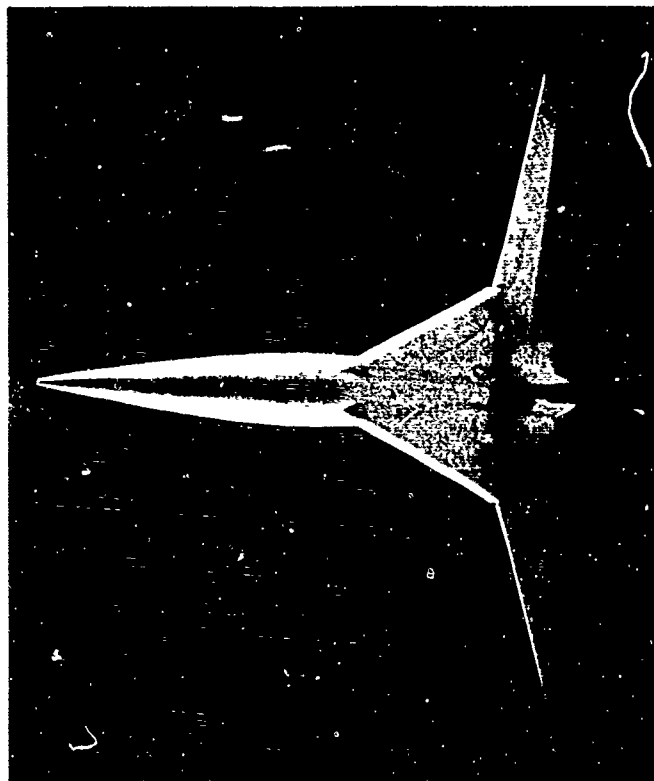
$$(k_{\alpha_0})_{\alpha} = 80 \text{ No. Model}$$

$$\left(\frac{L_R}{L_R} \right)_{\alpha_T} = .88$$

Figures D-22 through D-30 summarize the effects of airplane structural aeroelasticity on wing-body lift curve slopes, aerodynamic centers, and stabilizer and elevator effectiveness. Volume A-IV, Sect. 10 and Appx A, discuss the derivation of the airplane structural aeroelasticity effects. Figs. D-31 through D-33 show rigid airplane wing-body lift curve slopes, angle of attack at zero lift, and rigid tail lift curve slope. Fig. D-34 summarizes the increments in aerodynamic center due to maneuvering for the flexible airplane.

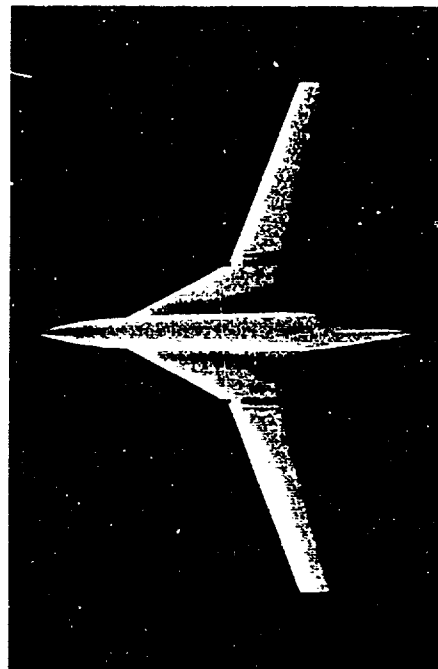
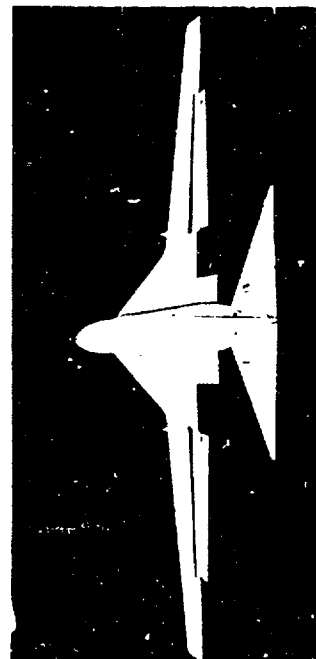


D-1 Low-Speed Wind Tunnel Model

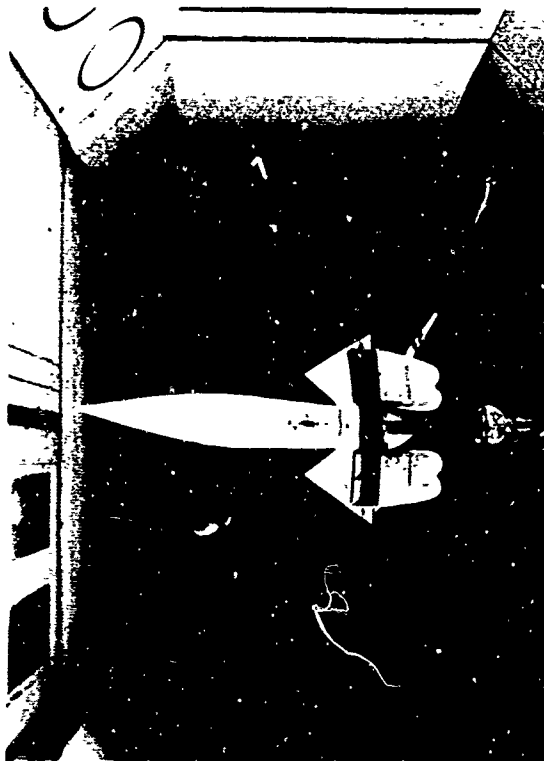
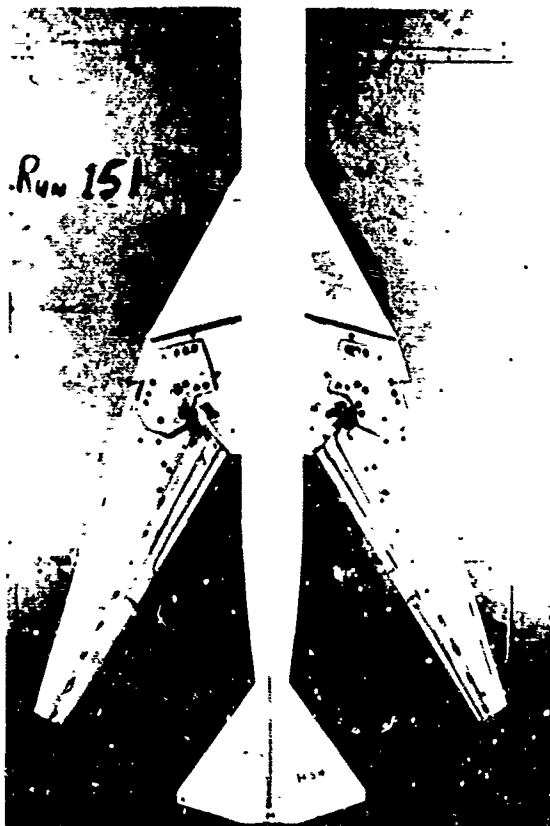


D-2 Comparison of Sharp and Rounded Stroke Leading-Edge

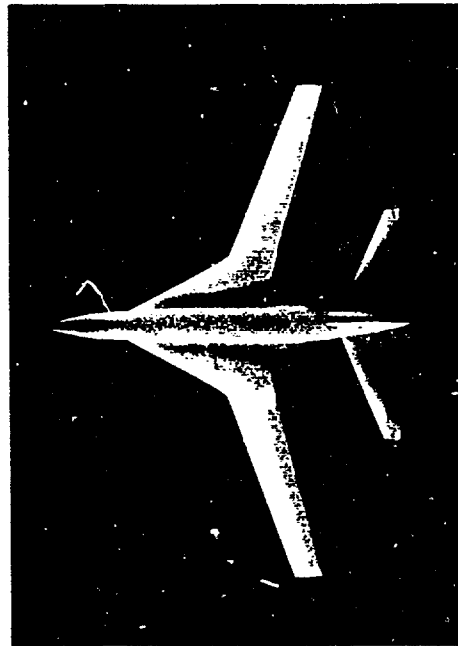
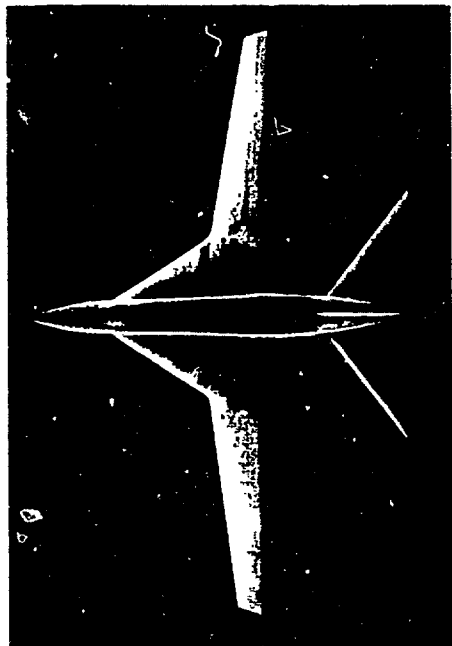


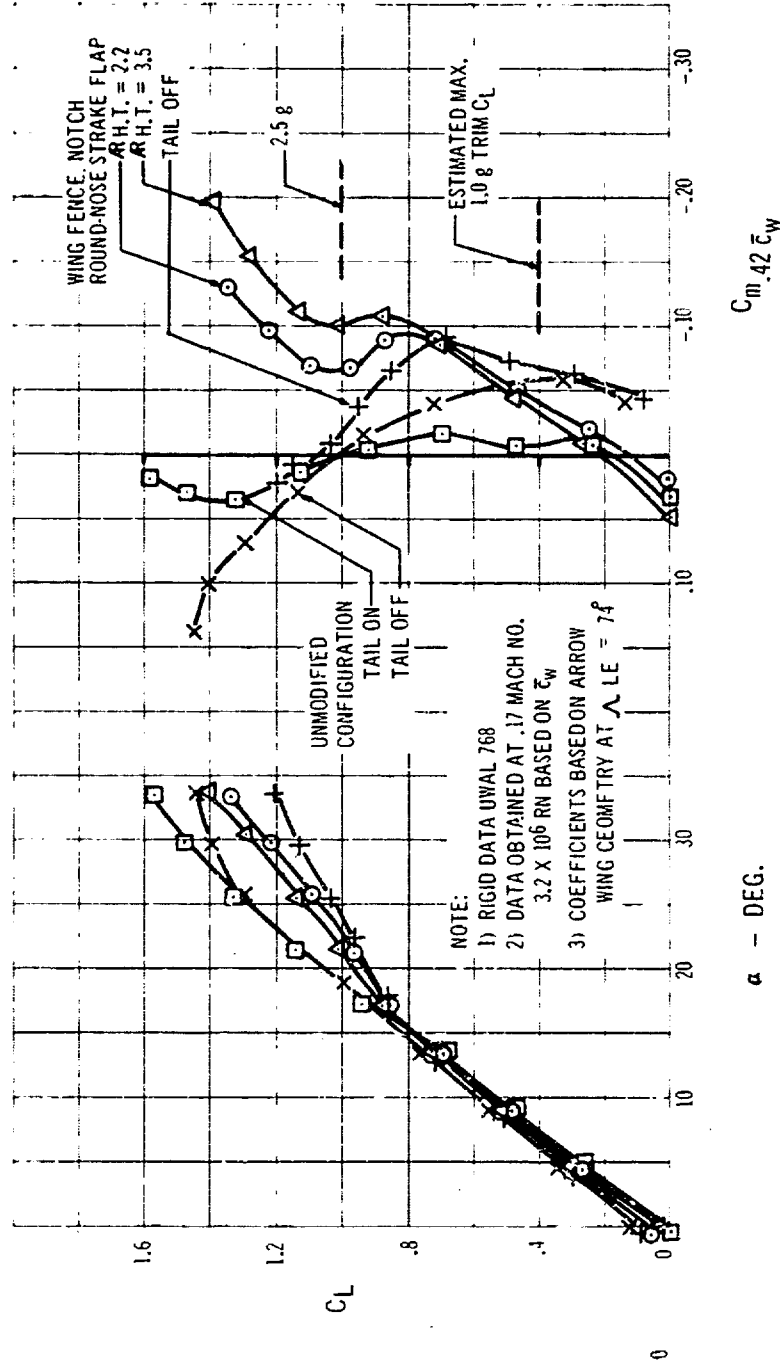


D-3 Low Speed Modifications, Fence, Notch, Round-Nose Strake Flap

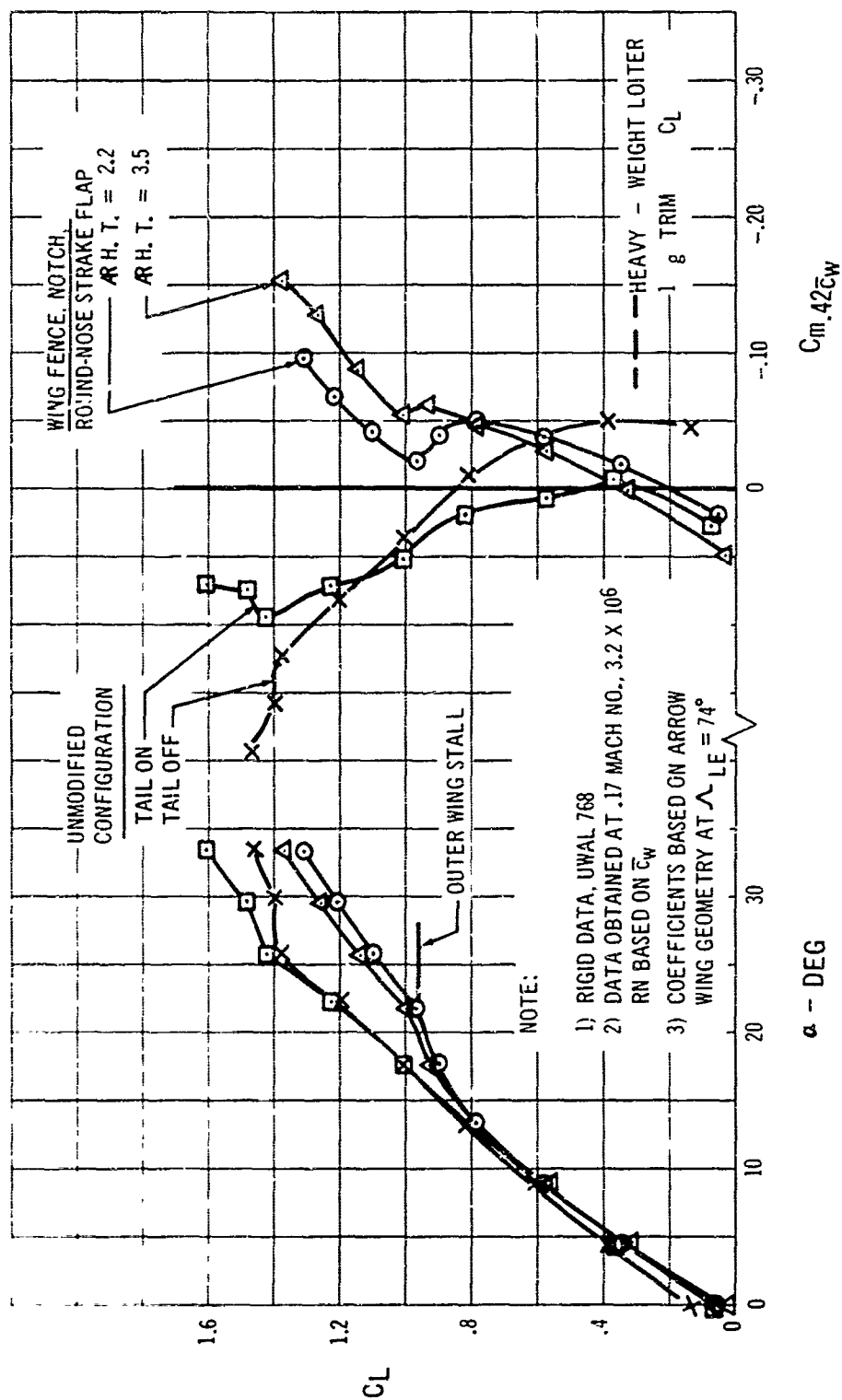


D-4 Configurations Providing Acceptable Longitudinal Stability Characteristics: 60° Stroke, M-Wing, Slotted Stroke with Leading-Edge Slats

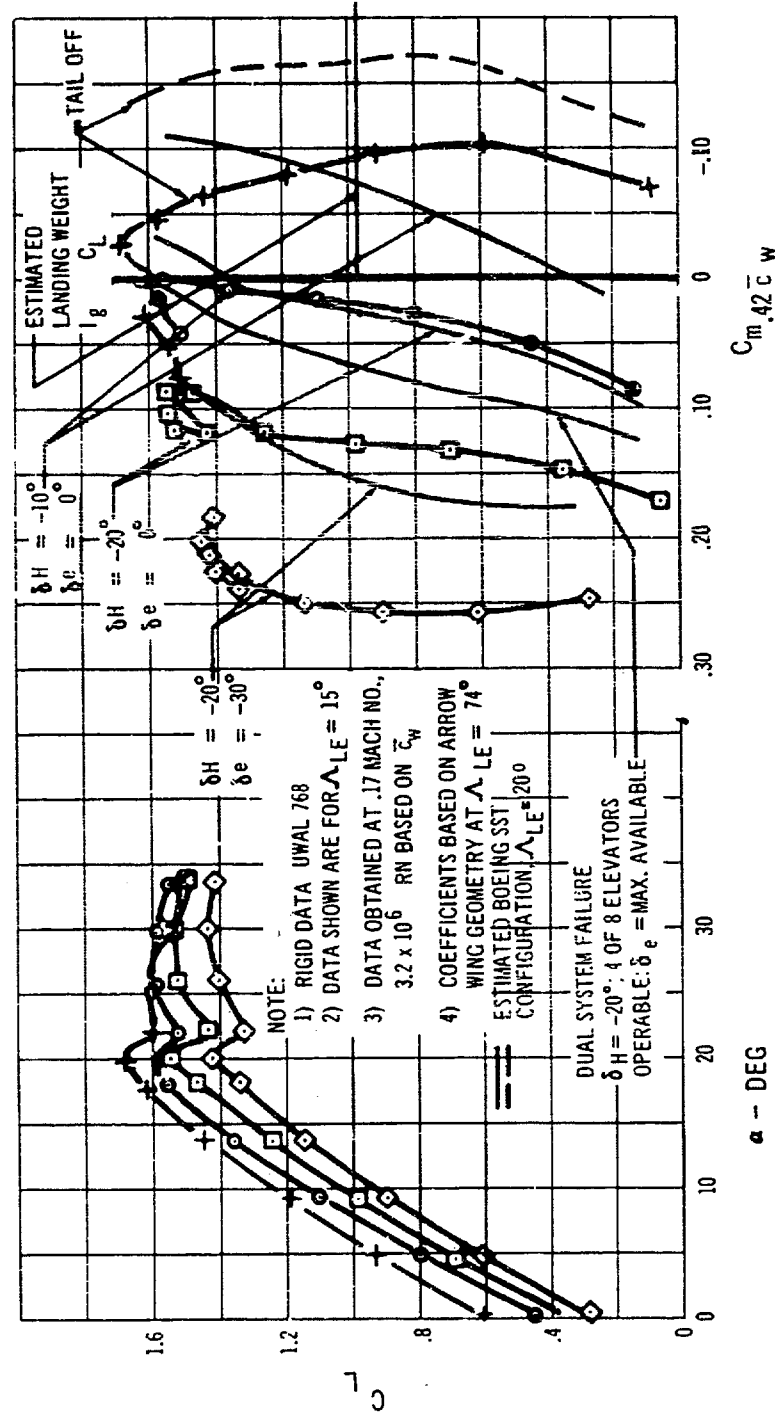




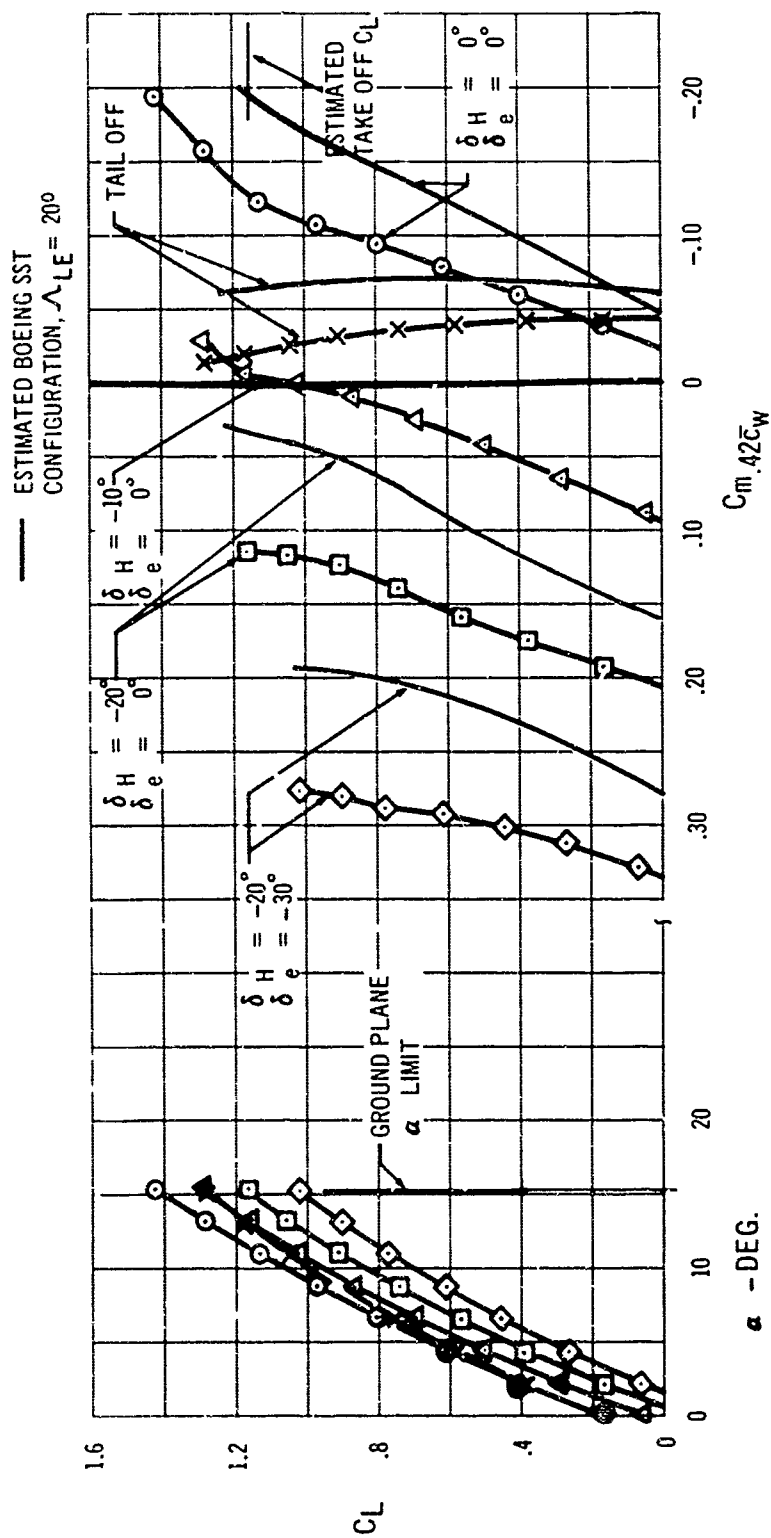
D-7 Effect of Strake Modifications on Static Longitudinal Stability, $\Lambda_{LE} = 42^\circ$, Flaps Up



D-8 Effect of Stroke Modifications on Static Longitudinal Stability, Loiter Configuration, $\angle LE = 30^\circ$, Flaps Up



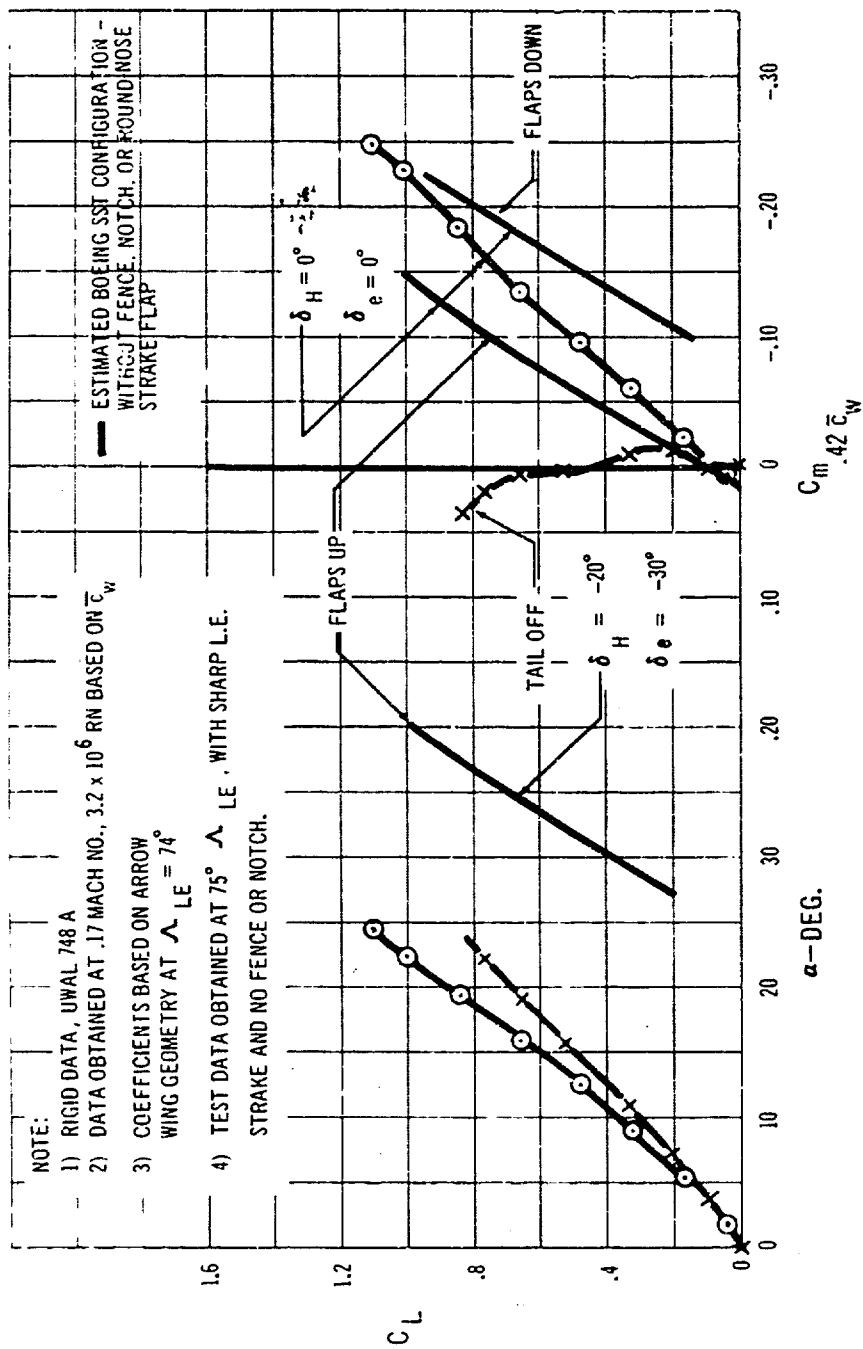
D-9 Static Longitudinal Stability and Control
 Low Speed, Landing - Flap Configuration



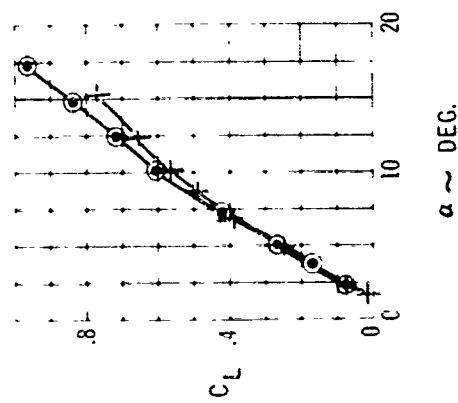
NOTE: 1) RIGID DATA, UWAL 768
 2) DATA SHOWN ARE FOR $\Lambda_{LE} = 15^\circ$
 3) DATA OBTAINED AT .17 MACH NO.,
 3.2×10^6 RN BASED ON \bar{c}_w

4) COEFFICIENTS BASED ON ARROW
 WING GEOMETRY AT $\Lambda_{LE} = 74^\circ$
 5) GROUND PLANE LOCATED AT
 $h_g/b \Lambda = 74^\circ = .237$

D-10 Static Longitudinal Stability and Control, Take-Off Flaps in Ground Effect



D-11 Static Longitudinal Stability Low Speed, $\Lambda_{LE} = 74^\circ$

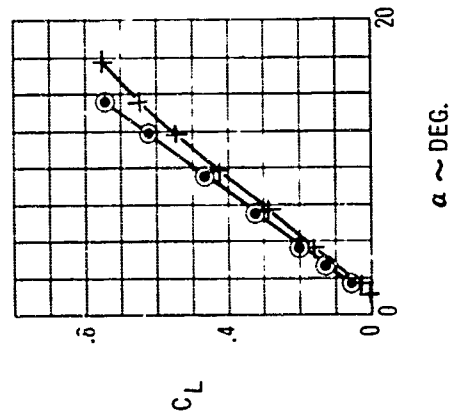
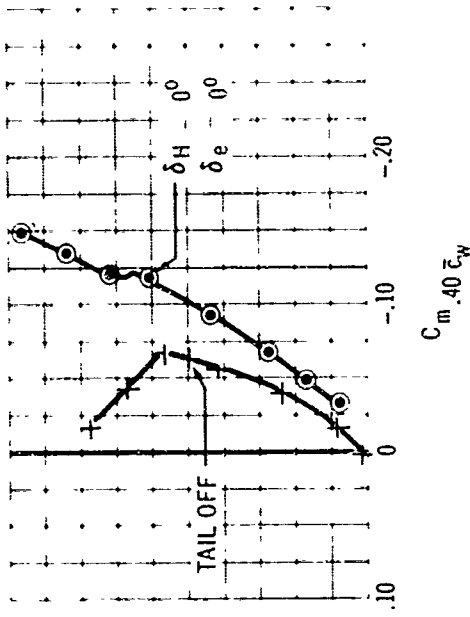


NOTE:

- 1) $q = 673$ PSF NOMINAL
- 2) $R_n = 3.02 \times 10^6$ BASED ON \bar{c}_w
- 3) COEFFICIENTS BASED ON ARROW WING GEOMETRY AT $\Lambda_{LE} = 74^\circ$
- 4) BOEING TRANSONIC TEST 814

$\alpha \sim \text{DEG.}$

D-12 Static Longitudinal Stability Transonic, $\Lambda_{LE} = 42^\circ$ $M = .85$

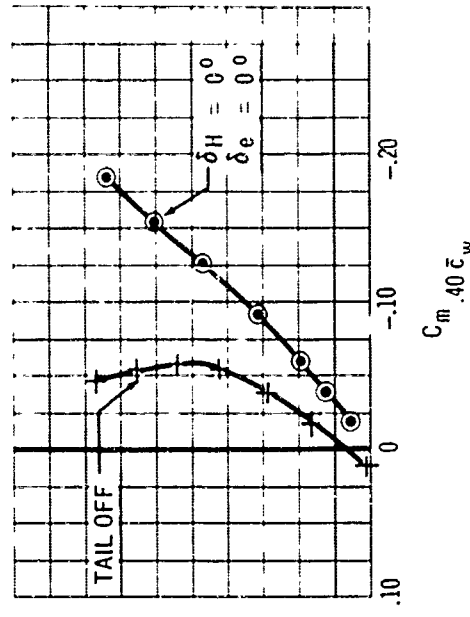


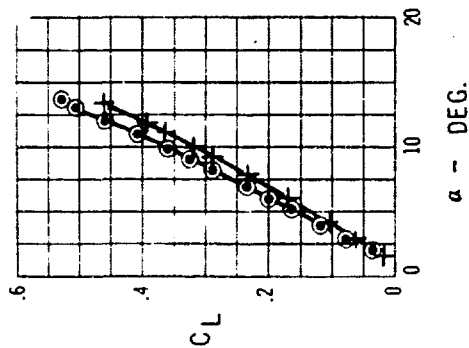
NOTE:

- 1) $q = 785$ PSF NOMINAL
- 2) $R_n = 3.2 \times 10^6$ BASED ON \bar{c}_w
- 3) COEFFICIENTS BASED ON ARROW WING GEOMETRY AT $\Lambda_{LE} = 74^\circ$
- 4) BOEING TRANSONIC TEST 814

$\alpha \sim \text{DEG.}$

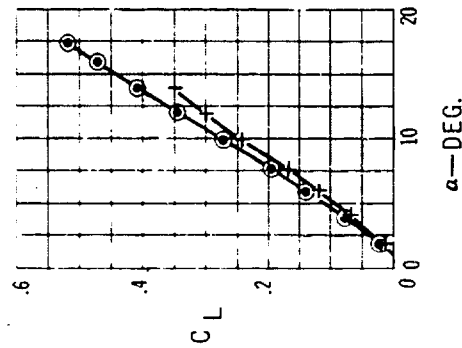
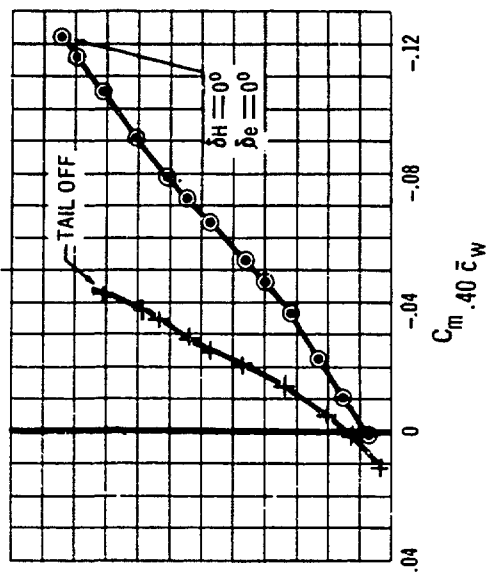
D-13 Static Longitudinal Stability Transonic, $\Lambda_{LE} = 60^\circ$ $M = 1.0$





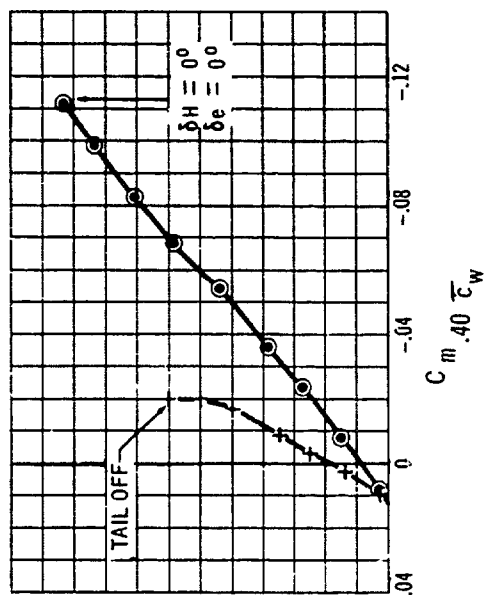
D-14 Static Longitudinal Stability Supersonic, $\Lambda_{LE} = 65^\circ$, $M = 1.3$

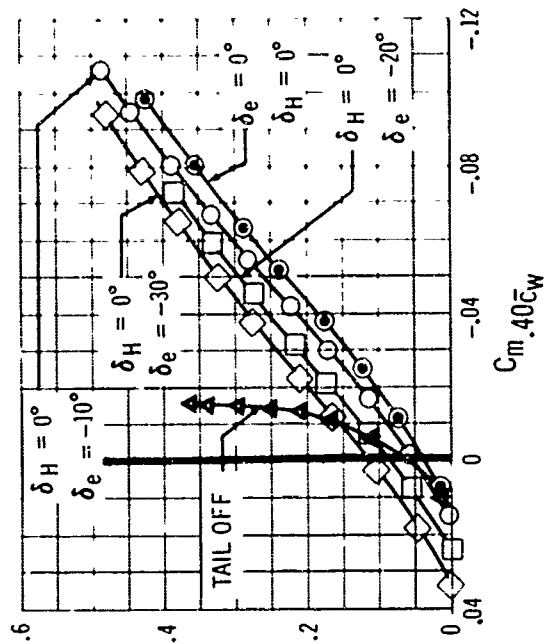
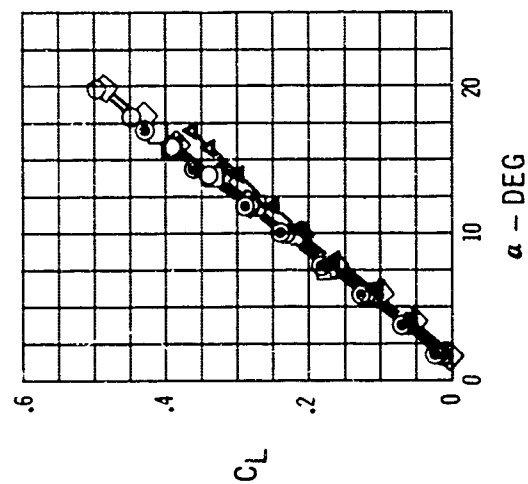
- NOTE:
- 1) THESE DATA UNCORRECTED FOR MODEL OR AIRPLANE AEROELASTICITY
 - 2) $q = 1500$ PSF NOMINAL
 - 3) $RN = 8.8 \times 10^6$ BASED ON \bar{c}_w
 - 4) COEFFICIENTS BASED ON ARROW WING GEOMETRY AT $\Lambda_{LE} = 74^\circ$
 - 5) BOEING SUPERSONIC TEST 218



D-15 Static Longitudinal Stability Supersonic, $\Lambda_{LE} = 74^\circ$, $M = 2.0$

- NOTE:
- 1) THESE DATA UNCORRECTED FOR MODEL OR AIRPLANE AEROELASTICITY
 - 2) $q = 1500$ NOMINAL
 - 3) $RN = 8.5 \times 10^6$ BASED ON \bar{c}_w
 - 4) COEFFICIENTS BASED ON ARROW WING GEOMETRY $\Lambda_{LE} = 74^\circ$
 - 5) BOEING SUPERSONIC TEST 218

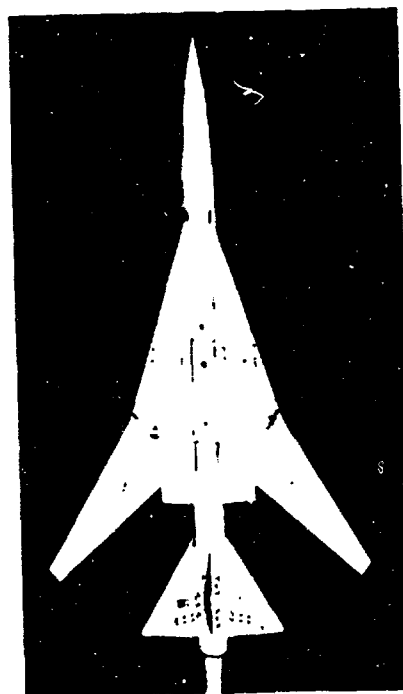
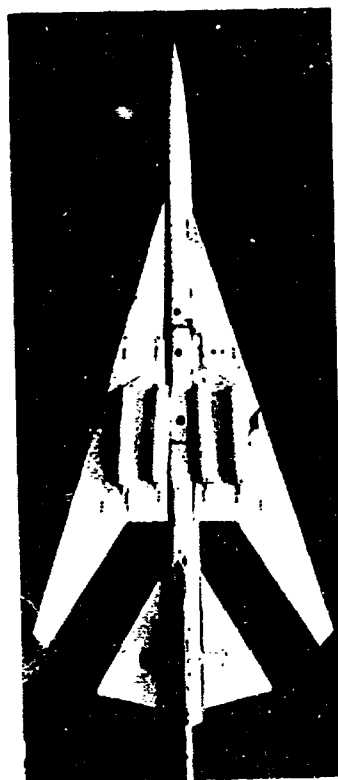




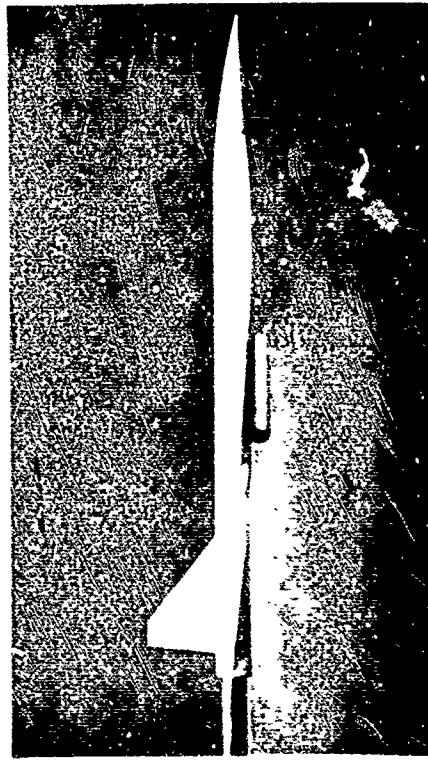
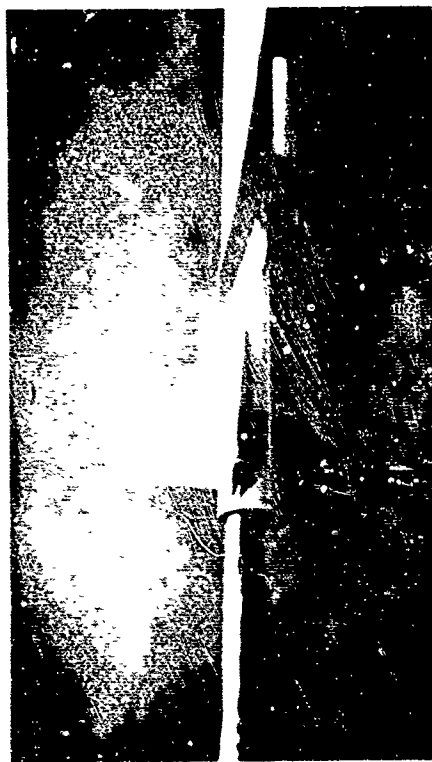
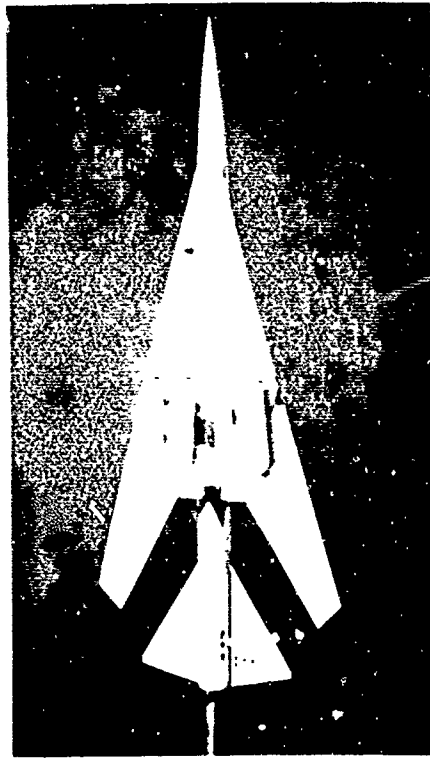
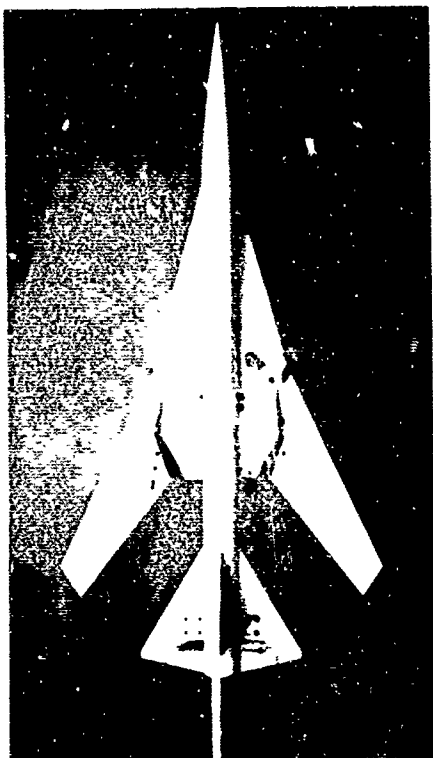
NOTE:

- 1) THESE DATA UNCORRECTED FOR MODEL OR AIRPLANE AEROELASTICITY
- 2) $q = 1500$ PSF NOMINAL
- 3) $RN = 10.1 \times 10^6$ BASED ON \bar{c}_w
- 4) COEFFICIENTS BASED ON ARROW WING GEOMETRY AT $\Lambda_{LE} = 74^\circ$
- 5) BOEING SUPERSONIC TEST 218

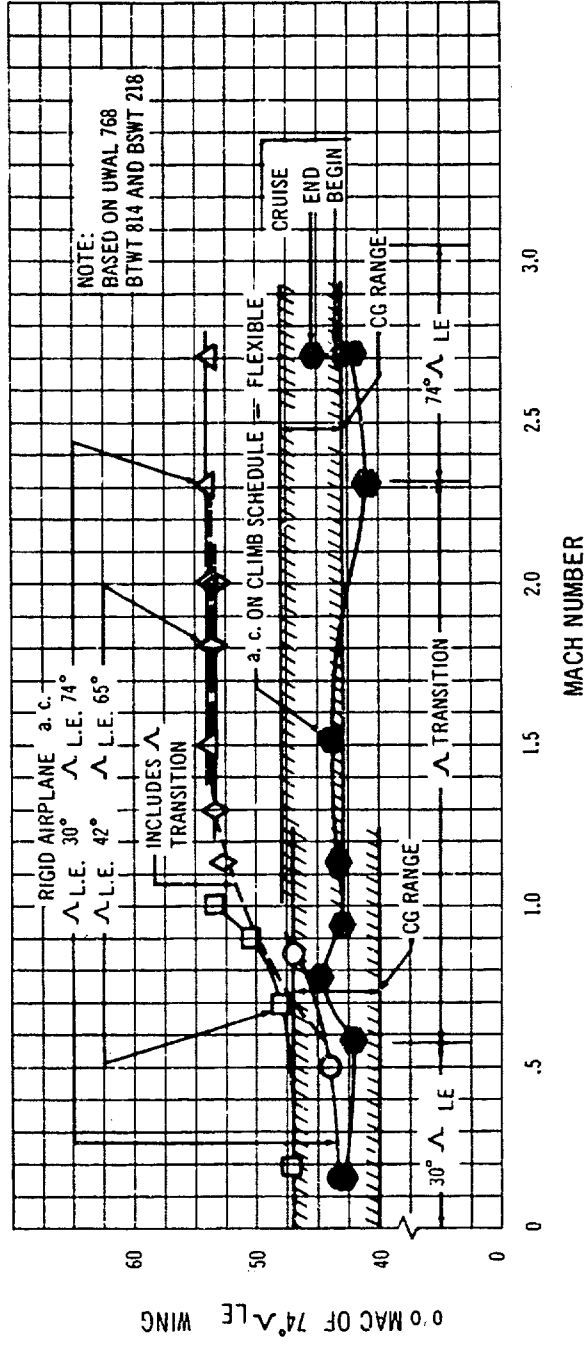
D-16 Static Longitudinal Stability and Control Supersonic, $\Lambda_{LE} = 74^\circ$, $M = 2.7$



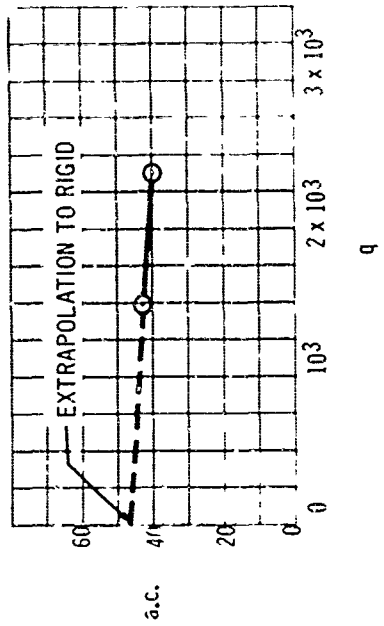
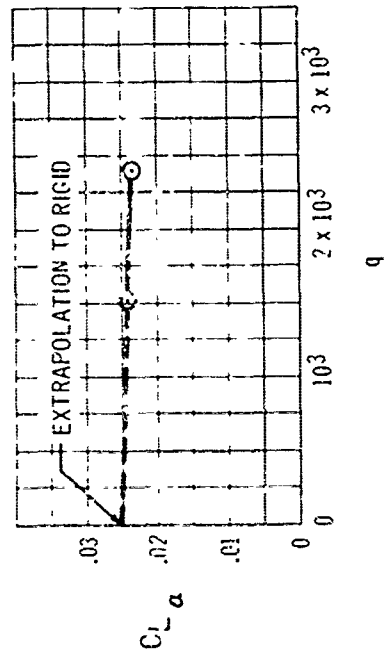
D-17 Model Configurations Tested in Transonic Wind Tunnel



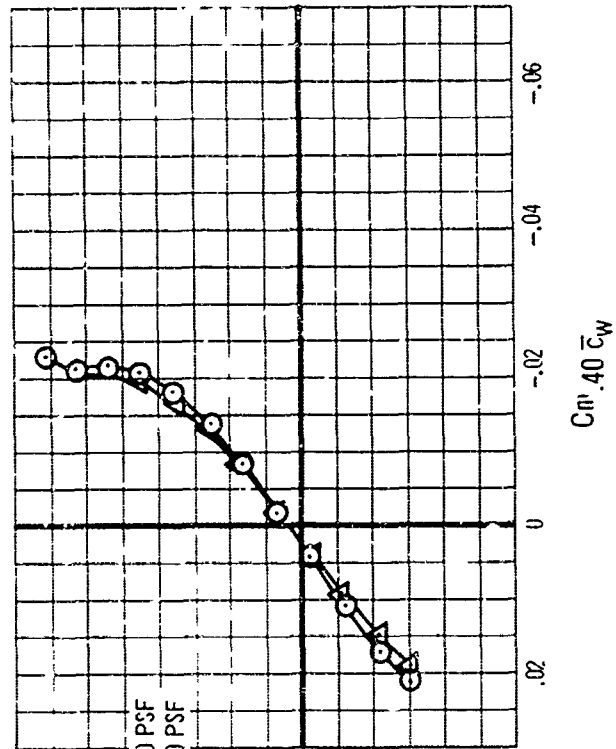
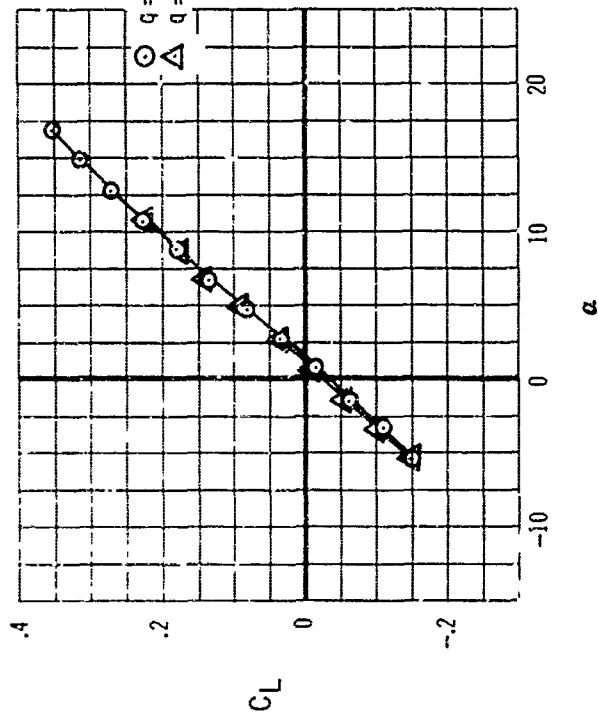
D-18 Model Configurations Tested in Supersonic Wind Tunnel



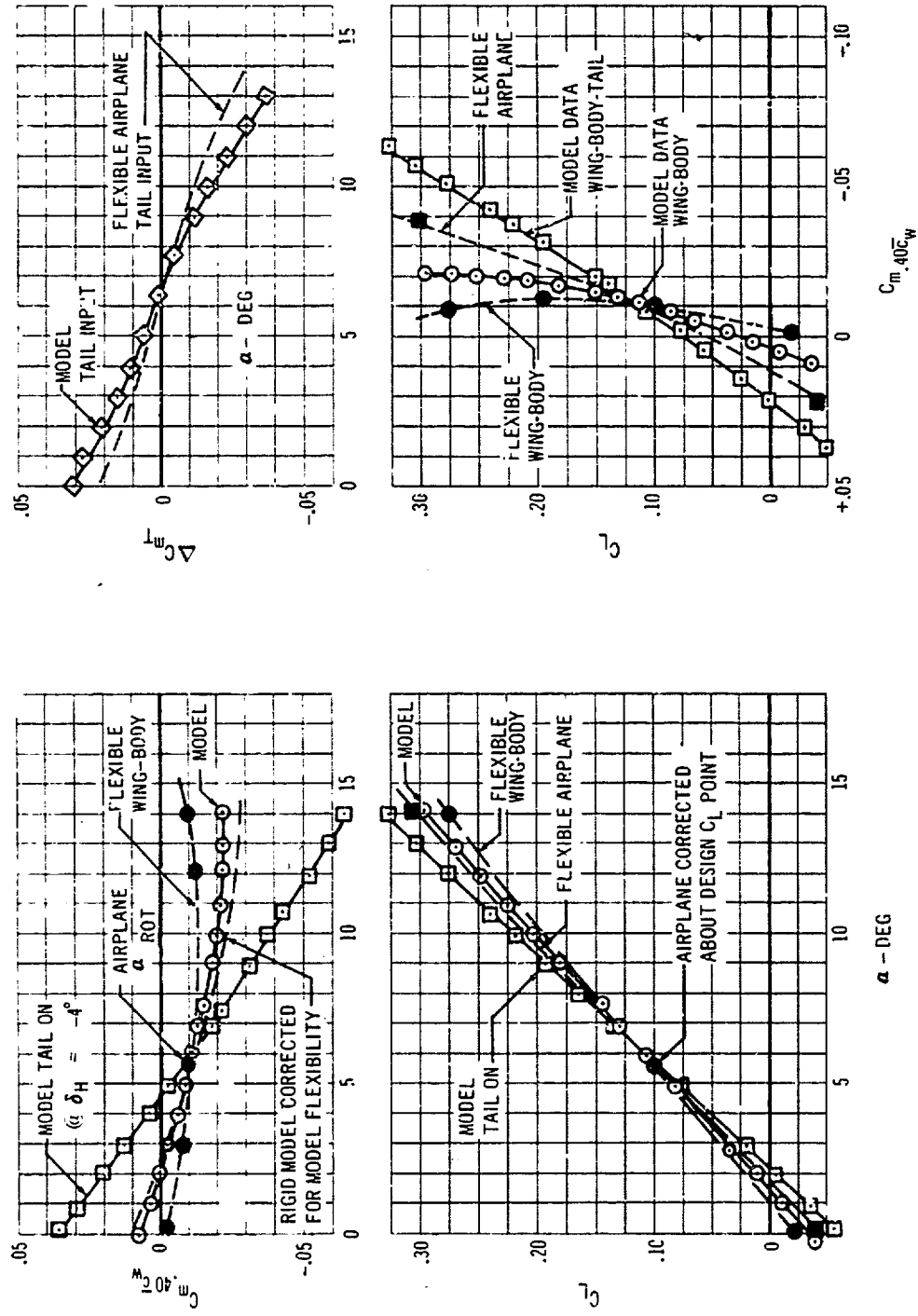
D-19 Tail-Off Aerodynamic Center, Center-of-gravity Relationship



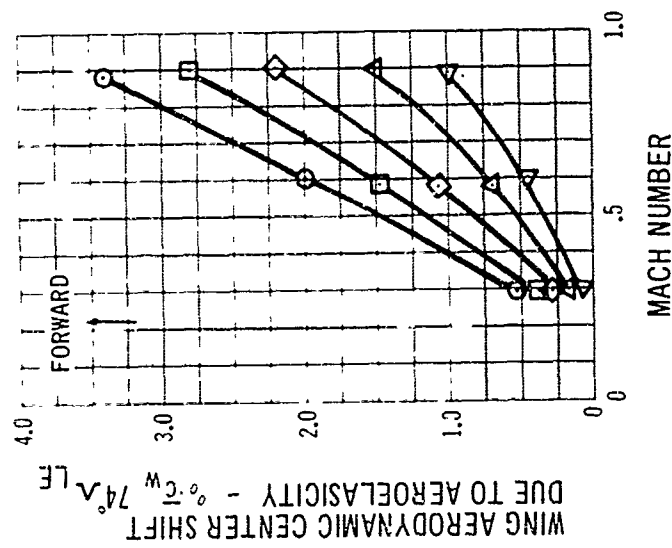
NOTE:
1. BASED ON BSWT 218



D-20 Supersonic Model Aeroelastic Effects, $M = 2.7$



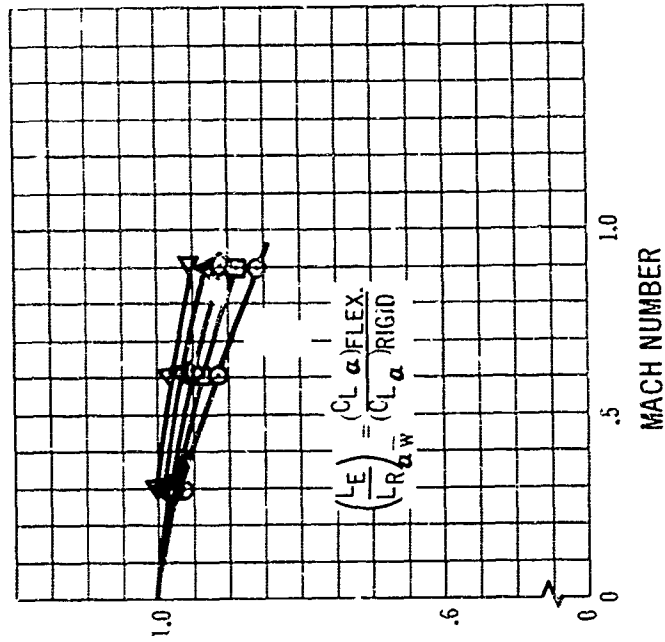
D-21 Application of Aeroelasticity Corrections to Static Longitudinal Stability Data, $M = 2.7$



NOTE: POINTS SHOWN ARE CALCULATIONS

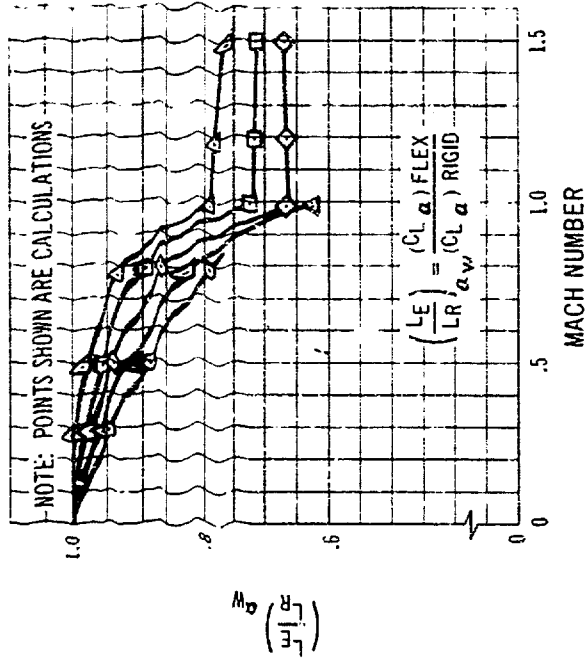
- SEA LEVEL
- 10,000 FT.
- ◇ 20,000 FT.
- △ 30,000 FT.
- ▽ 40,000 FT.

$$\left(\frac{L_E}{L_R} \right)_{a_w}$$

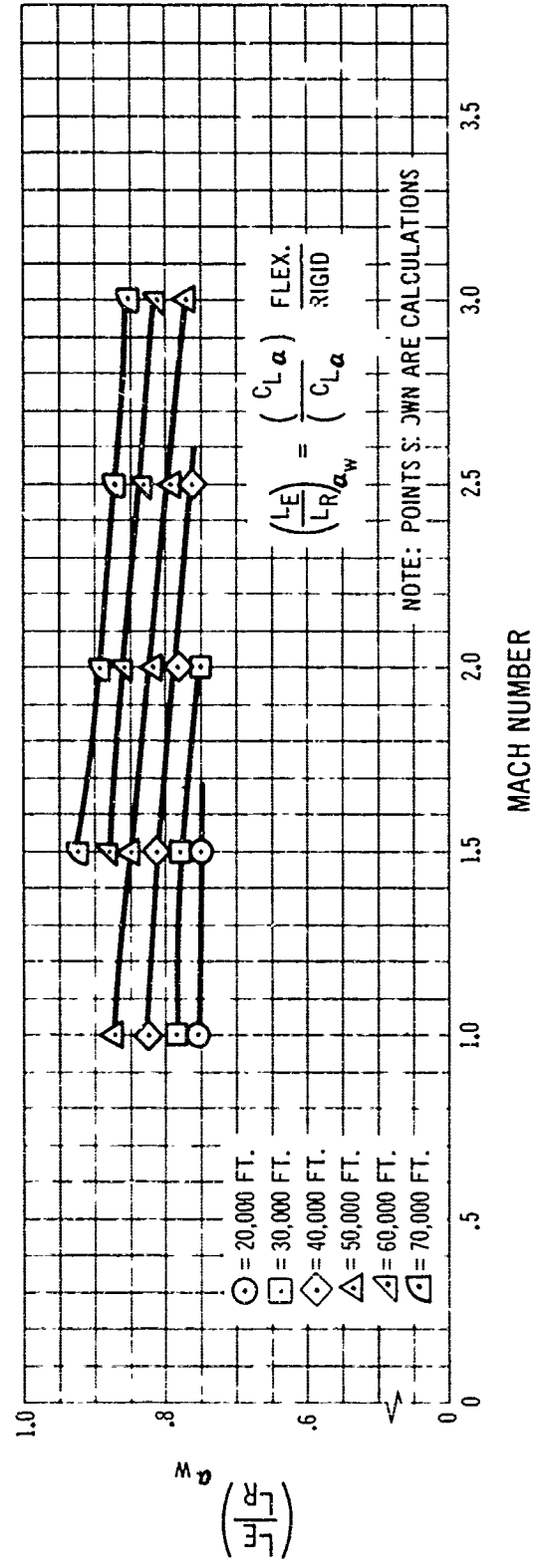


$$\left(\frac{L_E}{L_R} \right) = \frac{(C_{L\alpha})_{FLEX.}}{(C_{L\alpha})_{RIGID}}$$

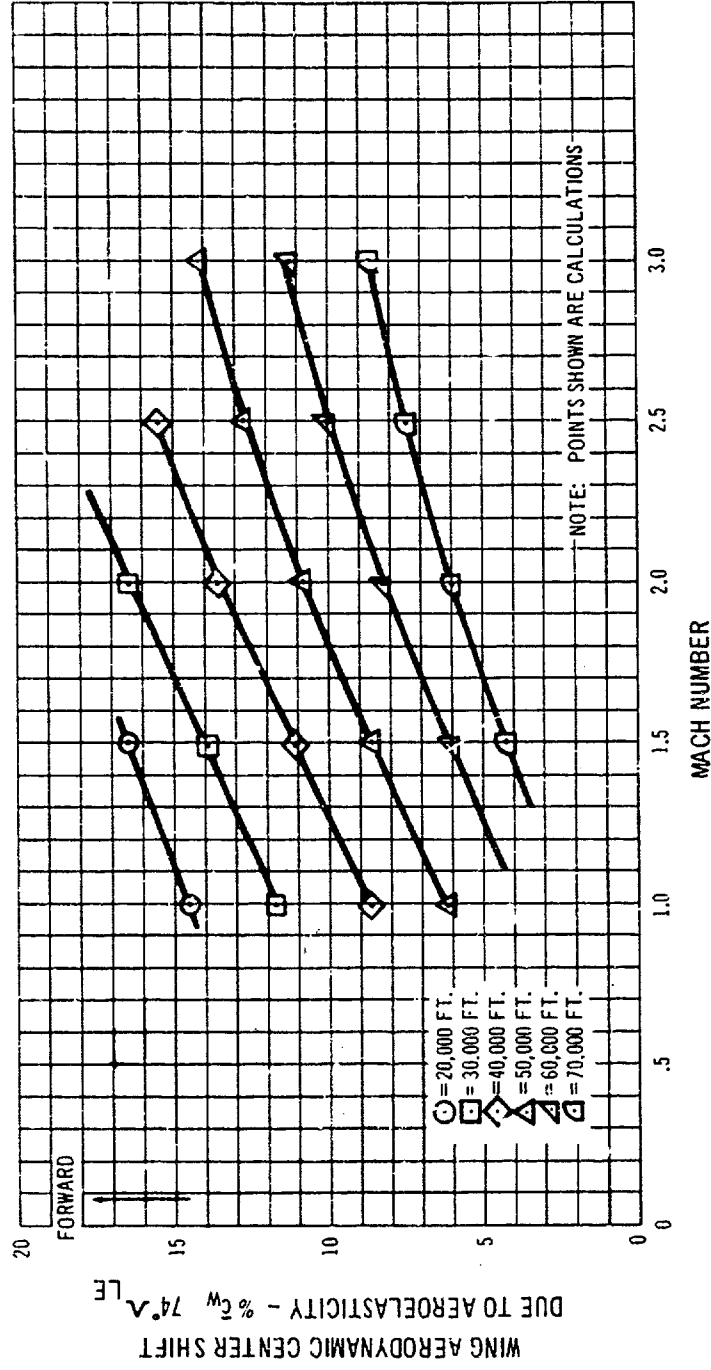
D-22 Wing Aeroelastic Effects, $\Delta LE = 25^\circ$



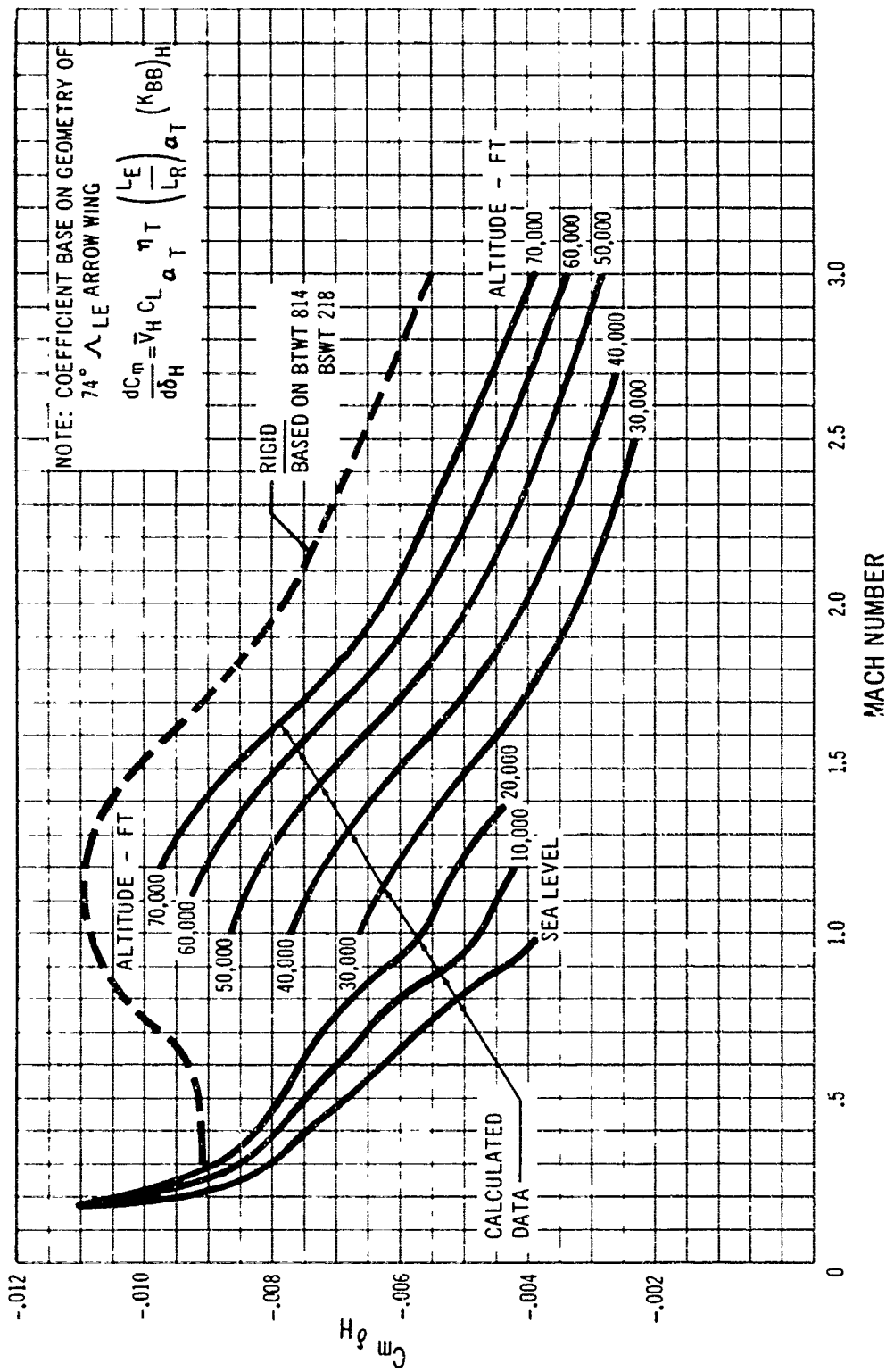
D6-2400-11 D/29



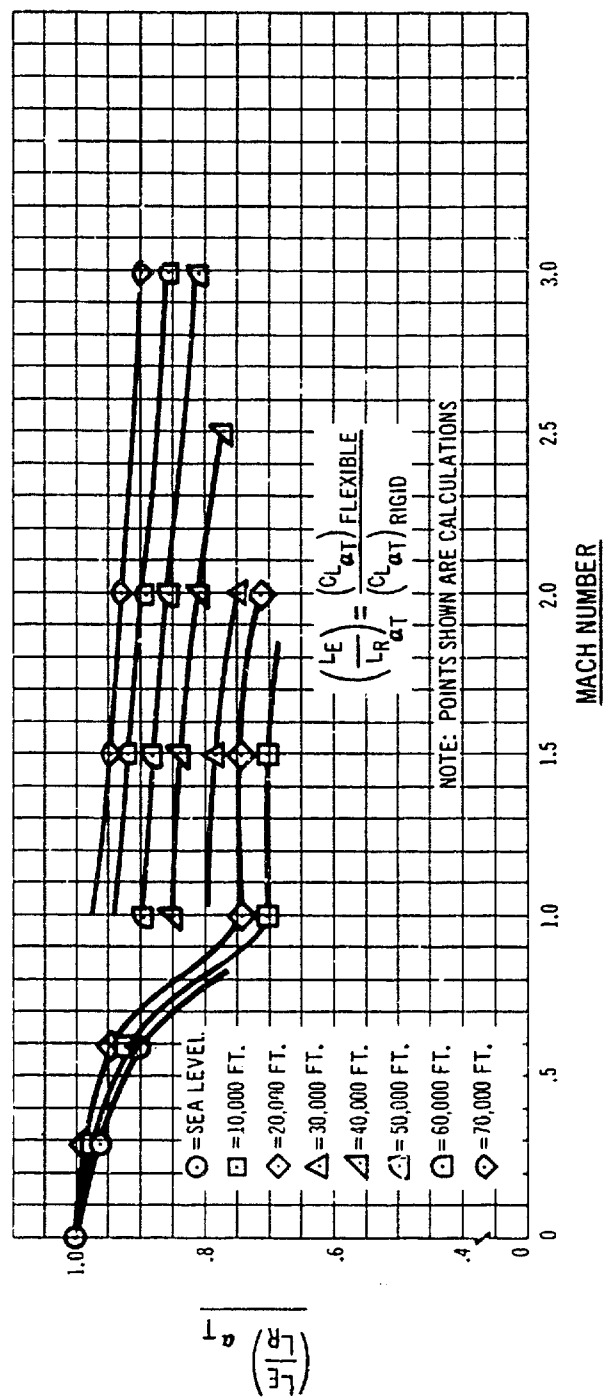
D-24 Wing Aeroelastic Factor, $\Lambda_{LE} = 74^\circ$



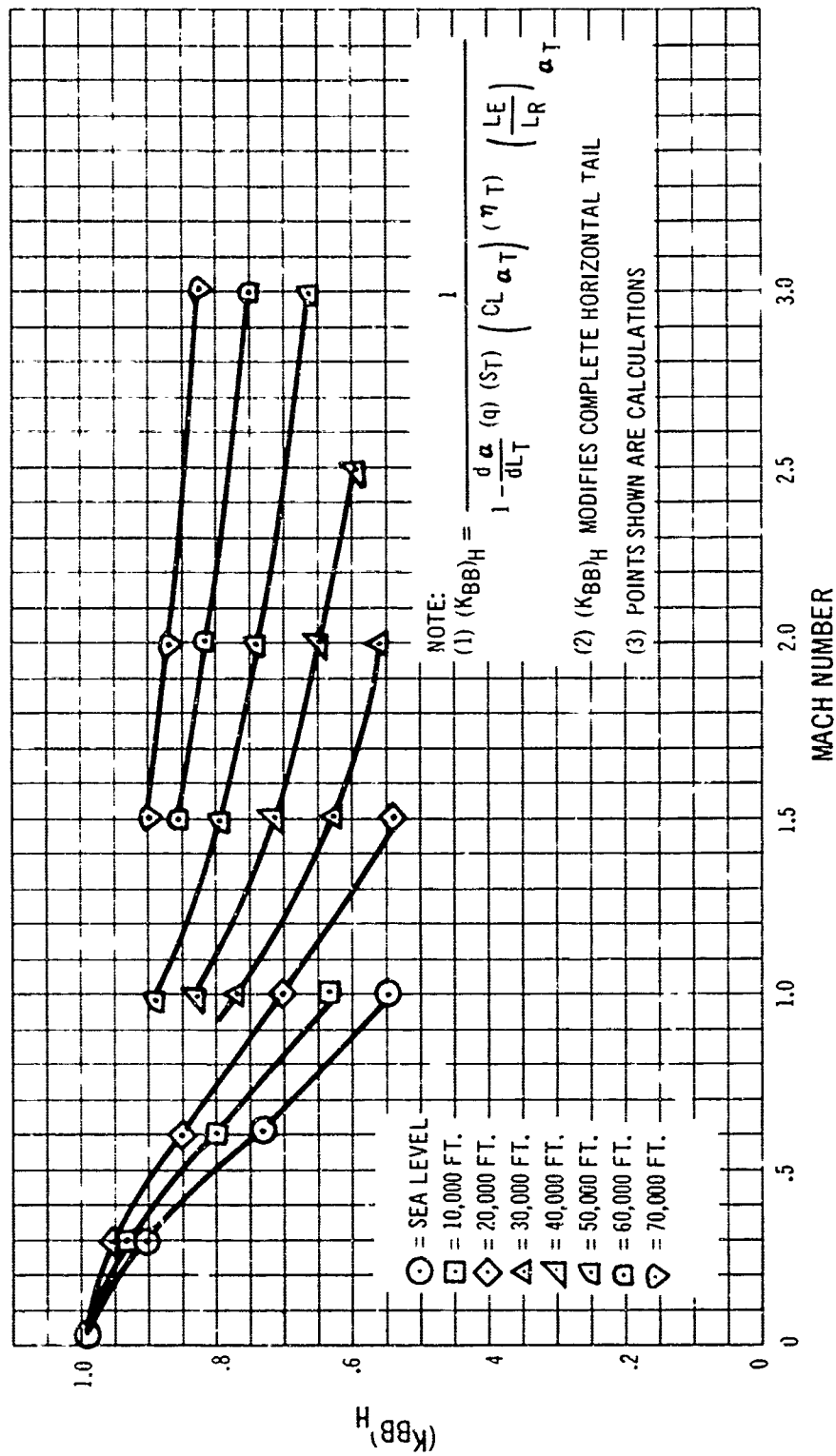
D-25 Wing Aerodynamic Center Shift Due to Aeroelasticity, $\Delta_{LE} = 74^\circ$



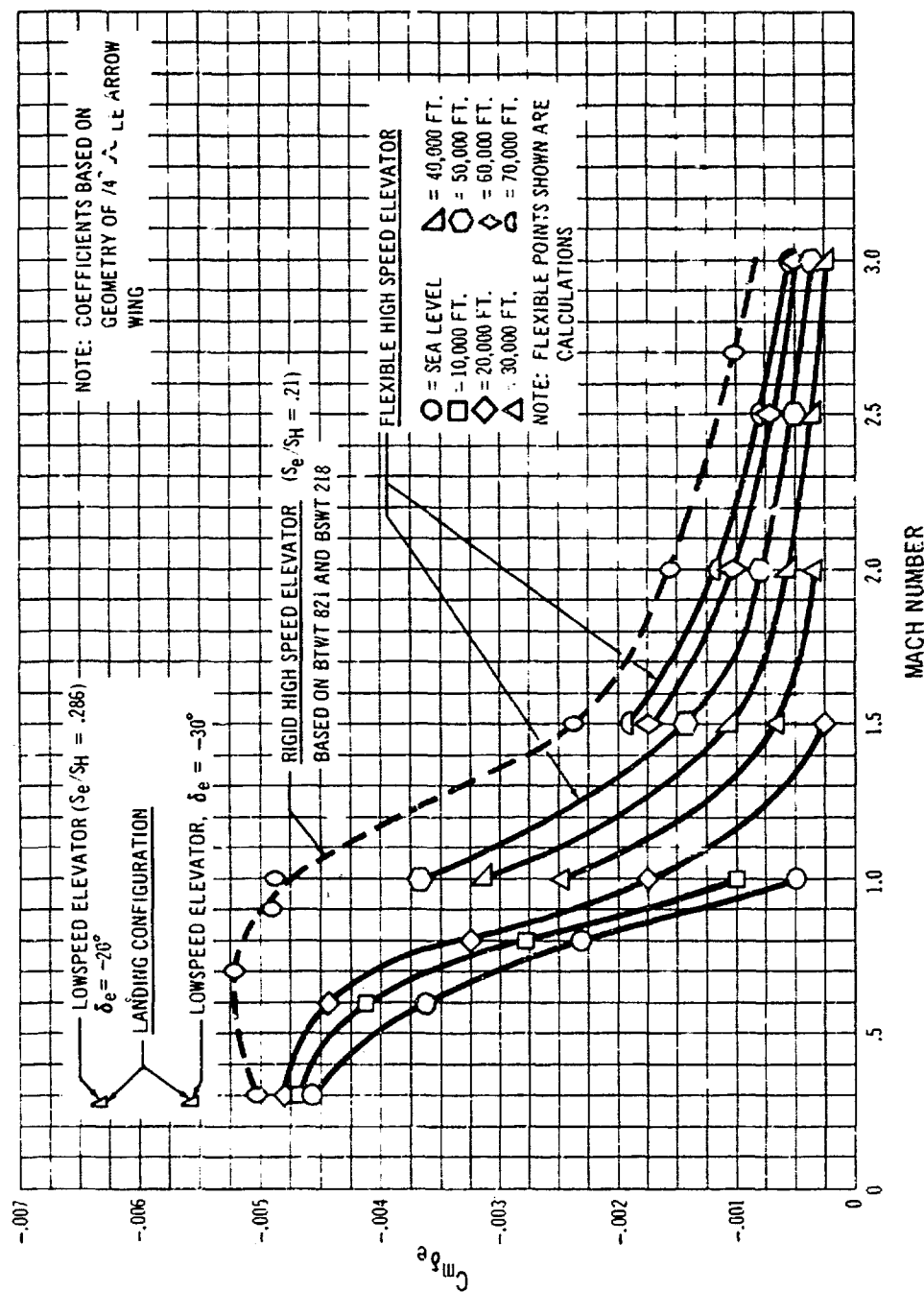
D-26 Horizontal Stabilizer Effectiveness, Rigid and Flexible



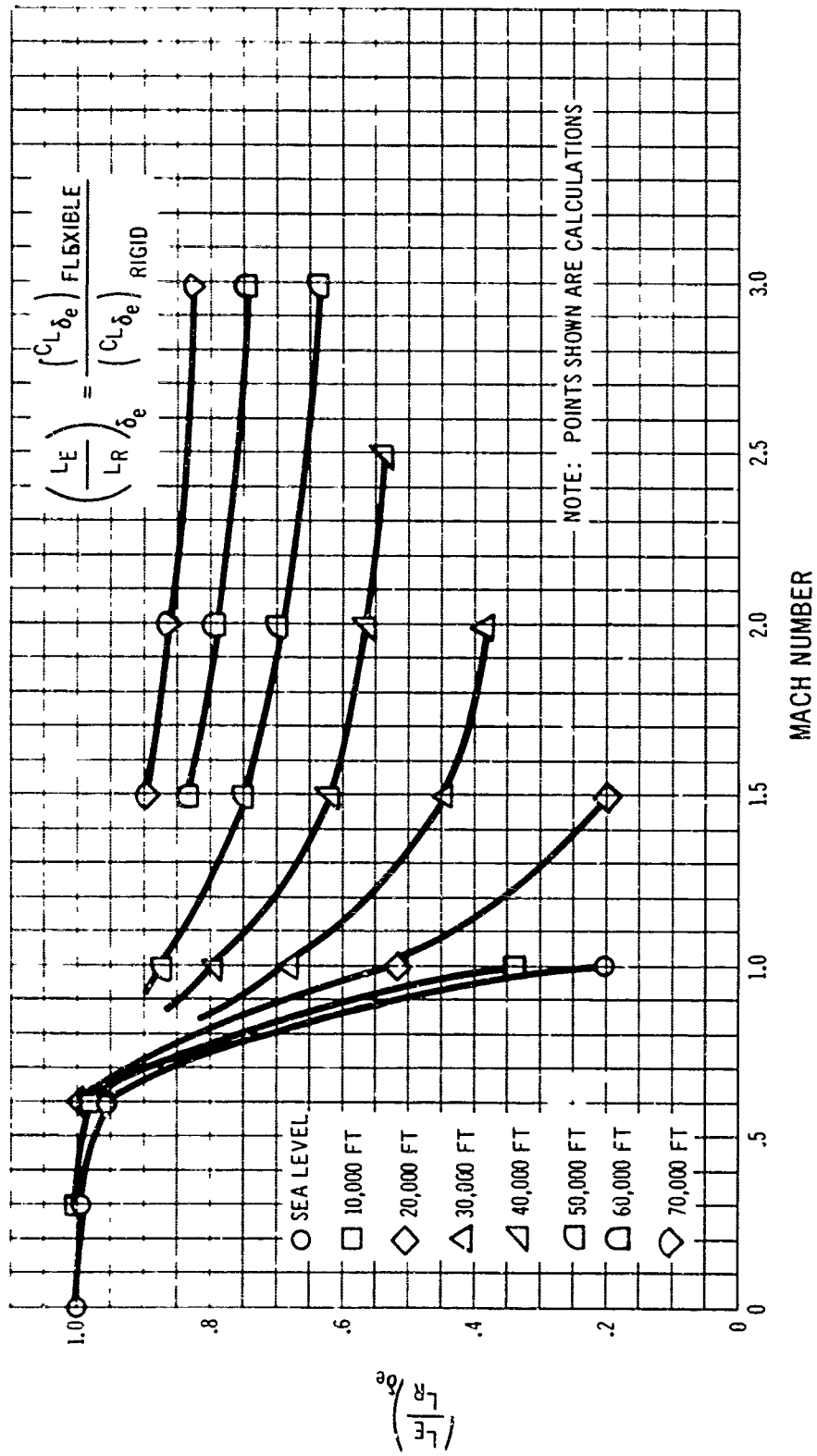
D-27 Horizontal Tail Aeroelastic Factor



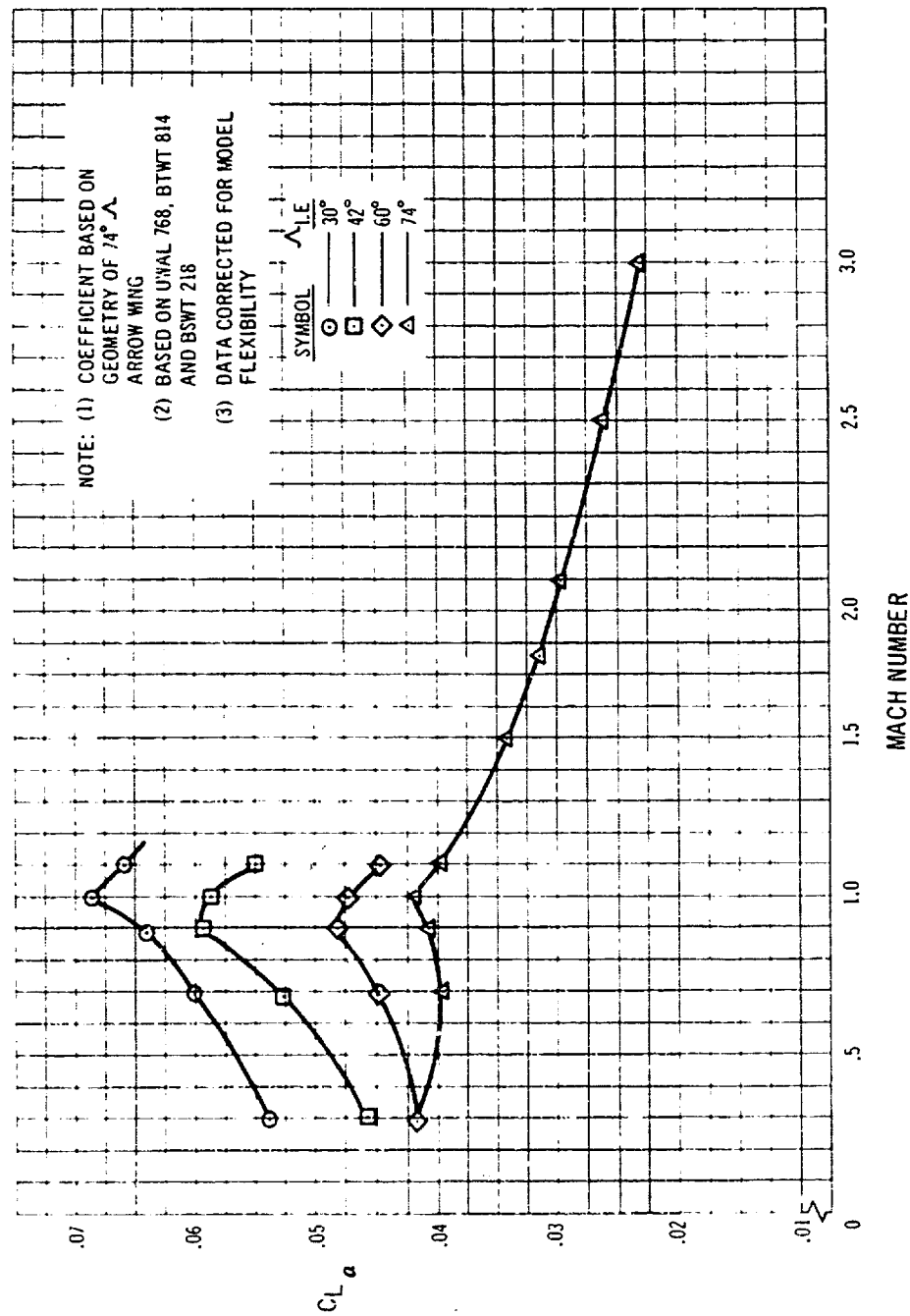
D-28 Aeroelastic Body - Bending Factor for Horizontal Tail



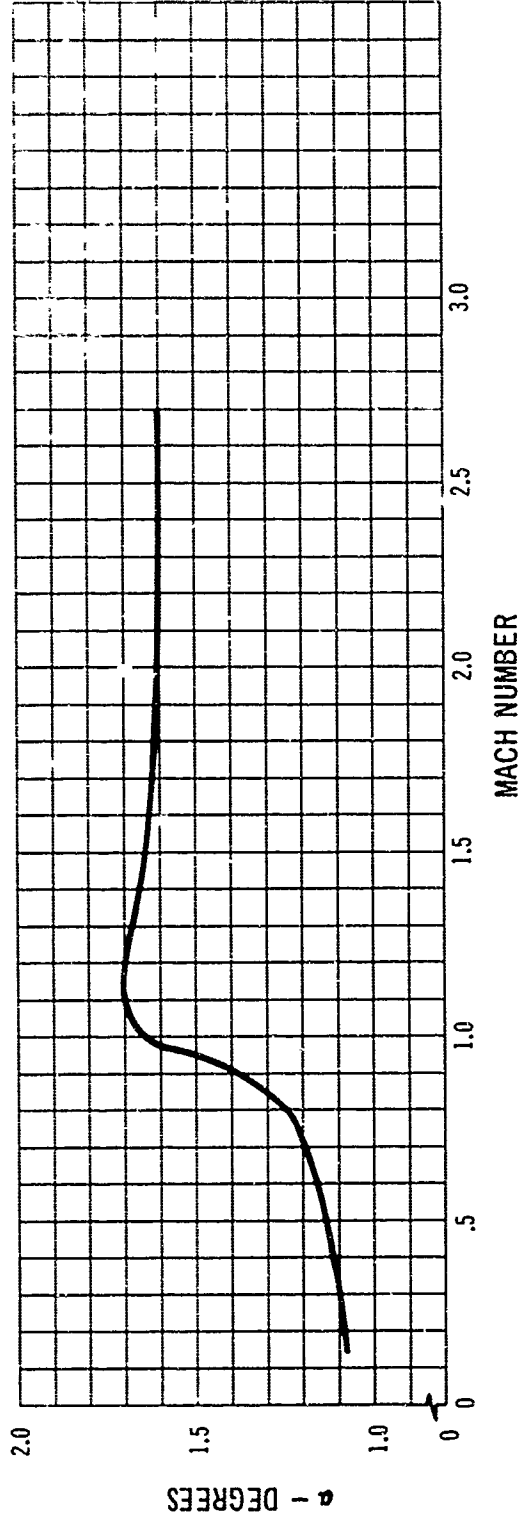
D-29 Elevator Effectiveness, Rigid and Flexible



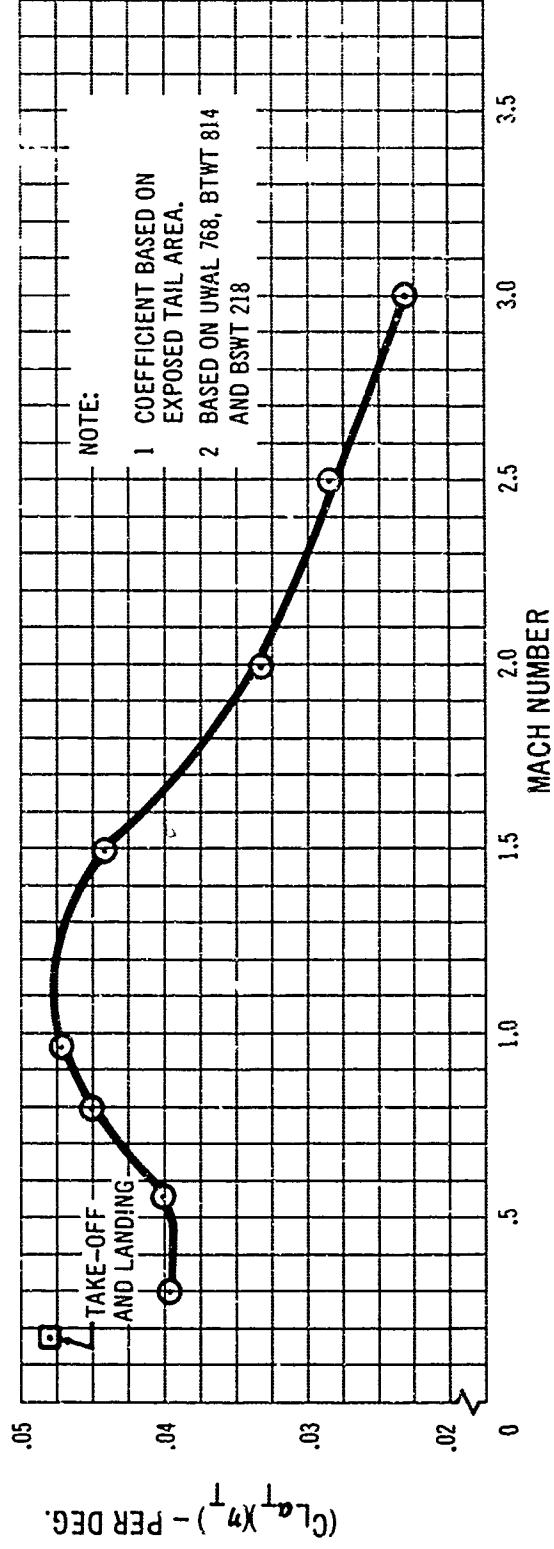
D-30 Elevator Aeroelastic Factor



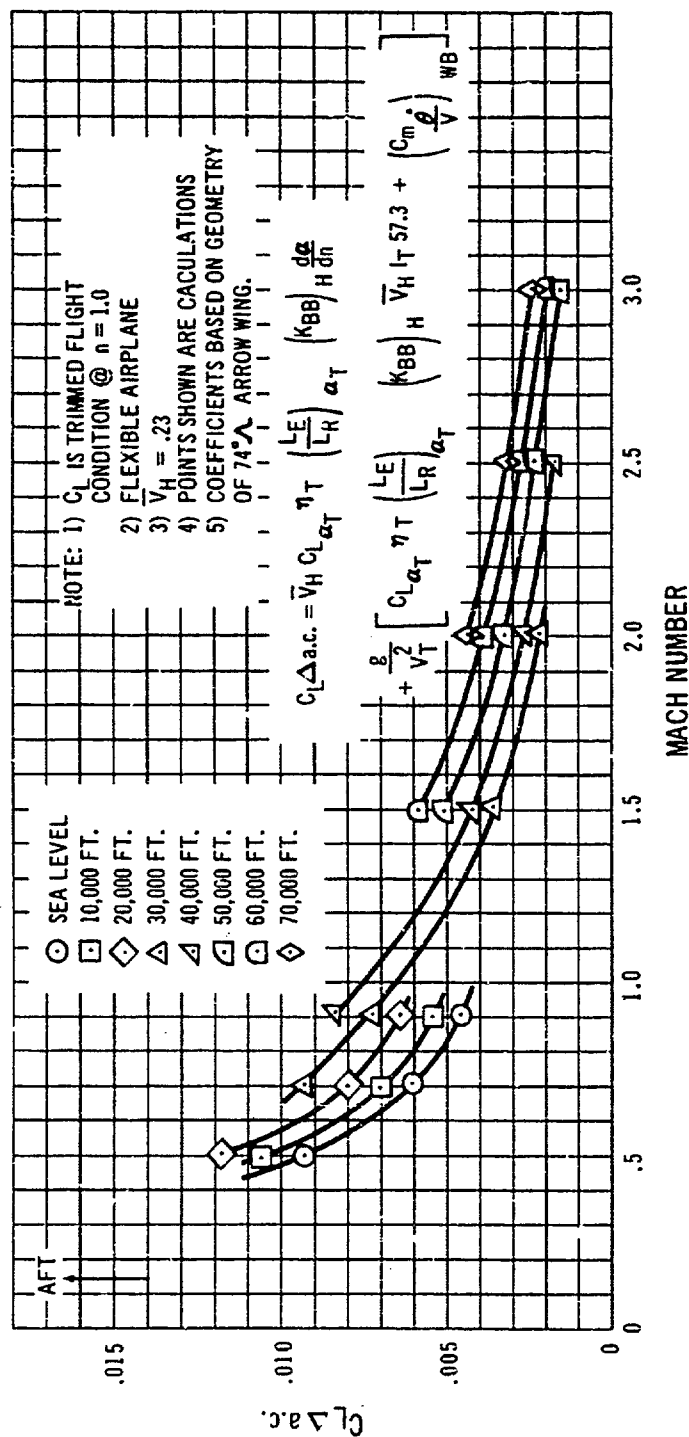
D-31 Wing Lift Curve Slope, Rigid



D-32 Angle of Attack at Zero Lift - Rigid Airplane



D-33 Horizontal Tail Lift Curve Slope, Rigid



D-34 Increment in Aerodynamic Center Due to Maneuver Effects (Wing, Tail Damping and Aft Body Inertia)

D7.4 Static Lateral-Directional Stability and Control Data

D7.4.1 LATERAL-DIRECTIONAL STABILITY

The vertical tail and ventral fin combination of the proposal configuration have been sized to provide good directional stability at all operating conditions in the flight envelope. The large ventral fin maintains directional stability at satisfactory levels at extreme angles of attack at the most critical maximum Mach number conditions. Figs. D-35 through D-37 show typical variations in directional stability with sideslip angle and angle-of-attack for three wing sweep angles (15 degrees, 45 degrees, and 74 degrees) at low speed. These data were obtained in wind tunnel tests of a Boeing SST low-speed model which is different from the proposal configuration in several minor details. The directional stability data shown in Section 7.2.2 have been adjusted to full scale by correcting for the longer fuselage nose and smaller vertical tail and ventral fin of the wind tunnel model. Except as noted, the data in this section are unadjusted wind tunnel measurements.

Fig. D-38 presents wind tunnel test data showing the variation in directional stability with sideslip angle and angle of attack at the critical cruise Mach number, 2.7, condition. The model moment center (.40 \bar{c}) for these data corresponds to the airplane aft CG limit (.47 \bar{c}), so that the wing-body data are directly applicable to the full-scale, rigid airplane. The model vertical tail and ventral \bar{V} 's however are different than those of the proposal configuration, so that the tail inputs shown are incorrect. The full scale characteristics shown in Section 7.2 have been corrected for the proper tail volume coefficients.

The following aeroelastic corrections have been applied to the wind tunnel test data:

$$C_{n\beta_E} = C_{n\beta_{(WB+H+NAC)}} + C_{n\beta_{VEN}} \left(K_{BB} \right)_{VEN} + C_{n\beta_v} \left(\frac{L_E}{L_R} \right)_v \left(K_{BB} \right)_v$$

Where $(K_{BB})_{VEN}$ is a factor on ventral tail lift due to body side bending. $(K_{BB})_v$ is a factor on vertical tail lift due to body side bending.

$\left(\frac{L_E}{L_R} \right)_v$ is a factor on vertical tail lift due to vertical tail flexibility.

$C_{l\beta_E} = C_{l\beta_R}$ (Difference is small since loss due to wing load change is opposed by change in dihedral.)

$$C_{Y\beta_E} = C_{Y\beta_{(WB+H+NAC)}} + \Delta C_{Y\beta_{VEN}} \left(K_{BB} \right)_{VEN} + C_{Y\beta_v} \left(\frac{L_E}{L_R} \right)_v \left(K_{BB} \right)_v$$

The above aeroelastic factors are presented in Figures D7-39 and D7-40.

Figures D-41 and D-42 present C_{δ} and C_{δ} variations with Mach number, wing sweep, flap deflection, and aeroelasticity. These data were obtained in low-speed, transonic, and supersonic wind tunnel tests of the models shown in Figs. D-55 and D-56.

D7.4.2 DIRECTIONAL CONTROL

Rigid wind tunnel data and flexible rudder effectiveness are shown in Fig. D-43.

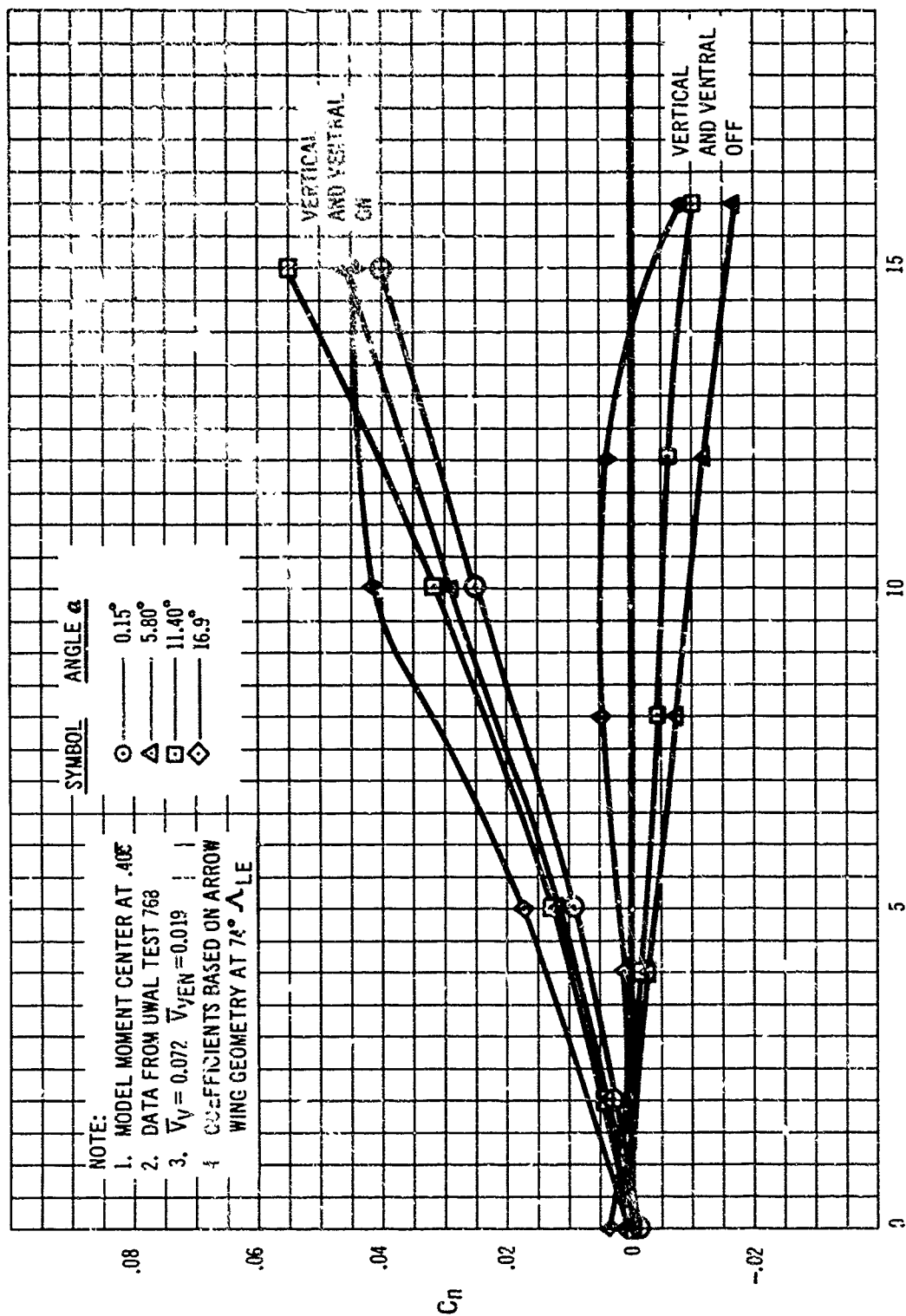
The following aeroelastic corrections were used:

$$C_{\eta E} = \left(C_{\eta \delta_r} \right)_E \delta_r$$

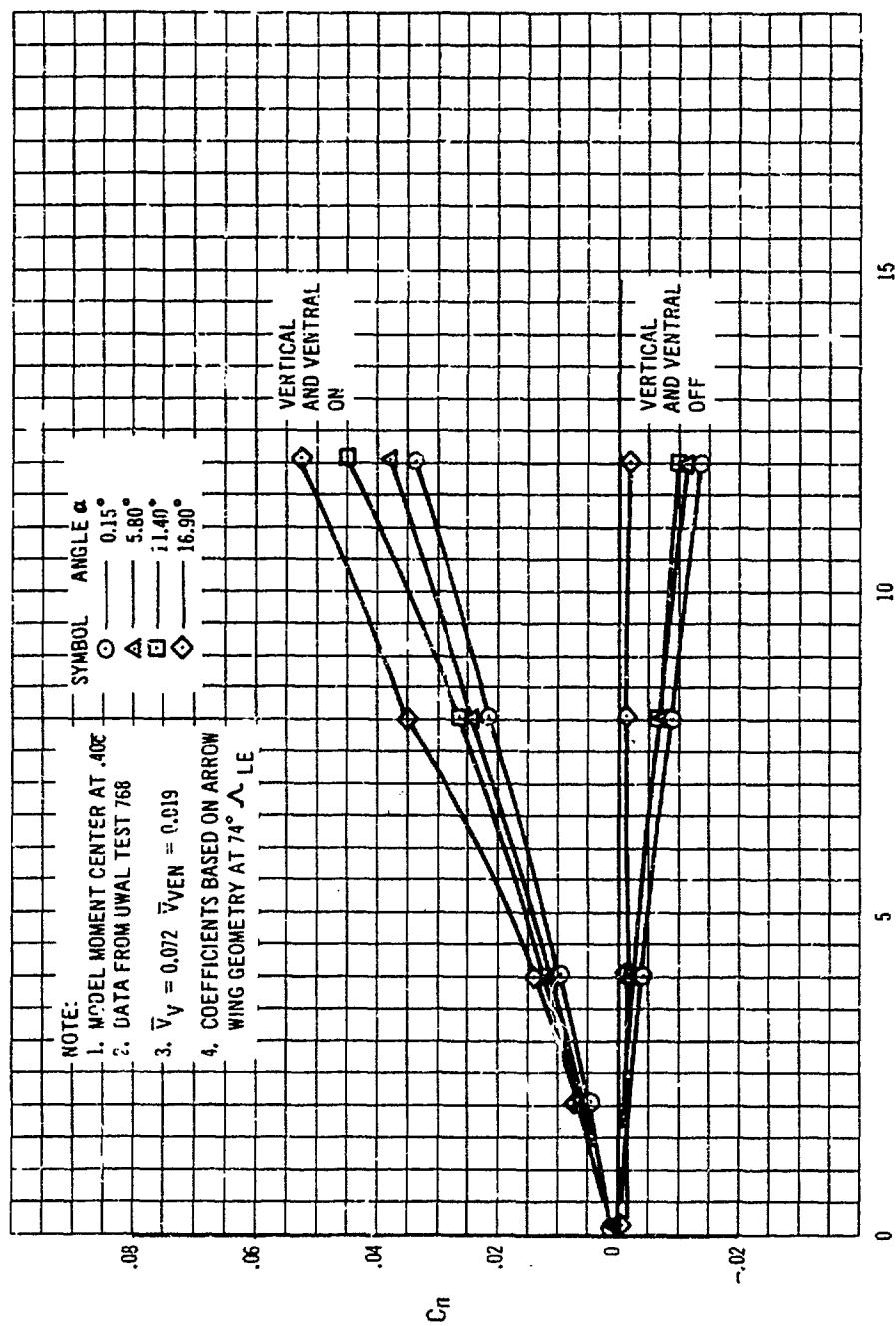
$$\text{where: } \left(C_{\eta \delta_r} \right)_E = \left(C_{\eta \delta_r} \right)_R \left(K_{SB} \right)_V \left(\frac{L_E}{L_R} \right) \delta_r$$

where $(K_{SB})_V$ is a factor on vertical tail lift due to body side bending. The elastic effect on rudder lift effectiveness, $\left(\frac{L_E}{L_R} \right) \delta_r$ is shown in Figure D-44.

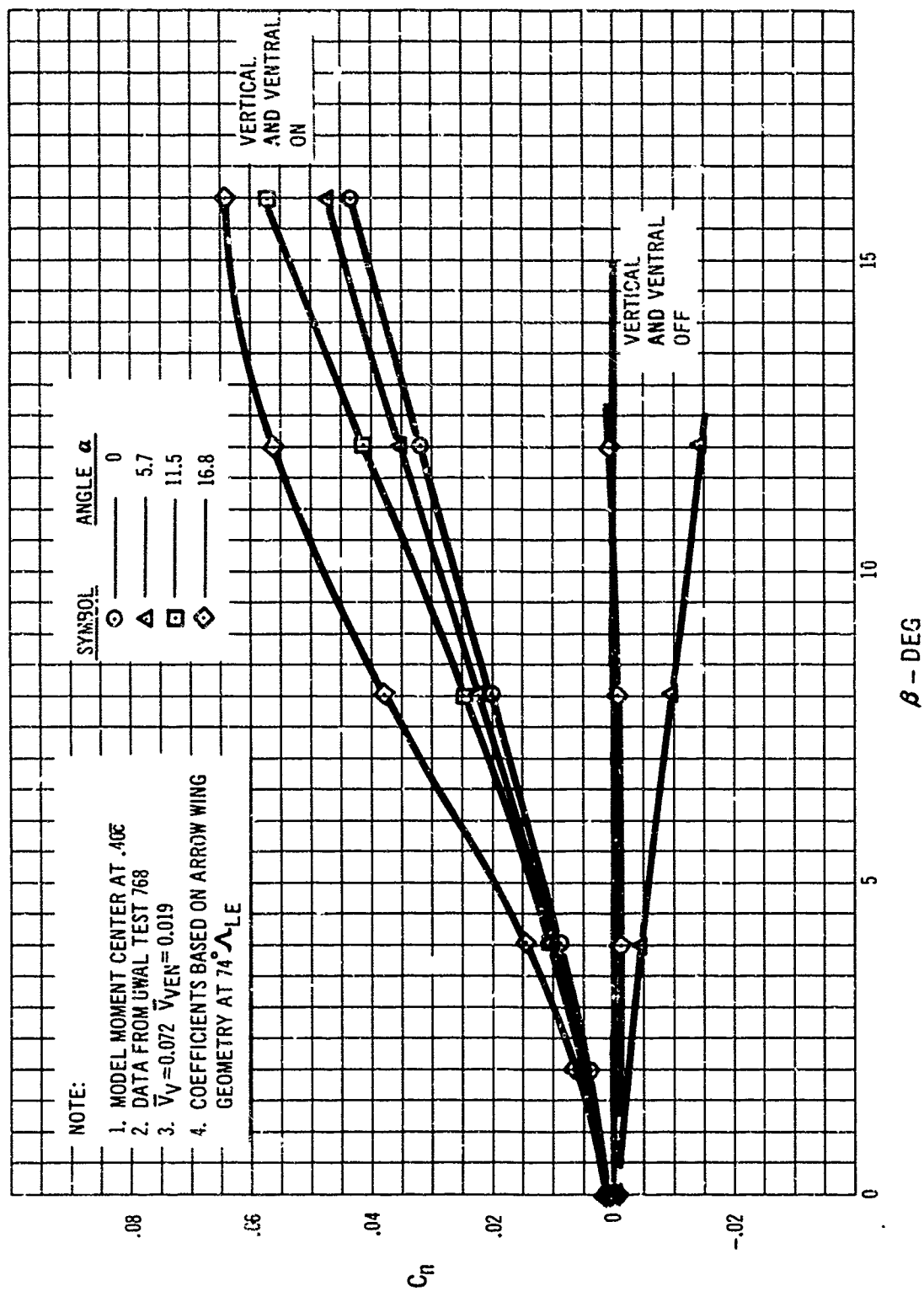
Figure D-45 summarizes the rudder travel limits. Fig. D-55 shows a photograph of one of the rudder configurations tested in the Boeing supersonic wind tunnel.



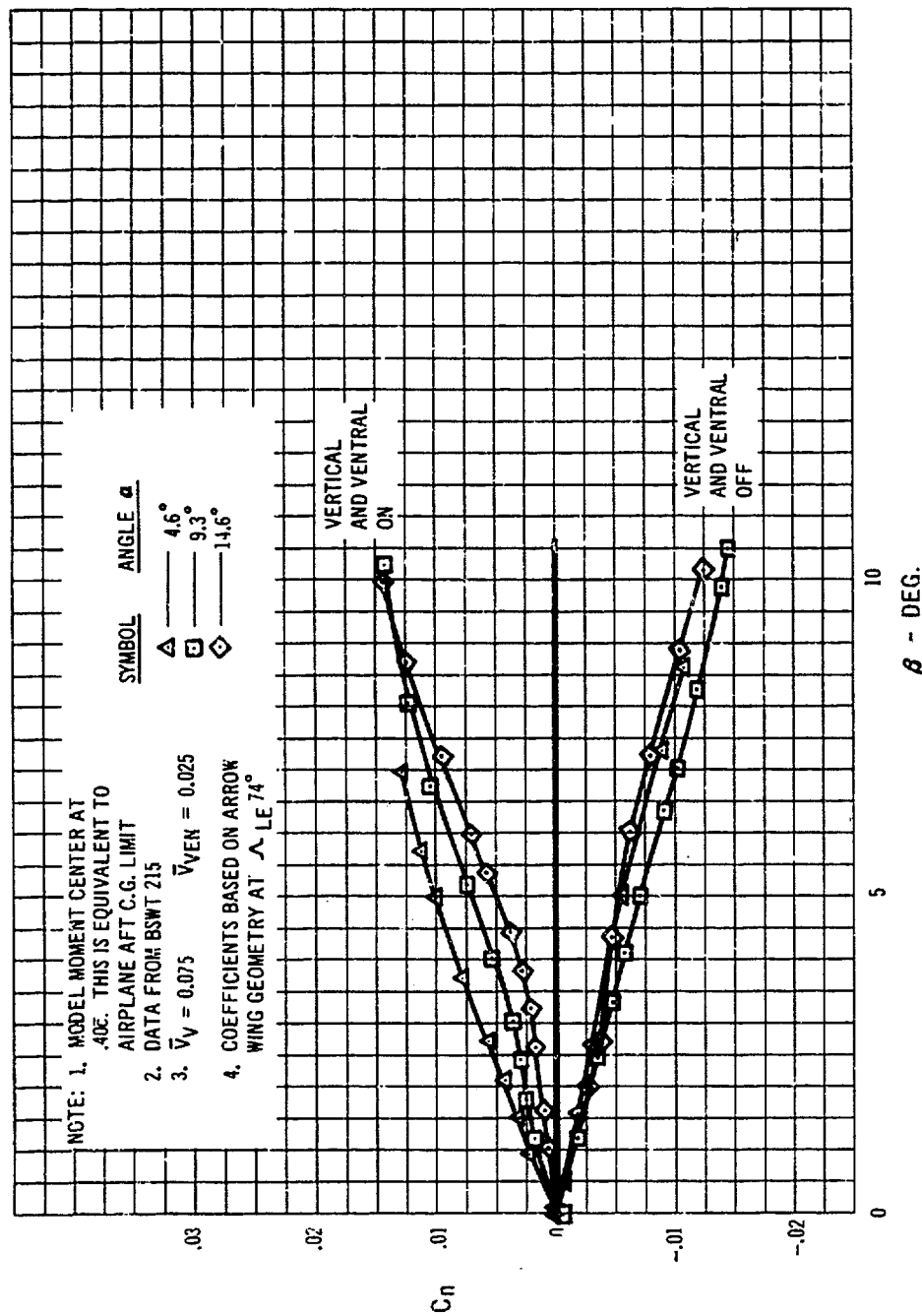
D-35 Yawing Moment Due to Sideslip, Low Speed $\Lambda_{LE} = 15^\circ$ β DEG Flaps Down



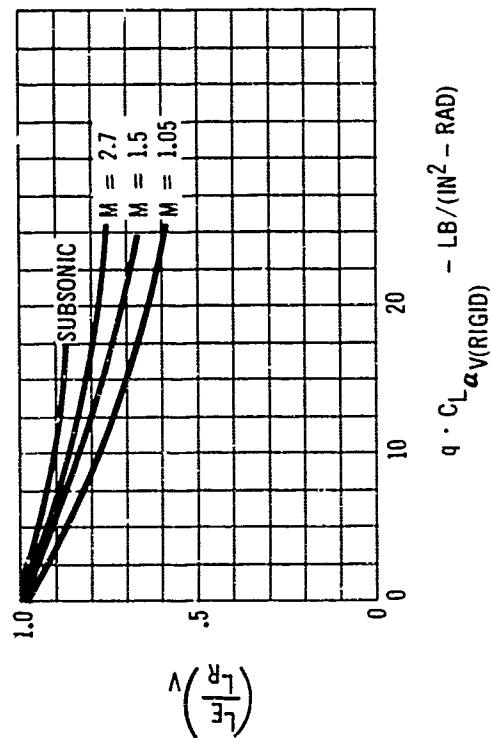
D-36 Yawing Moment Due to Sideslip, Low Speed, Δ LE = 45° , Flaps Up



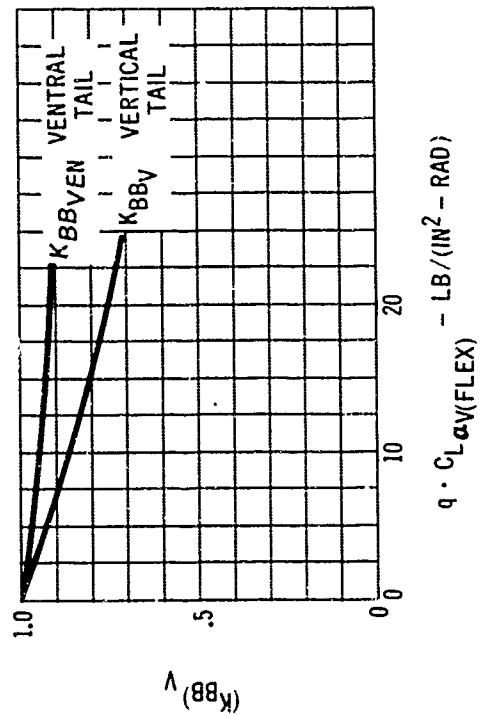
D-37 Yawing moment Due to Sideslip, Low Speed, $\Lambda_{LE} = 74^\circ$ Flaps Up



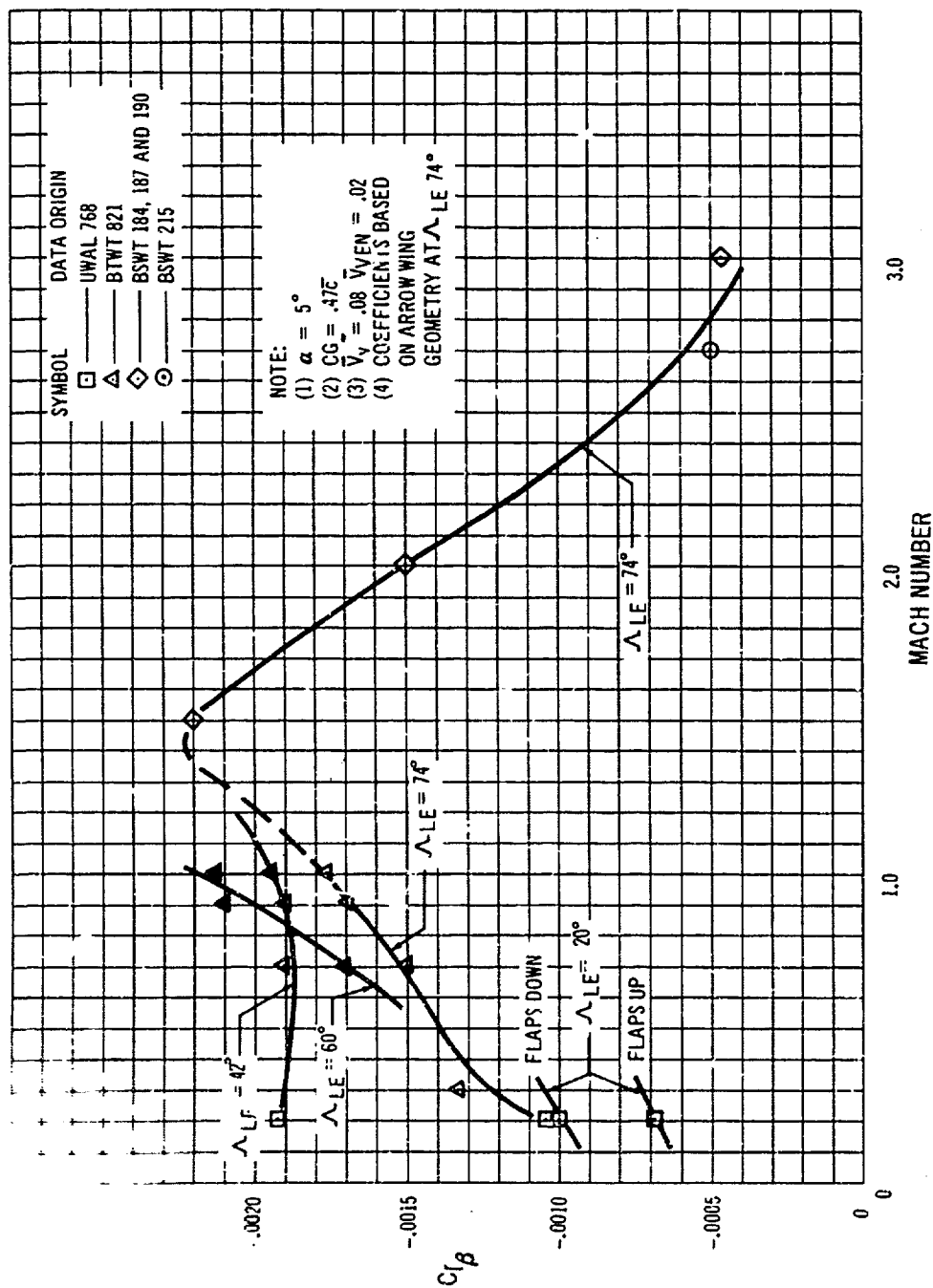
D-38 Yawing Moment Due to Sideslip, $M = 2.7$, $\Lambda_{LE} = 74^\circ$, Rigid



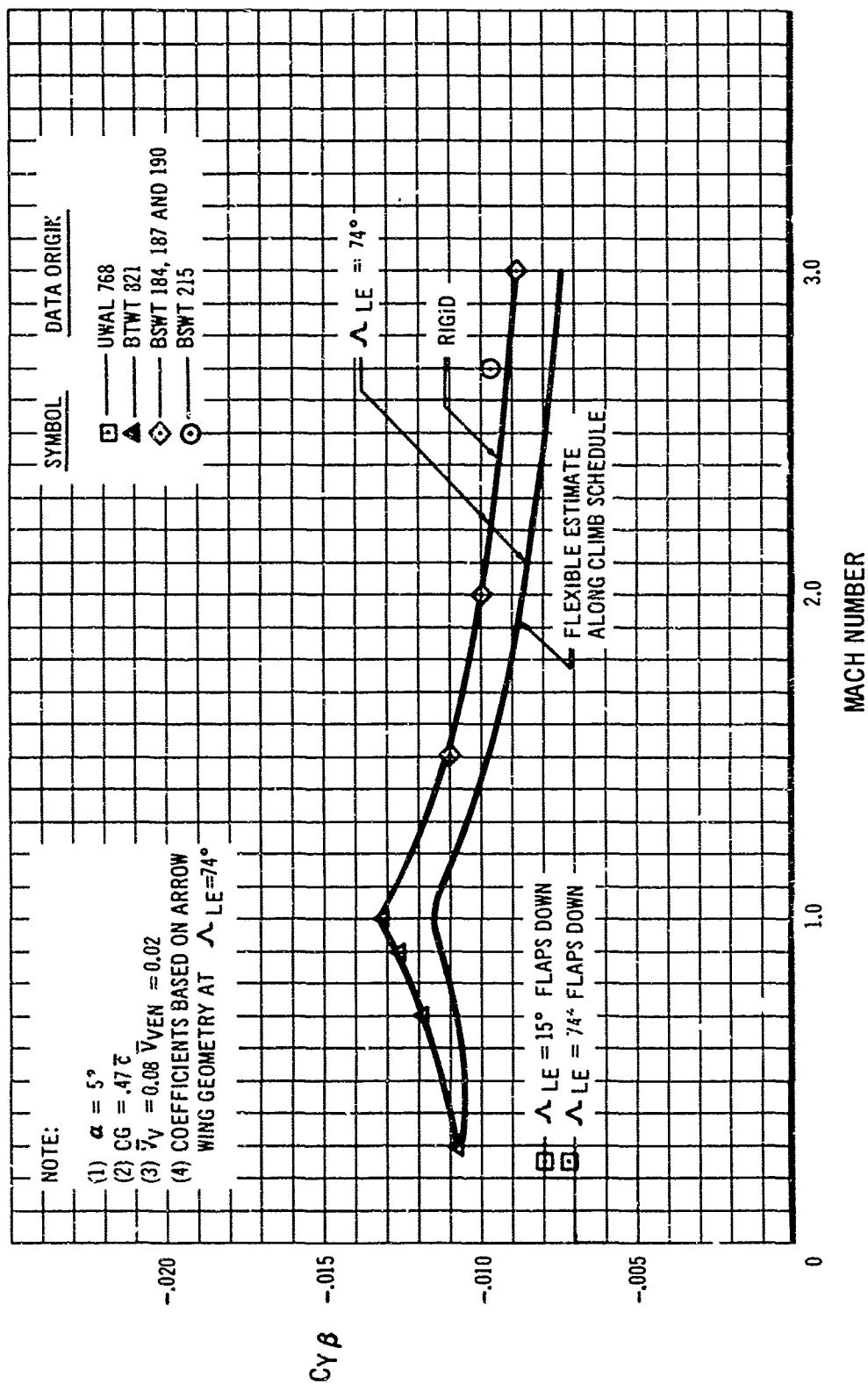
D-39 Vertical Tail Aeroelastic Factor



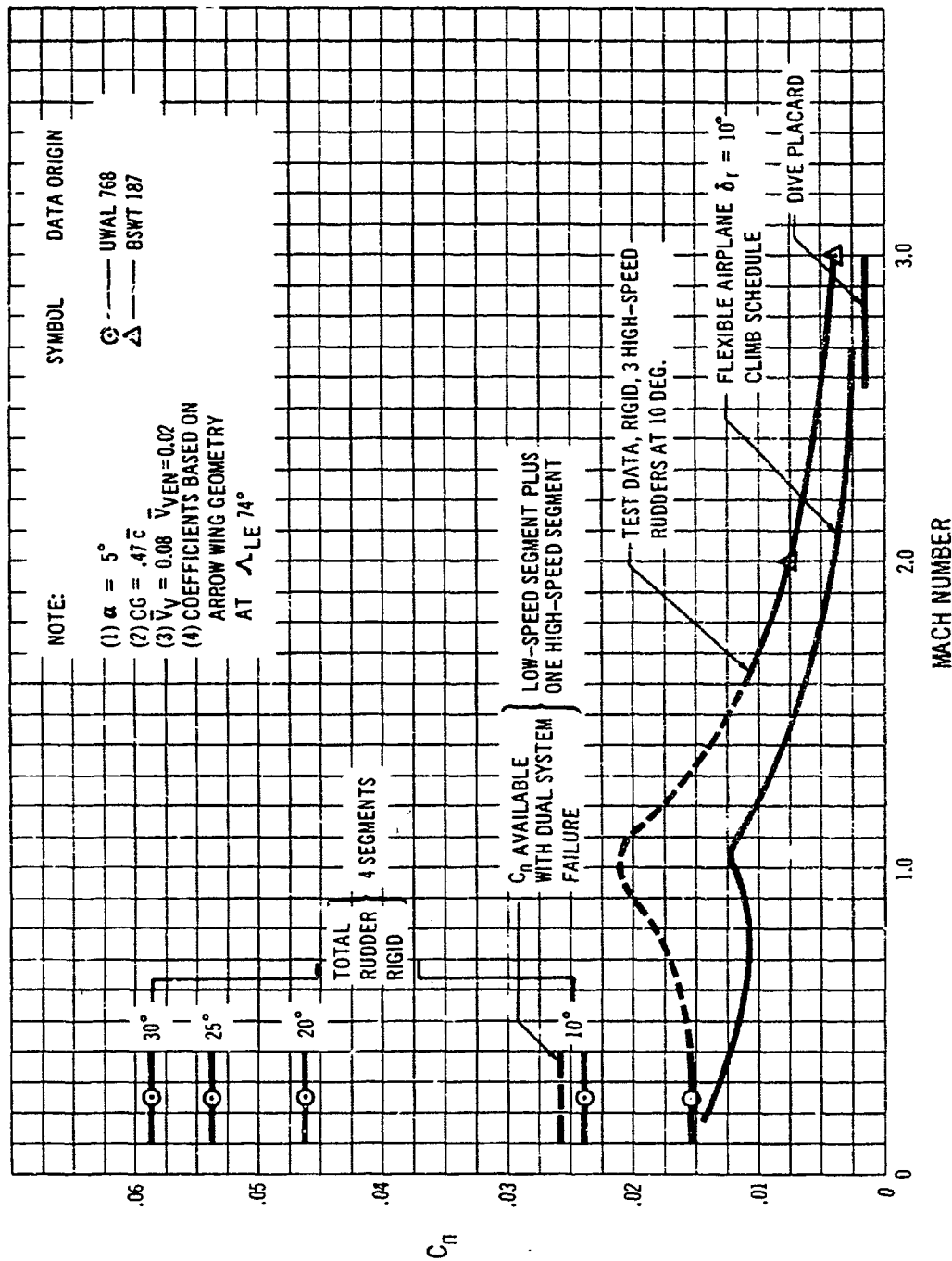
D-40 Aeroelastic Body Side Bending Factor



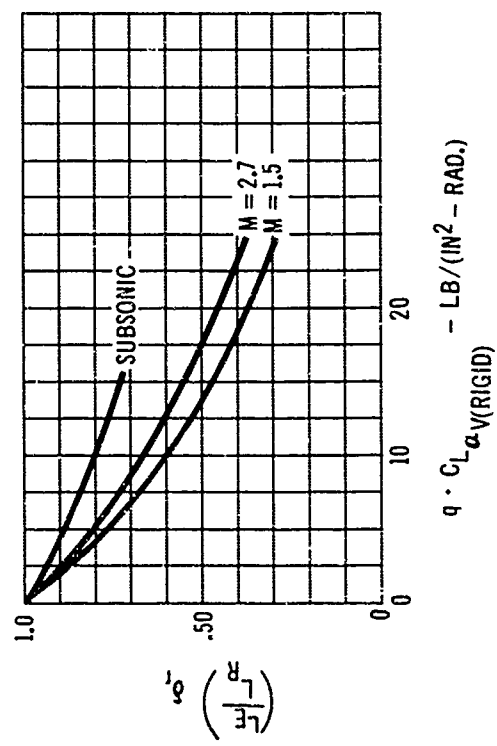
D-41 Dihedral Effect - C_{l_β} - Variation with Mach Number



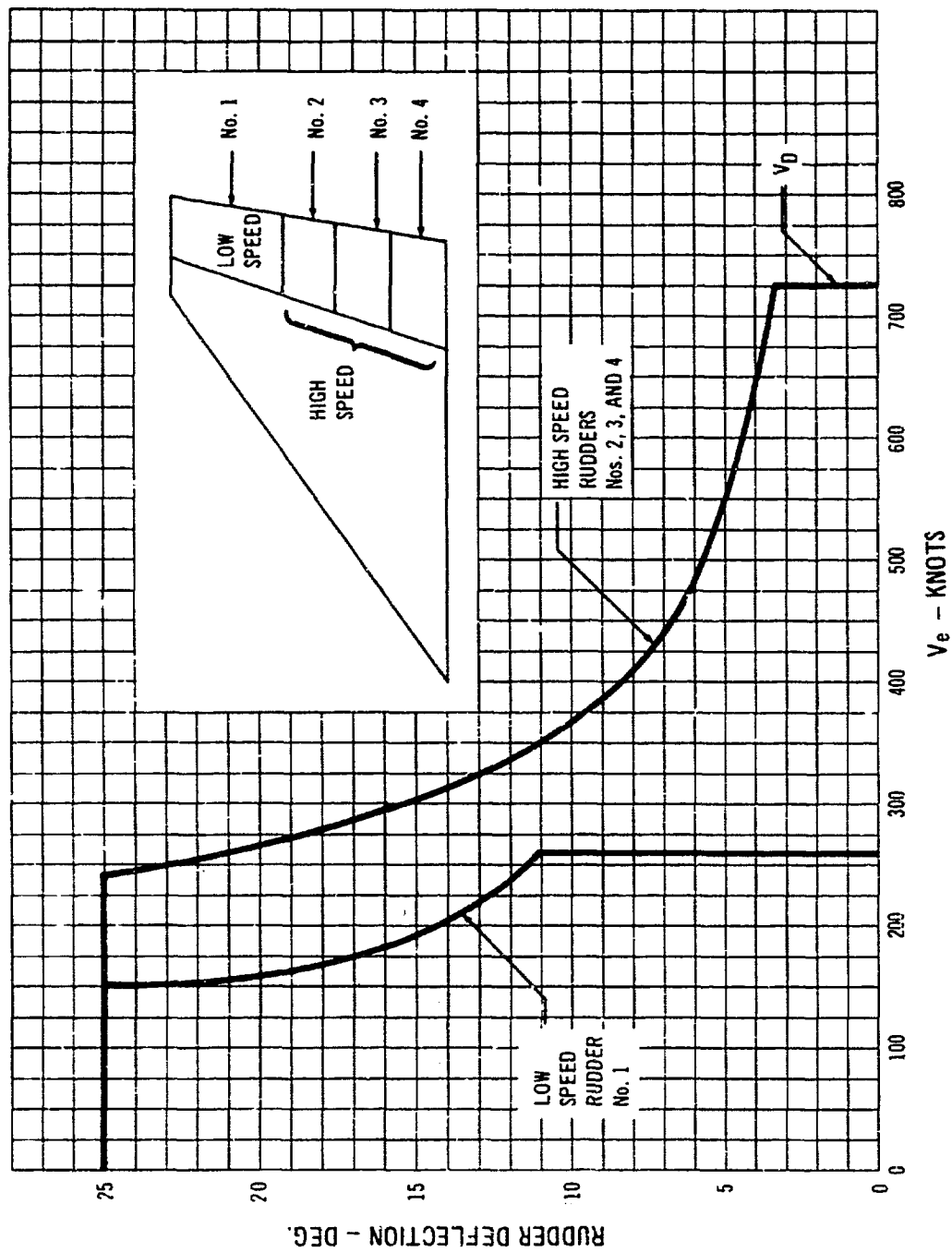
D-42 Side Force Variation with Sideslip - $C_{Y\beta}$ - versus Mach Number



D-43 Rudder Effectiveness, Rigid and Flexible



D-44 High Speed Rudder Aeroelastic Factor



D-45 Rudder Travel Limits

D7.4.3 LATERAL CONTROL

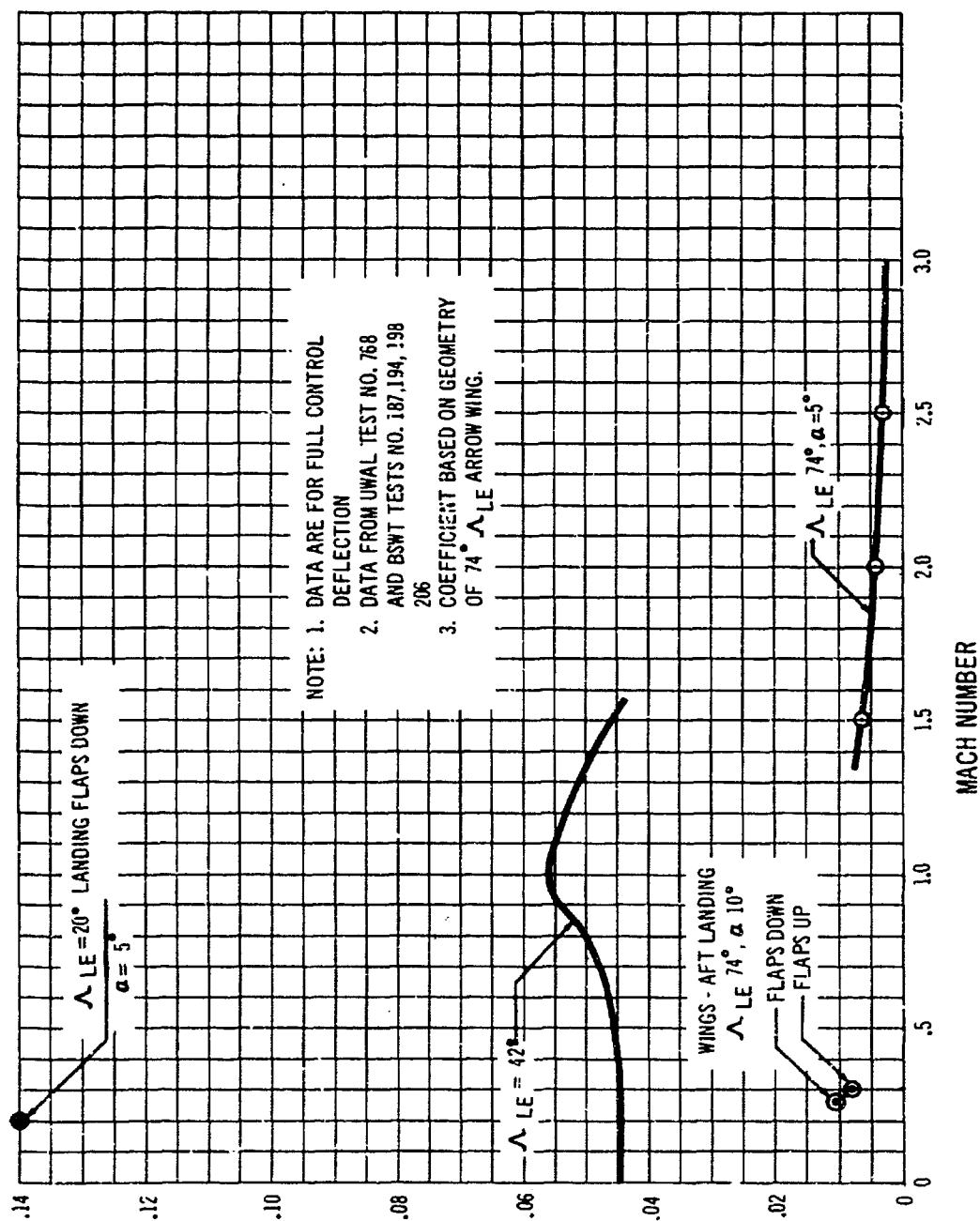
The spoiler-aileron configuration has been designed and sized to provide good lateral control power throughout the flight envelope. A considerable amount of wind tunnel testing has been done to evaluate many different wing spoiler arrangements. The top-plus-bottom spoiler design selected for the Boeing SST appears nearly optimum from the standpoint of control power and the yaw-to-roll relationship. Research is continuing in this area to develop further improvements in the lateral control system, particularly for the high-sweep, low-speed operation. For example, tests of spoiler-slot-deflector arrangements are scheduled to be conducted in the near future.

Rolling moment coefficients shown for the rigid airframe in Fig. D-46 were obtained from Boeing low-speed and supersonic wind tunnel tests. Fig. D-47 presents the maximum available rolling moment coefficients

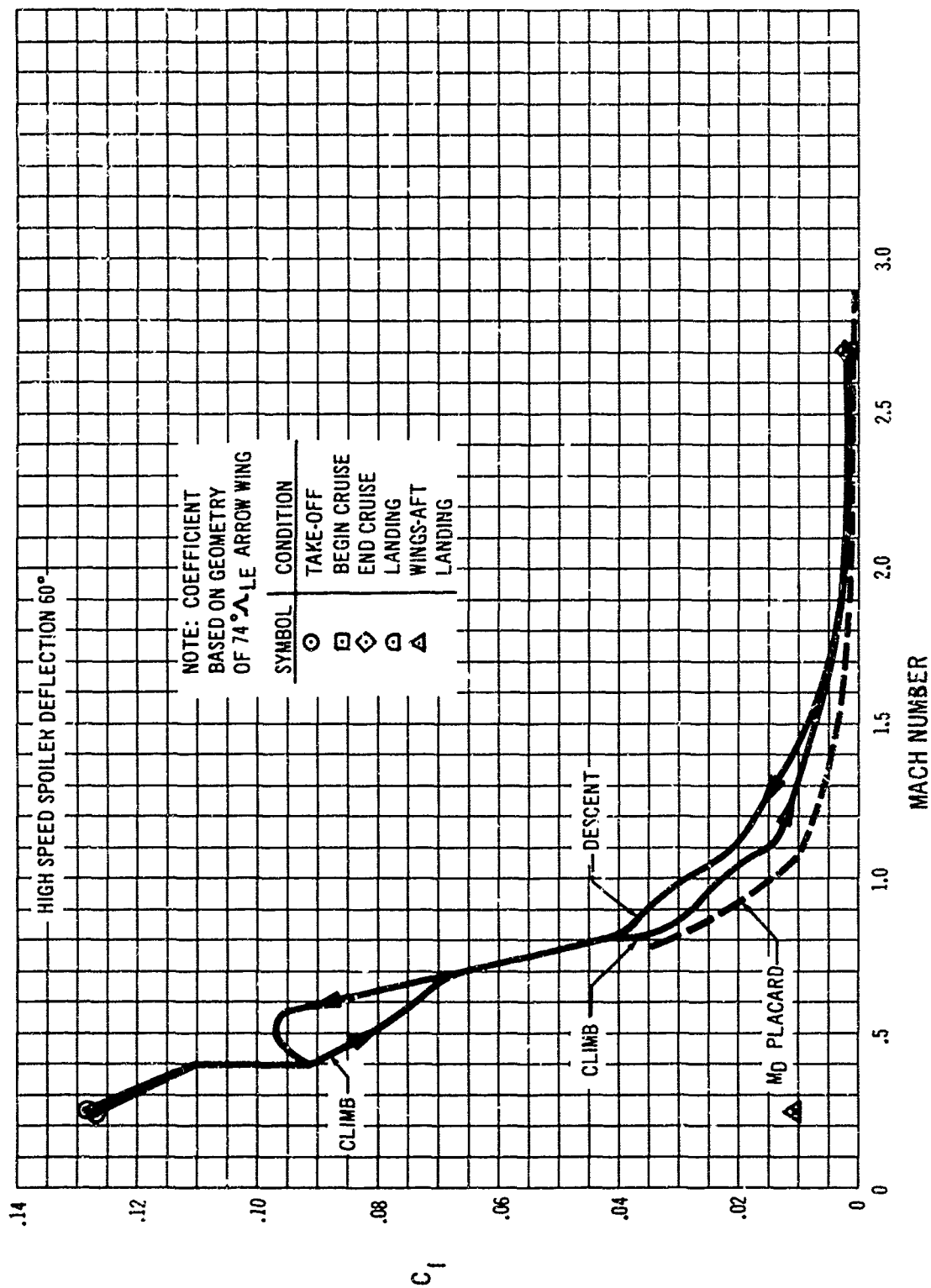
for the climb, descent, M_{10} , normal and wings-aft landing conditions for the flexible airplane. Corrections for aerodynamic elastic effects have been applied using the following equation: $C_{l_{\text{flex}}} = C_{l_{\text{rigid}}} \times R_t / R_{\text{flex}}$. Where $C_{l_{\text{flex}}}$ is the elastic coefficient, $C_{l_{\text{rigid}}}$ is the rigid coefficient and R_t / R_{flex} is the ratio of elastic-to-rigid rolling moment coefficient. This ratio is shown for ailerons and spoilers in Figs. D-48 through D-50.

The chosen arrangement of lateral control results in good rolling moment coefficient versus angle of attack relations for both wings-forward and wings-aft landings, as shown in Figs. D-51 and D-52. Yaw-to-roll ratios due to lateral control are shown in Figs. D-53 and D-54 for the most critical flight conditions.

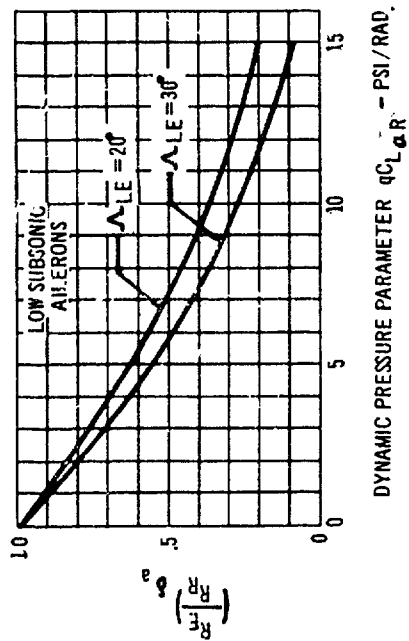
Figs. D-55 and D-56 present photographs of low-speed and supersonic wind tunnel test spoiler configurations.



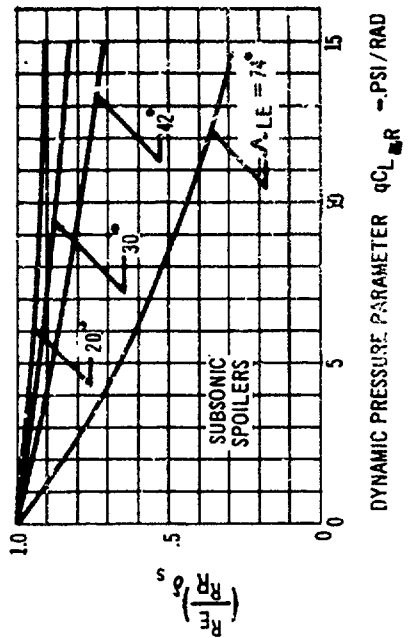
D-46 Maximum Rolling Moment Coefficients, Rigid Airplane



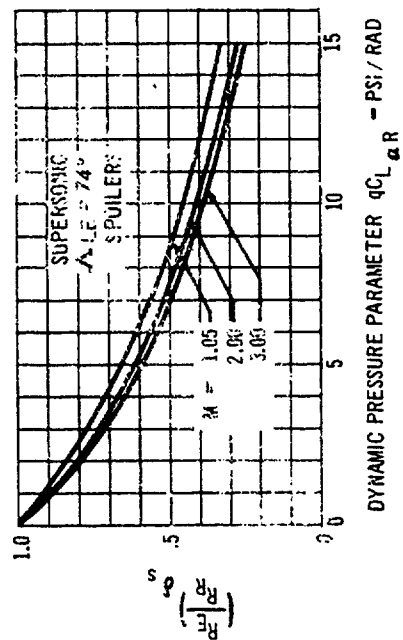
D-47 Maximum Rolling Moment Coefficient Available, Flexible Airplane



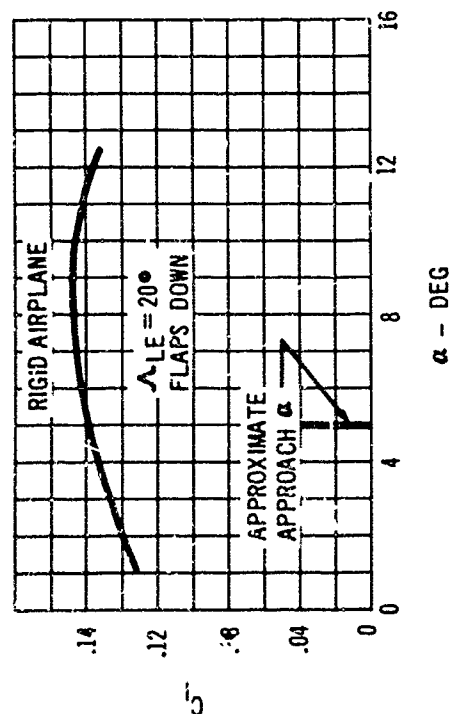
D-48 Aileron Aeroelastic Factor



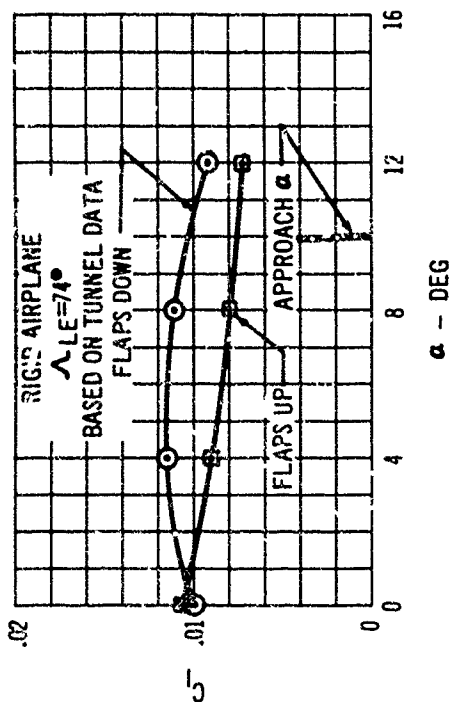
D-49 Spoiler Aeroelastic Factor



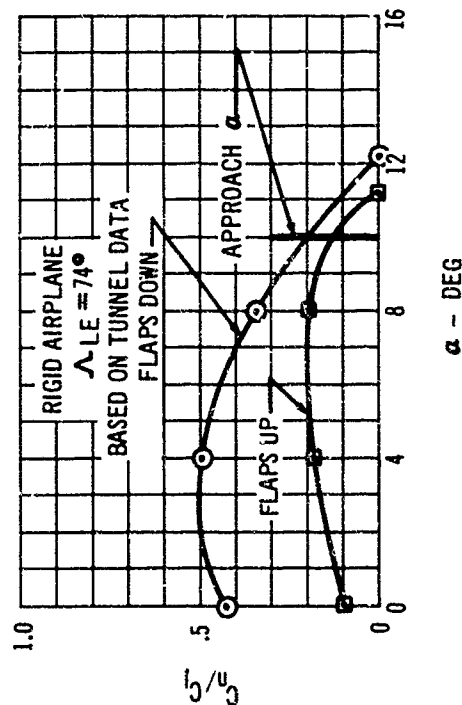
D-50 Spoiler Aeroelastic Factor



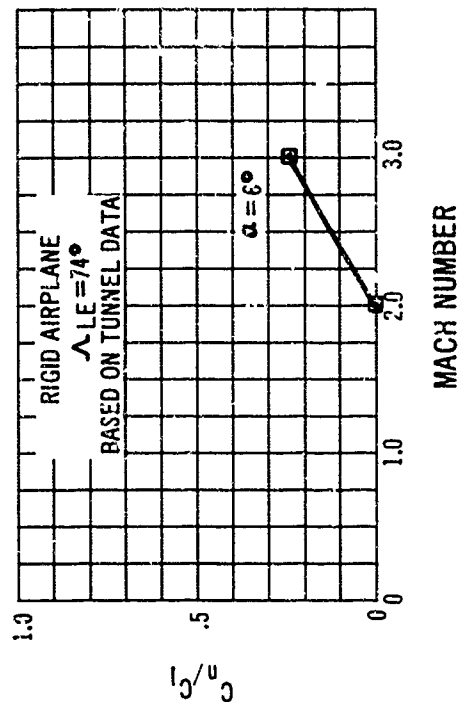
D-51 Low Speed Rolling Moment Coefficient (Wings Forward)



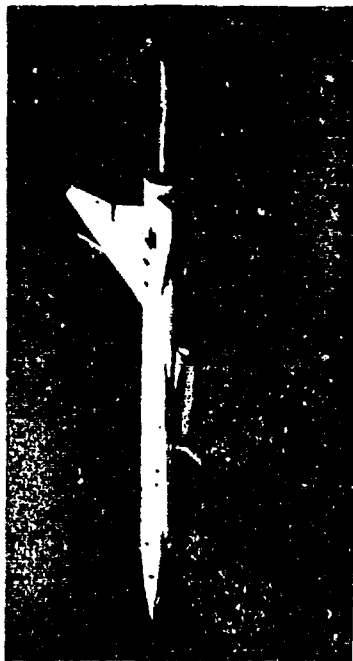
D-52 Low Speed Rolling Moment Coefficient (Wings Aft)



D-53 Low Speed Yaw To Roll Ratio For Maximum C_l



D-54 High Speed Yaw To Roll Ratio For Maximum C_l



D-55 Directional and Lateral Controls on Supersonic Model



D-56 D7-56 Lateral Controls on Low Speed Wind Tunnel Model

D7.5 Engine Inlet Shock Expulsion Data

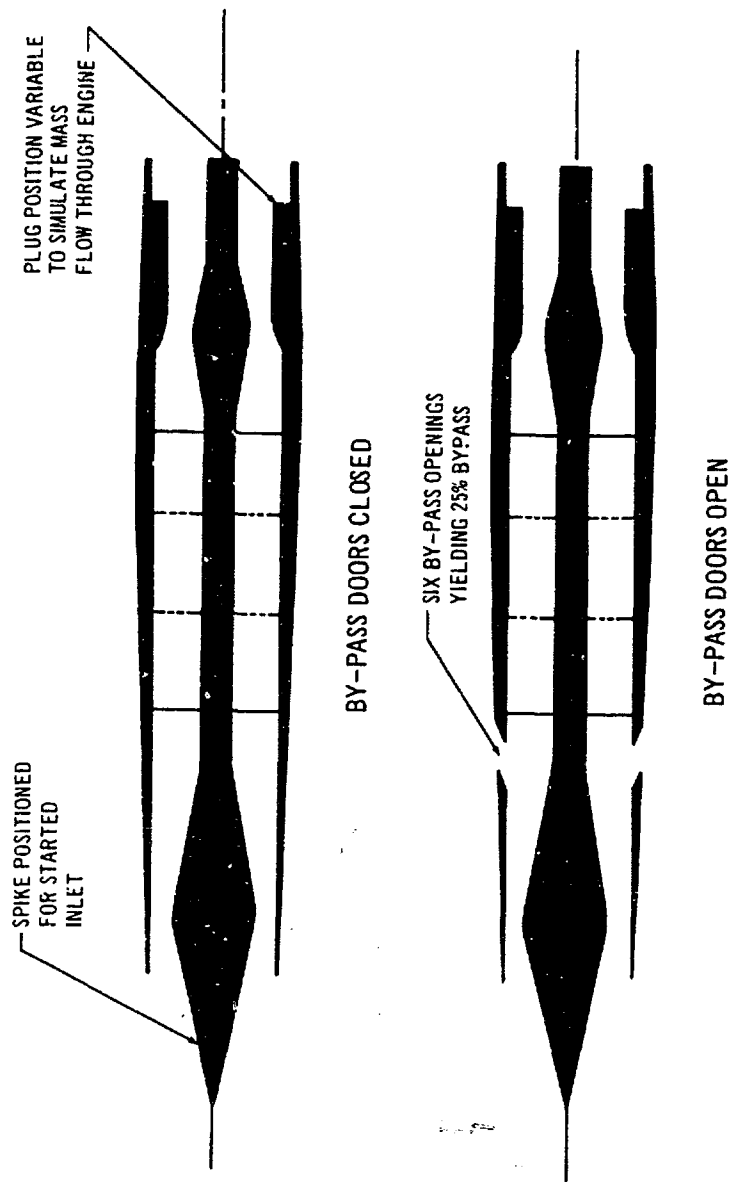
At subsonic speeds, the airplane dynamics following a sudden engine failure result primarily from asymmetric thrust and drag. The resulting airplane motions are small. In the supersonic regime, a sudden engine failure and/or inlet unstart results in inlet shock expulsion. This asymmetric shock pattern induces incremental moments and forces, the most important of which are the rolling, pitching and yawing moment increments. These moment increments are sensitive to engine spacing from the wing lower surface, fore and aft location, and lateral placement. The incremental forces and moments used in the analysis of sudden engine failure in Section 7.2.4.4 were determined from wind tunnel tests of inlet models simulating inlet unstart with by-pass doors closed (inlet buzz) and inlet unstart with by-pass doors open (stable shock pattern).

Supersonic wind tunnel tests of the Boeing proposal airplane with various nacelle locations were conducted to determine the expelled shock induced forces and moments. The nacelle locations varied from a forward position with the inlet face forward of the strake leading-edge to an aft position with the nacelle extending aft of the wing trailing edge. Lateral positions from just outboard of the wing pivot to the fuselage side were also investigated. The tests showed that the nacelle locations selected by considerations of drag and airplane arrangement were near optimum with regard to minimizing engine failure disturbances.

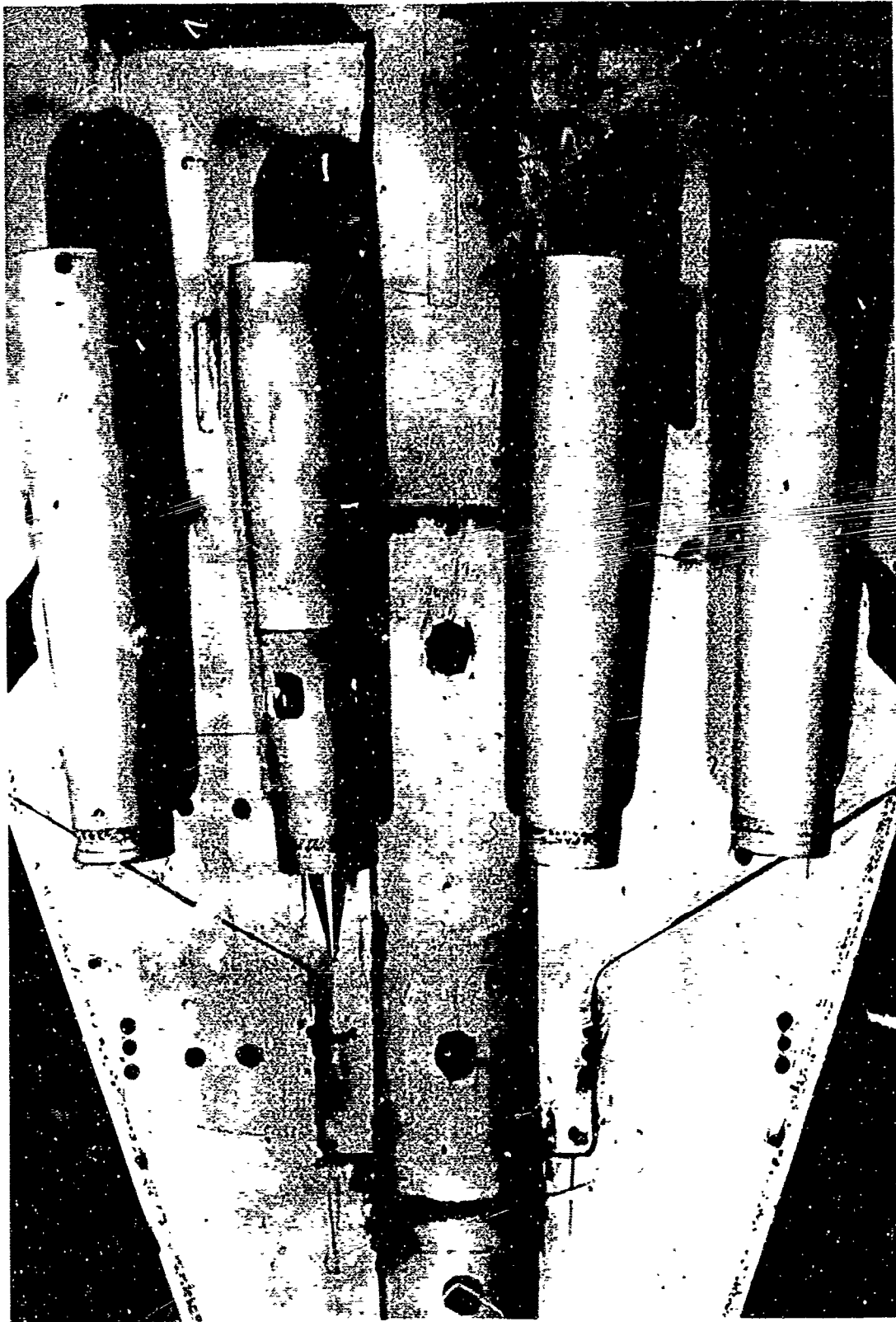
The inlet model used for these tests is shown in Fig. D-57. The upper sketch shows the simulation of inlet unstart with by-pass doors closed. The adjustable spike was flown in the design position and the adjustable plug in the aft end of the nacelle model was positioned to provide the correct engine mass flow with a started inlet. The lower sketch shows the model as flown to simulate the unstarted inlet with by-pass doors open. In this configuration the spike and plug position remained in the design location. Fig. D-58 shows the inlet model with by-pass doors open, installed on a wind tunnel model of the Boeing proposal airplane.

The Schlieren film strip in Fig. D-59 illustrates the inlet buzz experienced with the inlet model bypass doors closed. The upper still Schlieren photograph shows the by-pass-doors-closed model with the shock forward of the inlet face. Opening the by-pass doors stabilizes the flow and produces the flow shown in the lower Schlieren photograph in Fig. D-59.

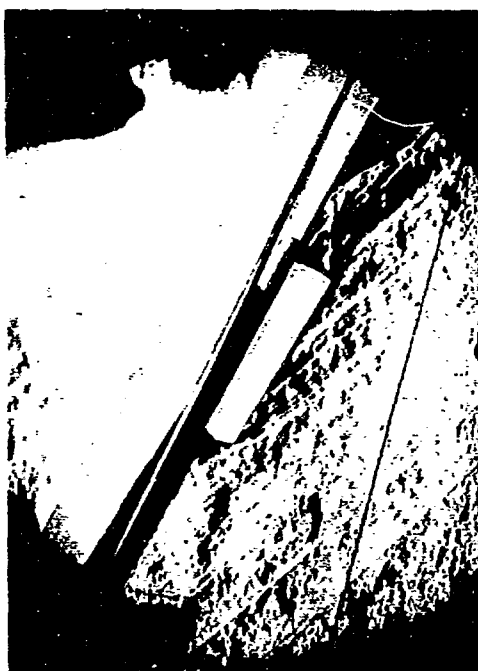
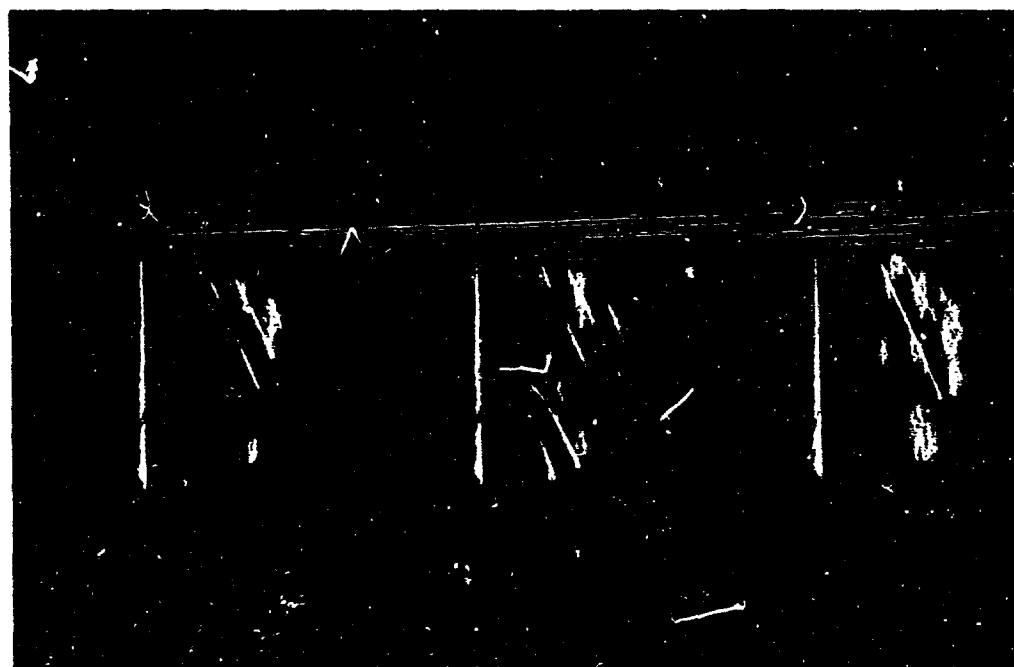
The incremental force and moment coefficients, based on the reference geometry ($\Lambda_{LE} = 74^\circ$) are shown in Figs. D-60 through D-71 for the nacelle location of the Boeing proposal airplane. The data are shown for cruise Mach number for both the inboard and outboard engines, with and without by-pass doors open. These data were used in analyzing the airplane motion following sudden engine failure, discussed in Section 7.2.4.4. The increments are very small due to the engine placement. As a result, inlet unstart or engine failure does not present a serious airplane handling problem.



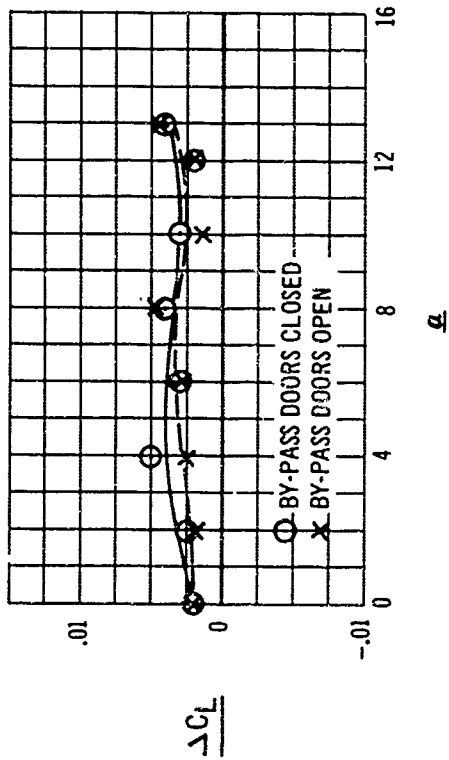
D-57 Sketch of Nacelle Model for Simulation of Inlet Unstart



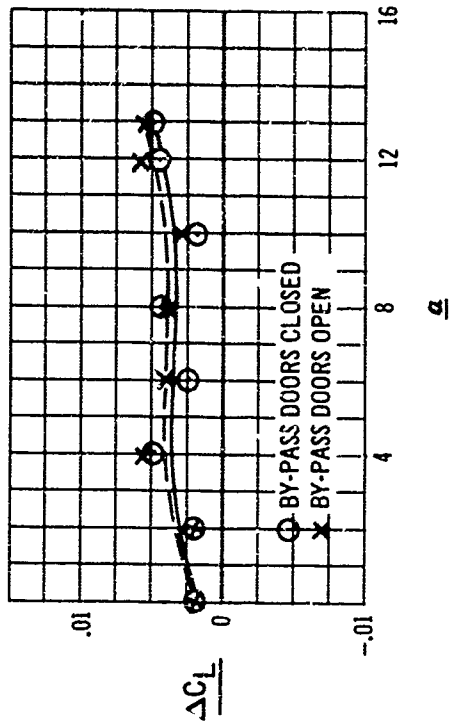
D-58 *Supersonic Stability and Control Inlet Unstart Test Model*



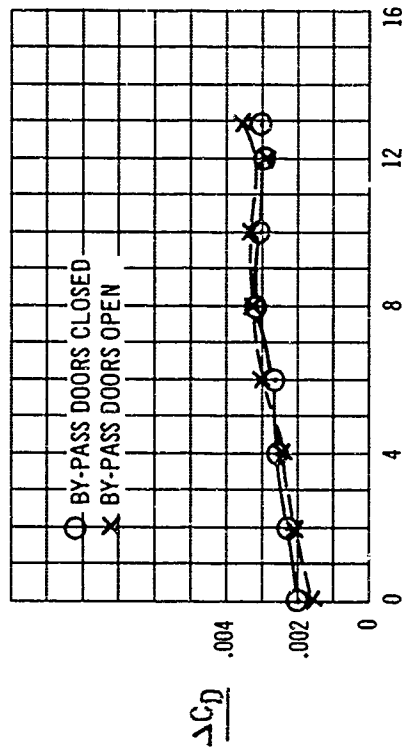
D:59 Shock Pattern with Inlet Unstart $M = 2.7, \alpha = 5^\circ$: Film Strip of Inlet Buzz (Left), By-Pass Doors Closed (Top), and By-Pass Doors Open



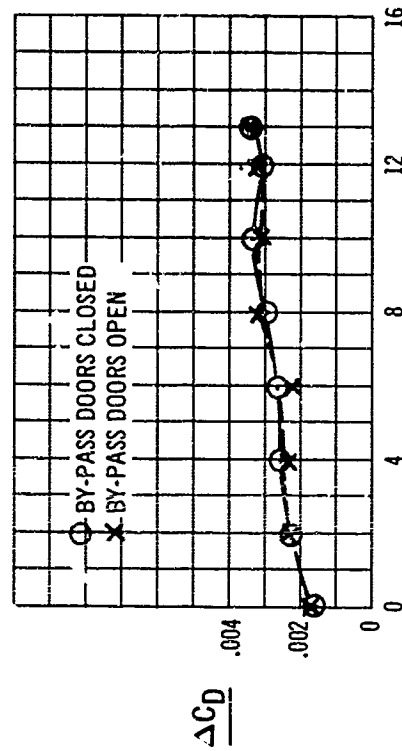
D-60 Effect of Left Outboard Inlet Unstart on Lift, Mach = 2.7



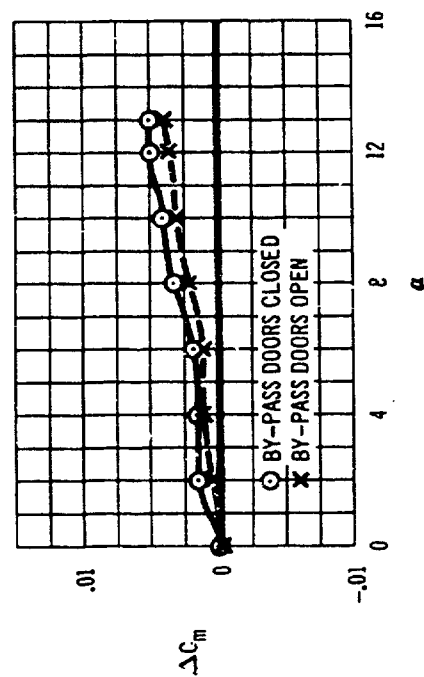
D-61 Effect of Left Inboard Inlet Unstart on Lift, Mach = 2.7



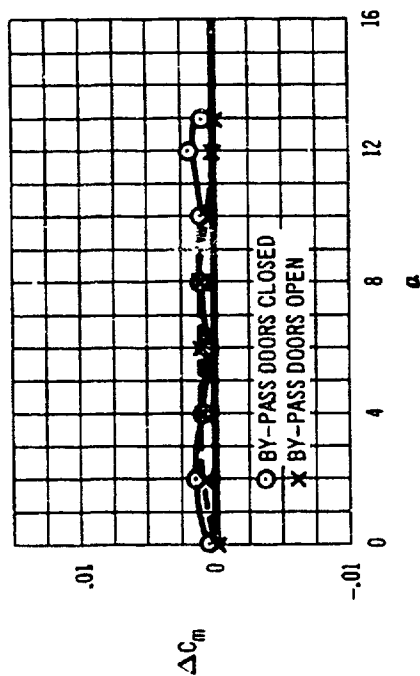
D-62 Effect of Left Outboard Inlet Unstart on Drag, Mach = 2.7



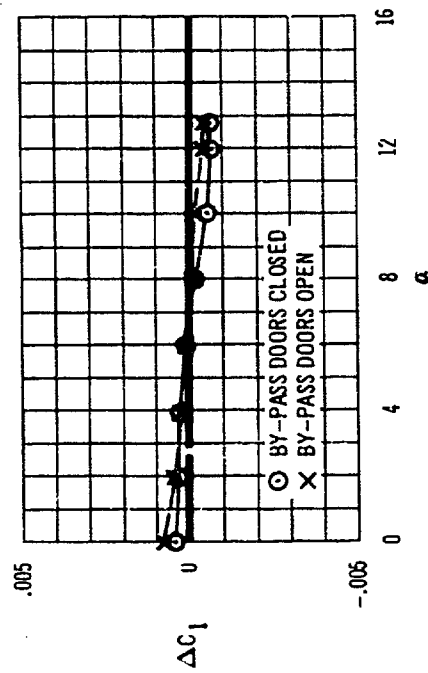
D-63 Effect of Left Inboard Inlet Unstart on Drag, Mach = 2.7



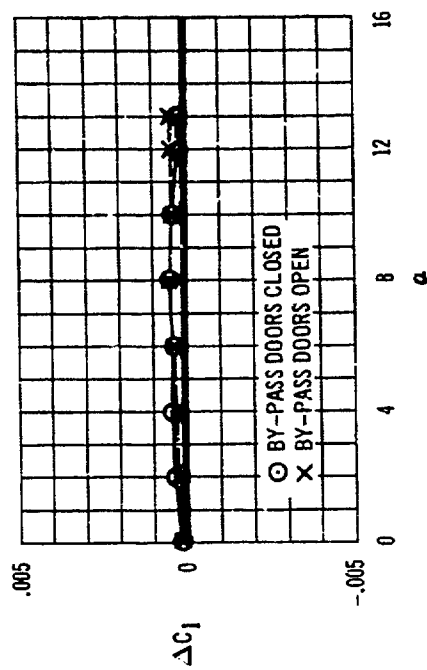
D-64 Effect of Left Outboard Inlet Unstart
on Pitching Moment, Mach = 2.7



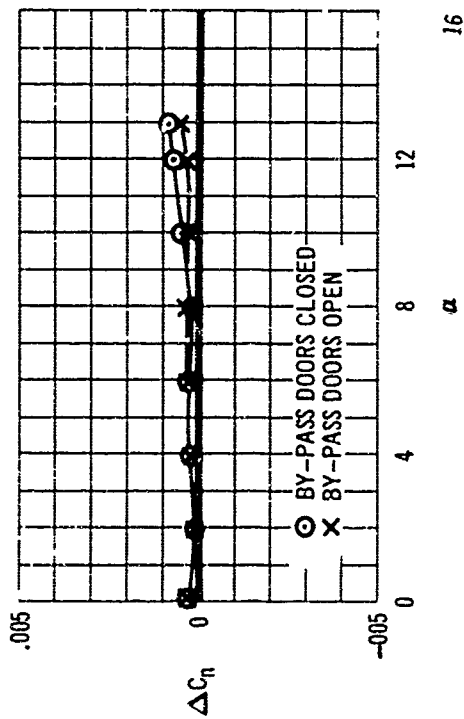
D-65 Effect of Left Inboard Inlet Unstart
on Pitching Moment, Mach = 2.7



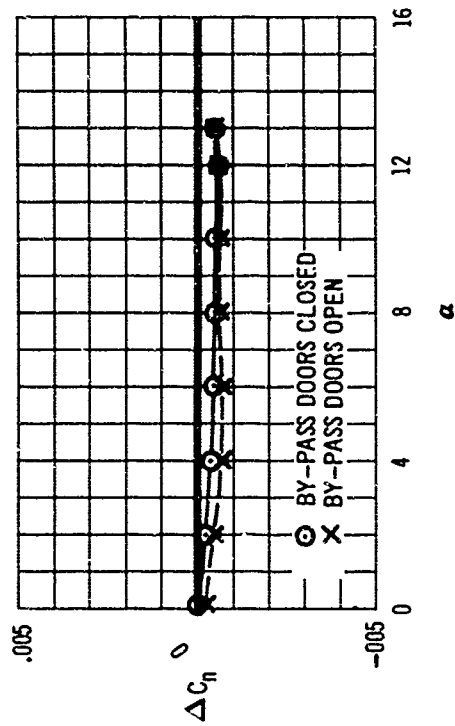
D-66 Effect of Left Outboard Inlet Unstart
on Rolling Moment, Mach = 2.7



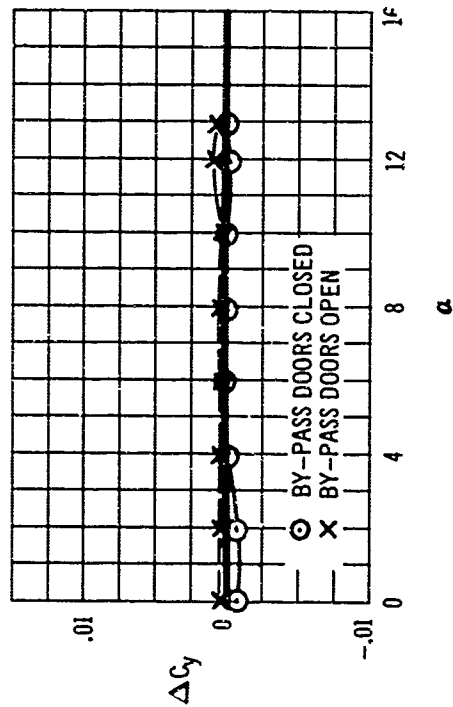
D-67 Effect of Left Inboard Inlet Unstart
on Rolling Moment, Mach = 2.7



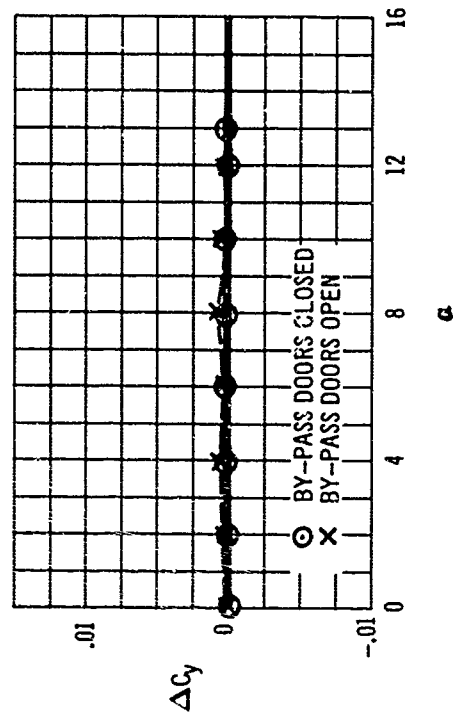
D-68 Effect of Left Outboard Inlet Unstart on Yawing Moment, Mach = 2.7



D-69 Effect of Left Inboard Inlet Unstart on Yawing Moment, Mach = 2.7



D-70 Effect of Left Outboard Inlet Unstart on Side Force, Mach = 2.7



D-71 Effect of Left Inboard Inlet Unstart on Side Force, Mach = 2.7

D7.6 Dynamic Stability Parameters

Unaugmented aerodynamic stability derivatives pertinent to the dynamic analysis of the Boeing SST handling qualities are presented in Figs. D-72 through D-121. These derivatives were calculated using standard methods (Refs. 42, 43 and 45). Wind tunnel tests performed in the Boeing supersonic and transonic tunnels as well as the University of Washington low speed tunnel provided the static characteristics used in estimating the majority of the dynamic derivatives. The models tested closely resemble the present Boeing SST configuration. In addition, dynamic test results for a similar variable-sweep configuration (Ref. 46) were utilized wherever applicable to provide the highest degree of accuracy in these estimates.

Aeroelastic corrections were obtained through extensive usage of high speed digital computing equipment. The methods used are detailed in The Structural Report, Volume IV. It has been assumed that the airplane must be considered elastic for purposes of dynamic stability analyses.

The data are presented in the following order:

Pitching moment ($C_{m,q}$, $C_{m,\dot{\alpha}}$)

Side force ($C_{Y,p}$, $C_{Y,r}$)

Rolling moment ($C_{l,p}$, $C_{l,r}$)

Yawing moment ($C_{n,p}$, $C_{n,r}$)

Elastic ratios (L_E/L_R), v_w , (R_E/R_R)_w

The last chart of each group of charts shows the applicable equation for estimating the elastic derivatives, except for the derivatives with trivial flexible effects.

The eight specific flight conditions which are used for describing airplane dynamic characteristics in Section 7.2.3 are shown along with the climb and descent schedules in Fig. D-122. In addition, the specific values of aerodynamic derivatives, dynamic parameters, as well as augmentation gains are presented in Tables D7/B through D7/I. It should be noted that the Boeing SST uses only simple rate damping for stability augmentation. The longitudinal derivatives have been based on the reference geometry of the wing having $\Delta_{1,E} = 74^\circ$. The lateral-directional derivatives have been based on the actual geometry of the wing under consideration. To convert the lateral-directional derivatives to the reference geometry the following equations are to be used:

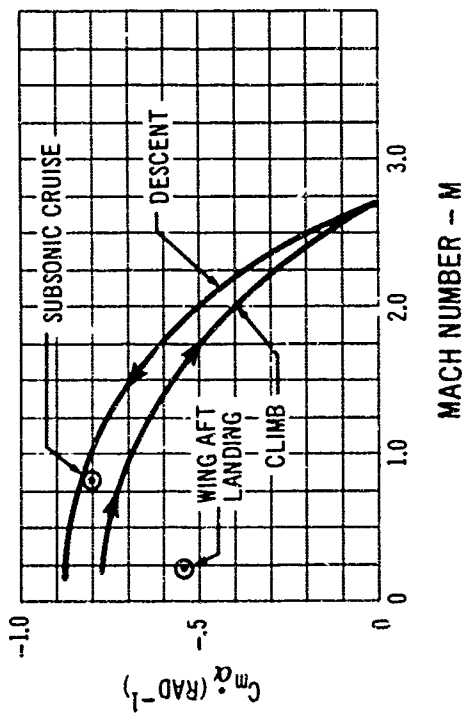
$$\left(C_{Y,p} \right)_{ref} = C_{Y,p} \left(\frac{S_{ref} b}{S b_{ref}} \right); \text{ also for } C_{Y,r}$$

$$\left(C_{l,p} \right)_{ref} = C_{l,p} \left(\frac{S_{ref}}{S} \right) \left(\frac{b}{b_{ref}} \right)^2; \text{ also for } C_{l,r}, C_{n,p}, C_{n,r}$$

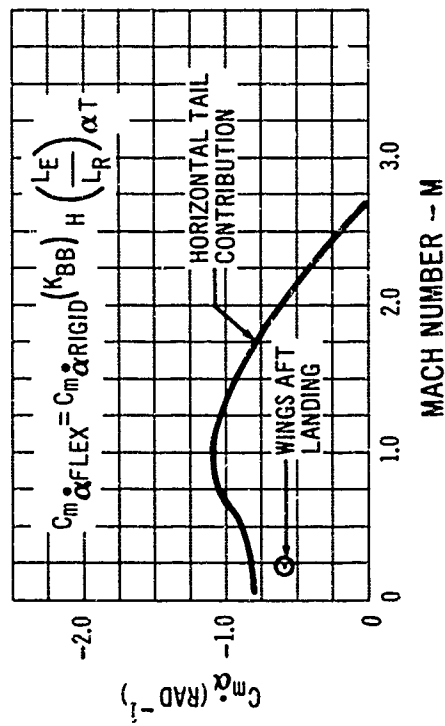
$$\left(C_{Y,\beta} \right)_{ref} = C_{Y,\beta} \left(\frac{S}{S_{ref}} \right)$$

$$\left(C_{l,\beta} \right)_{ref} = C_{l,\beta} \left(\frac{S_{ref} b}{S b_{ref}} \right); \text{ also for } C_{n,\beta}$$

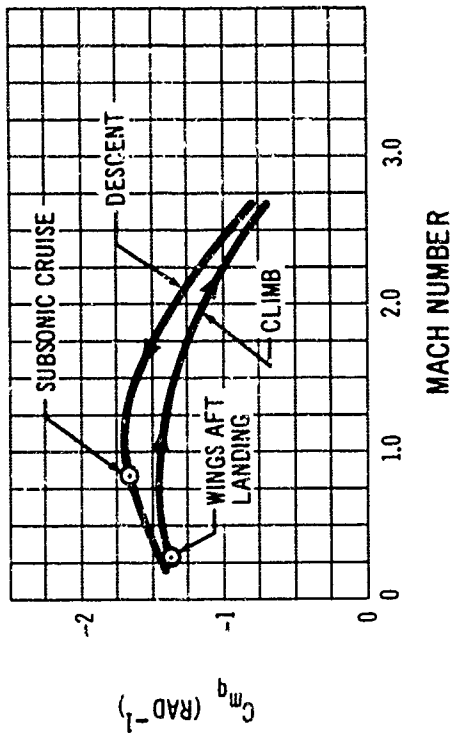
$$\left(C_{L} \right)_{ref} = C_L \left(\frac{S}{S_{ref}} \right)$$



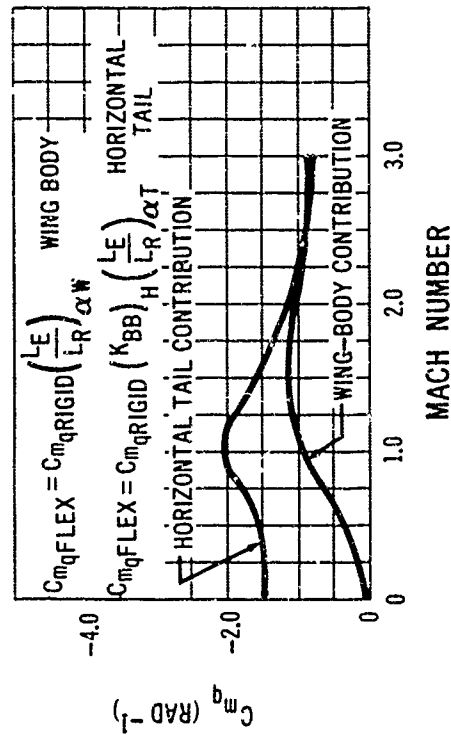
D-72 Pitching Moment Coefficient Due to Angle of Attack Rate, Flexible



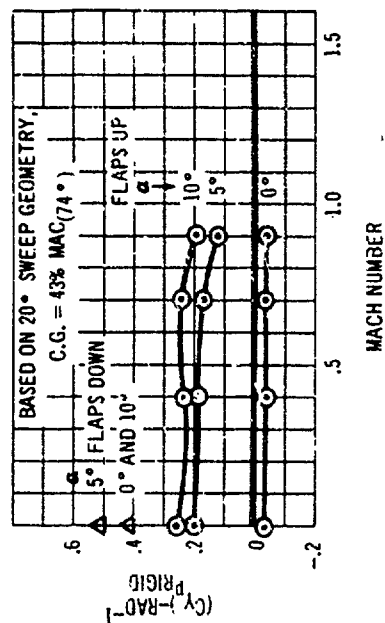
D-74 Pitching Moment Coefficient Due to Angle of Attack Rate, Rigid



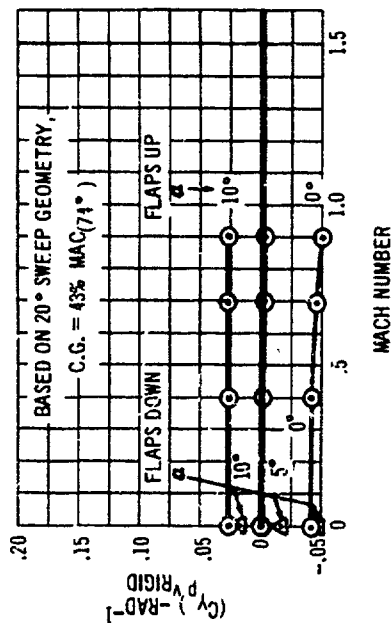
D-73 Pitching Moment Coefficient Due to Pitch Rate, Flexible



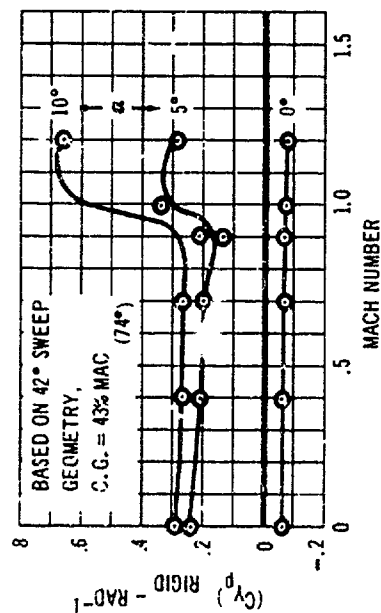
D-75 Pitching Moment Coefficient Due to Pitch Rate, Rigid



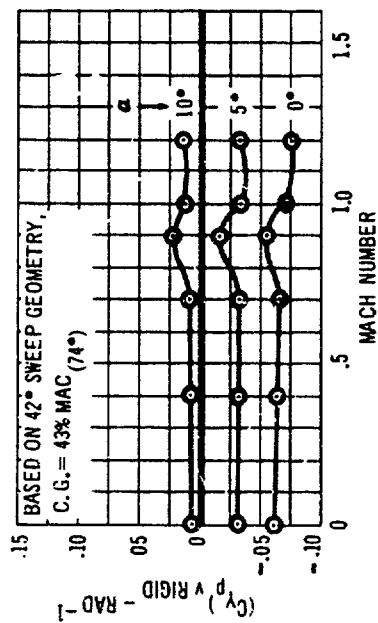
D-76 Estimated Side Force Coefficient Due to Roll Rate
 $\Lambda_{LE} = 20^\circ$, Rigid



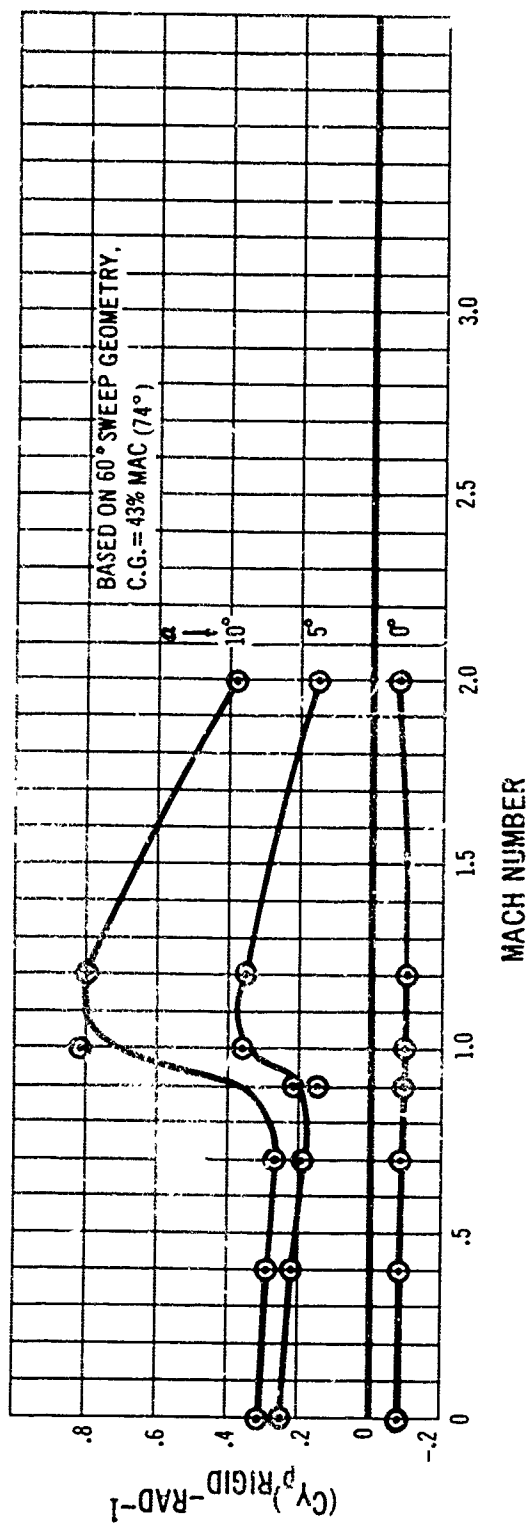
D-77 Estimated Vertical Tail Side Force Coefficient
 Due to Roll Rate, $\Lambda_{LE} = 20^\circ$, Rigid



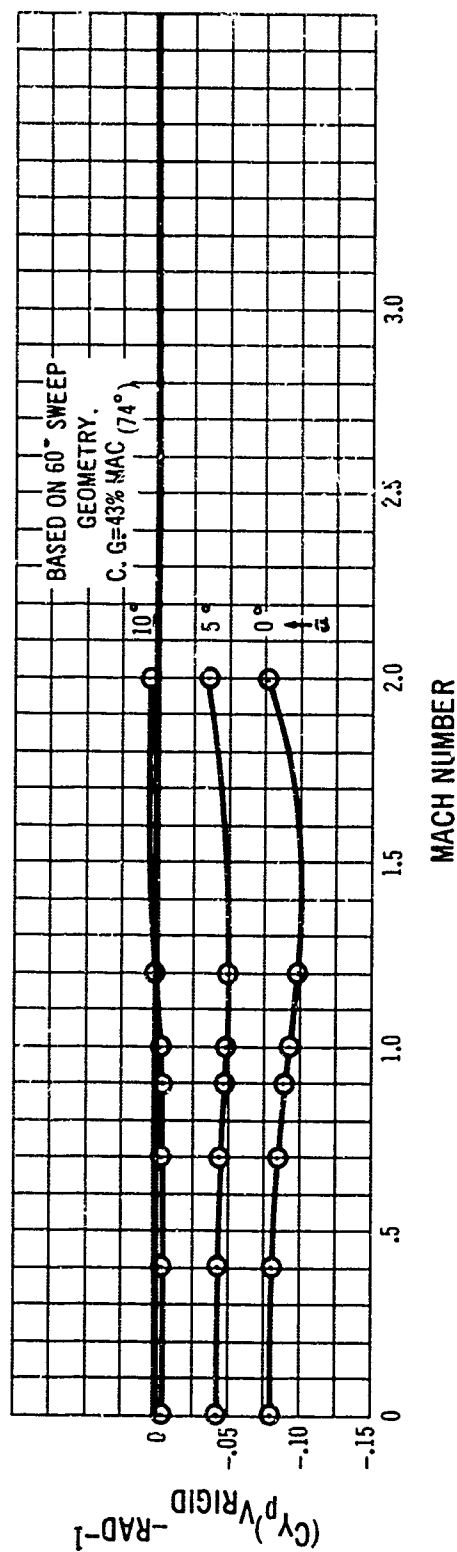
D-78 Estimated Side Force Coefficient Due To Roll
 Rate, $\Lambda_{LE} = 42^\circ$, Rigid



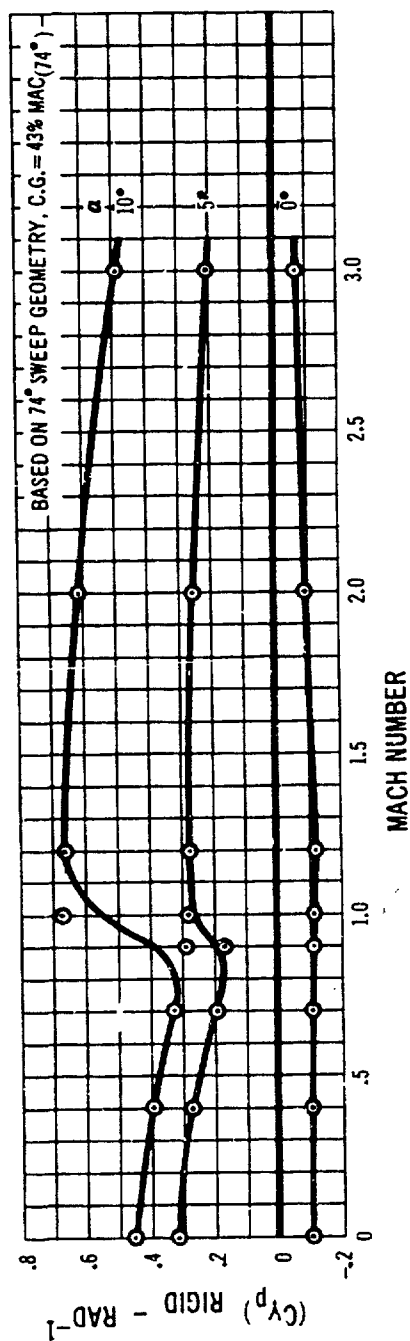
D-79 Estimated Vertical Tail Side Force Coefficient
 Due to Roll Rate, $\Lambda_{LE} = 42^\circ$, Rigid



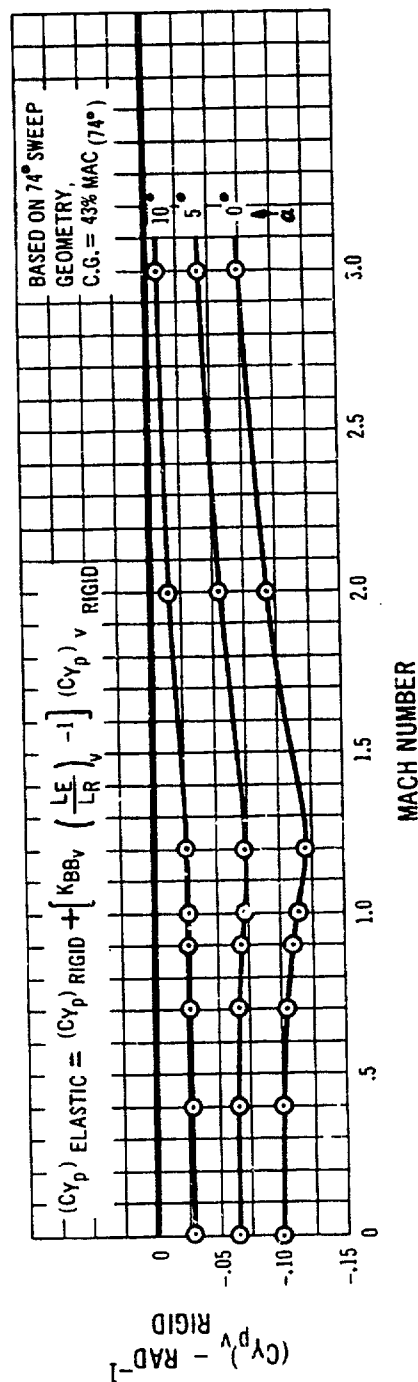
D-80 Estimated Side Force Coefficient Due to Roll Rate, $\Lambda_{LE} = 60^\circ$, Rigid



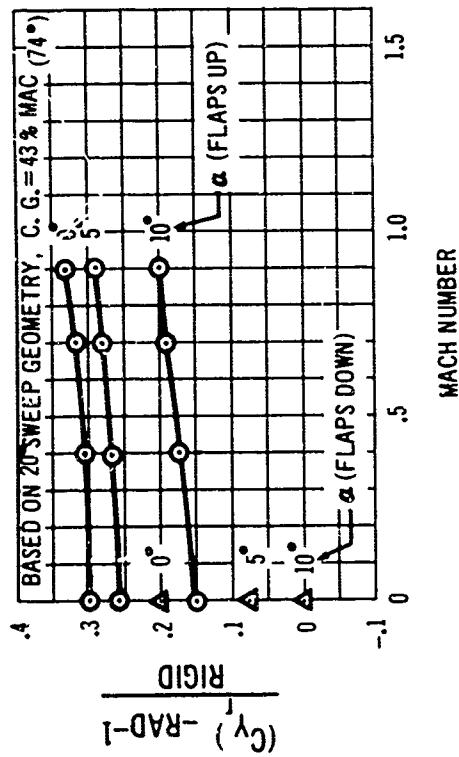
D-81 Estimated Vertical Tail Side Force Coefficient Due to Roll Rate, $\Lambda_{LE} = 60^\circ$, Rigid



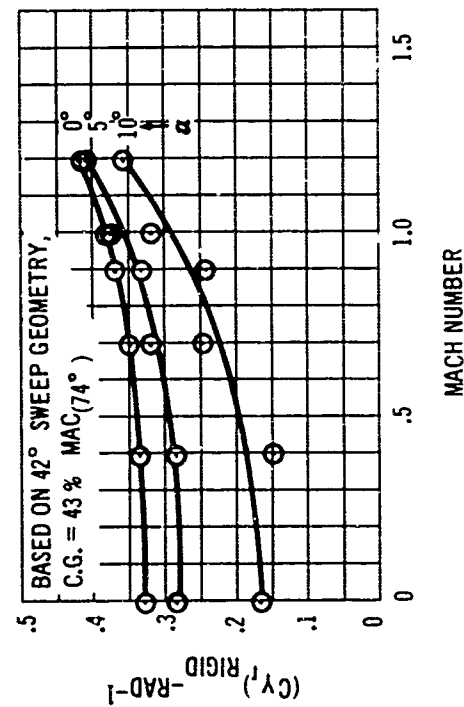
D-82 Estimated Side Force Coefficient Due to Roll Rate, $\Lambda_{LE} = 74^\circ$, Rigid



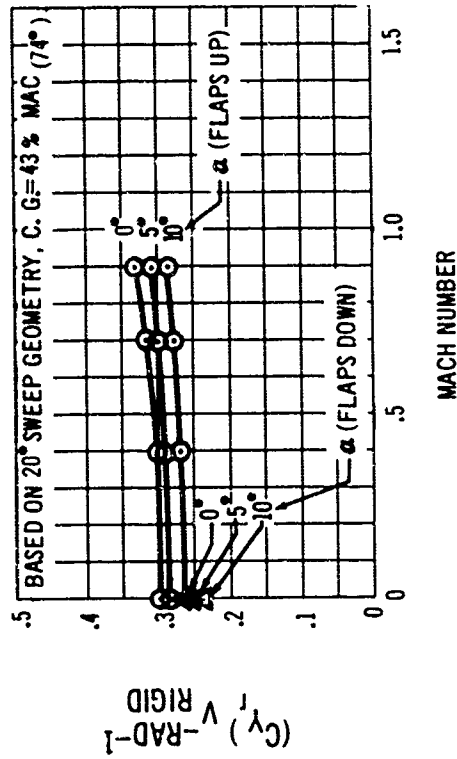
D-83 Estimated Vertical Tail Side Force Coefficient Due to Roll Rate, $\Lambda_{LE} = 74^\circ$, Rigid



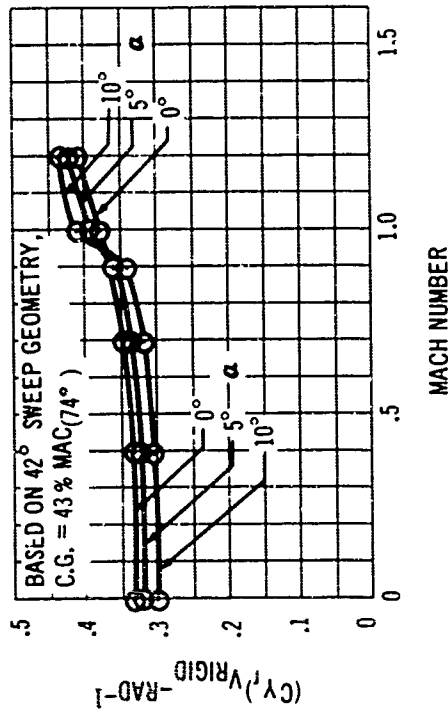
D-84 Estimated Side Force Coefficient Due to Yaw Rate, $\Lambda_{LE} = 20^\circ$, Rigid



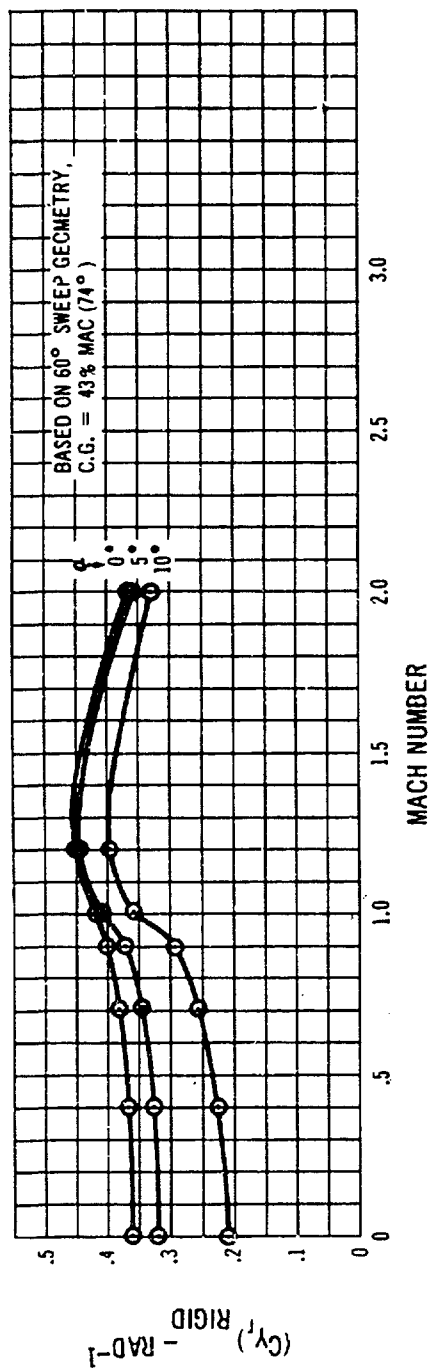
D-86 Estimated Side Force Coefficient Due to Yaw Rate, $\Lambda_{LE} = 42^\circ$, Rigid



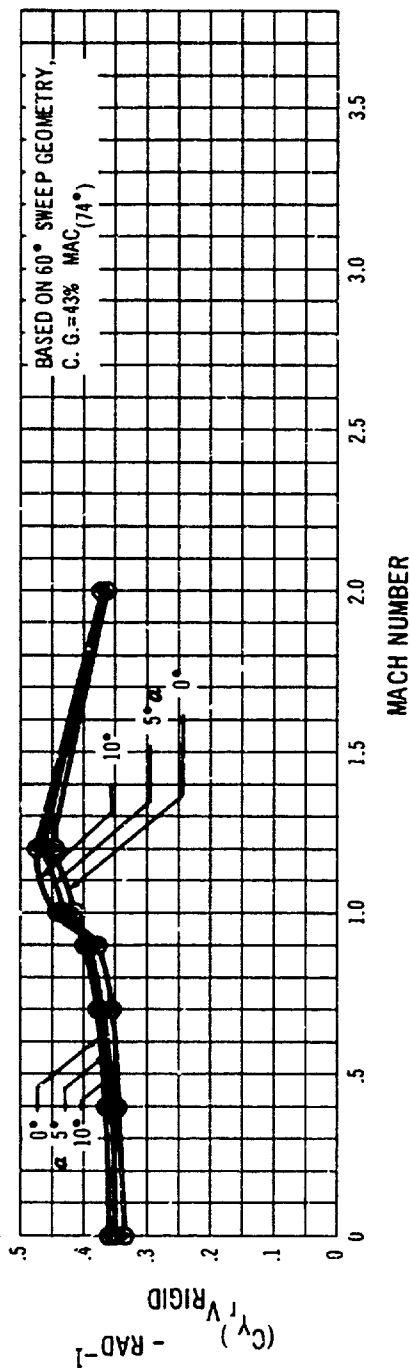
D-85 Estimated Vertical Tail Side Force Coefficient Due to Yaw Rate, $\Lambda_{LE} = 20^\circ$, Rigid



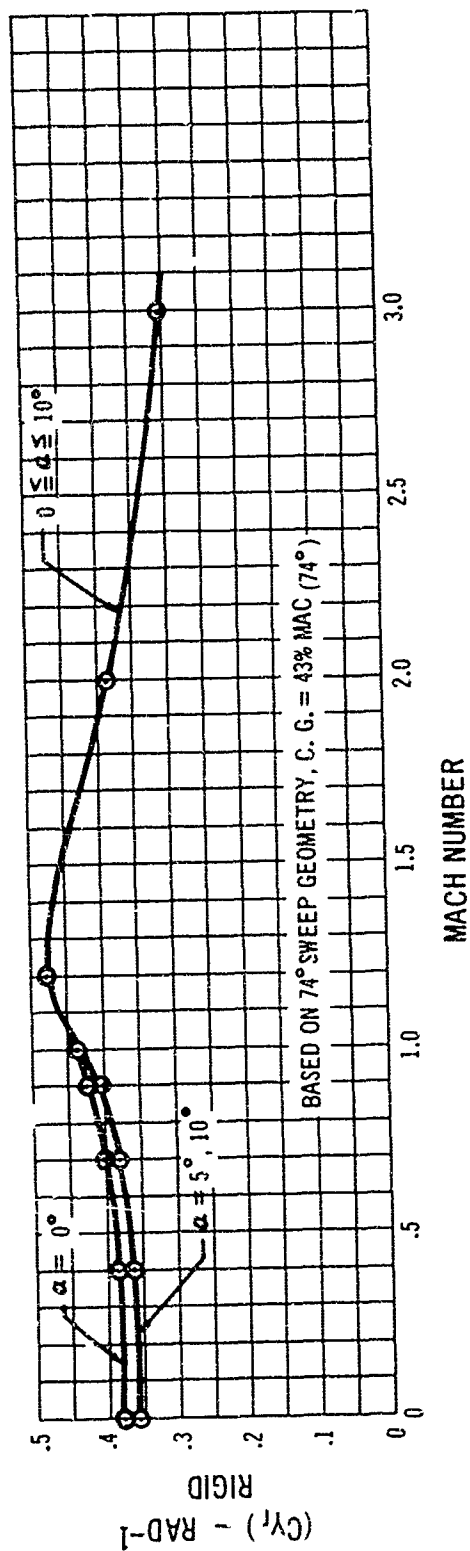
D-87 Estimated Vertical Tail Side Force Coefficient Due to Yaw Rate, $\Lambda_{LE} = 42^\circ$, Rigid



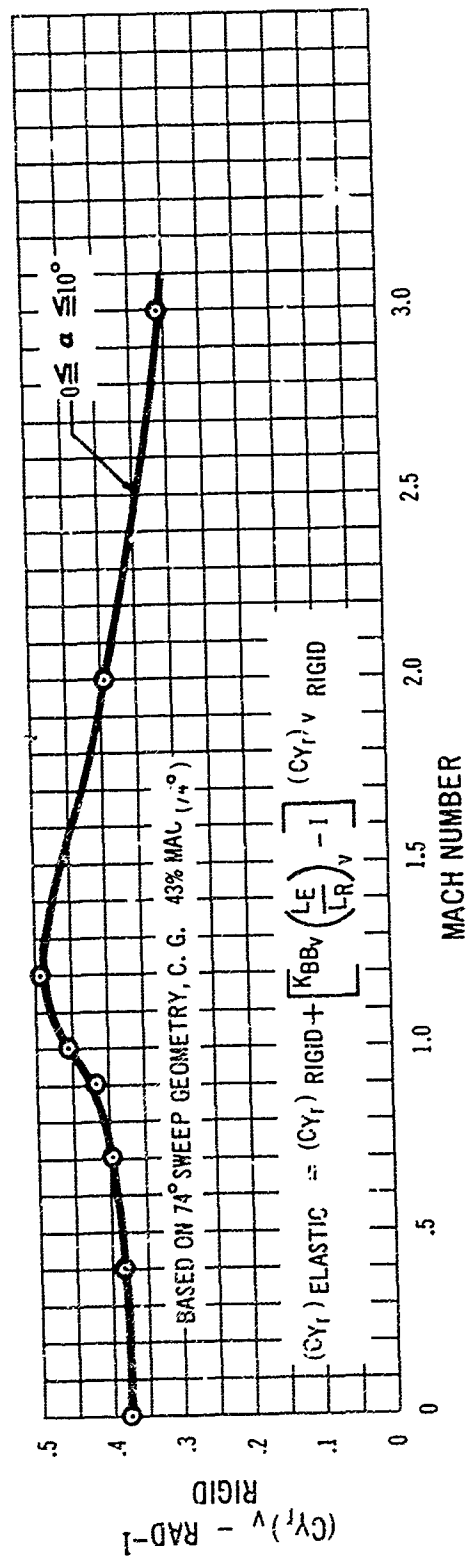
D-88 Estimated Side Force Coefficient Due to Yaw Rate, $\Lambda_{LE} = 60^\circ$, Rigid



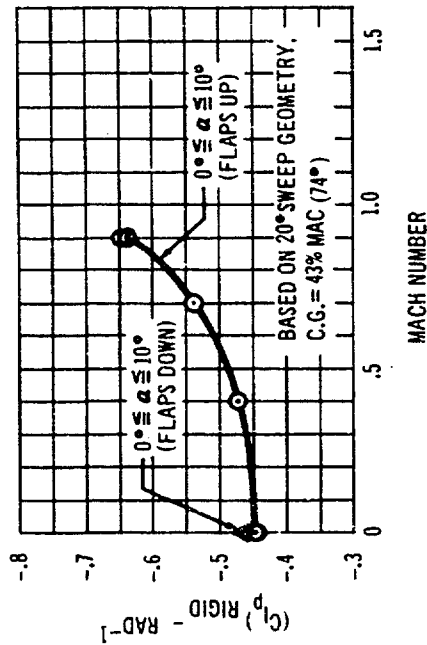
D-89 Estimated Vertical Tail Side Force Coefficient Due to Yaw Rate, $\Lambda_{LE} = 60^\circ$, Rigid



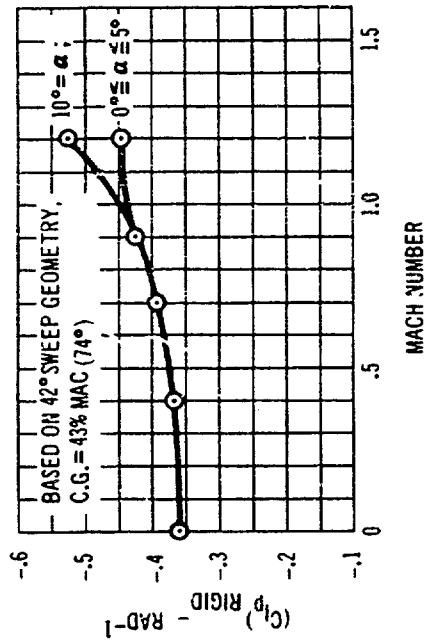
D-90 Estimated Side Force Coefficient Due to Yaw Rate, $A_{LE} = 74^\circ$, Rigid



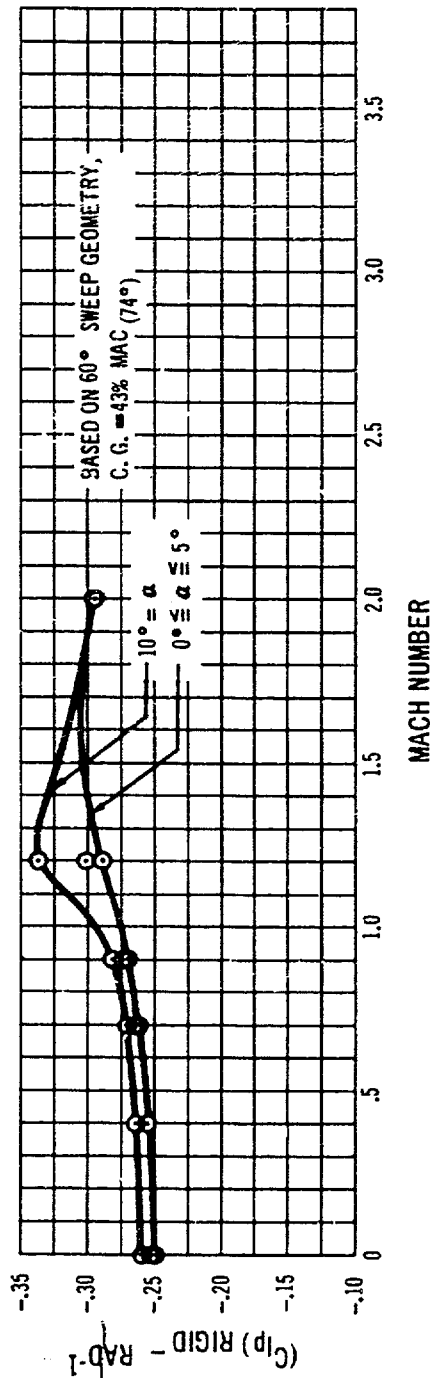
D-91 Estimated Vertical Tail Side Force Coefficient Due to Yaw Rate, $A_{LE} = 74^\circ$, Rigid



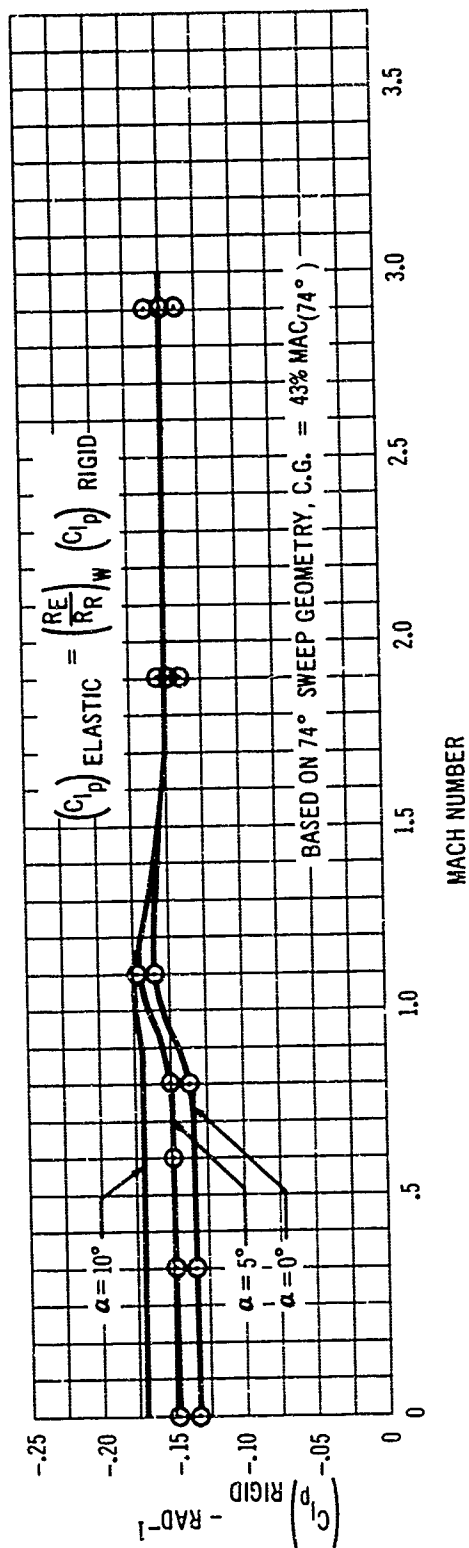
D-92 Estimated Rolling Moment Coefficient
Due to Roll Rate, $\Lambda_{LE} = 20^\circ$, Rigid



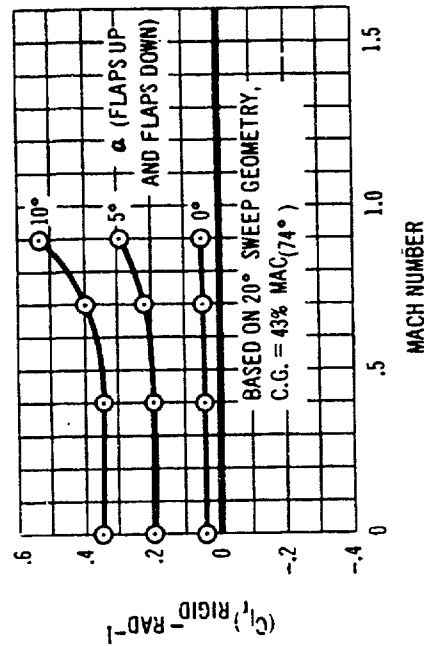
D-93 Estimated Rolling Moment Coefficient
Due to Roll Rate, $\Lambda_{LE} = 42^\circ$, Rigid



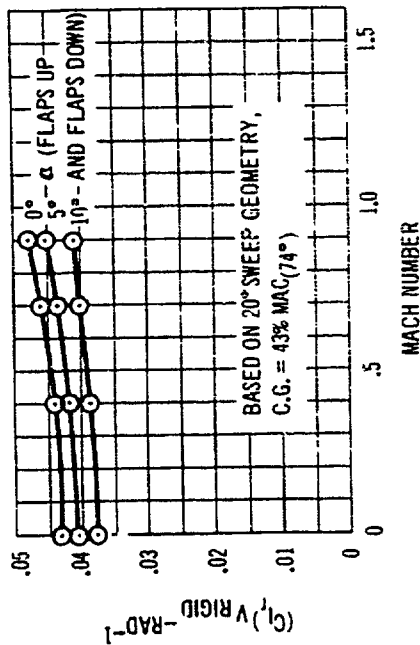
D-94 Estimated Rolling Moment Coefficient Due to Roll Rate, $\Lambda_{LE} = 60^\circ$, Rigid



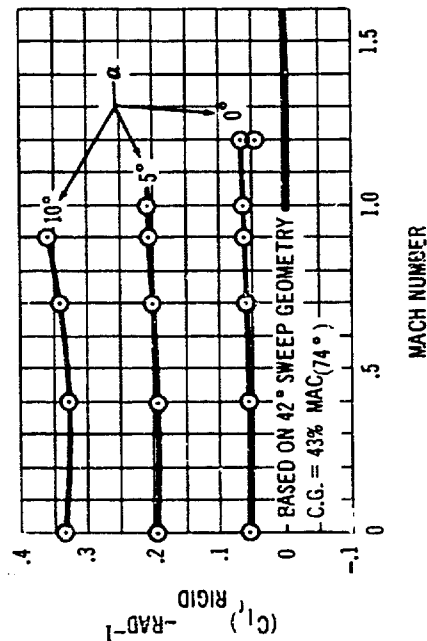
D-95 Estimated Rolling Moment Coefficient Due to Roll Rate, $\Lambda_L = 74^\circ$, Rigid



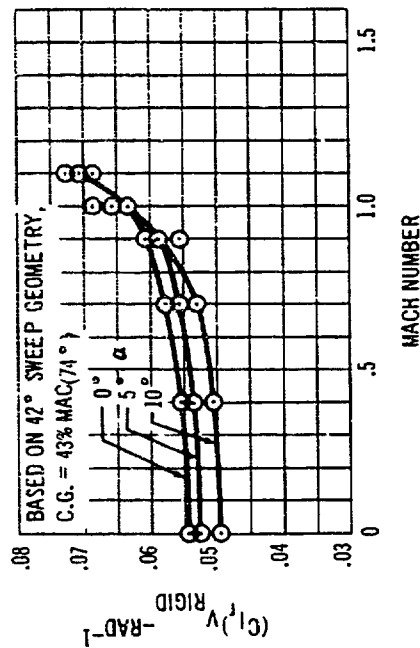
D-96 Estimated Rolling Moment Coefficient Due to Yaw Rate, $\Lambda_{LE} = 20^\circ$, Rigid



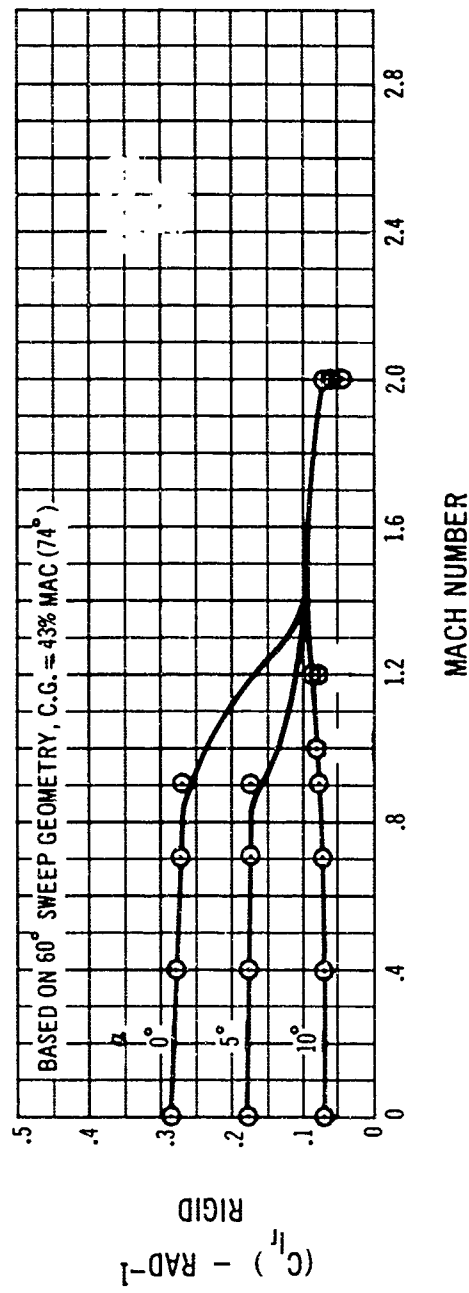
D-97 Estimated Vertical Tail Rolling Moment Coefficient Due to Yaw Rate, $\Lambda_{LE} = 20^\circ$, Rigid



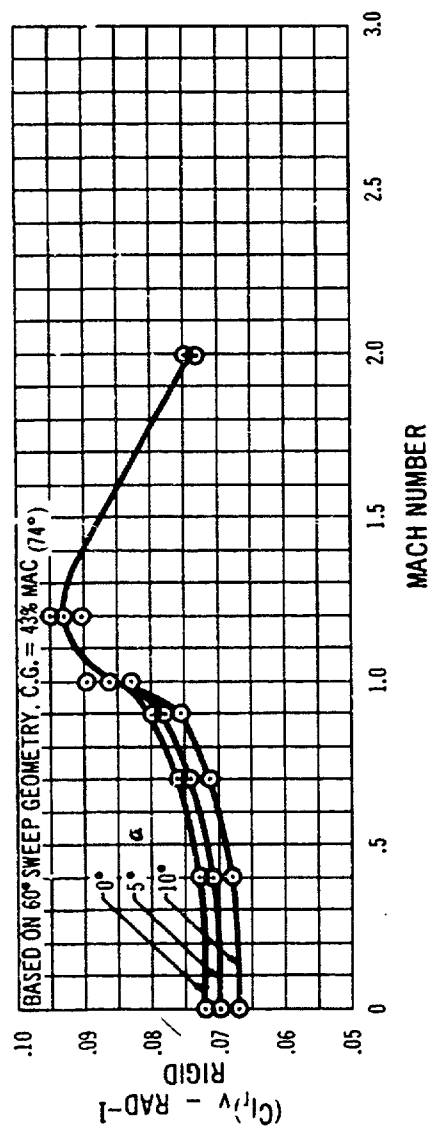
D-98 Estimated Rolling Moment Coefficient Due to Yaw Rate, $\Lambda_{LE} = 42^\circ$, Rigid



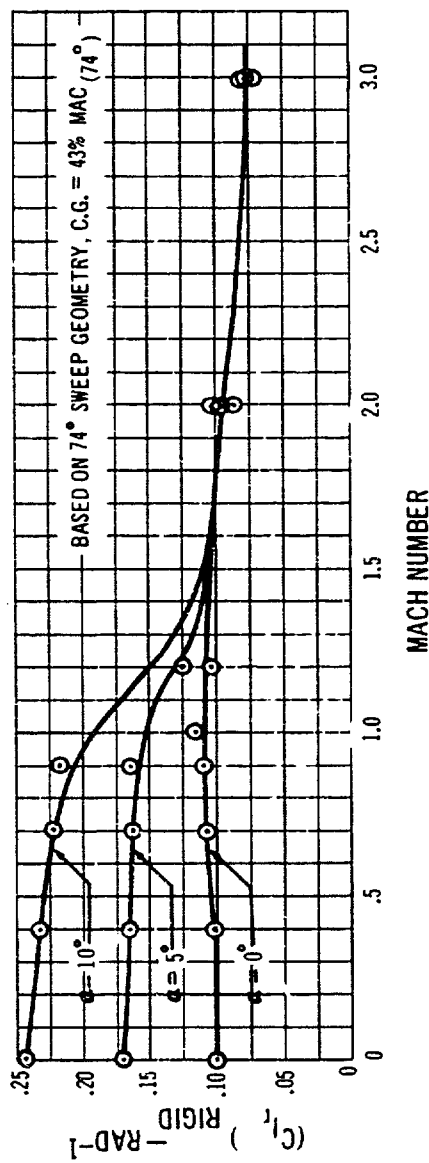
D-99 Estimated Vertical Tail Rolling Moment Coefficient Due to Yaw Rate, $\Lambda_{LE} = 42^\circ$, Rigid



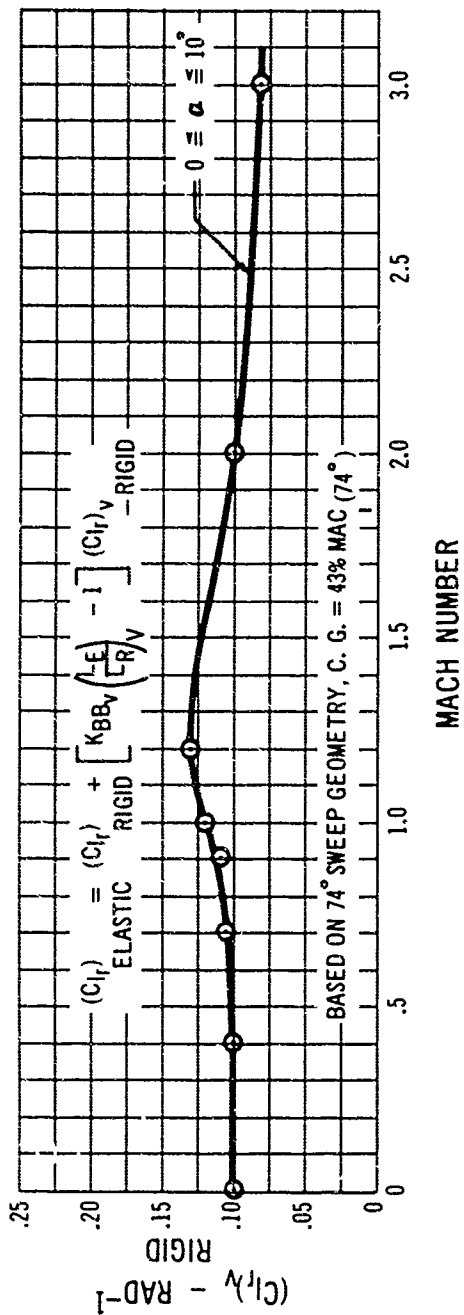
D-100 Estimated Rolling Moment Coefficient Due to Yaw Rate, $\Lambda_{LE} = 60^\circ$, Rigid



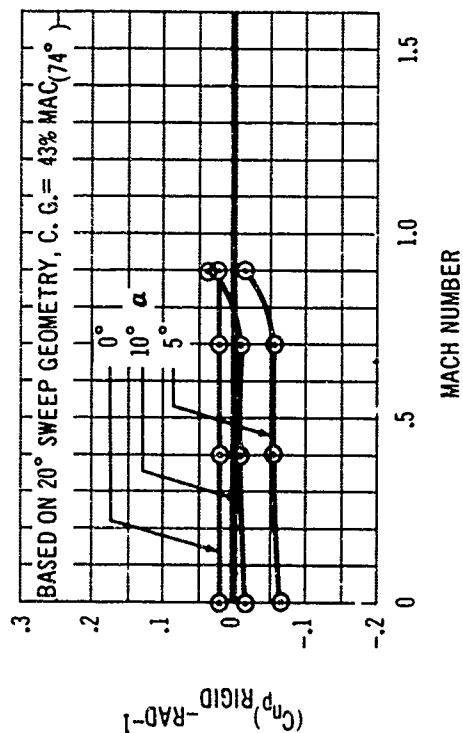
D-101 Estimated Vertical Tail Rolling Moment Coefficient Due to Yaw Rate, $\Lambda_{LE} = 60^\circ$, Rigid



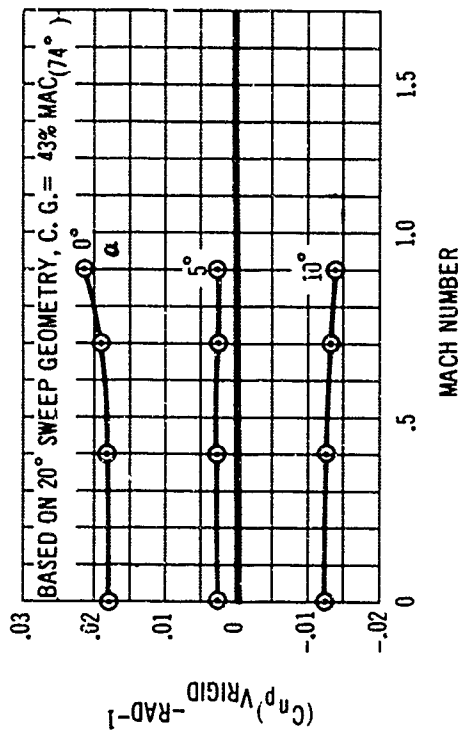
D-102 Estimated Rolling Moment Coefficient Due to Yaw Rate, $\Lambda_{LE} = 74^\circ$, Rigid



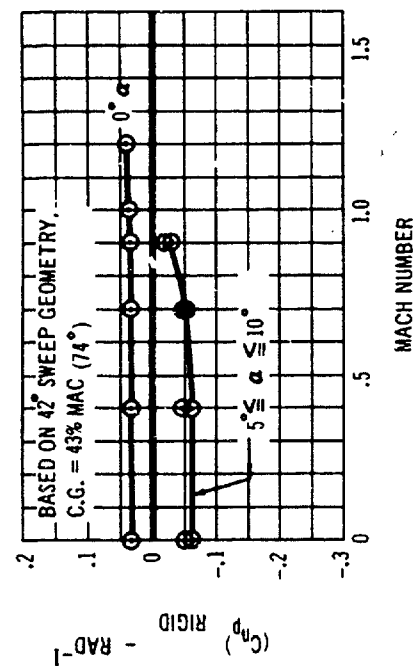
D-103 Estimated Vertical Tail Rolling Moment Coefficient Due to Yaw Rate, $\Lambda_{LE} = 74^\circ$, Rigid



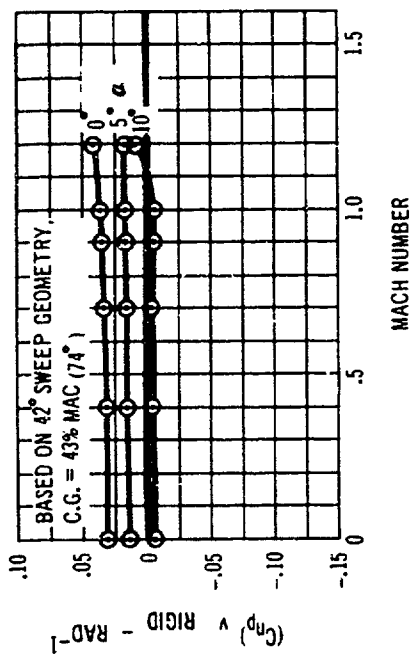
D-104 Estimated Yawing Moment Coefficient Due to Roll Rate, $\Lambda_{LE} = 20^\circ$, Rigid



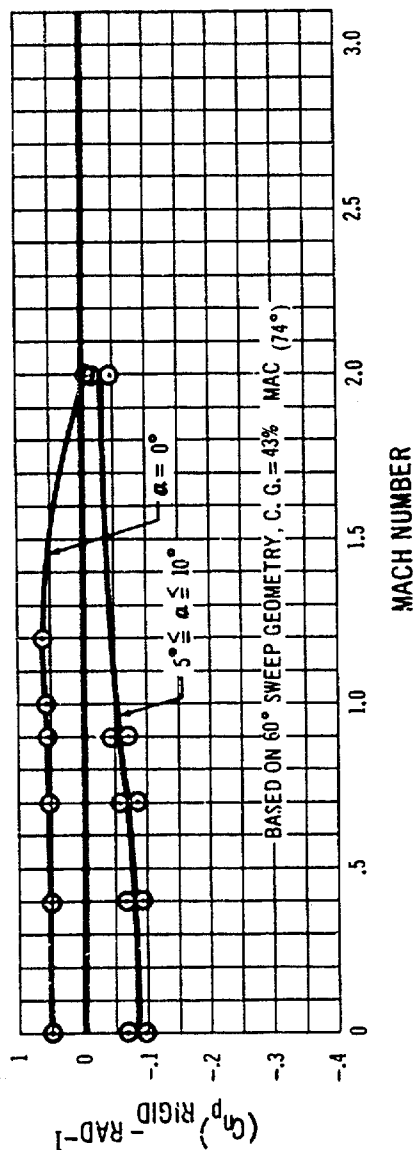
D-105 Estimated Vertical Tail Yawing Moment Coefficient Due to Roll Rate, $\Lambda_{LE} = 20^\circ$, Rigid



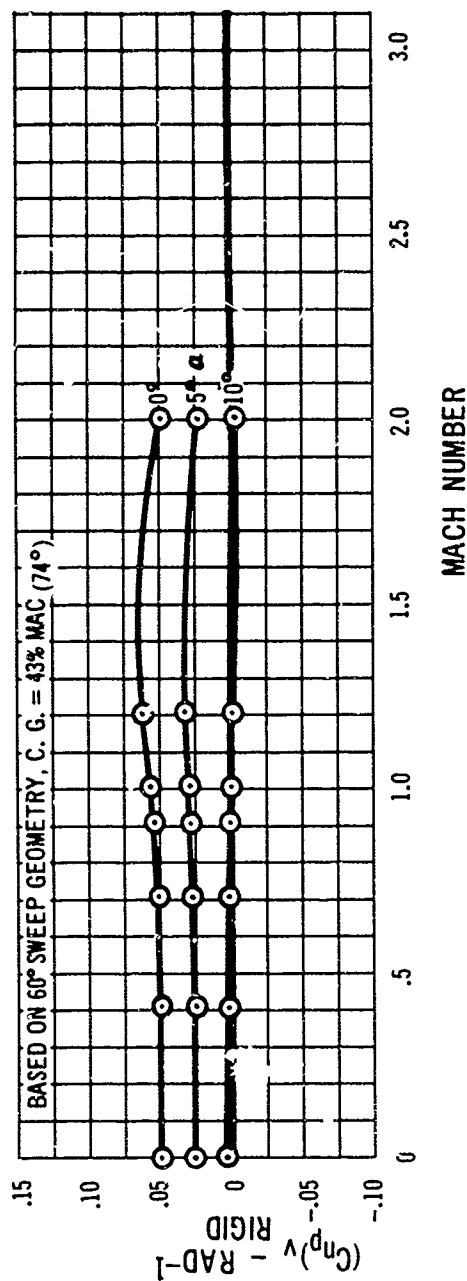
D-106 Estimated Yawing Moment Coefficient
Due to Roll Rate, $\Lambda_{LE} = 42^\circ$, Rigid



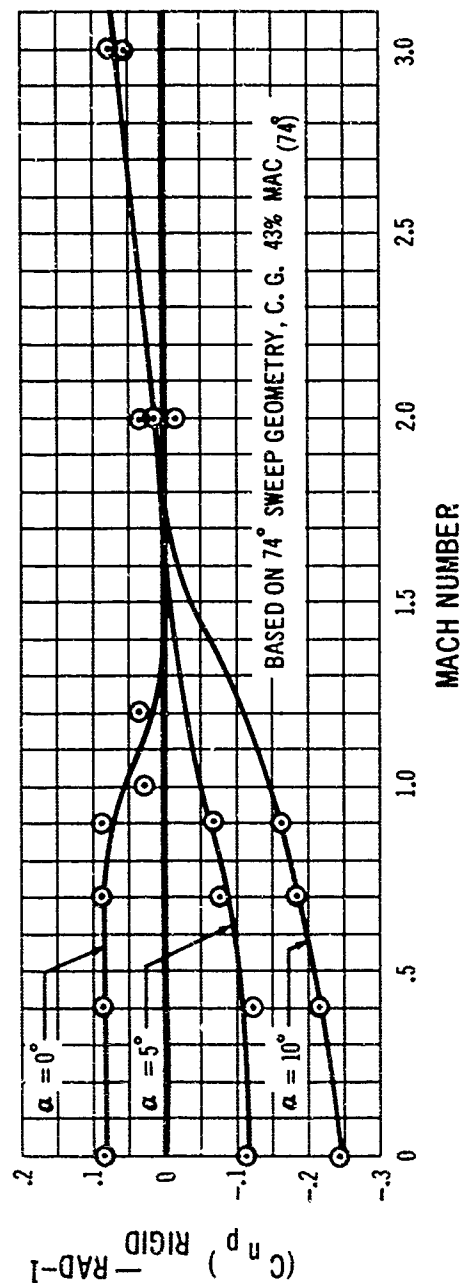
D-107 Estimated Vertical Tail Yawing Moment Coefficient
Due to Roll Rate, $\Lambda_{LE} = 42^\circ$, Rigid



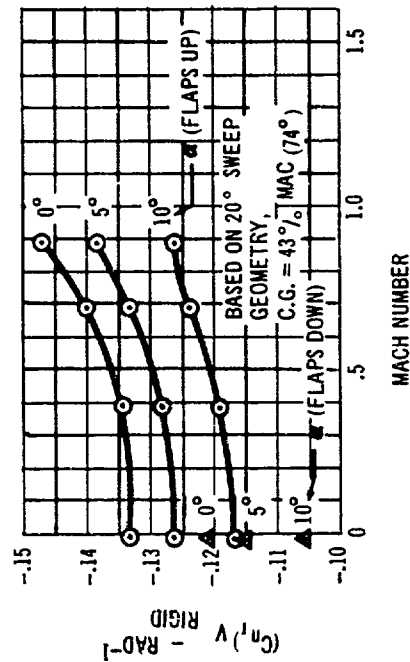
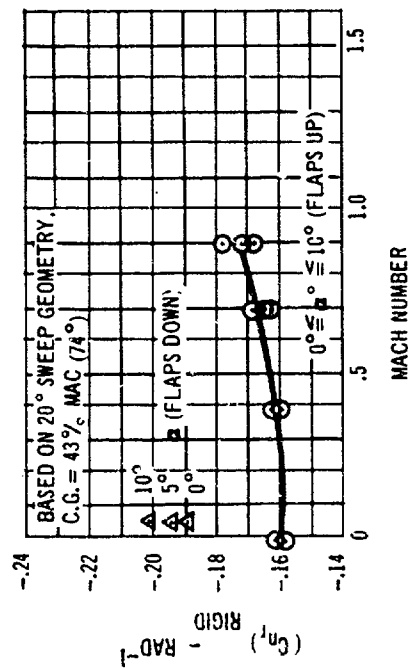
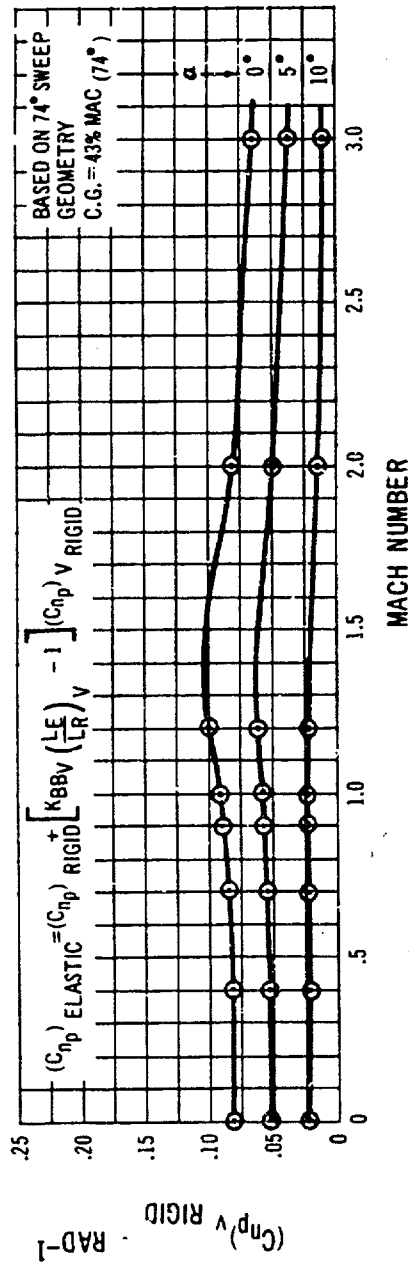
D-108 Estimated Yawing Moment Coefficient Due to Roll Rate, $\Lambda_{LE} = 60^\circ$, Rigid

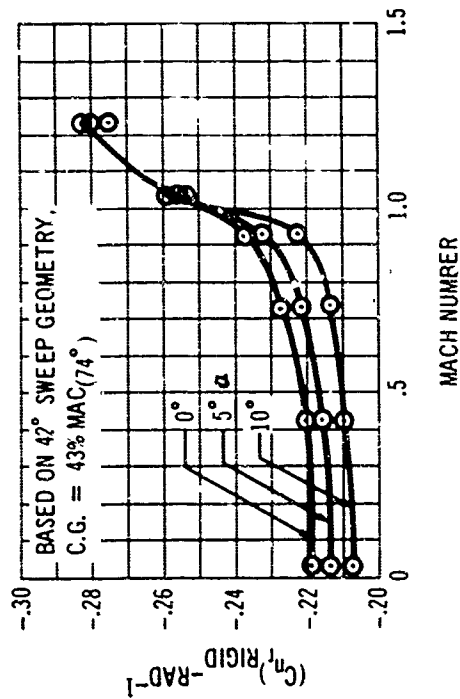


D-109 Estimated Vertical Tail Yawing Moment Coefficient Due to Roll Rate, $A_{LE} = 60^\circ$, Rigid

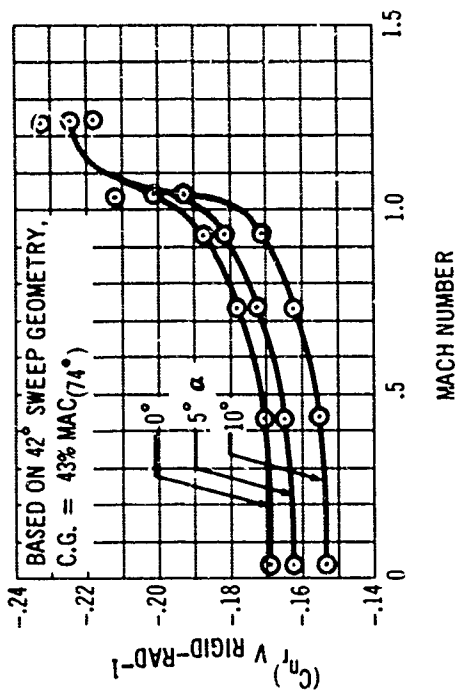


D-110 Estimated Yawing Moment Coefficient Due to Roll Rate, $A_{LE} = 74^\circ$, Rigid

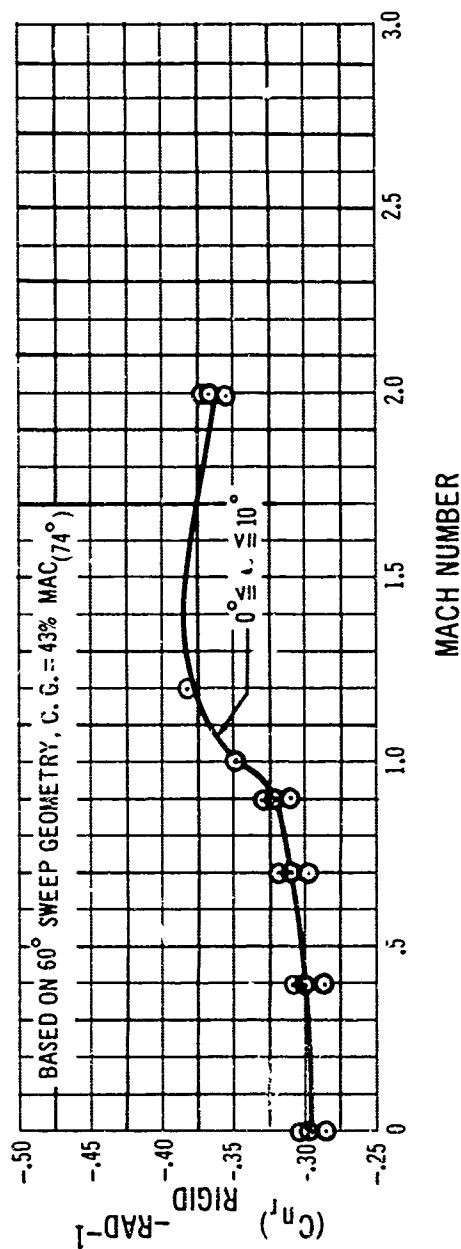




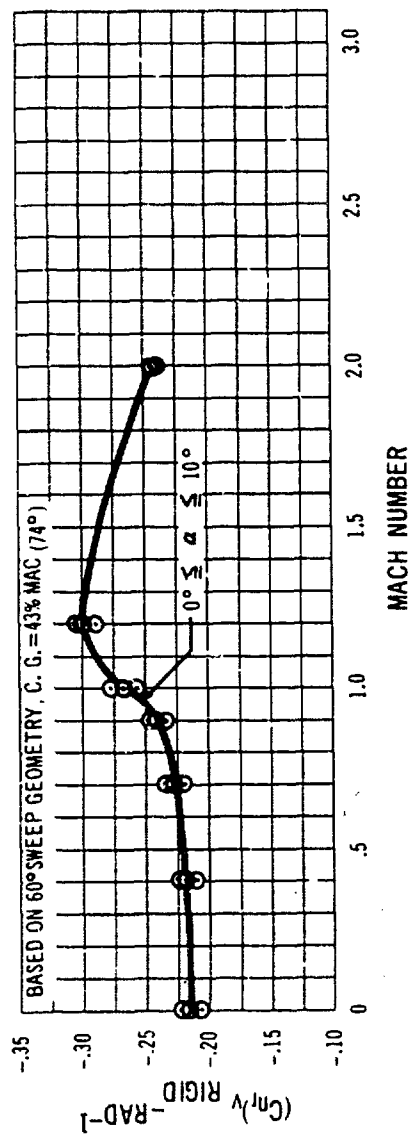
D-114 Estimated Yawing Moment Coefficient
Due to Yaw Rate, $\Lambda_{LE}=42^\circ$, Rigid



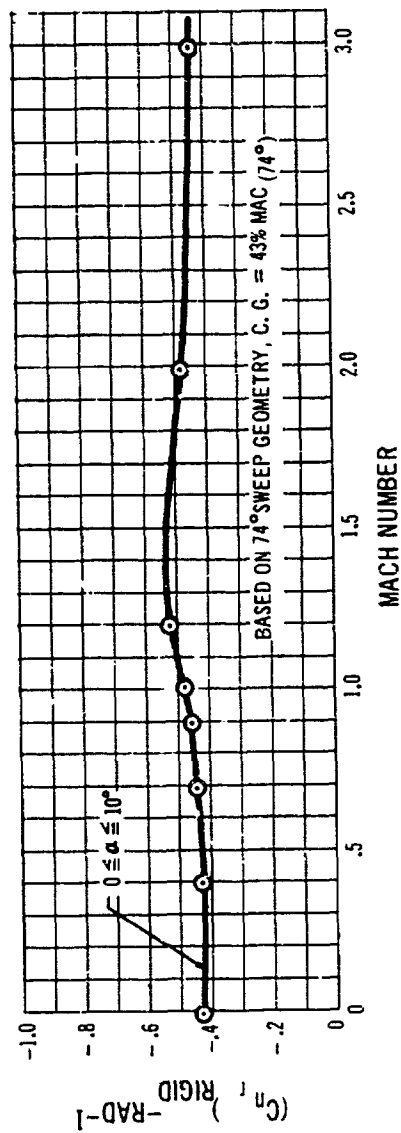
D-115 Estimated Vertical Tail Yawing Moment Coefficient
Due to Yaw Rate, $\Lambda_{LE}=42^\circ$, Rigid



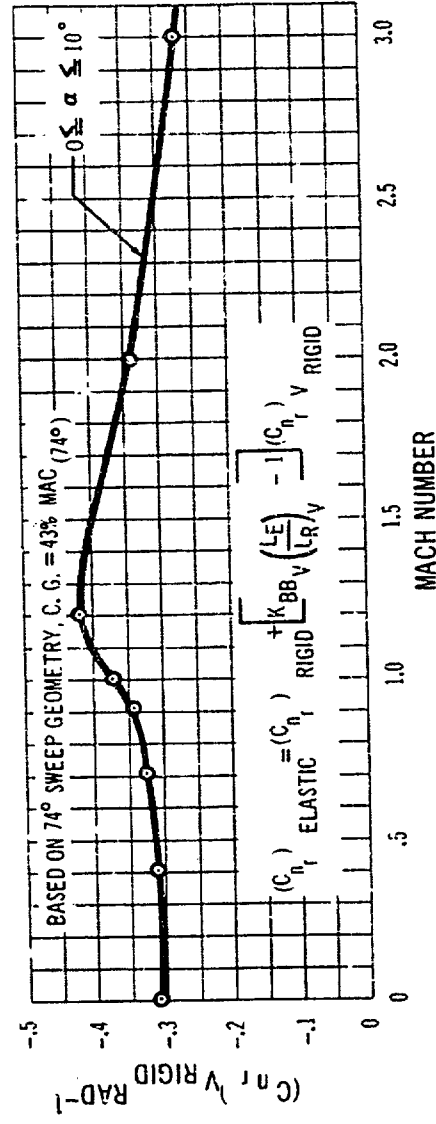
D-116 Estimated Yawing Moment Coefficient Due to Yaw Rate, $\Lambda_{LE}=60^\circ$, Rigid



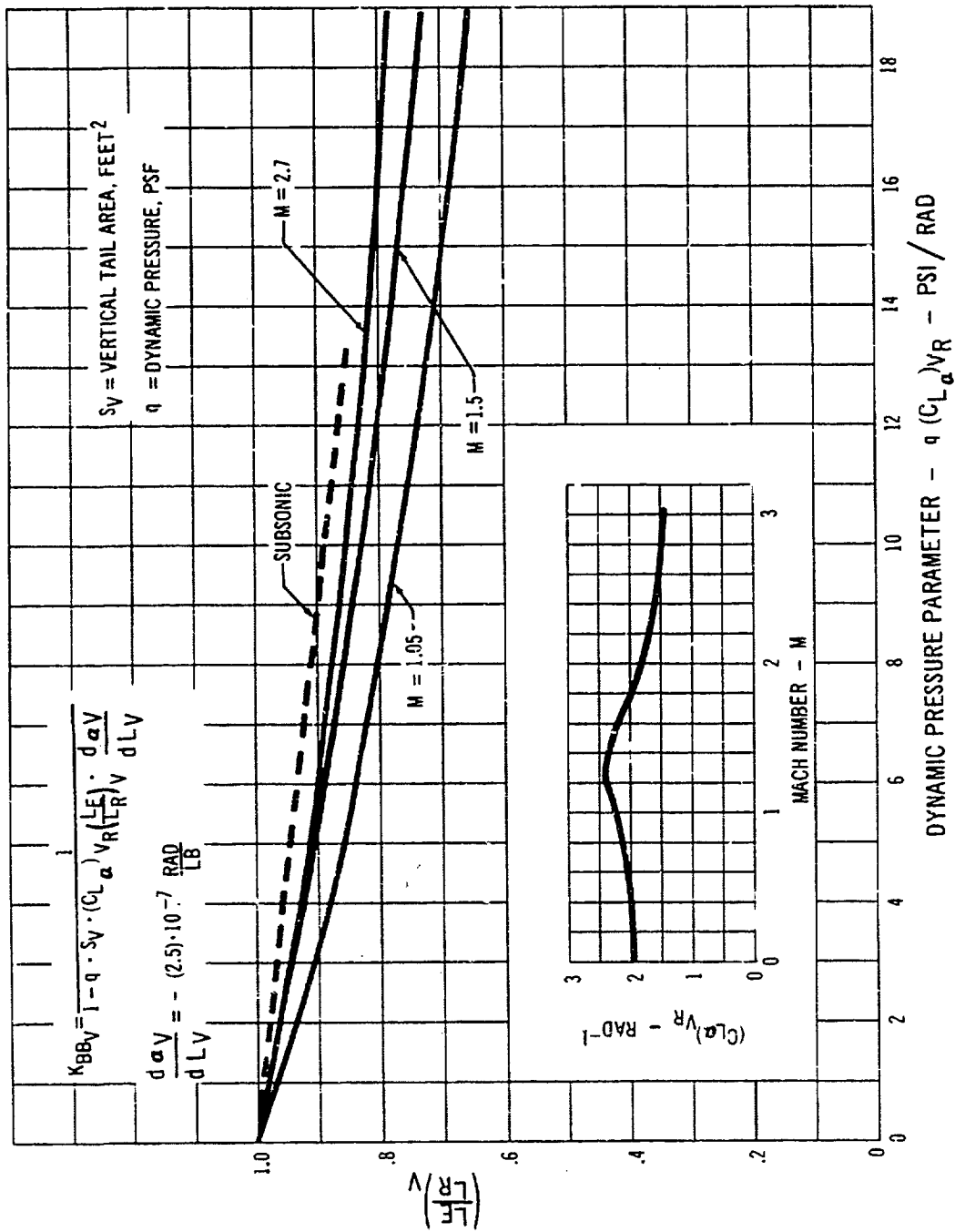
D-117 Estimated Vertical Tail Yawing Moment Coefficient Due to Yaw Rate, $\Lambda_{LE} = 60^\circ$, Rigid



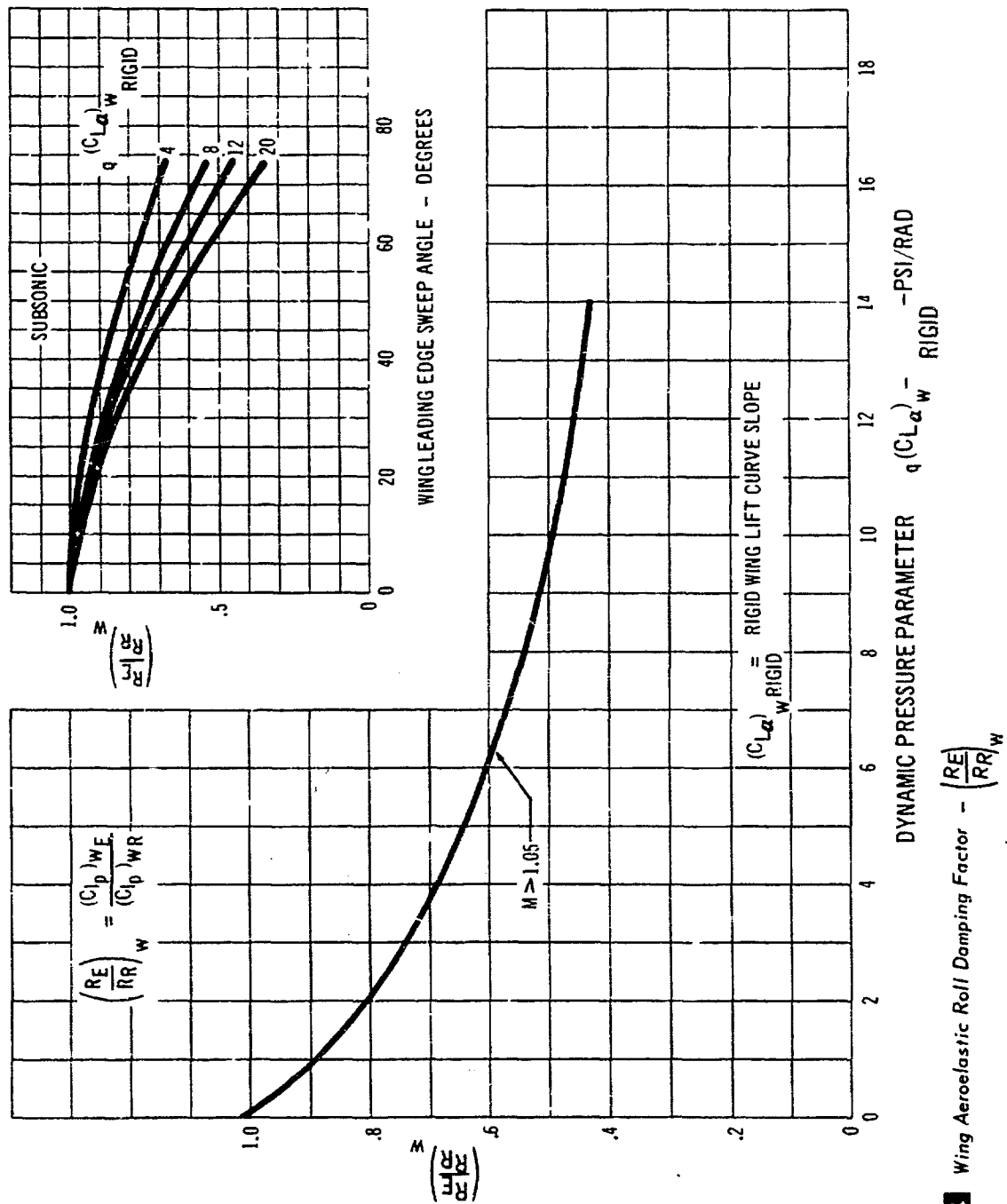
D-118 Estimated Yawing Moment Coefficient Due to Yaw Rate, $\Lambda_{LE} = 74^\circ$, Rigid



D-119 Estimated Vertical Tail Yawing Moment Coefficient Due to Yaw Rate, $\Lambda_{LE} = 74^\circ$, Rigid

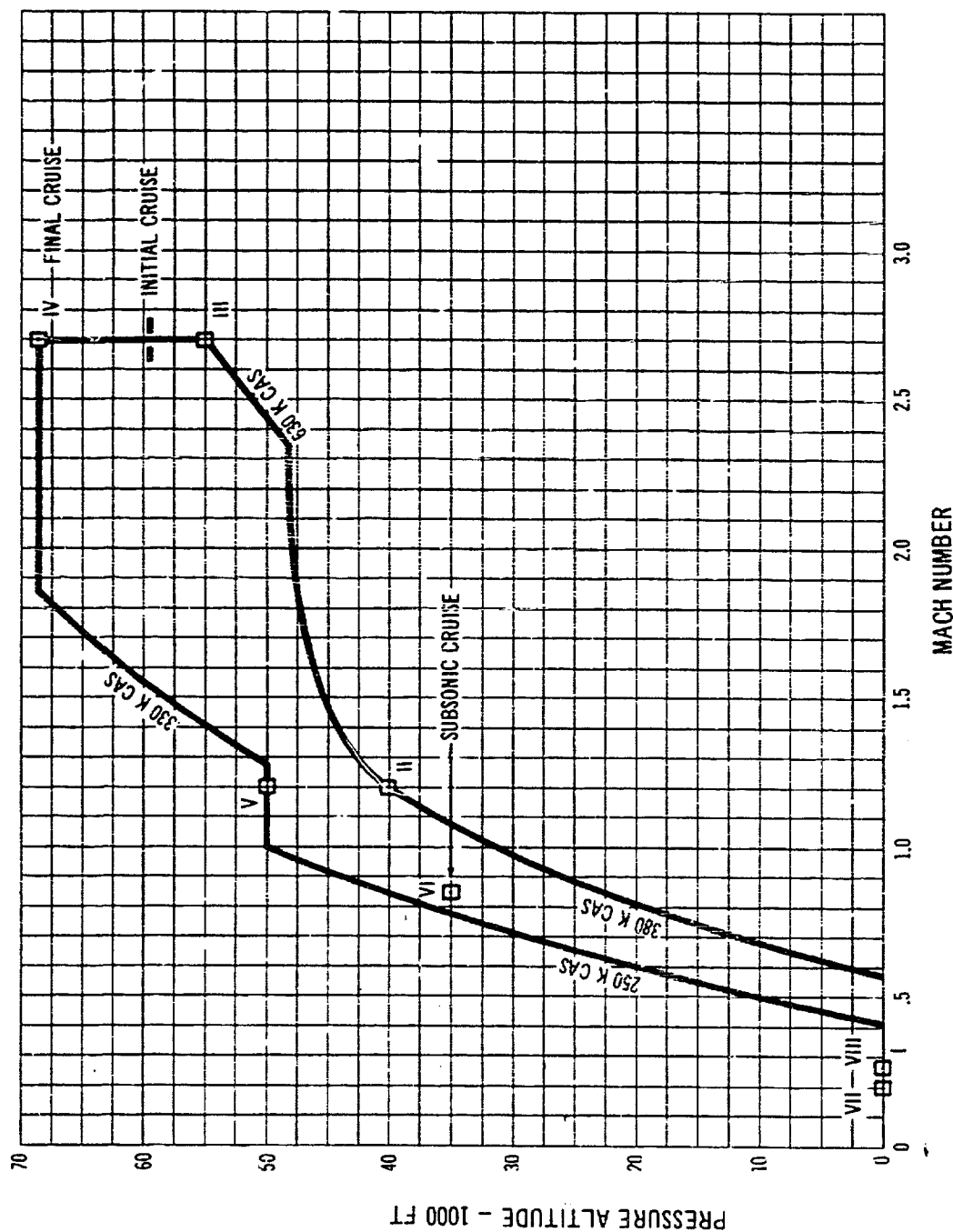


D-120 Vertical Tail Aeroelastic Factors, $\left(\frac{L_E}{L_R} \right)_V K_{BV}$



D-121

Wing Aeroelastic Roll Damping Factor - $\left(\frac{R_E}{R_R}\right)_w$



D-122 Flight Conditions Used in Dynamic Analyses on Climb and Descent Schedules

TABLE D7/B

AIRPLANE STABILITY DERIVATIVES FOR: I TAKE-OFF				DYNAMIC PARAMETERS FOR I TAKE-OFF			
ITEM	SYMBOL	VALUE	DIMENSION		UNAugMENTED AIRPLANE	AugMENTED AIRPLANE	
WEIGHT	W	426 000	LBS	DUTCH ROLL			
ALTITUDE	h	SEA LEVEL	FT	DAMPING RATIO	ζ_d	2301	458
REFERENCE GEOMETRY $\Delta_{LE}=14^\circ$				CYCLES TO HALF AMPLITUDE	C_h	.4666	214
WING AREA	S_w	4684	FT ²	RECIPROCAL OF CYCLES TO HALF AMPLITUDE	$1/C_h$	2.14	4.66
WING SPAN	b	86.33	FT	ROLL-YAW COUPLING PARAMETER $\frac{C_{\dot{\delta}_r}}{C_{\dot{\delta}_l}}$.957	
WING MAC	\bar{c}	64.52	FT	TIME TO HALF AMPLITUDE, SEC	T_h	4.777	
ACTUAL GEOMETRY $\Delta_{LE}=20^\circ$				DAMPED PERIOD, SEC	P_d	10.238	
WING AREA	S_w	3315	FT ²	UNDAMPED NATURAL FREQUENCY, CPS	f_{nd}	.1004	
WING SPAN	b	173.33	FT	ROLL TO SIDESLIP RATIO $\frac{C_{\dot{\delta}_r}}{C_{\dot{\delta}_l}}$		1.061	
MOMENTS OF INERTIA IN BODY AXES				ROLLING PARAMETER, DEG./FPS $\frac{I_{xx}}{I_{yy}}$.2195	21
	I_{xx}	5.29×10^8	SLUG FT ²				
	I_{yy}	12.8×10^6	SLUG FT ²	SPIRAL			
	I_{zz}	17.75×10^6	SLUG FT ²	TIME TO HALF AMPLITUDE, SEC	T_h		
	I_{xz}	$.43 \times 10^6$	SLUG FT ²	TIME TO DOUBLE AMPLITUDE, SEC	T_2	21.34	
INCLINATION OF STABILITY X AXIS FROM BODY REFERENCE X AXIS	ϵ_s	10	DEG	SHORT PERIOD			
POSITIVE DOWN	γ^p	164	KES	DAMPING RATIO	$\zeta_{s.p.}$	5542	5542
EQUIVALENT AIRSPEED	V^p	277	FT/SEC	DAMPED PERIOD, SEC	$P_{s.p.}$	8.93	8.93
TRUE AIRSPEED	V_T			UNDAMPED NATURAL FREQUENCY, CPS	$f_{n s.p.}$	1345	.1345
AIRPLANE TRIMMED LIFT COEFFICIENT ($C_L = \frac{W}{\rho S_w V^2}$)	C_L	1.0		PHUGOID			
ANGLE OF ATTACK AT TRIM	α_{TRIM}	10	DEG	DAMPING RATIO	ζ_p	1476	.1476
AIRPLANE LIFT CURVE SLOPE	$C_{L\alpha}$	3.205	RAD ⁻¹	DAMPED PERIOD, SEC	P_p	42.46	42.46
AERODYNAMIC TIME (LONGITUDINAL)	$\tau/2V_T$.1165	SEC				
STATIC LONGITUDINAL STABILITY	C_{m0}	-.272	RAD ⁻¹				
PITCH DAMPING DUE TO ANGLE OF ATTACK	$C_{m\dot{\alpha}}$	-.78	RAD ⁻¹				
PITCH DAMPING DUE TO PITCHING VELOCITY	$C_{m\dot{\alpha}}$	-1.38	RAD ⁻¹				
AERODYNAMIC TIME (LAT. - DIR.)	$b/2V_T$	3129	SEC				
STATIC DIRECTIONAL STABILITY	C_{n0}	.092	RAD ⁻¹				
EFFECTIVE DIRECTIONAL STABILITY	$C_{n\dot{\beta}}$.091	RAD ⁻¹				
SIDE FORCE DUE TO SIDESLIP	$C_{Y\beta}$	-.65	RAD ⁻¹				
YAW DAMPING DUE TO YAW RATE	$C_{n\dot{\beta}}$	-.19	RAD ⁻¹				
ROLL DUE TO YAW RATE	C_{lr}	.34	RAD ⁻¹				
SIDE FORCE DUE TO YAW RATE	$C_{Y\dot{\beta}}$.05	RAD ⁻¹				
YAW DUE TO ROLL RATE	C_{nr}	-.04	RAD ⁻¹				
ROLL DAMPING DUE TO ROLL RATE	$C_{l\dot{p}}$	-.47	RAD ⁻¹				
SIDE FORCE DUE TO ROLL RATE	$C_{Y\dot{p}}$.42	RAD ⁻¹				
*BASED ON ACTUAL GEOMETRY							

DAMPER DATA	SYMBOL	VALUE	DIMENSION
ROLL DAMPER GAIN EFFECTIVENESS	K_{δ_s}	0	DEG DEG SEC DEG ¹
YAW DAMPER GAIN EFFECTIVENESS	K_{δ_r}	1.5	DEG DEG SEC DEG ¹
PITCH DAMPER GAIN EFFECTIVENESS	K_{δ_e}	0	DEG DEG SEC DEG ¹
* BASED ON ACTUAL GEOMETRY			

TABLE D7/C

AIRPLANE STABILITY DERIVATIVES FOR II TRANSONIC CLIMB

ITEM	SYMBOL	VALUE	DIMENSION
WEIGHT	W	405000.	LIBS
ALTITUDE	h	40000.	FT
REFERENCE GEOMETRY $\Delta_{LE} = 4^\circ$			
WING AREA	S_w	4644.	FT ²
WING SPAN	b	86.33	FT
WING MAC	\bar{c}	64.52	FT
ACTUAL GEOMETRY: $\Delta_{LE} = 65^\circ$			
WING AREA	S_w	40500.	FT ²
WING SPAN	b	107.5	FT
MOMENTS OF INERTIA IN BODY AXES			
	I_{xx}	2.625 x 10 ⁶	SLUG FT ²
	I_{yy}	13.652 x 10 ⁶	SLUG FT ²
	I_{zz}	15.7 x 10 ⁶	SLUG FT ²
	I_{xz}	.385 x 10 ⁶	SLUG FT ²
INCLINATION OF STABILITY X AXIS FROM BODY REFERENCE X AXIS	ϵ_s	7.	DEG
POSITIVE DOWN	V_e	342.	KTS
EQUIVALENT AIRSPEED	V_e	1161.	FT/SEC
TRUE AIRSPEED			
AIRPLANE TRIMMED LIFT			
COEFFICIENT ($C_L = \frac{W}{q S_w}$)	C_L	.251	
ANGLE OF ATTACK AT TRIM	α TRIM	7.	DEG
AIRPLANE LIFT CURVE SLOPE	C_{L_α}	2.005	RAD ⁻¹
AERODYNAMIC TIME	$\tau/2V_T$.02779	SEC
STATIC LONGITUDINAL STABILITY	C_{m_α}	-.2005	RAD ⁻¹
PITCH DAMPING DUE TO ANGLE OF			
ATTACK	C_{m_p}	-.65	RAD ⁻¹
PITCH DAMPING DUE TO PITCHING			
VELOCITY	C_{m_q}	-1.41	RAD ⁻¹
AERODYNAMIC TIME (LAT. -DIR.)	$b/2V_T$.3129	SEC
STATIC DIRECTIONAL STABILITY	C_{Y_β}	.2	RAD ⁻¹
EFFECTIVE DIHEDRAL	C_{Y_β}	-.11	RAD ⁻¹
SIDE FORCE DUE TO SIDESLIP	C_{Y_β}	-.8	RAD ⁻¹
YAW DAMPING DUE TO YAW RATE	C_{Y_r}	-.35	RAD ⁻¹
ROLL DUE TO YAW RATE	C_{l_r}	.079	RAD ⁻¹
SIDE FORCE DUE TO YAW RATE	C_{Y_r}	.33	RAD ⁻¹
YAW DUE TO ROLL RATE	C_{Y_p}	-.13	RAD ⁻¹
ROLL DAMPING DUE TO ROLL RATE	C_{l_p}	-.15	RAD ⁻¹
SIDE FORCE DUE TO ROLL RATE	C_{Y_p}	.47	RAD ⁻¹
*BASED ON ACTUAL GEOMETRY			

DYNAMIC PARAMETERS FOR II TRANSONIC CLIMB

	UNDAUGHTED AIRPLANE	AUGMENTED AIRPLANE
DUTCH ROLL		
DAMPING RATIO	ζ_d	.03847
CYCLES TO HALF AMPLITUDE	C_h	2.8695
RECIPROCAL OF CYCLES TO HALF AMPLITUDE	$1/C_h$.3483
ROLL-YAW COUPLING PARAMETER $\frac{C_{Y_r}}{C_{l_r}}$.067
TIME TO HALF AMPLITUDE, SEC	$T_{1/2}$	10.462
DAMPED PERIOD, SEC	P_d	3.645
UNDAMPED NATURAL FREQUENCY, CPS	f_{nd}	.2745
ROLL TO SIDESLIP RATIO $\frac{C_{Y_p}}{C_{l_p}}$		2.747
ROLLING PARAMETER, DEG./FPS $104 \frac{1}{V_T} \frac{C_{Y_p}}{C_{l_p}}$.2732
SPIRAL		
TIME TO HALF AMPLITUDE, SEC	$T_{1/2}$	55.01
TIME TO DOUBLE AMPLITUDE, SEC	T_2	
SHORT PERIOD		
DAMPING RATIO	ζ_{sp}	.28
DAMPED PERIOD, SEC	P_{sp}	4.79
UNDAMPED NATURAL FREQUENCY, CPS	f_{sp}	.218
PHUGOID		
DAMPING RATIO	ζ_p	.218
DAMPED PERIOD, SEC	P_p	144.6
DAMPER DATA	SYMBOL	VALUE
ROLL DAMPER GAIN EFFECTIVENESS	K_{δ_s} $C_{l_{\delta_s}}$	5. .000025
YAW DAMPER GAIN EFFECTIVENESS	K_{δ_r} $C_{m_{\delta_r}}$	1.9 -.00094
PITCH DAMPER GAIN EFFECTIVENESS	K_{δ_e} $C_{m_{\delta_e}}$	3. -.00068
*BASED ON ACTUAL GEOMETRY		
		DIMENSION
		DEG/DEG-SEC DEG ¹
		DEG/DEG-SEC DEG ¹
		DEG/DEG-SEC DEG ¹

TABLE D7/D

AIRPLANE STABILITY DERIVATIVES FOR III END OF ACCELERATION

ITEM	SYMBOL	VALUE	DIMENSION
WEIGHT	W	380000	LBS
ALTITUDE	h	55000	FT
REFERENCE GEOMETRY $\Lambda_{LE}/4^\circ$			
WING AREA	S_w	4684	FT ²
WING SPAN	b	86.33	FT
WING MAC	\bar{c}	64.52	FT
ACTUAL GEOMETRY $\Lambda_{LE}/74^\circ$			
WING AREA	S_w	4684	FT ²
WING SPAN	b	86.33	FT
MOMENTS OF INERTIA IN BODY AXES			
	I_{xx}	1.85×10^6	SLUG FT ²
	I_{yy}	13.4×10^6	SLUG FT ²
	I_{zz}	14.82×10^6	SLUG FT ²
	I_{xz}	34×10^6	SLUG FT ²
INCLINATION OF STABILITY X AXIS			
FROM BODY REFERENCE X AXIS	ϵ_s	4.5	DEG
POSITIVE DOWN			
EQUIVALENT AIRSPEED	V_e	536	KTS
TRUE AIRSPEED	V_T	2615	FT/SEC
AIRPLANE TRIMMED LIFT			
COEFFICIENT: ($C_L = W/S_w$)	C_L	.0833	
ANGLE OF ATTACK AT TRIM	α TRIM	4.5	DEG
AIRPLANE LIFT CURVE SLOPE	$C_{L\alpha}$	1.319	RAD ⁻¹
AERODYNAMIC TIME	$\bar{c}/2V_T$.01234	SEC
(LONGITUDINAL)	$C_{m\alpha}$	-1015	RAD ⁻¹
STATIC LONGITUDINAL STABILITY			
PITCH DAMPING DUE TO ANGLE OF	$C_{m\dot{\alpha}}$	0	RAD ⁻¹
ATTACK			
PITCH DAMPING DUE TO PITCHING	$C_{m\ddot{\alpha}}$	-7	RAD ⁻¹
VELOCITY			
AERODYNAMIC TIME (LAT. DIR.)	$b/2V_T$.01651	SEC
STATIC DIRECT, ONAL STABILITY	$C_{n\beta}$.088	RAD ⁻¹
EFFECTIVE DIHEDRAL	$C_{l\beta}$	-.024	RAD ⁻¹
SIDE FORCE DUE TO SIDESLIP	$C_{y\beta}$	-.51	RAD ⁻¹
YAW DAMPING DUE TO YAW RATE	C_{nr}	-.36	RAD ⁻¹
ROLL DUE TO YAW RATE	C_{lr}	.055	RAD ⁻¹
SIDE FORCE DUE TO YAW RATE	C_{yp}	.23	RAD ⁻¹
YAW DUE TO ROLL RATE	C_{rp}	.038	RAD ⁻¹
ROLL DAMPING DUE TO ROLL RATE	C_{lp}	-.075	RAD ⁻¹
SIDE FORCE DUE TO ROLL RATE	C_{yp}	.2	RAD ⁻¹
*BASED ON ACTUAL GEOMETRY			

DYNAMIC PARAMETERS FOR III END OF ACCELERATION

	UNADJUSTED AIRPLANE	AUGMENTED AIRPLANE	
DUTCH ROLL			
DAMPING RATIO	ζ_d	.0875	
CYCLES TO HALF AMPLITUDE	C_h	1.256	
RECIPROCAL OF CYCLES TO HALF AMPLITUDE	$1/C_h$.796	
ROLL-YAW COUPLING PARAMETER	μ_{ry}	.9765	
TIME TO HALF AMPLITUDE, SEC	T_h	4.888	
DAMPED PERIOD, SEC	P_d	3.691	
UNDAMPED NATURAL FREQUENCY, CPS	f_{nd}	.258	
ROLL TO SIDESLIP RATIO	μ_{rl}	2.279	
ROLLING PARAMETER, DEG /FPS	$\mu_{rl} f_{nd}$.1443	
SPIRAL			
TIME TO HALF AMPLITUDE, SEC	T_h	93.01	
TIME TO DOUBLE AMPLITUDE, SEC	T_2		
SHORT PERIOD			
DAMPING RATIO	$\zeta_{s.p.}$.123	
DAMPED PERIOD, SEC	$P_{s.p.}$	4.2	
UNDAMPED NATURAL FREQUENCY, CPS	$f_{n.s.p.}$.240	
PHUGOID			
DAMPING RATIO	ζ_p	.1180	
DAMPED PERIOD, SEC	P_p	366.0	
		1178	
		374.5	
DAMPER DATA	SYMBOL	VALUE	DIMENSION
ROLL DAMPER GAIN EFFECTIVENESS	K_{δ_s}	5	DEG DEG SEC
	$C_{l\delta_s}$.000095	DEG ¹
YAW DAMPER GAIN EFFECTIVENESS	K_{δ_r}	1.9	DEG DEG SEC
	$C_{n\delta_r}$	-.000244	DEG ¹
PITCH DAMPER GAIN EFFECTIVENESS	K_{δ_e}	5	DEG DEG SEC
	$C_{m\delta_e}$	-.00017	DEG ¹
*BASED ON ACTUAL GEOMETRY			

TABLE D7/E

AIRPLANE STABILITY DERIVATIVES FOR IV END OF CRUISE

ITEM	SYMBOL	VALUE	DIMENSION
WEIGHT	W	246,000	LBS
ALTITUDE	h	68,500	FT
REFERENCE GEOMETRY $\Delta L E^2$			FT ²
WING AREA	S_w	4684	FT ²
WING SPAN	b	86.33	FT
WING MAC	c	64.52	FT
ACTUAL GEOMETRY $\Delta L E^2 = 74$			FT ²
WING AREA	S_w	4684	FT ²
WING SPAN	b	86.33	FT
MOMENTS OF INERTIA IN BODY AXES			
	I_{xx}	1.07×10^6	SLUG FT ²
	I_{yy}	10.1×10^6	SLUG FT ²
	I_{zz}	10.81×10^6	SLUG FT ²
	I_{xz}	$.22 \times 10^6$	SLUG FT ²
INCLINATION OF STABILITY X AXIS FROM BODY REFERENCE X AXIS	ϵ_s	5	DEG
POSTIVE DOWN	V_0	388	KTS
EQUIVALENT AIRSPEED	V_0	2620	FT/SEC
TRUE AIRSPEED			
AIRPLANE TRIMMED LIFT COEFFICIENT ($C_L = W/S_w$)	C_L	.1032	
ANGLE OF ATTACK AT TRIM	α	5	DEG
AIRPLANE LIFT CURVE SLOPE	$C_{L\alpha}$	1.49	RAD ⁻¹
AERODYNAMIC TIME (LONGITUDINAL)	$\tau/2V_0$.012336	SEC
STATIC LONGITUDINAL STABILITY	$C_{m\alpha}$	-.179	RAD ⁻¹
PITCH DAMPING DUE TO ANGLE OF ATTACK	$C_{m\dot{\alpha}}$	0	RAD ⁻¹
PITCH DAMPING DUE TO PITCHING VELOCITY	$C_{m\dot{\alpha}}$	-.81	RAD ⁻¹
AERODYNAMIC TIME (LAT. DIR.)	$b/2V_0$.01648	SEC
STATIC DIRECTIONAL STABILITY	$C_{n\beta}$.099	RAD ⁻¹
EFFECTIVE DIRECTIONAL	$C_{l\beta}$	-.026	RAD ⁻¹
SIDE FORCE DUE TO SIDESLIP	$C_{Y\beta}$	-.52	RAD ⁻¹
YAW DAMPING DUE TO YAW RATE	C_{nr}	-.39	RAD ⁻¹
ROLL DUE TO YAW RATE	C_{lr}	.064	RAD ⁻¹
SIDE FORCE DUE TO YAW RATE	C_{Yr}	.26	RAD ⁻¹
YAW DUE TO ROLL RATE	C_{nr}	.046	RAD ⁻¹
ROLL DAMPING DUE TO ROLL RATE	C_{lp}	-.095	RAD ⁻¹
SIDE FORCE DUE TO ROLL RATE	C_{Yp}	.23	RAD ⁻¹
*BASED ON ACTUAL GEOMETRY			

DYNAMIC PARAMETERS FOR IV END OF CRUISE

	UNADJUSTED AIRPLANE	ADJUSTED AIRPLANE
DUTCH ROLL		
DAMPING RATIO	ζ_d	.043
CYCLES TO HALF AMPLITUDE	C_h	1.304
RECIPROCAL OF CYCLES TO HALF AMPLITUDE	$1/C_h$.7665
ROLL-YAW COUPLING PARAMETER $\frac{C_{Yr}}{C_{nr}}$.9482
TIME TO HALF AMPLITUDE, SEC	T_h	5.475
DAMPED PERIOD, SEC	P_d	4.199
UNDAMPED NATURAL FREQUENCY, CPS	f_{nd}	.239
ROLL TO SIDESLIP RATIO $\frac{C_{Yr}}{C_{nr}}$		2.708
ROLLING PARAMETER, DEG./FPS $(\frac{C_{Yr}}{C_{nr}}) \frac{1}{V_0}$.2372
SPIRAL		
TIME TO HALF AMPLITUDE, SEC	T_h	138.4
TIME TO DOUBLE AMPLITUDE, SEC	T_2	
SHORT PERIOD		
DAMPING RATIO	$\zeta_{s.p.}$.099
DAMPED PERIOD, SEC	$P_{s.p.}$	3.81
UNDAMPED NATURAL FREQUENCY, CPS	$f_{s.p.}$.264
PHUGOID		
DAMPING RATIO	ζ_p	.095
DAMPED PERIOD, SEC	P_p	354
DAMPER DATA	SYMBOL	VALUE
ROLL DAMPER GAIN EFFECTIVENESS	K_{δ_s}	5
	$C_{l\delta_s}$.000005
YAW DAMPER GAIN EFFECTIVENESS	K_{δ_r}	1.9
	C_{nr}	-.000299
PITCH DAMPER GAIN EFFECTIVENESS	K_{δ_e}	5
*BASED ON ACTUAL GEOMETRY	$C_{m\delta_e}$	-.00072
		DIMENSION
		DEG DEG SEC
		DEG ¹
		DEG DEG SEC
		DEG ¹
		DEG DEG SEC
		DEG ¹

TABLE D7/F

AIRPLANE STABILITY DERIVATIVES FOR V TRANSONIC DESCENT

ITEM	SYMBOL	VALUE	DIMENSION
HEIGHT	h	245000.	LBS
REFERENCE GEOMETRY $\Lambda_{LE} = 4^\circ$	h	50000.	FT
WING AREA	S_w	4684	FT ²
WING SPAN	b	86.33	FT
WING VAC.	c	64.52	FT
ACTUAL GEOMETRY $\Lambda_{LE} = 65^\circ$			
WING AREA	S_w	4050.	FT ²
WING SPAN	b	107.5	FT
MOMENTS OF INERTIA IN BODY AXES			
	I_{xx}	1.3×10^6	SLUG FT ²
	I_{yy}	9.85×10^6	SLUG FT ²
	I_{zz}	10.92×10^6	SLUG FT ²
	I_{xz}	$.24 \times 10^6$	SLUG FT ²
INCLINATION OF STABILITY X AXIS FROM BODY REFERENCE X AXIS	ϵ_s	7.	DEG
POSITIVE DOWN	V_e	269.	KTS
EQUIVALENT AIRSPEED	V_T	1162.	FT/SEC
TRUE AIRSPEED			
AIRPLANE TRIMMED LIFT			
COEFFICIENT ($C_L = \frac{W}{q S_w}$)	C_L	.2065	
ANGLE OF ATTACK AT TRIM	α	7.	DEG
AIRPLANE LIFT CURVE SLOPE	$C_{L\alpha}$	2.29	RAD ⁻¹
AERODYNAMIC TIME	$\bar{c}/2V_T$.02776	SEC
(LONGITUDINAL)	$C_{m\alpha}$	-.314	RAD ⁻¹
STATIC LONGITUDINAL STABILITY			
PITCH DAMPING DUE TO ANGLE OF ATTACK	$C_{m\dot{\alpha}}$	-.78	RAD ⁻¹
PITCH DAMPING DUE TO PITCHING VELOCITY	$C_{m\dot{\alpha}}$	-1.73	RAD ⁻¹
AERODYNAMIC TIME (I.A., DIR.)	$b/2V_T$.04626	SEC
STATIC DIRECTIONAL STABILITY	$C_{n\beta}$.24	RAD ⁻¹
EFFECTIVE DIHEDRAL	$C_{Y\beta}$	-.11	RAD ⁻¹
SIDE FORCE DUE TO SIDESLIP	$C_{Y\beta}$	-.85	RAD ⁻¹
YAW DAMPING DUE TO YAW RATE	$C_{n\dot{\beta}}$	-.38	RAD ⁻¹
ROLL DUE TO YAW RATE	$C_{l\dot{\beta}}$.085	RAD ⁻¹
SIDE FORCE DUE TO YAW RATE	$C_{Y\dot{\beta}}$.37	RAD ⁻¹
YAW DUE TO ROLL RATE	$C_{n\dot{\rho}}$	-.12	RAD ⁻¹
ROLL DAMPING DUE TO ROLL RATE	$C_{l\dot{\rho}}$	-.18	RAD ⁻¹
SIDE FORCE DUE TO ROLL RATE	$C_{Y\dot{\rho}}$.47	RAD ⁻¹
*BASED ON ACTUAL GEOMETRY			

DYNAMIC PARAMETERS FOR V TRANSONIC DESCENT

	UNAugMENTED AIRPLANE	AUGMENTED AIRPLANE	
DUTCH ROLL			
DAMPING RATIO	ζ_d	.06175	
CYCLES TO HALF AMPLITUDE	$C_{\frac{1}{2}}$	1.783	
RECIPROCAL OF CYCLES TO HALF AMPLITUDE	$1/C_{\frac{1}{2}}$.561	
ROLL-YAW COUPLING PARAMETER	$\frac{C_{lr}}{C_{nr}}$.842	
TIME TO HALF AMPLITUDE, SEC	$T_{\frac{1}{2}}$	6.189	
DAMPED PERIOD, SEC	P_d	3.471	
UNDAMPED NATURAL FREQUENCY, CPS	f_{nd}	.2887	
ROLL TO SIDESLIP RATIO	$\frac{C_{lr}}{C_{nr}}$	3.071	
ROLLING PARAMETER, DEG./FPS	$\frac{C_{lr}}{C_{nr}}$.3881	
SPIRAL			
TIME TO HALF AMPLITUDE, SEC	$T_{\frac{1}{2}}$	74.53	
TIME TO DOUBLE AMPLITUDE, SEC	T_2		
SHORT PERIOD			
DAMPING RATIO	$\zeta_{s.p.}$.76	
DAMPED PERIOD, SEC	$P_{s.p.}$	4.18	
UNDAMPED NATURAL FREQUENCY, CPS	$f_{n.s.p.}$.248	
PHUGOID			
DAMPING RATIO	ζ_p	.232	
DAMPED PERIOD, SEC	P_p	177.	
		177.	
DAMPER DATA	SYMBOL	VALUE	DIMENSION
ROLL DAMPER GAIN EFFECTIVENESS	K_{δ_s}	5	DEG DEG SEC DEG ⁻¹
	$C_{Y\delta_s}$.000025	DEG ⁻¹
YAW DAMPER GAIN EFFECTIVENESS	K_{δ_e}	1.9	DEG DEG SEC DEG ⁻¹
	$C_{m\delta_e}$	-.00094	DEG ⁻¹
PITCH DAMPER GAIN EFFECTIVENESS	K_{δ_e}	3	DEG DEG SEC DEG ⁻¹
	$C_{m\delta_e}$	-.00087	DEG ⁻¹
*BASED ON ACTUAL GEOMETRY			

TABLE D7/G

AIRPLANE STABILITY DERIVATIVES FOR VI SUBSONIC CRUISE

ITEM	SYMBOL	VALUE	DIMENSION
WEIGHT	W	32000	LBS
ALTITUDE	h	35000	FT
REFERENCE GEOMETRY $\Lambda_{LE} = 4^\circ$			
WING AREA	S_w	4684	FT ²
WING SPAN	b	86.33	FT
WING MAC	\bar{c}	64.52	FT
ACTUAL GEOMETRY $\Lambda_{LE} = 42^\circ$			
WING AREA	S_w	3390	FT ²
WING SPAN	b	142.08	FT
MOMENTS OF INERTIA IN BODY AXES			
	I_{xx}	2.59×10^6	SLUG FT ²
	I_{yy}	12.02×10^6	SLUG FT ²
	I_{zz}	14.38×10^6	SLUG FT ²
	I_{xz}	$.35 \times 10^6$	SLUG FT ²
INCLINATION OF STABILITY X AXIS FROM BODY REFERENCE X AXIS			
POSITIVE DOWN	ϵ_s	3	DEG
EQUIVALENT AIRSPEED	V_e	274	KTS
TRUE AIRSPEED	V_T	826	FT/SEC
AIRPLANE TRIMMED LIFT COEFFICIENT ($C_L = W/q_{\infty}$)	C_L	.275	
ANGLE OF ATTACK AT TRIM	α_{TRIM}	3	DEG
AIRPLANE LIFT CURVE SLOPE	$C_{L\alpha}$	2.78	RAD ⁻¹
AERODYNAMIC TIME (LONGITUDINAL)	τ_{2V_T}	.039056	SEC
STATIC LONGITUDINAL STABILITY	$C_{m\alpha}$	-.203	RAD ⁻¹
PITCH DAMPING DUE TO ANGLE OF ATTACK	$C_{m\dot{\alpha}}$	-.81	RAD ⁻¹
PITCH DAMPING DUE TO PITCHING VELOCITY	$C_{m\dot{\alpha}}$	-1.70	RAD ⁻¹
AERODYNAMIC TIME (LAT. -DIR.)	$b/2V_T$.08661	SEC
STATIC DIRECTIONAL STABILITY	$C_{n\beta}$.18	RAD ⁻¹
EFFECTIVE DIRECTIONAL STABILITY	$C_{n\dot{\beta}}$	-.033	RAD ⁻¹
SIDE FORCE DUE TO SIDESLIP	$C_{Y\beta}$	-.85	RAD ⁻¹
YAW DAMPING DUE TO YAW RATE	$C_{Y\dot{\beta}}$	-.21	RAD ⁻¹
ROLL DUE TO YAW RATE	$C_{l\dot{\beta}}$	-.14	RAD ⁻¹
SIDE FORCE DUE TO YAW RATE	$C_{Y\dot{\beta}}$.3	RAD ⁻¹
YAW DUE TO ROLL RATE	$C_{Y\dot{\alpha}}$	-.037	RAD ⁻¹
ROLL DAMPING DUE TO ROLL RATE	$C_{l\dot{\alpha}}$	-.37	RAD ⁻¹
SIDE FORCE DUE TO ROLL RATE	$C_{Y\dot{\alpha}}$.084	RAD ⁻¹
*BASED ON ACTUAL GEOMETRY			

DYNAMIC PARAMETERS FOR VI SUBSONIC CRUISE

UNDAUGMENTED AIRPLANE		AUGMENTED AIRPLANE
DUTCH ROLL		
DAMPING RATIO	ζ_d	.0862
CYCLES TO HALF AMPLITUDE	C_H	1.142
RECIPROCAL OF CYCLES TO HALF AMPLITUDE	$1/C_H$.875
ROLL-YAW COUPLING PARAMETER	μ_R	.985
TIME TO HALF AMPLITUDE, SEC	T_H	5.276
DAMPED PERIOD, SEC	P_d	5.014
UNDAMPED NATURAL FREQUENCY, CPS	f_{n_d}	.2004
ROLL TO SIDESLIP RATIO	$\mu_{R/S}$.2794
ROLLING PARAMETER, DEG./FPS	$\mu_{R/S}$.0971
SPIRAL		
TIME TO HALF AMPLITUDE, SEC	T_H	68.76
TIME TO DOUBLE AMPLITUDE, SEC	T_2	
SHORT PERIOD		
DAMPING RATIO	$\zeta_{s.p.}$.42
DAMPED PERIOD, SEC	$P_{s.p.}$	5.758
UNDAMPED NATURAL FREQUENCY, CPS	$f_{n_{s.p.}}$.1913
PHUGOID		
DAMPING RATIO	ζ_p	.0306
DAMPED PERIOD, SEC	P_p	172.58
DAMPER DATA		
ROLL DAMPER GAIN	K_{δ_s}	0
EFFECTIVENESS	$C_{L\delta_s}$	
YAW DAMPER GAIN	K_{δ_r}	1
EFFECTIVENESS	$C_{m\delta_r}$.00095
PITCH DAMPER GAIN	K_{δ_e}	0
EFFECTIVENESS	$C_{m\delta_e}$	
*BASED ON ACTUAL GEOMETRY		

TABLE D7/H

AIRPLANE STABILITY DERIVATIVES FOR VII LANDING APPROACH				DYNAMIC PARAMETERS FOR VII LANDING APPROACH			
ITEM	SYMBOL	VALUE	DIMENSION	UNAugMENTED AIRPLANE	AugMENTED AIRPLANE		
WEIGHT	W	24400.	LBS				
ALTITUDE	h	SEA LEVEL	FT				
REFERENCE GEOMETRY $\Delta_{LE} = 74^\circ$							
WING AREA	S_w	4684	FT ²	ζ_d	.2824		.525
WING SPAN	b	86.33	FT	C_h	.3747		.179
WING MAC	c	64.52	FT	RECIPROCAL OF CYCLES TO HALF AMPLITUDE			
ACTUAL GEOMETRY $\Delta_{LE} = 70^\circ$				$1/C_h$	2.67		5.59
WING AREA	S_w	3315	FT ²	ROLL-YAW COUPLING PARAMETER $\frac{C_{\dot{\phi}}}{C_h}$.547		
WING SPAN	b	173.33	FT	TIME TO HALF AMPLITUDE SEC	3.90		
MOMENTS OF INERTIA IN BODY AXES	I_{xx}	2.25 x 10 ⁶	SLUG FT ²	DAMPED PERIOD, SEC	10.63		
	I_{yy}	9.25 x 10 ⁶	SLUG FT ²	UNDAMPED NATURAL FREQUENCY, CPS	.098		
	I_{zz}	11.21 x 10 ⁶	SLUG FT ²	ROLL TO SIDESLIP RATIO $\frac{C_{\dot{\phi}}}{C_h}$.574		
	I_{xz}	.26 x 10 ⁶	SLUG FT ²	ROLLING PARAMETER, DEG. FPS $\frac{C_{\dot{\phi}}}{C_h}$.1559		.1335
INCLINATION OF STABILITY Y AXIS FROM BODY REFERENCE X AXIS							
POSITIVE DOWN	ϵ_s	5	DEG	TIME TO HALF AMPLITUDE SEC	T_h		
EQUIVALENT AIRSPEED	V_e	125.	KTS	TIME TO DOUBLE AMPLITUDE, SEC	T_2		
TRUE AIRSPEED	V_T	211.	FT/SEC	SHORT PERIOD			
AIRPLANE TRIMMED LIFT COEFFICIENT ($C_L = W_{QSW}$)	C_L	.975		DAMPING RATIO	$\zeta_{s.p.}$.798
ANGLE OF ATTACK AT TRIM	α	5.	DEG	DAMPED PERIOD, SEC	$P_{s.p.}$		13.79
AIRPLANE LIFT CURVE SLOPE	$C_{L\alpha}$	3.6	RAD ⁻¹	UNDAMPED NATURAL FREQUENCY, CPS	$f_{n.s.p.}$.12
AERODYNAMIC TIME (LONGITUDINAL)	τ_{7V_T}	.15289	SEC	PHUGOID			
STATIC LONGITUDINAL STABILITY	$C_{m\alpha}$	-.198	RAD ⁻¹	DAMPING RATIO	ζ_p		.0274
PITCH DAMPING DUE TO ANGLE OF ATTACK	$C_{m\dot{\alpha}}$	-.88	RAD ⁻¹	DAMPED PERIOD, SEC	P_p		37.9
PITCH DAMPING DUE TO PITCHING VELOCITY	$C_{m\dot{\alpha}}$	-.41	RAD ⁻¹	DAMPER DATA			
AERODYNAMIC TIME (LAT. - DIR.)	$b/2V_T$.4107	SEC	ROLL DAMPER GAIN EFFECTIVENESS	K_{δ_s}		
STATIC DIRECTIONAL STABILITY	$C_{n\beta}$.11	RAD ⁻¹		$C_{\dot{\delta}_s}$	0	DEG DEG SEC DEG ⁻¹
EFFECTIVE DIHEDRAL	$C_{l\beta}$	-.74	RAD ⁻¹	YAW DAMPER GAIN EFFECTIVENESS	K_{δ_r}	1.5	DEG DEG SEC DEG ⁻¹
SIDE FORCE DUE TO SIDESLIP	$C_{y\beta}$.57	RAD ⁻¹		$C_{\dot{\delta}_r}$	-.0011	DEG DEG SEC DEG ⁻¹
YAW DAMPING DUE TO YAW RATE	$C_{n\dot{\beta}}$	-.19	RAD ⁻¹	PITCH DAMPER GAIN EFFECTIVENESS	K_{δ_e}	0	DEG DEG SEC DEG ⁻¹
ROLL DUE TO YAW RATE	$C_{l\dot{\beta}}$.24	RAD ⁻¹		$C_{\dot{\delta}_e}$		
SIDE FORCE DUE TO YAW RATE	$C_{y\dot{\beta}}$.069	RAD ⁻¹				
YAW DUE TO ROLL RATE	$C_{n\dot{\alpha}}$	-.06	RAD ⁻¹				
ROLL DAMPING DUE TO ROLL RATE	$C_{l\dot{\alpha}}$	-.47	RAD ⁻¹				
SIDE FORCE DUE TO ROLL RATE	$C_{y\dot{\alpha}}$.52	RAD ⁻¹				
*BASED ON ACTUAL GEOMETRY							

DYNAMIC PARAMETERS FOR VIII WINGS AFT LANDING APPROACH

ITEM	SYMBOL	VALUE	DIMENSION
WEIGHT	W	230000	LBS
ALTITUDE	h	0 (SEA)	FT
REFERENCE GEOMETRY $\Delta L_{REF}^{(0)}$			
WING AREA	S_w	4684	FT ²
WING SPAN	b	86.33	FT
WING MAC	\bar{c}	64.52	FT
ACTUAL GEOMETRY $\Delta L_{ACT} = 34^\circ$			
WING AREA	S_w	4684	FT ²
WING SPAN	b	86.33	FT
MOMENTS OF INERTIA BODY AXES			
	I_{xx}	1.05×10^6	SLUG FT ²
	I_{yy}	9.45×10^6	SLUG FT ²
	I_{zz}	10.05×10^6	SLUG FT ²
	I_{xz}	$.2 \times 10^6$	SLUG FT ²
INCLINATION OF STABILITY X AXIS FROM BODY REFERENCE X AXIS			
POSITIVE DOWN	δ	10	DEG
EQUIVALENT AIRSPEED	V_e	179.3	KTS
TRUE AIRSPEED	V_T	303	FT/SEC
AIRPLANE TRIMMED LIFT COEFFICIENT ($C_L = \frac{W}{q S_w}$)	C_L	.45	
ANGLE OF ATTACK AT TRIM	α_{TRIM}	10	DEG
AIRPLANE LIFT CURVE SLOPE	$C_{L\alpha}$	2.56	RAD ⁻¹
AERODYNAMIC TIME (LONGITUDINAL)	τ_{2V_T}	.1124	SEC
STATIC LONGITUDINAL STABILITY	$C_{m\alpha}$	-.335	RAD ⁻¹
PITCH DAMPING DUE TO ANGLE OF ATTACK	$C_{m\dot{\alpha}}$	-.73	RAD ⁻¹
PITCH DAMPING DUE TO PITCHING VELOCITY	$C_{m\dot{\theta}}$	-1.37	RAD ⁻¹
AERODYNAMIC TIME (LAT. - DIR.)	$b/2V_T$.1504	SEC
STATIC DIRECTIONAL STABILITY	$C_{Y\beta}$.2	RAD ⁻¹
EFFECTIVE DIHEDRAL	$C_{Y\dot{\beta}}$	-.17	RAD ⁻¹
SIDE FORCE DUE TO SIDESLIP	$C_{Y\beta}$	-.40	RAD ⁻¹
YAW DAMPING DUE TO YAW RATE	$C_{Y\dot{\beta}}$	-.41	RAD ⁻¹
ROLL DUE TO YAW RATE	$C_{l\dot{\beta}}$.23	RAD ⁻¹
SIDE FORCE DUE TO YAW RATE	$C_{Y\dot{\beta}}$.35	RAD ⁻¹
YAW DUE TO ROLL RATE	$C_{Y\dot{\phi}}$	-.73	RAD ⁻¹
ROLL DAMPING DUE TO ROLL RATE	$C_{l\dot{\phi}}$	-.177	RAD ⁻¹
SIDE FORCE DUE TO ROLL RATE	$C_{Y\dot{\phi}}$.42	RAD ⁻¹
*BASED ON ACTUAL GEOMETRY			

ITEM	SYMBOL	VALUE	DIMENSION
DUTCH ROLL			
DAMPING RATIO	f_d	.066	
CYCLES TO HALF AMPLITUDE	C_H	1.668	
RECIPROCAL OF CYCLES TO HALF AMPLITUDE	$1/C_H$.600	
1. YAW COUPLING PARAMETER $\frac{C_{Y\dot{\phi}}}{C_{l\dot{\phi}}}$	$\frac{C_{Y\dot{\phi}}}{C_{l\dot{\phi}}}$.653	
2. TO HALF AMPLITUDE, SEC	T_H	1.5	
DAMPED PERIOD, SEC	P_d	6.1	
UNDAMPED NATURAL FREQUENCY, CPS	f_{n0}	.243	
ROLL TO SIDESLIP RATIO $\frac{C_{Y\dot{\phi}}}{C_{l\dot{\phi}}}$	$\frac{C_{Y\dot{\phi}}}{C_{l\dot{\phi}}}$	3.0	
ROLLING PARAMETER, DEG./FPS $\frac{C_{Y\dot{\phi}}}{C_{l\dot{\phi}}}$	$\frac{C_{Y\dot{\phi}}}{C_{l\dot{\phi}}}$.565	
SPIRAL			
TIME TO HALF AMPLITUDE, SEC	T_H	28.5	
TIME TO DOUBLE AMP.ITUDE, SEC	T_2		
SHORT PERIOD			
DAMPING RATIO	$\zeta_{s.p.}$.5788	
DAMPED PERIOD, SEC	$P_{s.p.}$	6.34	
UNDAMPED NATURAL FREQUENCY, CPS	$f_{n s.p.}$.193	
PHUGOID			
DAMPING RATIO	ζ_p	.1634	
DAMPED PERIOD, SEC	P_p	47.52	
DAMPER DATA			
ROLL DAMPER GAIN EFFECTIVENESS	K_{δ} $C_{l\delta}$	6	DEG/DEG-SEC DEG ¹
YAW DAMPER GAIN EFFECTIVENESS	$K_{\dot{\beta}}$ $C_{Y\dot{\beta}}$	19 -.0014	DEG/DEG-SEC DEG ¹
PITCH DAMPER GAIN EFFECTIVENESS	$K_{\dot{\phi}}$ $C_{l\dot{\phi}}$	0	DEG/DEG-SEC DEG ¹
*BASED ON ACTUAL GEOMETRY			

ITEM	SYMBOL	VALUE	DIMENSION
WEIGHT	W	230000	LBS
ALTITUDE	h	0 (SEA)	FT
REFERENCE GEOMETRY $\Delta L_{REF}^{(0)}$			
WING AREA	S_w	4684	FT ²
WING SPAN	b	86.33	FT
WING MAC	\bar{c}	64.52	FT
ACTUAL GEOMETRY $\Delta L_{ACT} = 34^\circ$			
WING AREA	S_w	4684	FT ²
WING SPAN	b	86.33	FT
MOMENTS OF INERTIA BODY AXES			
	I_{xx}	1.05×10^6	SLUG FT ²
	I_{yy}	9.45×10^6	SLUG FT ²
	I_{zz}	10.05×10^6	SLUG FT ²
	I_{xz}	$.2 \times 10^6$	SLUG FT ²
INCLINATION OF STABILITY X AXIS FROM BODY REFERENCE X AXIS			
POSITIVE DOWN	δ	10	DEG
EQUIVALENT AIRSPEED	V_e	179.3	KTS
TRUE AIRSPEED	V_T	303	FT/SEC
AIRPLANE TRIMMED LIFT COEFFICIENT ($C_L = \frac{W}{q S_w}$)	C_L	.45	
ANGLE OF ATTACK AT TRIM	α_{TRIM}	10	DEG
AIRPLANE LIFT CURVE SLOPE	$C_{L\alpha}$	2.56	RAD ⁻¹
AERODYNAMIC TIME (LONGITUDINAL)	τ_{2V_T}	.1124	SEC
STATIC LONGITUDINAL STABILITY	$C_{m\alpha}$	-.335	RAD ⁻¹

CROSS REFERENCE INDEX

PROPOSAL DOCUMENTS - REQUEST FOR PROPOSAL (RFP)

This cross-reference index relates the paragraphs of the proposal documents to the Evaluation Factors and to the numbered paragraphs of the Request for Proposal. This index permits a reader to locate in the proposal documents each of the paragraphs which relate to any of the Evaluation Factors or any one of the paragraphs in the RFP.

The code uses the proposal document numbers as listed below:

Vol. No.

V-I Summary
A-I Airframe Work Statement
A-II Model Specification
A-III Aircraft Description
A-IV Structural Report
A-V Aerodynamic Report
A-VI Propulsion Report
A-VII Systems Report
A-VIII Ground Support Equipment Report
A-IX Test & Certification Plan
A-X Aircraft Mockup and DEI Plan
A-XI Flight Operation and Safety Management
M-I Management Controls
M-II Product Support Plan
M-III Preliminary Production Plan
M-IV Development & Production Cost
M-V Direct Operating Costs

Subject

Development Plan

V-I - paragraph 4.1
A-I - paragraph 2.1.6, 3.1.6
M-IV - paragraph 1.0, 1.3, 2.0, 6.0 and 7.0

If the reader wishes to know where paragraph 3.2.11.3 of the RFP, AUTOMATIC FLIGHT CONTROL SYSTEM, is described he will find the subject discussed in:

3.2.11.3 AUTOMATIC FLIGHT CONTROL SYSTEM

A-II - paragraph 8.4, 9.6
A-III - paragraph 9.7
A-VII - paragraph 3.3.3
A-IX - paragraph 4.2.6.3, 5.1.6.3
A-XI - paragraph 3.10

For example, if a reader is interested in Boeing's Development Plan as a part of the Master Plan as one of the evaluation factors, he will find this subject discussed in:

INDEX OF PROPOSAL DOCUMENTS TO EVALUATION FACTORS

MANAGEMENT

• MANAGEMENT & ORGANIZATION

Organization

V-I 4.2

M-I 1.2, 1.3, 2.0, 3.0, App. A

Manpower

V-I 5.3

M-I 4.2.3

• COMPANY COMPETENCE

V-I 6.0

M-I 1.6, 6.0

Financial Competence

M-I 6.6

Commercial Product Development

V-I 5.0

M-I 6.2, 6.3

Reliability & Quality of Products

M-I 6.4

Meeting Commitments

M-I 6.5

• FACILITIES (DEVELOPMENT & PRODUCTION)

V-I 5.1

A-I 2.1.9, 3.1.9

A-IX App. A, App. B

M-I 4.2.3.3

M-IV 1.2, 4.0, 8.0

• SUBCONTRACTING

V-I 4.3

M-I 1.4, 3.6 App. B

Selection

M-I 3.6

M-IV

Control

M-I 3.6, 3.7

M-II 6.3

• MASTER PLAN

V-I 4.0

M-I 1.5, 4.0

Development Plan

V-I 4.1

A-I 2.1.6, 3.1.6

A-IX

A-X

M-I 4.0

M-IV 1.0, 1.3, 2.0, 6.0, 7.0

Production Plan

V-I 4.1

A-X

M-I 4.0

M-IV 3.0, 6.0

• MANAGEMENT CONTROLS

A-I 2.1.7, 3.1.7

M-II All

Configuration

A-I 3.1.2.2

M-I 3.3

M-II 4.0, 6.4.2

Value Engineering

A-I 2.1.2.5, 3.1.2.5

M-II 5.4

PERT

A-IX 1.1, 2.2

M-II 2.2, 2.7

Safety

A-I 2.1.2.4, 3.1.2.4

A-VI 6.4

A-IX 3.1.1.2

M-II 5.3

Reliability

A-I 2.1.2.3, 3.1.2.4

A-VI 5.4, 9.0, 11.4.3

A-IX 1.2.2, 3.2

M-II 5.2

Maintainability

A-I 2.1.2.8, 3.1.2.8

A-VI 9.2, 11.4.3

A-IX 1.2.2, 3.2

M-II 5.5

M-III 2.0

Standardization

A-II 13.0

M-II 7.0

Quality Control

A-I 2.1.6.5, 3.1.6.6

A-IX 1.2.4, 3.4

M-II 6.0

Program Reporting & Documentation

M-I 5.0

M-V 12.0

INDEX OF PROPOSAL DOCUMENTS TO EVALUATION FACTORS (Continued)

TECHNICAL

• AIRCRAFT SYSTEM CONCEPT

A-I 1.0, 2.1, 3.1

Configuration

V-I 2.1

A-I 2.1.2.2

A-II 2.0

A-III All

A-V 5.0, 1.1, 2.0

A-VII 9.0

A-IX 3.1.1.1

A-XI 3.1

Ground System Compatibility

A-IX 1.2.3

M-III 4.0, 6.0

Reliability

A-I 2.1.2.3, 3.1.2.4

A-VI 6.4, 9.0, 11.4.3

A-IX 4.2.11, 5.1.11

M-II 5.2

Safety

A-IV 9.1

A-VII 7.0

A-IX 3.1.1.2, 3.3.8, 4.1.1.10,

4.2.1.12, 4.2.4.9,

5.1.1.13, 5.1.4.9

A-XI 1.1

Maintainability

A-I 2.1.2.8, 3.1.2.8

A-VI 9.2, 11.4.3

A-IX 1.2.2, 3.2

M-II 5.5

M-III 2.0

Sonic Boom & Noise

A-II 3.7, 14.2

A-V B3.3.7, B3.6.5, C6.3

A-VI 10.0, 13.0

A-VII 8.0

A-IX 3.1.1.3, 3.3.3, 4.1.1.11,

4.2.1.13, 5.1.1.4,

5.1.1.14

M-VI 5.2

• AERODYNAMICS

A-V All

Drag Analysis

A-V 6.1.2, C6.1.1

A-IX 3.1.1.1

Stability and Control

A-V 5.2.4, 7.0, D7.0, 1.5

A-IX 3.1.1.1

Airload Analysis

A-IV 4.1, 5.0

A-V 8.2

A-IX 3.1.1.1

Performance

V-I 2.2

A-II 14.0

A-III 1.0, 2.0

A-V 6.0, 3.0, B3.0, 1.2, 4.0,

2.0, A2.0, C6.1, 5.0, 8.0

A-VI 12.0

A-IX 3.1.1.1, 4.1.1, 4.2.1,

4.2.2, 5.1.1, 5.1.2

A-XI 2.0

• AIRFRAME DESIGN

A-I 2.2, 2.3, 3.2, 3.3

A-II 3.0

A-IV 8.0

M-I 4.2.4.3

Structures and Materials

V-I 2.5

A-II 4.0, 1.5

A-IV All

A-IX 3.1.2, 3.3.1

A-XI 3.8

M-IV 5.0, App. A, B, C, D, E,

F and G

Weights

V-I 2.6

A-II 3.3, 3.4

A-III 2.3

A-IV 4.1.1, 16.0

A-V 8.1

Flight Controls

V-I 2.7

A-I 2.6, 3.6

A-II 8.0

A-III 9.0

A-VII 3.0, 4.3

A-IX 3.1.6, 3.3.5, 4.1.6,

4.2.6, 5.1.6

A-XI 3.9, 3.10

M-I 4.2.4.3

INDEX OF PROPOSAL DOCUMENTS TO EVALUATION FACTORS (Continued)

• PROPULSION	Controls	• SYSTEMS
V-I 2.4	A-II 6.3, 6.4, 8.0	V-I 2.7
A-I 2.4, 3.4	A-III 7.4, 7.5	Environmental Control
A-II 6.0	A-V 7.1	V-I 2.7
A-III 7.0	A-VI 5.0	A-I 2.9, 3.9
A-VI All	A-VII 4.0	A-II 11.0
A-IX 3.1.4, 3.3.3, 4.1.4, 4.2.4, 5.1.4	A-IX 3.1.4.5	A-III 11.0
A-XI 3.4	Fuel System	A-VII 6.0
M-I 4.2.4.3	A-II 6.11	A-IX 3.1.9, 3.3.7, 4.1.9, 4.2.9, 5.1.9
	A-III 7.6	A-XI 3.5, 3.6
	A-VI 1.5, 2.8.3, 7.0, 9.1.3, 9.2.4	M-I 4.2.4.3
Engine	A-IX 3.1.4.5, 3.1.4.6, 4.1.4.3, 4.2.4.10, 5.1.4.10	
A-II 6.1.1, 2.6	A-XI 3.3	Secondary Power
A-III 7.2		V-I 2.7
A-VI 1.1, 2.0, 9.1.1, 9.2.1, 11.0	Starting System	A-I 2.5, 3.5
	A-II 6.7	A-II 7.0
Inlet	A-III	A-III 8.0
A-II 6.2.2	A-VI 5.3.1, 6.0, 9.1.2, 11.4.1	A-VII 2.0
A-III 7.1	A-IX 3.1.4.5, 4.2.4.2, 5.1.4.2	A-IX 3.1.5, 3.3.4, 4.1.5, 4.2.5, 5.1.5
A-V D7.5		A-XI 3.2
A-VI 1.3, 3.0, 9.1.4, 9.2.2	Thrust Reversal	M-I 4.2.4.3
A-IX 3.1.4.1, 3.1.4.5, 4.1.4.1, 4.2.4.1, 5.1.4.1	A-II 6.3, 2.6	
	A-III	Navigation & Communications
Installation	A-VI 4.3	V-I 2.7
A-II 6.1.5	A-IX 3.1.4.5, 4.2.4.8, 5.1.4.8, 3.1.4.3	A-I 2.7, 3.7
A-III 7.2, 7.3		A-II 9.0
A-VI 2.0, 1.2		A-III 10.0
A-IX 3.1.10		A-VII 5.0
		A-IX 3.1.7, 3.3.6, 4.1.7, 4.2.7, 5.1.7.1
		A-XI 3.11, 3.13, 3.14
		M-I 4.2.4.3

INDEX OF PROPOSAL DOCUMENTS TO EVALUATION FACTORS (Continued)

Computer & Data Processors		OPERATIONS AND ECONOMICS	
A-II 9.2.2, 9.3.1		Direct Operating	Handling Qualities
A-III		V-I 2.3	A-V 7.2
A-VII 5.0		A-I 2.1.2.1, 3.1.2.1	A-XI 2.0
A-IX 3.1.7.2, 4.3, App B		M-VI All	
M-III 5.0			Operation Flexibility
		Sales Price	V-I 2.2.1
Hydraulic & Pneumatic		V-I 3.0	A-XI 2.0, 3.0
A-II 7.3, 7.4		M-V 7.0	M-VI 5.0
A-III			Cockpit Facilities
A-VII 2.2, 2.3		Growth Potential	V-I 2.7
A-IX 3.1.5.2, 4.2.5.2, 5.1.5.4		A-V 1.3, 4.0	A-I 2.3, 3.3
A-XI 3.7		A-VI 11.6.3	A-II 5.0, 10.0
		M-VI 3.3	A-III 5.0
Instrumentation & Displays		Passenger & Cargo Accommodations	A-VII 4.0
A-II 5.5, 5.13, 6.10		A-I 2.8, 3.8	A-IX 3.1.3, 4.2.3
A-III 5.0		A-II 10.0	A-XI 3.0
A-VI 7.8		A-III 6.0	
A-VII 4.3, 5.0, 5.1.20		A-VII 9.0	• GROUND OPERATIONS
A-IX 4.1.1.1, 4.1.3.1, 4.1.3.2, 4.2.3.1, 4.2.3.2, 5.1.1.1, 5.1.3, 3.1.4.5		M-VI 3.0	A-I 2.10, 3.10
A-XI 3.12			A-II 12.0
			M-III All
		• FLIGHT OPERATIONS & SAFETY	
		V-I 2.2.1	Support Systems Concept
		A-XI All	A-VIII 1.0
• TEST & CERTIFICATION PLAN			M-III 1.0
A-I 2.1.4, 2.1.8, 3.1.4, 3.1.8		Safety	Airport Compatibility
A-IV 10.2.3.2, 10.2.5, 14.0		V-I	A-IV 15.5
A-VI 8.0		A-I 2.1.2.4, 3.1.2.4	M-III 4.0
A-VII 4.4, 10.0		A-VII 7.0	
A-IX All		A-XI 3.15	

Servicing	Maintenance	Training Plans
1.4.2	Phase II	A-I 2.12, 2.13, 3.12, 3.13
	V-I 4.1	A-XI 4.0
	A-I 1.2.2, 2.0	M-III 8.0, 9.0
	A-II Supp. S-1	
	M-I 4.2	
	M-V 1.1	
1.4.3	Phase III	
	V-I 4.1	
	A-I 1.2.3, 3.0	
	A-IX 2.3, 4.0	
	M-I 4.2	
	M-V 1.2	
1.5.1	Financial Participation	
	V-I 3.0	
	M-V 1.1, 1.2	
1.5.2	Research Credit as a Part of Manufacturers' Participation	
	M-V 1.1	
1.54	Contract Provisions	
	M-I 12.0	

INDEX OF PROPOSAL DOCUMENTS TO REQUEST FOR PROPOSAL PARAGRAPHS

1.4.2	• 2.1	GENERAL V-I 1.0	• 2.4	PAYLOAD PROVISIONS A-III 2.2 A-V 3.1
	• 2.2	RANGE AND PAYLOAD A-II 3.2.2, 14.1 A-III 2.2 A-V 3.0, B3.1.1	• 2.5	SONIC BOOM PRESSURES A-II 14.3 A-V 4.2, B3.4.5, B3.5.8, B3.6.5, C6.3 A-IX 4.1.1.11
1.4.3	2.2.1	Emergency Range A-V 3.1 A-XI B3.1.1		
	2.2.2	Fuel Reserves A-V 3.1 A-VI 7.0	• 2.6	NOISE A-II 3.7, 14.2 A-VI 10.0 A-VII 8.0 A-IX 4.2.1.13, 5.1.1.14
1.5.1	2.2.3	Additional Fuel Capacity A-V 3.1 A-VI 7.0		
1.5.2	• 2.3	SPEED V-I 2.2 A-II 3.2.5 A-III 2.4 A-V 8.5		
1.54				

INDEX OF PROPOSAL DOCUMENTS TO REQUEST FOR PROPOSAL PARAGRAPHS (Continued)

2.6.1	Takeoff Noise A-II 14.2 A-V B3.3.7, B3.3.8 A-VI 10.0 A-DX 4.1.1.11 A-XI 2.1.3	2.8.2	Instrument Approach Capability A-VII 3.3.3.3, 5.1.2.0	2.8.10	Go-Around Capability A-V 3.4.2 A-XI 2.5.2.3
2.6.2	Landing Noise A-II 14.2 A-V 3.4.1 A-VI 10.0 A-DX 4.1.1.11	2.8.3	Automatic Landing Capability A-VI 1.0 A-VII 3.3.3 A-XI 3.10.2.3	• 2.9	OPERATIONAL LIFE A-II 4.1.1
2.6.3	Ground Noise A-V 3.3.1 A-VI 10.0 A-VII 8.2.2	2.8.4	Wheel Loading A-IV 15.5	• 2.10	GROUND OPERATIONAL ENVIRONMENT A-VI 2.3, 6.1
2.7.1	Flying Qualities A-V 3.2, 7.2, B3.2 A-DX 4.2.1 A-XI 2.0	2.8.6	Takeoff and Landing Speeds A-II 3.2.7 A-III 2.4	• 2.11	MAINTAINABILITY A-I 2.1.2.8, 3.1.2.8 A-VI 9.2, 11.4.3, 11.6.4 A-VII 3.2.6 A-VIII M-II 5.5
2.7.2	Compatibility with Air Traffic Control System A-XI 1.0, 2.3.4, 2.5.1	2.8.7	Crosswind Capability A-V 7.0 A-XI 2.5.2.6	• 2.12	RELIABILITY A-I 2.1.2.3, 3.1.2.3 A-VI 9.1, 11.4.3 A-VII 2.2.6, 3.2.5, 6.5 M-II 5.2
2.8.1	Normal Approach and Landing Characteristics A-II 3.9 A-III 2.4 A-V 3.0 A-XI 2.1, 2.5	2.8.8	Landing Distances A-II 14.1 A-III 2.5 A-V 3.0, C6.2 A-XI 2.5	• 2.13	GROUND OPERATIONAL OBJECTIVES A-VIII 4.0

INDEX OF PROPOSAL DOCUMENTS TO REQUEST FOR PROPOSAL PARAGRAPHS (Continued)

• 2.14	TURNING RADIUS A-V B3.3.3	• 2.21	RADIATION MONITORING A-II 3.5.2	2.24.3	Preliminary Evaluation of En-Route Performance Characteristics During Typical Mission Profile A-VI 11.3 A-IX 4.0
• 2.15	PASSENGER COMPARTMENT WINDOWS A-II 4.4.4	2.22.1	Aircraft Fire Protection A-II 6.9 A-VI 2.10, 7.9.1 A-VII 7.3 A-IX 4.2.1.12	2.25.1	Engine Power Control and Ignition System A-VI 5.0, 5.3.1, 6.0 8.2.2
• 2.16	COCKPIT VISIBILITY A-VII 4.2	2.22.2	Crash Fire Prevention Measures A-VI 7.3.2 A-VII 7.3	2.25.2	Engine Lubrication System A-VI 2.3
• 2.17	FUEL CHARACTERISTICS A-II 6.11 A-VI 7.10	• 2.23	COMMUNICATIONS AND NAVIGATION EQUIPMENT A-I 2.7, 3.7 A-VII 5.0 A-IX 1.3.1, 4.1	2.25.3	Engine/Inlet Compatibility A-III 7.0, 7.1 A-VI 3.0 A-IX 3.1.4.1, 3.1.4.2, 3.1.4.5, 4.1.4.1, 4.2.4.1, 5.1.4.1
• 2.18	OVER-WATER PROVISIONS A-XI 3.15	• 2.24	100-HOUR DECISION POINT FLIGHT TEST REQUIREMENTS A-I 2.1.8, 3.1.8 A-IX 4.0	2.25.4	Automatic Sequencing of Engine and Inlet Control A-VI 5.2, 5.3
• 2.19	INFLIGHT CABIN NOISE A-II 3.7	2.24.1	Preliminary Evaluation of Handling Qualities A-IX 4.0	2.25.5	Aerodynamic Braking A-VI 4.3
• 2.20	FLIGHT CREW COMPLEMENTS, STATIONS AND FACILITIES A-II 4.2.2.2, 5.0 A-VII 4.0	2.24.2	Preliminary Evaluation of Takeoff and Landing Performance A-IX 4.0		

INDEX OF PROPOSAL DOCUMENTS TO REQUEST FOR PROPOSAL PARAGRAPHS (Continued)

• 3.2	AIRFRAME MANUFACTURER DATA REQUIREMENTS	3.2.3.4	Passenger Cabin A-I 2.8, 3.8 A-II 4.4.2.1, 10.0 A-III 6.0, 8.1.5 A-VII 9.0 A-IX 3.1.8	3.2.4.1	Materials and Construction A-II 4.1, 4.2, 4.3, 4.4 A-III 4.0 A-IV 2.4, 7.0, App. C M-IV 5.0
3.2.1	Work Statement - Airframe A-I All	3.2.3.5	Cargo Compartments A-I 2.8, 3.8 A-II 4.4.2.3, 10.0 A-III 6.0, 8.1.5 A-VII 9.0 A-IX 3.1.8	3.2.4.2	Flutter, Divergence & Control Characteristics A-IV 10.0, App. F A-IX 3.1.2.2, 3.3.1, 4.1.2.1, 4.2.2.1, 5.1.2.1
3.2.2	Specifications A-II All	3.2.3.6	Landing Gear System A-II 4.5 A-III 4.4 A-IV 15.0 A-XI 3.1.2.3, 3.8, 4.2.2.4	3.2.4.3	Vibration Program A-IV 2.7, 11.0 A-IX 3.3.1, 4.2.2.5, 5.1.2.2
3.2.3	Aircraft Description V-I 2.1 A-II 2.0, 3.0 A-III All A-V 1.1, 2.0 A-XI 3.1	3.2.3.7	Aircraft Lighting A-II 7.2.11 A-III 8.1.5 A-VII 2.4.8, 4.3.4	3.2.4.4	Dynamic Loads Data A-IV 2.3, 12.0, App. G A-IX 3.1.2, 3.3.1, 4.2.2.3, 5.1.2.1
3.2.3.1	General Arrangement Drawing A-II 2.1 A-III 3.0	3.2.4	Structural Data V-I 2.5 A-I 2.2, 3.2 A-II 4.0 A-III 4.0 A-IV 2.0, 2.1, 2.5, 2.6, 2.10, 2.11, 3.0, 4.0, 5.0, 6.0, 7.0, 8.0, 9.0, App. A, D, E A-IX 3.1.2, 3.3.1, 4.2.2, 5.1.2 M-I 4.2.4.3	3.2.4.5	Sonic Fatigue Program A-IV 2.8, 2.9, 13.0 A-IX 3.1.1.3, 3.1.2.4, 4.2.2.5, 5.1.2.2
3.2.3.2	Combined Inboard Profile and Fixed Equipment Drawing A-II 4.4, 2.2 A-III 3.2	3.2.3.3	Flight Deck Arrangement V-I 2.7 A-I 2.3, 3.3 A-II 4.4.2.3, 5.0, 10.0 A-III 5.0 A-VII 4.0 A-XI 3.1	3.2.4.6	Static and Fatigue Tests A-IV 2.10, 2.11, 9.0, 14.0 A-IX 3.1.2.3, 3.1.2.6, 3.1.2.7

INDEX OF PROPOSAL DOCUMENTS TO REQUEST FOR PROPOSAL PARAGRAPHS (Continued)

3.2.4.7	Aerodynamic Heating Data A-IV 2.1, 6.0, App. B A-VI 8.2.2	3.2.7.2	Flight Profile A-V 3.0, 7.0, D7.0	3.2.9.2	Controls A-II 6.3, 6.4 A-III 7.1, 7.3, 7.4 A-VI 5.0
3.2.4.8	Landing Gear A-II 4.5 A-III 4.4 A-IV 15.0 A-IX 3.1.2.3, 4.2.2.4	3.2.7.3	Variable Geometry A-V 5.1.3, 7.0	3.2.9.3	Engine Starting System A-II 6.7 A-III 7.4 A-VI 5.3.1, 6.0, 8.5, 9.1.2 A-VII 7.4, 7.5 A-DX 3.1.4.5, 3.3
3.2.5	Weight and Balance V-I 2.6 A-II 3.3, 3.4 A-III 2.3 A-IV 16.0 A-V 8.1	3.2.7.4	Additional Data A-V B3.0, 6.0, D7.0	3.2.9.4	Fuel System A-II 6.11 A-III 7.5 A-VI 1.5, 7.0, 8.6, 9.1.3, 9.2.4 A-DX 3.1.4.6, 5.1.4.10 A-XI 3.3
3.2.6	Aerodynamic Data A-III 2.0 A-V 2.0, A2.0, 4.0, C6.1, 8.0 A-IX 3.1.1.1, 3.1.2.2, 3.1.4.1, 3.1.4.3	3.2.9	Propulsion V-I 2.4 A-I 2.4, 3.4 A-II 6.0 A-III 7.0, 7.6 A-V 5.2.5 A-VI All A-IX 3.1.4, 3.3.3, 4.1.4, 4.2.4, 5.1.4 A-XI 3.4	3.2.9.5	Engine Installation A-II 6.2 A-III 7.2 A-VI 1.2, 2.0, 8.2 A-DX 3.1.4.5, 4.2.4.6, 5.1.4.7
3.2.7	Performance	3.2.9.1	Engines A-II 2.6, 6.1 A-III 7.0 A-V 5.1.1, 5.1.2 A-VI 1.1, 2.0, 4.3, 9.2.1, 11.0 A-IX 3.1.1.2, 3.1.4.5, 3.3.3, 4.1.1.10, 4.2.12, 5.1.4.9	3.2.9.6	Engine Inlet Configuration A-II 6.2.2 A-III 7.1 A-V D7.5 A-VI 1.3, 3.0, 8.3, 9.1.4, 9.2.2 A-DX 3.1.4.1, 4.2.4.1, 5.1.4.1
3.2.7.1	Report V-I 2.2 A-II 14.0 A-V 1.2, 3.0, B3.0, 4.0, C6.1 A-VI 11.3, 12.0 A-XI 2.0				

INDEX OF PROPOSAL DOCUMENTS TO REQUEST FOR PROPOSAL PARAGRAPHS (Continued)

3.2.10	Secondary Power	3.2.11	Flight Control System	3.2.11.4	Flight Instruments
	V-I 2.7		A-I 2.6		A-II 5.13.4, 6.10,
	A-I 2.5, 3.5		A-II 8.0		9.3
	A-II 7.0		A-III 9.0		A-III 5.3
	A-III 8.0		A-IX 3.1.6, 4.1.6,		A-VII 4.3, 5.0
	A-VII 2.0, 10.2		4.2.6, 5.1.6		A-IX 5.1.3
	A-IX 3.1.5, 3.3.4,		A-XI 3.9		A-XI 3.12
	4.1.5, 4.2.5,		M-I 4.2, 4.3		
	5.1.5				
	M-I 4.2.4.3	3.2.11.1	Design Data	3.2.11.5	Engine and Fuel System
			A-V 7.1		Instruments
			A-VII 3.2		A-II 6.10, 6.11.7
					A-III 5.3
					A-VI 2.5, 7.8
					A-VII 4.3
3.2.10.1	Hydraulic Systems	3.2.11.2	Control System Description	3.2.12	Navigation & Communications Equipment
	A-II 7.3		V-I 2.7		V-I 2.7
	A-III 8.2		A-I 2.6, 3.6		A-I 2.7, 3.7
	A-VII 2.2, 10.2.1		A-II 8.0		A-II 9.0
	A-IX 3.1.5.2, 4.2.5.1,		A-III 9.0		A-III 10.0
	5.1.5.4		A-VII 3.3		A-VII 5.0, 10.5
	A-XI 3.7		A-IX 3.1.6, 3.3.5,		A-IX 3.1.7, 3.3.6,
			4.1.6, 4.2.6,		4.1.7, 4.2.7,
			5.1.6		5.1.7
			A-XI 3.9		A-XI 3.11, 3.13, 3.14
3.2.10.2	Pneumatic System				
	A-II 7.4				
	A-VII 2.3				
3.2.10.3	Electrical System	3.2.11.3	Automatic Flight Control System	3.2.13	Computer and Data Processors
	A-II 7.2		A-II 8.4, 9.6		A-II 9.2.2, 9.3.1
	A-III 3.2, 8.1, 10.3		A-III 9.7		A-III 10.0
	A-VII 2.4		A-VII 3.3.3		A-VII 5.1.5
	A-IX 3.1.5.1		A-IX 4.2.6.3, 5.1.6.3		A-IX 4.3.1, App. B
	A-XI 3.2		A-XI 3.10		

INDEX OF PROPOSAL DOCUMENTS TO REQUEST FOR PROPOSAL PARAGRAPHS (Continued)

3.2.14	Environmental Control	3.2.15.3	Transparent Area Defogging, Defrosting, De-icing & Rain Removal	3.2.16	Noise Data
	V-I 2.7				A-II 3.6, 3.7
	A-I 2.9, 3.9				A-V B3.3.7, B3.3.8, B3.4.5, B3.5.8, B3.6.5
	A-II 11.0				A-VI 10.0
	A-III 11.0		A-II 11.7		A-VII 8.0
	A-VII 6.0, 10.6		A-III 5.2, 7.6		A-IX 3.1.1.3, 3.3.3, 4.1.1.11, 4.2.1.13, 5.1.1.14
	A-IX 3.1.9, 3.3.7, 4.1.9, 4.2.9, 5.1.9		A-VII 4.2.4		M-VI 5.2
	A-XI 3.6		A-IX 4.2.1.12, 5.1.1.13		
	M-I 4.2, 4.3		A-XI 3.5		
3.2.15	Safety Features	3.2.15.4	Fire Protection		
	A-I 2.1.2.4, 3.1.2.4		V-I 2.7	3.2.17	Ground Support Equipment
	A-III 6.1.1		A-II 6.9, 7.2.14, 7.3.12, 10.4.2		A-I 2.10, 3.10
	A-VII 7.0, 10.7		A-III 6.1.5, 7.2		A-II 4.1.7, 4.1.8, 4.1.9, 6.11.8, 7.2.7, 11.2.5, 12.0
	A-IX 3.3.8, 4.2.1.12		A-VI 2.10, 7.9.1		A-VIII All
3.2.15.1	Oxygen		A-VII 7.3		A-IX 3.1.10, 4.1.10, 5.1.10
	A-II 10.4.3, 10.5.5.		A-IX 4.2.1.12, 4.2.4.9		M-I 4.2.4.3
	A-III 6.3		M-I 4.2.4.3		
	A-VII 7.1			3.2.18	Systems Test Program
	A-IX 4.2.1.12, 5.1.1.13	3.2.15.5	Crash Fire Prevention Data		A-I 2.1.4, 3.1.4
3.2.15.2	Anti-icing		A-II 4.1.10		A-IV 10.2.5
	A-II 11.7		A-III 6.1.5		A-VI 8.0
	A-VII 4.2.4.5 7.2		A-VI 7.3.2		A-VII 4.4, 10.0
	A-IX 4.2.1.12		A-VII 7.3		A-IX 3.0
		3.2.15.6	Emergency Arrangements		
			A-II 10.4, 4.4.5.4, 5.3		
			A-III 6.1		
			A-VII 7.4		
			A-XI 3.15		

INDEX OF PROPOSAL DOCUMENTS TO REQUEST FOR PROPOSAL PARAGRAPHS (Continued)

3.2.19	Aircraft Flight Test Program A-I 2.1.8, 3.1.8 A-VI 8.0 A-IX 4.0, 5.0	4.1.2	Organization V-I 4.2 M-I 1.2, 2.0, App. A	• 4.7	VALUE ENGINEERING A-I 2.1.2.5, 3.1.2.5 M-II 5.4
3.2.19.1	Special Requirements - Sonic Boom and Noise A-VII 8.0 A-IX 4.1.1.11, 4.2.1.3, 5.1.1.14	• 4.2	MASTER PROGRAM PLAN V-I 4.1 A-VI 11.4.2, 11.6.2 M-I 1.4, 4.0	• 4.8	STANDARDIZATION A-II 13.0 M-II 7.0
3.2.20	Flight Simulator Program A-IX 6.0	• 4.3	REPORTS AND REPORT FREQUENCY A-IX 1.1 M-I 5.0 M-II 2.6 M-IV 12.0	• 4.9	QUALITY CONTROL A-I 2.1.6.5 A-IX 3.4 M-II 6.0
3.2.21	Aircraft Mockup & Design Engineering Inspection A-I 2.1.3, 3.1.3 A-II 1.9 A-X All M-I 4.2.4.3 M-IV 2.4, 3.1.5	• 4.4	PROGRAM EVALUATION REVIEW TECHNIQUE (PERT) A-IX 2.2 M-II 2.2, 2.7	• 4.10	RELIABILITY A-I 2.1.2.3, 3.1.2.3 A-IX 3.2 M-II 5.2
• 4.1	CONTRACTOR ORGANIZATION & MANAGEMENT M-I All	• 4.5	COST ESTIMATING & BUDGETING PROCEDURES A-IX 2.0 M-II 2.3, 2.4, 2.5, 2.6	• 4.11	PRODUCT SUPPORT PLAN M-III All
4.1.1	Management and Operation V-I 4.3, 5.3 A-I 2.1.7, 3.1.7 M-I 1.3, 2.0, 3.0, 4.2, 3.2, 6.0, App. B M-II 2.0	• 4.6	CONFIGURATION MANAGEMENT A-I 2.1.2.2, 3.1.2.2 M-I 3.3 M-II 4.0	4.11.1	Maintainability A-I 2.1.2.8, 3.1.2.8 A-VI 11.4.3 A-IX 3.2 M-II 5.5 M-III 2.0
				4.11.2	Support Plan A-I 2.11, 3.11 M-III 6.0, 10.0, 11.0, 12.0

INDEX OF PROPOSAL DOCUMENTS TO REQUEST FOR PROPOSAL PARAGRAPHS (Continued)

4.11.3	Warranty Program M-III 13.0	• 4.15	DEVELOPMENT COST DATA V-I 3.0 M-V All	4.16.3	Ground Support Equipment Cost M-V 8.0
4.11.4	Training A-I 2.12, 2.13, 3.12, 3.13 A-XI 4.0 M-III 8.0	4.15.1	Phase II - Airframe & Engine Costs M-V 2.0	• 4.18	DIRECT OPERATING COSTS V-I 2.2.2, 2.3 A-I 2.1.2.1 M-VI All
• 4.12	TOOLING A-I 2.1.6, 3.1.6 M-IV 1.0, 2.0, 3.0, 6.0, 7.0	4.15.2	Phase III - Airframe & Engine Costs M-V 3.0	4.18.1	Cost Factors M-VI 2.1, App. A
• 4.13	FACILITIES A-I 2.1.9, 3.1.9 A-IX App. A, App. B M-I 4.2.3.3 M-IV 1.2, 4.0, 8.0 M-V 10.0	4.15.3	Allocation of Costs by Government Fiscal Year M-V 4.0	4.18.2	Cost Computations M-VI 2.2, App. A
• 4.14	MATERIALS A-I 2.1.5, 3.1.5 A-IV 7.0 M-I 1.4 M-IV 1.3, 5.0	• 4.16	PRODUCTION COSTS M-V 5.0	• 5.0	SUMMARY DATA V-I All
		4.16.1	Work-in-Process Financial Requirements M-V 6.0		
		4.16.2	Estimated Sales Price of the Supersonic Transport M-V 7.0		